GeoFocus volume 13

Niels RAMEIL

Carbonate sedimentology, sequence stratigraphy, and cyclostratigraphy of the Tithonian in the Swiss and French Jura Mountains

A high-resolution record of changes in sea level and climate

Département de Géosciences - Géologie et Paléontologie - Université de Fribourg (Suisse)

DÉPARTEMENT DE GÉOSCIENCES – GÉOLOGIE ET PALÉONTOLOGIE
UNIVERSITÉ DE FRIBOURG (SUISSE)

Carbonate sedimentology, sequence stratigraphy, and cyclostratigraphy of the Tithonian in the Swiss and French Jura Mountains

A high-resolution record of changes in sea level and climate

THÈSE

présentée à la Faculté des Science de l'Université de Fribourg (Suisse)
pour l'obtention du grade de *Doctor rerum naturalium*

Niels RAMEIL

de Frankfurt a.M., Allemagne

Thèse N° 1493

Multiprint SA, Fribourg, 2005

Acceptée par la Faculté des Sciences de l'Université de Fribourg (Suisse)

---

sur la proposition de :

Prof. André STRASSER, Université de Fribourg (Suisse)

Prof. Daniel W.J. BOSENCE, Royal Holloway University of London (Angleterre)

Dr. Hansruedi BLÄSI, Universität Bern (Suisse)

et Prof. Norbert HUNGERBÜHLER, Université de Fribourg (Suisse) – *Président du jury*

Fribourg, le 21 octobre 2005

Le Doyen: Prof. Marco Celio

Directeur de thèse: Prof. André Stasser

“The sediments are a sort of epic poem of the Earth.”

Rachel Louise Carson (1907-1964), mentor of the American environmentalist movement

TABLE OF CONTENTS

ABSTRACT

The present study aims at a better understanding of the development of the Swiss and French Jura platform during the Jurassic/Cretaceous (J/K) boundary interval, with a special focus on the Tithonian stage. Nine reference sections were measured in the Jura Mountains of north-western Switzerland and eastern France, in the Helvetic Alps, and in the Subalpine Ranges in south-eastern France. Their palaeogeographic position was on the north-western margin of the Alpine Tethys. Six of the sections are located in platform, one in slope, and two in basin positions, covering an interval of about 11 Ma from the Late Kimmeridgian (152.2 Ma) to the Middle Berriasian (141.0 Ma). In the Jura Mountains, the sedimentary record consists of a succession of lagoonal and peritidal carbonates that represent a shallow-water carbonate platform. The (hemi)pelagic (re)sediments studied in SE France and the Helvetic Alps were deposited on the slope and in the adjacent basins.

Based on a detailed description and comprehensive sedimentological analysis of the reference sections the development and early diagenesis of the Late Jurassic/ Early Cretaceous carbonate platform are interpreted.

Stratiform, early dolomitization plays an important role in the Late Jurassic. Three different types of early diagenetic dolomite are observed and interpreted to represent three different dolomitization mechanisms: 1) a reflux-type mechanism that accounts for the majority of dolomite, 2) a dolomitization mechanism that depends on the presence of organic matter in burrow systems and is probably related to microbial mediation, and 3) dolomite that forms by evaporation near the surface of tidal flats. Massive dolomitization usually occurs in dolomite caps that define the upper parts of high-frequency shallowing-upward sequences.

Sedimentary sequences occur on different scales. The stratigraphic record of the measured sections can be subdivided in elementary, small-scale, medium-scale, and large-scale (3rd-order) sequences. These sequences are superimposed on long-term (2nd-order) sea-level changes. The studied interval begins in the Late Kimmeridgian – a period of maximum creation of accomodation space, followed by a long-lasting regression into the Early Cretaceous.

According to their estimated duration as inferred from biochronostratigraphic tie-points and their regular stacking pattern, medium-scale, small-scale, and elementary sequences can be interpreted in terms of cyclostratigraphy. Medium- and small -scale sequences are interpreted to represent the long and short eccentricity-cycle (400 and 100 ka respectively). Elementary sequences may in part relate to the 20 ka precession cycle but their record seems to be largely masked by noise that was generated by autocyclic processes, erosion, and/or non-deposition. Large-scale (3rd-order) sequence boundaries in the Jura Mountains usually consist of well-developed medium-scale sequence boundaries that were accentuated either by the superposition of the (orbitally induced) short-term fluctuations on the long-term trend in sea-level change and/or by regional tectonics.

Using litho- and sequence stratigraphic markers and clay mineral data, a detailed correlation for the Late Jurassic and earliest Cretaceous reference sections on the Jura platform is established. Based on some rare biostratigraphic tie-points, the litho- and sequence-stratigraphic record from the platform is then linked to a large-scale sequence-stratigraphic framework derived from the biostratigraphically well-defined basin sections. This allows for a verification of the established sequence- and cyclostratigraphic timeframe by projecting biozones from the basin onto the platform and to relate lithologic changes observed in the basin to events or environmental changes that are much better recorded on the platform. It turns out that the developed sequence- and cyclostratigraphic framework correlates well with various European sequence-stratigraphic studies and that the inferred timing from cyclostratigraphic analysis

is well in tune with the sequence-chronostratigraphic charts of Hardenbol et al. (1998). For the first time, this allows studying platform development and environmental change around the J/K boundary in the Swiss and French Jura Mountains within a high-resolution timeframe.

Clay mineral analysis reveals a Middle to Late Tithonian episode characterized by a very low abundance of kaolinite ("kaolinite minimum zone"). The low abundance of kaolinite is interpreted to indicate the "Late Jurassic dry phase" that is known from all over Europe. Based on the developed cyclostratigraphic timeframe, the duration of the Late Jurassic dry phase in the Jura Mountains is inferred to have lasted 8.4 Ma. Moreover, the detailed lithostratigraphic data allow for subdividing the dry phase into a dry phase *sensu stricto* (fully arid, desert-like climate) and a transition phase with a gradual change to semiarid, and winterwet conditions. A combination of sequence-, cyclo-, bio- and chronostratigraphic evidence supports the hypothesis that the beginning of the kaolinite minimum zone in the Jura Mountains is isochronous to the beginning of the kaolinite minimum zone in Dorset, southern England.

Possible drivers for these major climate changes are discussed. The scenario considered to be most consistent with the sum of all observations is a change in oceanic current patterns in the Greenland-Norwegian seaway. The change in oceanic current patterns was probably linked to a combination of changing geometry of the Greenland-Norwegian seaway due to high rift activity and long-term sea-level evolution, both supposedly linked to a plate-tectonic reorganization that precedes the opening of the northern North Atlantic.

Résumé

Cette étude a pour but une meilleure compréhension du développement de la plate-forme du Jura Suisse et Français à la limite Jurassique/Crétacé (J/K), avec un accent sur l'étude du Tithonien. Neuf coupes de référence ont été mesurées dans le Jura au nord-ouest de la Suisse et dans l'est de la France, dans les Alpes helvétiques et dans les Chaînes Subalpines au sud-est de la France. Leurs positions paléogéographiques étaient sur la marge nord-ouest de la Téthys Alpine. Six de ces coupes sont situées sur la plate-forme, une sur la pente et deux dans le bassin, couvrant un intervalle d'environ 11 Ma du Kimméridgien supérieur (155.2 Ma) au Berriasien moyen (141.0 Ma). Dans le Jura, l'enregistrement sédimentaire comprend une succession de carbonates lagunaires et péritidaux, qui représente une plate-forme carbonatée peu profonde. Les sédiments (hémi-) pélagique (remaniés) étudiés dans le sud-est de la France et dans les Alpes Helvétiques ont été déposés sur la pente et dans les bassins adjacents.

Basé sur une description détaillée et une vaste analyse sédimentologique des coupes de référence, le développement et la diagénèse précoce de la plate-forme carbonatée au Jurassique supérieur/Crétacé inférieur sont interprétés. La dolomitisation stratiforme précoce joue un rôle important dans le Jurassique supérieur. Trois types différents de dolomie précoce sont observés et interprétés. Ils correspondent à trois différents mécanismes de dolomitisation : 1) un mécanisme de type reflux qui explique la majorité de la dolomie, 2) un mécanisme de dolomitisation qui dépend de a présence de matière organique dans des terriers et est probablement relié à la médiation microbienne et 3) la dolomie qui se forme par évaporation près de la surface des estrans tidaux. La dolomitisation massive survient souvent dans des *dolomite caps* qui définissent les parties supérieures des séquences haute fréquence du type *shallowing upward*.

Les séquences sédimentaires existent à différentes échelles. L'enregistrement stratigraphique des coupes mesurées peut être subdivisé en séquences élémentaires, à court terme, moyen terme et long terme (3ème ordre). Ces séquences sont superposées à des changements du niveau marin de long terme (2ème ordre). L'intervalle étudié commence dans le Kimméridgien supérieur avec une période de création d'espace d'accommodation maximale, suivi par une longue régression dans le Crétacé inférieur.

Selon les durées estimées d'après des données biochr onostratigraphiques et un agencement régulier des bancs (*stacking pattern*), les séquences de moyen terme, court

terme et élémentaires peuvent être interprétés en terme de cyclostratigraphie. Les séquences de moyen terme et court terme sont interprétées comme le cycle de 1er ordre et 2ème ordre d'excentricité (400 et 100 ka respectivement). Les séquences élémentaires peuvent en partie être liées au cycle de précession (20 ka). Cependant leur enregistrement semble être largement masqué par le bruit qui a été généré par des processus autocycliques, l'érosion et/ou l'omission. Les limites de séquences de long terme (3ème ordre) dans le Jura sont souvent formés par des limites de séquence de moyen terme bien développées, accentuées par la superposition des fluctuations à court terme (lié à un contrôle orbital) sur l'évolution à long terme des changements du niveau marin et/ou par la tectonique régionale.

En utilisant des marqueurs lithostratigraphiques et séquentiels ainsi que les résultats des analyses des minéraux argileux, une corrélation détaillée pour les coupes de références du Jurassique supérieur et du début du Crétacé sur la plate-forme du Jura est établit. Basé sur de rares niveaux biostratigraphiques bien définis, l'enregistrement lithostratigraphique et séquentiel de la plate-forme est alors lié à un cadre séquentiel de long terme, déduit des coupes de bassin biostratigraphiquement bien définies. Cet approche permet une vérification du cadre séquentiel et cyclostratigraphique établis en projetant des biozones du bassin sur la plate-forme et de relier les changements lithologiques observés dans le bassin à des événements ou des changements paléoenvironnementaux, qui sont mieux enregistrés sur la plate-forme. Il en ressort que le cadre séquentiel et cyclostratigraphique développé se corrèle bien avec de nombreuses études de stratigraphie séquentielle à l'échelle Européen. Et que les durées estimées par l'analyse cyclostratigraphique sont bien en accord avec la charte chronostratigraphique et séquentiel de Hardenbol et al. (1998). Pour la première fois, cela permet d'étudier le développement de la plate-forme et les changements environnementaux autour de la limite Jurassique-Crétacé dans le Jura suisse et français dans un cadre à haute résolution.

Les analyses minéralogiques des argiles révèlent un épisode du Tithonien moyen au Tithonien supérieur, caractérisé par une très faible abondance de kaolinite (*kaolinite minimum zone*). La faible abondance de kaolinite indique la « phase aride du Jurassique supérieur » qui est connue dans toute l'Europe. Basée sur le cadre cyclostratigraphique développé, la durée de la phase aride du Jurassique supérieur dans le Jura est estimée à 8.4 Ma. De plus, les données lithostratigraphiques détaillées permettent de subdiviser la phase aride en une phase aride *sensu stricto* (aride, climat de désert) et une phase de transition avec un changement graduel vers des conditions semi-arides de type « méditerranéen ». Une combinaison des arguments séquentiels, cyclostratigraphiques, bio- et chronostratigraphiques supporte l'hypothèse que le début de la zone minimum à kaolinite dans le Jura est isochrone au début de la zone minimum à kaolinite dans le Dorset, au sud de l'Angleterre.

Des facteurs possibles pour ces changements climatiques majeurs sont discutés. Le scénario considéré comme le plus vraisemblable est un changement dans la courantologie du Proto-Atlantique. Ce changement était probablement lié à une combinaison d'une géométrie changeante du détroit entre Groenland et la Norvège dû à une forte activité de rifting et d'une évolution du niveau marin sur le long terme. Ces deux causes sont probablement liés à une réorganisation des plaques continentaux qui précède l'ouverture de la partie nord de l'Atlantique Nord.

Zusammenfassung

Die vorliegende Arbeit beschäftigt sich mit der Entwicklung der schweizer und französichen Jura Plattform im obersten Jura und der untersten Kreide, wobei das Tithon eine besondere Beachtung erfährt. Dazu wurden neun Referenzprofile im Juragebirge (NW-Schweiz und E-Frankreich), den Helvetischen Alpen und voralpinen Ketten in SE-Frankreich aufgenommen und untersucht. Die paläogeographische Position der aufgenommenen Profile ist am Nordwestrand der Alpinen Tethys, wobei sich sechs Profile auf der Plattform, eins auf dem Slope und zwei in Beckenposition befanden. Der untersuchte Zeitabschnitt umfasst etwa 11 Ma, vom späten Kimmeridge (152.2 Ma) bis ins mittlere Berrias (141.0 Ma). In dieser Zeit wurde im heutigen Juragebirge

eine Abfolge aus lagunären und peritidalen Plattform-Karbonaten abgelagert, während in SE-Frankreich und den Helvetischen Alpen (hemi)pelagische (Re)Sedimente des Slopes und des Beckens angetroffen werden.

Aufbauend auf einer detaillierten Beschreibung und umfassenden sedimentologischen Untersuchung der Referenzprofile werden die Entwicklung und frühdiagenetische Prozesse der oberjurassischen/ unterkretazischen Karbonat plattform nachvollzogen. Eine besondere Rolle splielt dabei frühdiagenetische, schichtparallelle Dolomitisierung. Drei verschiedene Dolomit-Typen werden beschrieben und deren Entstehungsmechnasimen diskutiert: 1) *Reflux*-Dolomit, der den grössten Volumenanteil der beobachteten Dolomitisierung ausmacht; 2) an Bioturbation gebundene Dolomitisierung, die an das Vorkommen organischer Substanz gebunden scheint und wahrscheinlich mikrobiell induziert ist und 3) Dolomit, der nahe der Karbonatwatt-Oberfläche durch Verdunstung entsteht. Durchgehende Dolomitisierung findet sich vor allem in *dolomite caps*, die in der Regel im oberen, stark regressiv geprägten Teil, von Verflachungssequenzen anzutreffen sind.

Die untersuchten Sedimente können in Ablagerungssequenzen verschiedener Ordnung unterteilt werden: Elementar-, „small-scale“, „medium-scale“ und „large-scale“-Sequenzen (3. Ordnung). Diese Ablagerungs-sequenzen unterschiedlicher Dauer überlagern sich gegenseitig und sind langfristigen Meeresspiegelschwan-kungen (2. Ordnung) untergeordnet. Der untersuchte Zeitabschnitt beginnt mit einem Intervall steigenden Meeresspiegels im späten Kimmeridge, bevor ein lang andauernder, regressiver Trend bis in die frühe Kreide einsetzt.

Aufgrund ihrer errechneten durchschnittlichen Dauer und des regelmässigen Stapelungsmusters lassen sich Elementar-, „small-scale“ und „medium-scale“-Sequenzen als Milankovitch-Zylen interpretieren. Dabei entsprechen die „small-scale“- und „medium-scale“-Sequenzen dem langen und kurzen Exzentrizitäts-Zyklus (400 ka bzw. 100 ka). Elemetanrsequenzen können teilweisem dem Präzessions-Zyklus (20 ka) zugeordnet werden, allerdings geht dieses hochfrequente Signal in den meisten Fällen in einem durch autozylische Prozesse, Erosion und Omission erzeugten Rauschen unter. In den Plattformprofilen bestehen „large-scale“-Sequenzgrenzen (3. Ordnung) aus gut entwickelten „medium-scale“-Sequenzgrenzen, welche entweder durch Überlagerungs-effekte von kurzfristigen Meeresspiegelschwankungen orbitalen Ursprungs und langfristigen Meeresspiegelsc hwankungen tektonoeustatischen Ursprungs, oder/und regionale Tektonik entstehen.

Mit Hilfe von lithologischen und sequenzstratigraphischen Leithorizonten, zusätzlich unterstützt durch Tonmineralanalysen, wird eine hochauflösende Korrelation der spätjurassischen und unterkretazischen Profile auf der Jura Plattform erstellt. Einige verstreute biostratigraphische Referenzpunkte in den Plattformprofilen erlauben es, den auf der Plattform etablierten sequenz- und zyklostratigraphischen Zeitrahmen mit der sequenzstratigraphischen Abfolge der Beckenprofilen zu verbinden, die den Vorteil einer wohl definierten Biostratigraphie aufweisen. Dies ermöglicht eine Überprüfung sequenz- und zyklostratigraphischen Zeitrahmens auf der Plattform, indem Biozonen vom becken auf die Plattform projeziert werden können und im Gegenzug die lithologiche Entwicklung der Beckenprofile mit Änderungen von Umweltbedingungen auf der Plattform in Zusammenhang zu bringen, welche dort wesentlich detaillierter überliefert sind.

Vergleicht man den entwickelten sequenz- und zyklostratigraphischen Zeitrahmen mit Literaturdaten, so stellt sich heraus, dass die sequenzstratigraphische Interpretation der untersuchten Profile grosse Ähnlichkeiten mit vielen Studien aus Europa zeigt und der zyklostratigraphische Zeitrahmen sehr gut mit den sequenz-chronostratigraphischen Tabellen von Hardenbol et al. (1998) übereinstimmt. Es ist folglich zum ersten Mal möglich die Entwicklung der Jura Plattform und sich ändernde Umweltbedingungen um die Jura/Kreide-Grenze in einem hochauflösenden Zeitrahmen nachzuvollziehen.

Die durchgeführten Tonmineralanalysen zeigen eine Phase von sehr geringem Kaolinitvorkommen (*kaolinite minimum zone*) im mittleren bis späten Tithon an. Deshalb wird diese Zeit als die Entsprechung einer spätjurassichen Trockenphase interpretiert, welche aus ganz Europa bekannt ist. Wendet man den entwickelten zyklostratigraphischen Zeitrahmen an, so ergibt sich eine Dauer der spätjurassichen Trockenphase von 8.4 Ma. Ausserdem lässt sich die Trockenphase in eine Trockenphase *sensu stricto* (vollarid, wüstenähnliches Klima) und eine Übergangsphase mit einem allmählichen Wechsel zu semiariden, winterfeuchten Bedingungen unter-teilen. Die Hypothese, dass der Beginn der spätjurassichen Trockenphase im Juragebirge und in Dorset (S-England) isochron ist wird durch eine Kombination aus sequenz-, zyklo-, bio- und chronostratigraphischen Argumenten gestützt.

Mögliche Ursachen für diese klimatischen Veränderungen werden diskutiert. Als wahrscheinlichstes Szenario wird eine Änderung des Strömungsmusters in der Grönland-Norwegischen Meeresstrasse angenommen. Die Änderung des Strömungsmusters wird vermutlich durch eine Kombination aus hoher Riftaktivität und langfristigen relativen Meeresspiegelschwankungen verursacht, welche wiederum mit einer plattentektonische Reorganisation in Verbindung steht, die der Öffnung des nördlichen Nordatlantiks vorausgeht.

ACKNOWLEDGEMENTS

Even if there is only one name mentioned on the title page, a PhD thesis is never the work of an individual – on the contrary! It was carried out with the help, both physical and moral, of a large number of colleagues, friends, and family. Without their continuous support, this thesis simply never would have been possible.

First of all, I would like to thank my "*Doktorvater*" André Strasser who accepted me as his PhD student in late August 1999. In the following years, I realized that I had the chance of being guided on the long leash – in the beginning, it felt even a little too long for that inexperienced student starting his thesis. However, very soon I began to appreciate the total liberty I had in exploring the Jura Mountains on my own tracks, knowing someone behind me to drag me back onto the main trail when I risked to get lost in intriguing but secondary details.

Thank you André, for your constant interest in my work, your active help in the field (specifically when my limited alpinistic skills risked to cut short sampling success) and for giving me the opportunity and liberty to widen not only my scientific, but also my geographical, lingual, and human horizons. I very much appreciated the open-door policy of your office, which actually is not only *open door*, but – far more important – also *open ear* and *open mind*. And, last but not least, thank you for the trust you had in me going through to the end of the project, even in times when I had partially lost it.

I further want to thank Dan Bosence (Royal Holloway College, London) and Hansruedi Bläsi (University of Berne) who agreed to be my co-referents. Discussions with Dan Bosence and his former PhD student Georg Warrlich helped to overcome my initial suspicion towards "virtual geology" (quantification and modelling) and thus added a fascinating field to my scientific interests. The PhD thesis of Hansruedi Bläsi on the "Portlandian" of the Jura Mountains was, even if some 25 years old, a solid basis to build my own research upon and a reliable guide where to head for.

During my time at Fribourg, I had the chance to work under great conditions. One the one hand, there was Christian Caron, the institute's director, whose never-ending quest for perfection, improvement of equipment and distributing it evenly among his charges has created a first-class research infrastructure. On the other hand, there were the senior members of the working group who taught me how to use it. I specifically like to thank: Heiko Hillgärtner for being my "career guide" (without knowing it) by showing to me what is possible in a PhD thesis while always keeping "two feet on the ground", Elias Samankassou for always having been willing to share his vast knowledge on microfacies, his help in measuring parts of the Dôle section, and his calm nature and good humour that considerately helped in several situations when I was close to panicking, Claude Colombié for great cooperation in dealing with the Late Kimmeridgian parts of my sections – during my thesis, now, and also in the future, I hope! Well, we still have to find an explanation for those "off-beat" 200 ka… and Wolfgang Hug for numerous valuable discussions on the lithostratigraphic, sequence-stratigraphic and palaeogeographic aspects of the Kimmeridgian/Tithonian transition and for sharing unpublished data with me. Thank you, Wolfgang, also for a warm welcome when I arrived at the institute in October 1999 and everybody else was on a two-week field trip. I hope the Fribourg-Porrentruy link will prove as fruit-bearing as it was for me in the future!

A big "Thank you" also goes to Thierry Adatte (University of Neuchâtel), who made possible an instant and fantastically efficient emergency program for clay mineral analyses when I thought myself trapped in an organizational dead-end. I would also like to thank him for his help in interpreting the raw data and his student(s) who did the sample preparation.

Stephan Dall'Agnolo (University of Fribourg / Federal Office for Water and Geology) gave me a brief but all the more efficient "learning-by-doing" introduction

to calpionellid biostratigraphy and Jürgen Remane (University of Neuchâtel) found both the interest and the time to come over to Fribourg in order to control and fine-tune the results, just a year before his untimely death in 2004.

I also like to thank Peter Baumgartner and Sébastien Bruchez (both University of Lausanne). The former gently agreed to measure stable isotopes in his lab and the latter carried them out – not only very efficiently but also introduced me to the laboratory techniques and patiently answered my numerous questions on the subject. When it came to data interpretation, Stefano Bernasconi (ETH Zurich) shared his vast knowledge on the subject in several fruitful discussions – either by e-mail or in town around a beer.

Jon Mosar (University of Fribourg) was always willing to give extra lessons on structural geology and plate dynamics to an ignorant carbonate sedimentologist. Some essential parts of chapter 8 are rooted in his knowledge on the opening of the North Atlantic and his state-of-the-art private library on this subject.

Caroline Pellaton and Michel Meyer (both former PhD students at the University of Geneva) drew my attention to the Clue de Taulanne and the Cirque des Avalanches sections, respectively.

Thanks to Raymond Plancherel, Daniel Oswald, and Luc Braillard, I received a crash-course in French geological vocabulary when I first arrived in Fribourg and nearly immediately began to assist with the teaching of the 1st-year *travaux pratiques*. I remember a good team that taught me much about my perception of geosciences and how to pass one's fascination for it to the students ("*Glaciers flow! Like that stiff white honey, the ice is neither hard, nor soft; it's… eeerr… plastic*").

As mentioned before, the institute was a great place to work at, not only because of the infrastructure but all the more due to the ambiance created by the scientific staff and PhD students: Bernard, Jürgen, Michèle, Jean-Pierre, Vincent, Sylvia, Folco, Sophie, Florence, Daniel (Oswald), Laurent, Cédric, Anna, Jessica, Lenni, Daniela, Giacomo "the Jazzman", Damien, Chantal, Andrea "il Professore", Claire (Blanc), Peter, Cécile, Kuno, Jonas, Claudius, Sébastien, Stéphanie, Maëlle, Daniel (Marty), and Sabina – hope to see you all at the next medieval-Nutella™-ski-film-weekend! And for those of you who still have to finish their theses: Good luck for your work!

Special "Thank Yous" go to Michèle and her *petites bestioles* – without your warmth the institute would be a much colder place to work at – and to Stéphanie for helping with the French *Resumé*.

There were also many students, who accompanied me during the last few years. In particular, a "Sorry" goes to Sophie Roulin for not having had advanced enough with my own research to help her to interpret the Poteu de Mié section for her diploma thesis and a big "Grazie" goes to Riccardo Mora for his help in the Gorges de Noirvaux, as well as for great discussions on geology, risotto, wine, and many good laughs.

Without our technical staff – Patrick Dietsché, Daniel Cuennet, Christoph Neururer, Jean-Paul "Polo" Bourqui, Françoise Mauroux, and Nicole Bruegger – any kind of scientific work would have been incredibly difficult. They helped with everything from bibliography, sawing samples, and preparing thin sections to organizing festivities, finding a place to keep the drinks cool, and that small but important good word and smile here and there.

Philippe Dubuis, the herdsman of the Dôle pasture, hosted me in his châlet right underneath the section in the field season of 2001, including *Café au berger* in the mornings and passionate discussions on world politics and the faith of our planet in front of the fireplace long into the nights, always accompanied by one or more glass(es) of Swiss White.

Then there were my friends – and I want to mention in particular the ex-crew of the G47, Marco & Bine, Hattes & Saho, André, and Claudia here – who supported me with open ears (respectively phone lines), enduring compassion and numerous attempts to cheer me up and side-drag me whenever I needed it. It simply felt (and feels!) good to have you around. Last but not least, a very special "Thank You" goes to Claire and the elves of the islands. I was really happy to know you at my side when life became as complicated as – and even worse – than this thesis.

The research presented in this GeoFocus volume was financed by the Swiss National Science Foundation (projects no. 20-56491.99 and 20-67736.02) and the University of Fribourg.

And, finally, to those whose contributions I did not mention here from sheer failure of memory or character, please accept my apologies. I owe you all a great debt.

Fribourg, 22. August 2005

1 - Introduction

In previous projects, the Fribourg sequence- and cyclostratigraphy working group carried out detailed analyses of Oxfordian to Kimmeridgian and Berriasian to Valanginian shallow-water sediments in the Swiss and French Jura (Pasquier 1995, Pittet 1996, Hillgärtner 1999, Dupraz 1999, Colombié 2002 and Hug 2003). Comparative studies were undertaken with shallow- and deep-water facies in France (Pasquier 1995, Pittet 1996, Hillgärtner 1999 and Colombié 2002), Spain (Pittet 1996), and Morocco (Hillgärtner 1999). By means of sequence stratigraphy and cyclostratigraphy, and within a relatively well-established chronostratigraphic framework (Hardenbol et al.1998), high-resolution correlations over far distances and between different palaeotectonic and palaeoclimatic regimes have been performed. In order to link these two "time-windows" to a 20 Ma record of highly detailed regional sedimentologic and stratigraphic data, a similar study for the Tithonian was necessary.

However, the Jurassic/Cretaceous (J/K) boundary interval is a long-standing problem in stratigraphy, being largely the result of stratigraphic difficulties caused by a lack of significant faunal turnover at either boundary of the Berriasian stage, and to extreme faunal provincialism as a consequence of the long-term (2^{nd}-order) Tithonian regression (Remane 1991). This is also true for the latest Jurassic and earliest Cretaceous of the Swiss and French Jura Mountains, where nearly 150 years of geological research resulted in a still unsatisfactory stratigraphic precision for the Tithonian Twannbach Formation ("Portlandian"). Due to the rareness of biostratigraphically valuable fossils, the definition of an accurate timeframework in peritidal carbonates demands the implementation of specially developed methods: sequence- and cyclostratigraphical interpretations, geochemical data, and biostratigraphic tie points are linked to produce a high-resolution correlation that reaches from the Late Kimmeridgian to the Middle Berriasian.

1.1 Objectives

The main objective of this study is **"*Closing the gap*"**, i.e. to link the working group's studies carried out in the Kimmeridgian (Colombié 2002) with those dealing with the Berriasian (Hillgärtner 1999, Pasquier 1995; cf. Fig.1.1). In order to achieve this, the following steps are important:

- to give a detailed description and comprehensive sedimentological analysis of the reference sections
- to understand the development of the ancient carbonate platform and the early diagenetic processes that were active
- to establish a sequence- and cyclostratigraphic timeframe for the Tithonian
- to set up a detailed correlation for the latest Jurassic and earliest Cretaceous reference sections in the Swiss and French Jura Mountains, and link it to biostratigraphically well-dated basin sections of the same age
- to use this precise stratigraphic framework in order to better understand the dynamics of Late Jurassic and Early Cretaceous climate and environmental change.

In order to guarantee the match of this study with the other studies of the Fribourg working group, its timeframe is extended to the Late Kimmeridgian so that a sufficient overlap exists with the sections of Colombié (2002). At the top of the studied interval, the work of Strasser (1994), dealing with the lowermost Cretaceous, was integrated

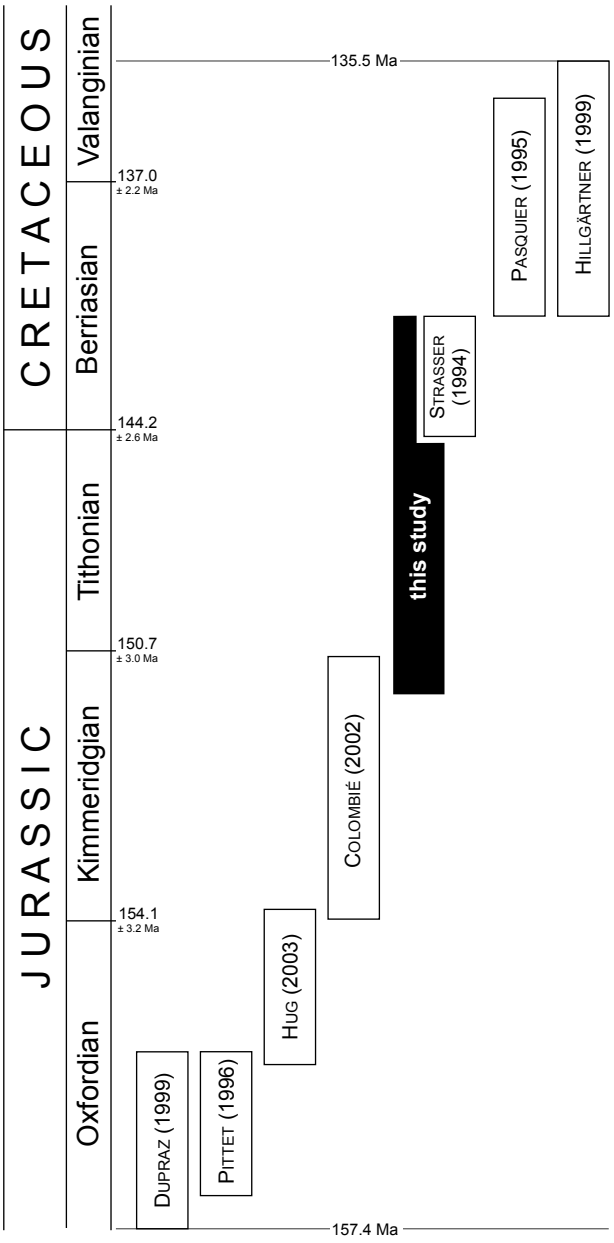

Fig. 1.1 - Stratigraphic range of studies carried out by the Fribourg sequence and cyclostratigraphic working group in the Swiss and French Jura Mountains. Numerical ages from Gradstein et al. (1994).

in order to reach the well-defined transgressive surface where the Berriasian-Valanginian sections studied by Hillgärtner (1999) and Pasquier (1995) begin (Fig.1.1).

1.2 General context

1.2.1 Study area

The main study area is located in the central and southern Jura Mountains, the *Jura vaudois* (north-western Switzerland) and the *Jura méridional* (eastern France) with the exception of one section that is located in the *Ajoie* area in northern Switzerland (Fig. 1.2a, b). The central and southern Jura Mountains belong to the folded Jura chain, the *Ajoie* area is part of the tabular Jura. One slope section is located in the Rhône valley and two basin sections in the French Subalpine ranges and the Helvetic Alps, respectively.

1.2.2 Palaeogeography

In the latest Jurassic and earliest Cretaceous, today's central and western Europe consisted of a patchwork of low-relief islands in a shallow continental sea at the northern (passive) margin of the Alpine Tethys (Fig. 1.3a and 1.4). Here, the Jura platform represented the central part of the North-Tethys platform.

Sedimentation from the Late Kimmeridgian to Middle Berriasian was characterized by shallow-marine and peritidal carbonates. During the Late Jurassic-earliest Cretaceous long-term regression, the platform was never far from exposure with maximum water depths of a few meters only. In times of humid climate, large islands such as the Armorican/Central Massif and Rhenish-Bohemian landmass were the source for significant siliciclastic influx into the Paris Basin and onto the northern Tethyan shelf. This is recorded e.g., in the Early Cretaceous Wealden deposits in southwestern England and the Paris Basin (Ziegler 1988), and the Goldberg Formation ("Purbeckian") on the Jura platform (Häfeli 1966).

The Vocontian and the Helvetic Rim Basin represent a branch of the Alpine Tethys which was bordered to the north and northwest by the Jura platform and to the south and southwest by the Corbières-Provence platform. The palaeogeographic position of Corsica and Sardinia is interpreted differently in plate-tectonic reconstructions (compare, e.g., Thierry et al. 2000 vs. Stampfli et al. 2002, or Fig. 1.3a vs. Fig. 1.4, respectively). Throughout the Late Jurassic and Early Cretaceous, this domain was characterized by hemipelagic to pelagic sedimentation with intermittent biodetrital influx from the surrounding platforms. In contrast to Kimmeridgian and Berriasian limestone-marl alternations, the strata of Tithonian age are relatively massive ("*Barre Tithonique*") or bedded with minor marly interbeds. In the center of the Vocontian Basin, Late Kimmeridgian and Tithonian hemipelagic carbonates are brecciated (Fig. 1.2b; see Remane 1970, Arnaud et al. 1984, Détraz et al. 1987, Séguret et al. 2001, Bouchette et al. 2001 for details).

The palaeolatitude of the Jura platform, according to palaeogeographic reconstructions (Stampfli & Borel 2002, Thierry et al. 2000, Dercourt et al. 1994, Smith et al. 1994, Fourcade et al. 1993, Ziegler 1988), was approximately 25˚ to 35˚ N. In the same reconstructions,

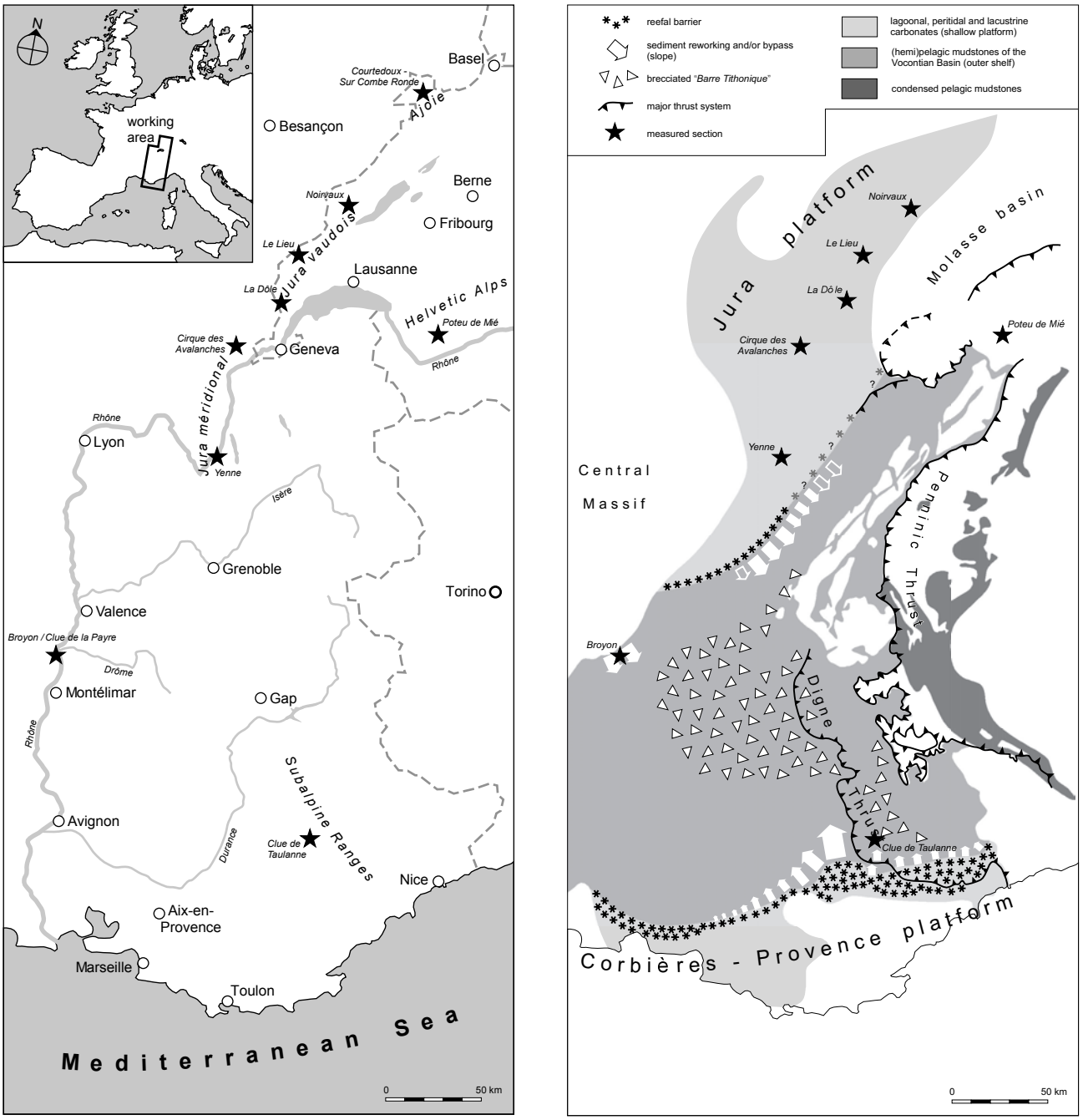

Fig. 1.2 - (a) Geographic overview of the working area, with locations of the measured sections. (b) Simplified facies distribution map of Late Tithonian sediments in the working area. After Debrand-Passard et al. (1984) and Séguret et al. (2001).

the Vocontian Basin was located 2° to 3° further to the south.

1.2.3 Global and regional tectonics

During the Late Jurassic, the supercontinent of Pangea did not exist anymore but, compared to the modern situation, the continents were still relatively close together (Ziegler 1988, Stampfli & Borel 2002; cf Fig. 1.4).

In the southern North Atlantic, the creation of oceanic crust had already begun in Middle Jurassic times and in the Early Tithonian (150 Ma), Iberia began to separate from North America (Schettino & Scotese 2002, Concheryo & Wise 2001). This event caused the formation of a new transform plate boundary between Iberia and Eurasia (Fig. 1.4), and the progressive transfer of left-lateral motion from the southern plate boundary (the former shear zone between Iberia and northern Africa) to this

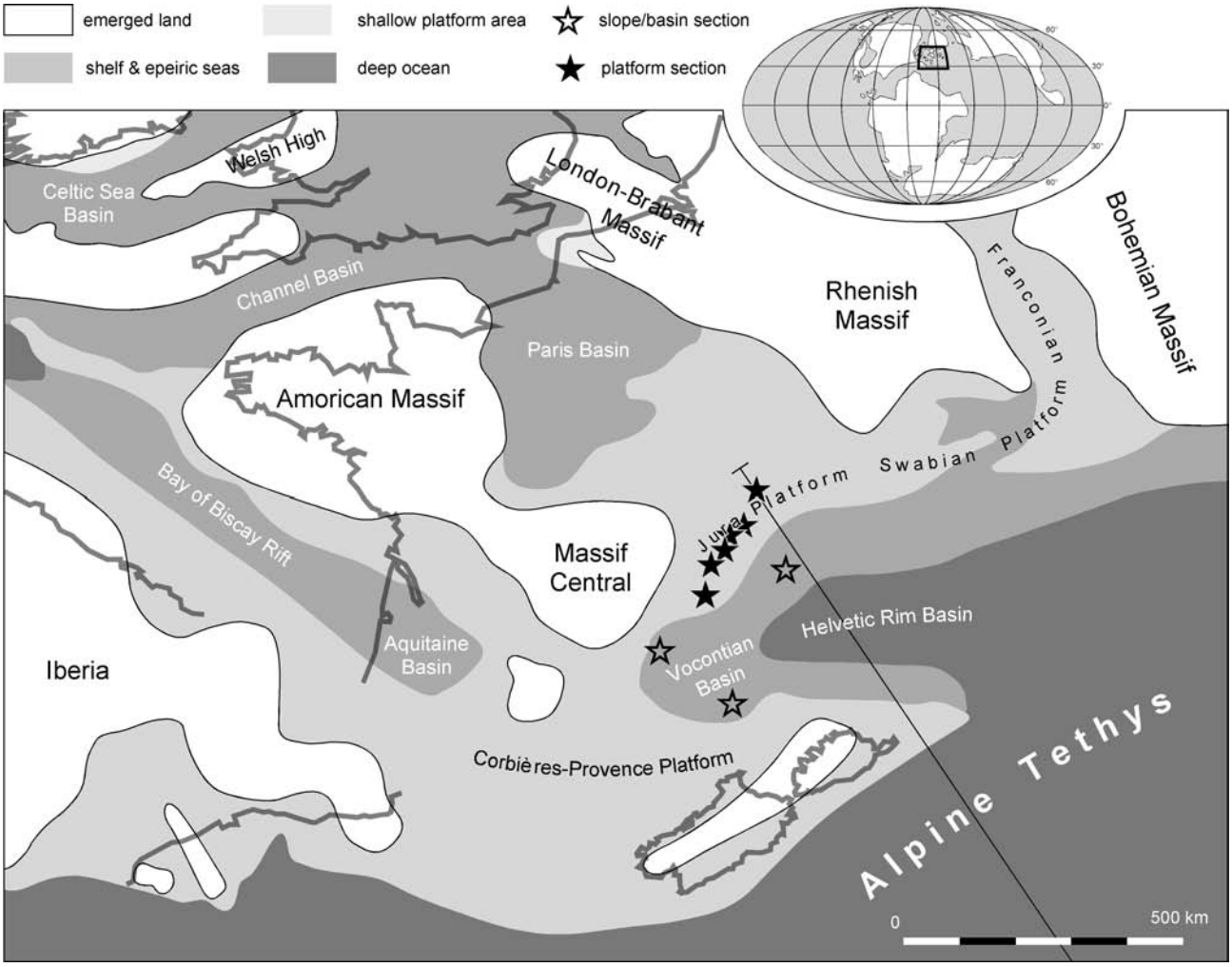

Fig. 1.3a - Early Tithonian (ca. 150 Ma) palaeogeography of western and central Europe. After Thierry et al. (2000). Global map after Smith et al. (1994). Note that the palaeogeographic position of Corsica and Sardinia is interpreted differently in other plate-tectonic reconstructions (e.g., Stampfli et al. 2002: cf. Fig. 1.4).

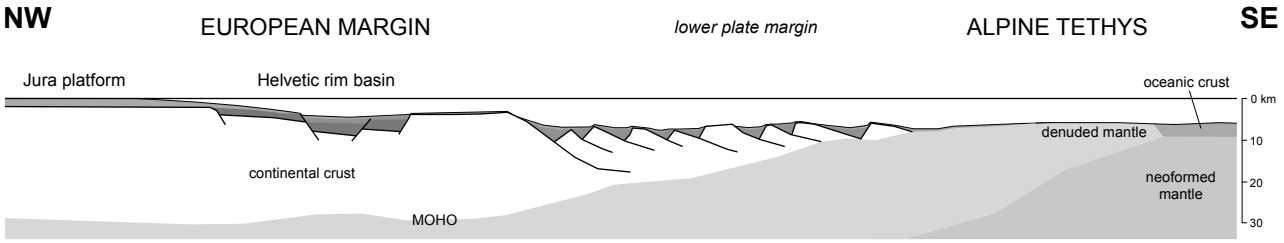

Fig. 1.3b - Sketch of the European margin during the Late Jurassic. After Stampfli et al. (2002).

newly constituted fault system. By the end of magnetic chron M21 (147.7 Ma, Middle Tithonian), any motion between Iberia and Africa had ceased, and the existing spreading center of the Alpine Tethys (Fig. 1.4) became extinct (Schettino & Scotese 2002).

Moreover, the Late Jurassic of NW Europe is a period of major rifting activity that was linked to the opening of the northern North Atlantic (see Chap. 8.3 for details).

The last tectonic event that had a major impact (deformation, erosion, karstification) on the studied sediments was the uplift and folding of the Jura Mountains during the terminal phase of the Alpine orogeny in the Tertiary (Trümpy 1980).

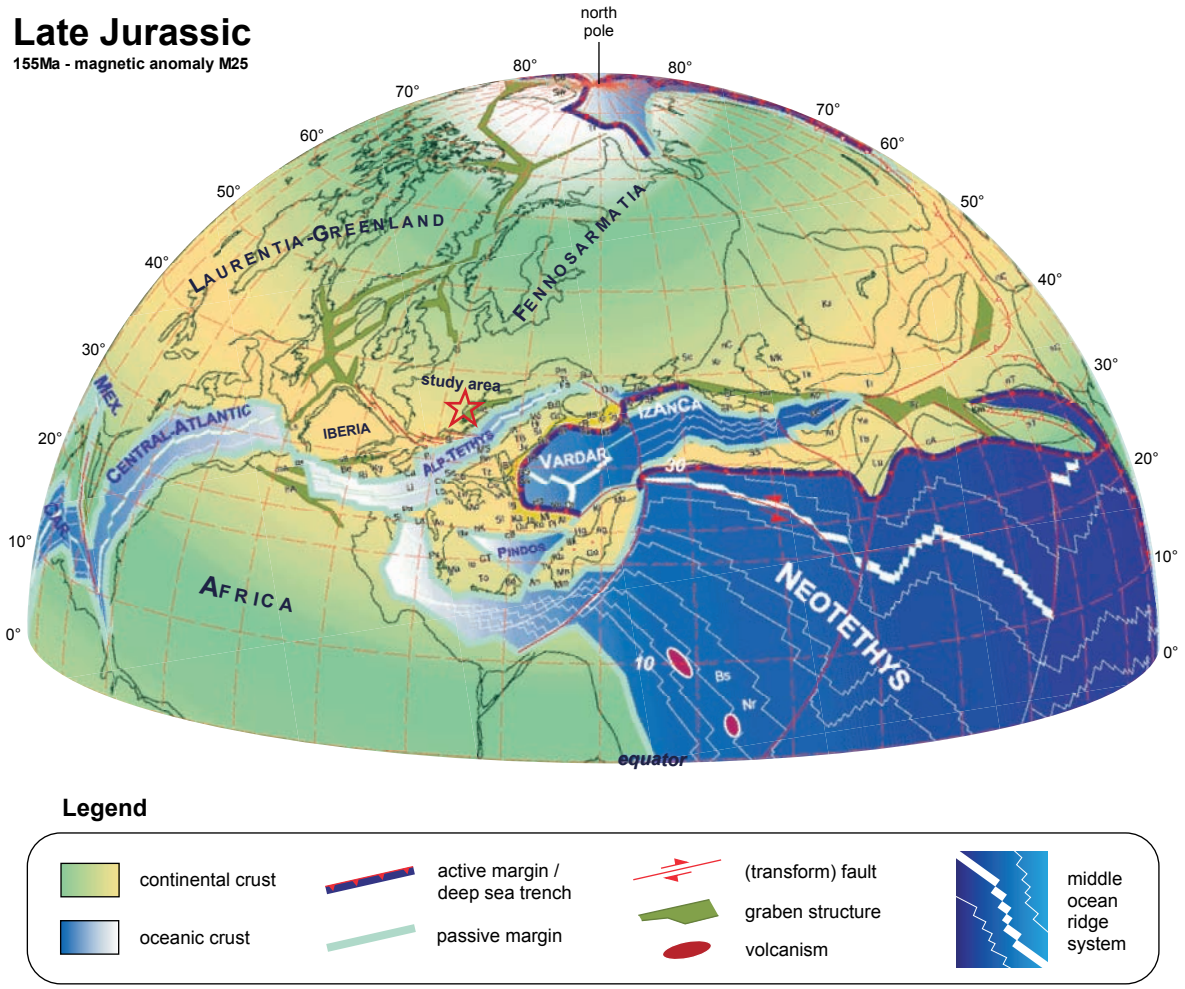

Fig. 1.4 - Plate tectonic reconstruction of the northern hemisphere during the Late Jurassic. From Stampfli & Borel (2002), modified.

1.2.4 Eustatic sea-level change

There are two distinct and widely recognized mechanisms of eustatic sea-level changes: the waxing and waning of polar icecaps and the changing volume of ocean basins due to the creation and destruction of oceanic ridges and swells (Hallam 1992). The latter process produces sea-level changes that are about three orders of magnitude slower than glacioeustatic changes. While they are most probably relevant to EXXON-type 1st- and 2nd-order sea-level changes, they cannot plausibly be invoked for 3rd-order changes. As the Jurassic world is generally accepted as lacking significant quantities of polar ice (see detailed discussion in Chap. 8), tectonoeustasy is the only possible mechanism that was able to drive long-term sea-level changes on the global scale (Hallam 2001).

According to Haq et al. (1987), the Kimmeridgian/Tithonian boundary interval was marked by a sea-level peak followed by a fall into the earliest Cretaceous (Fig. 1.5). The latest Jurassic and earliest Cretaceous in Europe is clearly regressive but such a regression is not evident in other parts of the world excepting New Zealand, although Surlyk (1991) reports a sea-level low in the Boreal basal Cretaceous. Consequently, the Tithonian regression is probably of only regional (European) extent, related to tectonic events in northwestern Europe (Hallam 2001; cf. Chap. 8.3)

Price (1999) presented evidence for episodes of cold or subfreezing polar climates during the Tithonian with a possible extent of polar ice sheets approximately one-third of those at the present day. It is thus possible that sea-level changes of 3rd-order and higher frequency have a glacioeustatic component (cf. discussion in Chap. 6). However, any glacially induced sea-level changes would have been no more than metre-scale (Hallam 2001).

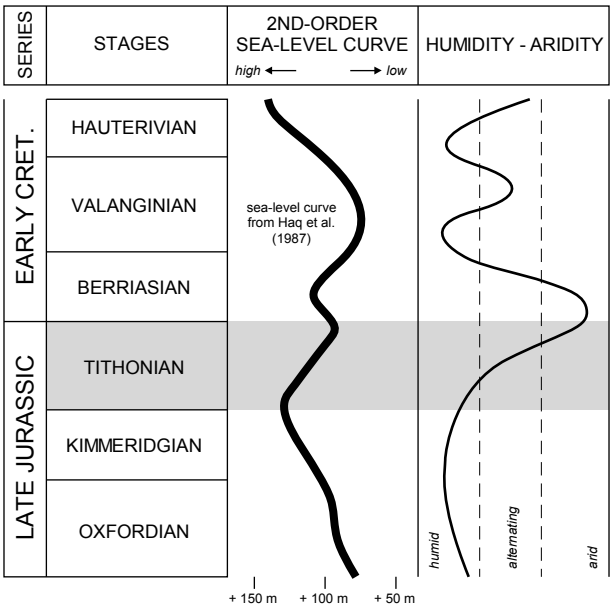

Fig. 1.5 - Long term sea-level trend and humidity-aridity cycles during the Late Jurassic and Early Cretaceous. From Price (1999), modified.

1.2.5 Palaeoclimatology

As mentioned above, the Jurassic world is generally accepted as lacking significant quantities of polar ice as it was a period of climatic maximum ("greenhouse world"; cf. Perlmutter & Mattews 1989). Average annual temperatures and humidity were supposed to have been significantly higher than today, with the N-S temperature gradient much smaller than present (e.g., Sellwood & Valdes 1997, Sellwood et al. 2000). However, there is evidence of regional and temporal changes (Fig. 1.5). This is discussed in more detail in Chap. 8.

1.3 The Tithonian of the Jura Mountains

1.3.1 Historic

Unlike all the other Late Jurassic and Early Cretaceous stages, the uppermost stage of the Jurassic derives its name not from any geographical location but from Greek mythology. Tithon was the son of Laomedon of Troy, who fell in love with Eos, Greek goddess of the dawn. His name finds his place in Mesozoic stratigraphy because this stage, the Tithonian, finds itself hand in hand with the dawn of the Cretaceous.

However, the application of this stage name to the latest Jurassic sediments in the study area began only recently. Due to the lack of biostratigraphically relevant fossils, there was a confusing multitude of different historic names for local formations and stages (Tab 1.1). Also on the European level, severe problems existed in correlating sections exactly. Thus, most correlations relied on mere lithostratigraphic features, assuming that facies changes are more or less isochronous. Finally, the existence of differing regional subdivisions (e.g., *sensu anglico – sensu gallico*) as well the unprecise use of (biostratigraphically defined) stage names and (lithostratigraphically defined) formation names resulted in a confusing variety of local stratigraphic subdivisions, with different authors using different names but meaning the same and vice versa.

In 1832, Thurmann introduced the terms *Kimméridgien* and *Portlandien* to the Swiss Jura (cf. Tab. 1.1) because he saw the *Marnes kimméridgiennes* and the *Calcaire portlandien* as lithologic equivalents to the type setions of the Kimmeridge Clay Formation and the "Portlandian" *sensu anglico* in Dorset, southern England. In the following, these terms were adapted by most of the Swiss and French geologists who worked in the area. Pidancet & Lory (1847) discovered the "Purbeckian" marls and defined them as the upper limit of the Jura Mountain's *Portlandien*. Some years later Etallon (1857, 1859, 1860) published a synthesis of the stratigraphy of the western Jura Mountains, followed by a new biostratigraphic subdivision of the Jura Mountains' Late Jurassic by Thurmann & Etallon (1861-64). Yet, Thurmann & Etallon apparently ignored the previously released biostratigraphic work of D'Orbigny (1842-49). They extended Thurmann's (1832) *Groupe Portlandien* to the lower limit of the *Astartien* (Late Oxfordian in today's terminology, cf. Tab. 1.1).

Jaccard (1869) found numerous non-marine fossils in the *Dolomies portlandiennes* and therefore considered these sediments as *Purbeckien inférieur* ("Lower Purbeckian") – a subdivision that did not survive in literature. Also Greppin's (1870) *Portlandien*, consisting of the *Calcaires compactes* and the *Calcaires en plaquettes* failed to achieve widespread acceptance.

Bourgéat (1888) published a synthesis for the *Jura méridional* (the southern, French Jura Mountains), and the stratigraphic chart presented by Rollier (1888) was very similar to the original one of Thurmann (1832): the "Purbeckian" marls as the upper limit and the top of the *virgula* Marls as the lower limit, whereas the zone of the *virgula* Marls was interpreted as uppermost *Kimméridgien*. In general, this mere lithologic subdivision is still in use nowadays, specifically for mapping purposes.

It was not before the beginning of the 20th century, that Salfeld (1913) noticed that the biostratigraphy introduced by D'Orbigny (1842-49) for the continental Late Jurassic does not match with the biostratigraphic zonation of the type sections in southern England. Much of the confusion caused by the competing *sensu anglico* and *sensu gallico* stratigraphies is rooted in this historical correlation error. Although the problem was now brought to awareness,

Thurmann (1832)	Thurmann & Etallon (1861-64)	Greppin (1870)	Bourgéat (1887)	Heim (1919)		Thalmann (1966) Häfeli (1966)	
PURBECKIEN	PURBECKIEN	PURBECKIEN	PURBECKIEN	PORTLANDIEN	PURBECKIEN	BER.	Goldberg Formation
GROUPE PORTLANDIEN — **I. Division** Calcaires portlandiennes	GROUPE PORTLANDIEN — VIRGULIEN — Epi-virgulien / Zone virgulienne / Hypo-virgulien	PORTLANDIEN	PORTLANDIEN		PORTL. s.str. (BONONIEN)	PORTL.	calcaire âpre / Twannbach Formation / *virgula* beds
		VIRGULIEN	VIRGULIEN	KIMERIDGIEN	VIRGULIEN (KIM. s.str.)	KIMMERIDGIEN	Grenznerineenbank / Reuchenette Formation
II. Division Marnes kimméridgiennes	STROMBIEN — Epi-strombien / Zone strombienne / Hypo-strombien	KIMMERIDGIEN	PTEROCERIEN		PTEROCERIEN		
GPE. CORALLIEN — **III. Division** Calcaires à Astartres	ASTRARTIEN — Epi-astartien / Zone astartienne / Hypo-astartien	SEQUANIEN	ASTARTIEN	LUSITANIEN	SEQUANIEN	SEQUANIEN	Verenaschichten

Jaccard (1869) Jura vaudois & neuchâtelois		Schardt (1891) Réculet / Vuache		Joukovsky & Favre (1913) Mont Salève		Aubert (1943) Vallée de Joux		Schär (1967) Lake Biel		Enay (2000) St-Germain-de-Joux		
PURBECKIEN INF. "Dolomies portlandiennes"	"calcaire âpre" (cell dolomite) / saccaroid dolomite / platy limestones	étage PORTLANDIEN	"partie supérieure" — marly and dolomitic zone, thin bedded	PORTL. SUP.	well-bedded oolites	PORTLANDIEN	extremly irregular series of interfingering compact limestone and dolomitic facies	Twannbach-Formation	**Upper Twannbach limestones**	**Tidalites de Vouglans**	well-bedded limestones and dolomites with frequent emersion features	TITHONIAN
PORTL. SUP.	marly and dolomitic limestones, mud-dominated facies		thick bedded limestones	PORTL. INF.	fossiliferous, oolithic breccia / reefal limestones / coral breccia				**Twannbach dolomite zone**			
PORTL. INF.	fossiliferous, compact limestones						*virgula*-beds		**Lower Twannbach limestones** / *virgula* beds	**Couches du Chailley / calcaires à tubulures**	bioturbated, massive to well-bedded limestones and dolomites	*gigas gravesiana*
PTEROCERIEN		KIMMERIDGIEN		KIMMERIDGIEN		KIMMERIDGIEN		Grenznerineenbank Reuchenette Fm.				*irius* KIM.

Tab. 1.1 – (*Upper part*) Evolution of the definition of "Portlandian" (French: "Portlandien") strata in the working area. Originally thought to be a (bio)stratigraphic equivalent of the English Portland Stone (Thurmann 1832), this was disproved by Salfeld (1913). In the following the term was applied in a more and more lithostratigraphic sense due to the lack of biostratigraphically relevant fossils. This consequently led to the mere lithological definition of the Twannbach Formation by Häfeli (1966). (*Lower part*) Some examples of local "Portlandian" subdivisions through time. Note the huge variety! Thus, a consistent lithological subdivision for the whole Jura chain is rather impossible.

Heim (1919) still based his work, to a large extent, on the publications of Greppin (1870). Frei (1925) added the *Grenznerineenbank* as a second marker horizon for the lower limit of the *Portlandien* in the Jura Mountains of the cantons of Neuchâtel and Berne, because the *virgula* Marls are hardly traceable in this area.

Enay (1965) defined the lithostratigraphic units of the *Couches de Chailley* (= *Calcaires à tubulures*) and the *Tidalites de Vouglans* in the southern Jura Mountains (*Jura méridional*). Häfeli (1966) introduced the name *Twannbach Formation*, for the "Portlandian" of the central Jura Mountains in order to emphasize the lithostratigraphic character of this stratigraphic unit and to avoid the chaos of similar names for different stages that had been established since the early 19th century. The base of the *Twannbach Formation* is well-defined by the *Grenznerineenbank* (Frei 1925) yet the upper limit ("*beginning of the Purbeckian*") is rather vague.

Newer studies focus more on the sedimentological reconstruction of the depositional area by comparing Jurassic lithofacies to recent carbonate environments and begin to interpret the lithological succession in terms of sequence stratigraphy. Bläsi (1980) carried out a regional study on the "Portlandian" of the Jura Mountains, looking in detail at the *virgula* Marls that define its lower limit. He presented a correlation that is based on clay minerals and the interpretation of depositional sequences. Bernier (1984) published a monograph on the *Kimméridgien* and *Portlandien* of the southern French Jura, providing micropalaeontological and sedimentological descriptions resulting in a very detailed lithostratigraphical approach. He was the first to mention and discuss the diachroneity of some lithologic formations in detail.

Détraz & Steinhauser (1988) and Détraz & Mojon (1989) were the first to present a sequence stratigraphic interpretation for the Jurassic and the Cretaceous, featuring a platform-basin transsect from the southern Jura Mountains to the French Prealps.

Meyer (2000) measured many sections in the southern Jura Mountains that were located close to the Late Kimmeridgian/Early Tithonian platform rim. He established a correlation and a 3rd-order sequence stratigraphic interpretation that allowed for putting up a local 3D model of the progradation pattern of the platform. In order to work with realistic distances he also provided a palinspastic reconstruction of the depositional area.

Enay (2000) gave a review on the ammonites found in the St-Germain-de-Joux area (southern Jura Mountains) and linked Late Kimmeridgian/Early Tithonian biostratigraphy to the local lithostratigraphy. However, even with this new data, biostratigraphic time control is still far from being satisfactory.

1.3.2 Lithostratigraphy

The historically grown multitude of homonyms and their inconsistent use for both, originally biostratigraphically defined stages and lithostratigraphically defined formations, demands for a clearly defined nomenclature.

Reuchenette Formation: formation that ends below the upper *virgula* Marls. It is more or less of Kimmeridgian age. In older publications the name "Kimmeridgian" (French: "*Kimméridgien*") is frequently used lithostratigraphically. It is not to be confused with the Kimmeridgian *sensu anglico* that includes the Kimmeridgian stage and parts of the Tithonian. In the measured sections, only parts of the upper Reuchenette Formation were measured that are characterized by thick-bedded lagoonal limestones with massive appearance.

Twannbach Formation: formation bounded by the upper *virgula* Marls and the first appearances of incipient palaeosols, green marls, and/or charophytes. It is more or less of Tithonian age. In older publications the name "Portlandian" (French: "*Portlandien*") is frequently used. It is not contemporaneous with the Portlandian *sensu anglico*. The lower boundary is also well defined by the *Grenznerineenbank* (Frei 1925, Dauwalder & Remane 1979) and a sharp change from the thick-bedded, massive limestones of the upper Reuchenette Formation to thinner-bedded limestones ("*Calcaires en plaquettes*"). Yet, the upper formation boundary is not clearly defined and is most probably diachronous.

Goldberg Formation: spans from the latest Tithonian/earliest Berriasian to the Middle Berriasian (boundary *subalpina/privasensis* Subzones). In older publications the name "Purbeckian" (French: "*Purbeckien*") is frequently used. It is not contemporaneous with the Purbeckian *sensu anglico*. The lower boundary is defined rather vaguely and is most probably diachronous (see above). Yet, the upper boundary is defined by a major emersion and a subsequent, well-developed transgressive surface that marks the beginning of the Pierre-Châtel Formation, found all over the study area.

Virgula Marls (= Marnes à virgules, Marnes à Exogyra virgula, virgula Mergel, virgula Schichten)

The *virgula* Marls are an important regional lithologic marker for the boundary between the Reuchenette Formation (± Kimmeridgian age) and the Twannbach Formation (± Tithonian age). A detailed study was carried out by Bläsi (1980). However, a major problem exists in the fact that this marly layer is a lithologic marker, i.e. a specific depositional environment represented by a characteristic facies. Such a marker horizon is not

necessarily isochronous, may be repetitive and must therefore be used with caution for correlational purposes. Indeed, Aubert (1950) reports two horizons from the Lac-de-Joux region and defines the strata in between as the *Virgulien*.

This double appearance, combined with the same name (homonym) for both horizons led to considerable problems in the past (cf., e.g., Gygi 1995). To avoid this confusion, the following terms will be used:

Lower *virgula* Marls for the horizon described by Marty (2003, 2004) in the Ajoie region and dated with ammonites to a Late Kimmeridgian age (*schilleri* Horizon of the *eudoxus* Zone).

Upper *virgula* Marls for the actual boundary-horizon between the Reuchenette and Twannbach formations that is located approximately at the Kimmeridgian/Tithonian boundary (lower *hybonotum* Zone).

Grenznerineenbank

In the *Jura neuchâtelois*, the upper *virgula* Marls are missing. Therefore, Frei (1925) defined the so-called *Grenznerineenbank* to act as formation boundary (see also Dauwalder & Remane 1979). However, this can be problematic in some places. E.g., the Noirvaux section is located just at the southern rim of this area and thus the *virgula* Marls are absent (see Fig. 4.11). Yet, Bläsi (1980) and Kettiger (1981) did not find a *Grenznerineenbank* in Noirvaux, whereas Mouchet (1995), based on Kettiger (1981), defines the thick bed from 88.2-90.2 m (banc 37 in Mouchet 1995) as *Grenznerineenbank*. Indeed, this bed contains some gastropods and also nerineans but not in a way that would distinguish it from other nerinean-bearing beds in the upper Reuchenette Formation.

Formations used in the southern Jura Mountains

The local formation names *Couches de Prapont, Couches de Chailley,* and *Tidalites de Vouglans* were introduced by Enay (1965) for the southern, French parts of the Jura Mountains. Bernier (1984) sticks for the greater part to the lithostratigraphy introduced by Enay (1965) but ends up with different thicknesses (specifically for the Avalanches section, cf. discussion in Chap. 4.3.1). Bernier (1984) also states that the base of the *Couches de Chailley* and the limit between the *Couches de Chailley* and the *Tidalites de Vouglans* is probably diachronous (p. 627 ff.).

The local formation names are given in the log of the Cirque des Avalanches section alternatively to the standard Reuchenette and Twannbach formations. However, a clear boundary between the *Couches de Chailley* and the *Tidalites de Vouglans* is difficult to define. Jaccard (1988) and Sudan (1997), working on the Noirvaux and the Lieu sections, respectively, stated that it is impossible to subdivide the two formations due to a repeated occurrence of their characteristic facies. Therefore, they use the names *Couches de Chailley* and *Tidalites de Vouglans* not as formation names but only as facies designations.

1.3.3 Biostratigraphy

Ammonites

The Jura Mountains are a key area for the correlation between the Tethyan and Boreal realms: located on the northernwestern rim of the Alpine Tethys, but also connected to the Boreal realm via the Paris Basin. They are populated by a mixture of both faunal realms (see, e.g., Schweigert 1993, Cariou & Hantzpergue 1997, Scherziger & Schweigert 1999, Colombié & Rameil submitted).

Some ammonites are reported from the upper Reuchenette Formation and around the Reuchenette/Twannbach boundary of the central Jura Montains (Thalmann 1966, Häfeli 1966, Meyer 1993, Hauser 1994, Meyer & Pittman 1994). Enay (1966, 2000) describes some ammonites from the St-Germain-de-Joux area (France) that define the biostratigraphic position of the Reuchenette/Twannbach Formation boundary in the southern Jura Mountains. However, the following parts of the Twannbach and most of the Goldberg Formations delivered no ammonites so far. Exceptional ammonite discoveries on the platform by Clavel et al. (1986) and Waehry (1989) allowed for dating the top of the Goldberg Formation as *jacobi/grandis* Zone and the major hiatus between top Goldberg and base Pierre-Châtel Formation to correspond approximately to the *subalpina* Zone (Deville 1991).

Other biostratigraphic markers

The sponge *Cladocoropsis mirabilis* is an important regional marker for the Kimmeridgian/Tithonian boundary interval. Mouchet (1995) described high abundances in the upper Reuchenette Formation of all measured sections and cores, just below the upper *virgula* Marls and the *Grenznerineenbank*. This is confirmed by own observations (see Fig. 7.1). However, it is not sure if the abundance of *Cladocoropsis mirabilis* in the upper Reuchenette Formation is really a biostratigraphic event or only a facies dependent effect.

The dasyclad algae *Clypeina jurassica* and *Campbelliella striata* have their first appearances simultaneously at the beginning of the *beckeri* Zone (Strohmenger et al. 1991). According to Flügel (1982), the association of *Clypeina jurassica, Campbelliella*

striata and *Salpingoporella annulata* is an indicator for the later part of the Late Jurassic.

Like dasyclad algae, some benthic foraminifera can be used to establish a relatively coarse biostratigrphy: the presence of *Alveosepta powersi* indicates the Late Kimmeridgian and the last appearance (LAD) of *Parurgonia* sp. the basal Tithonian (Bernier 1984, Cariou & Hantzpergue 1997). Yet, these species are highly facies dependent and not easily determined in thin section, so that this approach was not followed in this study.

Oertli (1959) established an ostracode biostratigraphy for the Late Jurassic of the Swiss Jura Mountains, but for the Late Kimmeridgian and Tithonian, this method has an even lower resolution than dasyclad algae and benthic foraminifera. However, from the Early Berriasian onwards, charophyte-ostracode assemblages are very useful regional biostratigraphic markers (see Mojon & Strasser 1987, Détraz & Mojon 1989 for details; application in Strasser 1994 and Strasser & Hillgärtner 1998).

Most of the biostratigraphic markers on the platform do not have the potential to furnish a high-resolution biostratigraphic framework that would be valuable in order to control sequence- and cyclostratigraphic interpretations. An exception are the Late Kimmeridgian *Cladocoropsis mirabilis* event and charophyte-ostracode assemblages in the Early and Middle Berriasian.

1.4 The Tithonian of the Vocontian Basin

1.4.1 Historic

Similar to the Jura Mountains, the Late Jurassic to Early Cretaceous basin deposits of SE France have been in the focus of research for a long time.

Among the first was Kilian (1889) who presented a remarkable study on the Late Jurassic and Early Cretaceous series of the region, featuring a large number of sections and palaeontologic descriptions. Already this author was impressed by the manifold features of resedimentation in the Vocontian Basin. Kilian (1895) was also the first one to use the term *pseudo-brèches* ("pseudobreccias") for the resediments of the Vocontian Basin. From the early days on, many researchers tried to explain the mechanism(s) that produced the pseudobreccias (e.g., Haug 1891, Goguel 1938, Gignout & Moret 1952, Remane 1960, 1966, 1970), an interest that continues until today (Raja Gabaglia 1995, Bouchette 2001, Séguret et al. 2001, Bouchette et al. 2001).

Yet, there are also numerous studies dealing with regional, palaeontological, and (bio)stratigraphical aspects (Goguel 1944, Tempier 1966, Remane 1967, Le Hégarat & Remane 1968, Cotillon 1968, 1974, Le Hégarat 1973, Beaudoin 1977, Cotillon et al. 1980, Debrand-Passard et al. 1984, Dromart & Atrops 1988, Dromart et al. 1993, Pellaton & Ullrich 1997, Bombadiere 1998, Bombadiere & Gorin 1998, 2000).

1.4.2 Lithostratigraphy

The Late Jurassic and Early Cretaceous of the Vocontian Basin is characterized by hemipelagic to pelagic sedimentation with intermittent biodetrital influx from the surrounding platforms. In contrast to Kimmeridgian and Berriasian limestone-marl alternations, the strata of Tithonian age are relatively massive ("*Barre Tithonique*") or bedded with only minor marly interbeds. In the center and on the slopes of the Vocontian Basin, Late Kimmeridgian and Tithonian hemipelagic carbonates are frequently brecciated (Fig. 1.2b). These "pseudobreccias" have been interpreted either as resediments or, in recent times, as the result of wave-oceanfloor interaction (for references, see Chap. 1.4.1)

1.4.3 Biostratigraphy

Ammonites

The Vocontian basin is part of the Tethyan faunal realm. In contrast to the Kimmeridgian and the Berriasian that are rich in ammonites (Le Hégarat 1980, Bulot 1995), ammonites are far less abundant in the Tithonian of the Vocontian Basin. Nevertheless, the Tethyan ammonite zonation that was developed on the northern and western margins of the Alpine Tethys (Hantzpergue 1983, Tavera 1985, Cecca & Sanantonio 1989, Cecca et al. 1989, Cecca & Enay 1991, Benzaggagh & Atrops 1995) can be applied. However, in terms of biostratigraphy, the Kimmeridgian/Tithonian boundary is not very well defined (Cecca & Zeiss 1994, Cariou & Hantzpergue 1997). At the present moment, several potential type localities for the Tithonian are in discussion but no agreement has been reached yet (pers. comm. G. Schweigert).

The correlation between the differing Boreal and Tethyan stratigraphic charts is still difficult (Fig. 1.6; for details see Kutek & Zeiss 1975, Gerasimov et al. 1975, Shulgina 1975, Hantzpergue 1993, 1995, Cecca 1999, Zeiss 2003) or, as boldly expressed by Atrops (1994) for the Early Kimmeridgian where similar problems exist, "difficult to entirely hypothetical".

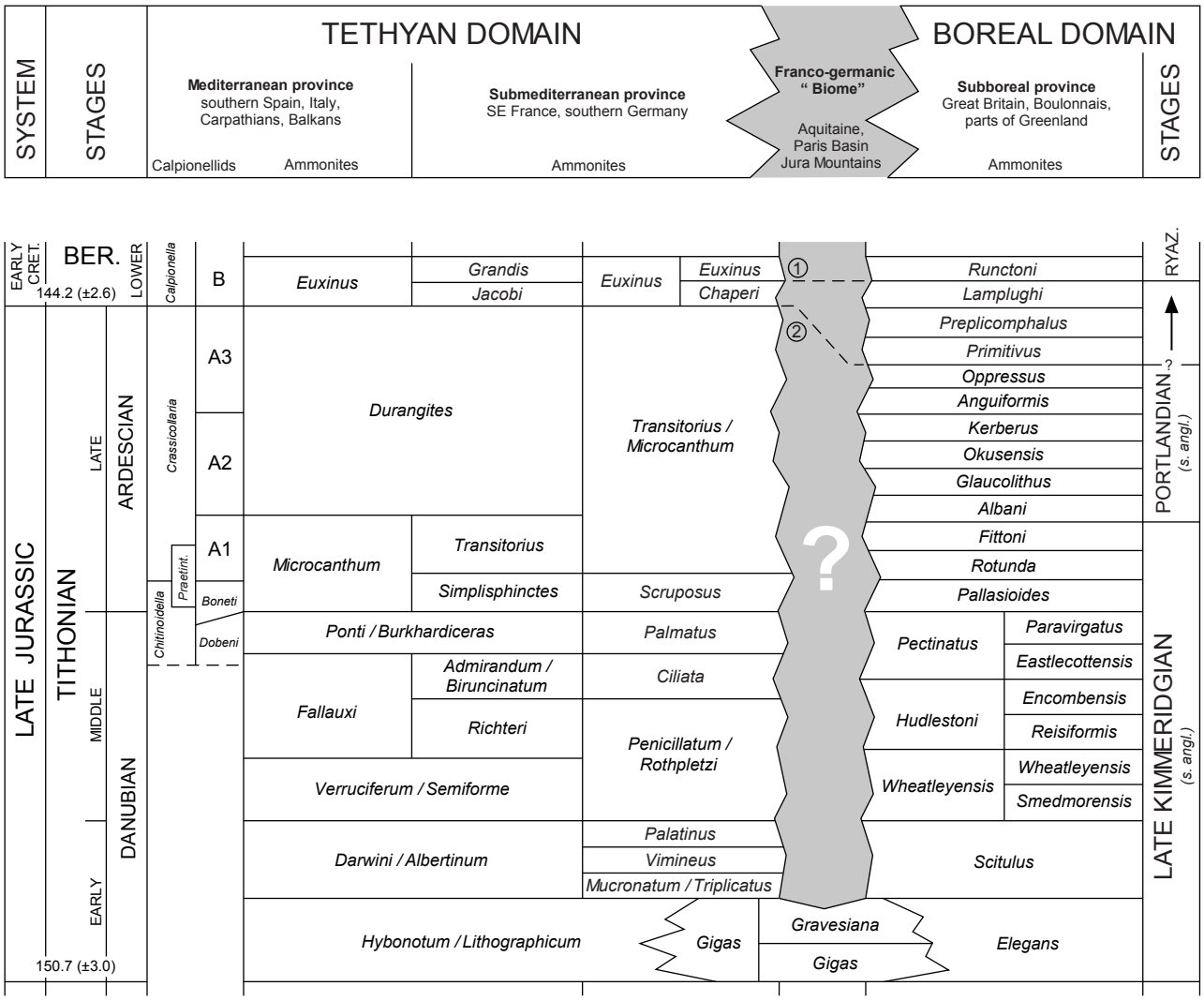

Fig. 1.6 - Biostratigraphy of the Tithonian. Note the divergent correlations between Tethyan and Boreal domains: (1) after Cariou & Hantzpergue (1997), (2) after Hardenbol et al. (1998). Note as well the differences between this chart and Fig. 1.9 for the correlation of calpionellid and ammonite zones in the Tethyan domain. From Cariou & Hantzpergue (1997), modified. Numeric ages after Gradstein et al. (1994).

Calpionellids

From the Middle Tithonian to the Valanginian, calpionellids are excellent index fossils in Tethyan pelagic carbonates. They were intensively studied by, e.g., Le Hégarat & Remane (1968), Remane (1985), Benzaggagh & Atrops (1995), and Remane (1998). The scheme applied in this study is based on Benzaggagh & Atrops (1995) for precalpionellids and on Remane (1985) and Remane in Cariou & Hantzpergue (1997) for calpionellids (Fig. 1.7). For SE France, this is still the widely accepted standard, even if there are recent studies on calpionellids biochronology (Grün & Blau 1996, 1997, Blau & Grün 1997, Pop 1997) that propose a revised zonation and also discuss critically the limitations of correlation of calpionellid zones with ammonite zones and absolute time scales (Blau & Grün 1997).

Microfossil assemblages

Compared to platform environments, where microfossils are more of value for palaeoenvironmental analysis, the microfossil assemblages of the Vocontian Basin yield stratigraphic information. Dromart & Atrops

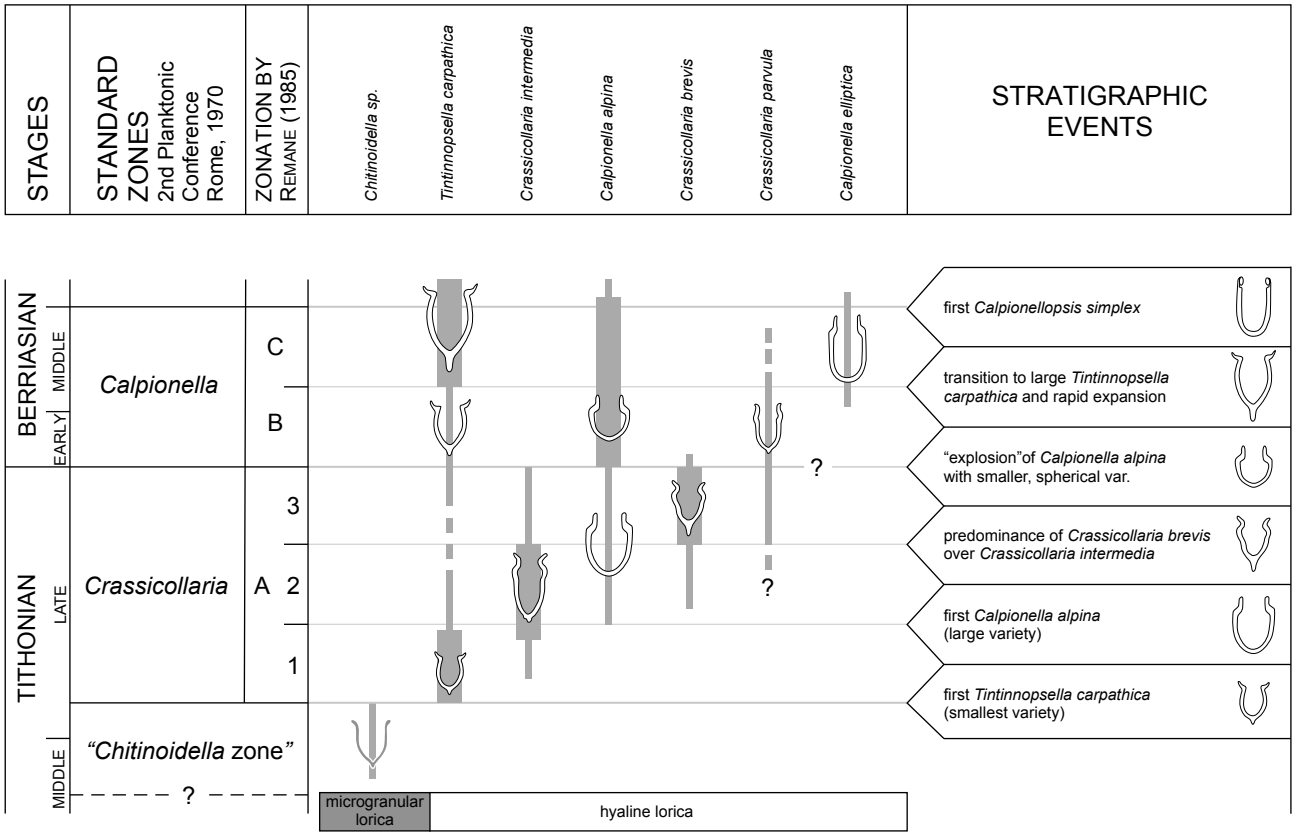

Fig. 1.7 - Calpionellid biostratigraphy. After Remane (1985) and Cariou & Hantzpergue (1997).

(1988) were the first to remark on this alternative method and established a stratigraphic chart. It covers the Middle and Late Jurassic, is based on the relative abundance of different microfossil groups, and is correlated to calpionellids and the standard Tethyan ammonite zonation (Fig. 1.8). Benzaggagh (2000) improved the original stratigraphic chart of Dromart & Atrops (1988).

The various microfossil zones are well-expressed in the two studied basin sections. In some cases, it was even possible to determine characteristic peaks in the abundance of a microfossil group that allow for a precise biostratigraphy on ammonite-zone level.

Combining ammonite, calpionellid, and microfossil assemblage stratigraphy, the biostratigraphic control in the basin sections is excellent. This is specifically true for the Clue de Taulanne section, whereas biostratigraphic resolution in the Poteu de Mié section is restricted due to a low sample density (see Chap. 4.3.3). The sequence-chronostratigraphic chart of Hardenbol et al. (1998; modified) gives an overview on the relationships between bio-, sequence-, and chronostratigraphy for both, the Tethyan and Boreal realms (Fig. 1.9).

1.5 Methodology

Field work

A total of 896 section metres have been logged and studied bed by bed, locally cm by cm if necessary. Every rock sample was cut. 816 etched slabs and 640 thin-sections were prepared to be examined under the binocular and the microscope, respectively, to determine depositional facies and early-diagenetic alteration. Cathodoluminescence was used to obtain more accurate data for selected samples. For the Yenne section, unpublished microfacies data of A. Strasser were used to complete the upper part of the section.

All samples carry a short letter combination that identifies the section and are numbered by from the base to the top, i.e. No135 represents the Noirvaux section, sample no. 135 counted from the base of the section. Exceptions are the Lieu and the Yenne section, where earlier work of Sudan (1997) and Strasser (1994) carried out the sampling for earlier projects that were incorporated in this study. All materials concerning this study (thin sections and selected rock slabs) are

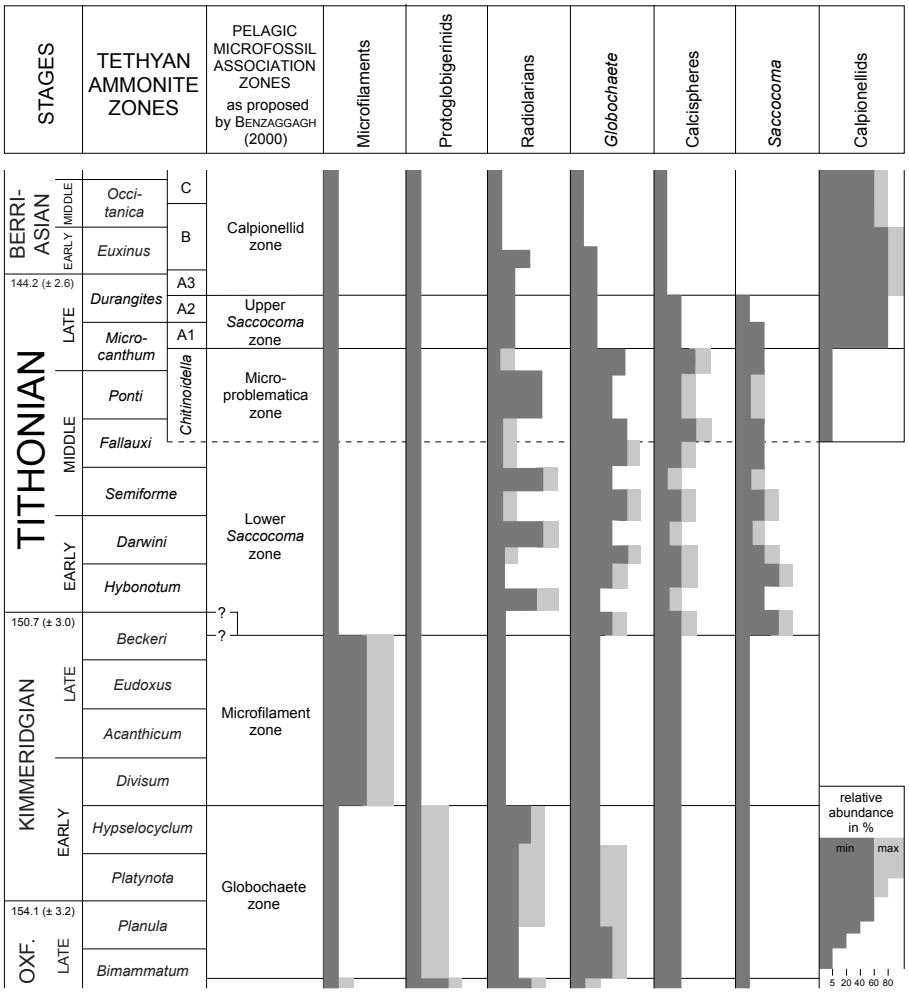

Fig. 1.8 - Late Jurassic to earliest Cretaceous microfossil association zonation of the north-western Tethys margin, referred to the standard Tethyan ammonite (and calpionellid) zones. Based on DROMART & ATROPS (1988), modified after BENZAGGAGH (2000) and own observations.

deposited in the Department of Geosciences, Geology and Palaeontology, at the University of Fribourg.

Stable isotope analysis

Stable-isotope analysis of 64 selected samples was carried out in the stable isotope laboratory of the University of Lausanne under the guidance of Sébastien Bruchez.

Rock powders were extracted with a dentist drill from etched slabs (effects of short-time surface etching with 10% HCl in order to remove saw dust from slab are negligible, pers. comm. S. BRUCHEZ), carefully avoiding large bio/intraclasts or cement veins. The powder was then homogenized. This "*modified whole rock*" analysis has shown to be representative for the overall isotopic signature, excluding biological fractionation and diagenetic signatures (PLUNKETT 1997).

Isotopes were measured with a FINNIGAN DELTA PLUS XL mass spectrometer with an attached GASBENCH II and a PAL autosampler. Rock powders are reacted with 100% phosporic acid at 90°C. The resulting CO_2 is then introduced into the GASBENCH II that consists essentially of a 50 m long capillary heated constantly to 70°C. Its function is to separate the CO_2 from water and other possible impurities, and subsequently send the treated gas in "continous flow" mode into the mass spectrometer, i.e. without interruptions and under variable pressure that depends on the original quantity of CO_2 from the sample. During the continuous flow, 10 measurements are taken for each sample. The thus obtained raw results are then corrected by comparison to an internal standard (Carrara Marble: 2.05 ‰ ä^{13}C and -1.75 ‰ ä^{18}O) that is measured regularly in between two samples. The internal standard is calibrated to the international standard NBS19 (1.95‰ ä^{13}C and -2.20‰ ä^{18}O). Finally, the mean value of the 10 corrected raw results is calculated and represents the C and O isotope values for a given sample.

Clay mineral analysis

Clay mineral analysis of 93 selected samples was carried out by Thierry Adatte, in his laboratory at the University of Neuchâtel. Because in clay mineral analysis, the methodology of sample preparation and the processing of raw data is an integral part of the interpretation, these are described separately in Chap. 5.2.1.

* * *

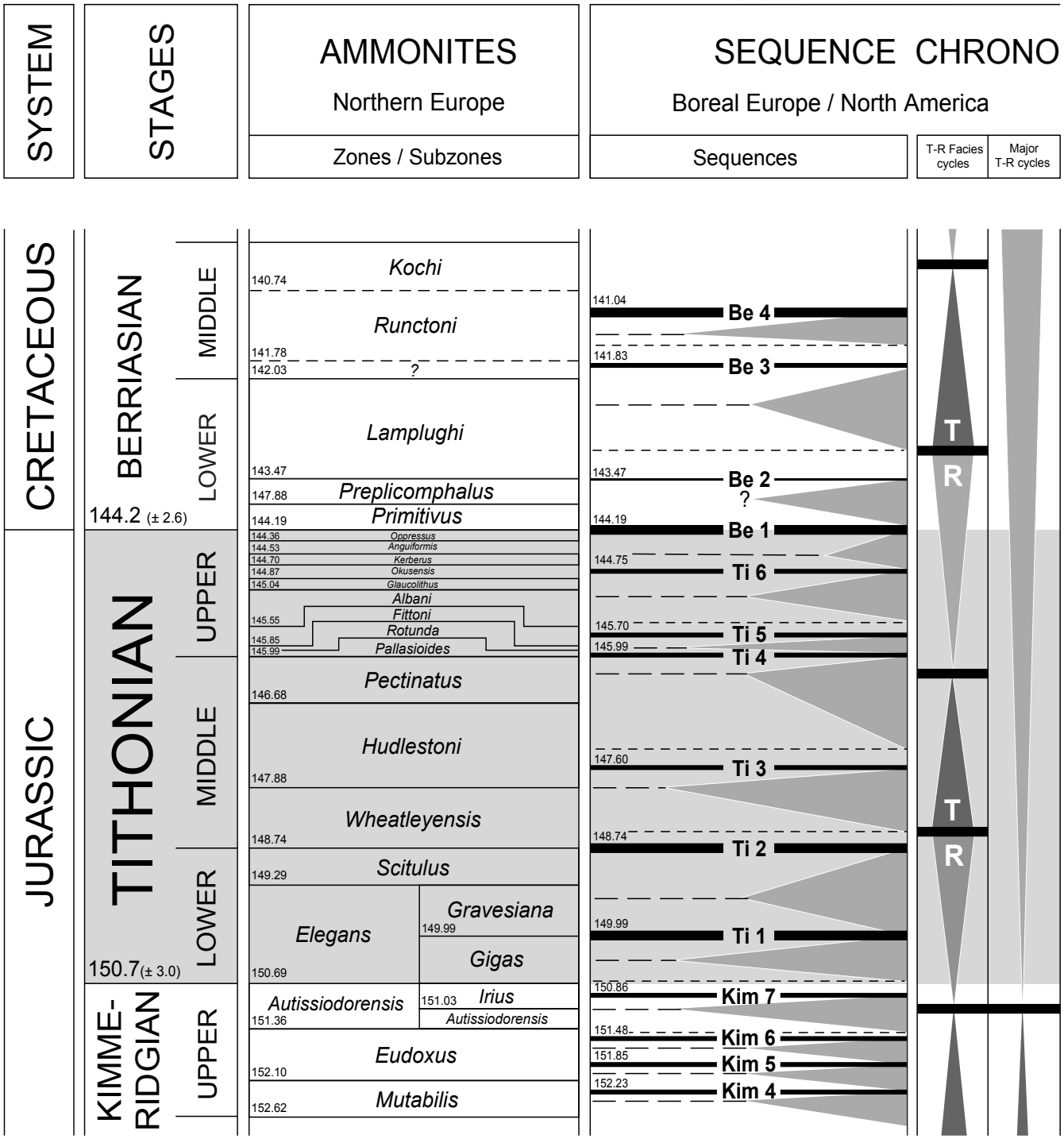

Fig. 1.9 - Sequence-chronostratigraphic chart for the studied interval after Hardenbol et al. (1998). Numeric ages from Gradstein et al.

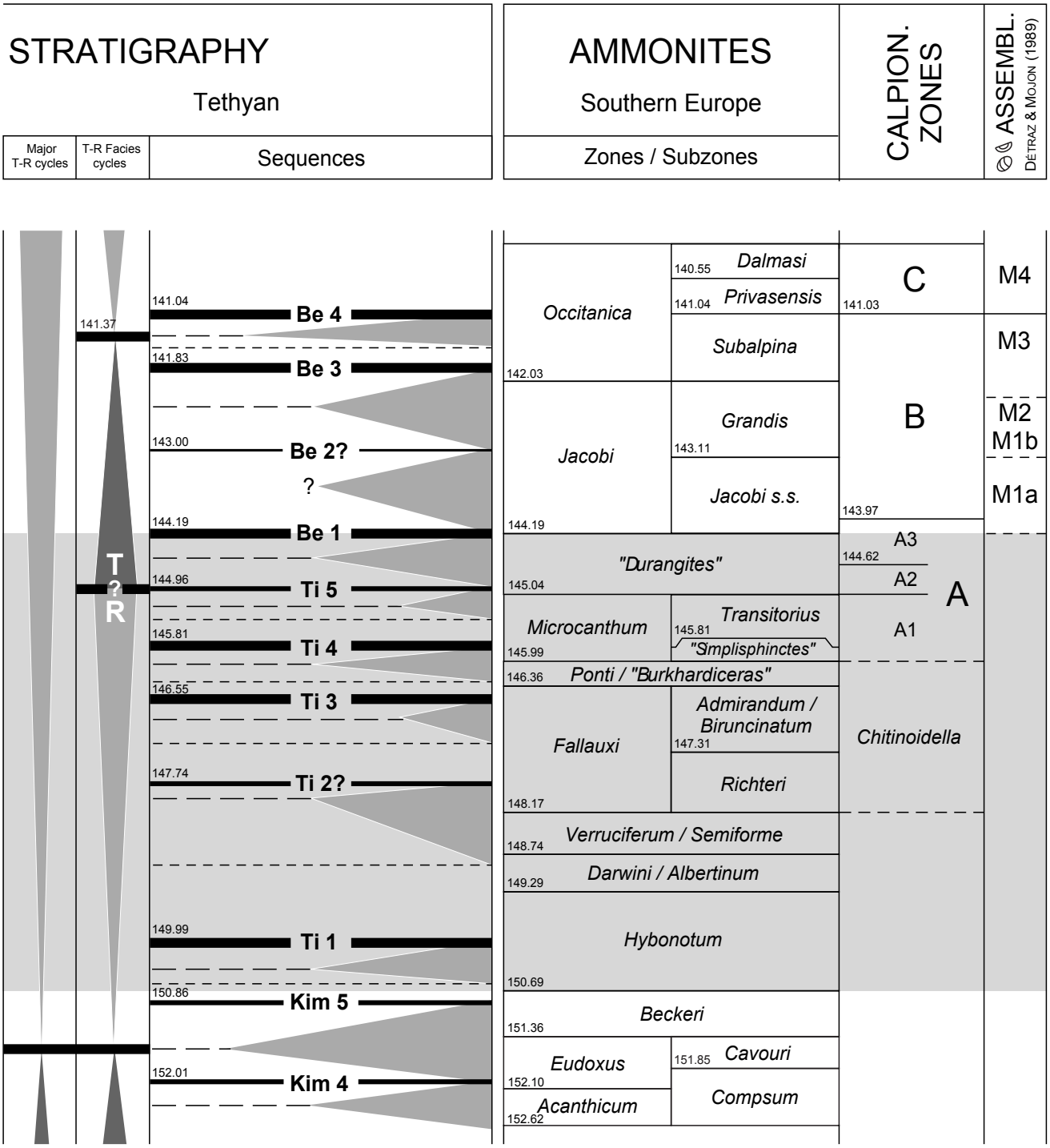
STRATIGRAPHY
Tethyan
Major T-R cycles
T-R Facies cycles
Sequences
AMMONITES
Southern Europe
Zones / Subzones
CALPION. ZONES
ASSEMBL.
DÉTRAZ & MOJON (1989)
141.04
Be 4
141.37
141.83
Be 3
143.00
Be 2?
?
144.19
Be 1
T
?
R
144.96
Ti 5
145.81
Ti 4
146.55
Ti 3
147.74
Ti 2?
149.99
Ti 1
150.86
Kim 5
152.01
Kim 4
Occitanica
140.55
Dalmasi
141.04
Privasensis
Subalpina
142.03
Jacobi
Grandis
143.11
Jacobi s.s.
144.19
"Durangites"
145.04
Microcanthum
145.99
Transitorius
145.81
"Simplisphinctes"
146.36
Ponti / "Burkhardiceras"
Fallauxi
148.17
Admirandum / Biruncinatum
147.31
Richteri
148.74
Verruciferum / Semiforme
149.29
Darwini / Albertinum
Hybonotum
150.69
Beckeri
151.36
Eudoxus
152.10
Acanthicum
152.62
151.85
Cavouri
Compsum
C
141.03
B
143.97
A3
144.62
A2
A1
A
Chitinoidella
M4
M3
M2
M1b
M1a

(1994).

2 - Facies analysis and interpretation

2.1 Definitions

Microfacies

The term microfacies includes the sum of all palaeontological and sediment-petrographic criteria that can be defined at a small scale, e.g., in a polished slab, acetate peel, or thin section using a binocular or an optical microscope (plain and/or polarized light) (Flügel 2004). Magnification allows for a better recognition of (micro)fossil content, small-scale sedimentary structures, and specifically the diagenetic history of an analyzed rock sample.

Facies

The term facies corresponds to the entity of all organic and inorganic characteristics of a sedimentary rock, such as colour, composition, texture, and sedimentary structures (Tucker & Wright 1990, Flügel 2004).

Facies zone

A facies zone is a depositional environment that is characterized by one or several related types of facies found in it. The term is used synonymously with the "facies belts" of Wilson (1975) and Flügel (1982). However, it avoids the notion of a linear geometry evoked by the latter.

Facies association/succession

Facies associations, as defined by Tucker & Wright (1990) represent "groups of facies occurring together" and reflect "the same general environments". Thus, they have a similar meaning as facies zone. However, this term may also be used to refer to vertical successions of related facies, and thus comprehends also the time interval during which a depositional environment is subject to a relatively continuous change (concordant deposition).

Nomenclature

Microfacies classification follows the standard nomenclatures for carbonates developed by Folk (1962) and Dunham (1962). Embry & Klovan (1971) enlarged Dunham's classification by additional divisions that take into account sediment-organism interactions, e.g., the presence of coarse reefal debris or sediment-binding organisms. However, this extension is only partly applied in the present work. As reefs are virtually non-existent in the investigated lagoonal sediments, the few potential float- and rudstones were classified according to Dunham's (1962) original classification scheme as wacke-, pack-, and grainstones. Additionally, this allows for using the Dunham microfacies column of the detailed sections (cf. Chap. 4) as an energy proxy, with marls and mudstones representing the relatively lowest and grainstones the relatively highest energy levels.

2.2 Approach

At a first glance, the Twannbach Formation is a rather monotonous, relatively thin-bedded succession of pure carbonates that spans over about a hundred meters of thickness. It consists exclusively of shallow-lagoonal to tidal-flat limestones and dolomites, which implies a strongly reduced variety on the level of facies zones. At a closer look, however, this monotony turns out to be a complex pattern of a multitude of different types of peritidal facies that form rhythmical facies successions.

The (micro)facies classification scheme applied here was developed in accordance with the primary aim of this study: monitoring high-frequency relative sea-level oscillations. It is based on standard facies divisions from literature (e.g., Flügel 2004, Wilson 1975), as well as on the experience the Fribourg sequence- and cyclostratigraphy working group accumulated over the last ten years while working in the Jura Mountains — notably the studies

dealing with the underlying Kimmeridgian (Colombié 2002) and overlying Berriasian strata (Hillgärtner 1999, Pasquier 1995) served as a working basis.

In order to avoid numerous repetitions and thus further an easier access to this work, this chapter does not strictly follow the scientific standard of clearly separating description and interpretation. Basic elements and features of carbonate (micro)facies and their generally accepted interpretations (e.g., Scholle et al. 1983, Walker & James 1992, Flügel 2004) are considered as "given" facts and are therefore directly used as a basis for further interpretation in the following chapters.

2.3 Constituents

As this thesis deals mainly with platform carbonates, and platform facies is far more diverse than in the basin, this chapter will essentially concentrate on constituents of shallow-marine carbonates. A summary of basin facies is given in Chap. 2.6.

2.3.1 Non-skeletal carbonate grains

Peloids (Pl. 1/1-4)

Peloids are rounded to well rounded, micritic clasts without internal structure. Two different types are distinguished (cf. Colombié 2002): **Type-1 peloids** (Pl. 1/4) range from 10 to approx. 60 µm in diameter and show no sharply defined rim ("cloudy appearance"). In general, type-1 peloid assemblages are almost perfectly sorted. They are observed either in intergranular pore space or in microcavities – commonly as "peloidal cement" between type-2 peloids, bio- and/or intraclasts – or as sediment-forming components in highly restricted lagoonal or tidal-flat environments and are assumed to be of cyano- or nano(?)bacterial origin (Chafetz 1986, Sun & Wright1989, Kazmierczak et al. 1996, Tribovillard 1998, Folk & Chafetz 2000).

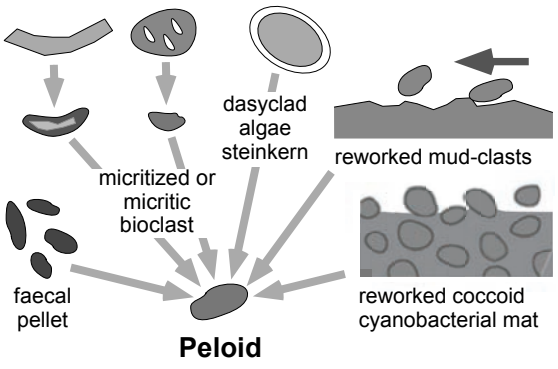

Fig. 2.1 - Possible origin of peloids. After Tucker & Wright (1990), modified.

Type-2 peloids (Pl. 1/3, 1/4) are much more abundant, usually bigger and poorer sorted than type-1 peloids (cf. Sun & Wright 1989). Their diameter typically ranges from approx. 50 µm to 1 mm. Rims are sharply defined and in some cases slightly darker than the rest of the peloid. Due to their broad spectrum of possibly reworked, (micritized bio)clastic, faecal, or steinkern origin (Bathurst 1966, Kobluk & Risk 1977, Macintyre 1985, Sun & Wright1989, Tucker & Wright 1990, Reid & Macintyre 1998, Reid & Macintyre 2000, Peterhänsel 2003, Samankassou et al. 2005; cf. Fig 2.1), they appear in a wide range of different facies. In high-energy grainstones, as well as in medium-energy packstones, they are frequently associated with oncoids, intraclasts, and occasionally ooids. In mud-supported low-energy sediments type-2 peloids are easily passed over because of their poor contrast with respect to the micritic matrix. Yet, in low-energy environments they generally represent a high percentage of burrow-filling material. (cf. Chap. 2.4.2).

There is no clear difference between type-2 peloids and small mudstone-intraclasts (see below).

Oncoids (Pl. 7)

Since the Lower Twannbach Formation is very similar to the Upper Reuchenette Formation in terms of facies associations, the observed oncoid types are essentially the same as described by Colombié (2002): **type-1 oncoids** (Pl. 7/1, 4) are of spherical to irregularly-formed contour with a diameter that varies from 1 mm to 3 cm (typically about 1 cm). They consist mainly of a relatively thick cortex; the nucleus may be absent (or invisible due to sectioning effects?). The cyanobacteria *Bacinella irregularis* plays an important role in constructing the micritic or peloidal laminae which make up the cortex. Laminae may be continuous or discontinuous (cf. Dahanayake 1977). Commonly, the outer rim of these oncoids is not sharply defined ("cloudy growth"). This type is equivalent to the type II oncoids defined by Dahanayake (1977) and is thought to have formed under relatively calm conditions and frequent short phases of low sediment supply: each lamina is assumed to represent a period favouring bacterial growth. The bigger an oncoid is and the more irregular its shape, the less agitation it experienced during its formation. **Type-2 oncoids** (Pl. 7/2) consist of a micritic nucleus that is encrusted by one or two concentric laminae, frequently containing *Bacinella irregularis*. In size and texture they resemble type-1 oncoids. According to the classification of Dahanayake (1977), these oncoids could

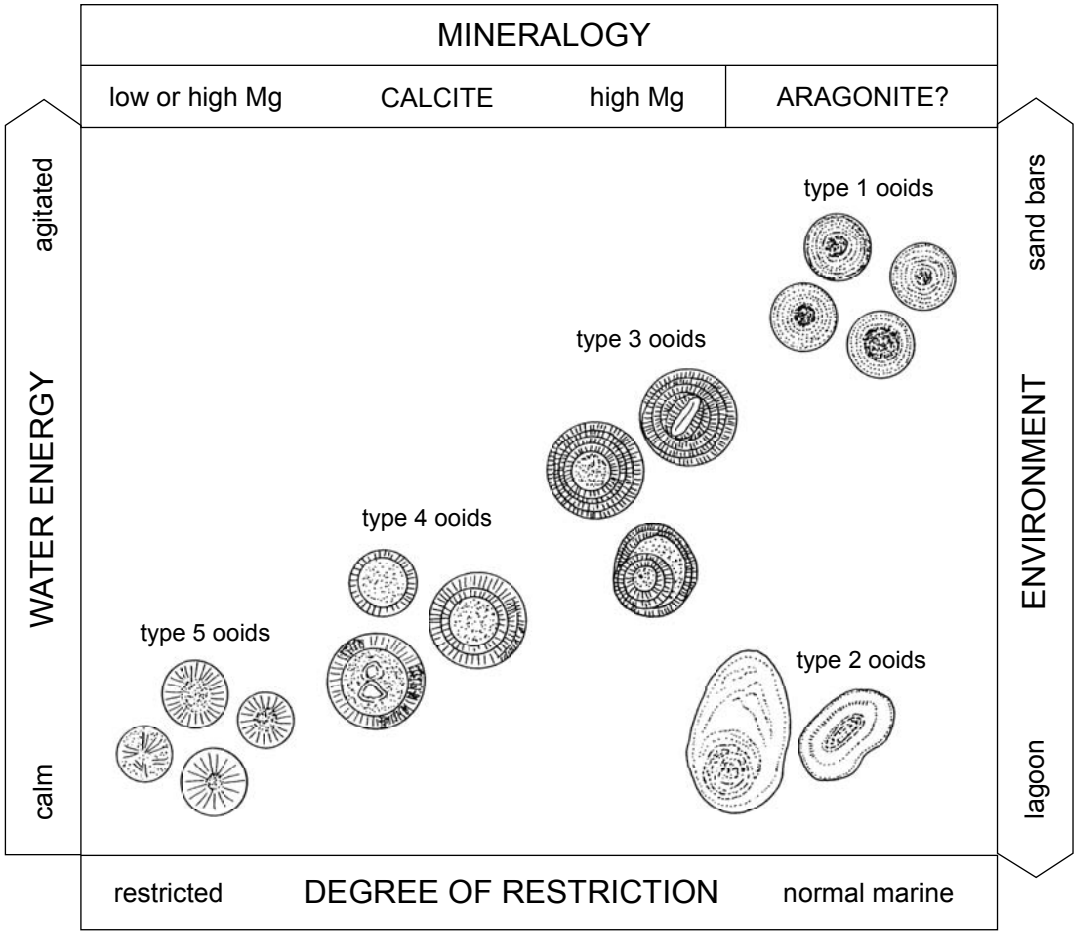

Fig. 2.2 - Schematic representation of inferred mineralogy, water energy, and depositional environment of different ooid types from the Upper Jurassic and Lower Cretaceous. Type 6 ooids represent a mixture of different elements from types 1-5. From Strasser (1986), modified.

be described as superficial type II. Type 1 and 2 oncoids are observed predominantly in the muddy, low-energy lagoonal sediments of the Late Kimmeridgian, specifically in the lower half of the Cirque des Avalanches section ("calcaires à oncolithes" of Bernier 1984). In contrast to the types 1 and 2 that show a contribution of *Bacinella irregularis* to different extent, **type-3 oncoids** (Pl. 7/3) are micritic and generally lack a laminated cortex, nucleus, or any other visible internal structure. As an exception, in some cases a small central cavity filled by sparitic cement is observed. Frequently, type 3 oncoids are surrounded by a thin, diffuse film of micrite of darker colour than the internal part. This film, as well as the central cavity, might be traces of microbial activity. Their comparatively small mean diameter of 0.5 to 10 mm and their generally well rounded, elliptical form suggest that type 3 oncoids formed in a continuously agitated environment, which was nevertheless appropriate for oncoid growth. They resemble type-1 oncoids that "*are difficult to recognize due to a process of reconstitution of mineral matter which modifies their laminated character*" (Dahanayake 1977, p. 346). This type is the most abundant in the examined sediments, commonly accumulated in grainstones and packstones of high or medium-energy environments.

Ooids (Pl. 1/5, 6)

Ooids are spherical to elliptical coated grains, generally with a diameter below 2 mm. They consist of concentric calcareous cortices growing around a (bio)clastic nucleus of various origin and composition (Flügel 1982, Tucker & Wright 1990). Ooids are known to form, most probably by microbiological mediation, in a multitude of marine, lacustrine, or fluviatile environments. This is reflected by differing microfabrics and primary mineralogies (Richter 1983, Strasser 1986). Nevertheless, most known fossil ooids are interpreted to originate from shallow marine environments. Modern marine ooid formation takes place in tropical and subtropical waters, periodically agitated by tidal currents, typically at depths of 1-5 m (max. 10-

15 m). The water is supersaturated with respect to $CaCO_3$ and temperature never drops below 18-20° C. Also, a slightly elevated salinity seems to favour ooid formation. Yet, ooids are easily transported, i.e. attention has to be paid to not over-interpret occurrences that may be of allochtonous origin.

Ooids are relatively rare in the Twannbach Formation. All found specimens are clearly associated with marine faunas or deposited in a marine context. Different types of ooids are observed; they correspond to the types 1 to 6 of the classification scheme developed by Strasser (1986) for the Purbeckian (cf. Fig. 2.2). In accordance to the Kimmeridgian (Colombié 2002), no type-5 ooids were found.

The rare occurrence of ooids in general and the predominance of type-4 ooids (cortex of only one to four laminae, with a relatively big nucleus) indicate a general tendency to low-energy restricted lagoonal environments. However, due to the scarcity of freshwater-indicating fossils in the Portlandian (cf. Chap. 2.3.2), elevated salinity is a more probable restriction factor than the brackish conditions Strasser (1986) proposed for the Purbeckian.

Lithoclasts (Pl. 1/1, 2; 11/5-7, 12/2, 3a, b)

Two general types of lithoclasts are distinguished: *intraclasts* are defined as syn-sedimentarily reworked components of slightly consolidated sediment and derive from the same general environment as the host-rock.

Extraclasts consist of reworked fragments of a fully consolidated (and often significantly older) sedimentary and/or crystalline rock eroded in an environment foreign to the host sediment. Extraclasts were not found. This fact suggests that the Jura platform in Late Jurassic times was distal with respect to any potential source area, or that the low source-area relief was too low to build up a sufficient energy gradient for seaward transport. Palaeogeographical reconstructions (Ziegler 1988, 1990; Vercoutere & van den Houte 1993, Smith et al. 1994) confirm this reasoning.

In contrast to extraclasts, **intraclasts** are very abundant in the studied shallow marine sediments. They are mainly represented by slightly rounded mudclasts in tidal environments and high-energy bioclastic bars and vary from a few mm to up to 5 cm in diameter. Alternating low-energy conditions and comparably high current velocities, as well as outer bank erosion of meandering tidal channels are thought to be the main sources for these clasts. Platy, commonly laminated fragments in tidal-flat environments ("*mudchips*", "*flat-pebble conglomerates*"; cf. Pl. 11/5-7) result from the reworking of inter- and supratidal microbial mats during major storms (Demicco & Hardie 1994).

Black pebbles (Pl. 1/2; 12/2, 3a, b) are a particular form of lithoclasts. In most cases they display all the characteristics of intraclasts: they are predominantly micritic and commonly plastically deformed and/or rounded. Yet, they show intensive black staining. Observed black pebble diameters fall in the same range as mentioned for intraclasts and thus match well with observations from the Portlandian-Purbeckian of the Lake Biel area (Häfeli 1966). However, Joukovsky & Favre (1913) report diameters of up to 30 cm from the Purbeckian of Mt. Salève south of Geneva.

Although isolated black pebbles may be found in any stratigraphic position throughout the examined sections, they are mostly related to inter/supratidal facies and specifically to "multicoloured breccias" (cf. Chap. 2.4.3): accumulations of reworked clasts of various colour and origin that occur predominantly on top of emersion/erosion surfaces. This is consistent with the observations of Strasser & Davaud (1983) from the Purbeckian.

The black colour is either the result of a high pyrite content, commonly present as microscopic framboids, interpreted to be the result of bacterial decomposition of organic matter (Häfeli 1966) and/or is caused by degraded organic matter itself, fixed by adsorption to carbonate crystal surfaces (Strasser & Davaud 1983, Strasser 1984). The main blackening process is interpreted to have happened in the vadose or phreatic zone, where dissolved, colloidal or very fine particulate organic matter is adsorbed to carbonate crystal surfaces in a reducing, slightly alkaline chemical environment. The interaction of adsorption and simultaneous, early cementation enables a durable fixation of the organic matter, resulting in a high resistance to oxidation (thus decolouration) (Strasser & Davaud 1983).

These blackened and early cemented carbonates may then be eroded, transported, and re-deposited. Consequently, the occurrence of black pebbles alone is not a direct sign for an in-situ emersion, yet the black pebbles are most probably related to a nearby island or coastline. Thus, horizons rich in black pebbles are interpreted to indicate a preceding drop in relative sea level below platform top, followed by flooding and reworking ("*transgressive lag deposit*", cf. Chap. 2.4.3 and Chap. 4.1).

Coprolites

Coprolites are relatively rare in the investigated sediments. The only clasts that were unequivocally identified as coprolites are *Favreina* sp. (Pl. 2/6; 13/5), which are interpreted as shrimp faeces. Their occurrence (preservation?) is commonly linked to highly restricted lagoonal settings.

2.3.2 Skeletal carbonate grains

Calcareous algae (Pl. 4, 5)

Calcareous algae are not a systematic division of algae but "*constitute a highly artificial group comprising various benthic and planktonic algae (...), which are capable of removing carbon dioxide from the water in which they live and secreting or depositing carbonate around the algal body (thallus)*" (Flügel 2004, p. 404) and therefore have a significant preservation potential. In the examined sediments, **dasyclad green algae** are the most important calcareous algae that act as source for skeletal carbonate grains. As mm- to cm-sized, calcifying, photosynthetic plants, dasyclads are most abundant in shallow, protected lagoonal environments (Flügel 1977). However, they may also be found in associations indicating more open marine conditions.

Their most common representatives are (in order of decreasing frequency):
Campbelliella striata (Pl. 4/2a, b; 5/3)
Clypeina sulcata (ex *C. jurassica*) (Pl. 4/1a, b; 5/4)
Salpingoporella sp. (Pl. 5/1a, b)

Other dasyclads include:
Acicularia sp. (Pl. 5/2)
Macroporella sp. (Pl. 4/3a, b)
Heteroporella sp. (Pl. 5/2)
Likanella sp.

If dasyclad green algae are abundant in a sample, their occurrence is commonly monospecific, respectively clearly dominated by one single species: either *Campbelliella striata* or *Clypeina sulcata* (ex *C. jurassica*, cf. Granier & Deloffre 1993). This underlines a general tendency towards restricted environments in the deposition area of the Twannbach Formation (cf. Bläsi 1980, p. 32f.). An extensive overview on the diversity and palaeoecology of dasyclad green algae from the Kimmeridgian and Portlandian of the Jura Mountains is given in Bernier (1984).

Charophytes (Pl. 2/7) are macrophytic, green algae that grow predominantly in oligotrophic freshwater environments. Selective calcification takes place exclusively at the female reproductive organs (oogons) and near stem nodes and internodes (Flügel 2004). Despite a predominance of intertidal and supratidal sediments, only some occasional, single charophyte oogons were found in the Upper Reuchenette and the Twannbach Formations ("Late Kimmeridgian and Portlandian") of the examined sections. This is in sharp contrast to their repetitive occurrence in the Goldberg Formation ("Purbeckian") (cf. Chap. 4, Yenne section and Strasser 1994). Moreover, the Goldberg Formation is the only one of the examined formations to contain some proven freshwater lake sediments – indicated by the occurrence of charophyte oogons *and* stem nodes (stems are quickly destroyed when transported) as well as the absence of marine fauna. This may be interpreted as relatively dry palaeoclimatic conditions during the deposition of the Upper Reuchenette and the Twannbach Formations (cf. Chap. 8).

Calcispheres are easily overlooked due to their small diameter of 20 to 150 µm. They play no important role in platform top sediments whereas they are more abundant in basinal limestones (cf. Chap. 2.6). In platform environments, there are two opinions with regard to their systematic position: Marszalek (1975) observed modern calcispheres in Florida Bay and showed them to be cysts of dasyclad algae (*Acetabularia* sp.), whereas Keupp (1991) interprets them as cysts of open-marine dinoflagellates.

Microbes and associated binding and encrusting organisms

A variety of bacteria with phototrophic and heterotrophic metabolisms is involved in the process of sediment binding and encrustation. In the intertidal and supratidal realm, their activity is expressed in micritic laminar, generally undulated ("wavy"), stromatolitic crusts (Pl. 13/1). Cloudy, unstructured growth forms, commonly occurring in subtidal low-energy environments under normal or restricted marine conditions are interpreted as thrombolite (Pl. 6/6; cf. Dupraz & Strasser 1999).

Various other organisms, some with an uncertain systematic status, contribute to shallow lagoonal sediment binding and encrusting. All of them seem to occur predominantly in ecological niches that also favour oncoid growth:

Cayeuxia sp. (Pl. 6/2) is a porostromate algae that was formerly regarded as belonging to the group of green algae. Newer publications attribute it to the group of cyanobacteria (Leinfelder et al. 1993, Dupraz 1999).

Bacinella irregularis, related to the group of cyanobacteria, occurs rarely in isolated form. If it is present, it contributes to oncoid growth, or it is associated in clusters with the more frequent *Lithocodium aggregatum* that is considered as an encrusting foraminifer (Schmid & Leinfelder 1996). However, some occurrences of isolated *Lithocodium* are also observed. This supports the interpretation that the two organisms belong to different systematic groups (cf. Dupraz & Strasser 1999).

Thaumatoporella sp. (Pl. 6/1) shows affinities to green algae and red algae (Leinfelder et al. 1993). This characteristic, easily-to-be-identified encruster is commonly found reworked in coarse, oncoid-bearing packstones and grainstones.

Tubiphytes is relatively rare on the platform but much more common in the studied basin sections. It is therefore described in Chap. 2.6.

Bivalves

Bivalves were found in all observed environments, commonly as reworked shell fragments. Local concentrations of oysters may indicate brackish influences.

Brachiopods

Preferring open marine environments, brachiopods are found only sporadically in the examined sections. This is in concordance with the results of Colombié (2002). The general development of the Jura platform from relatively open marine lagoons close to the platform rim during the Early Kimmeridgian (richer in brachiopods) to the more restricted internal lagoons and tidal flats of the Tithonian reflects the general trend of platform progradation to the south.

Echinoderms

Crinoids make up only a very small percentage of the observed echinoderms. To the most part this group is represented by spines and plates of sea urchins (Pl. 2/2); a fact that reflects a shallow lagoonal depositional system. Their abundance varies in the different facies types and is – together with the overall biota diversity – an important indicator to faunal restrictions: living echinoderms are strictly stenohaline, i.e. very intolerant to salinity changes. Consequently, they indicate relatively open marine settings, either in muddy low-energy facies or in carbonate sands. However, due to its porous internal structure, echinoderm debris is easily transported by currents and may therefore occasionally be found even in highly restricted environments.

Bryozoans

Bryozoans are colonial, sessile suspension feeders that prefer stenohaline habitats. Thus, only very few reworked specimens were found in the mostly restricted, internal lagoons of the Portlandian.

Corals

Corals are very rare in the examined lagoonal sediments. No build-ups were observed in the studied sections; only infrequent, usually reworked specimens were found (Pl. 2/1). However, in the Cirque des Avalanches section, a massive, coral-bearing part just below the measured section is interpreted as a lagoonal patch reef (cf. Fig. 4.17 and Meyer 2000; Bernier 1984).

Serpulids (Pl. 6/5)

Serpulids are suspension feeding polychaete worms that live in a calcareous tube, which is attached to a hard substrate. In lagoonal settings, they have the potential to construct considerable bioconstructions. Yet, only sporadic occurrences were found encrusting bivalve and gastropod shell debris. This points to prevailing soft-bottom conditions.

Gastropods (Pl. 2/3; 8/1)

Like bivalves, gastropods occur in all facies zones. However, solitary nerinean gastropods are rather found in low-energy environments with normal marine conditions, whereas small, thin-walled, high-spiralled gastropods seem to be more abundant in restricted environments, comparable to the modern ceritid gastropods. Locally, reworking (cf. Chap. 2.2.1 lithoclasts) produces mixed skeletal/non-skeletal conglomerates, which may consist to a high percentage of reworked gastropod shells ("shell beds", Pl. 2/3).

Ostracodes

Ostracode valves are omnipresent in the platform sediments and are most abundant in muddy, restricted lagoonal environments (Détraz & Mojon 1989). Peloidal pack- to grainstones showing parallel texture and containing a high percentage of closed carapaces – indicating live burial – are interpreted as storm layers (tempestites) (Pl. 11/4 and Azerêdo et al. 2002).

Sponges

In the platform sections, no entire parts of siliceous sponges were found, whereas sponge **spicules** may be highly abundant, even dominant, in low energy lagoonal environments. The most abundant forms are "rhaxes", monaxone spicules of oval or somewhat bean-shaped diameter (Pl. 2/4). They are attributed to the siliceous demosponge *Rhaxella* (Dupraz 1999). Tetraxone and triaxone spicules are less abundant and are also attributed to the group of siliceous sponges. None of the identified spicules are still showing their original mineralogical composition, i.e. the siliceous material was dissolved and replaced by calcite during diagenesis.

After having passed for an algae, and as some kind of coral, ***Cladocoropsis mirabilis*** Felix (Pl. 2/5) is today interpreted as a hypercalcified branching sponge (Termier et al. 1977, Termier & Termier 1977) a typical dweller of Late Jurassic low-energy, somewhat "polluted", "sub-lagoonal" back reef habitats. According to Flügel (1974),

it colonized the "inner shelf", yet in relatively open conditions just behind a protecting barrier. Leinfelder et al. (1996) report *Cladocoropsis* patch-reefs from Late Jurassic ramp deposits in southern Portugal.

These literature data match very well with observations from the studied sections. *Cladocoropsis* is frequently associated with oncoids, peloids, small intraclasts, and encrusting organisms and occurs predominantly in mud-dominated lithologies. A massive occurrence of *Cladocoropsis mirabilis* is a valuable indicator for relatively open conditions and probably also for relative proximity to the platform rim. It is clearly most abundant in the thick-bedded limestones of the upper Reuchenette Formation (Late Kimmeridgian) and always related to normal marine or only slightly restricted environments.

Benthic foraminifera (Pl. 3)

A variety of benthic foraminifera is observed in the studied shallow-water carbonates. The majority among them belongs to the sub-orders Textulariina and Miliolina. Four major associations of foraminifera can be distinguished, reflecting different palaeoecological conditions. They are differentiated by presence or absence of marker species and overall diversity:

a) A low diversity with a clear predominance of miliolid foraminifera (Pl. 3/10) is typical for restricted to highly restricted milieus.

b) Quasi monospecific occurrences of *Everticyclammina* sp. (in association with oysters and ostracodes; Pl. 3/11) can be found in dark, marly limestones. They represent restricted low-energy conditions; the also quasi monospecific abundance of small oysters (*Exogyra virgula*) and the increased input of fine siliciclastics are interpreted to reflect a brackish influence, probably under a more humid climate.

c) An assemblage of *Nautiloculina, Everticyclammina, Pseudocyclammina, Alveosepta, Valvulina*, and *Anchispirocyclina* is typical for restricted to normal marine conditions under both, high- and low-energy conditions.

d) Kurnubia, Parurgonia, Kiliania, and *Lenticulina* are indicators for relatively open, normal marine conditions. The highest concentration of these genera can be found in the high-energy back-reef sediments of the Cirque des Avalanches section (5-65m, Fig. 4.17).

In contrast to its normal habitat, the deeper external platform or ramp at a depth of several 10s of m (Flügel 2004), *Conicospirillina* sp. shows a reverse behaviour in the Lieu section: it is most abundant in (highly) restricted facies, even in the intertidal domain (cf. Sudan 1997).

Detailed studies on benthic Mesozoic foraminifera are provided by Septfontaine (1981) and, specifically for the Kimmeridgian and Portlandian of the French Jura Mountains, by Bernier (1984). In his diploma thesis, Sudan (1997) studied the stratigraphic distribution and palaeoecology of foraminifera in the Lieu section.

2.3.3 Lime mud

A micritic matrix makes up the vast majority of rock volume. This general predominance of mud-supported sediments is typical for shallow water low-energy environments, i.e. lagoons separated from the open ocean by a barrier.

Although it is impossible to demonstrate for the studied sections, it is assumed that the primary calcareous material was directly produced by marine organisms or by biological mediation. For example, in recent isolated carbonate platforms off the Belize coast, the fraction from 4-125 µm consists mainly of fragments of *Halimeda*, corals, and molluscs. The fraction < 4 µm (micrite s.s.) consists of aragonite needles (2-6 µm in length), which are interpreted to derive from decayed calcareous algae (*Penicillus, Halimeda*) and nanograins (< 1 µm) (Gischler & Zingeler 2002). Nanograins are most probably produced by boring micro-organisms such as fungi and/or bacterial activity and may represent the main volume of carbonate mud (Reid & Macintyre 1998, 2000; Reid et al. 1990, 1992).

2.3.4 Other constituents

Quartz

The quartz content of the investigated sediments is very low, generally below 1% (cf. Colombié 2002, Persoz 1982). However, its distribution is clearly facies dependent. Maximum values are reached in the most restricted environments, respectively in the intertidal and supratidal domain (Pl. 10/3; 13/3a, b). Quartz grains are small – in general about 50 µm in diameter or smaller – and mostly angular, except for some rare singular, well rounded, bigger grains. These grains are most probably related to input of mature siliciclastic sediments from distant landmasses, such as the Massif Central or the Rhenish Massif (cf. Fig. 1.3a) and were transported by rivers and ocean currents.

For the angular, silt-sized particles two different origins are proposed: Clay and silt particles of approximately 5 to 50 µm in diameter are commonly lifted from dry desert surfaces by wind and suspended in the air as **aeolian dust**.

The finest particles can remain suspended for weeks and travel thousands of kilometres, whereas particles of 20 µm or larger remain in the atmosphere only minutes to hours and may travel a few tens to hundreds of kilometres (PÉWÉ 1981).

Consequently, layerwise concentrations of fine, (sub)angular quartz grains in tidal flat tempestites and clay to silt-sized layers on mud-cracked emersion surfaces are interpreted to be predominantly of aeolian origin. On modern tidal flats in (semi)arid environments, aeolian sediment typically contains about 60% detrital dolomite with a grain size of about 30 µm across, with quartz silt in the same size range (SHINN 1983).

Yet, fine angular quartz grains that are evenly dispersed in the muddy matrix of lagoonal sediments may either be of aeolian, or **authigenic** origin (cf. Chap. 2.4.4). A possible source supplying the SiO_2 for the neoformation of quartz crystals would be siliceous sponge spicules that are frequent in the studied lagoonal sediments. However, according to the results of XRD-analyses carried out by MOUCHET (1995), quartz grains found in the Kimmeridgian of the central Jura are of purely detritic origin. As no major diagenetic differences exist, the same can be assumed for the Portlandian.

Clay minerals

Concentrations of clay minerals are relatively rare in the pure limestones and dolomites of the Kimmeridgian and Tithonian. They appear either in well-defined marly intervals that are traditionally used for regional correlation (lower and upper *virgula* Marls), or as marl/clay-seams separating two beds of pure carbonate, thus indicating a discontinuity. Clay minerals comprise mainly illite, chlorite, kaolinite, and mixed-layer minerals.

Marl seams become more abundant in the Purbeckian (Goldberg Formation). Their typical colour is greenish-grey (yellow or reddish-grey when oxidized; cf. DECONINCK & STRASSER 1987). Dark brown to nearly black colour is caused by the presence of organic matter and pyrite. The Purbeckian TOC content varies from 0.1-0.3% (DECONINCK & STRASSER 1987).

Organic Matter

Dark marly limestones and marls typically yield small fragments of charred organic matter. In the Dôle section, a black clay band containing cm-size plant remains was found. However, most organic matter is finely dissipated (cf. Chap. 2.4.4, *Black facies*).

Pyrite

Pyrite is usually linked to the occurrence of organic matter as it can form by the bacterial degradation of the latter (sulphate reduction, cf. JØRGENSEN 1983). It usually precipitates in framboids (commonly linked to bioclastic grains, cf. Chap. 2.4.4, *Black facies*) or cubic crystals.

Glauconite/Chamosite

Occurrences of glauconite, respectively chamosite are restricted to some dolomitized intervals of Late Kimmeridgian age. They appear as small, sub-millimetric, green grains embedded in sucrosic dolomite. For this project, no geochemical analyses were carried out in order to determine the exact mineralogy. According to VAN HOUTEN & PURUCKER (1984), glauconite is a mineral typically occurring in deeper, open-marine settings, whereas chamosite represents its shallow-marine, lagoonal counterpart.

Evaporites

Due to their easy dissolution, no evaporites are materially preserved. After dissolution, crystal molds were filled with calcite cement, creating pseudomorphs. The encountered morphologies point either to replacive in-sediment growth (lozenge-shape gypsum crystals – Pl. 13/4, halite cubes – Pl. 13/5,), or evaporite nodules (gypsum/anhydrite? – Pl. 13/6) that form in sabkhas. Generally, sediments displaying evaporitic features are barren of any fauna, or show at best a highly restricted association of ostracodes and various transported bioclasts.

2.4 SEDIMENTARY STRUCTURES

2.4.1 Hydrodynamically formed structures

Lamination (Pl. 11/1-4; 13/3a)

Laminated sediments form by different processes and in a multitude of sedimentary environments. However, for their preservation, the absence of burrowing fauna is essential, because in abundance of burrowing organisms all primary structures are quickly homogenized. Consequently, lamination will be preserved predominantly in anoxic basin conditions, or in supra- and upper intertidal coastal environment, where burrowing organisms are either totally absent, or at least rare. Even if a shallow intraplatform basin with bituminous laminites is known to exist in the Late Kimmeridgian of the southern Jura Mountains (cf. BERNIER 1984) this facies-type was not encountered in the measured sections. Consequently (and in accordance with observations on modern tidal flats) all laminations, graded or ungraded, thick or thin, with or without cross-bedding, are interpreted to have been originally deposited in supra-

and upper intertidal settings as a result of spring or storm tide deposition. Also microbial trapping and binding of grains may be implicated to a certain extent, indicating relatively quiet phases between two high-energy events (Pl. 11/1&2).

Cross bedding (Pl. 1/2)

Cross bedding is a sedimentary structure related to the migration of (carbonate) sand bodies under uni- or multi-directional current with relatively high velocities. Foreset-beds observed in samples and outcrops are of cm to dm scale.

Lenticular and flaser bedding (Pl. 11/7)

Lenticular bedding and flaser bedding are diagnostic features for periodically switching, opposed current directions, i.e. tidal environments, usually in very shallow water. In the examined sediments, their distinctive geometries, as originally described from siliciclastic sediments, translate into micrite-pelsparite alternations with frequent bioclast occurrence (mainly ostracodes, cf. Pl. 11/4 and 11/7). In outcrop view, these structures commonly are not clearly expressed and may look rather similar to heavily bioturbated ("nodular") mud and wackestones that were subject to strong compaction.

Wave ripples

Cm-sized wave ripples evidence wave action in a very shallow lagoonal to intertidal context.

Keystone vugs and plane bedding (Pl. 8/3)

Keystone vugs are fenestrae in a well-sorted grainstone that are commonly arranged like a string of pearls. Their formation is attributed to the entrapment of air bubbles between quickly settling grains in the swash and back wash zone of beaches. Plane bedding, that usually accompanies the appearance of keystone vugs, results from upper flow-regime conditions while the waves washed over the beach.

Erosion (Pl. 8/2)

Erosion of semi-consolidated sediment may be indicated by truncated bedforms. It is generally caused by a sudden rise of energy related to storms, waves, tides, laterally migrating channels, or changes in base level.

Grading (Pl.1/2; 13/3a)

Normal or inverse grading is related to changing energy conditions during event deposits or tides.

Bimodal grain-distribution

Carbonate sands with bimodal grain distributions have possibly been deposited under pronounced tidal influence (cf. Colacicchi et al. 1975). The bimodal distribution reflects flood and ebb currents of different velocities. Some unequivocal examples are found in sandy tidal channel fills. Others in shallow marine carbonate sands are interpreted with caution as grain-size distributions in carbonates heavily depend on the type of skeletal grains available (Flügel 2004).

2.4.2 Biogenic structures

Bioturbation and -perforation

Bioturbation is very frequent in the studied interval. Burrows can usually easily be distinguished from muddy matrix due to a difference in colour, texture, or by differential dolomitization (cf. Chap. 3). Burrows filled with packstones or grainstones are interpreted as "tubular tempestites" sensu Wanless et al. (1988). Nodular limestones (Pl. 8/4) are interpreted as the result of intense bioturbation. If there is a significant difference in colour and/or texture between burrow fill and matrix, heavily bioturbated limestones may resemble "pseudobreccias" (Pl. 16/3; cf. Horbury & Qing 2004). Bioturbation types were not studied in detail, only the characteristic, Y-shaped *Thalassinoides* were determined where possible (e.g., nicely visible from below on the bedding planes of the Cirque des Avalanches section, 70-75 m). Hard-substrate bioperforation (*Trypanites*) was found only on one surface (Noirvaux section, 124.5 m). However, as most of the sections do not expose the sedimentary surfaces, it is likely that more bioperforation is present than indicated in the section logs.

Levels of intense bioturbation and/or bioperforation may indicate a low sedimentation rate or omission phases.

Microbial sedimentation

Biofilms and microbial mats can trap grains on their surface and precipitate carbonates in a multitude of conditions from subtidal to supratidal environments (Riding 2000).

The most evident microbial structures in Late Jurassic carbonates are s**tromatolites** (Pl. 13/1). The term "stromatolite" is rather vaguely defined (Riding 1999). In this study, stromatolites are understood as rocks made up of mm-scale flat or undulating ("wavy") laminae that probably formed under microbial influence. As a matter of fact, all stromatolites in the investigated sections grew in the upper intertidal or supratidal zone and are more or less

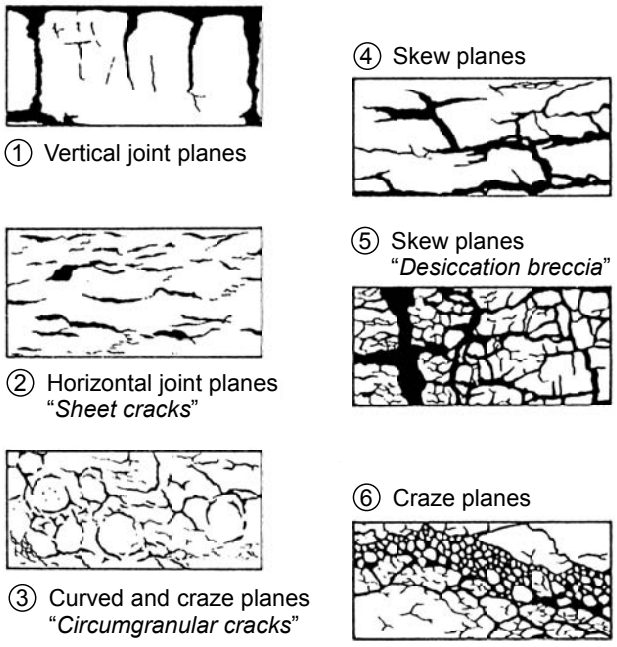

Fig. 2.3 - Different morphologies of shrinkage cracks in lime mud related to desiccation and pedogenesis (from Freytet & Plaziat 1982).

dolomitized (Pl. 13/2). This is deduced from their regular association with desiccation structures. Additionally, the dolomitization type suggests penecontemporaneous dolomite formation triggered by evaporation (cf. Chap. 3). Commonly platy, but otherwise structureless, sucrosic dolomites are observed in association with tidal-flat facies. It is assumed that at least parts of this platy dolomite were originally stromatolites. As secondary dolomitization tends to be fabric destructive (cf. Chap. 3), it is assumed that the more delicate laminations were lost during the recrystallization process.

Algal mats form the accretion surface of stromatolites, but can also occur as mm-thick, sediment-binding blankets ("*stick-on layers*", cf. Pl. 6/4, 11/1, 2). If not dolomitized they show a clotted microtexture, resembling type-1 peloids.

Thrombolites (Pl. 6/6) have a macroscopically clotted fabric, consisting of irregular patches of mm- to cm-scale. Each patch ("clot") shows a micropeloidal internal structure and is separated from the neighbouring patch by micritic sediment (or sediment grains, or sparite; cf. Dupraz 1999, Dupraz & Strasser 1999). Thrombolites may form m-scale "doughnut-like masses" (small mounds) in low-energy environments marked by slow sedimentation rates (Riding 2000, Leinfelder et al. 1996). Such a small mound was found in the Cirque des Avalanches section (64 m), its internal structure can be described as somewhere between "layered thrombolite" (lT) and "poorly structured thrombolite" (sT) according to the classification by Schmid (1996).

2.4.3 Structures indicating subaerial exposure

Desiccation cracks

Desiccation features are very common in the studied sediments. They result from the (repeated) shrinkage of carbonate mud or cryptalgal mats when drying under subaerial conditions. Different morphologies (Fig. 2.3, Pl. 9) are present, each one typical for a distinct level in tidal environments, respectively a distinct stage in soil development:

Deep prism cracks separating polygons of several tens of cm diameter are typically present in intertidal environments, commonly with extensive growth of cryptalgal mats (Fig. 2.7; Pl. 9/1a, b). Polygon edges in sediments with extensive growth of cryptalgal mats are typically rimmed with tepee-like pressure ridges (Pl. 9/2a, b). Cm-scale polygons of **shallow mudcracks** (Pl. 9/3a-c) occur predominantly in upper intertidal to supratidal laminites (Fig. 2.7). During the desiccation process the polygon surface may deform to a concave shape. These little depressions act as sediment traps; specifically for windblown clay- and silt-sized grains (e.g., sample Do160).

Sheet cracks (Fig. 2.3; Pl. 12/1) are common in desiccated algal mats of the supratidal algal marsh (Fig. 2.7). Well developed **circumgranular cracks** and **skew planes** (Fig. 2.3) are structures that are typically related to incipient soil formation, for which a longer period of subaerial exposure is necessary. Mature palaeosols were not found, however, **desiccation breccias** developing from a dense network of skew and craze planes indicate longer periods of emersion and are an important source for intraclasts (Freytet & Plaziat 1982).

Tepee(like) structures, pressure ridges (Pl. 9/2a)

Tepee structures form by expansive growth of early cements (subtidal hardgrounds), microbial mats (inter- and supratidal, Pl. 9/2a, b), and/or evaporites (supratidal sabkha) in a host sediment (Demicco & Hardie 1994). In the observed cases, tepee structures are always associated with other emersion-related structures and/or facies.

Birdseyes

Although "birdseyes" (and "fenestrae") are non-genetic terms they are most commonly associated with peritidal environments (Shinn 1983). Some authors also include root- or worm-tubes in this category. In this work, however, birdseyes are understood exclusively as mm-scale cavities in carbonate mud that are created by active algal/microbial growth and/or by trapping of gases released during the decomposition of organic matter. These kinds of birdseyes occur characteristically in the

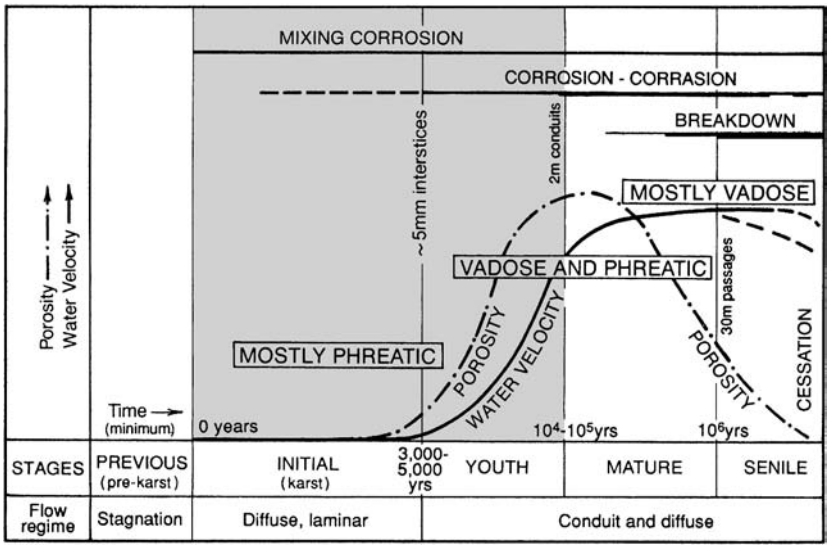

Fig. 2.4 - Stages of karst evolution in carbonate rocks (from Esteban & Wilson 1993). Represented here is a tight carbonate formation with only capillary interstices or joints as pre-karstic permeability pathways that allow initial water flow. Many systems start from phreatic conditions with laminar flow, with only mixing corrosion possible and slow porosity development. The grey area marks the initial and youth stages in the evolution of a karst system (mean conduit diameter lower than 2 m). The karst phenomena observed in the field were of a maximum diameter of several dm.

upper intertidal and supratidal zone.

Infill sediment

Fine-grained infill sediment forms geopetal structures in intergranular voids (Pl. 8/1). It is related to a drop in energy, allowing for the deposition and infiltration of fine-grained sediment that was subject to constant winnowing before. Infill sediment commonly comes along e.g., with vadose cementation (Pl. 10/1) or other emersion indicators and, in consequence, is interpreted to be related to emersion. As a stand-alone, however, it is no unequivocal indicator for subaerial exposure.

Evaporite pseudomorphs (Pl. 13/3-6)

Evaporites precipitate in hypersaline environments and are therefore indicating close-to-emersion or clearly supratidal settings if they are found in association with other sedimentary structures implying sabkha environments. In the examined sediments, no evaporites are materially preserved: the crystals were dissolved and their molds filled with calcite cement ("pseudomorphs"). The encountered morphology of crystal molds points either to replacive in-sediment growth (halite cubes, lozenge-shape gypsum crystals), or evaporite nodules (gypsum/anhydrite?) that form in supratidal sabkhas (cf. Demicco & Hardie 1994).

Karst-related structures

Karst is the product of subaerial (terrestrial and coastal) exposure of carbonates rocks, recognizable by features produced by dissolution, precipitation, erosion, sedimentation, and collapse in a variety of surface and subsurface landforms, and cave deposits consisting of both cements and sediments. Starting from bedding planes, fractures, or intergranular porosity, karst systems create additional porosity by dissolution (corrosion), erosion (corrasion), and incasion (collapse). Most of the corrosion results from carbonation of atmospheric CO_2 and the formation of carbonic acid. Another important process – specifically for the initial stages of karstification in deep phreatic environments – is mixing corrosion. This process results from the mixing of two waters with different partial CO_2 pressures, e.g., groundwater and meteoric water. Other particular cases are corrosion by non-atmospheric CO_2, humic, sulphuric, or organic acids, cooling corrosion, pressure corrosion, and biocorrosion (Esteban & Wilson 1993).

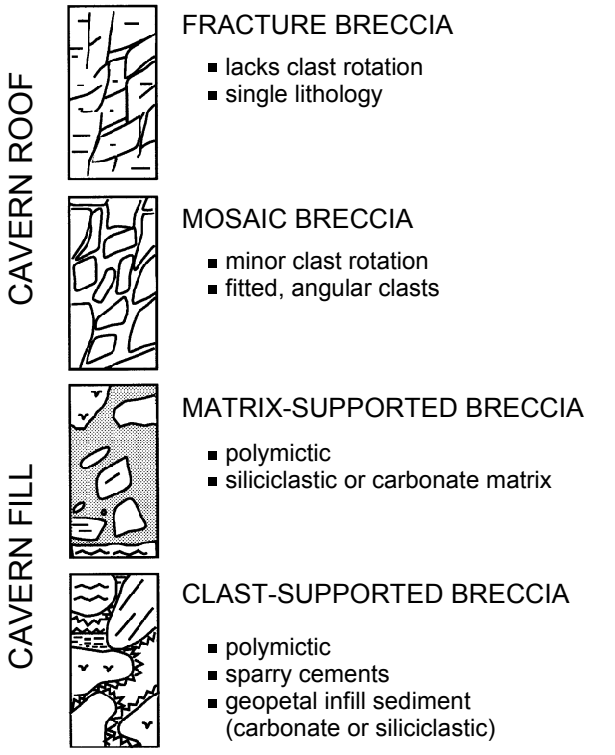

Fig. 2.5 - Schematic representation of karst-breccia types (from Canter et al. 1993, modified).

In the studied sections, all observed **solution cavities** ("*karst pockets*") that are related to carbonate dissolution have a diameter of less than 1 m (e.g., Pl. 10/6). In many cases, only **microkarst**ic features (mm-scale dissolution, filling, and cementation of joints, Pl. 10/5) are developed. This means that only the initial and youth stages of karst evolution were reached (Fig. 2.4). To determine the age of karstification is of high relevance for a sequence- and cyclostratigraphic approach, but of course very difficult. Karst pockets that are filled with matrix- or clast-supported breccia consisting of intraclasts and a marly matrix (Fig. 2.5) are likely to be related to an early-stage (Late Jurassic) karstification, whereas pockets with reddish clay filling are probably reflecting later phases of karstification under Tertiary warm and humid conditions.

In contrast to karst in carbonates rocks, **gypsum karst** evolves much faster due to that mineral's far higher solubility. Consequently, all encountered traces of gypsum karst represent the senile stage ("breakdown", Fig. 2.4) of karst evolution, mainly as collapse breccias of different scales. **Local in-situ brecciation**, as found e.g., in the Lieu section (Pl. 13/7), usually shows a mosaic-like texture indicating that the clasts are still more or less in place (cf. Fig. 2.5). In mature karst systems, this breccia facies is typical for the cave roof (Canter et al. 1993). Here, it is interpreted to be related to the dissolution of small underlying evaporite occurrences by meteoric water.

The removal of voluminous, bedded evaporite successions leads to the development of **large intrastratal collapse breccias** (Scholle et al. 1992, 1993). Such collapse breccias are found at the top of the Dôle section (Figs 4.14 and 4.15). In the field, they present a several m-thick massive body composed of angular intraclasts and clods (cm to m size), with clods still showing their original bedding planes. The lateral succession of clods forms folded surfaces, and some clods are even internally folded. The breccia is matrix- to clast-supported; some geopetal interclast voids with horizontal lower surface and filled with sparite cement indicate the (at least partly) infill character of grey micritic matrix. According to Canter et al. (1993), these breccia facies are typically polymictic and represent cave fill sediments in carbonate karst (Fig. 2.5). However, the breccia being made up exclusively of intraclasts from the surrounding carbonate facies, locally with clods still in lateral association, and the placement on top of a several m thick succession of sabkha facies are strong arguments for *in-situ* formation related to evaporite dissolution.

To reconstruct the timing of dissolution and collapse is problematic, particularly whether the evaporite removal happened synsedimentary or late diagenetic, e.g., during the Tertiary uplift of the Jura Mountains. Studying Triassic evaporites in Crete (Greece), Pomoni-Papaioannou & Karakitsios (2002) found that brecciation is a multistage process, starting right after deposition, but mainly taking place during recent uplift and renewed groundwater flow ("telogenetic alteration"). Intrastratal collapse breccias in Permian sediments that are related to Tertiary surficial or telogenetic alteration are described by Scholle et al. (1992, 1993).

Resedimentation: (multicoloured) breccias

Multicoloured breccias are sedimentary breccias of polygenic origin. They are composed of angular or rounded clasts (mm- to cm-scale) of various colours (black, brown, and beige) in a micritic, frequently dolomitized matrix of grey or beige colour. Dark-colour clasts often show "corroded" rims (Pl. 12/3a), there may also be borings (Pl. 12/3b), Fe-crusts, or *Microcodium* (Bläsi 1980). Multicoloured breccias are always found in association with other indicators of inter- or supratidal deposition. Most commonly they form flat, lenticular bodies on a tidal flat surface.

The incorporated black pebbles are a sign of nearby emersion (Strasser & Davaud 1983, Strasser 1984; cf. Chap. 2.4.4). Light-coloured clasts are usually eroded from the underlying peritidal strata. Thus, multicoloured breccias are interpreted as coarse storm deposits in (mostly supra-)tidal environments. A detailed analysis of microfacies and 3-dimensinonal architecture of multicoloured breccia deposits from the Portlandian of the Swiss and French Jura Mountains is given in Bläsi (1980).

Thick bodies of breccia, either plain or multicoloured, are interpreted as deposition of reworked material in drainage channels during longer periods of emergence. Their substratum may show a channel-like geometry (Pl. 10/7) but this is not always apparent. In any case, well developed emersion features like mudcracks and vadose diagenesis, or even hints to fully continental conditions such as charophyte occurrence and/or incipient palaeosols are present under the breccia bed. This type of breccia is found only in the upper part of the Yenne section (Goldberg Formation, "Purbeckian").

Microcodium

Microcodium is formed by 20 to 70 μm wide and 100 to 800 μm long calcite prisms that are arranged in corn-cob like colonies (Pl. 10/3). *Microcodium* typically corrodes limestones in terrestrial environments and is commonly associated with (micro)karst features, root casts, pedogenic nodulization, or desiccation breccia (Pl. 16/1). After a long history of controversial interpretations, the origin of this sedimentary structure is still uncertain. Widely accepted theories relate the formation of

Microcodium to a symbiotic association of bacteria and fungi or root calcification of certain plants (Klappa 1978, Morin 1993, Košir 2004).

The presence of non-reworked *Microcodium* is an unequivocal proof for continental conditions, i.e. a vadose zone underlying a surface of subaerial exposure (Klappa 1978, Freytet & Plaziat 1982, Esteban & Klappa 1983).

Microcodium was found in one interval in the Noirvaux section (138.5-140 m) that is interpreted to be a sequence boundary zone. However, it is not clear if this *Microcodium* occurrence reflects a longer lasting Late Jurassic phase of emergence and pedogenesis, or if it is related to regional Tertiary uplift and erosion.

Rhizoturbation

Rhizoliths (root structures) appear as root casts or rhizocretions (concretions precipitated around roots). Root casts are mm-sized tubular, branched voids or linings of decayed roots. The decayed root is usually replaced by fine sparitic cement, with a surrounding micritic carbonate lining ("sheath"; cf. Pl. 10/4 and 16/1b) as a result of the biochemical activities of the living plants or the post-mortem decay of organic root material (Esteban & Klappa 1983). Rhizocretions consist of mm-scale concentric micrite nodules, commonly surrounded by root casts and alveolar structures. Rhizocretions were not observed in the studied sections, whereas root casts (locally associated with *Microcodium*) occur repeatedly together with other features indicating vadose diagenesis. For a detailed classification of root structures see Klappa (1980).

Continental stromatolites

A laminated crust was found in the same interval of the Noirvaux section that also contains root casts and *Microcodium*. It is about 500 µm thick, runs parallel to the bedding planes and consists of fibro-radial calcite crystals that show undulating alternations of dark and light layers (Pl. 10/2). Freytet & Plaziat (1982) relate this microstructure to continental stromatolites, which are formed by the cyanobacteria of the genus *Schizothrix* and *Phormidium* (cf. Colom 1961, Freytet & Verrecchia 1998).

Calcretes

The absence of calcretes in the Portlandian is in sharp contrast to their relative abundance in the Purbeckian (Strasser & Davaud 1982, Davaud et al. 1983). This can be interpreted in terms of a relatively drier Portlandian palaeoclimate (cf. Chap. 8). An overview of calcrete phenomena and formation is given in Wright & Tucker (1991).

Palaeosols

Palaeosols, respectively incipient palaeosols were only found in the upper parts of the Yenne and the Dôle sections (Goldberg Formation, "Purbeckian" – Early-Middle Berriasian). In the Dôle section, two mm- to cm-thick red-brown carbonaceous marls, overlain by a patchy cornieule crust are interpreted as thin, immature soils that developed under a semi-arid, Mediterranean climate. In the Yenne section, Strasser (1994 and unpubl. data) reports two palaeosol horizons (Fig. 4.19). According to E.J. Anderson (pers. comm.), also the boundary interval between the Goldberg and the Pierre-Châtel Formations (Fig. 4.19 and Pl. 20/4) is a well developed palaeosol. It consists of a dark grey to brown carbonaceous marl matrix with nodular texture, incorporating black and unblackened limestone pebbles with a diameter of up to 20 cm. It thus resembles the 'Great Dirt Bed' that marks the base of the Purbeckian *sensu anglico* in Dorset, southern England (Francis 1986). Overviews of palaeosols and pedogenic features are given in Wright (1994).

Lacustrine carbonates

In parallel to the distribution of palaeosol horizons, Strasser (1994 and unpubl. data) reports lacustrine deposits from the upper part of the Yenne section (Goldberg Formation, "Purbeckian"). These are limestones and marls that probably formed in coastal lakes and lack any clearly marine biota but contain ostracodes, charophytes (oogons and stems), and freshwater gastropods (Mojon & Strasser 1987, see also Freytet & Verrecchia 2002).

2.4.4 Early diagenetic effects

Early diagenesis is defined as the part of diagenetic history of a sediment that takes place shortly after deposition. It is essentially marked by compaction (geometric rearrangement of constituents), cementation, and alteration (mineral transformations, dissolution).

Involved processes depend on depositional environment and external factors. Thus, their traces can eventually furnish details about the regional post-depositional history (e.g., Plunkett 1997, Tucker 1993). In the present study, early diagenesis was only looked at with the objective to obtain further indications of sea-level and climate changes. The analytical methods that were used comprise thin-section petrography (plane and cross-polarized) and stable-isotope analysis.

Cementation

Cementation is the initial process leading to sediment lithification. Environment and composition of pore fluids cause precipitation of characteristic cement types (e.g., Moore 1989, Tucker & Wright 1990, Flügel 2004). Subaerial exposure and influence of meteoric waters can lead to rapid cementation of carbonates (Wright 1994, Tucker & Wright 1990). In grainstones, special attention is given to cements with asymmetric crystal habits that indicate precipitation in vadose environments (Moore 1989). These include pendant (Pl. 10/1) and meniscus cements. The former are unequivocal indicators for the vadose zone, in contrast to the latter that may form by different processes in the vadose or shallow subtidal zone. "Real" meniscus cements precipitate exclusively in the vadose zone and are either sparitic or micritic. They clearly follow the geometry of water-to-surface adhesion-patterns caused by the surface tension of water. Meniscus-type grain bridges that probably originate from microbial mucilage binding are of micritic texture and can also form in shallow subtidal environments (Pl. 8/5; Hillgärtner et al. 2001). However, they may also show a much more complicated geometry that resembles pedogenic alveolar structure (Esteban & Klappa 1983). As a conclusion, Hillgärtner et al. (2001) state that micritic meniscus-type grain bridges alone are no valid proof of emersion.

A special case of vadose diagenesis is the "*vadose compaction*" of oolitic grainstones, as described by Clark (1980) for pisolitic grainstones from the Permian Zechstein Basin: sediment that escaped early cementation becomes subaerially exposed and flushed with freshwater. Under these conditions, preferential leaching takes place at grain contacts and eventually leads to a tightly compacted texture with virtually no intervening porosity, characterized by well-defined isopachous sparry cements. Presence of this texture suggests that the grains were originally composed of a mineral unstable in freshwater (high-Mg calcite or aragonite), otherwise vadose compaction probably would not have occurred.

In marine-phreatic environments, early cementation is commonly associated with omission phases, or phases of reduced sediment accumulation and intensified percolation of pore fluids through the sediment. These cements characteristically display fibrous and micritic crystal-fringes. Such synsedimentary cementation can lead to the formation of firm- and hardgrounds (cf. Shinn 1969), which consecutively are subject to biogenic and/or chemical alteration (bioperforation, encrusting, Fe-staining, etc., see Pl. 8/4, 12/2, and Fürsich 1979).

Compaction

Initial compaction of unconsolidated sediment is due to dewatering and changes in packing density. These processes can be observed at a burial depth of just one metre, whereas plastic deformation of grains, grain crushing, and pressure solution (stylolites, overpacking) start at burial depths of approximately 100 m (Flügel 2004). The compactional behaviour of a given sediment depends on dynamic, inherited and inhibiting factors. When trying to deduce 'external' influences, such as sea-level and climate changes, from differences in compaction, inherited factors (sedimentary fabric, architecture and mineralogy of skeletal grains, clay content, grain-size, -shape, and -sorting) and inhibiting factors (preburial cementation and dolomitization) play the most important roles.

Dolomitization and dedolomitization

Dolomitization (dolomite caps) plays an important role in the sedimentary architecture of the Jura Mountains' Portlandian. This is why dolomitization and dedolomitization processes are treated in a separate chapter (Chap. 3).

Black facies (Pl. 3/11; 16/4)

Dark grey to nearly black, marly and often dolomitic limestones ("*black facies*") stick out from the mainly bright, cream-coloured carbonate succession. In sedimentary environments, blackening is essentially the result of bacterial decomposition of organic matter and resulting precipitation of pyrite (framboids). Pyrite framboids or pyritized microfossils on outcropping rock surfaces and/or close to superficial joints may be altered by oxidation and thus show a colour varying from rusty brown to bright orange to red (Pl. 16/4).

Blackening typically takes place in anoxic bottom waters or anoxic sediment in stagnant bays, lakes, ponds, or channels with varying salinity (Strasser 1984) and in the presence of iron sulphides (Jørgensen 1983, Berner 1989). Terrigenous influence seems to be an important factor in the process of blackening, not only for the input of iron, which is commonly adsorbed on clay and silt grains, but also for the influx of particulate organic matter and dissolved nutrients (phosphates, nitrates). The elevated nutrient level leads to increased primary productivity, which in turn causes higher oxygen consumption by benthic organisms and aerobic bacteria (Hallock & Schlager 1986). Eventually, this leads to an eutrophication of the environment, anaerobic degradation of organic matter by sulphate reducing bacteria and, consequently, to the formation of pyrite, specifically in a protected lagoonal environment with low water exchange.

The typical faunal assemblage of oysters and pyritized agglutinating benthic foraminifera in these sediments fits well into the scenario described above. Oysters are known to be rather tolerant to salinity drops caused by freshwater input, the latter also providing fine-grained siliciclastic material, particulate organic matter and dissolved nutrients

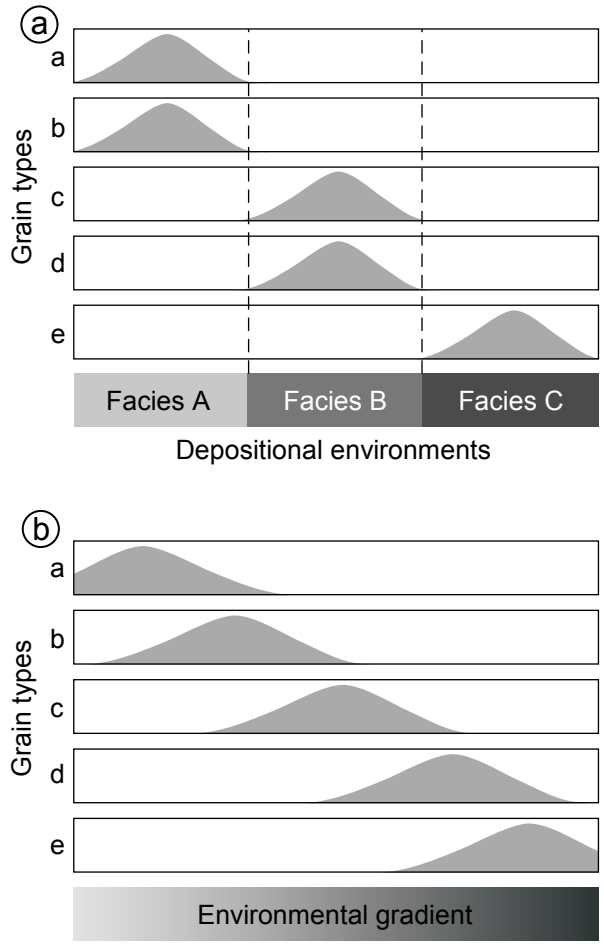

Fig. 2.6 - a) Microfacies divisions of depositional environments tend to create an illusion of discontinuous distribution of grain-type abundance (either in space or time). b) In nature, however, the spatial and/or stratigraphic distribution and relative abundance of grain types is the result of a unidirectional environmental gradient. Although samples from different geographic or stratigraphic positions may share no grain types in common, they are genetically related to one another as part of the same unbroken dynamic continuum (after Spence & Tucker 1999).

(see above). Additionally, monospecific mass occurrences (e.g., *Nanogyra nana, Evertycyclammina* sp.) and a low faunal diversity indicate an ecologically stressed environment. The frequent occurrence of entire sea urchin plates implies a rather calm environment. However, it is not clear if the stenohaline echinoderms actually lived in these conditions, or if their plates were imported without being broken or rounded.

Due to their characteristic colour, facies, and geomorphologic aspect ("soft weathering"), these horizons are easily recognizable and are traditionally used for lithological correlation. The upper *virgula* Marls are the most important example for this (Aubert 1950a, b; Bläsi 1980).

2.5 Platform facies

Standard microfacies divisions (e.g., Folk 1962, Dunham 1962, Wilson 1975, Flügel 2004) tend to create an illusion of clearly separated facies and facies zones. In nature, however, the spatial and/or temporal distribution is the result of an unidirectional environmental gradient, i.e. laterally correlating facies or facies of the next older, respectively the next younger bed are not sharply separated but genetically related to one another as part of the same unbroken dynamic continuum (Fig. 2.6, Spence & Tucker 1999). This has to be kept in mind when setting up facies models for any depositional environment.

Therefore, Spence & Tucker (1999) propose an alternative approach, based on computer optimized similarity coefficient matrices of relative grain-type abundances, which allows for quantified statements on genetic facies-relation and describing environmental gradients. This elegant approach is, despite its rather non-illustrative nature, definitely closer to reality and is definitely of advantage if primary research-targets are minute environmental reconstruction and smooth integration of data into numeric modelling. Yet, the aims of this study are primarily the development of a sequence- and cyclostratigraphic timeframe for the Tithonian as a part of a larger project covering the Late Oxfordian to Early Valanginian. Consequently, compatibility with earlier work of the Fribourg working group, based on methodology described by Strasser et al. (1999), is essential, and it was chosen to stay with the standard divisions. A second argument favouring a qualitative, respectively semi-quantitative approach was the large amount of time a point-counting approach for the 640 analyzed thin sections would have demanded. If of appropriate resolution, microfacies divisions are likewise a rather reliable tool for identifying high-frequency transgressive-regressive trends. Additionally, by working with qualitative data, it was by far easier to incorporate the less detailed (but nonetheless important) data from 816 etched slabs, as well as from detailed section logs and field observations. The facies types identified in this study are described in Tab. 2.2.

2.5.1 Facies zones

Seven facies zones (FZ) are differentiated in this study and are numbered from proximal to distal positions (Fig. 2.8a, 2.9). Facies zones 1-5 represent platform environments, facies zones 6 and 7 slope and (hemi)pelagic environments.

FZ1 - continental

Continental deposits are rare in the studied sections. They are restricted to thin green and black marl seams

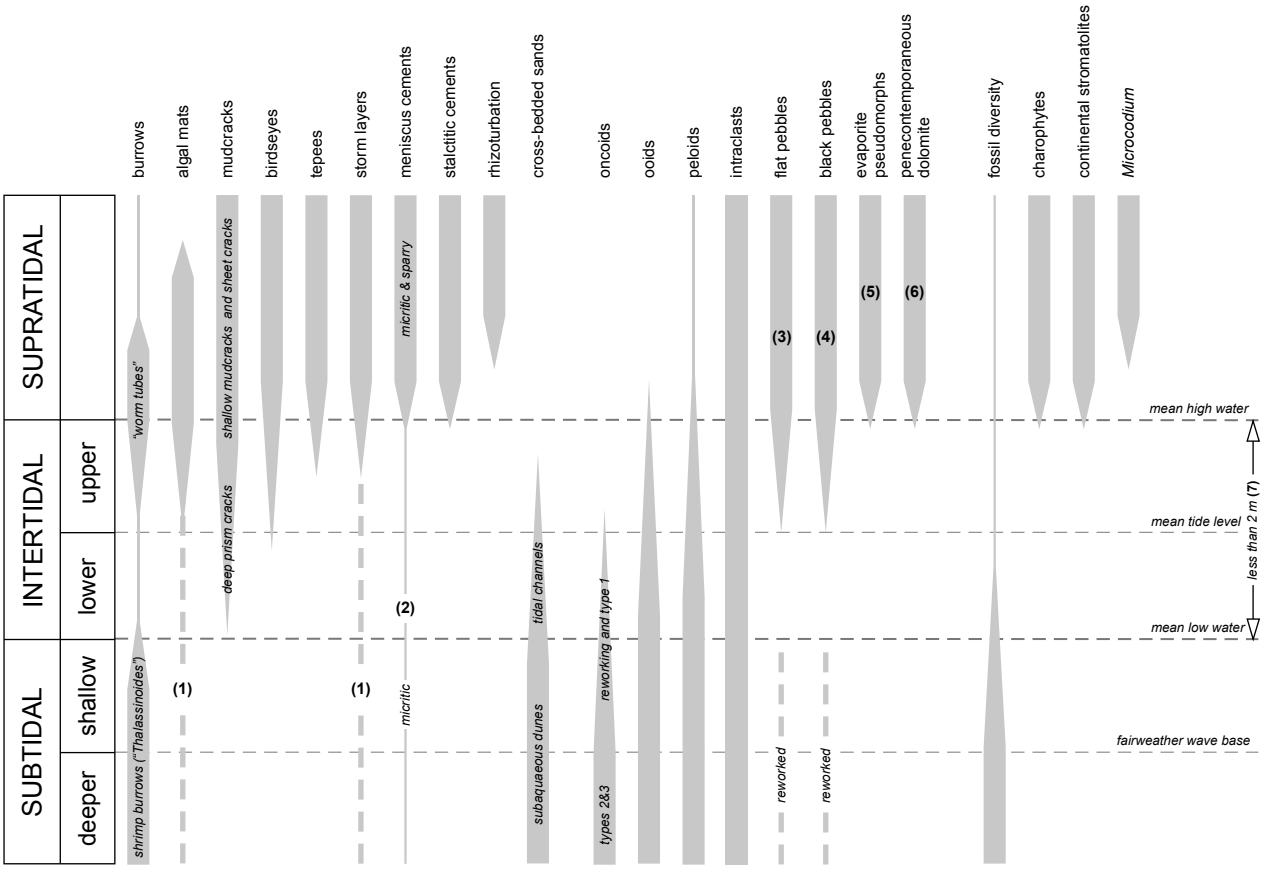

1) present during time of deposition, but usually not preserved due to constant burrowing and reworking (Shinn 1983)
2) micritic meniscus-type grain bridges that probably originate from microbial mucilage binding (Hillgärtner et al. 1999)
3) "*mud chips*", reworked algal laminites (Demicco & Hardie 1994, Shinn 1983)
4) indicative of nearby emersion (Strasser & Davaud 1983, Tucker & Wright 1990)
5) under arid climate, at the intertidal-supratidal transition (Shinn 1983)
6) "*sabkha dolomite*" or "*evaporatic dolomite*"; small rhombs with high $\delta^{18}O$-values
7) most ancient carbonate peritidal settings were microtidal, i.e. characterized by an amplitude lower than 2 metres (Pratt & James 1992)

Fig. 2.7 - Compilation of tidal flat diagnostic criteria, classified in accordance with their genetic processes and typical relative water depth.

and charophyte-ostracode bearing limestones that are interpreted as coastal lakes (Strasser 1994). All other indications of continental environments are restricted to reworking of continentally derived material and alteration of limestones. They are commonly manifested as black pebbles and (immature) palaeosols, karstification and/or other indications of vadose diagenesis. The extent of limestone alteration suggests, however, that the huge majority of the intervals where continental conditions prevailed were of relative short duration.

FZ2 - Coastal / tidal domain

The coastal and tidal domains include all environments with intertidal to supratidal characteristics. This can be sabkhas, tidal flats featuring laminated microbial mats, stromatolitic and/or microbial encrusting/binding with desiccation and dissolution features or, more rarely, beaches with characteristic laminations. Their proximal situation with respect to the continental domain is manifested by increased terrigenous influence.

Sabkhas develop under arid climate at the interface between the continental and tidal domain. Though clearly supratidal in location, the formation of evaporites depends on sea-water recharge, powered by evaporative pumping (Schreiber & El Tabakh 2000). Sabkha sediments are often chalky carbonates and show evaporite pseudomorphs and signs of haloturbation when analyzed under the microscope.

Tidal flats are essentially subdivided according to the prevailing grain size as mudflats and/or (mixed) sandflats, either intertidal or supratidal. A clear distinction of intertidal and supratidal environments in the fossil record can be difficult if characteristic sedimentary structures are

absent or not (fully) preserved. The most important factors for distinction are the lack of laminations and storm layers in intertidal sediments (due to permanent reworking), the geometry of desiccation cracks, as well as the occurrence of tepee structures and birdseyes (Fig. 2.7). The exact boundary between lower intertidal and shallow subtidal is even harder to define, as long as the subtidal environment does not show clearly lagoonal features.

FZ3 - internal lagoon – restricted to highly restricted, tidally influenced

This facies zone is the most common in the Portlandian of the Swiss and French Jura platform. Internal lagoons occupy the entire protected to highly restricted realm of the platform. Diversity of fauna and flora commonly is reduced due to increased or decreased salinity (evaporation or freshwater input). As the Tithonian is interpreted to be relatively arid (cf. Chap. 8), the role of brackish water as an environmental stress factor is assumed to be minimal during this epoch. Additionally, the microfacies zonation within the internal lagoons seems rather similar to the environmental successions of the modern Persian Gulf described by Hughes Clarke & Keij 1973; cf. Tab. 2.1). Contrasting to the Tithonian, reduced faunal diversity during the Kimmeridgian and Berriasian may be related to freshwater input caused by a more humid, monsoonal climate (cf. Colombié 2002, Strasser 1988, Deconinck & Strasser 1987, Strasser 1986, Strasser & Davaud 1982).

In general, the facies displays intense bioturbation by few types of organisms and euryhaline fauna such as bivalves, gastropods, ostracodes, serpulids, and small miliolid foraminifera. However, the taphonomic influence of tidal currents can be the reason for the abundance of echinoderm fragments (usually stenohaline organisms) in internal lagoons. In the shallowest subtidal and intertidal areas, flaser-bedding is a characteristic sedimentary structure.

FZ4 – normal marine lagoon – high-energy settings ("open"), low-energy settings ("protected")

This facies zone is characterized by open marine conditions with normal salinity and relatively low turbidity. Depositional environments range from high-energy lagoons (exposed to waves and/or currents) to lagoons that are protected, but not restricted in diversity of marine life. Limestone textures vary between grain- and mudstone, accordingly. Fauna and flora generally are diverse, specifically foraminifera, which are represented by trocholins, large textulariids, large miliolids, and cyclamminids. All three types of oncoids are abundant, type, size and form being dependent on energy conditions. Patchy growth and sediment binding by micro-encrusters occur when sedimentation rates are low (cf. Fig. 2.8b). In normal marine, protected environments dasycladacean algae are common. In contrast, higher-energy settings that are influenced by tidal currents show reworking, dominance of echinoderm fragments, bivalve and brachiopod shells, and peloids.

Normal marine environment
High-variety assem blage of sten ohaline or ganisms. At appr ox. 48‰ salinity ther e is a ver y mark ed change i n fauna and flora. Above this point all coral, alcyonarians, echinoids, and melobesoid algae disappear, together with most of the perforate and arenaceous foraminifera.
Restricted environment
Approx. 50-70‰ salinity: fauna dominated by imperforate foraminifera and gastropods
Highly restricted environment
> 70‰ salinity: "faunal deserts", only some cyprideid ostracods

Tab. 2.1 – Subdivisions of normal marine, restricted, and highly restricted environments in the modern Persian Gulf, according to Hughes Clarke & Keij (1973). Whilst this subdivision is based on changes in salinity, it is certain that the faunal character is also very much dependant on diurnal and/or seasonal fluctuations in water temperature. In general, there is a fairly close parallelism between increasing salinity and increasing temperature fluctuation as both characterize rather shallow water.

FZ5 - barrier

During the Late Kimmeridgian and the Tithonian, the platform-barrier of the Jura platform was a mixture of reefs and high-energy subtidal bars with occasional indications for emergence. Biogenically constructed reefs of the barrier zone were not observed in this study, but have been described by, e.g., Fookes (1995), Détraz & Mojon (1989), Détraz (1989), Bernier (1984), Bernier & Gaillard (1980), and Steinhauser (1969) in laterally equivalent strata.

The barriers are composed of open-marine carbonates dominated by ooids, peloids, diverse foraminifera, coarse bioclastic rubble and intraclasts, echinoderms, and microencrusters. Typical is the reworked habit of the constituents. Shoaling may be indicated by beaches or vadose diagenesis. During the Early Berriasian ("Purbeckian"), barriers may also be formed by isolated islands where prolonged subaerial exposure is indicated by the formation of palaeosols and caliche (Davaud et al. 1983).

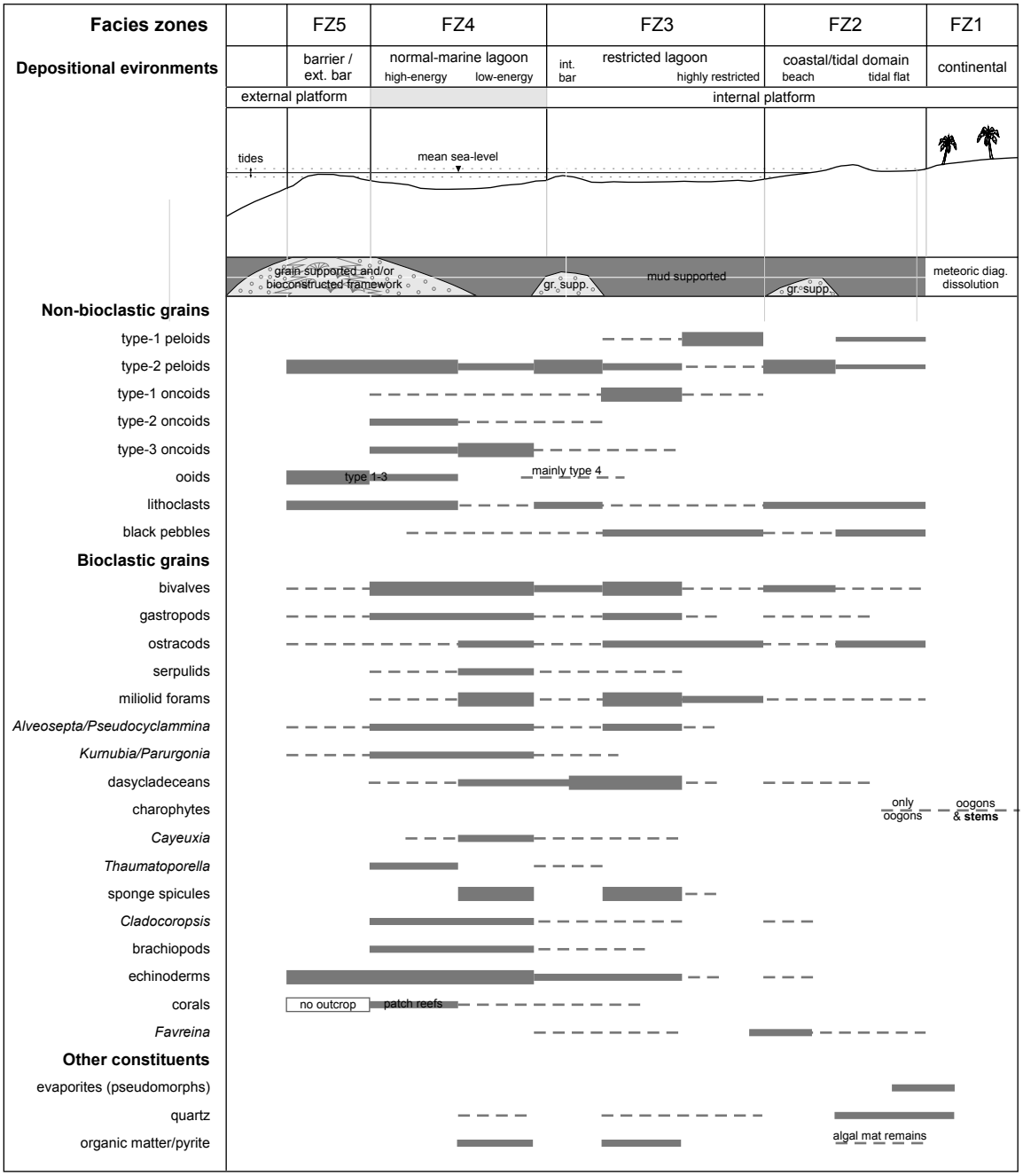

Fig. 2.8a - Facies model for the Upper Kimmeridgian and Tithonian showing the distribution of mud- and grain-supported facies and characteristic constituents.

2.6 Slope and basin facies

Basin facies is much more uniform than platform facies (Tab. 2.3). Additionally, the slope and basin environments of the Vocontian basin were subject to major resedimentation during the Late Jurassic. Consequently, the basin section were measured in less detail than the platform sections. Here, the principal goal was to set up a sequence stratigraphic interpretation linked to biostratigraphy (ammonites, calpionellids, and microfossil assemblages) that can eventually be correlated to the platform.

In contrast to the Early and Middle Kimmeridgian (Colombié 2002) and the Middle Berriasian to Valanginian (Hillgärtner 1999), the studied sections do not consist of marl-limestone alternations but of massive,

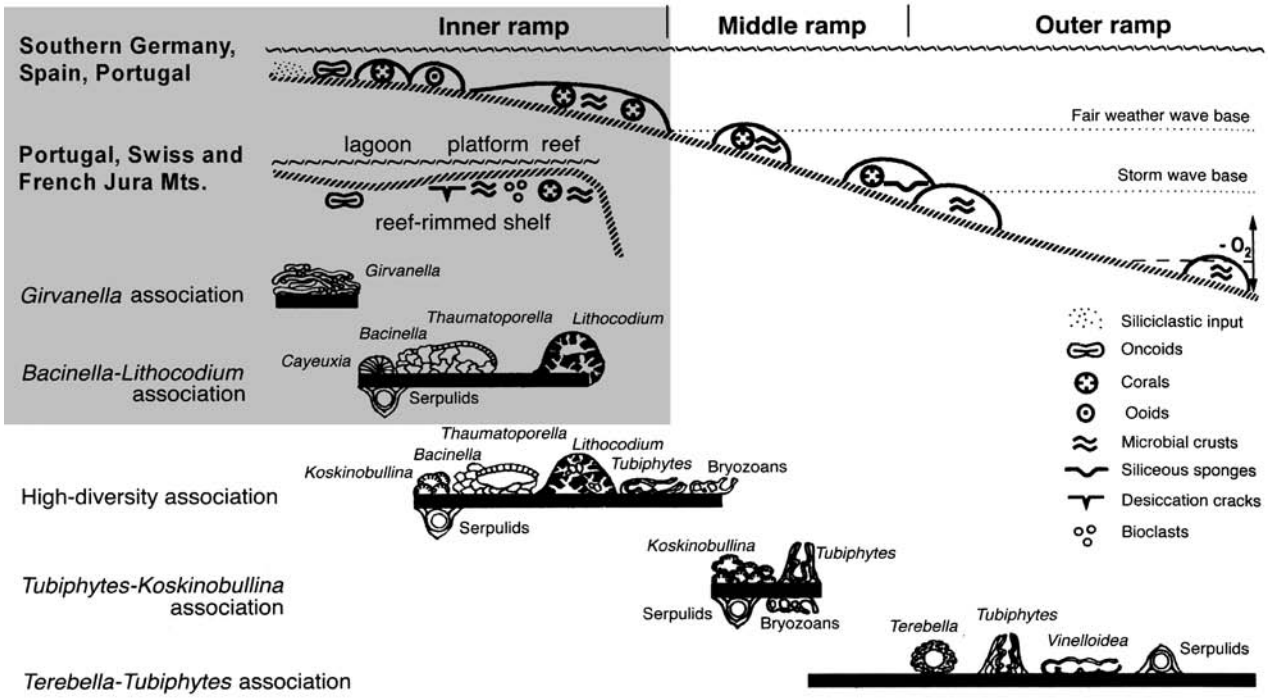

Fig. 2.8b - Distribution of micro-encruster associations in Late Jurassic reefs developed in different parts of carbonate ramps. Modified after SCHMID (1996). The grey square marks the encountered associations and highlights the proximal/internal position of the studied sections (Late Kimmeridgian to Early Berriasian; cf. Pl. 6). The 'high-diversity association' is typical for the more open and deeper lagoonal and ramp-environments of the Middle Berriasian to Valanginian (cf. HILLGÄRTNER 1999).

bedded limestones. Marly intercalations are rare. The most important interruptions of the quiet, hemipelagic sedimentation are resediments in form of mud flows, debris flows, grain flows, and turbidites.

2.6.1 Bioclastic grains

Foraminifera

Compared to platform environments, benthic foraminifera are relatively rare in the studied basin sections. Most probably, most of the specimens with agglutinated and porcelain tests were exported from the platform (Pl. 19/5) and thus furnish no palaeoecologically valuable information. Yet, foraminifera with hyaline test (*Lenticulina* sp., *Conicospirillina* sp., *Nodosaria* sp.) are typical inhabitants of the external platform to shallow basin and can be found all over the basin sections.

Tubiphytes (Pl. 17/8) is one of the most common microproblematica in Late Palaeozoic and Mesozoic limestones and has been attributed to various algal groups, cyanobacteria, as well as sponges and hydrozoans (RIDING & GUO 1992). SCHMID (1995) regards the Jurassic and Early Cretaceous *Tubiphytes*-variety as a foraminifer living in symbiosis with cyanobacteria. It prefers open-marine conditions and can be abundant in proximal platform talus and slope deposits as well as in sponge mounds in deeper ramp settings (FLÜGEL 2004).

The planktonic foraminifer *Protoglobigerina* sp. (Pl. 17/2) is known from the Liassic to the Early Cretaceous. As blooms of planktonic foraminifera are essentially linked to increased nutrient supply, the occurrence of *Protoglobigerina* sp. in Late Jurassic basin sediments is episodical. These organisms are rare in the studied sections.

Calcispheres

Calcispheres are small, hollow globules with diameters of 20 to 100 µm. Their test is made of calcite, commonly displaying several layers with differing texture (hyaline, microgranular, and/or fibroradial; Pl. 17/4). According to KEUPP (1991), calcispheres in basin sediments are interpreted as calcitic cysts of dinoflagellates. A possible use for biostratigraphy is discussed in BENZAGGAGH & ATROPS (1996).

Radiolarians

Radiolarians are unicellular marine planktonic protozoans that construct a skeleton of amorphous silica (opaline). Two groups of different morphology occur:

Facies	Facies description (Dunham)		Non-skeletal constituents, fabrics & early diagenetic features	Fossil content	Interpretation of depositional environment	Facies zone
CONTINENTAL DOMAIN						
lake	M	(bio)micrite		ostracodes, **charophyte stems** & oogons, **lack of marine fossils**	freshwater lake	**FZ1**
diss brecc	W/P	intramicrite	angular clasts and clods (cm to 10s of cm size), clods still showing original bedding, partly folded, some geopetal structures (interclast voids with horizontal lower surface and filled with sparite cement) indicateinfill character, at least partly, of muddy matrix; dolomitization/dedolomitization	as function of afflicted facies	dissolution breccia	**FZ1**
marl	m	green marl				**FZ1**
		black marl				**FZ1**
TIDAL/COASTAL DOMAIN						
sabkha						
sbk1	M	micrite	**intrasedimentary evaporite growth horizons**, chalky habit, bioturbation, peloidal storm layers, Qtz, silt-sized dust (of aeolian origin?), (de)dolomitization	rare ostracodes	sabkha with preserved layerwise storm and aeolian deposits	**FZ1-2**
sbk2	M	micrite	**evaporite nodules**, chalky habit, haloturbation, bioturbation, peloidal storm layers, Qtz, silt-sized dust (of aeolian origin?), (de)dolomitization		sabkha, most primary features destroyed by haloturbation, evoporite dissolution and reprecipitation	**FZ1-2**
tidal flat						
tf1	M/B	(intra/pel) micrite	**reworked evaporite clasts, peloids**, normal grading, lamination, microbial mats	rare ostracodes	storm-influenced supratidal flat / algal marsh, neighbouring sabkha	**FZ2**
tf2	M/W-B	laminated biolithite	**prominent lamination caused by microbial mats**, type-1 peloids, intraclasts (mostly laminated mudchips), Qtz.; lamination, peloidal & Qtz-grain tempestite layers, surface-parallel orientation of elongated clasts, birds eyes (commonly with vadose silt fillings), erosion surfaces, worm tubes, desiccation cracks, tepee structures, frequent occurrence of small evaporite pseudomorphs	rare ostracodes, miliolid foraminifera, and assorted allochtonous bioclasts (e.g., bivalves, dasycladacean fragments)	storm-influenced supratidal to uppermost intertidal, channel levees and algal marsh	**FZ2**
tf3	M	vaguely laminated micrite	**vague lamination predominantly caused by tempestites and some microbially stabilized layers**, intraclasts (mostly laminated mudchips), type-1 peloids, worm tubes peloidal/ Qtz/bioclast tempestites, surface-parallel orientation of elongated clasts, desiccation cracks; frequent occurrence of small evaporite pseudomorphs and wide-spread penecontemporaneous? dolomitization (small rhombs)	rare ostracodes, and assorted allochtonous bioclasts (e.g., bivalves, dasycladacean fragments)	storm-influenced upper intertidal flat	**FZ2**
tf4	M	vaguely laminated, bioturbated micrite	**vague lamination predominantly caused by tempestites with some microbially stabilized layers, partly destroyed by burrowing organisms:** worm tubes and crab burrows; peloidal tempestites, surface-parallel orientation of elongated clasts, microscopic desiccation features; penecontemporaneous? dolomitization (small rhombs)	rare ostracodes, miliolid foraminifera, and assorted allochtonous bioclasts (e.g., bivalves, dasycladacean fragments)	storm-influenced (lower) intertidal flat	**FZ2**
tf2-4 (*dol*)	–	laminated dolomite	visible **lamination** caused by alternating dolomitization intensity and/or rhomb sizes, locally traced by thin brownish colour bands caused by differing Fe-oxide content; bioturbation (worm tubes and other), 100% dolomitized, **crystalline aspect**	rare ostracodes and assorted allochtonous bioclasts	completely dolomitized tidal flat of facies tf2-4	**FZ2**
tf5	M	micrite	**empty, texture-less mudstone**, rare type-1 peloids, intraclasts (mostly laminated mudchips), and qtz.; birds eyes (commonly with vadose silt fillings), bioturbation (worm tubes and other), **frequent occurrence of small evaporite pseudomorphs** and dolomitization (small & medium-sized rhombs)	rare ostracodes, rare charophyte oogons and rare assorted allochtonous bioclasts	supratidal to uppermost intertidal mudflat, tidal ponds transition to facies tf3	**FZ2**
tf6	W-P/G	pelmicrite (sparite)	rock **composed mainly of type 1&2 peloids**, some type-3 oncoids and intraclasts, bioturbation, peloidal tempestites, flaser bedding, locally micritic meniscus cements, and/or penecontemporaneous? dolomitization (small rhombs)	**very sparse and restricted fauna & flora,** some ostracodes (commonly with articulated valves, i.e. live burial), *Favreina*, microbioclasts, rare gastropods, bivalves and charophyte oogons, **absent (or rare) echinoderms**	intertidal mixed flat to sand flat, subject to significant tidal currents and occasionally reworked by storms transition to facies rl1	**FZ2**
reworking / storm-related deposits						
mc brec	P	intramicrite	clasts: **black pebbles (clast margins may be decoloured), intraclasts of various origin**, large elongated clasts oriented predominantly parallel to underlying sediment surfaces, normal graded, top commonly with (algal) lamination matrix: worm tubes, commonly dolomitized & containing qtz., birds eyes (with frequent vadose silt fillings), small tepee-like structures, desiccation cracks	rare bioclasts of allochtonous origin	reworking of blackened sediment that was deposited in isolated, stagnant ponds and various otherlithologies; deposition in shallow depressions on upper intertidal/supratidal flat related to longer emersion periods → reliable sequence-boundary indicator	**FZ2**
fpc	P	intramicrite	**mainly composed of (laminated) mudchips**, commonly oriented subparallel to underlying sediment surfaces or imbricated, type 1&2 peloids, matrix may be dolomitized	rare ostracodes and *Favreina*	reworking of upper intertidal/supratidal flat's uppermost, microbially stabilized layer and redeposition in immediate surroundings	**FZ2**
wash	P	bio-(intra) micrite	intraclasts, Type-2 peloids; **erosional base, gradation, lamination (cm-scale)**, microbially stabilized layers, ripples marks	**assorted allochtonous bioclasts which indicate significantly more open (lagoonal) conditions compared to the surrounding tidal flat facies**	tempestite washovers on tidal flat	**FZ2**
beach						
bch	(P)-G	pel/intra/oo/ bio-sparite	moderately sorted and (sub)rounded type-2 peloids and intraclasts, ooids (predominantly type 4), type-1 peloids as geopetal infill; **plane bedding, keystone vugs**, possible vadose diagenesis	changing amounts of (sub)rounded bivalves, benthic foraminifera, dasycladacean algae, and gastropods, rare echinoderms and *Cladocoropsis*	beach	**FZ2**
tidal channel						
tch	G	pel/bio/onco/ intra-sparite	type-2 peloids, type-3 oncoids, intraclasts, **channel geometry, bimodal grain distribution, (cross bedding)**	bivalves, gastropods, ostracodes, foraminifera, **rare echinoderms**	tidal channel fill in tidal flat (Le Lieu and Noirvaux sections) or shallow subtidal bar environment (Cirque des Avalanche section)	**FZ2**

Tab. 2.2a – (this page and facing page) Principal facies occurring in the studied platform sections (Parts 1 and 2).

Facies	Facies description (DUNHAM)		Non-skeletal constituents, fabrics & early diagenetic features	Fossil content	Interpretation of depositional environment		Facies zone
LAGOON							
highly restricted lagoon							
hrl1	M	micrite	**empty, texture-less mudstone without evaporites and signs of emersion**, bioturbation (worm tubes, crab burrows); dolomitization (commonly as diagenetic halo around burrows)	rare ostracodes and spiculae, rare allochtonous bioclasts, **echinoderms absent (or very rare)**	highly restricted lagoon (or tidal ponds?), "*faunal deserts*", transition to mudflat tran-sitions to facies tf3 & tf5		**FZ3**
hrl2	P-(G)	pel/oo-micrite	**type-2 peloids, ooids (mainly type 4), and qtz. in muddy matrix**; penecontemporaneous? dolomitization (small rhombs)	**fossil-barren**: very rare bivalves, ostracodes, and miliolid forams, **echinoderms absent**	highly restricted interbar lagoon		**FZ3**
hrl3	M-W	oncomicrite	**type-3 oncoids** with fuzzy rim, dolomitization (medium-sized rhombs)	**fossil-barren**: rare ostracodes (some with articulated valves) and miliolid forams, **echinoderms absent**			**FZ3**
hrl4	W-P (B)	biolithit/ algal bindstone	predominantly type-1 (and some type-2) peloids, microbially stabilized surfaces cause undulatory-like "bedding"; solution seams, **dm-scale mound geometry**	algal filaments, microbioclasts, **echinoderms absent**	small algal build-up in highly restricted lagoon		**FZ3**
restricted lagoon							
rl1	W-P	bio-(pel) micrite	peloids (predominantly type 1), qtz., clay minerals (→ solution seams), bioturbation, flaser bedding	**dominant microbioclasts** , some bivalves, gastropods, miliolid forams, ostracodes, and spiculae, rare dasycladacean fragments, **rare to common echinoderms** (commonly as entire sea-urchin plates)	shallowest subtidal influenced by tidal currents, transition to lower intertidal mudflat/mixed flat transition to facies tf6		**FZ3**
rl2	W-(P)		type-2 peloids, some oncoids (type 3, rarely type 1&2) and intraclasts; bioturbation, dolomitization (locally burrow-related)	gastropods, bivalves, ostracodes, spiculae, benthic forams (mainly miliolid), rare dasycladacean algae debris, and serpulids, **rare echinoderms**	transitions to facies rl5/6		**FZ3**
rl3	M-W(P)		type-2 peloids, micritization, dolomitization (commonly burrow-related)	**abundant** bivalves (**oysters**), gastropods, some ostracodes & spiculae, miliolid forams, rare, **rare to common echinoderms**	(brackish?) lagoon		**FZ3**
rl4	(m)M -W	biomicrite	**marly micrite of dark gray colour with blackened type-2 peloids, pyrite, particulate organic matter**; bioturbation, dolomitization,	**blackened agglutinating forams**, bivalves, gastropods, ostracodes, locally oysters and plant remains, **rare to common echinoderms** (commonly as entire sea-urchin plates)	restricted, dysoxic lagoon, possible freshwater influence		**FZ3**
rl5	M-W		some type-2 peloids (commonly as burrow fill); bioturbation, burrow-related dolomitization	**abundant ostracodes and/or spiculae**, some miliolid foraminifera, bivalves, gastropods, **rare echinoderms**	transition to facies rl2		**FZ3**
rl6	(M)W-P		some type-2 peloids, rare type-3 oncoids; bioturbation, rarely dolomitized	**abundant dasycladacean algae**, some benthic forams, ostracodes, spiculae, gastropods, bivalves, and *Cayeuxia*, **rare echinoderms**			**FZ3**
rl7	M-W		rare-frequent oncoids; bioturbation (*Thalassinoides*), dolomitization	**primarily bivalves, gastropods, ostracodes, and spiculae**, some benthic foraminifera (commonly miliolid), rare dasycladacean algae, brachiopods, and *Cladocoropsis*, **rare to common echinoderms**	transition to facies lowEl1		**FZ3**
rl8	W-P(G)	pel-oo-micrite (sparite)	**type-2 peloids, ooids (mainly type 4)**, locally oncoids and intraclasts **in muddy matrix**; graded layers, bioturbation, micritization, ferrigenous rims	bivalves, ostracodes, gastropds, benthic foraminifera, locally dasycladacean algae, rarely *Cladocoropsis*, **rare to frequent echinoderms**	interbar lagoon		**FZ3**
rl9	W-P	onco-(bio) micrite	**abundant oncoids (types 1, 2 and/or 3)**, some intraclasts; bioturbation (with type-2 peloids as burrow fill)	dasycladacean algae, *Lithocodium/ Baccinella*, benthic forams, gastropods, ostracodes, spiculae; rare bivalves, *Cladocoropsis*, and *Cayeuxia*, **rare to common echinoderms**	facies with predominantly type-1/2 oncoids and common echinoderms represents transition to normal marine lagoon		**FZ3**
rl9	W-P	onco-(bio) micrite	**abundant oncoids (types 1, 2 and/or 3)**, some intraclasts; bioturbation (with type-2 peloids as burrow fill)	dasycladacean algae, *Lithocodium/ Baccinella*, benthic forams, gastropods, ostracodes, spiculae; rare bivalves, *Cladocoropsis*, and *Cayeuxia*, **rare to common echinoderms**	facies with predominantly type-1/2 oncoids and common echinoderms represents transition to normal marine lagoon		**FZ3**
internal bar							
inbar1	G	pel/bio-intra sparite	**abundant type-2 peloids** and (commonly elongated) intraclasts, locally ooids; **cross bedding, poorly sorted** (→ immature sediment), large elongated intraclasts commonly oriented parallel to reactivation surfaces; micritization, overpacking, **locally emersion features**	common bivalves, gastropods, dasycladacean algae, rare ostracodes and benthic forams, **rare or absent echinoderms**	small, short-lived, partly emersive bar in very shallow restricted lagoon, probably tidally influenced	internal bars in shallow restricted lagoon; constituents reflect ecology of neighbouring low-energy areas; increasing matrix content (G → P/W), preserved burrows, and/or microbially stabilized surfaces are interpreted as indicators of bar deactivation (subfacies ↓Fz)	**FZ3**
inbar2	(P)-G	bio-pel sparite	**abundant type-2 peloids**, varying amounts of intraclasts, locally oncoids, ooids, **poorly sorted, subrounded grainstones** (→ immature sediment); **emersion features and/or black pebbles**	**abundant dasycladacean fragments**, rel. high foram diversity, gastropods, bivalves, rare occurrences of *Thaumatoporella, Cladocoropsis, Cayeuxia* & spiculae, **rare or absent echinoderms**	small, short-lived, partly emersive bar or very shallow, restricted interbar lagoon, probably tidally influenced		**FZ3**
inbar3	G	pelsparite	**predominantly type-2 peloids**, some intraclasts, **cross-bedded, well sorted, well rounded** (→ mature sediment)	**well rounded bioclastic debris**: dasycladacean algae, *Favreina*, rare gastropods, ostracodes and miliolid foraminifera, **rare or absent echinoderms**	peloid sand bar in restricted lagoon, probably tidally influenced		**FZ3**
inbar4	(P)-G	(bio)-oo/pel sparite	**ooids** (predominantly type 4), **type-2 peloids**, some aggregate grains and intraclasts; **cross-bedded**; some samples show emersion features and/or black pebbles	common dasycladacean fragments, benthic foraminifera, gastropods, & bivalves; rare occurrences of *Thaumatoporella, Lith./Bacc.,* & *Favreina*, **rare or absent echinoderms**	ooid shoal in shallow, restricted lagoon, probably tidally influenced		**FZ3**
inbar5	P-G	pel-onco-(bio) sparite	**oncoids (predominantly type 3), type-2 peloids; cross-bedded** (commonly badly visible); ferrigenous rims and dolomitization in some samples	frequent dasycladacean algae, varying amount and diversity of benthic foraminifera, gastropods, ostracodes, rare occurrences of *Baccinella, Cayeuxia* & spiculae, **(absent to) rare echinoderms**	bar or restricted interbar lagoon, probably tidally influenced		**FZ3**
inbar6	P-G	onco-pel-(bio) sparite	**oncoids (predominantly type-1&2)**, type-2 peloids; **cross-bedded** (commonly badly visible); infrequent ooids	**abundant *Lithocodium/Baccinella*-associations**, frequent dasycladacean algae, rel. high foram diversity, common gastropods, bivalves, *Cayeuxia*, rare *Thaumatoporella* & *Cladocoropsis,* **rare echinoderms**	bar or restricted interbar lagoon, probably tidally influenced, transition to normal marine lagoon with varying energy		**FZ3**
normal marine lagoon – low energy settings ("protected lagoon")							
lowEl1	M-W	biomicrite	rare-frequent oncoids; bioturbation (*Thalassinoides*), dolomitization	**primarily bivalves, gastropods, ostracodes, and spiculae**, diverse benthic foraminifera, , commonly dasycladacean algae *and Cladocoropsis*, rare brachiopods, serpulids, bryozoans, and corals, **frequent to abundant echinoderms**	transition to facies rl7	lagoon with a salinity close to normal marine (relatively free water exchange) but protected by a barrier from the open sea	**FZ4**
lowEl2	W-P		type-2 peloids, locally oncoids; **heavily bioturbated**	**abundant microbioclasts**, some bivalves, ostracodes, and spiculae, **abundant echinoderms**			**FZ4**
lowEl3	W-P	bio-pel micrite	**type-2 peloids**; bioturbation, dolomitization (commonly burrow-related)	**varying bioclastic composition**: gastropods, bivalves, ostracodes, spiculae, diverse benthic forams, dasycladacean algae debris, and serpulids, rare bryozoans, **frequent to abundant echinoderms**			**FZ4**
lowEl4	W-P	bio-onco micrite	**type-3 oncoids**; bioturbation, dolomitization	some bivalves (inocerams, oysters, ...), gastropods, diverse benthic foraminifera, ostracodes, *Cayeuxia*, rare dasycladacean algae, **abundant echinoderms**			**FZ4**

Facies	Facies description DUNHAM		Non-skeletal constituents, fabrics & early diagenetic features	Fossil content	Interpretation of depositional environment	Facies zone
normal marine lagoon – high energy settings ("open lagoon")						
hiEl	P-G	onco/bio/pel sparite (micrite)	oncoids (type 1, 2 & 3), type-2 peloids, intraclasts; micritization, (heavy) bioturbation, **yellowish-brownish colour due to high Fe-content / Fe envelopes**	bivalves (inocerams, oysters, ...), brachiopods, gastropods, ostracodes, diverse benthic forams, and serpulids, *Cladocoropsis, Thaumatoporella*, and *Baccinella*, **frequent to abundant echinoderms**	abandoned bar and/or interbar lagoon under normal marine conditions	**FZ4**
hiEl			oncoids (type 1, 2 & 3), type-2 peloids; incrustations (*Baccinella*)	bivalves, diverse benthic forams, Tubiphytes , *Thaumatoporella*, *Cayeuxia*, and *Baccinella*, rare dasycladacean algae, **frequent to abundant echinoderms**		**FZ4**
hiEl	(P)-G	pel-bio-(intra)-sparite	type-2 peloids, some oncoids, ooids, and intraclasts, moderately sorted; bioturbation	abundant and diverse benthic forams, , *Cladocoropsis, Thaumatoporella*, rare bivalves, ostracodes, and bryozoans, **frequent to abundant echinoderms**		**FZ4**
external bar						
exbar1	G	pel/bio/intra/ onco sparite	varying composition: type-2 peloids, (incrusted) intraclasts ↔ oncoids, and rare ooids; micritization, **cross bedding**	bivalves, benthic forams, brachiopods, some ostracodes, rare dasycladacean algae debris, **frequent to abundant echinoderms**	bar in platform-rim position	**FZ5**
exbar2	G	oo-(pel-bio-onco) sparite	**well sorted, well rounded, cross-bedded grainstones** composed of **ooids**, type-2 peloids (micritized ooids?), (incrusted) intraclasts ↔ oncoids; micritization possible	relatively rare bivalves, gastropods, diverse benthic forams, gastropods, *Cayeuxia*, and *Baccinella*, rare ostracodes and dasycladacean algae debris, **frequent to abundant echinoderms**		**FZ5**

Tab. 2.2a – Principal facies occurring in the studied platform sections (Part 3).

Sub-facies	Afflicted environments	DUNHAM	Sedimentary structures & diagnostic features	Interpretation of diagenetic environment	Facies zone
ALTERATION / EARLY DIAGENESIS					
FG *HG*	lagoonal environments	M-P	FG: intense bioturbation, Fe-staining HG: boring, incrusting, multiphase bioturbation, Fe-staining	firmground/hardground, condensation	**FZ3-4**
(↓*E*)	high-energy facies and bars	(P)-G	infill sediment (commonly type-1 peloids), geopetal structures, preserved burrows, microbially stabilized surfaces	abandonment of high-energy environment, stabilization of mobile sediment	**FZ3-5**
(*em*)	high-energy facies and bars	(P)-G	meniscus and pendant cements, freshwater cements, infill sediment (commonly type-1 peloids), geopetal structures	emersion, subaerial exposure	**FZ2-5**
	tidal and shallow lagoonal environments	M-P	polygonal mudcracks and/or other desiccation features, infill sediment, geopetal structures, meteoric cements	emersion, subaerial exposure	**FZ2-4**
(*ped*)	tidal and shallow lagoonal environments	M-P	roots, root casts, *Microcodium*, circumgranular cracks ("nodulization"), brecciation (rhizoturbation), infill sediment, geopetal structures, meteoric cements	(initial) pedogenesis	**FZ2-3**
(*dol*)	tidal and (shallow) lagoonal environments	M-W(P)	slight – complete dolomitization of muddy matrix (medium-sized, commonly zoned rhombs)	early diagenetic dolomitization (by seepage reflux and/or tidal pumping?) in shallow burial position	**FZ2-3**
(*dedol*)	tidal and shallow lagoonal environments	?	"cornieule" showing complete, mostly fabric-destructive recrystallization	early diagenetic dedolomitization by meteoric waters under continental conditions	**FZ1**

Tab. 2.2b – Alteration and early diagenetic occurring in the studied platform sections.

Facies	Facies description DUNHAM		Non-skeletal constituents & sedimentary structures	Fossil content	Interpretation of depositional environment	Facies zone
SLOPE / BASIN						
resediments (allochtonous to parautochtonous)						
B1	W-P	intramicrite	abundant large intraclasts, up to 20 cm in diam., matrix supported; erosive lower surface	in function of initial composition of reworked sediment, mostly normal pelagic fauna (cf. facies B6) with rare to common occurrence of platform biota	channeled debris flow in slope position (Broyon, Clue de Taulanne sections)	**FZ6**
B2	(P)-G	intra-pel-sparite (micrite)	type-2 peloids, small intraclasts (grain supported); erosive lower surface,	in function of initial composition of reworked sediment, mostly normal pelagic fauna (cf. facies B6) with rare to common occurrence of platform biota	channeled turbidite in slope position (Broyon section)	**FZ6**
B3	(P)-G	pelsparite	type-2 peloids, some (small) intraclasts; slightly erosive lower surface, fining upward	in function of initial composition of reworked sediment, mostly normal pelagic fauna (cf. facies B6)	minor grainflow (Clue de Taulanne, Poteu de Mié sections)	**FZ6**
B4	(P)-G	pelsparite	type-2 peloids, intraclasts; erosive lower surface, grading, plain bedding, current ripples	in function of initial composition of reworked sediment, mostly normal pelagic fauna (cf. facies B6) with rare to common occurrence of platform biota	turbidite in toe-of-slope or basin-floor position (Clue de Taulanne, Poteu de Mié sections)	**FZ7**
B5	M-W	bio-intra-mictite	common to frequent (rounded) intraclasts, up to 1 cm in diam., floating in matrix; uneven, wavy (folded?) bedding planes	in function of initial composition of reworked sediment, mostly normal pelagic fauna (cf. facies B6)	minor mudflow / slump	**FZ6-7**
autochtonous sediments						
B6	M-W	bio-(intra)-micrite	rare intraclasts, type-2 peloids; even bedding; bioturbation	varying amounts of radiolarians, calpionellids, calcispheres, *Globochaetes*, echinoderms (*Saccocoma*), benthic foraminifera, proto-globigerinids, ostracodes, sponge debris & spiculae, filaments, ammonites, belemnites	basin floor (or stable slope) with normal pelagic sedimentation below storm wave base, low detritic influence	**FZ(6-)7**
B7	M-W marl	biomicrite	type-2 peloids, quartz, clay; even bedding, bioturbation	varying amounts of radiolarians, calpionellids, calcispheres, *Globochaetes*, echinoderms (*Saccocoma*), benthic foraminifera, proto-globigerinids, ostracodes, sponge debris & spiculae, filaments, ammonites, belemnites	basin floor (or stable slope) with normal pelagic sedimentation below storm wave base, increased detritic influence (as a result of a change in climatic / tectonic regime?)	**FZ(6-)7**

Tab. 2.3 – Principal facies occurring in the studied slope and basin sections.

Spumellaria and *Nassellaria* (Pl. 17/1). The changing abundance of radiolarians (Pl. 19/3) within a defined microfossil assemblage is of regional biostratigraphic use (Dromart & Atrops 1988, Benzaggagh 2000, cf. Fig. 1.8). Dissolved silica from radiolarian skeletons probably is the main source for chert nodules in the basin sections.

Globochaetes

Globochaetes are fibroradial calcite spheres with a diameter of 10 to 100 µm and thus show a characteristic cross under polarized light (Pl. 17/3a, b). They are interpreted as calcified cysts of unicellular planktonic green algae (Lombard 1945). Their changing abundance (as part of a microfossil assemblage) is of regional biostratigraphic use (Dromart & Atrops 1988, Benzaggagh 2000, cf. Fig. 1.8).

Calpionellids

Calpionellids are small (50-200 µm), bell-shaped organisms that are characteristic for Tethyan pelagic limestones from the Middle Tithonian to the Valanginian. Although their systematic position is unknown (Remane 1985), they are excellent index fossils in the above-mentioned time interval (Pl. 18). Calpionellids can occur in high abundances (up to rock-building) in autochthonous, fine grained carbonates of the studied basin sections (Pl. 19/4). Their biostratigraphy is explained in Chap. 1.4.3.

Filaments

Filaments (Pl. 19/1) are interpreted as larval or juvenile shells of pelagic thin-shelled (posidoniid?) bivalves (Flügel 2004). The thin, curved elements show a single-layered or multi-layered calcitic prismatic microstructure. Their changing abundance (as part of a microfossil assemblage) is of regional biostratigraphic use (Dromart & Atrops 1988, Benzaggagh 2000, cf. Fig. 1.8).

Saccocoma

The distribution and abundance of planktonic crinoids had three culminations during the Mesozoic. Their first appearance (*roveocrinoids*) in the Alpine-Mediterranean region was from the Late Ladinian to the Early Carnian. The first record of *Saccocoma* (Pl. 17/6) is from the late Middle Jurassic. Mass occurrences in Tethyan open-marine limestones (Pl. 19/2) as well as in epicontinental shelf carbonates (e.g., in the famous lithographic limestone of Solnhofen, Germany) extend from the Kimmeridgian to the Middle Tithonian (Flügel 2004). A third maximum is observed during the Late Cretaceous. The changing abundance of *Saccocoma* (as part of a microfossil assemblage) and its quasi-disappearance in the Late Tithonian is of regional biostratigraphic importance (Dromart & Atrops 1988, Benzaggagh 2000, cf. Fig. 1.8).

Sponges

Siliceous sponges are typical dwellers of the deeper external ramp and the slope. Transported fragments that are in the process of decomposition are called 'tuberoids' (Flügel & Steiger 1981). The presence of perforations and encrustations (Pl. 17/9) indicates that these fragments rested a certain time on the sediment surface in a semi-lithified state before their burial in carbonate mud. Mass occurrences of tuberoids appear usually in the proximity of sponge reefs (Flügel & Steiger 1981). Another mode of sponge preservation is the replacement of the siliceous sponge skeleton with calcite or pyrite (Pl. 17/10).

Cephalopods (Pl. 17/7)

Belemnites, ammonites, and aptychi (ammonite mandibles) are abundant in the lower part of the Clue de Taulanne section (Kimmeridgian to earliest Tithonian). During most of the Tithonian and Early Berriasian, cephalopod remains are rare; they reappear in the condensed sediments at the section top (Middle Berriasian). In the Poteu de Mié section, only some rare specimens were found (Roulin 2001). The ammonite fauna and stratigraphy of the Clue de Taulanne section was studied by Pellaton & Ullrich (1997).

2.6.2 Reworked sediments (Pl. 19/5-7; 21/2)

The "sedimentary breccias" of the Vocontian Basin and the involved resedimentation processes have been subject to discussion for a long time (e.g., Remane 1970, Beaudoin 1977, Arnaud et al. 1984, Détraz et al. 1987). Eventually, Bouchette et al. (2001) and Séguret et al. (2001) proposed an alternative interpretation for the formation of the "breccias" in the basin center, involving wave-oceanfloor-interaction.

The scope of this study was neither a new approach to the study of resedimented carbonates, nor the verification of the wave-oceanfloor-interaction theory. So these sediments were not studied in detail. However, as mass flows are most likely to occur at the beginning of a drop in relative sea-level (Sarg 1988, Haq 1991, Vail et al. 1991), resedimented beds are of relevance for sequence stratigraphic interpretation. Detailed analyses of the different resedimented facies are given in Strohmenger & Strasser (1993) for the Broyon section and Pellaton & Ullrich (1997) for the Clue de Taulanne section.

Mud- and debris-flows

Mud-flow facies is characterized by subangular to subrounded limestone clasts that are floating in a micritic matrix (Pl. 19/6). The clasts, as well as the background sediment contain typical hemipelagic or pelagic fossil assemblages. Mud-flow deposits are interpreted to be of parautochtonous character because they contain only monomictic clasts that were derived from older sediments within the basin (Pellaton & Ullrich 1997). Large parts of the Clue de Taulanne section consist of this facies.

Debris-flows contain a higher percentage of clasts and have a less cohesive rheology than mud-flows that can result in grading (fining-up or coarsening-up). In the Broyon section, debris-flows show a large-scale channel-geometry (Pl. 21/2) and a clearly erosive lower surface.

Mud-flows and debris-flows usually originate from slides and slumps by liquefaction of the primary lime mud. Mud-flow dominated deposits can locally grade into debris-flow dominated deposits and vice versa. There is no sharp boundary between the two end members (see Einsele 1991 for discussion).

Grain-supported resedimented carbonates

A grain-supported texture indicates high water energy and winnowing of lime mud during deposition. These deposits contain subangular to subrounded limestone clasts, peloids, and fossils. On the upper slope (Broyon), intraclast-fossil grainstones are composed mainly of intraclasts with a typical deep-marine, pelagic fossil assemblage, whereas abundant echinoderms were obviously imported from open platform environments. They are interpreted as channelized grain-flow deposits on a bypass-slope during sea-level lowstands (Strohmenger & Strasser 1993) and may correspond to the "fluxoturbidites" described by Schlager & Schlager (1973).

In the Clue de Taulanne section, a peloid-grainstone was found that clearly shows the Bouma-intervals B and C (plane bedding and current ripples) over a sharply defined basal surface (Pl. 19/7). Consequently, it is interpreted as calcarentic turbidite. Recently, authors that worked in a more regional context have proposed that similar calcarentic deposits may be in effect distal tempestites. (Raja Gabaglia 1995, Pellaton & Ullrich 1997, Bouchette et al. 2001, Séguret et al. 2001).

2.6.3 Facies zones

FZ6 - slope

Background sedimentation on the slope is of hemipelagic to pelagic type, similar to FZ7. The essential difference to the basin is a far greater percentage of platform-derived material and an emphasis on erosion and resedimentation. Gravitational processes such as slumps and submarine slides, mud- and debris-flows, grain-flows and turbidity currents transport exported platform material and eroded slope deposits downslope.

During the Middle and Late Tithonian a bypass-slope had developed in the Broyon area, with debris- and grain-flows running down the slope in wide channels. This resulted in a heavily reduced thickness of the Tithonian.

FZ7 - basin

Sedimentation is of a hemipelagic to pelagic type. Constituents are dominated by an association of radiolarians, filaments, calpionellids, globochaetes, sponge remains, calcispheres, ammonites, and planktonic echinoderms. Locally, mass-flow deposits that import platform detritus such as debris-flows and turbidity currents may arrive on the basin floor.

2.7 Facies model

In order to facilitate the understanding of the architecture of large-scale depositional systems and their lateral and temporal variations as well as the prevailing environmental conditions, sedimentological models are developed. These generalized, interpretative facies models are based on the study of associations of litho-, micro-, bio-, ichno-, and diagenetic facies of sedimentary rocks which, in an uniformitarian approach, are compared with facies associations in modern sedimentary environments (e.g., Wilson 1975, Flügel 1982, Scholle 1983, Tucker & Wright 1990, Tucker et al. 1990, Walker 1992, Flügel 2004).

The depositional model that was developed for the present study draws in particular from personal actuosedimentological observations made in Florida Bay, the tidal flats of Andros Island (Bahamas), and tidal flats and sabkhas in southern Tunisia. The result is a two-dimensional facies model for the Tithonian of the Swiss and French Jura platform that is a modified version of the standard "rimmed carbonate platform model" ("Wilson model": Wilson 1975, Flügel 2004; Fig. 2.8a). A three-dimensional block-diagram (Fig. 2.9) is used to better illustrate the lateral coexistence of different depositional environments on the Late Jurassic passive continental margin.

However, it has to be kept in mind that such models are highly schematic and rarely reflect the real depositional diversity. They are also static and thus cannot illustrate gradual environmental or climatic change – e.g., the development from mud-dominated Late Kimmeridgian

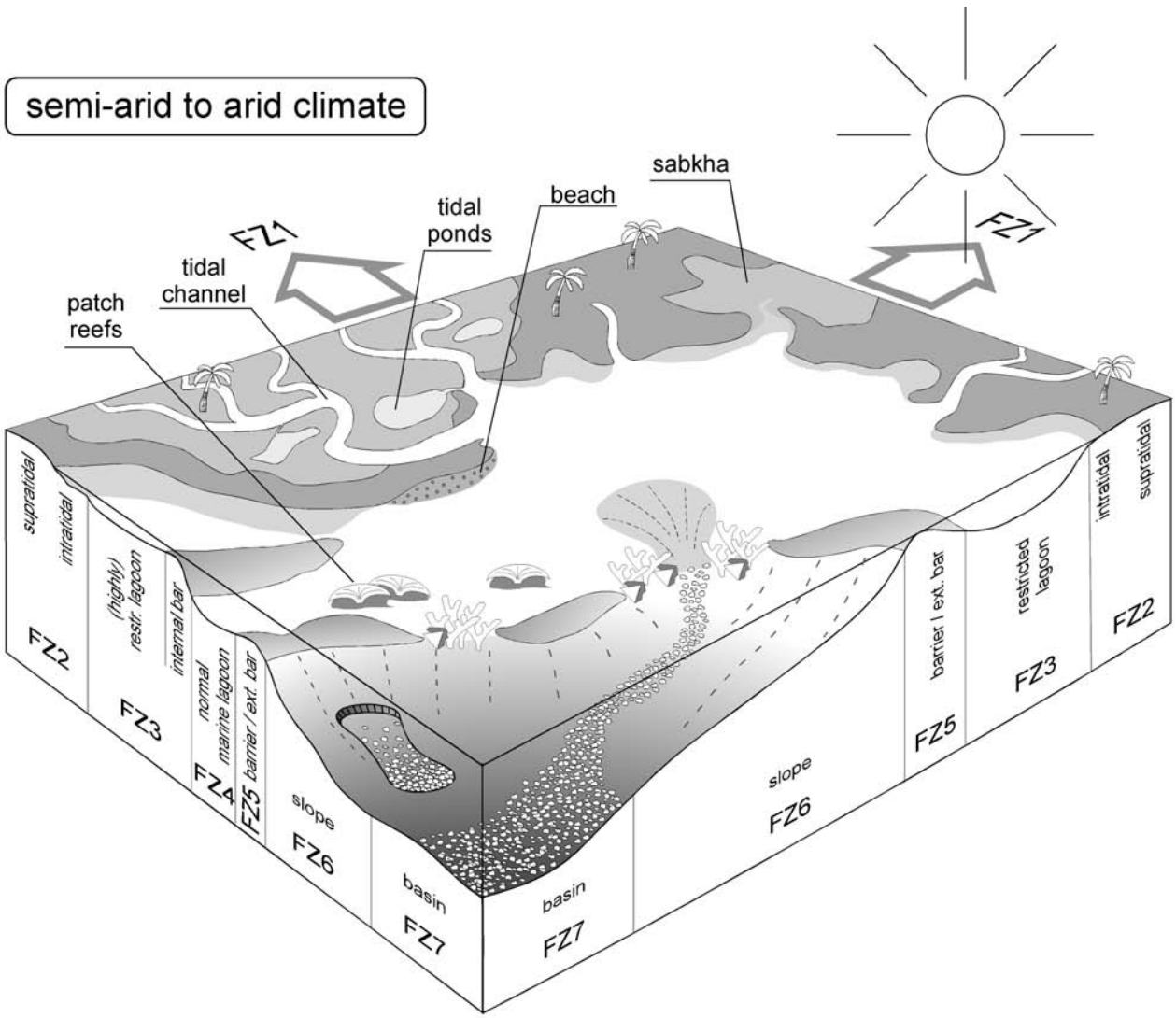

Fig. 2.9 - Block diagram showing the spatial relations (no scale) between the different facies zones studied.

lagoons over the Tithonian and Early Berriasian tidal flat and sabkha successions to the installation of a Middle Berriasian carbonate ramp; all related to changes in tectonics, sea-level, and climate (cf. COLOMBIÉ 2002, HILLGÄRTNER 1999, DÉTRAZ & MOJON 1989, DÉTRAZ & STEINHAUSER 1988).

* * *

3 - Dolomitization and dedolomitization

Despite being the focus of research for several decades, the origin of dolomite is still controversial, often addressed as "*The Dolomite Problem*" (e.g., McKenzie 1991, Warren 2000, Machel 2002). Dolomite is an unusual mineral: it is common – or even frequent – in platform carbonates throughout the geologic record, but rare in Holocene sediments. Moreover, it is nearly impossible to precipitate in the laboratory at earth surface conditions without the help of bacterial mediation. Fossil dolomite is known to have formed in a multitude of different settings: from continental to deep marine, from synsedimentary to late/deep burial, and from meteoric water to mixed water or hypersaline brines. In the last years, the role of bacterial mediation has been increasingly documented (e.g., Vasconcelos & McKenzie 1997, Burns et al. 2000, van Lith et al. 2003a, b).

Consequently, a large number of explications and models of dolomite formation have been put forward, modified and/or rejected over the years (cf. Machel & Mountjoy 1986, Hardie 1987, Warren 2000), without being able to explain all aspects of dolomitization to full satisfaction yet.

It is neither the purpose of this study to delve deeply into the details of the various, complex, and even not yet fully understood mechanisms leading to the dolomitization of carbonate platforms, nor to furnish a full-scale diagenetic study. However, dolomitized sediments play a key role in deciphering the facies architecture of the examined Upper Jurassic and Lower Cretaceous sediments. This leads directly to the question: What kind of links do exist between dolomitization, stacking pattern, and high-frequency oscillations of relative sea-level? Hence, the development of a conceptual model on dolomitization patterns and their underlying mechanisms is a crucial step towards the understanding of the evolution of the Jura platform.

3.1 Dolomitization

In this study, three different types of dolomite are distinguished, based on their texture after Sibley & Gregg (1987) and the typical depositional environment where they occur. The texture-based classification is also of use for the interpretation of dolomite origin.

3.1.1 Type-1 dolomite ("matrix dolomite")

Type-1 dolomite (Pl. 14/1) is a matrix-replacive, medium grained (50-500 μm), planar-e to planar-s type dolomite (Tab. 3.1). Intensity of dolomitization varies from isolated rhombs floating in the matrix to idiotopic and hypidiotopic mosaic textures (cf. Tab. 3.1). A small test series of cathodoluminescence (CL) was run on hypidiotopic mosaic texture type-1 dolomites in order to reveal potential ghost structures that might give information on the microfacies of the replaced limestone. Unfortunately, no such structures were found. Dolomite crystals often show a "cloudy centre - clear rim" geometry (Pl. 14/1). In the examined test series the clear rims generally display a brighter CL (dark orange) than the cloudy centre (dull mottled CL).

This type of dolomite makes up by far the biggest volume of dolomitized sediments in the measured sections. It always occurs in stratiform geometries in the uppermost part of a shallowing-upward lagoonal/peritidal sequence, typically with a sharp (slightly erosive) upper contact surface and a more diffuse lower contact (dolomite cap). Dolomite caps occur in different stages of development; ranging from a slightly dolomitized single bed to completely dolomitized rock successions with thicknesses of up to 8 m. In the field, well developed

"Planar" or "idiotopic" dolomite - obvious rhombs typical for penecontemporaneous to early diagenetic dolomitization during initial (shallow) burial	**"Nonplanar" or "xenotopic" dolomite - nonrhombic** typical for dolomitization during deeper burial
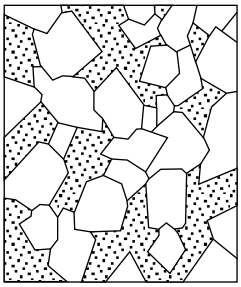 **Planar-e (euhedral)** most of the dolomite crystals are euhedral rhombs, crystal-supported framework with intercrystalline areas filled by another mineral or porous (as in sucrosic texture). Idiotopic Mosaic	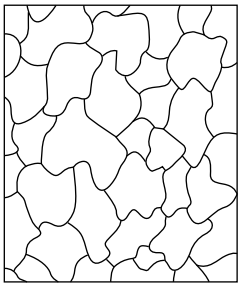 **Nonplanar** closely packed anhedral crystals with mostly curved, lobate, serrated, or otherwise irregular intercrystalline boundaries. Preserved crystal face junctions are rare and crystals often have undulatory extinction in crossed polarized light Xenotopic Mosaic
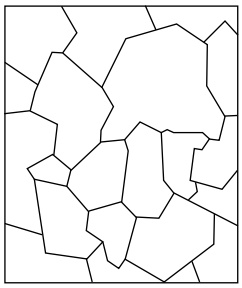 **Planar-s (subhedral)** most dolomite crystals are subhedral to anhedral with straight, compromise boundaries and many crystal face junctions. Low porosity and/or intercrystalline matrix Hypidiotopic Mosaic	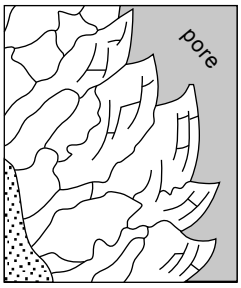 **Nonplanar - Cement** pore lining of saddle-shaped or baroque dolomite (subset of nonplanar anhedral shown above). Preserved crystal face junctions are rare and crystals often have undulatory extinction in crossed polarized light Xenotopic Cement

Tab. 3.1 - Common dolomite textures emphasizing the effect of temperature (in general as a function of burial depth) on the style of dolomite development (after Gregg & Sibley 1984, Sibley & Gregg 1987, and Warren 2000). The investigated Late Kimmeridgian-Tithonian dolomites and dolomitic limestones show exclusively planar-e and/or planar-s textures. This strongly suggests penecontemporaneous or early diagenetic (i.e. shallow burial) dolomite formation. For details refer to text.

dolomite caps are easily recognizable: they tend to show softer weathering (Pl. 20/1, 3) and a darker colour (dark beige with brownish or greenish hues) than the over- and underlying limestones. Microfacies at the diffuse lower contact frequently reflects (highly) restricted lagoonal environments. Higher up in the dolomite cap, dolomitization is usually fabric-destructive, so that in most cases no microfacies features of the precursor rock are preserved. Yet, these dolomites are commonly platy and may show remains of lamination, birdseyes, and tepee structures—indicative of tidal flat environments. Here, type-1 dolomites are frequently intercalated with type-3 dolomites (Pl. 14/4), thus creating the laminated/platy aspect. In the uppermost part of a dolomite cap, leaching may occur.

3.1.2 Type-2 dolomite ("burrow dolomite")

Type-2 dolomite (Pl. 14/2) is a replacive, fine to medium grained (20-100 μm), predominantly planar-s (subhedral) dolomite (Tab. 3.1). Type-2 dolomitization occurs in patches of *Thalassinoides*-like geometries. The rock texture is thus very similar to the "grey pseudobreccias" described by Horbury & Qing (2004) from the Carboniferous of the Lake District (U.K.), and the dolomite-mottled Ordovician Tyndall Limestone from Manitoba, Canada (Gingras et al. 2004). The patches show a relatively sharp dolomite-matrix boundary. However, a "diagenetic halo" (Gingras et al. 2004) can usually be observed around the burrow-like dolomite patches: floating dolomite rhombs that rapidly decrease in numbers in a few mm-wide zone next to a dolomite-matrix boundary (cf. Pl. 14/2). Within the dolomitized patches, Fe-nodules or pyrite commonly occur. Locally, this changes the colour of the entire dolomite-patch to rusty brown or dark grey in contrast to the cream-colored limestone matrix (Pl. 16/3). Other typical "inclusions" within the patches are peloids (cf. Pl. 14/2) and echinoderm debris that were not dolomitized. There are also various examples of geopetal calcite cements in the upper part of dolomite patches. Considering the various inclusions and the partially filled character of dolomitized patches, type-2 dolomite seems to replace a precursor burrow fill. In

contrast to type-1 and type-3 dolomites, type-2 dolomite can be found in any position within a shallowing-upward sequence. Thus, there are all stages between only burrows dolomitized and completely dolomitized rocks.

Due to the sharp contrast in colour and texture this kind of dolomite-mottled limestone is sometimes called "pseudobreccia" (Horbury & Qing 2004). The phenomenon is particularly common in the Upper Reuchenette and the Lower Twannbach Formations of the Swiss and French Jura Mountains. In the southern Jura this led to the denomination of the local "*Calcaires à Tubulures*" (also "*Couches de Chailley*") Formation (Enay 2000, Bernier 1984).

3.1.3 Type-3 dolomite ("tidal-flat dolomite")

Type-3 dolomite (Pl. 14/3) consists of fine grained (10-60 μm), euhedral rhombs (planar-e type; cf. Tab. 3.1). However, in comparison to type-1 dolomite ("matrix dolomite") crystal shape is relatively badly defined. Type-3 dolomitization predominantly occurs in laminated sediments that usually show various signs of emersion. Laminated type-3 dolomites frequently occur in the upper part of dolomite caps that mainly consist of type-1 dolomite. The original lamination is preserved by alternations in dolomitization intensity of laminae and rhomb diameter (Pl. 14/4).

3.1.4 Late diagenetic dolomite and dolomitic cements

The vast majority of the dolomite in the measured platform sections is matrix-replacive dolomite, with isopachous overgrowth rims (cloudy center, clear rim crystals; cf. Pl. 14/1). The zonation that is already visible in normal light is unequivocally confirmed by cathodoluminescence analysis: the overgrowth shows a substantially brighter orange than the dull center. Apart from the overgrowth rims, only negligible amounts of void-filling dolomitic cements were found.

The basin sections are virtually free of dolomite. Only a single saddle dolomite was found in sample CT 11 of the Clue de Taulanne section as burrow fill (Pl. 14/7). Radke & Mathis (1980) postulate that saddle dolomite formation takes place at temperatures higher than 80°C (60-150°C) and thus imply a deeper burial origin – or a hydrothermal origin at shallower depths – for this type of dolomite. This is consistent with the burial history of the basin sediments (Deconinck & Debrabant 1985).

3.2 Dedolomitization

3.2.1 Type-1 dedolomite

Type-1 dedolomite can be found anywhere in the measured sections. It consists of rhomb-shaped pores that are either completely filled with calcitic microsparite or (more frequent) consisting of a thin crystalline, rhomb-shaped calcite rim with a micrite fill (Pl. 15/1). Apparently, leaching started from the inside of dolomite crystals. All type-1 dedolomites seem to be leached or recrystallized type-1 dolomites ("matrix dolomites"), mostly of planar-e geometry (cf. Tab. 3.1).

According to Nordeng & Sibley (2003), the process of dolomitization is rather sensitive to timing: There is a rather long induction period for dolomite formation in marine pore fluids. During this period metastable precursor minerals are developed, which may progress into more stable dolomite or be destroyed if a change in pore-water chemistry occurs, as induced for example through meteoric influx. Another possibility for type-1 dedolomite formation would be selective dissolution of unstable ferroan dolomite that post-dated the dolomitization process (Purser et al. 1994a, b) and formed during burial (Warren 2000).

3.2.2 Type-2 dedolomite

Type-2 dedolomites are completely recrystallized rocks that show a large variation in their appearance. However, the common factor is that, in contrast to type-1 dedolomites, absolutely no traces of rhomb-shaped crystals are left. They are always sparitic with widely varying crystal diameters and may be of sucrosic character (Pl. 15/2-4). A special type of type-2 dedolomite is cellular/vuggy sparite ("*cornieules*", Warrak 1974), either showing remains of tidal-flat like lamination (Pl. 15/4, 16/2a), or comprised of intergrown millimetric nodules that form a 3-dimensional grid without a clear preferential direction (Pl. 16/2b). Vugs can be empty or filled with red-brown, only partly lithified clay (Pl. 16/2a, b).

The main volume of dedolomite is found in the Upper Twannbach and basal Goldberg Formation (Dôle, and specifically Lieu section). Some isolated dedolomitized beds are found in the Lower Twannbach Formation (e.g., Noirvaux section 138.5m, Cirque des Avalanches section 178m). Type-2 dedolomitization is completely absent in the upper Reuchenette Formation.

3.3 Stable Isotope Analysis

Stable isotope data yield useful information for interpreting depositional and diagenetic histories of carbonates, when regarded in a stratigraphic context: Depleted ^{18}O isotopic compositions in carbonates can either result from an increase in temperature of precipitation (burial), or reflect isotopically depleted subsurface waters (Lohmann 1988). The $\delta^{18}O$ values of meteoric waters vary within a broad range, reflecting the combination of numerous variables such as latitude, altitude, windward/leeward effects, prevailing weather patterns, or temperature.

Under an arid climate, $\delta^{18}O$ values may be slightly heavier directly below an exposure surface due to evaporative precipitation of calcite and/or dolomite. Strong variations in $\delta^{13}C$ associated with relatively stable $\delta^{18}O$ values (*meteoric calcite line*, Lohmann 1988) are typical for meteoric diagenesis, with the *meteoric calcite line* defining the $\delta^{18}O$-calcite value characteristic of meteoric water. At localities were an organic-rich soil is developed, meteoric waters will inherit a depleted $\delta^{13}C$ signal from isotopically light soil-gas CO_2. As these waters infiltrate the vadose zone and flow through the phreatic lens, rock-water interaction will produce a progressive shift in the $\delta^{13}C$ composition related to the distance from this surface (Fig. 3.1). Bulk compositions of alteration products will be isotopically enriched and have more positive $\delta^{13}C$ with increasing stratigraphic depth relative to the exposure surface (Allan & Matthews 1977, 1982; Videtich & Matthews 1980). The intensity of this $\delta^{13}C$ isotopic signature in comparable geochemical/environmental conditions is a function of the subaerial exposure time and degree of pedogenic alteration (Yang 2001, Joachimski 1994).

However, a few cautionary notes are to be considered in the interpretation of isotope data. First, all the isotopic analyses carried out in this study are modified whole rock analyses. I.e., in some cases rocks of 100% dolomite were analyzed, whereas in the case of partial dolomitization, a mixture of dolomite, calcareous matrix, and microfossils were analyzed. In either case, multiple generations of cement or dolomite (if present) are analyzed as a single population, and the measured isotopic composition thus represents an average of all isotopic compositions in the sample. Furthermore, the complexity of sedimentological and diagenetic factors in shallow-marine environments – such as facies, primary porosity, permeability, type and extent of vegetation cover, duration of exposure, and late diagenetic alteration (Joachimski 1994) – complicates the interpretation of the data.

Despite of these difficulties, the analytical method has been used successfully in the identification of exposure surfaces in Jurassic and Cretaceous carbonates of the Jura platform (Joachimski 1994, Pasquier 1995, Plunkett 1997, Hillgärtner 1999). In the absence of sedimentary evidence some subaerial exposures may even be identified exclusively by isotopic signatures.

Limestones and Dedolomites

Regarding the fields where the measured samples plot in the $\delta^{18}O/\delta^{13}C$-crossplot (Fig. 3.1), there seems to be no great influence of late diagenetic cements. This is in perfect correspondence with microscopic observations and literature data, giving a maximum burial depth in the southern Jura Mountains of 1000 m (Trümpy 1980).

Limestones from lagoonal and tidal domains plot well within the field of Kimmeridgian-Tithonian bulk-rock samples from pelagic carbonates (Bartolini et al. 1996, Padden et al. 2002). However, two samples from restricted lagoonal facies show positive $\delta^{18}O$, which can be interpreted as a result of evaporation under hot and arid conditions. Furthermore, compared to the pelagic reference carbonates, four samples from restricted lagoon environments and one deposited in the tidal domain are slightly depleted in ^{13}C ($\delta^{13}C < +1.0‰$). A possible explanation for this shallow-water depletion is the input of isotopically light CO_2 from respiration of marine and terrestrial organic matter, freshwater discharge, and/or $CaCO_3$ withdrawal during water-mass residence on the extensive shallow platform (Patterson & Walter 1994). The outliers are interpreted to represent the changing water conditions in the generally restricted lagoonal system of the Late Jurassic. A concentration of data points around +2‰ $\delta^{18}O$ / +2‰ $\delta^{13}C$ might define the isotopic signature of limestone bulk-rock precipitated from normal-marine sea water.

Limestone samples that show signs of emersion and/or (meteoric-)vadose diagenesis all plot at the negative end of the measured $\delta^{18}O$-spectrum. Their majority (cf. Chap. 2.4.3 and 2.4.4) varies between -4.27‰ to -5.96‰ $\delta^{18}O$ and +1.96‰ to -0.10‰ $\delta^{13}C$, only one extreme value goes as low as -2.0‰ $\delta^{13}C$ (Fig. 3.1). They thus plot very well within the field of soil carbonates from monsoonal environments as defined by Cerling (1984). The low $\delta^{18}O$ values are due to contamination with isotopically light meteoric waters (Lohmann 1988). The $\delta^{18}O$ values of type-2 dedolomites all are strongly negative (-3.57‰ to -6.14‰) and plot in the same range as those of vadose limestones (Fig 3.1), respectively in the fields for soil carbonates from continental, monsoonal, and coastal

Fig. 3.1 – (facing page) $\delta^{18}O/\delta^{13}C$ (PDB) crossplot. The meteoric vadose samples were identified by microscope analysis. Calculation of normal marine sea water dolostones (bulk rock): $\delta^{18}O$dol-cal = +3 per mil (cf. review in Budd 1997).

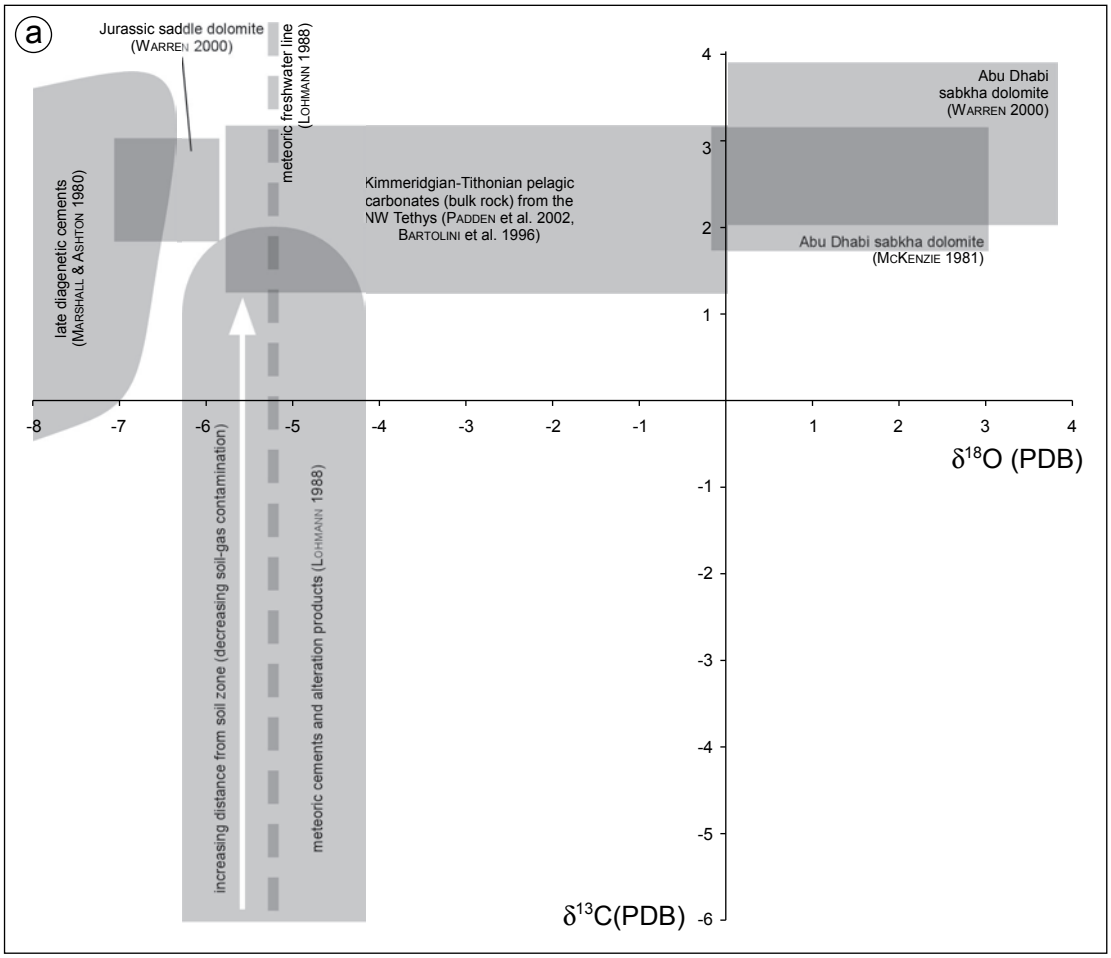
a
Jurassic saddle dolomite (Warren 2000)
meteoric freshwater line (Lohmann 1988)
late diagenetic cements (Marshall & Ashton 1980)
Kimmeridgian-Tithonian pelagic carbonates (bulk rock) from the NW Tethys (Padden et al. 2002, Bartolini et al. 1996)
Abu Dhabi sabkha dolomite (Warren 2000)
Abu Dhabi sabkha dolomite (McKenzie 1981)
increasing distance from soil zone (decreasing soil-gas contamination)
meteoric cements and alteration products (Lohmann 1988)
δ18O (PDB)
δ13C(PDB)

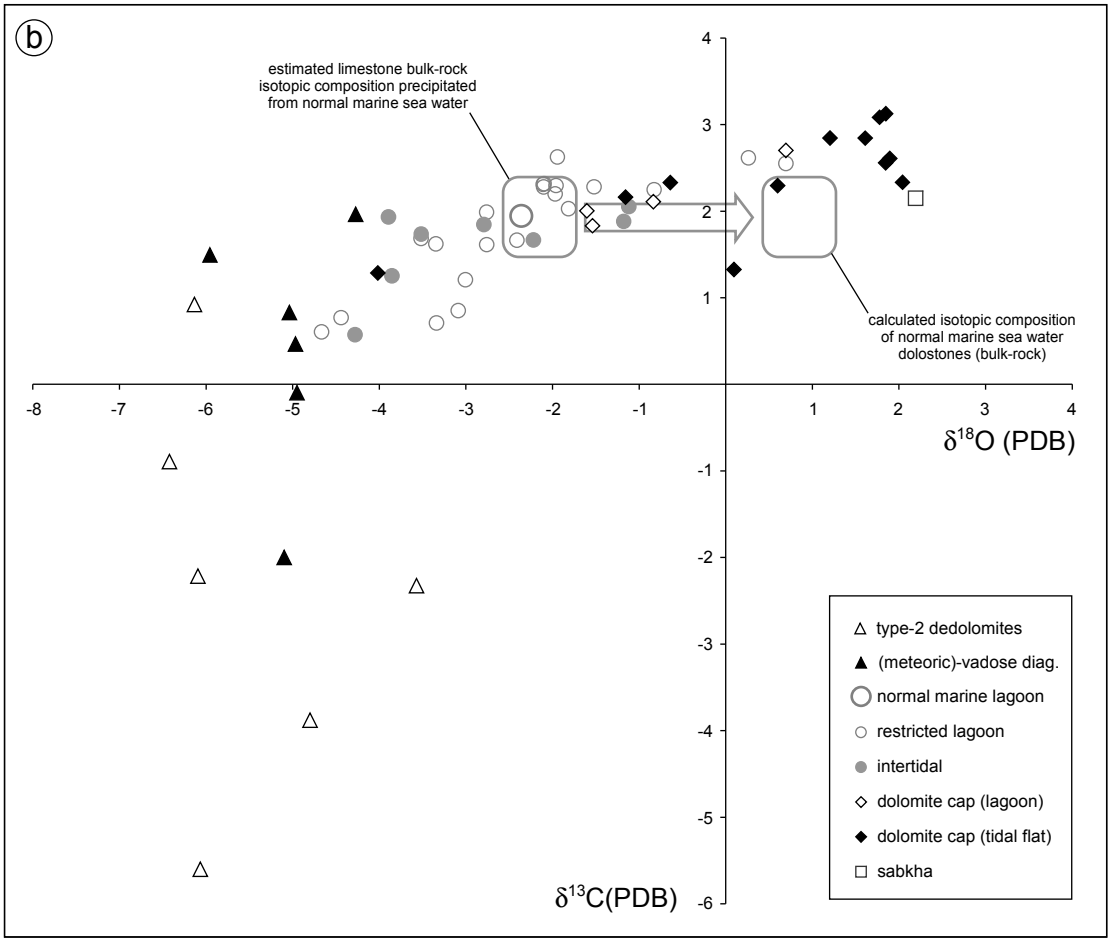
b
estimated limestone bulk-rock isotopic composition precipitated from normal marine sea water
calculated isotopic composition of normal marine sea water dolostones (bulk-rock)
δ18O (PDB)
δ13C(PDB)
type-2 dedolomites
(meteoric)-vadose diag.
normal marine lagoon
restricted lagoon
intertidal
dolomite cap (lagoon)
dolomite cap (tidal flat)
sabkha

FACIES	(Meteoric)-vadose diagenesis	Tidal domain	Restricted lagoon	Normal mar. lagoon	Dolomite cap (lagoonal facies)	Dolomite cap (tidal facies)	Sabkha
No. of samples	(n = 12)	(n = 8)	(n = 21)	(n = 1)	(n = 4)	(n = 12)	(n = 1)
mean $\delta^{18}O$	-5.28 (= *meteoric calcite line*, LOHMANN 1988)	-2.86	-2.32	-2.36	-0.82	0.59	2.19
mean $\delta^{13}C$	min -5.60, max 1.96 dependant on soil-gas contamination	1.62	1.83	1.95	2.16	2.40	2.15

Tab. 3.2 – Mean isotope values for carbonates of different facies. Dedolomites are comprised in the column "(Meteoric)-vadose diagenesis".

environments as defined by CERLING (1984). This fact implies that they were also subject to alteration by meteoric waters. Yet, their $\delta^{13}C$ values are highly variable and range from +0.92‰ to as low as -5.60‰ $\delta^{13}C$. This suggests that limestones showing a vadose overprint were flushed by ^{18}O-depleted rainwater only during short-termed emersions, whereas type-2 dedolomitization obviously is related to longer periods of subaerial exposure that allowed for the development of an organic-rich soil cover. Under these conditions, low $\delta^{18}O$ rain water percolating through the soil would be additionally charged with light, organically derived ^{12}C and cause a low $\delta^{13}C$ in the type-2 dedolomites.

As a result, vadose limestones and type-2 dedolomite form a vertical trend in the $\delta^{18}O/\delta^{13}C$-crossplot (Fig. 3.1). This trend, the "*meteoric calcite line"* of LOHMANN (1988), encompasses the majority of variations present in a single meteoric water system. Since the isotopic composition of meteoric water varies geographically (BOWEN & WILKINSON 2002, CRAIG & GORDON 1965), the $\delta^{18}O$ value of the *meteoric calcite line* must be determined individually for each sequence and location studied (LOHMANN 1988). For this study, an average *meteoric calcite line* was calculated from all samples that had undergone alteration by meteoric waters ($\delta^{18}O$ = -5.28‰, mean value of all vadose limestones and type-2 dedolomites; cf. Tab. 3.2).

Dolomites

Many of the dolomite values plot in the range of Persian Gulf sabkha dolomites (Fig. 3.1) and thus seem to indicate dolomitization by evaporated sea water. Furthermore, this hypothesis can be validated by a second approach.

During sea-water evaporation, the remaining brine typically becomes enriched in ^{18}O. As the oxygen isotopic composition of dolomite is usually derived from the dolomitizing fluid rather than from the precursor rock (LAND 1980, BANNER et al. 1988), dolomites with enriched oxygen isotopic values are most probably precipitated from brines with high $\delta^{18}O$ values. Thus, dolomites with enriched oxygen isotopic values are usually interpreted to indicate precipitation from higher salinity waters (MELIM & SCHOLLE 2002).

The equilibrium fractionation between dolomite and water at low temperatures is unknown (LAND 1980). As a result, interpretation of $\delta^{18}O$ data must follow other lines of reasoning. A common method is to calculate the equilibrium isotopic composition of calcite for a particular fluid and temperature, and then assume a value for $\Delta^{18}O$ (= $\delta^{18}O_{dolomite}$ - $\delta^{18}O_{calcite}$ on the PDB scale), in order to derive an estimate of the equilibrium isotopic composition of dolomite from that fluid at that temperature (BUDD 1997). Estimations of $\Delta^{18}O$ values ranging from 2‰ to 6‰ have been put forward by a number of authors (cf. review in BUDD 1997), but a mean value that is widely accepted to work with is 3‰. This is also matches Holocene data presented by MITCHELL et al. (1987) and MAZULLO et al. (1995).

If this calculation is done for the estimated normal-marine limestone bulk-rock composition (see above), it becomes evident that a significant cluster of tidal-flat dolomites (a mixture of type-1 and type-3 dolomite), as well as one sabkha limestone are heavier than the calculated normal seawater dolomite (Fig. 3.1b). Consequently, they were precipitated from evaporated sea water of elevated salinity. However, some of the dolomites also show isotopic compositions close to the normal seawater dolomite or are even further depleted in ^{18}O. On the one hand, this is probably an effect caused by the modified whole rock sampling (a mixture of dolomite and calcitic matrix is measured), and on the other hand it is possible that in these sample the influence of late diagenetic dolomite formation and recrystallization, characterized by generally lower $\delta^{18}O$ values (cf. REINHOLD 1998), begins to play a significant role.

An extra series of five pairs of limestone matrix and dolomitized burrows (type-2 dolomite) was measured in order to see if the selective dolomitization of burrows was also caused by the percolation of meso- or hypersaline

brines, similar to type-1 and type-3 dolomites (Fig. 3.2). The diagram reveals that the burrow dolomites were probably precipitated from sea water with the same isotopic composition (and thus salinity) as the micritic limestone matrix (see also Fig. 3.3a). The slightly elevated $\delta^{13}C$ values of the dolomites may be a hint to a dolomitization process involving organic matter (cf. Chap. 3.5.3). In any case, it seems evident that the type-2 dolomites precipitate by another dolomitization mechanism than type-1 and type-3 dolomites.

3.4 Discussion of dolomitization and dedolomitization patterns

3.4.1 Timing of dolomitization

In the platform sections, exclusively dolomicrospar (type-3 dolomite, "*tidal flat dolomite*") and host replacive, hypidiotopic-rhombic dolomite (type-1 and -2 dolomite, "*matrix and burrow dolomite*") were found. Dolomite mosaics with planar crystal boundaries (idiotopic) indicate growth temperatures below 50-60°C (i.e. shallow burial), while those with non-planar boundaries (xenotopic) form at temperatures superior to 50-60°C (deeper burial; cf. Tab. 3.1).

Furthermore, a cloudy-center clear-rim texture – commonly occurring within the dolomites of the platform sections (cf. Pl. 14/1) – is considered as typical for many sparry dolomites that form at lower temperatures (Warren 2000). This texture suggests multistage dolomite generation. The cloudy center often represents penecontemporaneous or early post-depositional dolomite precipitation, while the clear rim forms by continuing growth during (shallow) burial.

Another indication for the early timing of platform dolomitization comes from the oncoid-rich limestones of the upper Reuchenette Formation at Cirque des Avalanches. In these oncoid-wackestones to -packstones, the matrix is dolomitized by medium-grained, idiotopic, zoned dolomite rhombs (type-1 dolomite, "*matrix dolomite*"; Pl. 14/6). The oncoids, however, are not affected by dolomitization, except for a relatively well defined outer part of the cortex. This can be interpreted in the way that dolomitization happened when the oncoid surface was

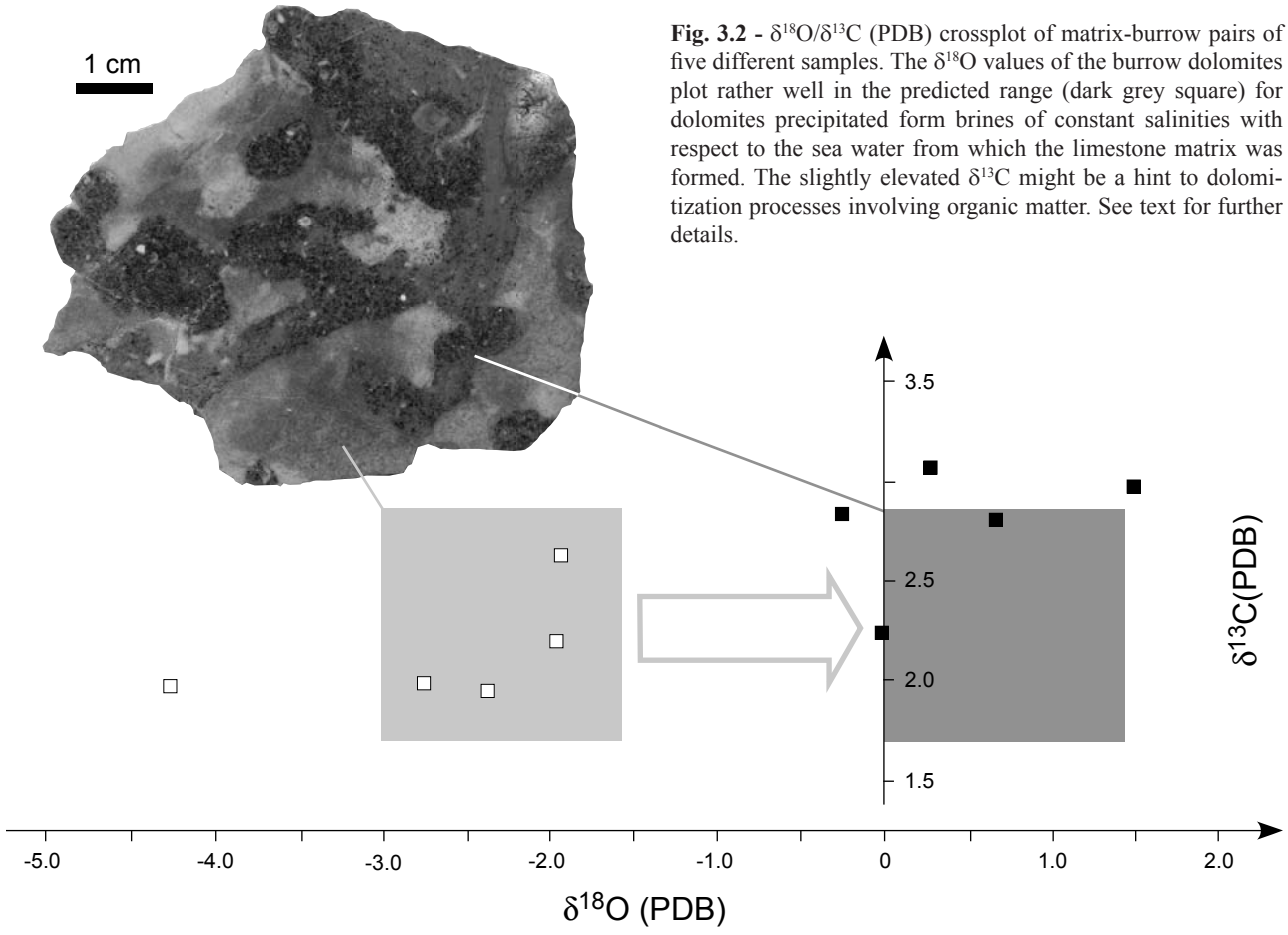

Fig. 3.2 - $\delta^{18}O/\delta^{13}C$ (PDB) crossplot of matrix-burrow pairs of five different samples. The $\delta^{18}O$ values of the burrow dolomites plot rather well in the predicted range (dark grey square) for dolomites precipitated form brines of constant salinities with respect to the sea water from which the limestone matrix was formed. The slightly elevated $\delta^{13}C$ might be a hint to dolomitization processes involving organic matter. See text for further details.

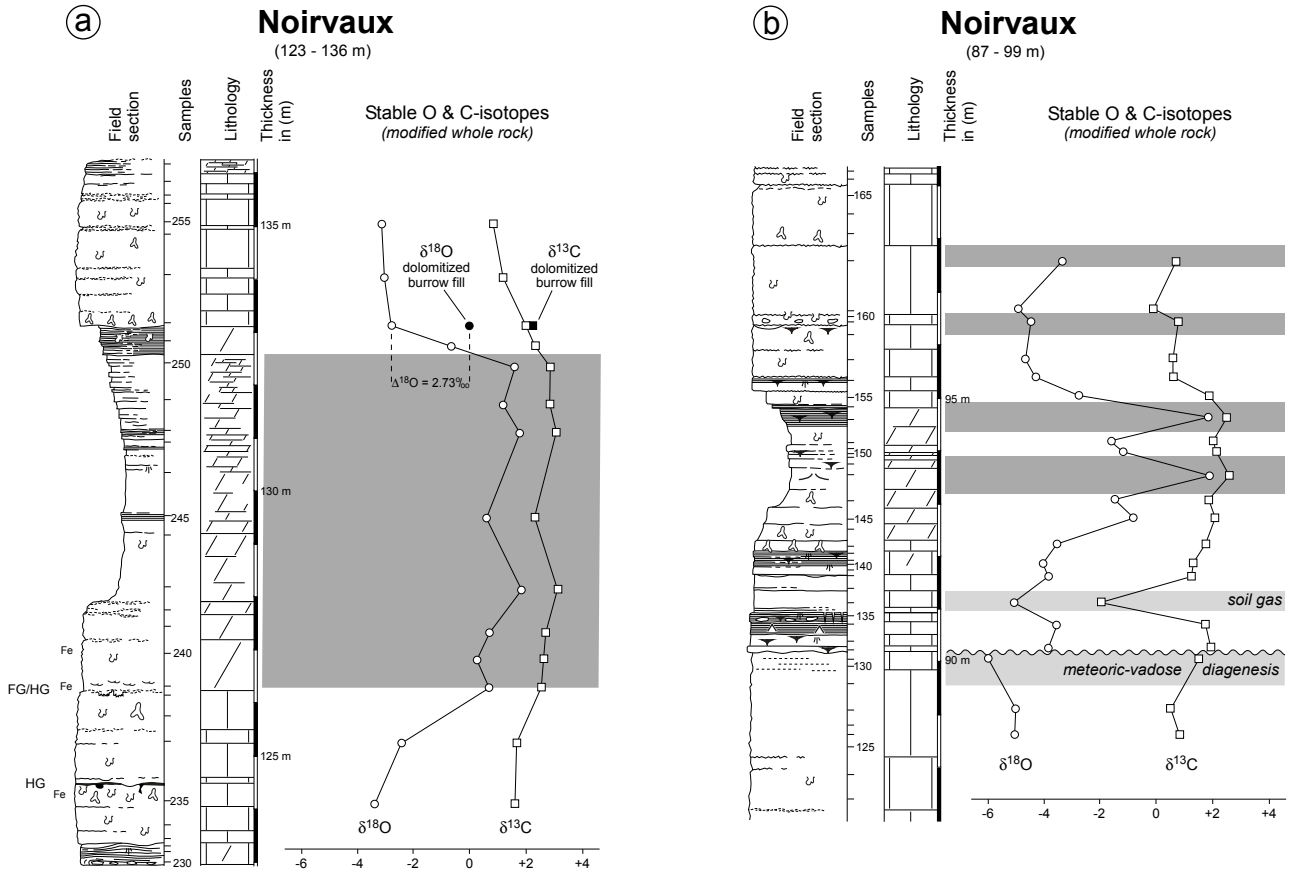

still permeable for the dolomitizing fluid. I.e., the timing of the dolomitization process was penecontemporaneous or early post-depositional – in any case *very* early with respect to diagenetic history.

3.4.2 Stratigraphic patterns

According to Warren (2000), different dolomitization mechanisms produce differing isotopic signatures with respect to $\delta^{18}O$ values and their spatial variation. Therefore, stratigraphic stable isotope analyses were carried out in three selected dolomite caps in order to gain information on the role of evaporated sea water as dolomitization fluid (Fig. 3.3). Furthermore, the stable isotope analyses help to verify the sedimentological interpretation of subaerial exposure, as well as the relationships between subaerial exposure, soil gas contamination, and dedolomitization.

Type-1 dolomite makes up by far the biggest volume of dolomitized sediments in the measured sections. It always occurs in stratiform geometries in the uppermost part of a shallowing-upward lagoonal/peritidal sequence, typically with a sharp (slightly erosive) upper contact surface and a more diffuse lower contact (Fig. 3.3a). Within a dolomite cap that consists mainly of type-1 dolomite, there are frequently intercalations of type-3 dolomite, usually accompanied by laminated texture and sedimentary signs of emersion (Fig. 3.3a, b and Pl. 14/3, 4). These changes in dolomitization type and sedimentary facies are commonly found at the end of both a small-scale thinning-upward trend and an interval of increasing or high $\delta^{18}O$ values. This is interpreted to reflect high-frequency shallowing-upward sequences, i.e. one dolomite cap can be composed of one or several shallowing-upward sequences. This interpretation will be of importance for the sequence- and cyclostratigraphic interpretation of the sections (Chap. 4 and 7).

In Fig. 3.3a (Noirvaux section from123-136 m), a drastic positive shift of $\delta^{18}O$ of about 4‰ (PDB) followed by relatively constant values over the entire dolomite cap indicates a relatively uniform influence of evaporated sea-water. However, according to a $\delta^{18}O$ minimum at ca. 129.5 m and a laminated interval that also translates in the weathering morphology, the cap can be divided into two subunits. An interesting detail in this specific dolomite cap is the lower boundary: Unlike the usual downward-transition from type-1 dolomite to a dolomitized limestone with floating rhombs and a decrease in $\delta^{18}O$ (cf. Fig. 3.3b, 94-92 m), a firm- or hardground separates dolomites from lagoonal limestones and high from low $\delta^{18}O$ values (Fig. 3.3a, 126.3 m). A similar case was observed in the Dôle section at 120 m (Fig. 4.15). The early cemented

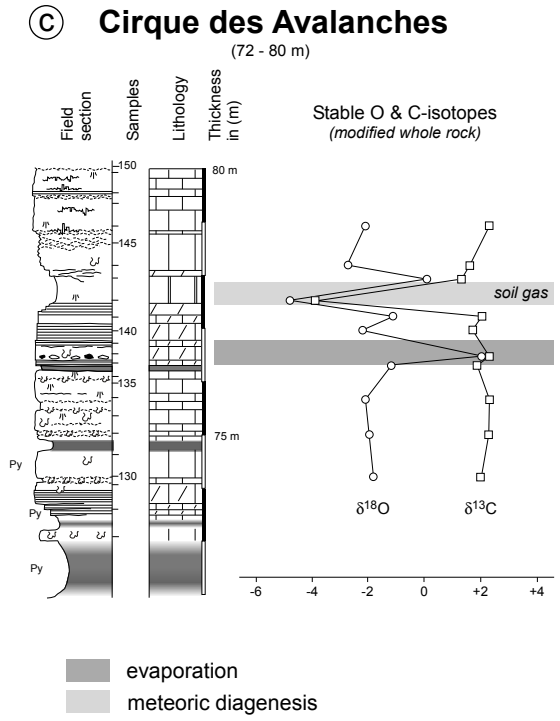

Fig. 3.3 - (above and facing page) Stable isotope analysis of three selected dolomite caps. For details, refer to text. For legend, see Fig. 4.6a.

surface obviously acted as an aquitard with respect to the dolomitizing fluid. This is an additional indication that type-1 dolomitization was an early process. If the cemented surface acted as an aquitard for the brine percolating in the sediments above, these sediments must still have been permeable, i.e. probably uncemented, or at least not fully cemented, respectively compacted. On the other hand, the normal, gradual transition would imply a percolation of the dolomitizing brines from above. In the case of not fully compacted peritidal sediments (i.e. very shallow burial), the most relevant fluid source for early dolomitization is sea water that infiltrates the sediment/water or sediment/air interface (Fig. 3.4). Sedimentary evidence like tepee structures and evaporite pseudomorphs (Fig. 3.3b) underlines the existence of arid conditions that favour extensive evaporation, specifically in shallow water-bodies. Also, the isotopic composition of the dolomites (Chap. 3.3) support elevated salinity of sea water due to evaporation.

The sum of this evidence (like sharp, partly erosive upper boundaries, in general transitional lower boundaries and the evaporitic, downward decreasing $\delta^{18}O$ isotope signature of the investigated dolomite caps), leads to a model of shallow seepage reflux (Adams & Rhodes 1960, Budd 1997, Warren 2000) with common emersion events, during which, under hot and arid conditions, evaporitic, penecontemporaneous type-3 dolomites would precipitate as laminated supratidal crusts (Carballo et al. 1987).

The second analyzed dolomite cap from the Noirvaux section (Fig. 3.3b) is much more complex than the one described above. As already mentioned, this dolomite cap shows the typical transitional downward decrease of dolomitization intensity (and corresponding $\delta^{18}O$ values). In contrast to the example of Fig. 3.3a that is characterized by a relative homogenous isotopic signature over the entire thickness of the dolomite cap, Fig. 3.3b clearly shows two sharp peaks. The evaporitic influence is expressed with an $\delta^{18}O$ excursion of about +6‰. In terms of fluid flow this can either be interpreted as a shallower infiltration depth (that might be due to shorter periods of evaporation), or as meteoric influence on the tidal-flat sediments at around 94 m. Similar to the example of Fig. 3.3a, the isotope signature indicates, in congruence with stacking pattern and weathering morphology, that the cap can be divided into two subunits.

In Fig. 3.3c a supratidal, multicoloured breccia coincides with a single, sharp $\delta^{18}O$ peak. As dolomites in supratidal sediments usually are of type-3, this peak is not interpreted as seepage reflux, but as evaporation on a supratidal flat.

If Fig. 3.3a represents a model dolomite cap, the examples of Fig 3.3b and 3.3c were chosen because they display some particular details. In the Noirvaux section, an eye-catching erosion surface separates the Reuchenette and Twannbach formations at 90 m (Figs. 3.3b and 4.11; Pl. 20/1). This erosion surface is not only defined by an abrupt change in facies and weathering colour, but microfacies analysis also reveals microkarstic features (Fig. 4.11). Stable isotopes indicate a negative shift in $\delta^{18}O$ but a relatively undisturbed trend in $\delta^{13}C$. The low $\delta^{18}O$ suggests meteoric influence on the karstified rocks. The virtually non-existent change in $\delta^{13}C$ can either be interpreted in a way that colonization by land plants was absent or played only a minor role, or that a hypothetically present soil-gas-contaminated horizon was eroded. Sedimentary and correlational evidence favour the second interpretation (cf. Chap. 4, Noirvaux section). Another argument for the reasoning of substantial erosion at this surface is the existence of a horizon with a similar $\delta^{18}O$ signature, but heavily depleted $\delta^{13}C$ values (soil gas contamination) just 1 m above the erosion surface.

In the Cirque des Avalanches section, the evolution of a relatively thin dolomite cap is terminated by a bed of type-2 dedolomite (Fig. 3.3c). According to Allan & Matthews (1982), parallel shifts in $\delta^{18}O$ and $\delta^{13}C$ are typical for diagenetic alteration in mixed, meteoric-marine environments. However, for the type-2 dedolomites observed in this study, a prominent role of soil-influenced meteoric diagenesis is assumed in the recrystallization

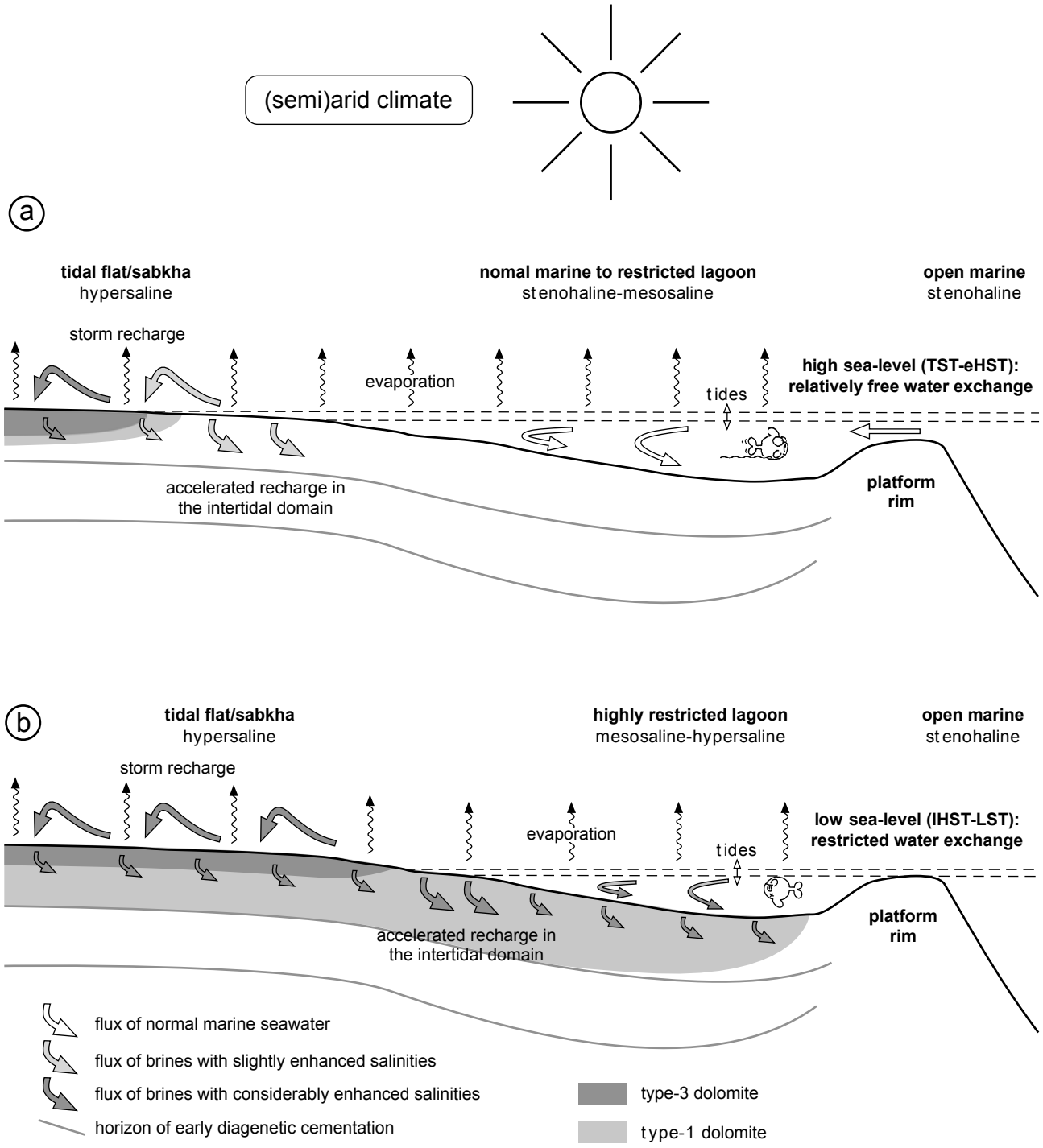

Fig. 3.4 - Hypothetical sketch (no scale) to explain the observed dolomitization patterns: a) during high relative sea-level (TST-eHST; cf. Fig. 4.1) the lagoon is in relatively free water exchange with the open ocean. Dolomitization of burrows may occur, but no, or only negligible amounts of matrix dolomite will be produced in shallow lagoonal settings. b) A sea-level drop causes the (emerged?) platform rim to limit water exchange between the lagoon and the open ocean, leading to mesosaline to hypersaline conditions in the lagoon. Due to the higher brine density and/or the accelerating effect of burrows the in intertidal (cf. Fig. 3.5), reflux-type dolomitization will kick off in not fully consolidated lagoonal lime mud ("brine reflux dolomite" sensu Warren 2000, "penesaline dolomite" sensu Qing et al. 2001). Horizons of early diagenetic cementation (e.g., firm- and hardgrounds) may act as aquitards with respect to the percolating brine, leading to stratiform dolomitization. See text for detailed discussion.

process: In the Dôle section, recrystallized laminated dedolomitic crusts (Fig. 4.15, Pl. 16/2a) are clearly associated with red-brown clay-layers that are interpreted as incipient soils. Type-2 dedolomitization is always associated with large-scale sequence boundaries.

3.5 Dolomitization model(s)

"*...to conclude that there are dolomites and then there are dolomites will come as no revelation. Nonetheless, the message is worth repeating...*" (Hardie 1987)

In his study of the "Portlandian", Bläsi (1980) explained the dolomites of the Jura Mountains to have formed by schizohaline dolomitization, or "mixing zone" dolomitization – a model that was widely accepted during the late 1970s and early 1980s, until criticized by Machel & Mountjoy (1986) and Hardie (1987); see also Melim et al. (2004) for a recent view on the topic.

Newer research on early post-depositional dolomitization of carbonate platforms emphasizes the role of reflux mechanisms and interplay between reflux and thermal convection (Whitaker et al. 1997, Melim & Scholle 2002, Jones et al. 2002, 2004).

3.5.1 Type-1 dolomite: dolomitization by seepage reflux

Judging from their stratal geometries and isotopic signature (Warren 2000), the majority of the observed type-1 dolomites fit perfectly into a reflux-type model. The original model of Newell et al. (1953) and Adams & Rhodes (1960) uses dense hypersaline brines from evaporite lagoons near the coastline that sink into the platform and dolomitize the underlying sediments. Yet, evaporite deposits only start to play an important role in the Upper Twannbach and Lower Goldberg Formations (Dôle and Lieu sections).

Simms (1984) and Kaufman (1994) have shown that reflux systems can work with sea water of only slightly increased salinity: Simms (1984) modelled reflux in carbonate platforms with brines of only 42‰ salinity and predicted the existence of such a reflux system in the Great Bahama Bank that was eventually documented (e.g., Whitaker & Smart 1993, Whitaker et al. 1994). Sun (1994) reasoned that during ice-free periods with small amplitudes in high-frequency sea-level change, carbonate platforms switch to "keep-up mode" over tens of millions of years, because their potential of carbonate production by far exceeds normal rates of platform subsidence. Thus, platforms are able to prograde extensively, creating vast platform-top areas with metre-scale cyclic peritidal successions, which, in turn, would allow for frequent inundation of extensive supratidal surfaces by storm-driven marine waters. These waters had to traverse the vast shallow-water area of the platform top. Consequently, if under (semi)arid climate conditions evaporation is sufficiently high, a "mesosaline" fluid (35 to 120‰, i.e. below gypsum saturation; Kirkland & Evans 1981) is generated that represents a potential source for refluxing brines. Such salinities are indicated by the presence of restricted marine carbonate facies and

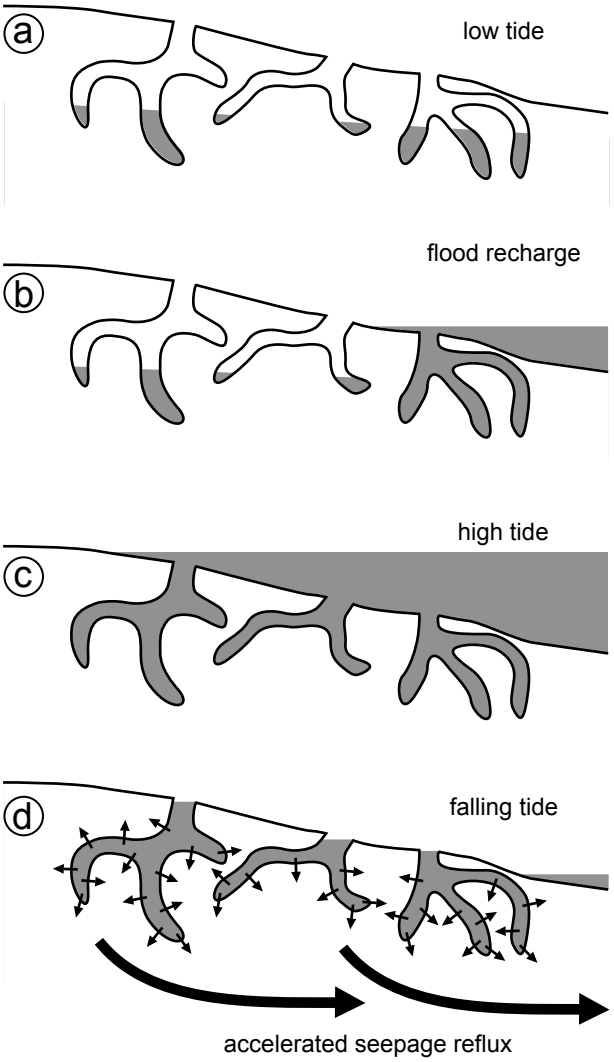

Fig. 3.5 - Accelerating effect of bio- and/or rhizoturbation on seepage reflux: burrows and hollow root debris, partly empty at low tide (a), are rapidly filled by flood tide (b, c) forming a perched reservoir ensuring percolation of dolomitizing fluid (sea water of elevated salinity) during falling tide (d). After Baltzer et al. (1994).

biota and the absence of massive evaporite deposits (Qing et al. 2001). Dolomites that are interpreted to form by reflux of mesosaline brines were described by Qing et al. (2001) from the Early Jurassic of Gibraltar and by Melim & Scholle (2002) from the Permian Capitan Formation of Texas and New Mexico. Qing et al. (2001) proposed to call this type of dolomitization "*penesaline dolomites*", referring to Adams & Rhodes' (1960) term for evaporated sea water with salinities varying from 72 to 199‰.

While the observed dolomite caps clearly fulfil all criteria to have formed through "*penesaline dolomitization by seepage reflux*", there remains still an unanswered question: Why is there a succession of dolomite caps and not one thick body of reflux dolomite? Qing et al. (2001) and Mutti & Simo (1994) proposed that repeated high-frequency sea-level falls are able to drive the dolomitizing fluid into the platform. This hypothesis is not fully convincing because even if they are high-frequency in geological terms, these sea-level changes happen to occur over thousands of years and thus should in the first place shift the whole system laterally (cf. Fig. 3.4) rather than actively drive fluids into the sediment. Much more likely mechanisms for actively driving sea-water into the platform are storm recharge on tidal flats (Fig. 3.4) and the development of perched reservoirs in the intertidal domain twice a day (Fig. 3.5).

However, according to Machel (2002), the efficiency of reflux mechanisms is different during transgressive and regressive periods, i.e. high-frequency sea-level changes are indeed able to influence the rate of dolomitization. Taking into account all observed features, the following qualitative model is proposed:

During transgressive phases, there is relatively free water inflow on the platform. Lagoons stay normal marine to slightly restricted, but shallow marine life flourishes. Storms regularly drive lagoon water on the adjacent tidal flats where it is concentrated by evaporation and contributes to the formation of dolomite crusts (type-3 dolomite) (Fig. 3.4a).

With relative sea level falling, the water exchange with the open ocean becomes more and more restricted, the salinity of lagoon water increases to a point where it is hostile for most marine life (Fig. 3.4b). However, as the platform rim – that is assumed to act as the separating barrier – probably consisted of a relatively loose chain of reefal mounds and oolite bars (Détraz & Mojon 1989, Meyer 2000), no complete isolation of the lagoon will take place that would allow for the development of massive evaporite deposits. However, salinity is elevated enough to create a brine of sufficient density to start a reflux flow. With the next transgression, water exchange is rehabilitated and the system switches back to the state as shown in Fig. 3.4a, while the mesosaline brine can continue to sink in, respectively flow seawards ("latent reflux", Jones et al. 2002). According to Whitaker (pers. comm.), a reflux mechanism that is "switched on and off" by high frequency sea-level changes should produce only shallow, but repeated infiltration horizons – repeated dolomite caps in a peritidal limestone succession like the ones found in the measured sections. Furthermore, horizons of early cementation may act as seals and hinder brines from sinking and thus force them to migrate laterally (Fig. 3.4b).

From the Early Berriasian onwards, the spatial distribution of calcrete crusts on the Jura platform implies the development of a barrier island chain (Strasser & Davaud 1982, Davaud et al. 1983). With this much more efficient barrier against water exchange, the lagoons were almost completely cut off and the massive evaporites of the Goldberg Formation could precipitate. Later dissolution of those evaporites then led to the formation of the collapse breccias found in the upper parts of the Dôle and Lieu sections.

3.5.2 Type-3 dolomite: evaporitic tidal flat dolomite

Type-3 dolomites are interpreted to be an analogue to penecontemporaneous dolomitic crusts known from recent and Holocene tidal flats (e.g., Shinn et al. 1965, Carballo et al. 1987, Mazullo et al. 1987). These dolomites typically form cm-thick supratidal crusts formed at or right below the sediment surface. Dolomite crystals are small, euhedral to subhedral rhombs which range in size from < 1 to 5 µm (Budd 1997). Every aspect in terms of facies, texture, and average crust thickness relates perfectly to the Late Jurassic type-3 dolomite intercalations in type-1 dolomite caps. The bigger size of type-3 dolomite crystals (Chap. 3.1.3) may in part be a result of ongoing post-burial growth and/or a type-1 dolomite overprint.

The formation of their Holocene and recent counterparts is accomplished by active tidal pumping of sea water of normal or slightly elevated salinity. Although a certain amount of evaporation and/or sulphate reduction cannot be ruled out, these processes seem to be of secondary importance (Carballo et al. 1987). $\delta^{18}O$ values of Holocene dolomite crusts range from 1.5‰ to 3.2‰ (PDB) (Carballo et al. 1987, Mazullo et al. 1987) and thus plot right in the range of most important cluster of measured Late Jurassic tidal-flat dolomite (Fig. 3.1b). Also, the cm-thick, discontinuous layers of type-2 dedolomite ("*laminated cornieule*", Pl. 16/2a) that are intercalated in sabkha sediments at the top of the Dôle section (148-153m) most probably represented such dolomite crusts.

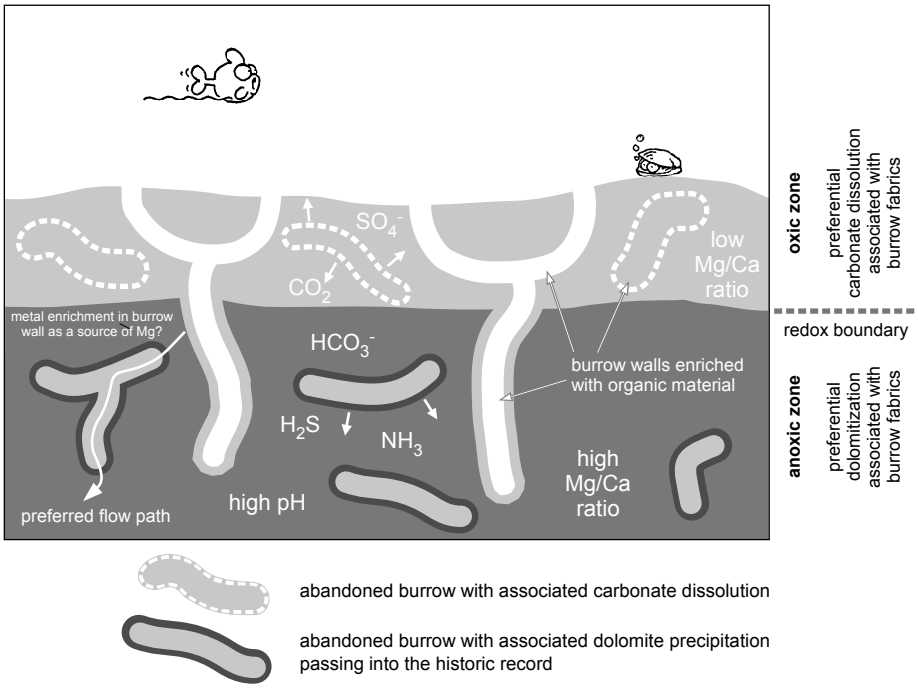

Fig. 3.6 - Schematic diagram illustrating the geochemical characteristics of the oxic and anoxic zones in a subaqueous (marine) substrate and the resulting differential dolomitization associated to burrows. After Gingras et al. (2004). For detailed explanation refer to text.

3.5.3 Type-2 dolomite: organically mediated dolomite precipitation in burrows

Dolomitized burrows are a relatively widespread phenomenon and were described by, e.g., Purser (1975), Gingras et al. (2004), and Horbury & Qing (2004). In contrast to type-1 and type-3 dolomites, burrows filled with type-2 dolomite can be found in any position within a shallowing-upward sequence, i.e. they follow a completely different stratigraphic distribution pattern. This and the completely different isotopic signature – not supporting the influence of concentrated brines but suggesting the involvement of organic matter in the dolomitization process (Fig. 3.2) – make it obvious that an independent dolomitization mechanism was at work.

Burrowing organisms significantly alter the sediment substrates in various ways. The alterations not only include physical parameters like modification and redistribution of grain size, compaction, and sorting, but also biochemical modifications by the incorporation of localized, concentrated organic matter in the form of mucous or faecal pellets that provide excellent substrates for bacterial colonization. Open burrows or burrows filled with coarse (bio)clastic material ("*tubular tempestites*", Wanless et al. 1988) thus act as open conduits to the sediment-water interface but can maintain a variety of chemical microenvironments that may extend several cm into the sediment surface (Gingras et al. 2004). Close to the surface and in burrows that still communicate with the sediment-water interface, the microbial oxidation of organic material (respiration) produces CO_2. Depending on geochemical conditions, increased CO_2 activities can enhance carbonate dissolution during early diagenesis, while free SO_4^{2-} ions inhibit dolomite precipitation and may lower the Mg/Ca ration by bonding with Mg^{2+} ions (Fig. 3.6). It is known that dolomite formation preferably occurs in reducing environments and in the presence of microbes that promote dolomitization (Vasconcelos & McKenzie 1997, van Lith et al. 2003a, b). CO_2 and NH_3 are common products in this geochemical setting and both react with water. The reaction of ammonia raises pH ($NH_3 + H_2O \leftrightarrow NH_4^+ + OH^-$) which, in turn, increases the activity of the bicarbonate ion (HCO_3^-) that favours the direct precipitation of dolomite (Gingras et al. 2004, Lippmann 1973).

In reducing environments, SO_4^{2-} ions are consumed by sulphate reducing bacteria and the inhibitory effects of these ions are removed from the system. This combination of elevating pH and lowering SO_4^{2-} levels is the key to the early diagenetic precipitation of dolomite in burrow systems (Gingras et al. 2004). Under these geochemical conditions, dolomite crystals precipitate under microbial mediation (van Lith et al. 2003b). Metal enrichments

in the organic burrow lining may additionally facilitate dolomite precipitation (Mirsal & Zankl 1985).

The geochemical conditions favourable for dolomite precipitation may infiltrate into the surrounding micritic matrix and thus can produce a diagenetic halo, i.e. floating dolomite rhombs next to a dolomite-matrix boundary (Pl. 14/2). The halo usually spreads only a few mm into the surrounding limestone and blends without a sharp transition into the matrix (Pl. 14/5). However, a limestone with dolomitized burrows can in a later phase undergo type-1 dolomitization so that all transitions from "*only burrows dolomitized*" to "*matrix and burrows dolomitized*" can be observed in the studied sediments.

* * *

4 - Sedimentological interpretation and sequence analysis

"...sequence stratigraphy must be viewed as a tool or approach rather than a rigid template. The conceptual stratigraphic models are based on first principles and it is the understanding of these first principles rather than memorization of the model that is the key to the successful application of sequence stratigraphy."

Posamentier & James (1993)

4.1. Introduction

Sequence stratigraphy was initially put forward by a research group of EXXON (Vail et al. 1977) as a tool to understand and predict the dynamics and resulting stratal geometries of sedimentary systems in the search for petroleum reservoirs. It is a conceptual model that explains stratigraphic patterns and the evolution of sedimentary basins mainly as the effects of large-scale eustatic sea-level changes (e.g., Vail 1987, Posamentier et al. 1988, 1992, Posamentier & James 1992, Posamentier & Allen 1993, Hunt & Tucker 1992, 1995, Kolla et al. 1995, Miall 1986, 1991, 1997, Nystuen 1998). As the initial model was essentially developed on the basis of seismic studies on passive continental margins, one of the major problems was the low vertical resolution of the source data, which only resolve major lithological changes and stratigraphic geometries. With technical advance in seismic and computing equipment, and with detailed field analogue studies, higher-quality data of lithological variations can now be obtained. However, even in relation to modern high-resolution seismics, outcrop-based studies offer a higher level of detail and the advantage of working with real rocks and surfaces. Yet, a common drawback is the lack of information on geometries of large-scale sediment bodies in outcrop.

Over the years, the initial concepts of sequence stratigraphy were refined by integrating the results of numerous case studies, which led not only to a continuous questioning and redefinition of principles and terms and an ever finer stratigraphic subdivision for different sedimentary environments, but also to the development of different schools of thought or models, depending on how sequences are identified and subdivided, and on the interpretation of which kinds of processes have controlled the genesis of stratigraphic sequences and sequence boundaries. E.g., the o*riginal EXXON model* of Vail et al. (1977); the *genetic sequences* of Galloway (1989); the *T-R sequences* of Embry (1993, 1995); the *base-level cycles* of Cross (1991) and Cross & Lessenger (1998); the *regime theory* of Thorne & Swift (1991a, b) that led to the *accommodation-supply model* of Schlager (1993) (for a detailed review see Nystuen 1998). Eventually, it has been realized that eustatic variations are not necessarily the dominating factor controlling the formation of stratigraphic sequences in tectonically unstable settings or in carbonate systems (e.g., Posamentier & Allen 1993, Schlager 1989, 1991, 1993, Hubbard 1988,

Cloetingh 1988). Also, the validity of global correlations of apparently eustatic events as presented in global cycle charts (Haq et al. 1988) was questioned (Miall & Miall 2001, Miall 1999, 1992, 1991).

Some time ago, the concepts of sequence stratigraphy were also applied to smaller-scale systems (Mitchum & Van Wagoner 1991) and the terminology was proposed to be entirely independent of scale (Posamentier et al. 1992). Yet, a major problem is the unfeasibility of scaling down the simplistic sequence-stratigraphic model and applying it to different kinds of environments without modification. On the other hand, modern cyclostratigraphy, originating from the analysis of m-scale sedimentary cycles (cf. Chap. 6), seeks to reconcile large-scale, basin-wide processes with Milankovitch-type climate variations (Perlmutter & Matthews 1990, 1992) and the concepts are applied also to platform environments (e.g., Goldhammer et al. 1990). However, no systematic terminology exists in cyclostratigraphic concepts for complex depositional sequences (called "sedimentary cycles" in these approaches) in platform environments, which genetically compare well with "depositional sequences" sensu Vail et al. (1991).

Although the fundamental controlling processes and the scale of time and space are not the same, sedimentary systems show a comparable logic in the response to accommodation changes on all scales. For the time being, the numerous concepts undergo continuous modification, and many authors apply customized terminologies suiting their specific case.

4.2. Depositional sequences

When Sloss (1963) introduced the concept of depositional sequences, he defined sequences as stratigraphic units that are "*traceable over major areas of a continent and bounded by unconformities of interregional scope*". Vail et al. (1977) adjusted this definition for working with smaller units and seismic data. These authors defined a depositional sequence as a "*stratigraphic unit composed of a relatively conformable succession of genetically related strata and bounded at its top and base by unconformities or their correlative conformities*". This definition is essentially based on stratal geometry and therefore well suited for seismic interpretation. Subsequently, it has been accepted in numerous key publications (e.g., Van Wagoner et al. 1988, Posamentier et al. 1988, Emery & Myers 1996, Miall 1997). The definition furthermore avoids any reference to the origin of a depositional sequence even though Vail et al. (1977) clearly expressed their conviction that eustatic sea-level fluctuations were the dominant control.

There are numerous criteria to identify and interpret depositional sequences. Sedimentological analysis provides various parameters such as deepening-up (transgressive) and shallowing-up (regressive) trends in general facies evolution, variations in ecological indicators, interpretation of beds and discontinuities, and vertical variations in bed thickness and stacking patterns. Specific analyses of diagenetic features, stable isotope or geochemical signatures, and the study of clay-mineral abundance/composition and palynofacies can yield supporting evidence (e.g., D'Argenio et al. 2004, Colombié 2002, Rameil et al. 2000, Hillgärtner 1999, Plunkett 1997, Pittet & Gorin 1997, Pasquier 1995, Budd et al. 1995, Joachimski 1994). A detailed description of the various sequence identification criteria and their interpretation is given in Hillgärtner (1999, p. 51ff.).

4.2.1 Applied sequence model and terminology

The Fribourg Approach is a combination of sequence- and cyclostratigraphic aspects developed for studying depositional sequences on shallow-water carbonate platforms, but its principles are generally applicable. Methodology and reasoning for interpretation are summarized in Strasser et al. (1999) and Strasser et al. (2000) and explained by using examples from the Late Oxfordian and Berriasian of the Jura Mountains. The terminology used in this approach evolved from the experience accumulated in the Fribourg working group during more than a decade of high-resolution outcrop studies in Mesozoic carbonate platform environments of the Swiss and French Jura Mountains (Hug 2003, Colombié & Strasser 2005, 2003; Colombié 2002, Hillgärtner 1999, Strasser & Hillgärtner 1998, Pittet & Strasser 1998a, b, Pasquier & Strasser 1997, Pittet 1996, Pasquier 1995, Strasser 1994). It is partly based on Vail et al. (1991) and adapted to the specific study conditions where:

1) it is impossible to directly determine the geometry of large-scale sediment bodies;
2) discontinuity surfaces can be traced (physically) only for limited distances (outcrop scale, i.e. meters to 100s of meters);
3) reference sections supply data about environmental dynamics on the platform, and complementary sections provide information on contemporaneous basinal dynamics.

The main difference of this model to the sequence-stratigraphic model (Vail et al. 1977, Vail et al. 1991) is the self-similarity of depositional sequences at all scales. The nomenclature for high-frequency sequence analysis introduced by Mitchum & Van Wagoner (1991) took into

account the superposition of different orders of sea-level change. Yet, it seems too clumsy to be useful in outcrop scale (Hillgärtner 1999) as it assumes that systems tracts and sequence sets, for example, are measures of larger-scale sea-level trends and are defined by different progradation-aggradation ratios and terminations of seismic reflectors (Mitchum & Van Wagoner 1991, Emery & Myers 1996). The direct observation of such features is extremely difficult in field-based studies with restricted outcrop conditions.

The Fribourg Approach thus avoids terms such as "systems tract" or "parasequence", which would imply specific architectures and scales. Here, the smaller-scale depositional sequences with their changing sedimentological characteristics and their typical stacking pattern, are the units from which short-term and long-term relative sea-level evolution is interpreted (Strasser et al. 1999).

Another important point is the assumption that characteristic deposits and discontinuity surfaces that define a depositional sequence are independent of the temporal scale of relative sea-level change. I.e., on all scales, deposits that indicate, e.g., relative deepening and/or opening of the system are called "transgressive deposits" (**TD**) (Fig. 4.1a). They correspond to the phase where accommodation increases during relative sea-level rise, after an initial flooding of a relatively shallower substrate. The discontinuity depicting the initial flooding is termed "transgressive surface" (**TS**). Just after the initial flooding, carbonate production is still in "start up*"* mode (Kendall & Schlager 1981) and thus the TS is commonly characterized by reworked clasts ("lag deposit"), an abrupt increase in mean grain diameter, and minor erosion ("transgressive surface of erosion (TSE)", Nummedal & Swift 1987, Bhattacharya 1993, Caron et al. 2004; also termed "ravinement surface" by Swift 1968). The "start up*"* phase is equivalent to the "lag time" of Strasser (1991).

With increasing water depth and the recovery of the carbonate factory, conditions become ideal for maximum carbonate production and thus the previously created accommodation space begins to fill up ("catch up*"* phase, Kendall & Schlager 1981). This is when the thickest beds are created on the top of a shallow-water carbonate platform (Strasser et al. 1999). Intensively bioturbated and/or marly intervals, or distinct omission surfaces testify to the most open-marine conditions that correspond to the fastest rise in relative sea-level. If a distinct single surface is developed, this is denoted as "maximum flooding surface" (**MFS**) (Fig. 4.1a). In the case of repeated maximum flooding surfaces, or an interval that lacks distinct surfaces, but clearly shows the most open-marine conditions, the term "maximum flooding zone" (**MFZ**) is used. A more general term for both "maximum flooding surface" and "maximum flooding zone" is "maximum flooding" (**MF**) (Fig. 4.1a). It is important to notice that this definition of maximum flooding differs from the original definition of Vail et al. (1977). While the original maximum flooding surface was defined geometrically as the seismic surface that marks maximum transgression, i.e. the surface that separates retrograding from prograding sediment packages, the maximum flooding (surface) in this approach represents the sedimentological expression of the most open-marine conditions. I.e. if the two concepts are applied to the same (seismic-scale) sediment succession, the two differently defined maximum floodings will not necessarily be represented by the same surface, respectively seismic reflector.

After the maximum flooding, beds thin upwards and indicate shallowing trends that correspond to a slow-down in relative sea-level rise and an initial fall. They are depicted as "highstand deposits" (**HD**) (Fig. 4.1a). During this phase, the carbonate platform usually is in "keep up" mode (Kendall & Schlager 1981). If the production of carbonates matches the creation of accommodation space, the platform will grow predominantly vertically (aggradation). However, in the standard case, the production of carbonates is higher than the creation of accommodation space, so the highstand deposits usually build towards the basin (progradation).

Commonly, the highstand deposits are terminated by a discontinuity surface, or an interval indicating subaerial exposure: the "sequence boundary" (**SB**) or the "sequence boundary zone" (**SBZ**) (Fig. 4.1a). Theoretically, this surface or interval corresponds to the time of fastest relative sea-level fall and, thus, to destruction of accommodation space. Thus, the possibility to create subaerial exposure is highest.

Most SBZs on the large scale reflect times of general relative sea-level fall and thus correspond to deposits that are attributed to the late highstand systems tract and/or to the early lowstand systems tract (Vail et al. 1977). Because of shallow depositional environments on the studied platform, deposits representing a low relative sea-level usually are very thin or not developed at all. Additionally, it is very difficult to distinguish, in terms of facies, deposits that correspond to a lowstand in relative sea-level ("lowstand deposits", **LD**), from deposits that formed during the initial phase of the subsequent transgression ("early transgressive deposits", **eTD**) (Fig. 4.1a). In the traditional sequence stratigraphic model, the sediments of the lowstand systems tract are located below the platform edge on the slope. Thus, in order to avoid confusion, all deposits that are located between well-developed SB and TS and thus correspond to a low sea level and/or the beginning of the subsequent

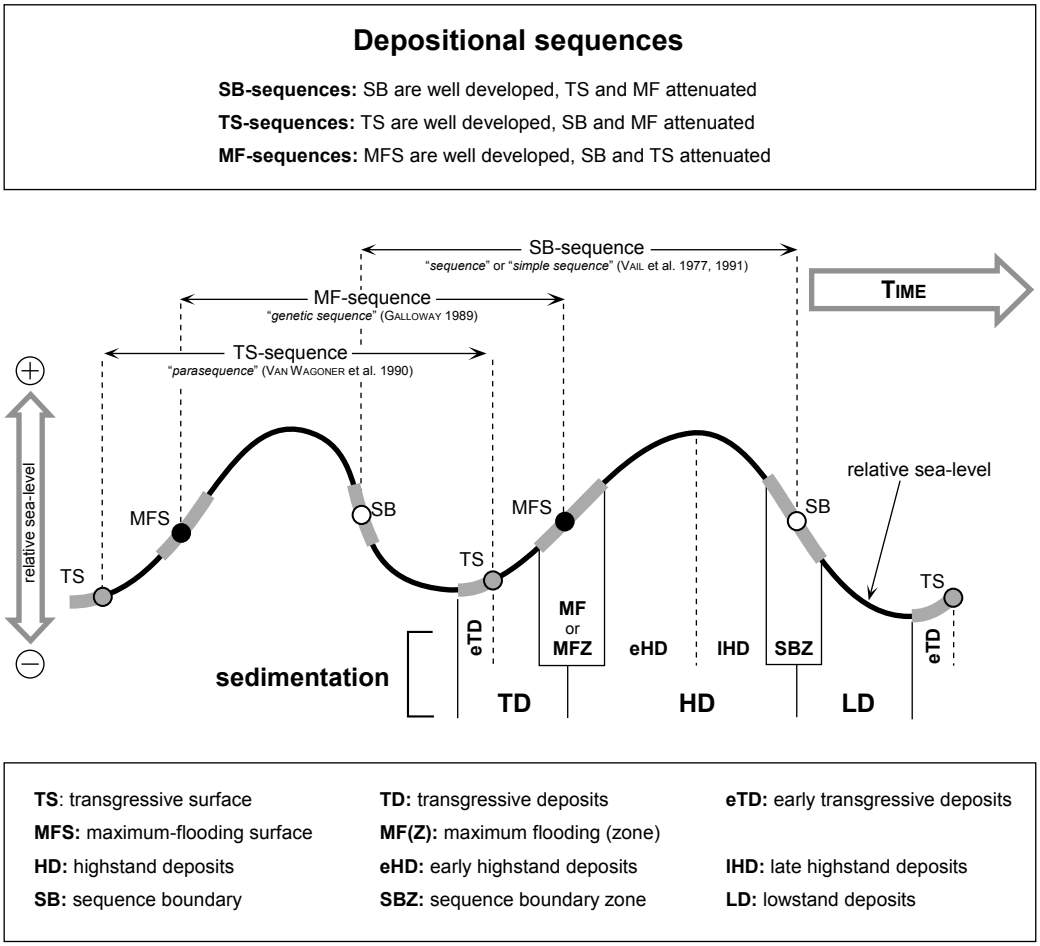

Fig. 4.1a - Sequence model. The theoretical position of characteristic deposits and discontinuity surfaces is independent of the time scale and amplitude of relative sea-level change. For more details on the terms used and the development of the concept refer to text. Based on Hillgärtner (1999) and Hug (2003).

Fig. 4.1b - (facing page) Examples for SB-, TS-, MF-, and aggrading sequences. Note that, even if the examples have been carefully chosen, these are real sequences from the sections measured for this work, so they may to a certain extent display characteristics of more than one only sequence type (see text for discussion). For legend, refer to Fig. 4.6a.

transgression are labelled early transgressive deposits (eTD). These deposits have the lowest preservation potential and tend to be eroded and reworked during the subsequent transgression (Walker 1995). Consequently, transgressive surfaces in many cases coincide with the sequence-bounding exposure surfaces (**SB/TS**). Schlager (1999), with reference to the type-1 and type-2 sequence boundaries defined by Vail et al. (1977, 1984), proposed that the flooding surface between highstand deposits and the overlying transgressive deposits, without evidence of sea-level fall or lowstand deposits in between, as a third type of sequence boundary for carbonate successions. Another special type of discontinuity surface that is unique to carbonate platforms and ramps are "drowning unconformities" (Schlager 1989). They are rooted in the phenomenon of "give up" (Neumann & Macintyre 1985), which means a major reduction or even a cessation of carbonate production after a rapid rise in relative sea-level. As under favourable conditions the production and accumulation rates of carbonate platforms easily outpace any rise in relative sea-level (Kendall & Schlager 1981), a give-up or drowning usually goes hand in hand with a significant change in geological and/or environmental conditions.

A specific feature in the studied platform sections is fabric destructive dolomitization that commonly masks microfacies and sedimentary features indicating supratidal conditions (cf. Fig. 4.2). Consequently, dolomite caps are interpreted as sequence boundary zones (SBZ) – lacking hard evidence, but backed up by the general context and/or lateral correlations.

Example for a SB-sequence

Yenne section (19.5-23.7m)

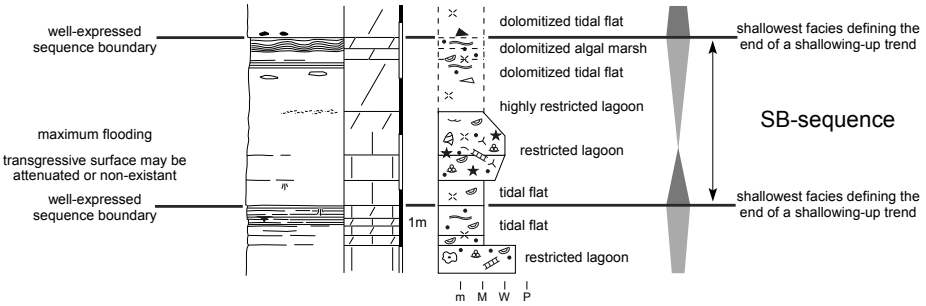

Example for a TS-sequence

La Dôle section (87-92m)

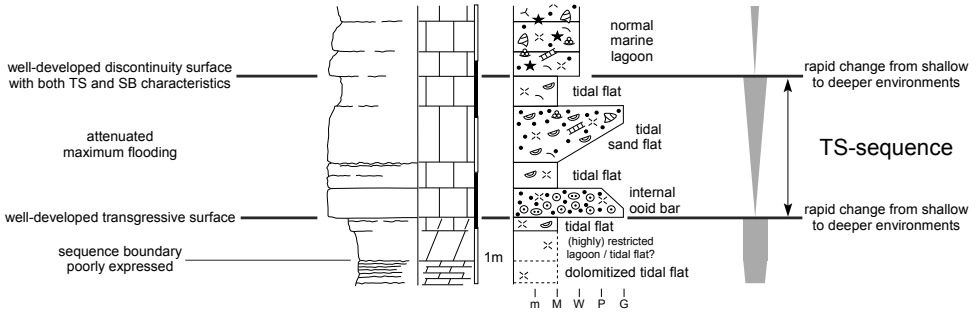

Example for a MF-sequence

Noirvaux section (6.7-12m)

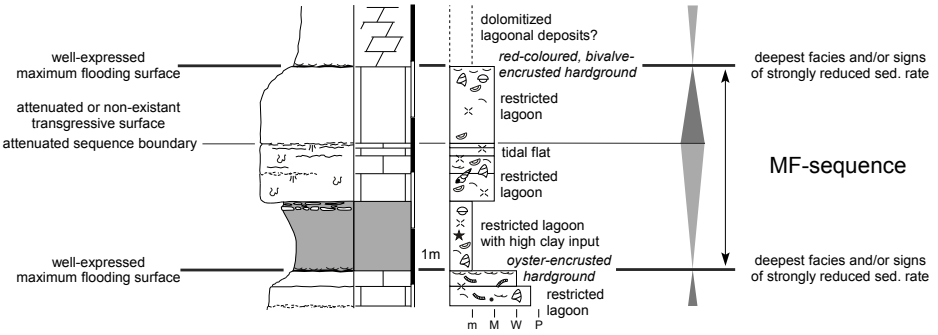

Example for an aggrading sequence

La Dôle section (110-115m)

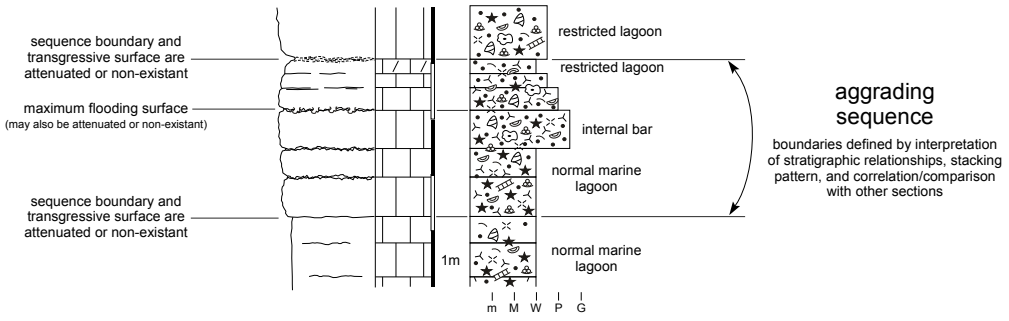

For similar reasons, previous workers have suggested that the surface underlying transgressive deposits is the most appropriate discontinuity to choose for delimiting a sequence: Arnott (1995), Hunt & Tucker (1995) and Naish & Kamp (1997) placed sequence boundaries above regressive deposits (either forced or normal regressive systems tracts) and beneath transgressive deposits because the transgressive surface of erosion (TSE) is typically extensive, easily identifiable in sections (either outcrops or cores), and, by its very nature, usually well preserved in the stratigraphic record. Although the TSE may form a sharp, widespread lithologic boundary in the stratigraphic record, Demarest & Kraft (1987) argued that this surface should not be regarded as a hiatus between depositional sequences when it does not coincide with the regressive surface of erosion (= sequence boundary sensu Vail et al. 1977).

4.2.2 Types of depositional sequences

Unifying all high-frequency depositional sequences as, e.g., "*parasequences*" (Mitchum & Van Wagoner 1991) means neglecting important sedimentological information. Vail et al. (1991) introduced the term "*simple sequence*" to describe small (elementary) depositional sequences, but the term was never accepted by the scientific community, mainly because a clear concept integrating them into the sequence-stratigraphic model was missing.

Four descriptive types of high-frequency depositional sequence in the sections of the Jura platform can be differentiated on the basis of their characteristic facies evolution and the enhancement or attenuation of characteristic discontinuity surfaces (Fig. 4.1b; cf. Strasser et al. 1999, Hillgärtner 1999). Rather than shallowing or deepening, facies evolution may also indicate changes from more open-marine to more restricted conditions and vice versa. The environmental significance, however, is comparable to that of bathymetric changes.

Deepening-shallowing sequences defined by sequence boundaries (SB-sequences)

In this sequence type, facies evolution through time indicates that water depth first increased, then decreased. In shallow-water carbonate-dominated sedimentary environments their evolution is commonly asymmetric, i.e., many depositional sequences are composed of a thin deepening-up and a thick shallowing-up part (e.g., Strasser 1988, Jones & Desrochers 1992; Pratt et al. 1992). Transgressive lag-deposits at the base of such sequences are common, resulting from the time when, for example after an emersion, carbonate production was in start-up mode (Kendall & Schlager 1981). The shallowing-up trend is due to the high production and accumulation rates of carbonate platform systems which — as long as environmental conditions are favourable — easily outpace any relative sea-level rise ("*catch-up phase*", Kendall & Schlager 1981). The shallowing-up trend may additionally be enhanced by the deceleration of sea-level rise and a subsequent fall. If relative sea-level drops below the depositional surface and non-consolidated sediment is eroded, the resulting erosion surface is classified as regressive surface of erosion (RSE, Caron et al. 2004) and interpreted as the boundary of the depositional sequence (SB). Prolonged emersion can lead to vadose cementation. If the climate is humid enough, a prolonged emersion may also produce chemical dissolution of carbonate grains ("leaching"), (incipient) pedogenesis, and karstification. This type of depositional sequence corresponds to the definition of classical sequence stratigraphy (Vail et al. 1987) where the sequence boundaries form during relative sea-level fall. However, the boundaries of such sequences may also be subtidal or intertidal surfaces that reflect the relatively shallowest conditions within the sequence. Deepening–shallowing sequences that never reach intertidal or supratidal facies have been termed "subtidal cycles" by Osleger (1991). Shallowing-up sequences can also be created by progradation or migration of sedimentary systems (e.g., Ginsburg 1971; Pratt & James 1986) without being related to sea-level fall. However, if supratidal facies and/or vadose diagenesis are directly superimposed on subtidal sediments, or if regressive surfaces of erosion can be correlated over large distances, relative sea-level fall must be involved (Strasser 1991).

Deepening-shallowing sequences defined by flooding surfaces (TS-sequences)

These sequences display a comparable internal facies evolution as the sequences described above. The main difference is that the bounding discontinuities mark a rapid facies change from the relatively shallowest (or most restricted) to deeper (or more marine) sedimentary environments ("*transgressive surfaces*"). As these surfaces are the most visible in the field and as evidence of subaerial exposure may lack or may not be well expressed, they define the depositional sequence. Facies changes related to sea-level fall or maximum flooding may be identified but are either too subtle to develop a well-marked bedding plane, or pre-existing surfaces may have been eroded during sea-level fall or the following transgression ("*transgressive surface of erosion*", Nummedal & Swift 1987, Bhattacharya 1993, Caron et al. 2004; also termed "*ravinement surface*" by Swift 1968). Such sequences are usually strongly asymmetric (cf. Fig. 4.1b) can be compared to the "*parasequences*" of Van Wagoner et al. (1990), which are defined as being bounded by marine flooding surfaces (cf. Fig. 4.1a).

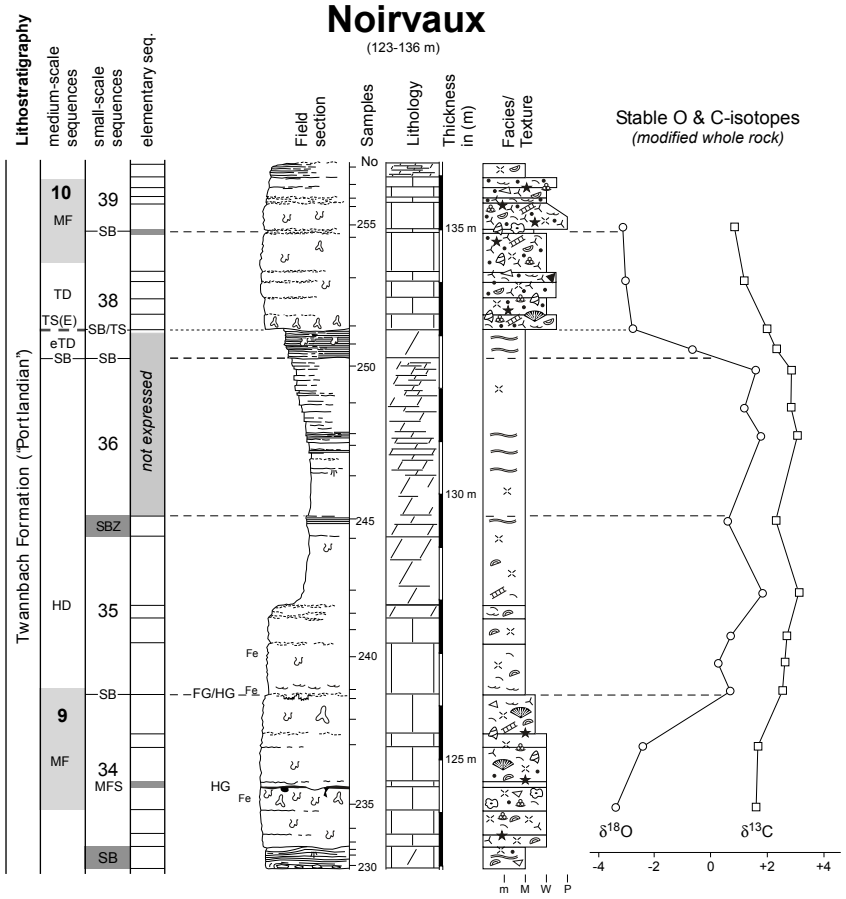

Fig. 4.2 - Sequence-stratigraphic significance of dolomite caps. With the predominant dolomitization mechanism controlled by sea-level changes, most of the observed dolomites relate to medium-scale (late) highstand deposits (cf. Chap. 3). Yet, due to the fabric destructive nature of dolomitization, most sedimentary evidence for identifying a sequence-bounding discontinuity surface is destroyed. So, it is not clear how to interpret the transgressive surface of erosion (TSE) at 133.1 m or the base of the dolomitized laminites at 132.6 m. Is the TSE to be interpreted as SB/TS or only as TS? Where exactly is the bed (or the surface) representing maximum regression? And which significance (if at all) has the sharp surface at the base of the dolomitized laminites? In this specific case, stable isotope analysis helps to solve the problem: Maximum lagoonal restriction, characterized by high $\delta^{18}O$ values (cf. Chap. 3), is reached in sample No250. This is followed by a rapid drop back to the "base level" of about -3‰, reflecting a stepwise opening of the sedimentary system. Consequently, the base of the dolomitized laminites represents the point of maximum regression, i.e. a medium-scale sequence boundary (SB). Consequently, the TSE must be the related medium-scale TS and the laminites in between can be denominated as early transgressive deposits (eTD). See text for definitions and discussion of the application of sequence stratigraphic nomenclature.

Shallowing-deepening sequences defined by maximum flooding and/or condensation (MF-sequences)

In such sequences, facies evolution shows an inverse trend (shallowing-deepening) and surfaces of maximum-flooding are best marked in the field. Bioturbation may be abundant around these surfaces, suggesting low sedimentation rates. Other maximum-flooding surfaces are developed as firm- or hardgrounds, partly with fossil or mineral encrustations, suggesting strongly reduced sedimentation rates. MF-sequences may be completely subtidal but most examples in this study show a thin, poorly expressed interval of inter/supratidal facies in between the two bounding maximum-flooding surfaces. This type of sequences can be compared to the "*genetic sequences*" defined by Galloway (1989) (cf. Fig. 4.1a).

Aggrading sequences

Facies changes in meter-scale depositional sequences are in some cases too subtle to allow identification of a shallowing-up or deepening-up trend. Furthermore, if the depositional environment was constantly subtidal, bounding discontinuities only indicate omission or minor erosion and thus yield no substantial information if the surface was formed during a rapid sea-level rise or a sea-level drop cutting a lagoon off from sediment supply.

However, when such intervals occur in a vertical context of repetitive facies changes between clearly identified depositional sequences of a similar scale, they can be classified as sequences. In such cases, analyses of isotopic composition, clay minerals, palynofacies, or, as in most cases in this study, of the general context with lateral correlations can yield information on the environmental significance of the sequence.

These four types of platform sequence are to be regarded as models or end members in a continuous spectrum of sequence architectures. In reality, any given sequence can combine features of the above-mentioned type-sequences to a different extent. For example, in transitional zones where the long-term trend of relative sea-level changes from rise to fall, all types of discontinuities can be well expressed. It may occur that a MF-sequence overlaps with a subsequent SB-sequence. The attribution to either sequence type has to be done according to the most appropriate interpretation of the long-term sea-level trend, on the basis of lateral correlations and the best marked bounding surfaces. In the same way, aggrading sequences do not show typical characteristics of any sequence type. However, seen in the context of relative sea-level changes and surrounding, unequivocally defined sequence types, all sequences can be interpreted as being on the more transgressional or more regressional long-term trend. Consequently, and following the model, most sequences can be attributed to TS-, MF-, or SB-sequences. In places where all discontinuities are equally well expressed, SBs are chosen as delimiting boundaries.

Basinal sequences

Basinal settings are characterized by only one type of depositional sequence. These sequences cannot be compared with their counterparts found on the platform. In terms of microfacies, they show little internal variation and consist either of marl-limestone alternations, or, when lacking relevant quantities of marl, are merely recognizable by changes in bed thicknesses or stacking patterns.

Marl-limestone alternations may have different origins: Many are interpreted to result from climatically induced changes in planktonic carbonate productivity and/or detritic input of clays (e.g., Einsele & Ricken 1991, Pittet et al. 2000, Mattioli & Pittet 2002, Pittet & Mattioli 2002, Colombié 2002). Pittet & Strasser (1998) and Colombié & Strasser (2003) showed that cyclical phases of export of carbonate mud from the platform to the basin may also contribute. In contrast to these externally forced mechanisms, Ricken (1986), Munnecke & Samtleben (1996), Westphal et al. (2000, 2002, 2004a, b), and Munnecke & Westphal (2004) proposed differential diagenesis during burial. In some, but specifically in larger-scale depositional sequences, lowstand deposits consist of relatively thick packages of resedimented carbonates (cf. Strohmenger & Strasser 1993). Major maximum floodings can be expressed through sediment starvation, i.e. condensed sections and/or discontinuity surfaces that display evidence for condensation (e.g., iron/manganese crusts, glauconite, fossil concentrations, and bioturbation). Such variability can be interpreted in terms of changes in relative sea-level, climate, and sedimentation rate.

4.2.3 Hierarchy and stacking of depositional sequences

In all studied sections the depositional sequences are stacked in a hierarchical pattern. Four hierarchies of sequence are recognized:

Elementary sequences

These sequences are the smallest units recognizable in the field. They commonly correspond to one bed, bounded by discontinuity surfaces. On a first look, vertical facies distributions in single beds may seem to be rather homogenous. On a closer look, however, deepening-shallowing trends or shallowing-up trends of facies evolution can be identified in many cases (SB- or TS-sequences). These depositional sequences represent the record of the shortest cycle of visible environmental change. The thickness of elementary sequences usually ranges from a few centimeters to a few 10s of centimeters. In the upper Reuchenette Formation, maximum thicknesses of several meters are attained. Beds that can be clearly attributed to event deposits (tempestites, turbidites, etc.) are not considered as elementary sequence.

Small-scale (composite) sequences

Small-scale sequences are composed of 2 to 6 elementary sequences. They frequently show a well-defined deepening-shallowing facies evolution (SB- or TS-sequences), but shallowing-deepening trends also occur (MF-sequences). In a few cases the hierarchical stacking of different types of elementary sequence composing small-scale sequences shows clearly a notion of self-similarity. Asymmetry in the facies evolution (shallowing vs. deepening) is frequently developed (Strasser 1991). In a small-scale deepening-shallowing sequence, elementary deepening-shallowing sequences are predominant and the shallowing-up trend becomes especially evident at the upper boundary of a composite sequence. The inverse pattern is true for shallowing-deepening sequences.

If expressed at all, small-scale sequences in basinal settings commonly are defined by thickening-upwards or thinning-upwards trends of a set of 4 to 6 limestone beds. These trends are often subtle and only observable in parts of the studied sections. Small-scale sequences on

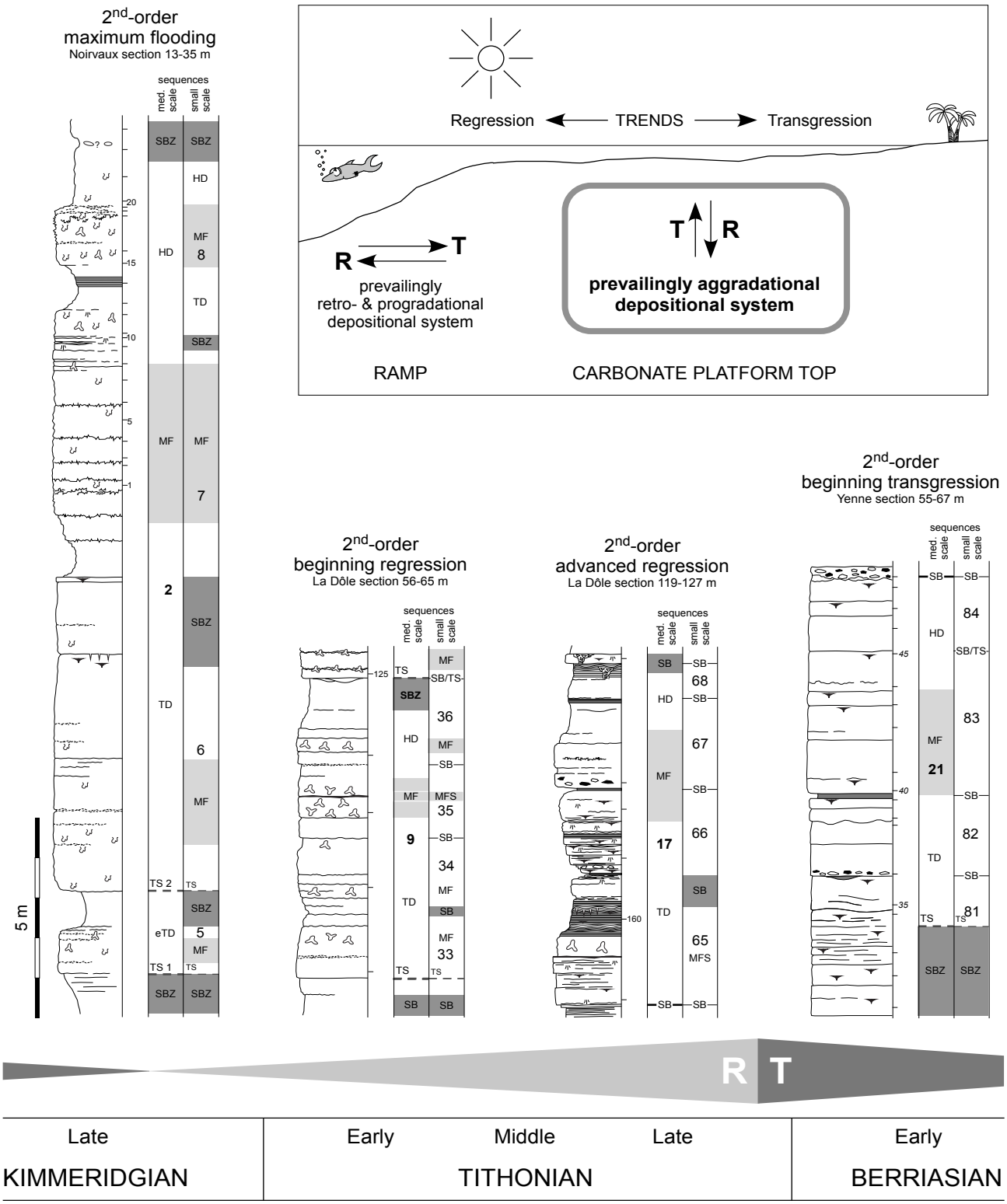

Fig. 4.3 - In flat carbonate platform interiors, sea-level changes translate prevailingly into aggradational patterns. Lateral variations in stratal geometries are very gradual, unlike in marginal settings, where retro- and progadational patterns will develop (D'Argenio 1999). Four typical examples for the evolution of medium-scale sequence architecture from the studied platform sections document this principle. Note that the 2nd-order T/R-cycles translate mainly into thickness differences (due to differing rates in accommodation gain), whereas the general facies evolution from the open-marine to restricted, bioturbated lagoons of the Late Kimmeridgian to the tidal flats of the Late Tithonian/Early Berriasian seems to reflect the overall southward progradation of the platform. This pattern is ended with a major transgression in the Early Berriasian (base of the open-marine Pierre-Châtel Formation on the southern Jura platform and a switch to marly sedimentation in the basin).

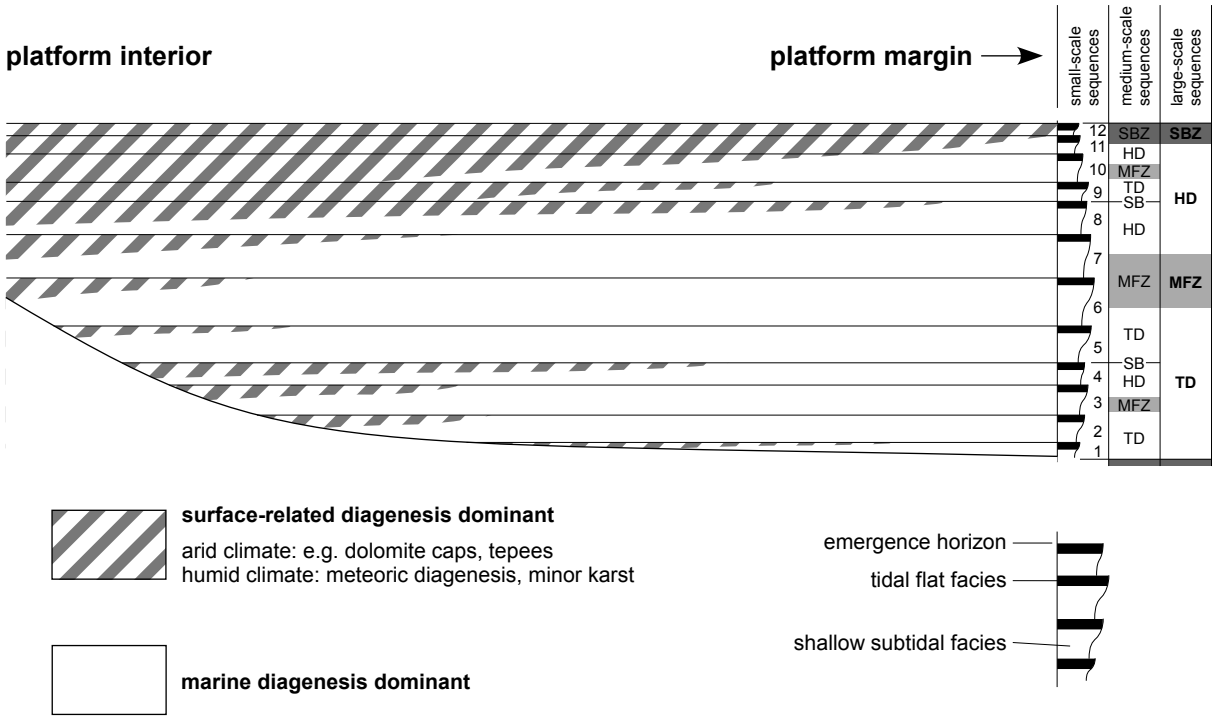

Fig. 4.4 - Generalized scheme indicating the lateral and vertical variations in early diagenesis linked to small-, medium-, and large-scale sequences. The type of subaerial (or surface-related) diagenesis depends very much on climate with dolomite caps characterizing more arid climate, and meteoric cements and palaeokarst features typical of a more humid climate. After Purser et al. (1994).

the platform and in the basin measure from a few tens of centimeters to a few meters.

Medium-scale (composite) sequences

Medium-scale sequences generally are composed of 4 small-scale composite sequences (Fig. 4.3, Pl. 20/3). If a smaller number of small-scale composite sequences builds up the medium-scale sequence, this is always accompanied by evident features of erosion or non-deposition. Facies evolution is comparable to those of the small-scale composite sequences but usually shows a higher degree of complexity. Additionally, medium-scale sequences are delimited by well-developed discontinuity surfaces (which may be multiplied, see below) testifying to exposure or condensation (SB/TS-sequences). Commonly, they display a rather symmetric deepening-shallowing facies evolution and a well developed MF. Thickening-up of beds and small-scale sequences may appear in the lower part, thinning-up in the upper part. Another common phenomenon at the base and the top is dolomitization. At the base, dolomitization is limited to early transgressive deposits, whereas considerable parts of the highstand deposits, in rare cases even the majority of the medium-scale sequence, can be dolomitized (dolomite caps, cf. Figs 4.2 and 4.4, see also Chap. 3). In some cases a characteristic stacking of different sequence types, in a similar way as in large-scale composite sequences, can be observed (see discussion below).

Medium-scale sequences in the basin can only be detected on the basis of abrupt changes in the stacking pattern of the small-scale sequences. This is expressed by changes in thickness of limestone and/or marl layers, which mirror general changes in sedimentation rate and changes in the ratio of lime versus clay sedimentation. Sudden variations of this type can be marked by small slumps or turbidites, indicating different environmental conditions at the boundaries of these sequences. A gradual increase of marls towards the center of the sequence can be present. In many cases, however, changes in colour and weathering aspect that delimit sequences are the only evidence and point to changing contents of trace elements such as iron or clay content. The thickness of medium-scale composite sequences on the platform and in the basin varies from a few meters to a few tens of meters.

Large-scale (composite) sequences

Large-scale sequences are composed of several medium-scale sequences (in most cases 2 or 3). They are characterized by a deepening-shallowing facies evolution, with individual trends either symmetrically expressed,

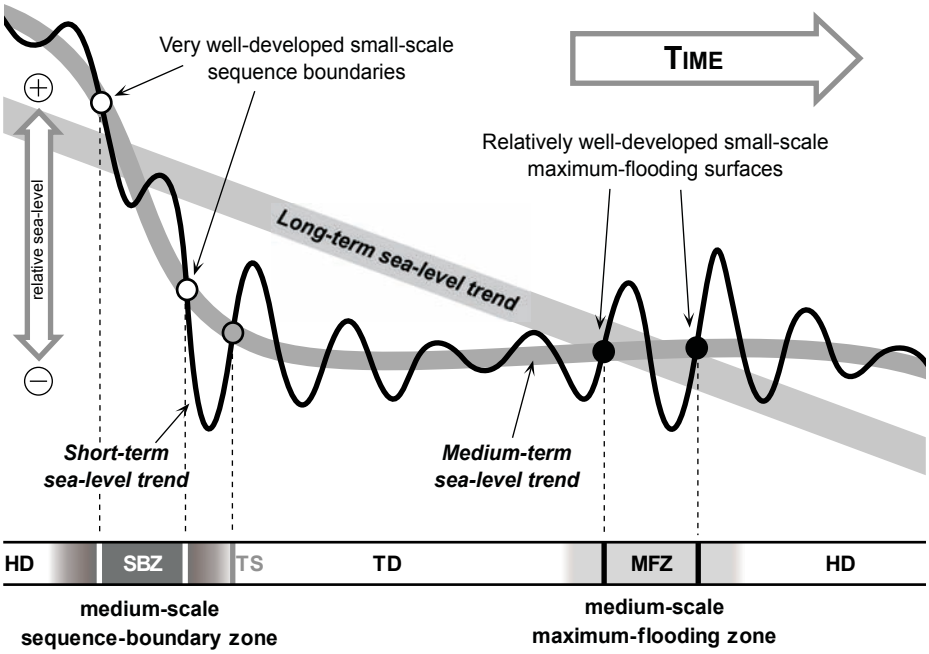

Fig. 4.5 - Superimposed relative sea-level changes of different orders can lead to the enhancement (shown here) or attenuation of trends in sea-level change. The changes in amplitude and phase-relations of small-scale sequences create well-expressed or attenuated zones of repeated, characteristic discontinuity surfaces rather than single unconformities on the large scale ("3rd order"). After Strasser et al. (1999).

or either of the two trends can predominate. Large-scale sequences are bounded by well-developed exposure surfaces (SB-sequences). In some cases, subsequent transgressive surfaces are equally or even better expressed than the sequence boundaries (SB/TS-sequences). Commonly, the exposure surface defining a large-scale sequence boundary is underlain by a succession of inter- to supratidal facies (that is frequently dolomitized; Fig. 4.4). However, it is rarely one single unconformity that defines a large-scale sequence boundary, but rather a zone of repetitive surfaces (Fig. 4.5). These surfaces themselves define smaller-scale sequences, commonly of the deepening-shallowing type. Small-scale deepening-shallowing sequences bounded by flooding surfaces (TS-sequences) are usually well expressed in the deepening phase (TD) of the large-scale sequence and are overlain by shallowing-deepening sequences (MF-sequences) in the overall deepest and/or most open facies (MF). Here, small-scale sequences commonly attain their greatest thicknesses. Small-scale sequences of the highstand deposits (HD), deposited during the large-scale shallowing trend, tend to be bounded by exposure surfaces (SB-sequences) and frequently display a thinning-up evolution.

Large-scale sequences in the Vocontian Trough are delimited by significant event deposits (turbidites or slumps). Lowstand deposits tend to be relatively thick and massive with influx of platform-derived detritus. Towards the maximum flooding clay content and indications for condensation usually become more abundant. In both settings, large-scale sequences measure several tens of meters. They correspond to 3rd-order sequences of the traditional sequence stratigraphic model (e.g., Vail et al. 1991).

Stacking pattern: the result of superposition of relative sea-level changes

The different sequence-types described above are arranged in the following way:

- large-scale sequences are superimposed on a long-term transgressive or regressive trend ("2nd-order sequences" of Vail et al. 1991 or "T/R facies cycles" sensu Hardenbol et al. 1998, cf. Fig 1.9)
- 1 large-scale sequence usually consists of 2 or 3 medium-scale sequences
- 1 medium-scale sequence usually consists of 4 small-scale sequences
- 1 small-scale sequence consists of 2 to 6 elementary sequences

By the superposition of sequences of different scale (i.e. different order), complex stacking patterns develop that are defined by changes in thicknesses of sequences and beds, facies development (deepening/shallowing trends), and the enhanced or attenuated expression of discontinuity surfaces (Fig. 4.3 and 4.5). Characteristic

Lithology

- marl
- marly limestone
- limestone
- dolomitic limestone
- dolomite
- dedolomite
- cornieule
- breccia
- chert nodules

Texture

m	marl
M	mudstone
W	wackestone
P	packstone
G	grainstone

Relative abundance

- present
- common
- frequent
- abundant
- dominant (rarely applied)

Key Surfaces

- omission/condensation
  deduced from sedimentological evidence such as hard-grounds, firmgrounds, or heavily bioturbated horizons
- emersion
  deduced from sedimentological and/or microfacies, e.g. desiccation cracks, bird's eyes, incipient pedogenesis
- erosion surface (major / minor / with reworking)
  deduced from outcrop observations
- vadose diagenesis
  deduced from microfacies interpretation, e.g. microkarstic features and/or vadose cements (partly in combination with infill sediment and leaching)
- FG/HG firmground / hardground

Bathymetry

- supratidal
- intertidal
- subtidal

Sedimentary structures

- root casts
- *Microcodium* sp.
- firm-, hardground
- bird's eyes
- tepee structures
- desiccation cracks
- evaporite pseudomorphs
- circum-granular cracks
- keystone vugs
- bioturbation (*undifferentiated*)
- *Thalassinoides* sp.
- worm tubes
- cross bedding (foresets)
- low angle cross bedding
- plane bedding
- abrupt change in grain diameter
- current ripples
- wave ripples
- flasery aspect
- nodular aspect
- solution seams
- stylolitic contact

Facies - descriptive elements

- peloids
- ooids
- oncoids
- *Favreina* sp.
- intraclasts
- black pebbles
- bioclasts (undifferentiated)
- ammonites
- belemnites
- gastropods
- brachiopods
- bivalves
- oysters
- inoceramus
- corals
- coral debris
- sponge spicules
- *Cladocoropsis mirabilis*
- *Cayeuxia* sp.
- *Lithocodium / Bacinella*
- serpulids
- bryozoans
- foraminifera
- dasyclad algae
- charophytes
- ostracodes
- echinoderms
- plant fragments
- fish remains
- microbial mats

Non-calcareous grains

Qtz	quartz
Py	pyrite
Fe	Fe-crusts or red staining
Ch	chamosite

Fig. 4.6a - Legend for all logs of the measured sections.

stacking patterns can be correlated over 10s of kilometers. Therefore, and on the account of the inferred bathymetric changes, they can be attributed to the superposition of different orders of changes in relative sea-level.

This superposition of relative sea-level changes not only creates depositional sequences at different scales, but also leads to multiplication of their characteristic discontinuity surfaces (Fig. 4.5). Thus, a sequence boundary of, e.g., a large-scale sequence will frequently not consist of one well-marked surface but of a repetitive group of regressive discontinuity surfaces, each of them bounding small-scale or elementary sequences (cf. Montañez & Osleger 1993, Pasquier & Strasser 1997). Such clusters of surfaces are referred to as "*maximum-flooding zone*" (**MFZ**), or "*sequence-boundary zone*" (**SBZ**). Theoretically, also a "*transgressive-surface zone*" (**TSZ**) can be defined. However, as medium- and large-scale transgressive surfaces are usually well expressed in the studied sections, they are numbered as $\mathbf{TS_1}$, $\mathbf{TS_2}$, etc., with the last well-expressed TS dividing early transgressive deposits (eTD) from transgressive deposits (TD).

Increasing or decreasing amplitudes, asymmetry, and varying phase relationships of the sea-level curves can enhance or attenuate the formation of such zones (cf. Hillgärtner 1999, Strasser et al. 1999). When a small-scale relative sea-level fluctuation is superimposed on a larger-scale sea-level rise, the flooding will be enhanced, whereas the small-scale sea-level fall will be attenuated (Fig. 4.5). Consequently, MF-surfaces will be marked better in the resulting sedimentary record than sequence boundaries. Sequence boundaries, in contrast, will be enhanced when falling trends of different orders are combined, and transgressive surfaces will be underlined when different orders of initial flooding are synchronous. If high-frequency fluctuations of high amplitude are superimposed on a rapidly falling long-term sea-level trend, accommodation space is available, if at all, only for a short time during the high-frequency sea-level rises. The preservation potential of such sequences will be rather low and the sedimentary record may be incomplete ("missed beats" sensu Goldhammer et al. 1990, see also Chap. 6). During moderate- to low-amplitude fluctuations, however, the intensity of condensation or exposure in a surface zone increases towards the strongest rate of sea-level rise or fall on the long-term trend, respectively. This leads to the extreme expression of SBZs with quasi non-existing MFs when reaching peak regression of the Late Jurassic long-term regressive trend (cf. Fig. 4.3).

4.3. Sections

In order to avoid the multiple (re-)appearance of the section panels and therefore unnecessarily increasing the size of this thesis, observations, microfacies data, and interpretation are all integrated: i.e. the figures presented in this chapter already display the detailed results from sequence- and cyclostratigraphic interpretation (Chaps. 4 and 6) and depositional sequences in the far left columns are already numbered according to the best-fit correlation put forward in Chap. 6.

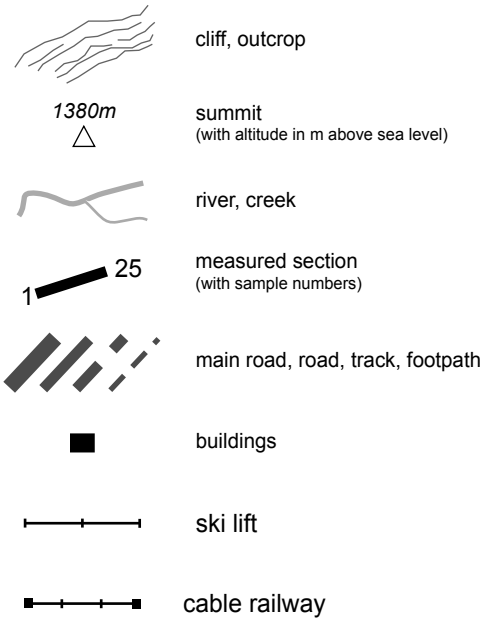

Fig. 4.6b - Legend for all figures describing geographical positions of the measured sections.

Sections are treated in the order platform – slope – basin, in each category from NE to SW (following the approximate direction of the Late Jurassic continental margin and today's extension of the Jura Mountains; cf. Fig. 1.3). The section logs are mostly self-explanatory, and only the most prominent or controversial features are described in this chapter.

4.3.1 Platform sections

Courtedoux – Sur Combe Ronde *(Figs 4.7, 4.9)*

located approximately 4 km W of Porrentruy (JU)

National topographic map of Switzerland 1 : 25 000, sheet 1182 *Ste-Croix*

Base of section: X: 568 950
Y: 249 990

The outcrop of Courtedoux – Sur Combe Ronde was created in early 2002, by the Section of Archaeology and Palaeontology of the Cantonal Culture Office of the Canton

Jura that constantly monitors the construction works on the new A16 motorway ("Transjurane") in the Ajoie region (Fig. 4.7). The scientists quickly realized that they had discovered one of the – or even the – biggest sauropod tracksite of Jurassic age in Europe (Marty 2003, 2004, Marty et al. 2003). The dinosaur-track bearing surface is a laminated tidal flat showing various signs of emersion. In addition to this spectacular discovery, several ammonites found in subtidal parts of the section allow for an exact biostratitigraphic dating down to subzone/horizon level (cf. Fig. 4.8). Beds are nearly horizontal and thus give a unique access to huge surfaces that are studied in detail by the Section of Archaeology and Palaeontology. In order to match the graphic style of this study, the section presented here was redrawn from the highly detailed, original log measured by the Section of Archaeology and Palaeontology (W. Hug, pers. comm.).

Lithostratigraphy and sedimentology

Due to the dip of outcropping beds oriented subhorizontally to the land surface, the outcrop exposes a section of only about 9 m thickness. Yet, it shows a very characteristic and varied facies succession: Its base consists of 1 m of intertidal and supratidal flat environment that also includes the main sauropod track surface (level 1000, Fig. 4.9a, b). Then a 4 m-succession of mostly subtidal wacke-, pack-, and grainstones with rare coral rubble follows. In the upper 4 m of the section the style considerably changes and is predominated by hardgrounds and marl layers that contain up to 20% chamosite. At about 12 m, further search has yielded a bored, coral-bearing horizon. The thick marl layer at 8 m is highly fossiliferous with millions of *Exogyra virgula*. In the Ajoie region, this bed is known as "the *virgula* Marls". However, due to excellent biostratigraphic control (Fig. 4.8) it is clear that these "*virgula* Marls" are definitely older than their counterpart that defines the boundary between the Reuchenette and the Twannbach formations in the Central Jura. They are thus called "lower *virgula* Marls" in this study.

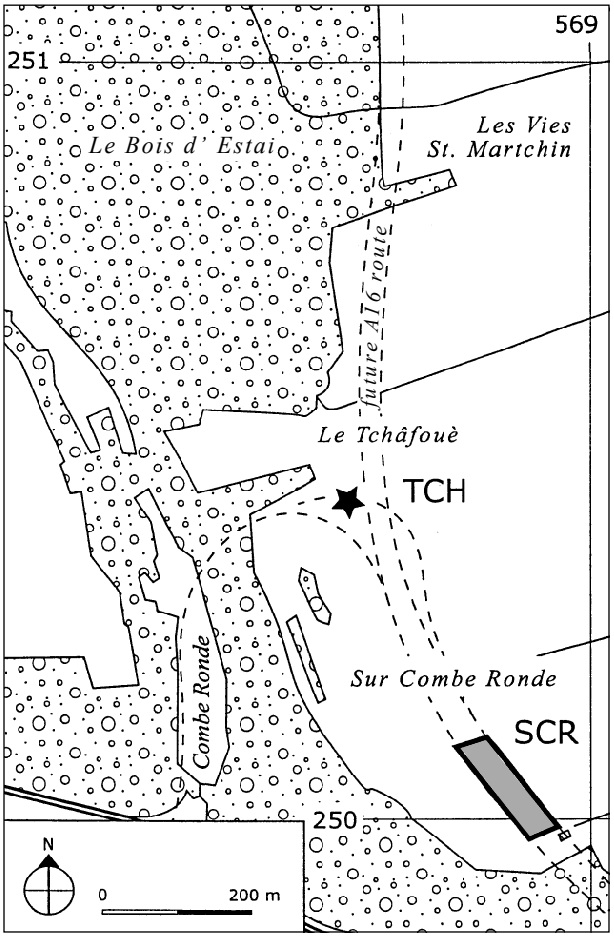

Fig. 4.7 - Location of the "Sur Combe Ronde" (SCR) and "Le Tchâfouè" (TCH) excavations near Courtedoux. The future route of the A16 motorway is marked in dashed lines. From Marty (2003), modified. For legend see Fig. 4.6b.

Biostratigraphy

The Courtedoux – Sur Combe Ronde section furnished several cephalopods that allowed for an excellent biostratigraphic control (Marty 2004, 2003, Marty et al. 2003).

Orthaspidoceras schilleri
Aspidoceras calenatum
Physodoceras longispinum
?*Paracoeroceras* sp.
Nautiloidea indet.
Ammonoidea indet.

Thus, the section can be dated to the Late Kimmeridgian, around the boundary of the *Mutabilis* and *Eudoxus* Zones. The interval between layer 2400 and layer 4000 represents the *Schilleri* Horizon of the *Lallierianum* Subzone, uppermost *Mutabilis* Zone.

Sequence stratigraphy

The section is too short to run a valid sequence- and cyclostratigraphic analysis. Nevertheless, 3 small-scale sequences can be defined. The package of tidal flat facies at the base of the section could relate to a larger-scale SB and the hardground- and marl-dominated sedimentation in the upper part to a larger-scale MF. Surprisingly, the characteristic lithostratigraphic succession and stacking pattern of the Courtedoux – Sur Combe Ronde section corresponds literally bed-by-bed to the lower parts of the Noirvaux section (Fig. 4.11). The age of the interval in question at Noirvaux, estimated from cyclostratigraphic analysis (Chap. 6), fits perfectly, too. Consequently, it was chosen to regard the correlation as valid, allowing for denomination and numbering of depositional sequences

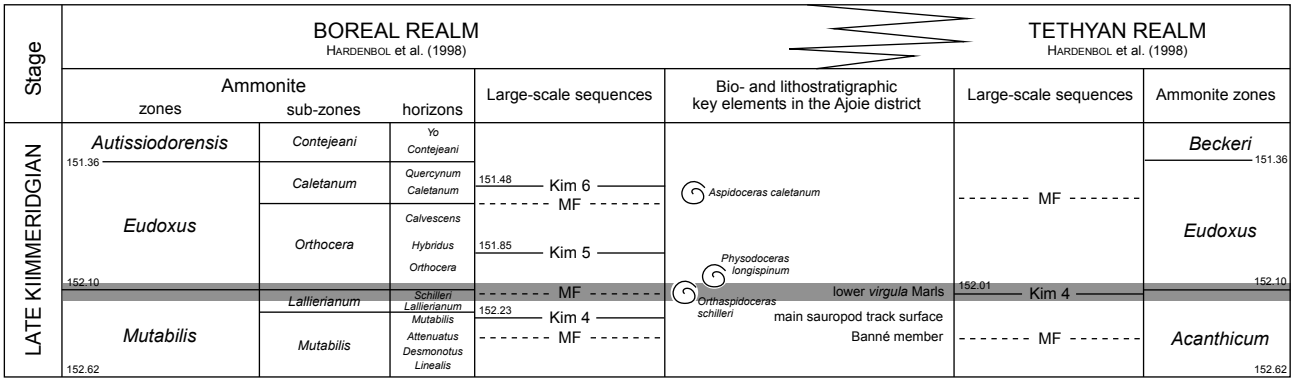

Fig. 4.8 - Chrono-, bio-, and lithostratigraphic context and key elements of the Late Kimmeridgian in the Ajoie district (after Marty et al. 2003). Numeric ages after Hardenbol et al. (1998).

on all scales. Vice versa, the Courtedoux – Sur Combe Ronde section adds an excellent biostratigraphic pin point to the other studied sections.

Noirvaux *(Figs 4.10, 4.11)*

approx. 4 km N of S^{te}-Croix (VD),
13 km NW of Yverdon-les-Bains (VD)

National topographic map of Switzerland
1 : 25 000, sheet 1182 *S^{te}-Croix*

Base of section: X: 529 450
Y: 190 025

A complete section from the *Gorge de Noirvaux* was first published by Rittener (1902). Bläsi (1980), working on the "Portlandian", analyzed the upper half of the section (starting at the hardground at 63.3 m, this study). Kettiger (1981) measured the lower part of the section, beginning at the top of the Argovian (Middle Oxfordian) up to the upper Reuchenette Formation (condensed interval at 77.2 m, this study). Later on, Mouchet (1995) essentially presented a simplified version of the detailed work of Kettiger (1981), and placed the section within a regional relationship.

Lithostratigraphy and sedimentology

The section begins with the characteristic, marly interval of the lower *virgula* Marls (cf. Courtedoux – Sur Combe Ronde section) at the parking lot north of the Noiraigue Bridge (Figs. 4.10 and 4.11). The massive cliff at the bridge marks the beginning of the Upper Reuchenette-Formation, characterized by a lagoonal succession of thick-bedded mud- and wackestones with intercalated dolomitic intervals, also yielding a prominent interval of cross-bedded peloid-grainstones (ca. 50-63 m) that are interpreted to have been deposited under high-energy, normal-marine conditions (external bar). The upper limit of these grainstones is defined by thin tidal flat deposits and a sharp (erosional?) discontinuity surface (62.7 m), which, in turn, is directly followed by a heavily bored hardground (63.3 m). The bed in between these two surfaces is heavily bioturbated with iron staining linked to the burrows. With dark burrow-fill in contrast to cream-coloured matrix the texture of the bed resembles to a "*pseudobreccia*" sensu Horbury & Qing (2004). On the facing (northern) wall of the gorge that is unaffected by recent road-construction, this interval (discontinuity surface & hardground) translates into a well-developed step. Above, the thick-bedded lagoonal mud- to packstones of the Upper Reuchenette-Formation continue for another 27 m until the sharply defined limit. They were deposited under restricted to normal marine conditions and represent a time of maximum accommodation and minimum ecological restriction.

The definition of the Reuchenette / Twannbach Fm. boundary in Noirvaux has been discussed controversially for decades. This is because of the absence of the upper *virgula* Marls. Thus, according to Rittener (1902), the "Portlandian" of the S^{te}-Croix area is nothing but "*the normal continuation of the ordinary Late Kimmeridgian*" and a precise limit between these two stages "*cannot be established*". Bläsi (1980) also mentions the lacking marker bed but, eventually, by reasoning with thickness and the usual presence of a well-defined hardground at the lower limit of the upper *virgula* Marls, he chose the above-mentioned hardground at 63.3 m as the probable formation boundary.

Another regional lithological marker for the Reuchenette/Twannbach boundary is the so-called "*Grenznerineenbank*" (Frei 1925, Häfeli 1966, Thalmann 1966, Dauwalder & Remane 1979), located just below the upper *virgula* Marls. Bläsi (1980) and Kettiger (1981) correspondingly state that this marker-bed is absent in

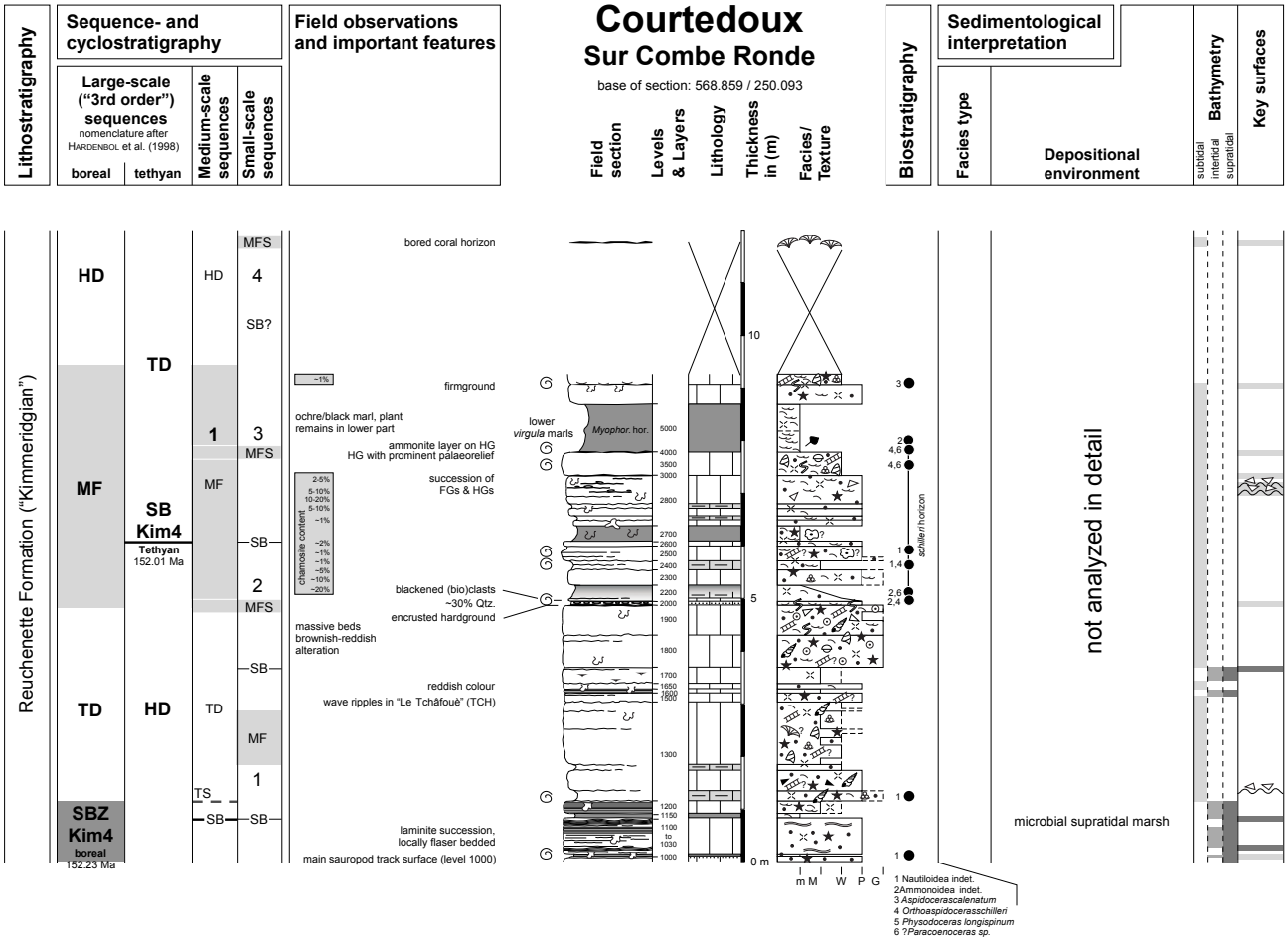

Fig. 4.9a - Detailed section log, biostratigraphy, sedimentological, and sequence-stratigraphic interpretation of the Courtedoux - Sur Combe Ronde excavation. Lithological data from the Section de Paléontologie, Porrentruy (W. Hug, pers. comm.). Biostratigraphic data from Marty (2004).

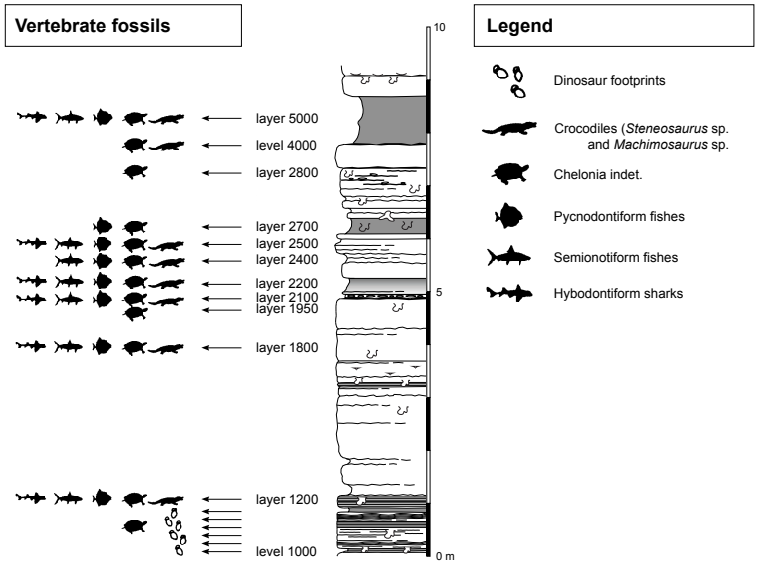

Fig. 4.9b - Vertebrate fossils found in the Courtedoux - Sur Combe Ronde excavation. Level numbers represent sedimentologic surfaces, whereas layer numbers represent beds. After Marty (2003, 2004).

Noirvaux. Mouchet (1995, in Annex 2.2.4), however, argues that "*bed 37 containing Nerineans, regionally marks the Kimmeridgian/Portlandian boundary*". Mouchet's (1995) bed 37 corresponds to the interval from 67.7 m to 70.2 m of this study, delimited by sharp surfaces and its upper half rich in gastropods. Thus, after Mouchet (1995), the upper surface (70.2 m) would represent the boundary between the Reuchenette and the Twannbach Formation.

In this study, however, the lithologic record is interpreted in an alternative way: a well-marked discontinuity surface at 90 m (Fig. 4.11) is interpreted to represent the lithological formation boundary. This erosive surface is not only defined by an abrupt change in facies, stacking pattern and weathering colour (Pl. 20/1), but microfacies analysis also reveals microkarstic features just below the surface. Additionally, stable isotope analysis (Fig. 3.3b) underlines meteoric influence with a major negative shift in $\delta^{18}O$ but a relatively undisturbed trend in $\delta^{13}C$. Consequently, a certain thickness of sedimentary record is supposed missing in this place. Based on regional high-resolution correlations (Chap. 7), this distinct, but apparently local emersion is postulated to be time-equivalent to the upper *virgula* Marls of other sections in the central and southern Jura Mountains and thus represents the boundary between the Reuchenette and the Twannbach Formation (cf. discussion in Chap. 6).

Above this sharply defined surface, the sedimentary architecture becomes completely different. In comparison with the thick-bedded, mostly lagoonal upper Reuchenette Formation, the Twannbach Formation is characterized by a decrease in average bed thickness and a complex pattern of more proximal peritidal facies successions with a variety of emersion indicators and repeated dolomite caps. The prevailing sedimentary environments are shallow, (highly) restricted lagoons and tidal flats.

The outcrop ends on top of the cliff against a meadow, indicating softer morphology. The upper part of the Twannbach Formation is not exposed in the Noirvaux section. This is why Bläsi (1980), assuming a complete section with the formation boundary about 27 m lower than in this study, found the sedimentological evolution of Noirvaux "*not comparable*" to other sections of Tithonian age.

A thickness of 70 m confirms the observations of Rittener (1902), who gave a thickness of approximatively 60 m for the "Portlandian" of the Noirvaux section. Also Jaccard (1988, p. 96) mentions that Noirvaux is "…*very incomplete. Actually, the upper part of the Portlandian, at least 20 m, perhaps even 50 m, is eroded*…". According to the geological map of Kettiger (1981, Pl. I.B and I.D), this is the effect of a thrust that runs parallel to the local fold axes and placed the upper part of the section just aside softer sediments of Early Cretaceous and Tertiary age that form the Grand Suvagnier meadows (Fig. 4.10).

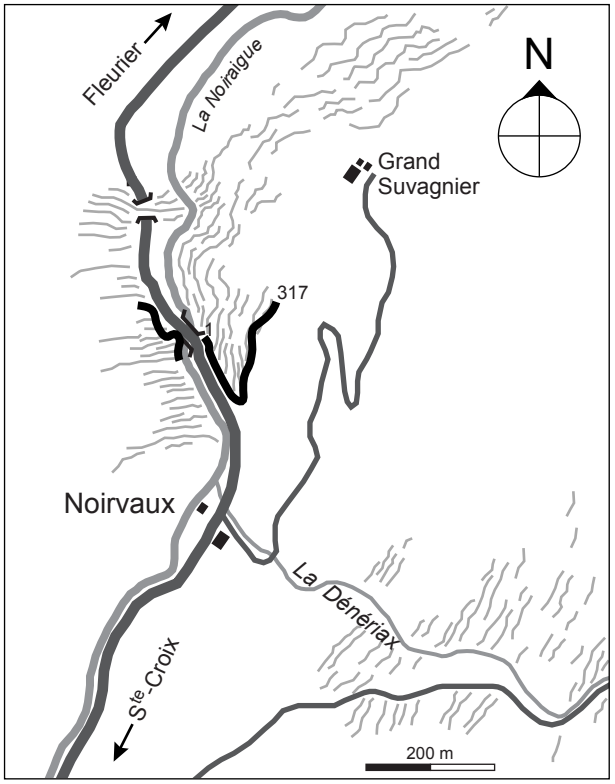

Fig. 4.10 - Location of the Noirvaux section. For legend see Fig. 4.6b.

Biostratigraphy

No fossils of value for a high-resolution biostratigraphic analysis were found. Oertli (1959) dated the "*yellowish-brownish marl layer on the western side of the bridge*" (X: 529 400 / Y: 190 050) with ostracodes as Sequanian (= Late Oxfordian) and considered it to be the *humeralis* Marls (Fig. 4.11 at 8 m). This interpretation seems to be based on (unfortunately erroneous) lithostratigraphy, because the only biostratigraphically relevant ostracode that is contained in the sample in question, *Schuleridea triebli* Steghaus 1951, has a range from the Late Oxfordian to the Early Tithonian. If, alternatively, the yellowish-brownish marl layer is considered as an equivalent to the lower *virgula* Marls that date around the *mutabilis/eudoxus* ammonite-zone boundary (cf. Courtedoux – Sur Combe Ronde section, this chapter), as proposed in this study, Oertli's (1959) range chart becomes even more consistent for a second ostracode, *Schuleridea* n.sp. Also lithostratigraphic evidence speaks for the new interpretation: The actual *humeralis* Marls directly underlie the Verena Oolite, which is situated approximately 70 m below the yellowish-brownish marl layer in question (Kettiger 1981, confirmed by own observations).

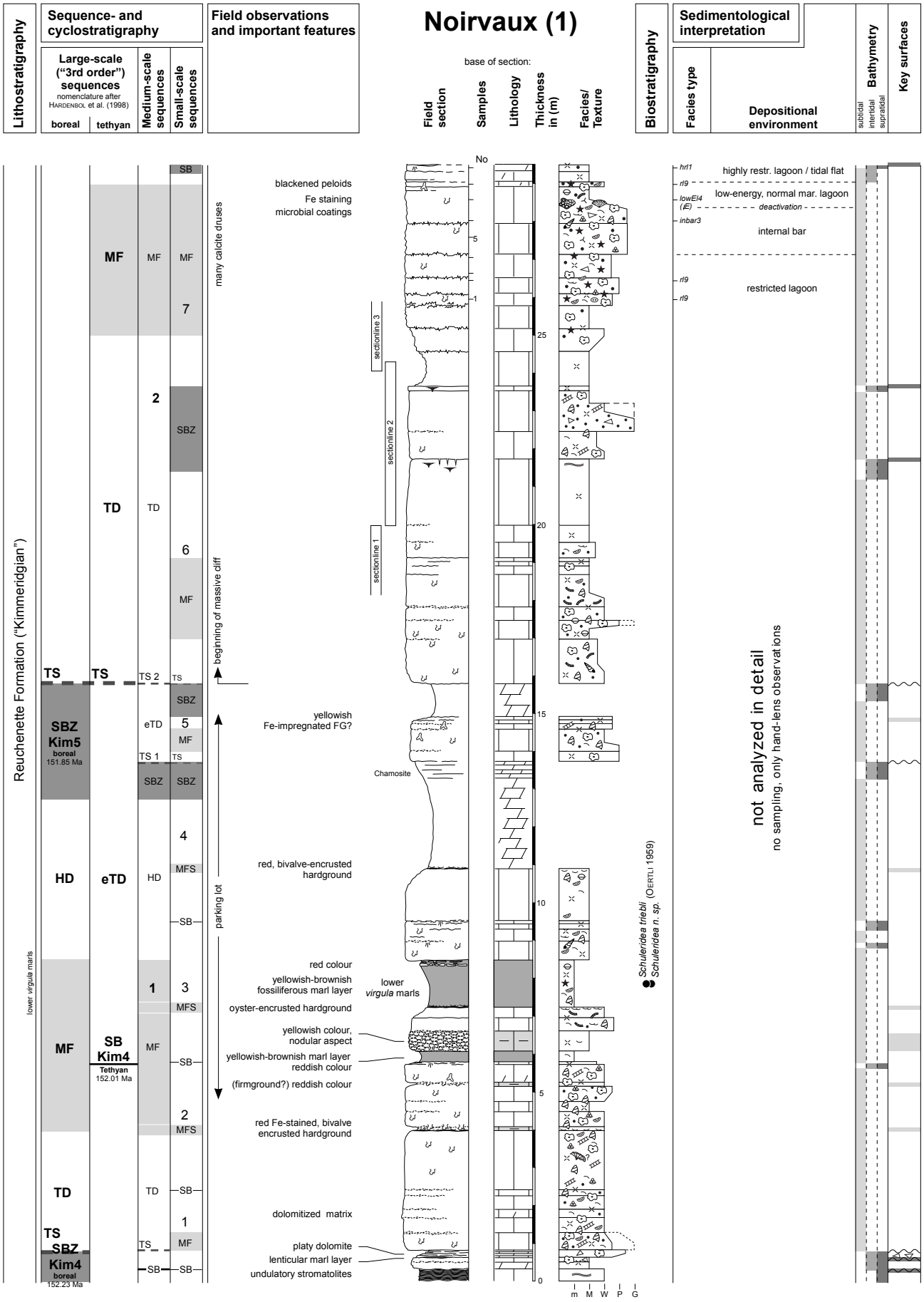

Fig. 4.11 - (this page and the five following pages) Sedimentological and sequence-stratigraphic interpretation of the Noirvaux section.

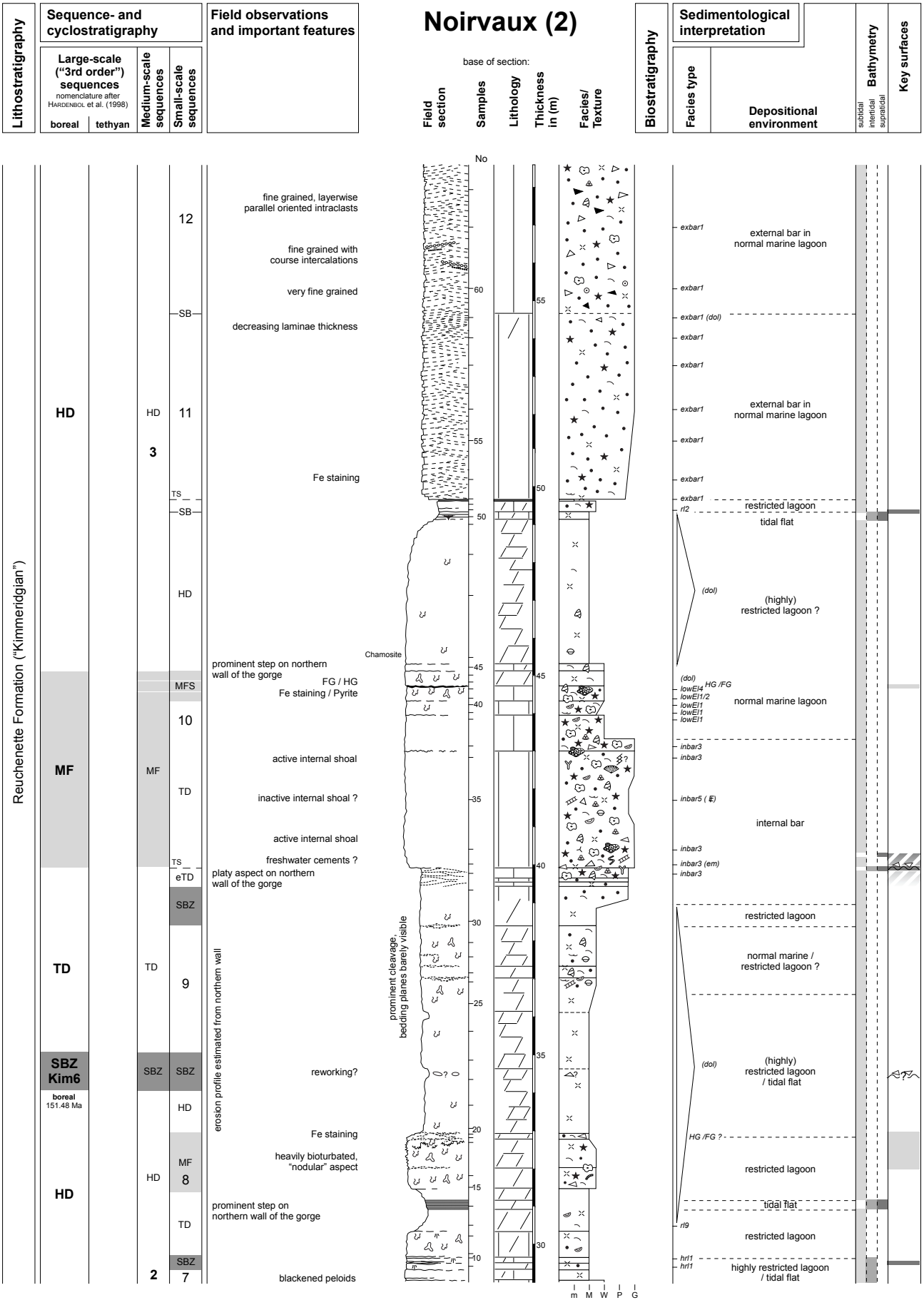
Noirvaux (2)
base of section:
Lithostratigraphy
Sequence- and cyclostratigraphy
Large-scale ("3rd order") sequences
nomenclature after HARDENBOL et al. (1998)
boreal
tethyan
Medium-scale sequences
Small-scale sequences
Field observations and important features
Field section
Samples
Lithology
Thickness in (m)
Facies/ Texture
Biostratigraphy
Sedimentological interpretation
Facies type
Depositional environment
Bathymetry
subtidal
intertidal
supratidal
Key surfaces
Reuchenette Formation ("Kimmeridgian")
HD
MF
TD
SBZ Kim6
boreal
151.48 Ma
HD
fine grained, layerwise parallel oriented intraclasts
fine grained with course intercalations
very fine grained
decreasing laminae thickness
Fe staining
prominent step on northern wall of the gorge
FG / HG
Fe staining / Pyrite
active internal shoal
inactive internal shoal ?
active internal shoal
freshwater cements ?
platy aspect on northern wall of the gorge
erosion profile estimated from northern wall
reworking?
Fe staining
heavily bioturbated, "nodular" aspect
prominent step on northern wall of the gorge
blackened peloids
Chamosite
prominent cleavage, bedding planes barely visible
external bar in normal marine lagoon
restricted lagoon
tidal flat
(highly) restricted lagoon ?
normal marine lagoon
internal bar
restricted lagoon
normal marine / restricted lagoon ?
(highly) restricted lagoon / tidal flat
restricted lagoon
tidal flat
restricted lagoon
highly restricted lagoon / tidal flat
m M W P G

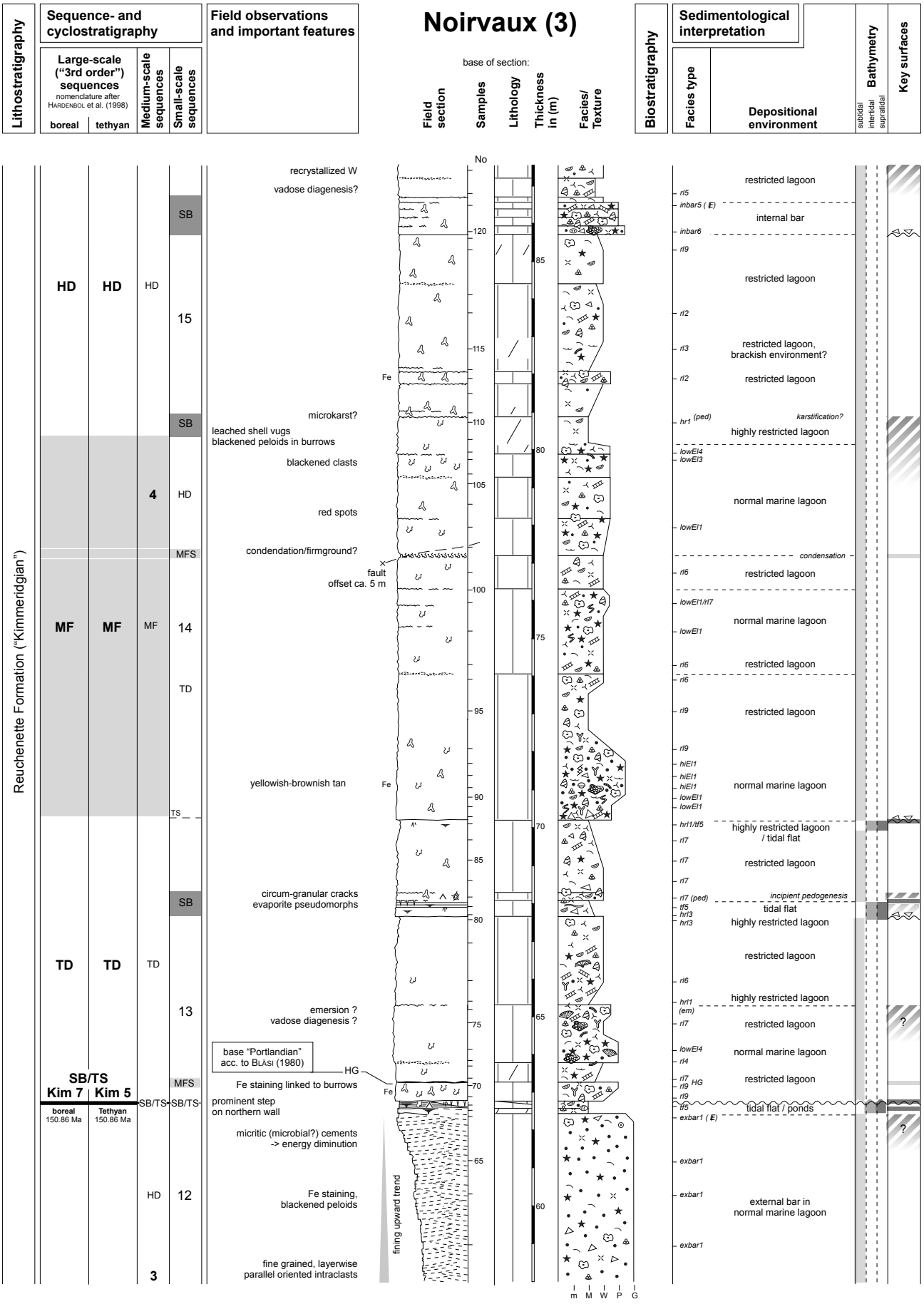
Noirvaux (3)
base of section:
Lithostratigraphy
Sequence- and cyclostratigraphy
Large-scale ("3rd order") sequences
nomenclature after HARDENBOL et al. (1998)
boreal
tethyan
Medium-scale sequences
Small-scale sequences
Field observations and important features
Field section
Samples
Lithology
Thickness in (m)
Facies/ Texture
Biostratigraphy
Sedimentological interpretation
Facies type
Depositional environment
Bathymetry
subtidal
intertidal
supratidal
Key surfaces
Reuchenette Formation ("Kimmeridgian")
HD
HD
MF
MF
TD
TD
SB/TS
Kim 7
Kim 5
boreal
150.86 Ma
Tethyan
150.86 Ma
recrystallized W
vadose diagenesis?
microkarst?
leached shell vugs
blackened peloids in burrows
blackened clasts
red spots
condendation/firmground?
fault
offset ca. 5 m
yellowish-brownish tan
circum-granular cracks
evaporite pseudomorphs
emersion ?
vadose diagenesis ?
base "Portlandian" acc. to BLASI (1980)
HG
Fe staining linked to burrows
prominent step
on northern wall
micritic (microbial?) cements
-> energy diminution
Fe staining,
blackened peloids
fining upward trend
fine grained, layerwise
parallel oriented intraclasts
restricted lagoon
internal bar
restricted lagoon
restricted lagoon,
brackish environment?
restricted lagoon
karstification?
highly restricted lagoon
normal marine lagoon
condensation
restricted lagoon
normal marine lagoon
restricted lagoon
restricted lagoon
normal marine lagoon
highly restricted lagoon
/ tidal flat
restricted lagoon
incipient pedogenesis
tidal flat
highly restricted lagoon
restricted lagoon
highly restricted lagoon
restricted lagoon
normal marine lagoon
restricted lagoon
tidal flat / ponds
external bar in
normal marine lagoon
m M W P G

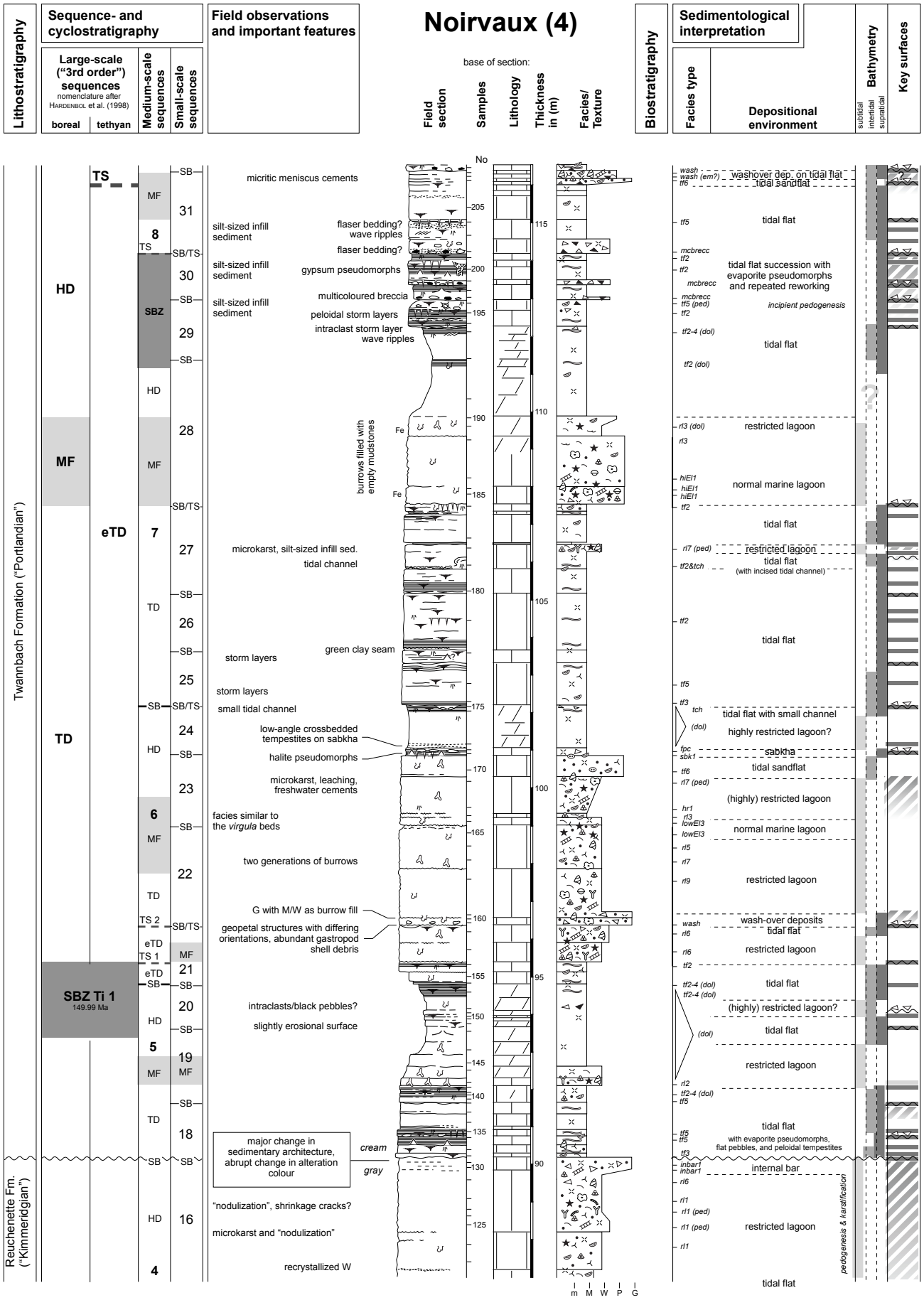
Noirvaux (4)
base of section:
Lithostratigraphy
Sequence- and cyclostratigraphy
Large-scale ("3rd order") sequences
nomenclature after HARDENBOL et al. (1998)
boreal
tethyan
Medium-scale sequences
Small-scale sequences
Field observations and important features
Field section
Samples
Lithology
Thickness in (m)
Facies/ Texture
Biostratigraphy
Sedimentological interpretation
Facies type
Depositional environment
Bathymetry
subtidal
intertidal
supratidal
Key surfaces
Twannbach Formation ("Portlandian")
Reuchenette Fm. ("Kimmeridgian")
TS
HD
MF
eTD
TD
SBZ Ti 1
149.99 Ma
micritic meniscus cements
silt-sized infill sediment
flaser bedding? wave ripples
flaser bedding?
gypsum pseudomorphs
multicoloured breccia
peloidal storm layers
intraclast storm layer wave ripples
burrows filled with empty mudstones
microkarst, silt-sized infill sed.
tidal channel
green clay seam
storm layers
small tidal channel
low-angle crossbedded tempestites on sabkha
halite pseudomorphs
microkarst, leaching, freshwater cements
facies similar to the virgula beds
two generations of burrows
G with M/W as burrow fill
geopetal structures with differing orientations, abundant gastropod shell debris
intraclasts/black pebbles?
slightly erosional surface
major change in sedimentary architecture, abrupt change in alteration colour
cream
gray
"nodulization", shrinkage cracks?
microkarst and "nodulization"
recrystallized W
washover dep. on tidal flat
tidal sandflat
tidal flat
tidal flat succession with evaporite pseudomorphs and repeated reworking
incipient pedogenesis
restricted lagoon
normal marine lagoon
tidal flat with small channel
highly restricted lagoon?
sabkha
(highly) restricted lagoon
wash-over deposits
internal bar
pedogenesis & karstification
m M W P G

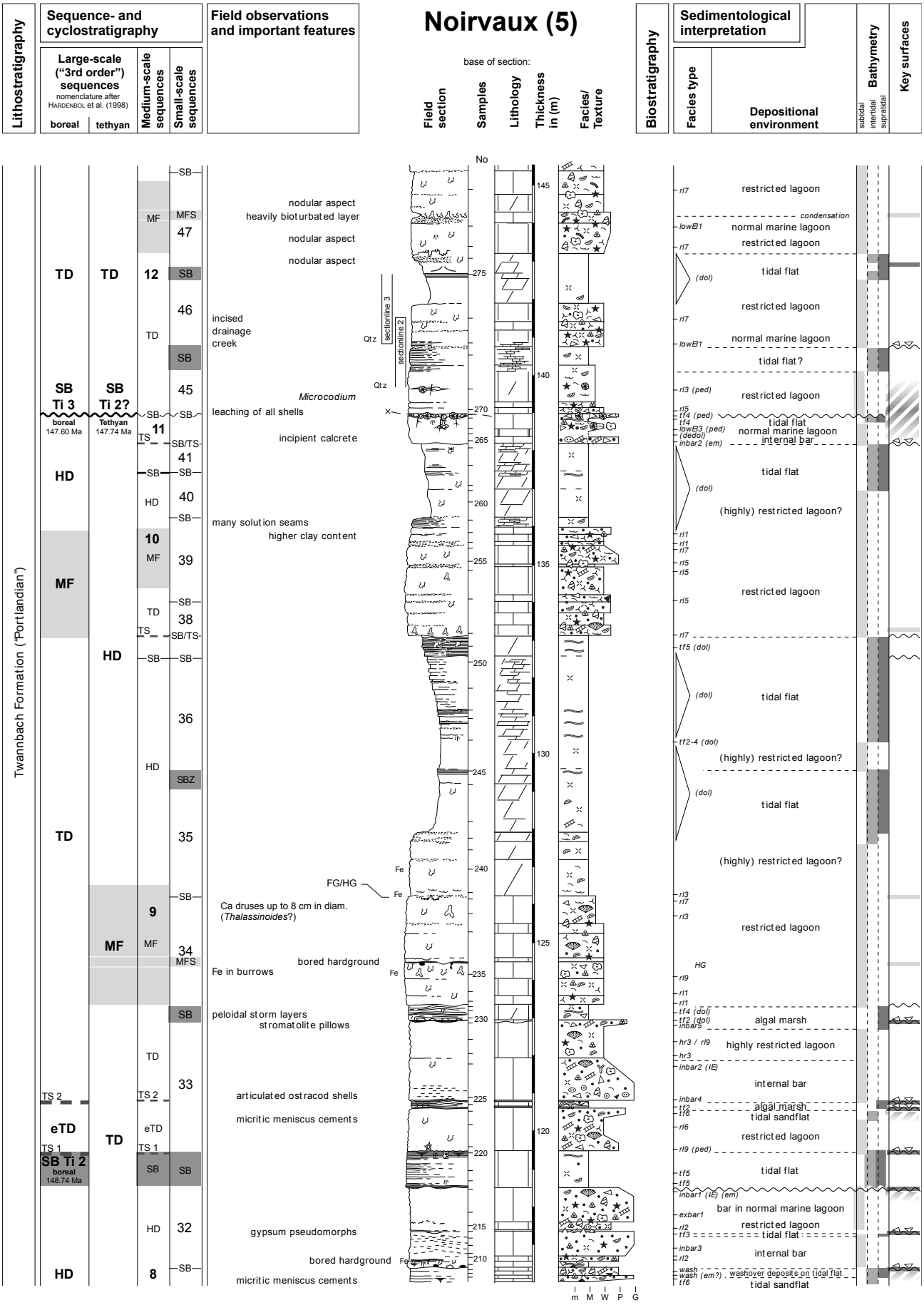
Noirvaux (5)
base of section:
Lithostratigraphy
Sequence- and cyclostratigraphy
Large-scale ("3rd order") sequences
nomenclature after HARDENBOL et al. (1998)
boreal
tethyan
Medium-scale sequences
Small-scale sequences
Field observations and important features
Field section
Samples
Lithology
Thickness in (m)
Facies/ Texture
Biostratigraphy
Sedimentological interpretation
Facies type
Depositional environment
Bathymetry
subtidal
intertidal
supratidal
Key surfaces
Twannbach Formation ("Portlandian")
TD
HD
MF
SB Ti 3
boreal
147.60 Ma
SB Ti 2?
Tethyan
147.74 Ma
SB Ti 2
boreal
148.74 Ma
eTD
TS 1
TS 2
SB
MFS
TS
SB/TS
SBZ
nodular aspect
heavily bioturbated layer
incised drainage creek
Qtz
sectionline 3
sectionline 2
Microcodium
leaching of all shells
incipient calcrete
many solution seams
higher clay content
FG/HG
Fe
Ca druses up to 8 cm in diam. (Thalassinoides?)
bored hardground
Fe in burrows
peloidal storm layers
stromatolite pillows
articulated ostracod shells
micritic meniscus cements
gypsum pseudomorphs
bored hardground
micritic meniscus cements
restricted lagoon
condensation
normal marine lagoon
tidal flat
tidal flat?
normal marine lagoon internal bar
(highly) restricted lagoon?
algal marsh
highly restricted lagoon
internal bar
tidal sandflat
bar in normal marine lagoon
washover deposits on tidal flat
m M W P G

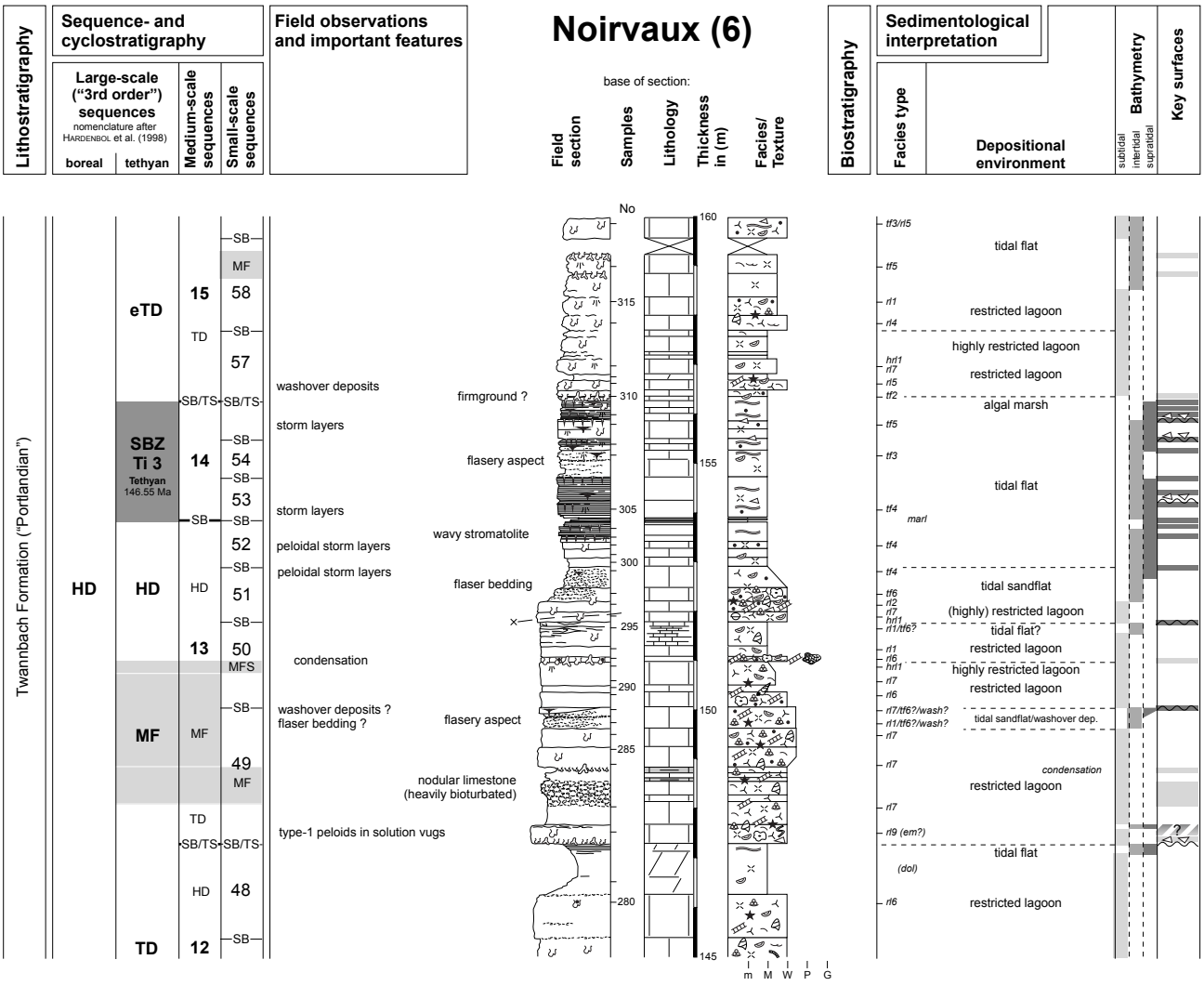

Sequence stratigraphy

Regarding the sequence stratigraphic interpretation (left column) of the Noirvaux section's base (Fig. 4.11), the out of phase-relationship of the Tethyan and the Boreal sequence stratigraphic patterns (SB $Kim4_{Boreal}$ - SB $Kim4_{Tethyan}$ - SB $Kim5_{Boreal}$) is puzzling at first. Medium- and small-scale MFs are well-developed in this interval in the form of Fe-stained and encrusted hardgrounds and bioturbated to nodular limestones.

SB $Kim5_{Boreal}$ is followed by a major transgression that is primarily characterized by a substantial gain in accommodation space. This produces the thickest medium- and small-scale sequences that were found in the measured sections (16-90m). This interval probably defines a period of MF in long-term (2^{nd} -order) sea-level evolution. Within this 2^{nd}-order MF, SB $Kim5_{Tethyan}$ (= SB $Kim7_{Boreal}$) is defined by a brief, but marked excursion from normal marine lagoons with relatively high water energy ("open lagoons") to subaerial exposure and non-deposition, respectively erosion.

The sedimentological expression of the 2^{nd}-order MF ends abruptly at the above-mentioned, well-marked discontinuity surface at 90 m (Fig. 4.11) that also acts as formation boundary. Despite its karstic and pedogenic features, it is only interpreted as medium-scale SB (evidence from regional correlation, cf. Chap. 7). The next large-scale sequence boundary (SB Ti1) is found in the dolomite cap a few metres above. Beginning with the base of medium-scale sequence 5, medium- and small-scale sequences show a lower average thickness than below and are much more characterized by peritidal environments, repeated emersions, and sequence boundaries hidden in dolomite caps and/or with pronounced subaerial exposure. An exception to the rule are well-developed MFSs of small-scale sequences 34, 47, and 50 that are at the same time situated in MFZs of medium- and/or large-scale sequences (see also Chap. 4.2.3).

The presence of SB $Ti2?_{Tethyan}$ (SB $Ti3_{Boreal}$) is underlined by evidence for plant colonization: a layer and pockets of brecciated limestone with rhizoliths and frequent

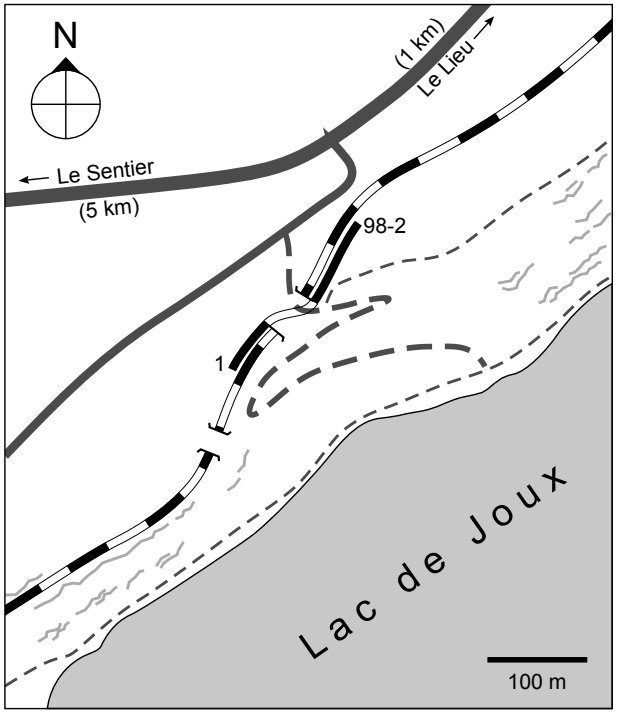

Fig. 4.12 - Location of the Lieu section. For legend see Fig. 4.6b.

Microcodium (Pl. 10/3 and 16/1a, b). Additionally, in a dedolomitized layer just below the *Microcodium*-bearing breccia, a structure was found that resembles the initial stages of laminar calcrete-formation by roots (Pl. 10/2) as described by Alonso-Zarza (1999). Even if the *Microcodium*/laminar calcrete association was found at a large-scale sequence boundary where prolonged emersion is nothing unusual, it remains unclear if it formed in the Late Jurassic or during the long-lasting emersion/erosion caused by Cretaceous-Tertiary uplift in this area. According to various authors (e.g., Klappa 1978, Freytet & Plaziat 1982, Freytet & Verrecchia 1998), most *Microcodium* and continental stromatolite appearances are reported from Late Cretaceous and Tertiary sediments.

At the top of the section, medium-scale sequence 14 is among the thinnest found in the measured sections (Pl. 20/2). The reduced thickness ("telescoping") of small-scale sequences is caused by extremely low rates of accommodation gain that define large-scale SBZ $Ti3_{Tethyan}$ that is the most pronounced large-scale SB of Tithonian age on the Jura platform.

Le Lieu *(Figs 4.12, 4.13)*

Originally measured for a diploma thesis by Sudan (1997) at the Institute of Geology in Fribourg, this section was completely re-measured, re-interpreted and re-sampled for clay mineralogical analysis. Existing thin sections from the diploma project were used for microfacies analysis. Additional specimens were taken where the original sample density was considered insufficient. In this way, many details were added, specifically in the lower 30 m of the section, where outcrop conditions are excellent.

approx. 15 km SW of Vallorbe, on the north shore of the Lac de Joux

National topographic map of Switzerland
1 : 25 000, sheet 1221 *Le Sentier*

Base of section: X: 510 570
Y: 165 910

Lithostratigraphy and sedimentology

The section begins approximately in the middle between two tunnels on the railway track along the shore of the Lac de Joux that links Le Pont with Le Sentier (Fig. 4.12). Its base is defined by the "*La Côte*"-thrust that repeats the Twannbach Formation in this locality (Sudan 1997). The outcropping sedimentary record thus starts in the lower part of the Twannbach Formation; the boundary between the Reuchenette and the Twannbach Formation is not exposed along the railroad tracks. Yet, according to Aubert (1941), this boundary, expressed as the *virgula* Marls, can be found some 10s of metres down the slope towards the lake. The section runs through the eastern tunnel and ends in a morphological depression used as a meadow and stands in contrast to the forested, hard limestone ridge that is cut by the tunnel. This morphological depression is known all over the Jura as the *Combe purbeckienne*, the "Purbeckian depression" that is caused by the weathering of the relatively soft sediments of the Goldberg Formation.

Lithologically, the section can be subdivided into two parts: The lower part (most of the Twannbach Formation, 0-55 m) consists of a succession of more or less restricted, commonly heavily bioturbated, mud-supported limestones of lagoonal origin, internal bars, and tidal flats. Then, around 55 m, a rapid change takes place from a normal marine lagoon to a tidally influenced internal bar (showing a bimodal grain-size distribution), and eventually to a tidal flat with an incised and filled-up tidal channel. The following part (upper part of the Twannbach Formation and parts of the Goldberg Formation, 55-89 m) is characterized mainly by intertidal to supratidal deposition with abundant emersion features and evaporite pseudomorphs (tidal flats and sabkhas). The uppermost 20 m are subject to complete type-2 dedolomitization (cf. Chap. 3.2.2) and dissolution breccias, both testifying to long-term emersion.

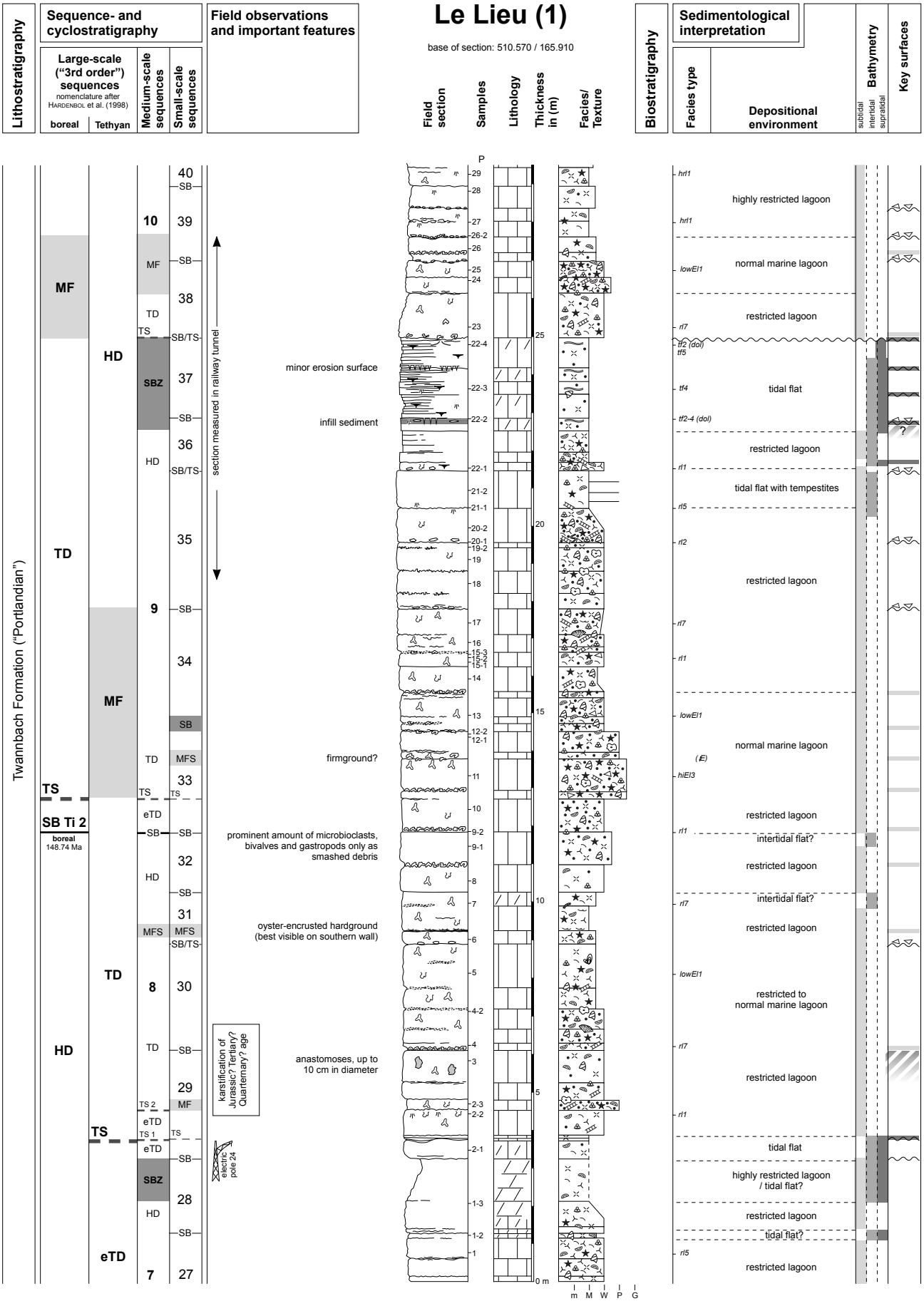

Fig. 4.13 - (this page and the two following pages) Sedimentological and sequence-stratigraphic interpretation of the Lieu section.

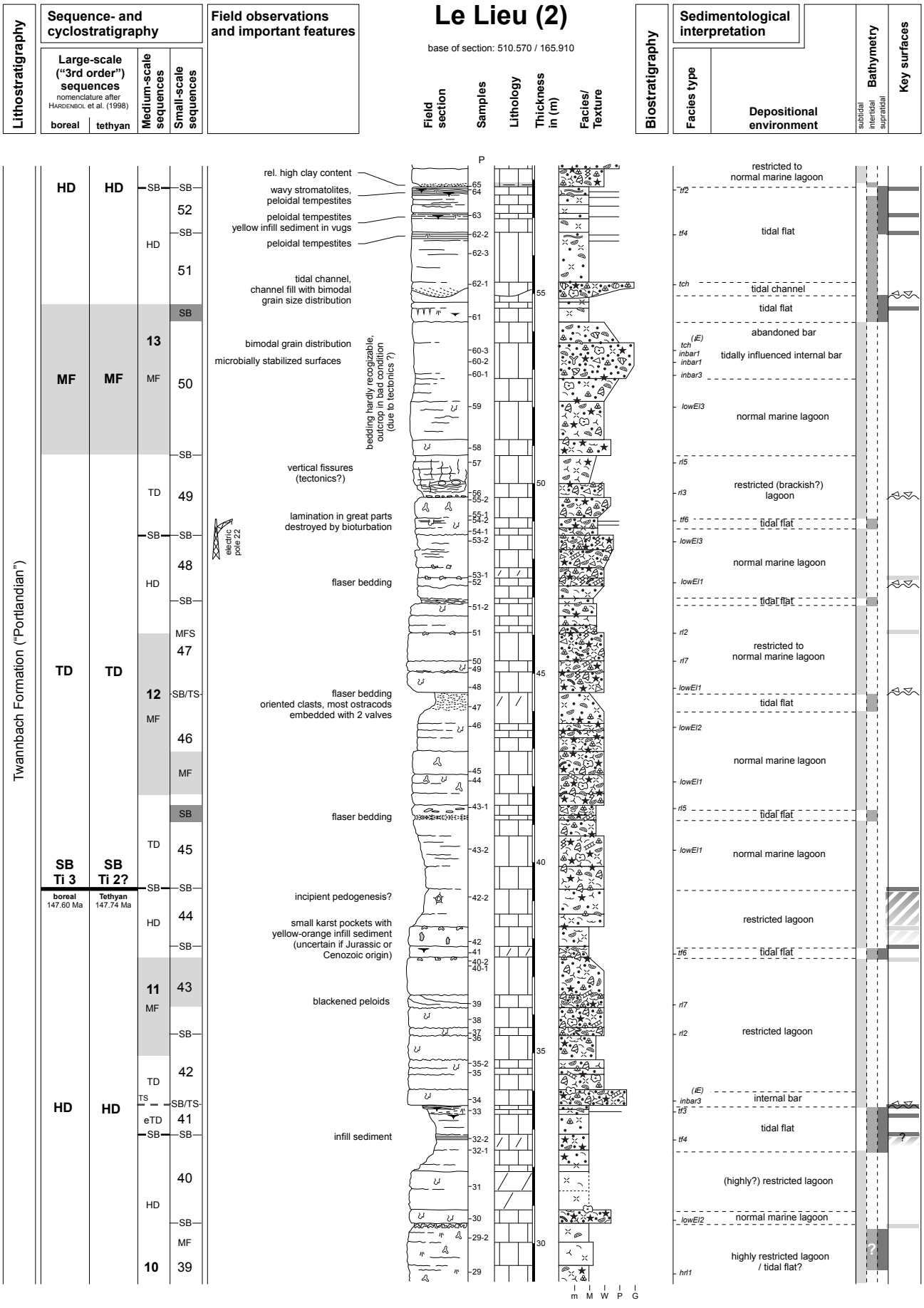
Le Lieu (2)
base of section: 510.570 / 165.910
Lithostratigraphy
Sequence- and cyclostratigraphy
Large-scale ("3rd order") sequences
nomenclature after HARDENBOL et al. (1998)
boreal
tethyan
Medium-scale sequences
Small-scale sequences
Field observations and important features
Field section
Samples
Lithology
Thickness in (m)
Facies/ Texture
Biostratigraphy
Sedimentological interpretation
Facies type
Depositional environment
Bathymetry
subtidal
intertidal
supratidal
Key surfaces
Twannbach Formation ("Portlandian")
HD
MF
TD
SB Ti 3
SB Ti 2?
boreal 147.60 Ma
Tethyan 147.74 Ma
HD
rel. high clay content
wavy stromatolites, peloidal tempestites
peloidal tempestites
yellow infill sediment in vugs
peloidal tempestites
tidal channel, channel fill with bimodal grain size distribution
bimodal grain distribution
microbially stabilized surfaces
bedding hardly recogizable, outcrop in bad condition (due to tectonics ?)
vertical fissures (tectonics?)
lamination in great parts destroyed by bioturbation
electric pole 22
flaser bedding
flaser bedding
oriented clasts, most ostracods embedded with 2 valves
flaser bedding
incipient pedogenesis?
small karst pockets with yellow-orange infill sediment (uncertain if Jurassic or Cenozoic origin)
blackened peloids
infill sediment
restricted to normal marine lagoon
tidal flat
tidal channel
tidal flat
abandoned bar
tidally influenced internal bar
normal marine lagoon
restricted (brackish?) lagoon
tidal flat
normal marine lagoon
tidal flat
restricted to normal marine lagoon
tidal flat
normal marine lagoon
tidal flat
normal marine lagoon
restricted lagoon
tidal flat
restricted lagoon
internal bar
tidal flat
(highly?) restricted lagoon
normal marine lagoon
highly restricted lagoon / tidal flat?
m M W P G

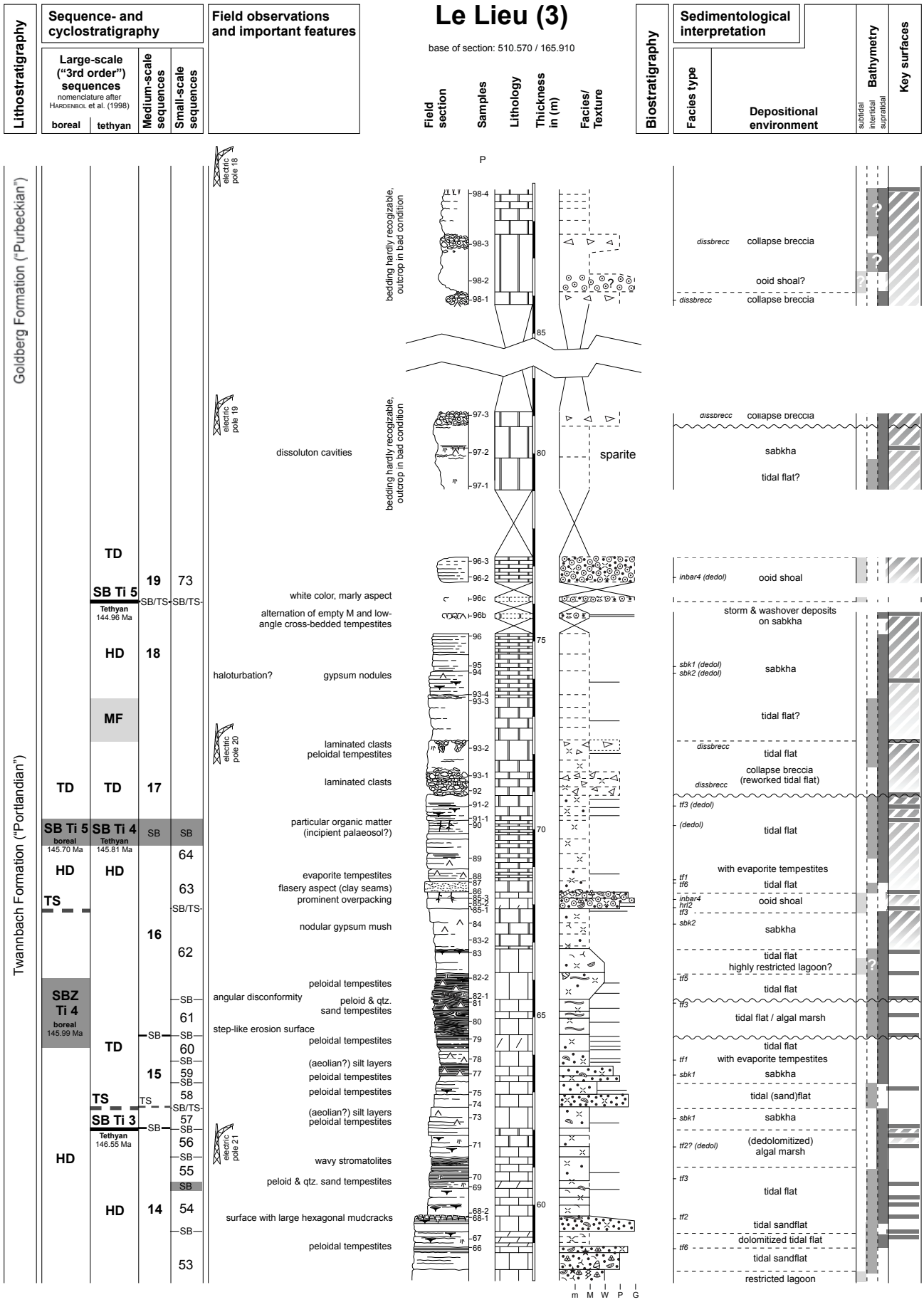
Le Lieu (3)
base of section: 510.570 / 165.910
Lithostratigraphy
Goldberg Formation ("Purbeckian")
Twannbach Formation ("Portlandian")
Sequence- and cyclostratigraphy
Large-scale ("3rd order") sequences
nomenclature after HARDENBOL et al. (1998)
boreal
tethyan
Medium-scale sequences
Small-scale sequences
Field observations and important features
Field section
Samples
Lithology
Thickness in (m)
Facies/ Texture
Biostratigraphy
Sedimentological interpretation
Facies type
Depositional environment
Bathymetry
subtidal
intertidal
supratidal
Key surfaces
TD
SB Ti 5
Tethyan
144.96 Ma
HD
MF
TD
TD
SB Ti 5
boreal
145.70 Ma
SB Ti 4
Tethyan
145.81 Ma
HD
HD
TS
SBZ Ti 4
boreal
145.99 Ma
TD
TS
SB Ti 3
Tethyan
146.55 Ma
HD
HD
19
18
17
16
15
14
73
64
63
62
61
60
59
58
57
56
55
54
53
SB/TS
SB
TS
electric pole 18
electric pole 19
electric pole 20
electric pole 21
bedding hardly recognizable, outcrop in bad condition
dissoluton cavities
white color, marly aspect
alternation of empty M and low-angle cross-bedded tempestites
haloturbation?
gypsum nodules
laminated clasts peloidal tempestites
laminated clasts
particular organic matter (incipient palaeosol?)
evaporite tempestites
flasery aspect (clay seams)
prominent overpacking
nodular gypsum mush
peloidal tempestites
angular disconformity
peloid & qtz. sand tempestites
step-like erosion surface
peloidal tempestites
(aeolian?) silt layers
peloidal tempestites
peloidal tempestites
(aeolian?) silt layers
peloidal tempestites
wavy stromatolites
peloid & qtz. sand tempestites
surface with large hexagonal mudcracks
peloidal tempestites
sparite
collapse breccia
ooid shoal?
collapse breccia
collapse breccia
sabkha
tidal flat?
ooid shoal
storm & washover deposits on sabkha
sabkha
tidal flat?
tidal flat
collapse breccia (reworked tidal flat)
tidal flat
with evaporite tempestites
tidal flat
ooid shoal
sabkha
tidal flat
highly restricted lagoon?
tidal flat
tidal flat / algal marsh
tidal flat
with evaporite tempestites
sabkha
tidal (sand)flat
sabkha
(dedolomitized) algal marsh
tidal flat
tidal sandflat
dolomitized tidal flat
tidal sandflat
restricted lagoon
m M W P G

Biostratigraphy

No fossils of use for biostratigraphic interpretation were found.

Sequence stratigraphy

In the lower part of the section, small- and medium-scale sequences are well expressed. Medium-scale sequence boundary zones are manifest as tidal-flat facies with or without dolomitization (medium-scale sequences 7-10). Small-scale maximum flooding surfaces are best expressed in an interval around a large-scale MF that also attenuated the boundary between medium-scale sequences 8 and 9. Beginning with medium-scale sequence 11, dolomite caps start to play a less central role in indicating SBs, and tidal-flat facies and emersion indicators become more important. E.g., medium-scale SB11, that is also a large-scale SB, is indicated by circumgranular cracks and incipient pedogenesis. Maybe even the small karst pockets 1.5 m below the SB were caused by the sea-level drop creating the sequence boundary, but the age of their formation could not be determined. Also beginning with medium-scale sequence 11, bioturbation and the physical expression of small-scale MFS diminishes.

From the top of medium-scale sequence 13 upwards the section is dominated by inter- and supratidal deposits. The average thickness of medium- and small-scale sequences drops dramatically and reaches an absolute minimum in medium-scale sequence 15. The tidal-flat succession is only interrupted by either medium-scale transgressive deposits or small-scale transgressive deposits during a medium-scale MF (e.g., medium-scale sequences 16, 19), both consisting of peloid- or ooid-grainstones. Numerous indicators for subaerial exposure and vadose diagenesis prove the repeated emersion of the platform at all scales of SBs during this interval.

The meter-thick collapse breccia just above large-scale SB $Ti4_{Boreal}$ (SB $Ti5_{Tethyan}$) is interpreted to be related to evaporites that were deposited during the initial accommodation gain of the following large-scale transgression (Tucker 1999).

La Dôle *(Figs 4.14, 4.15)*

With an altitude of 1677 m, *La Dôle* is one of the Jura's summits that is easily identified from afar by its relatively isolated position and the eye-catching radar station that SKYGUIDE, Switzerland's civil and military air navigation service, installed on top of it (cf. Fig. 4.14). High above the city of Nyon and the shores of Lake Geneva, its east-facing cliff exposes a complete section from the Late Kimmeridgian to the Early Berriasian.

approx. 12 km NW of Nyon (VD)

National topographic map of Switzerland
1 : 25 000, sheet 1260 *Col de la Faucille*

Base of section: X: 497 350
Y: 142 825
approx. 1530 m asl

Previous studies on this section include Pidancet & Lory (1847), Lagotala (1920), and Bläsi (1980).

Among the measured platform sections, the Dôle section is the only one that consists of a completely natural cliff. Following thousands of years of weathering, the stacking pattern of depositional sequences translated nearly perfectly into outcrop morphology (cf. Pl. 20/3).

Due to the rugged terrain, the section had to be measured in several subsections (section lines a-e; Fig. 4.14) that were eventually summarized in one log. The upper part of section line (d) was only measured for stacking pattern and general facies associations because the upper part of the couloir is rather steep and not easily accessible. Detailed study and sampling were therefore carried out at section line (e), which is a succession of several small outcrops along the foot-path on the crest. The top (124-158 m) of the log (Fig 4.15) is consequently a composite section of section lines (d), (e) and (e_2). Despite of minor changes in thickness and different weathering aspects in the cliff (section line d) and on the crest (section lines e and e_2), a bed-by-bed correlation between the section lines is easily possible.

Lithostratigraphy and sedimentology

The section begins above a minor fault (Fig. 4.14b, c) that was already mentioned by Lagotala (1920, Pl.1), but is not marked in recent geological maps of the area. The basal 20 m of the section belong to the upper Reuchenette Formation and form a relatively massive succession that builds the base of the northern part of the La Dôle cliff. The facies of thick-bedded wacke- to grainstones reflects a comparatively high-energy environment with normal marine to restricted lagoonal conditions and abundant shoals. This part ends with a thinning-up sequence, which is followed by a major change in sedimentation: after a heavily bioturbated interval featuring Fe-staining and two well-developed hardgrounds follows a dark-grey marly interval, yielding pyrite, blackened microfossils (cf. Pl. 3/11 and 16/4), wood fragments, and small oysters. This facies succession indicates an initial omission/condensation succeeded by a phase of dysoxic, restricted conditions. The abundance of oysters is a possible hint to changing salinities, e.g., by freshwater input. In

accordance with Bläsi (1980), this interval is interpreted as the upper *virgula* Marls, defining the boundary between the Reuchenette and the Twannbach formations. Yet, Lagotala (1920, p. 2f.) stated that "…*it was impossible to find determinable fossils, therefore the* virgula *Marls could not be tracked down*".

On top of the upper *virgula* Marls, the Twannbach Formation begins with its typical complex pattern of peritidal facies successions and a decrease in average bed thickness. A particular detail in this section is that large parts of the Twannbach Formation show stratiform dolomitization. The prevailing sedimentary environments are shallow, (highly) restricted lagoons and tidal flats. From 98 to110 m, a thick interval of laminites is found, showing a multitude of emersion indicators such as tepee structures, bird's eyes, root casts, multicoloured breccia, and pedogenesis/karstification. It represents a long time of tidal flat / algal marsh conditions, interrupted by longer periods of subaerial exposure during continental conditions. After the following transgression, lagoonal conditions are re-established, transiently, before the environments switch back to tidal-flat and sabkha sedimentation for the rest of the section.

Beginning at 140 m, parts of the carbonates are dedolomitized and show cornieule-texture. This recrystallization does not follow bed geometries and ends at 148 m with a surface showing prominent solution features. The cornieules are interpreted to result from vadose diagenesis during longer periods of subaerial exposure. These sediments correspond to the so-called "*calcaire âpre*" (Jaccard 1869). If present, they are used to delimit the top of "Portlandian", respectively the Twannbach Formation (see Häfeli 1966, Thalmann 1966, Bläsi 1980). In the Dôle section, the Goldberg Formation begins with soft, laminated, chalky sabkha sediments that are exposed along the footpath from Col de Porte to the Dôle summit. The massive limestone body west of the footpath (Fig. 4.14b, c) is composed of angular clasts and clods (cm to 10s of cm size). Many of the clods still show their original bedding, some are folded. Interclast voids frequently show a horizontal (geopetal) lower surface that divides the sparite-filled void from a muddy matrix. This indicates an (at least partly) infill-character of the muddy matrix. The whole, several m-thick massive bed is interpreted as a collapse breccia that resulted from the dissolution of underlying evaporites. The timing of the dissolution process is difficult to determine (cf. discussion in Chap. 2.4.3). However, in this specific case, the plastic deformation of some m-scale clasts that still show the original bedding would rather speak for early dissolution, when the evaporite-covering carbonates were not yet fully lithified.

Biostratigraphy

No fossils of use for biostratigraphic interpretation were found.

Sequence stratigraphy

In the predominantly lagoonal Reuchenette Formation, large-scale sequence boundary SB $Kim5_{Tethyan}$ (SB $Kim7_{Boreal}$) is only expressed as a thin intercalation of tidal-flat facies. All other large-scale sequence boundaries of the Twannbach Formation (SB $Ti1\text{-}5_{Tethyan}$, respectively SB $Ti1\text{-}6_{Boreal}$) are linked to dolomite caps of different extent. Of these SBs, SBZ $Ti3_{Tethyan}$ is by far the most pronounced; it lies within the above-mentioned thick interval of laminites from 98 to 110 m with various markers of prolonged subaerial exposure. Another well-pronounced SB is the SB Be1 (148 m). In contrast to SBZ $Ti3_{Tethyan}$ it is mainly defined by diagenetic overprinting and dissolution. This is also the case for SB $Be2_{Boreal}$ that is interpreted to be located at the base of the above-mentioned collapse breccia. Yet, massive evaporites that are essential for the development of a collapse breccia of the observed scale need accommodation space to be deposited. According to Sarg (2003) and Tucker (1999), given the right conditions (arid climate and a restricted basin), massive evaporites most probably develop during the initial phase of long-term transgressions when relative sea-level is still low but the creation of new accommodation space already started. Indeed, according to the sequence-chronostratigraphic charts of Hardenbol et al. (1998), the latest Tithonian – Early Berriasian corresponds to the transgressive part of a 2nd-order T-R facies cycle.

Despite all the differences in their lithologic successions (cf. Chap. 1) the Dôle section shows many similarities with the Noirvaux and the Lieu sections: medium- and small-scale sequences of the upper Reuchenette Formation are rather thick. With the beginning of the Twannbach Formation, their thicknesses decrease. Similar to the Lieu section, small-scale sequences in the lower part of the Twannbach Formation show heavy bioturbation and well-expressed MFs where they coincide with medium- and large-scale maximum floodings (57-75 m). Other similarities to the Lieu and the Noirvaux sections are the attenuation of medium-scale sequence boundary 8, the considerably reduced thicknesses ("telescoping") of small-scale sequences around SBZ $Ti3_{Tethyan}$, and tidal-flat facies and emersion indicators becoming more important in the upper part of the Twannbach Formation. Yet, in the Dôle section, dolomite caps play a more important role in sequence architecture.

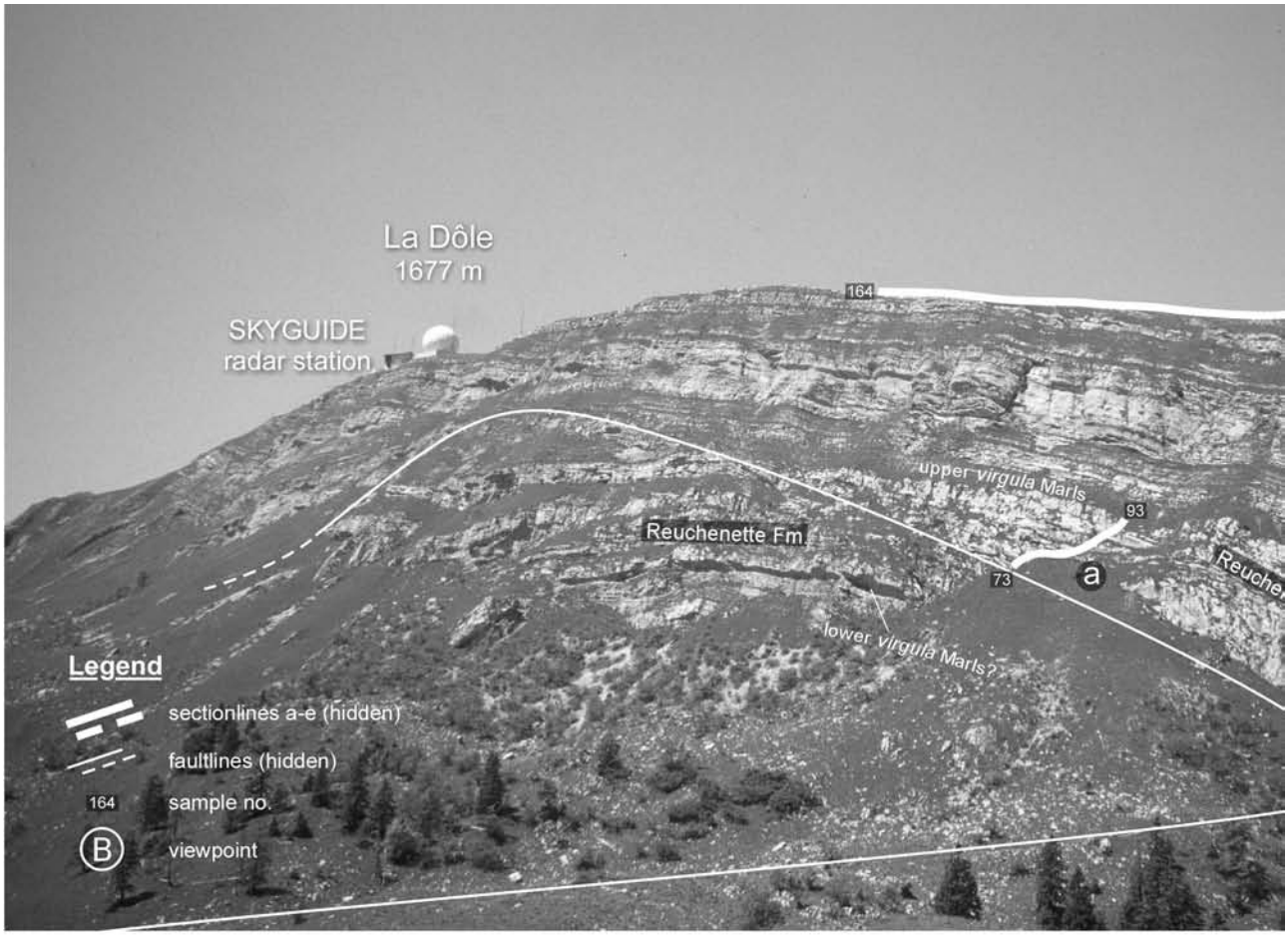

Fig. 4.14a - (above) The Dôle cliff seen from the East. Photograph was taken from viewpoint A.

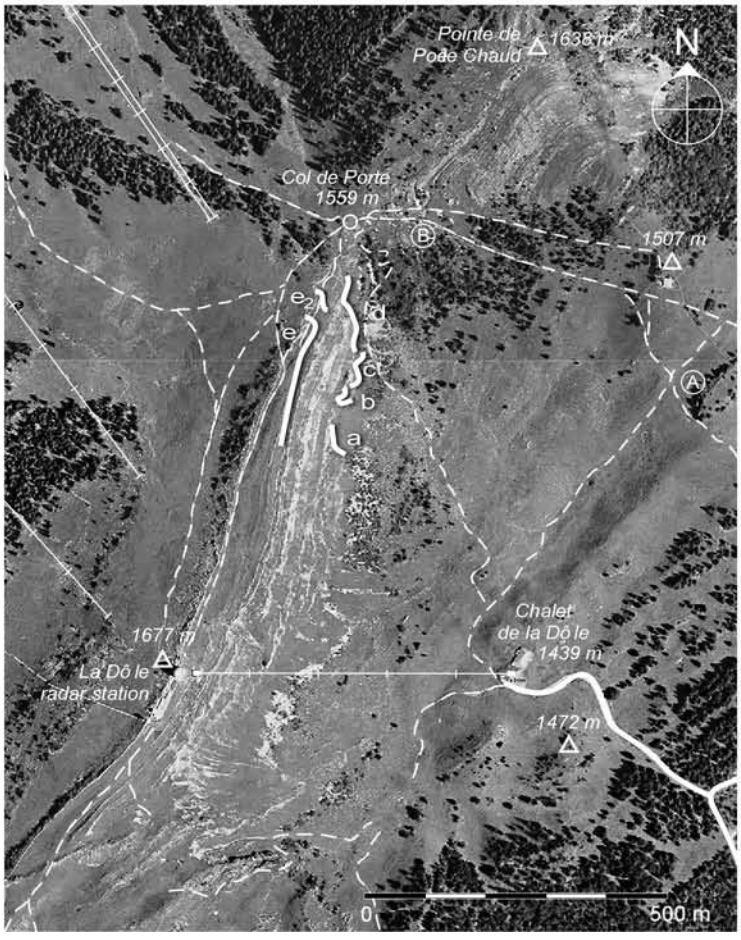

Fig. 4.14b - (left) Aerial view of the Dôle cliff and its surroundings.

Fig. 4.14c - (right) The Dôle cliff seen from the North. Photograph was taken from viewpoint B.


collapse
breccia
Col de Porte
1559 m
B
e
197
e2
Twannbach Fm.
163
d
94
116
133
132
b
117
c

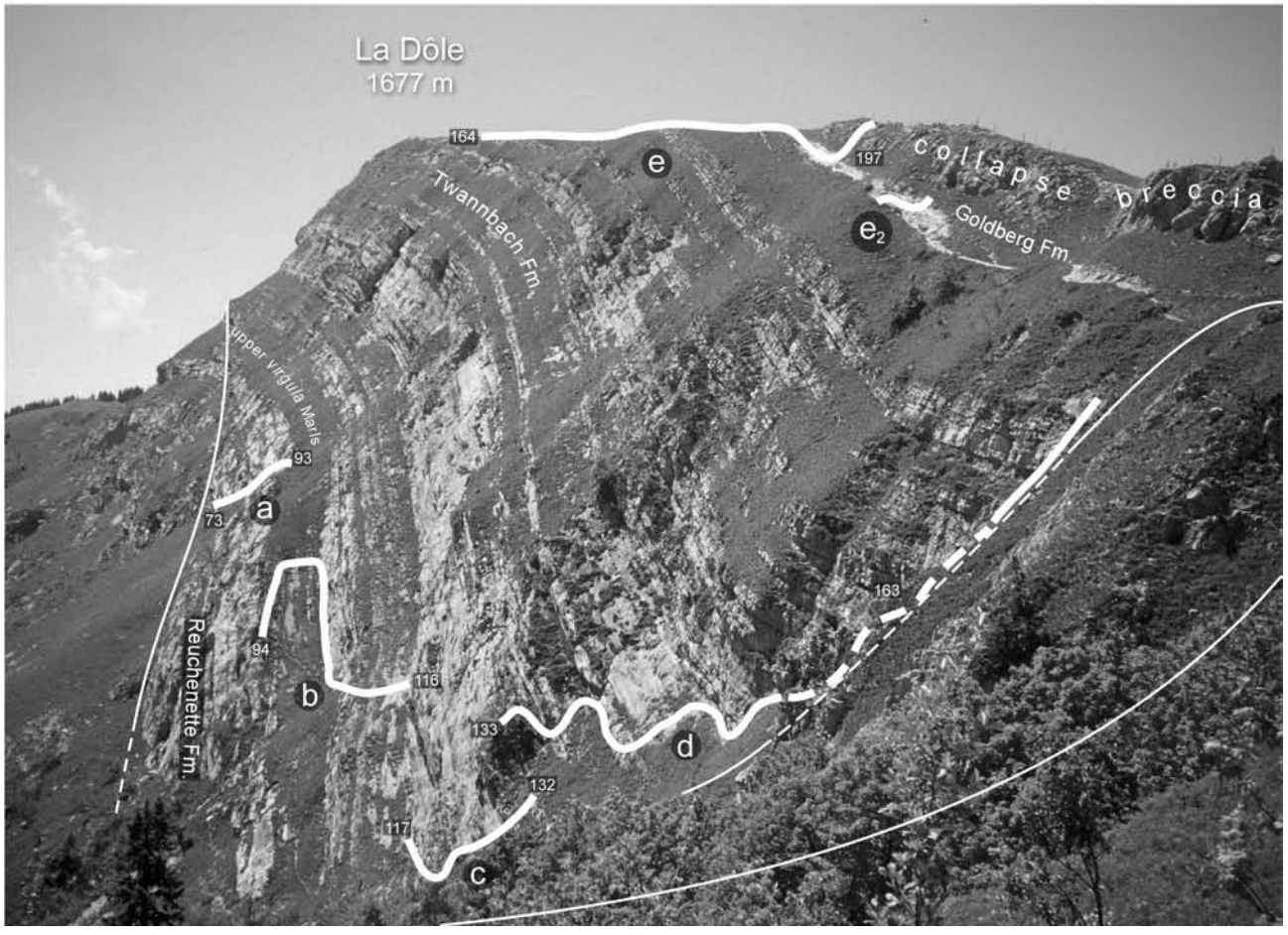
La Dôle
1677 m
164
e
197
collapse breccia
Twannbach Fm.
e2
Goldberg Fm.
upper Virgula Marls
93
73
a
163
Reuchenette Fm.
94
b
116
133
d
132
117
c

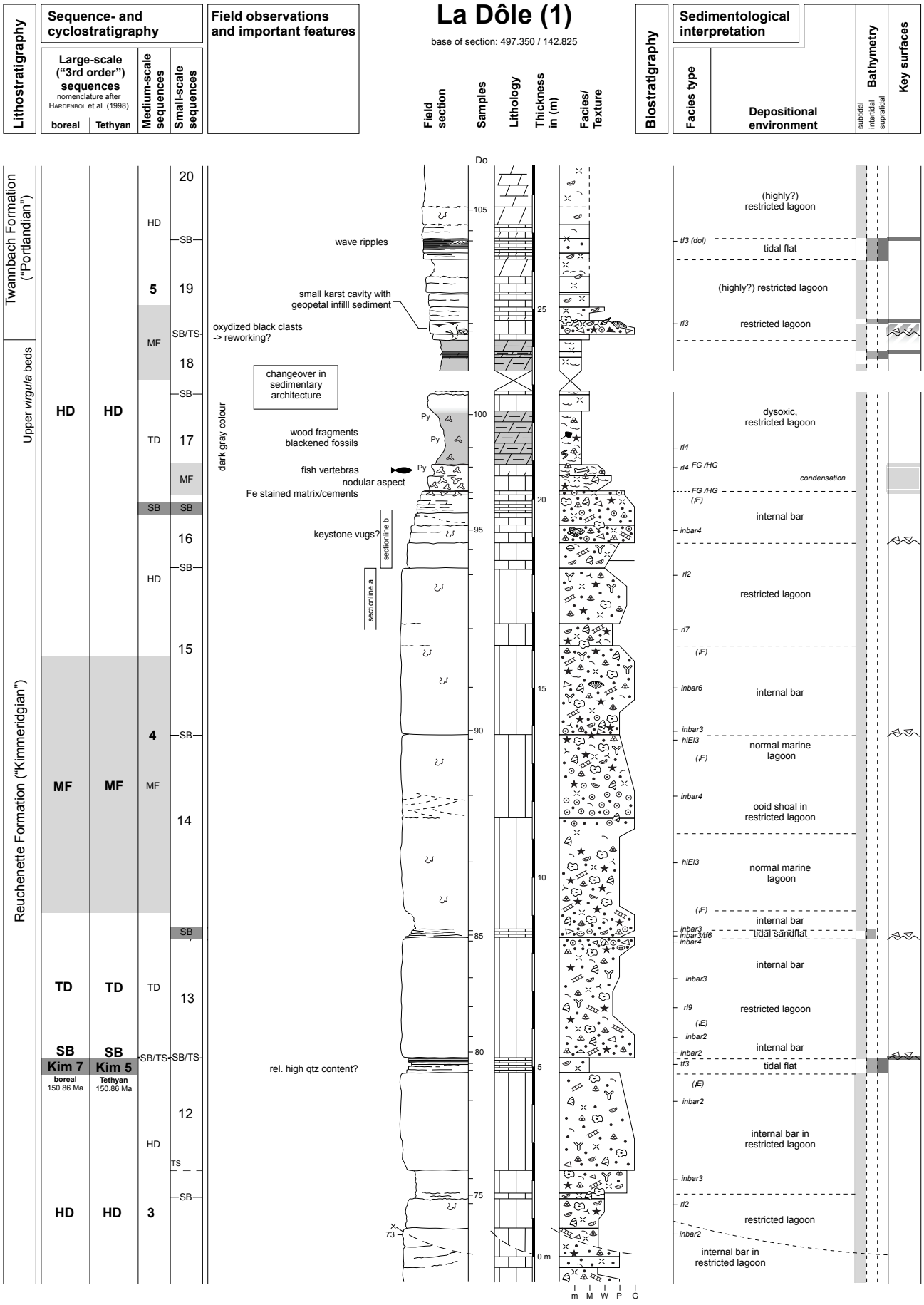

Fig. 4.15 - (this page and the five following pages) Sedimentological and sequence-stratigraphic interpretation of the Dô le section.

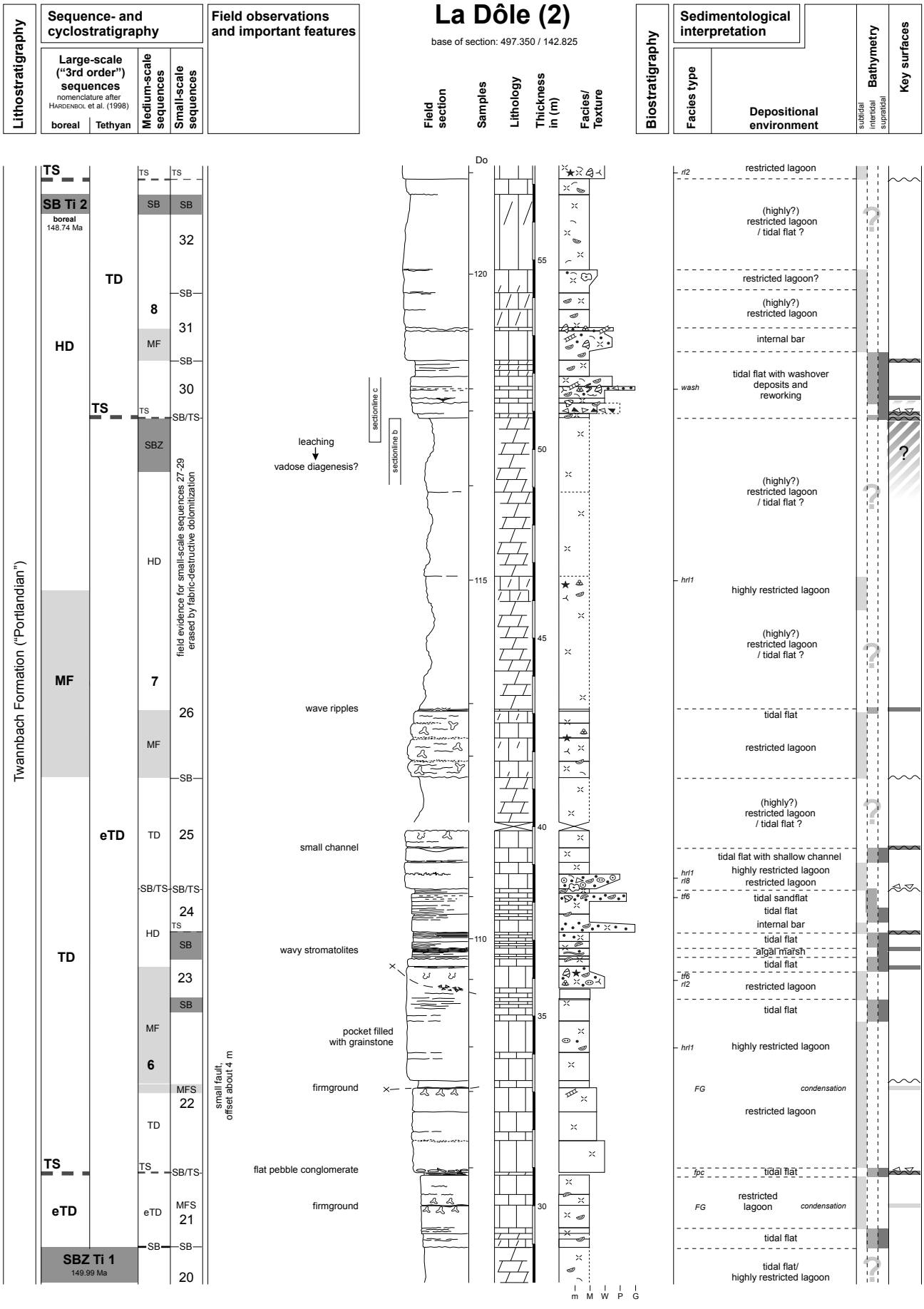
La Dôle (2)
base of section: 497.350 / 142.825
Lithostratigraphy
Sequence- and cyclostratigraphy
Large-scale ("3rd order") sequences
nomenclature after Hardenbol et al. (1998)
boreal
Tethyan
Medium-scale sequences
Small-scale sequences
Field observations and important features
Field section
Samples
Lithology
Thickness in (m)
Facies/ Texture
Biostratigraphy
Sedimentological interpretation
Facies type
Depositional environment
Bathymetry
subtidal
intertidal
supratidal
Key surfaces
Twannbach Formation ("Portlandian")
TS
SB Ti 2
boreal
148.74 Ma
TD
HD
MF
eTD
SBZ Ti 1
149.99 Ma
SB
MFS
SBZ
field evidence for small-scale sequences 27-29 erased by fabric-destructive dolomitization
sectioniine c
sectioniine b
leaching
vadose diagenesis?
wave ripples
small channel
wavy stromatolites
pocket filled with grainstone
firmground
flat pebble conglomerate
small fault, offset about 4 m
Do
m M W P G
restricted lagoon
(highly?) restricted lagoon / tidal flat ?
restricted lagoon?
(highly?) restricted lagoon
internal bar
tidal flat with washover deposits and reworking
highly restricted lagoon
tidal flat
tidal flat with shallow channel
tidal sandflat
algal marsh
condensation
tidal flat/ highly restricted lagoon

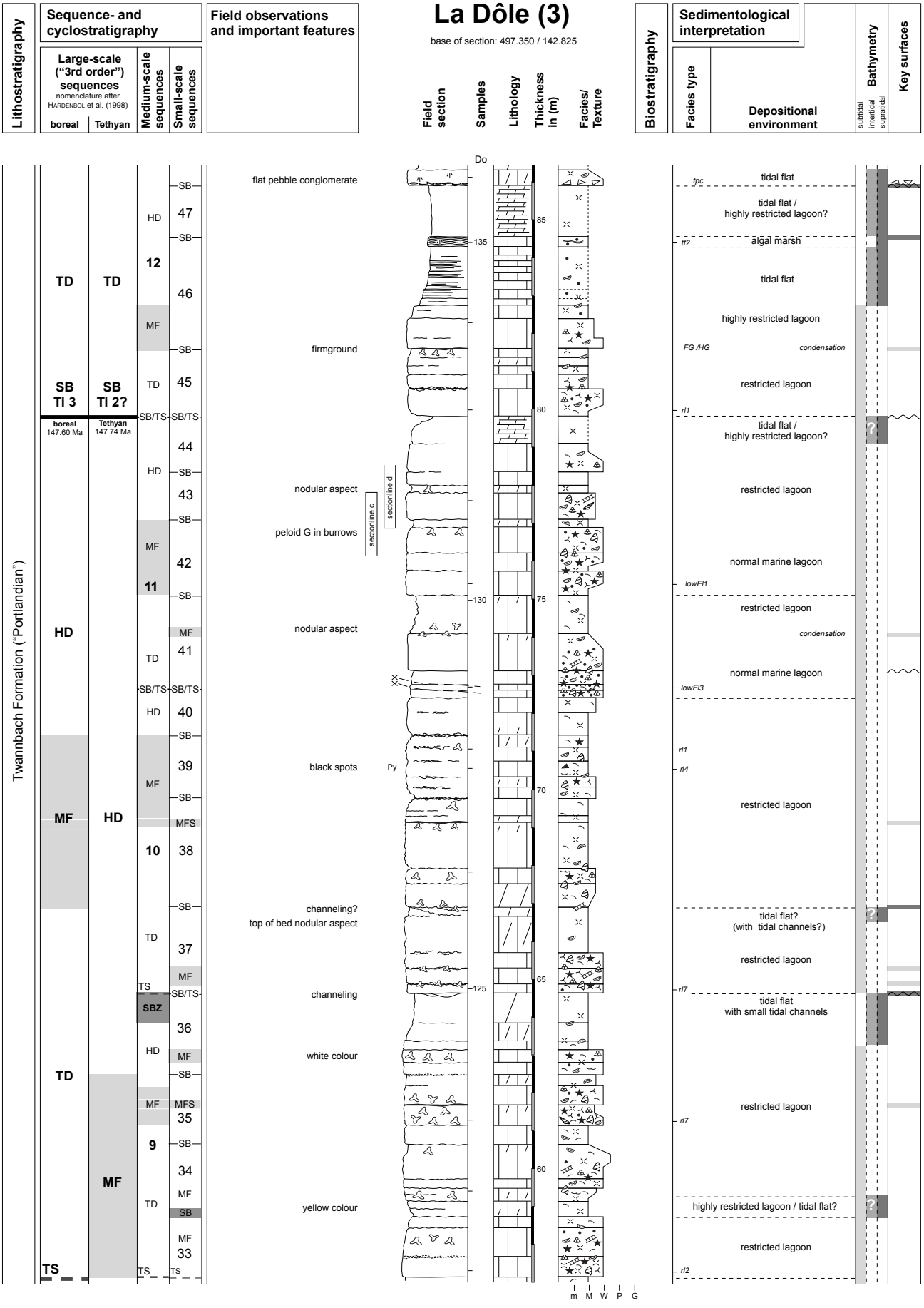
La Dôle (3)
base of section: 497.350 / 142.825
Lithostratigraphy
Sequence- and cyclostratigraphy
Large-scale ("3rd order") sequences
nomenclature after Hardenbol et al. (1998)
boreal
Tethyan
Medium-scale sequences
Small-scale sequences
Field observations and important features
Field section
Samples
Lithology
Thickness in (m)
Facies/ Texture
Biostratigraphy
Sedimentological interpretation
Facies type
Depositional environment
Bathymetry
subtidal
intertidal
supratidal
Key surfaces
Twannbach Formation ("Portlandian")
TD
HD
MF
SB
Ti 3
Ti 2?
boreal
147.60 Ma
Tethyan
147.74 Ma
SBZ
TS
SB/TS
MFS
Do
flat pebble conglomerate
firmground
nodular aspect
peloid G in burrows
sectionline c
sectionline d
nodular aspect
black spots
Py
channeling?
top of bed nodular aspect
channeling
white colour
yellow colour
85
80
75
70
65
60
135
130
125
m M W P G
fpc
tidal flat
tidal flat / highly restricted lagoon?
tf2
algal marsh
tidal flat
highly restricted lagoon
FG /HG
condensation
restricted lagoon
rl1
tidal flat / highly restricted lagoon?
restricted lagoon
normal marine lagoon
lowEl1
restricted lagoon
condensation
normal marine lagoon
lowEl3
rl1
rl4
restricted lagoon
tidal flat? (with tidal channels?)
restricted lagoon
rl7
tidal flat with small tidal channels
restricted lagoon
rl7
highly restricted lagoon / tidal flat?
restricted lagoon
rl2

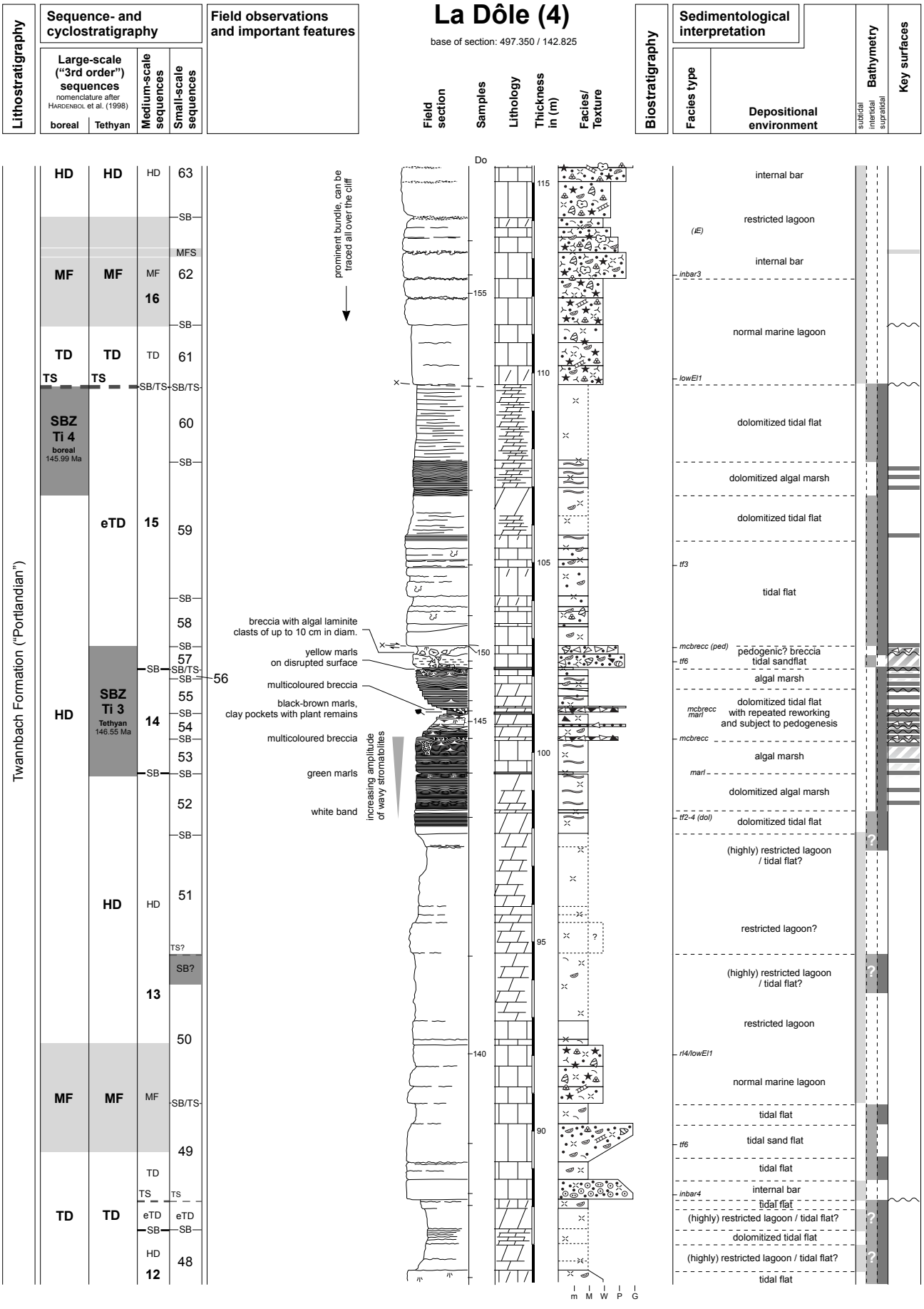
La Dôle (4)
base of section: 497.350 / 142.825
Lithostratigraphy
Sequence- and cyclostratigraphy
Large-scale ("3rd order") sequences
nomenclature after HARDENBOL et al. (1998)
boreal
Tethyan
Medium-scale sequences
Small-scale sequences
Field observations and important features
Field section
Samples
Lithology
Thickness in (m)
Facies/ Texture
Biostratigraphy
Sedimentological interpretation
Facies type
Depositional environment
Bathymetry
subtidal
intertidal
supratidal
Key surfaces
Twannbach Formation ("Portlandian")
HD
MF
TD
TS
SB/TS
SB
MFS
eTD
SBZ Ti 4
boreal
145.99 Ma
SBZ Ti 3
Tethyan
146.55 Ma
prominent bundle, can be traced all over the cliff
breccia with algal laminite clasts of up to 10 cm in diam.
yellow marls on disrupted surface
multicoloured breccia
black-brown marls, clay pockets with plant remains
multicoloured breccia
green marls
white band
increasing amplitude of wavy stromatolites
m M W P G
internal bar
restricted lagoon
(iE)
inbar3
normal marine lagoon
lowEl1
dolomitized tidal flat
dolomitized algal marsh
tf3
tidal flat
mcbrecc (ped)
pedogenic? breccia
tf6
tidal sandflat
algal marsh
mcbrecc marl
dolomitized tidal flat with repeated reworking and subject to pedogenesis
mcbrecc
marl
tf2-4 (dol)
(highly) restricted lagoon / tidal flat?
rl4/lowEl1
tidal sand flat
inbar4

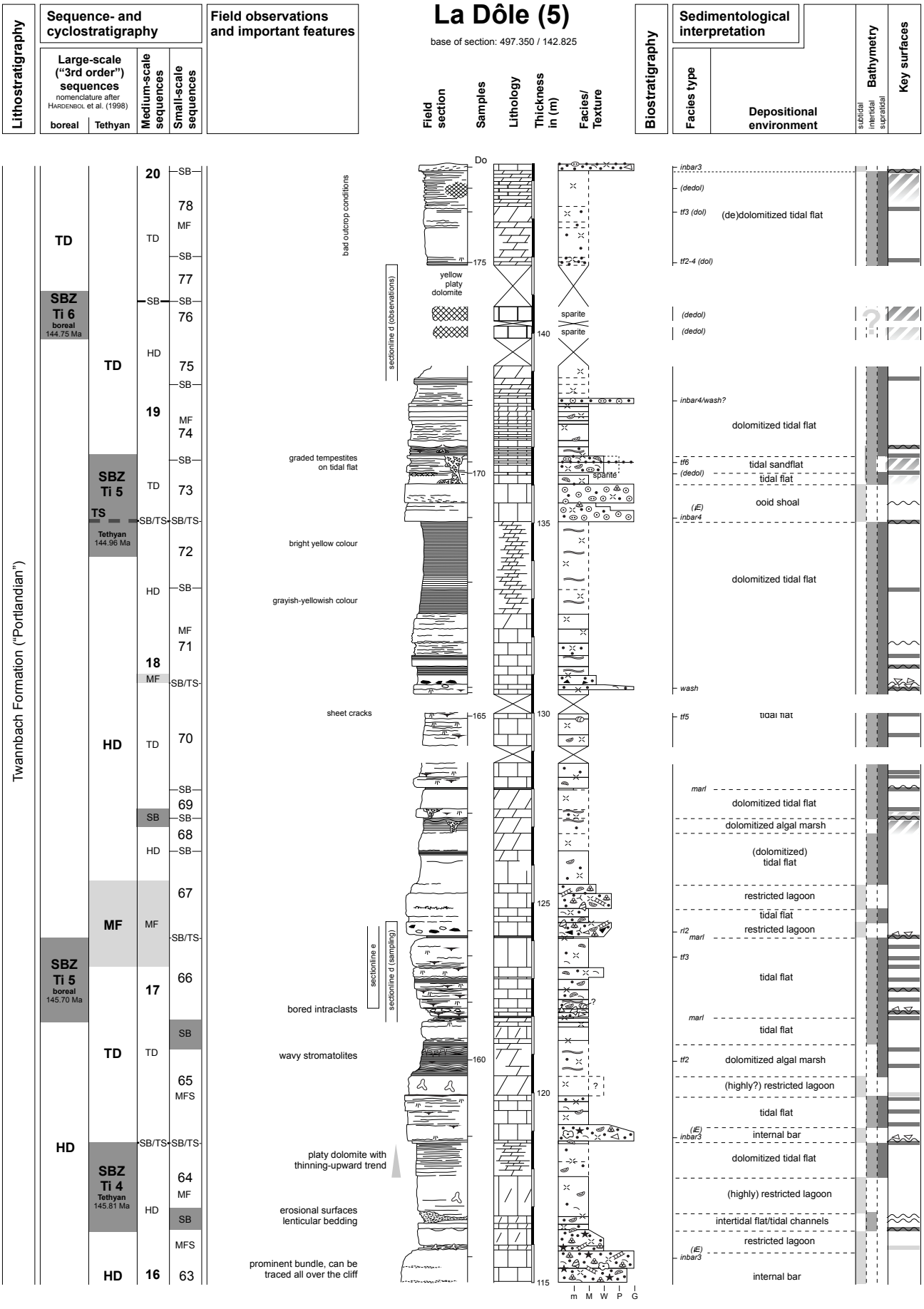
La Dôle (5)
base of section: 497.350 / 142.825
Lithostratigraphy
Sequence- and cyclostratigraphy
Large-scale ("3rd order") sequences
nomenclature after HARDENBOL et al. (1998)
boreal
Tethyan
Medium-scale sequences
Small-scale sequences
Field observations and important features
Field section
Samples
Lithology
Thickness in (m)
Facies/ Texture
Biostratigraphy
Sedimentological interpretation
Facies type
Depositional environment
Bathymetry
subtidal
intertidal
supratidal
Key surfaces
Twannbach Formation ("Portlandian")
TD
SBZ Ti 6
boreal
144.75 Ma
TD
SBZ Ti 5
TS
Tethyan
144.96 Ma
HD
MF
SBZ Ti 5
boreal
145.70 Ma
TD
HD
SBZ Ti 4
Tethyan
145.81 Ma
HD
20
78
MF
TD
77
76
HD
75
19
MF
74
73
72
HD
MF
71
18
MF
70
69
68
HD
67
MF
66
17
65
MFS
64
MF
HD
63
16
SB
SB/TS
Do
175
140
135
130
125
120
115
bad outcrop conditions
yellow platy dolomite
sectionline d (observations)
sparite
graded tempestites on tidal flat
bright yellow colour
grayish-yellowish colour
sheet cracks
bored intraclasts
wavy stromatolites
platy dolomite with thinning-upward trend
erosional surfaces lenticular bedding
prominent bundle, can be traced all over the cliff
sectionline e
sectionline d (sampling)
m M W P G
inbar3
(dedol)
tf3 (dol)
(de)dolomitized tidal flat
tf2-4 (dol)
inbar4/wash?
dolomitized tidal flat
tf6
tidal sandflat
tidal flat
(lE)
inbar4
ooid shoal
wash
tf5
marl
dolomitized algal marsh
(dolomitized) tidal flat
restricted lagoon
rl2
tf3
tf2
(highly?) restricted lagoon
inbar3
internal bar
(highly) restricted lagoon
intertidal flat/tidal channels

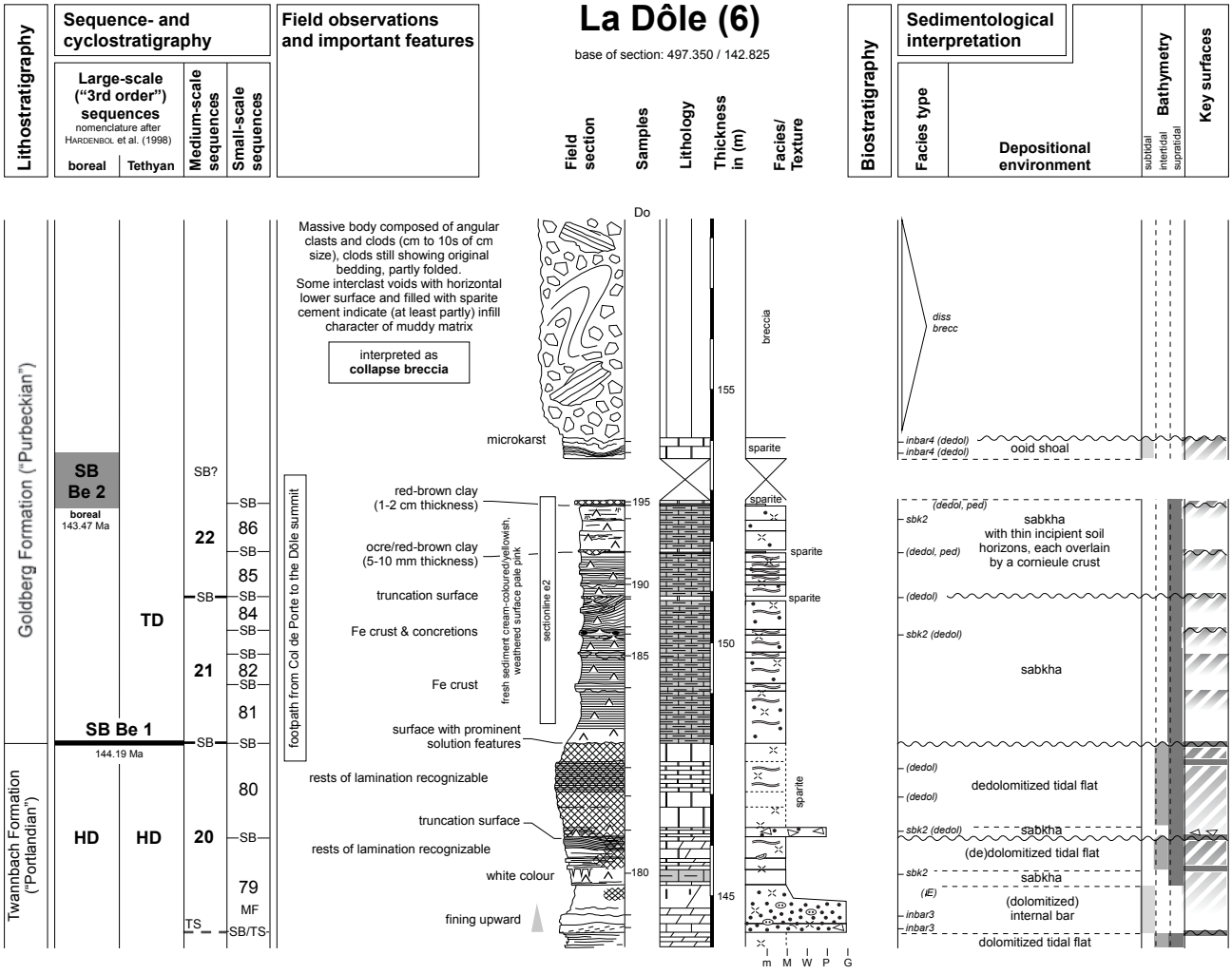

Cirque des Avalanches *(Figs 4.16, 4.17)*

approx. 12 km N of Bellegarde-sur-Valsérine (France), 25 km W of Geneva

Institut Géographique National (IGN), TOP 25, sheet 3329 O: *Bellegarde-sur-Valsérine / Grand Cret d'Eau* 1 : 25 000

Base of section: X: 868.375
Y: 2140.675

The Cirque des Avalanches section was already described by Bernier (1984) and Meyer (2000). Along a small forest road running from the village of Champfromier onto the plateau of the *Forêt de Champfromier* (Fig. 4.16), it exposes Oxfordian to Early Tithonian strata. For this study, only the upper part (Late Kimmeridgian – Early Tithonian) was measured, starting some 100 m down the road from the little roadmen's cabin, with the first clearly developed beds that onlap on a massive, patch-reef like structure (Fig. 4.17, see also Meyer 2000). The outcrop ends at the viewpoint on the edge of the *Forêt de Champfromier* plateau.

Lithostratigraphy and sedimentology

Enay (1965) introduced a lithostratigraphic subdivision for the southern Jura Mountains that differs from the northern Jura lithostratigraphy (Thalmann 1966, Häfeli 1966). This lithostratigraphy was, in turn, modified by Bernier (1984). Later on, Bernier's (1984) new nomenclature was adopted by Enay (2000), yet, specifically in the Cirque des Avalanches section, the two schemes differ considerably in thicknesses and stratigraphic position of lithologic units bearing identical names. E.g., Bernier (1984) states that his "*Calcaires de la Sémine"* correspond to the *"Banc à momies intermédiaire"* of Enay (1965), which is definitely not true for the Cirque des Avalanches section. Compared to Bernier's (1984, Fig. 46) interpretation, the *Calcaires de la Sémine* of Enay (2000) are situated approximately 50 m

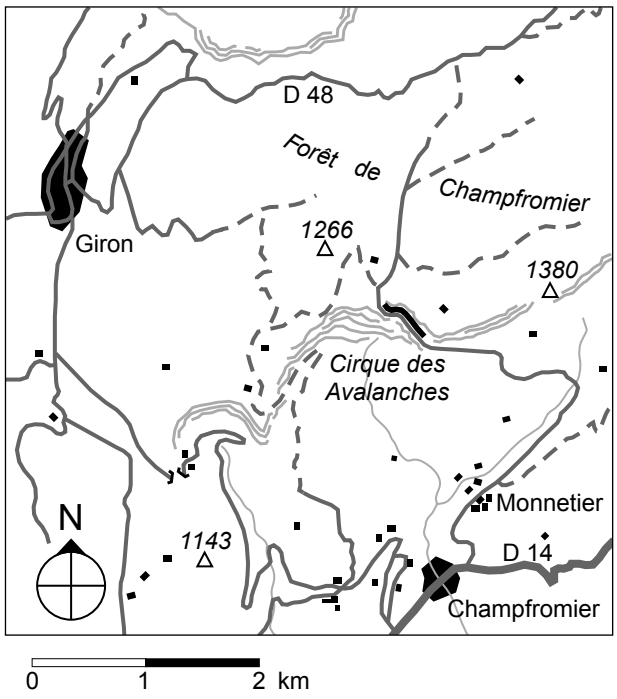

Fig. 4.16 - Location of the Cirque des Avalanches section. For legend see Fig. 4.6b.

higher in the stratigraphic column, extending the *Couches de Prapont inférieures* to a thickness of more than 50 m and reducing the *Couches de Prapont supérieures* to some 14 m. The local lithostratigraphic names used in this study (Fig. 4.17) – except for the "*Marnes grises*" (Meyer 2000) – follow Enay (2000), who provides a brief but very useful lithological description of each lithologic unit and its approximate thickness in the region.

The section is divided into two major parts that correspond to the Reuchenette and the Twannbach formations. The lower part of the section begins with bedded dolomites onlapping on a patch-reef that are overlain by a thick succession of lagoonal pack- to grainstones that indicate relatively open (close to normal marine, high-energy) conditions. Rich in oncoids and ooids at the base (6-17 m), they reflect a high-energy backreef environment with ooid bars, probably relatively close behind the platform rim. The following 37 m (17–54 m) are dominated by oncoid pack- and grainstones, indicating a change to a more proximal (but slightly deeper) lagoonal system. Beginning at 54 m, ooids begin to re-appear, at first reflecting internal bars (54-61 m) and then again more open marine, tidally influenced conditions (61-67.5 m). After the local subdivision of Enay (2000), this thick-bedded, high-energy interval with frequently barely visible bedding-planes is called the "*Couches de Prapont*", subdivided into a lower part ("*inférieur*") and an upper part ("*supérieur*") by the well-developed emersion horizons of the "*Calcaires de la Sémine*" (49-54 m). Enay (2000) reports multicoloured breccias, rhizoliths, calcrete fragments, and green marls from this level in nearby locations. According to P. Skelton (pers. comm.), the *Couches de Prapont* in the region also yield small biostromes of diceratid rudists. However, no rudists were discovered in the examined section.

The upper part of the section begins with a sharp change in energy regime and sedimentary environments. It is expressed by a sudden switch above 67.5 m (Fig. 4.17) from peloid grainstones to dark, marly mudstones ("*Marnes grises*" Meyer 2000, "*Marnes des Abergements*" Enay 2000) with heavily bioturbated calcareous interbeds (67.5-73.5 m). The dark colour of the marls and the virtual absence of bioturbation, in contrast to the heavily burrowed interbeds, were probably caused by a lack in oxygenation (dysaerobic conditions). A small microbialite build-up at the top of the *Couches de Prapont supérieures* (63.5 m; cf. Pl. 6/6) might be a first hint for diminishing water-exchange. Pure microbialite reefs, which contain hardly any macro-organisms, normally occur in deep ramp settings and tolerate dysaerobic conditions (Leinfelder et al. 1993, Leinfelder & Schmid 2000). Yet, in this case, the build-up is intercalated between a shallow open-marine bar-system at the base and tidally influenced peloidal dunes on top. It probably reflects a short period of complete isolation from the rest of the lagoon system, potentially caused by the high mobility of the surrounding bar systems.

The lower part of the Twannbach Formation (= "*Couches de Chailley*", Enay 2000) (73.5 m – top section) consists of a succession of muddy lagoonal and tidal-flat sediments with intercalated dolomite caps, very similar to the lower part of the Twannbach Formation as described for other platform sections. The upper part of the Twannbach Formation (= "*Tidalites de Vouglans*", Bernier 1984) is not exposed.

Biostratigraphy

No fossils suitable for a biostratigraphic framework on ammonite-zone level were found. Bernier (1984) tried to establish a coarse biostratigraphy based on microfossils that is not very useful for a high-resolution approach like in the present study. However, Enay (1965, 1966, 2000) mentions some ammonites found in the region that, due to his precise facies descriptions, can be approximated to certain levels in the Cirque des Avalanches section. He reports an *Aulacostephanus eudoxus* from the base of the coral patch-reef near the Prapont Bridge that probably was more or less contemporaneous to the one in Cirque des Avalanches. Furthermore, *Gravesia gravesiana*, *Gravesia irius*, and *Gravesia gigas* were found, with *Gravesia irius* always associated with the heavily bioturbated limestones ("*Calcaires à tubulures*"-facies of the *Couches de Chailley*) at the base of the Twannbach Formation. Thus, Enay (2000) states that it is obvious

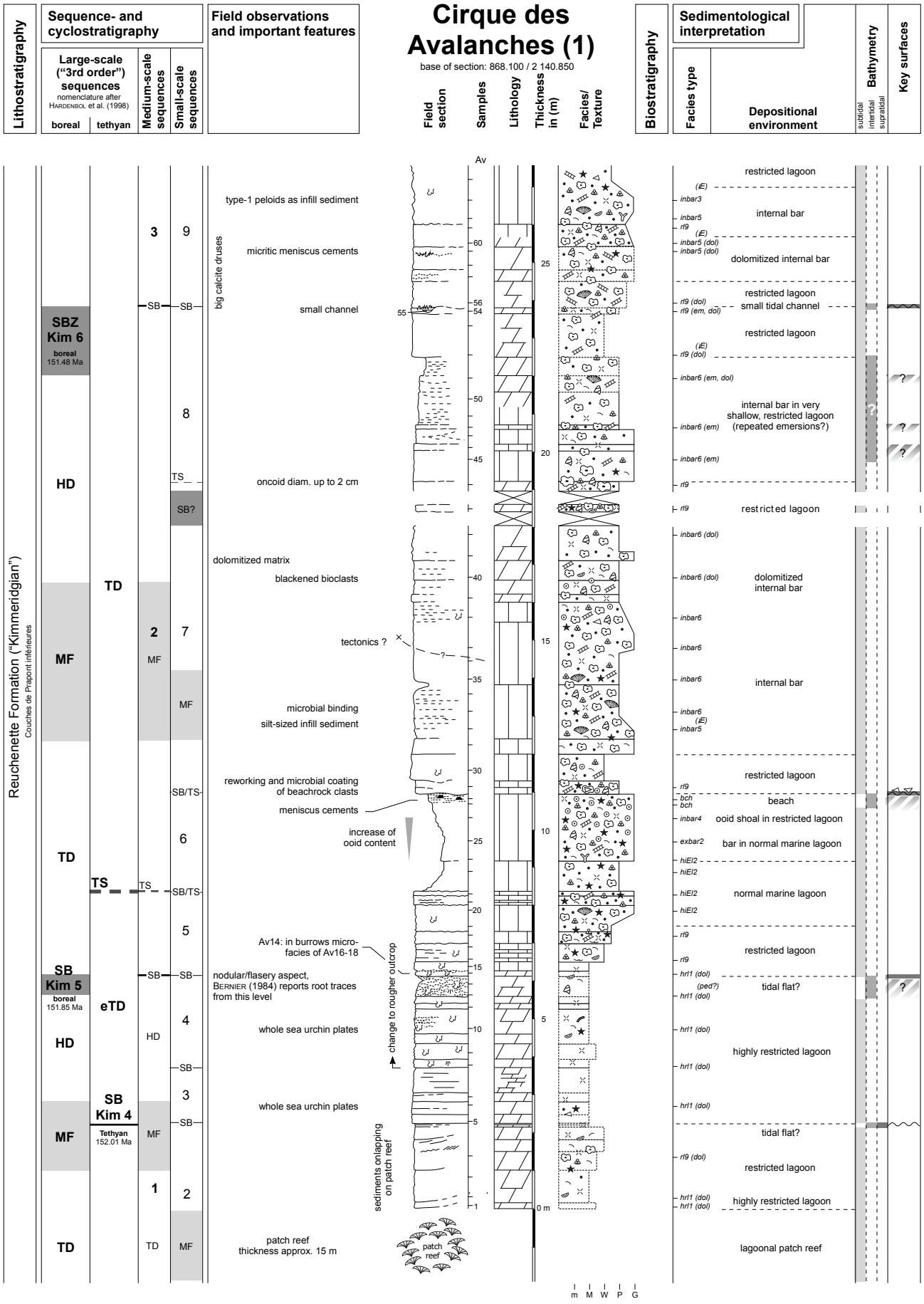

Fig. 4.17 - (this page and the three following pages) Sedimentological and sequence-stratigraphic interpretation of the Cirque des Avalanches section.

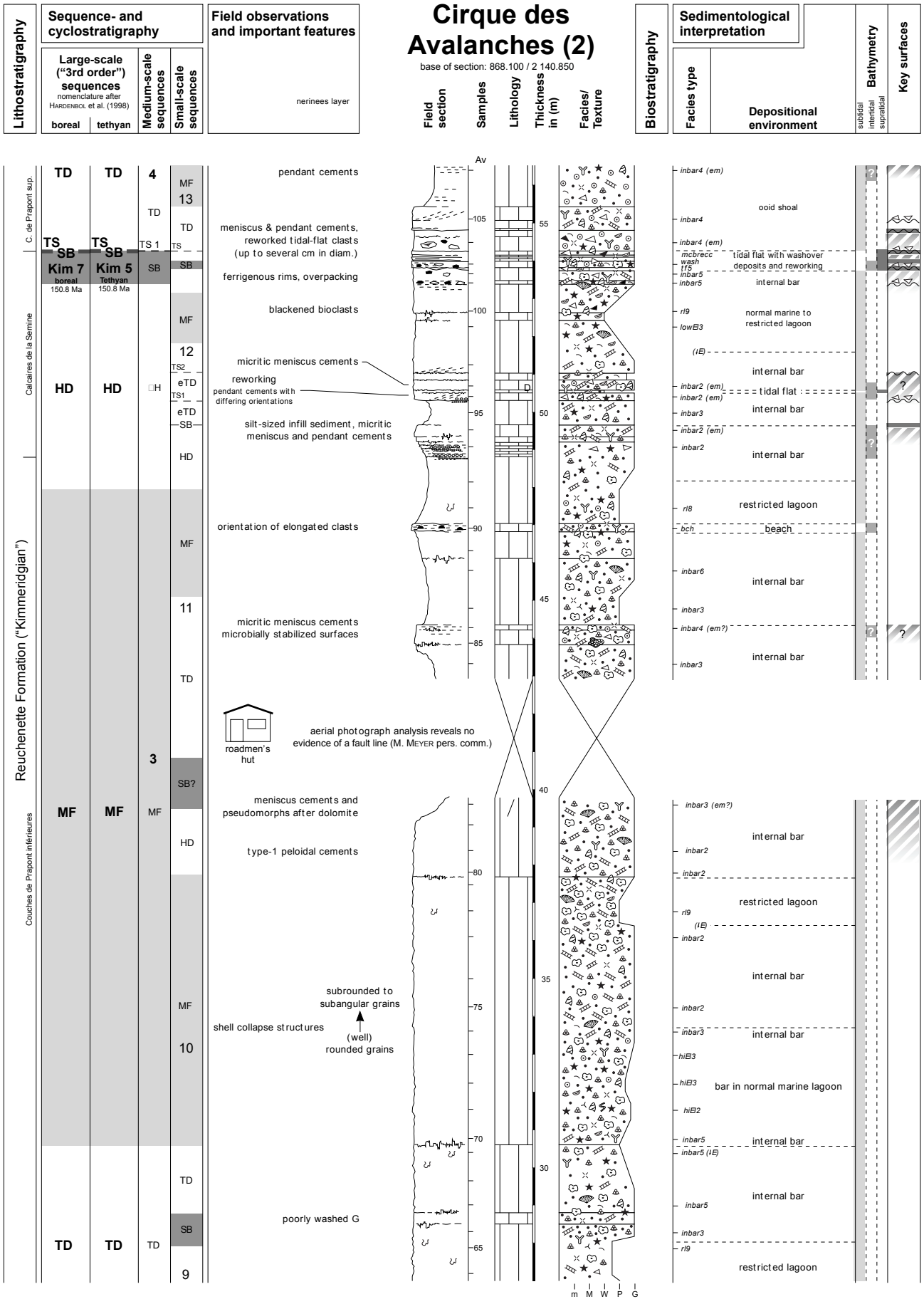
Cirque des Avalanches (2)
base of section: 868.100 / 2 140.850
Lithostratigraphy
Sequence- and cyclostratigraphy
Large-scale ("3rd order") sequences
nomenclature after HARDENBOL et al. (1998)
boreal
tethyan
Medium-scale sequences
Small-scale sequences
Field observations and important features
nerinees layer
Field section
Samples
Lithology
Thickness in (m)
Facies/ Texture
Biostratigraphy
Sedimentological interpretation
Facies type
Depositional environment
Bathymetry
subtidal
intertidal
supratidal
Key surfaces
Reuchenette Formation ("Kimmeridgian")
C. de Prapont sup.
Calcaires de la Semine
Couches de Prapont inférieures
Kim 7
boreal
150.8 Ma
Kim 5
Tethyan
150.8 Ma
pendant cements
meniscus & pendant cements, reworked tidal-flat clasts (up to several cm in diam.)
ferrigenous rims, overpacking
blackened bioclasts
micritic meniscus cements
reworking
pendant cements with differing orientations
silt-sized infill sediment, micritic meniscus and pendant cements
orientation of elongated clasts
micritic meniscus cements microbially stabilized surfaces
roadmen's hut
aerial photograph analysis reveals no evidence of a fault line (M. MEYER pers. comm.)
meniscus cements and pseudomorphs after dolomite
type-1 peloidal cements
subrounded to subangular grains
shell collapse structures
(well) rounded grains
poorly washed G
ooid shoal
tidal flat with washover deposits and reworking
internal bar
normal marine to restricted lagoon
tidal flat
restricted lagoon
beach
bar in normal marine lagoon
m M W P G

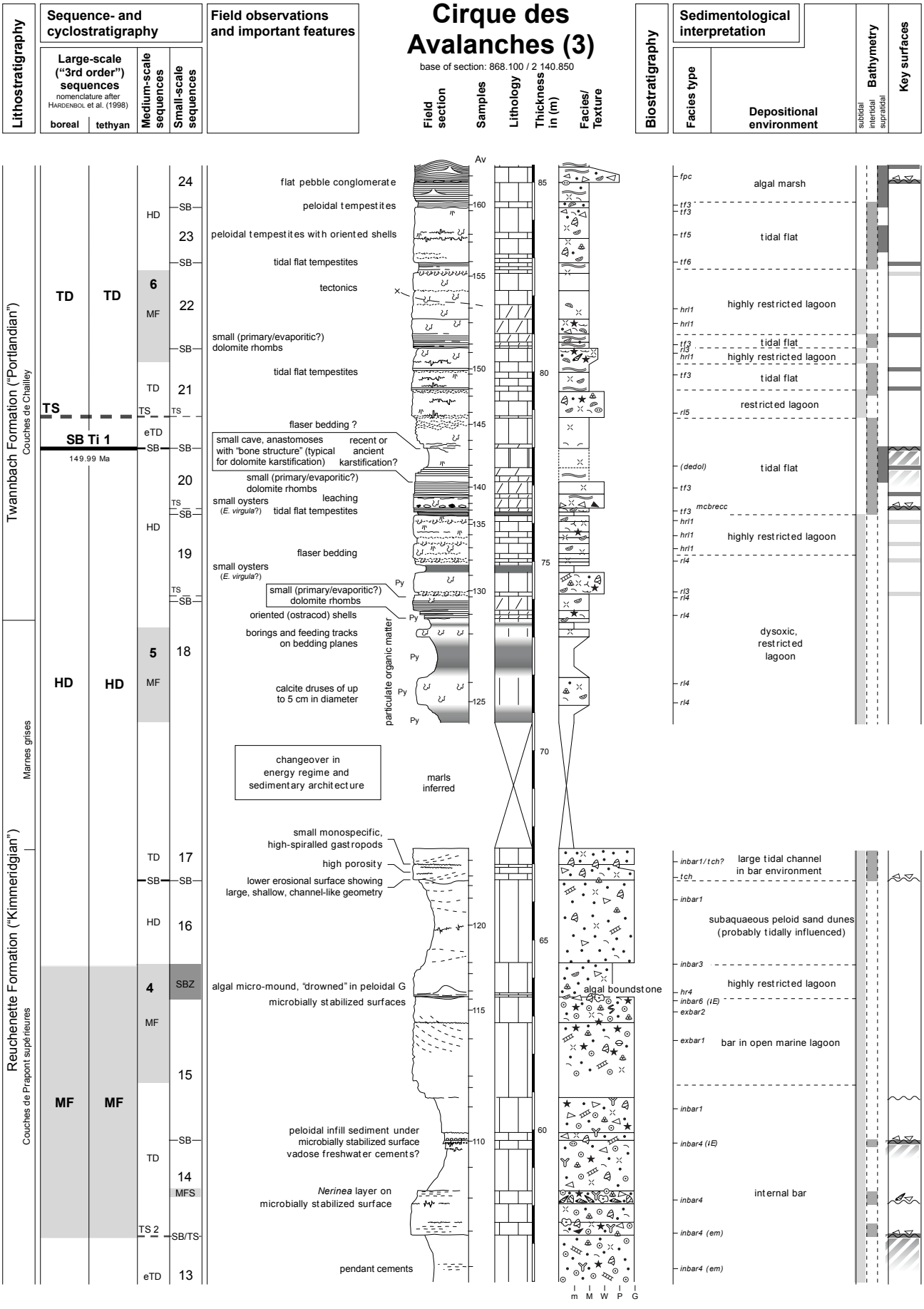
Lithostratigraphy
Sequence- and cyclostratigraphy
Large-scale ("3rd order") sequences
nomenclature after HARDENBOL et al. (1998)
boreal
tethyan
Medium-scale sequences
Small-scale sequences
Field observations and important features
Cirque des Avalanches (3)
base of section: 868.100 / 2 140.850
Field section
Samples
Lithology
Thickness in (m)
Facies/ Texture
Biostratigraphy
Sedimentological interpretation
Facies type
Depositional environment
Bathymetry
subtidal
intertidal
supratidal
Key surfaces
Twannbach Formation ("Portlandian")
Couches de Chailley
Marnes grises
Reuchenette Formation ("Kimmeridgian")
Couches de Praporit supérieures
TD
HD
MF
TS
SB Ti 1
149.99 Ma
SB
eTD
MFS
SB/TS
TS 2
flat pebble conglomerate
peloidal tempestites
peloidal tempestites with oriented shells
tidal flat tempestites
tectonics
small (primary/evaporitic?) dolomite rhombs
flaser bedding ?
small cave, anastomoses with "bone structure" (typical for dolomite karstification)
recent or ancient karstification?
small oysters (E. virgula?)
leaching
flaser bedding
oriented (ostracod) shells
borings and feeding tracks on bedding planes
particulate organic matter
calcite druses of up to 5 cm in diameter
changeover in energy regime and sedimentary architecture
marls inferred
small monospecific, high-spiralled gastropods
high porosity
lower erosional surface showing large, shallow, channel-like geometry
algal micro-mound, "drowned" in peloidal G
microbially stabilized surfaces
peloidal infill sediment under microbially stabilized surface
vadose freshwater cements?
Nerinea layer on microbially stabilized surface
pendant cements
algal boundstone
algal marsh
tidal flat
highly restricted lagoon
restricted lagoon
dysoxic, restricted lagoon
large tidal channel in bar environment
subaquaeous peloid sand dunes (probably tidally influenced)
bar in open marine lagoon
internal bar
m M W P G

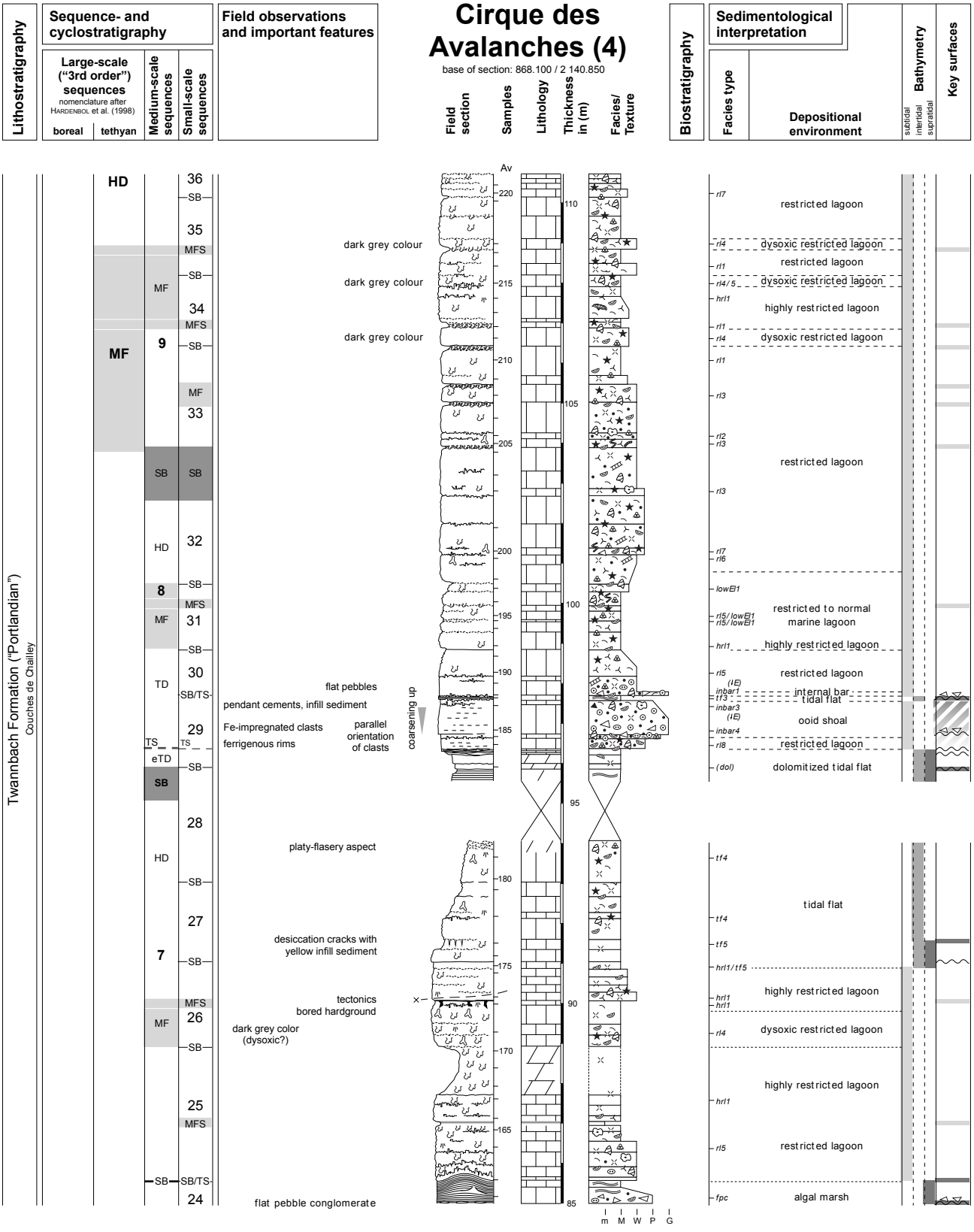
Cirque des Avalanches (4)
base of section: 868.100 / 2 140.850
Lithostratigraphy
Sequence- and cyclostratigraphy
Large-scale ("3rd order") sequences
nomenclature after Hardenbol et al. (1998)
boreal
tethyan
Medium-scale sequences
Small-scale sequences
Field observations and important features
Field section
Samples
Lithology
Thickness in (m)
Facies/ Texture
Biostratigraphy
Sedimentological interpretation
Facies type
Depositional environment
Bathymetry
subtidal
intertidal
supratidal
Key surfaces
Twannbach Formation ("Portlandian")
Couches de Chailley
HD
MF
SB
TS
eTD
MFS
TD
dark grey colour
flat pebbles
pendant cements, infill sediment
Fe-impregnated clasts
ferrigenous rims
parallel orientation of clasts
coarsening up
platy-flasery aspect
desiccation cracks with yellow infill sediment
tectonics
bored hardground
dark grey color (dysoxic?)
flat pebble conglomerate
restricted lagoon
dysoxic restricted lagoon
highly restricted lagoon
restricted to normal marine lagoon
internal bar
tidal flat
ooid shoal
dolomitized tidal flat
algal marsh
m M W P G

that the *Couches de Chailley* begin in the uppermost Kimmeridgian (top *beckeri/autissiodorensis* Zone) and the age of the *Couches de Prapont* corresponds in large parts to the *beckeri* Zone.

Bernier (1984) and Enay (2000) refer to the marly interval (67-73.5 m) as an equivalent of the *Marnes des Abergements*. However, the palynological dating carried out by Meyer (2000) shows that the *Marnes des Abergements* in their type locality (cf. Bernier 1984) are most probably located in the *mutabilis* Zone (beginning Late Kimmeridgian). Meyer (2000) refers to the marly interval of the *Cirque des Avalanches* section as "*Marnes grises*" (grey marls), because the palynomorph assemblage points to a latest Kimmeridgian or Early Tithonian age and therefore excludes any isochroneity with the *Marnes des Abergements*. Apparently, this marly interval, located exactly at the point of a major change in sedimentary architecture (Reuchenette-Twannbach boundary) and also very close to the Kimmeridgian/Tithonian boundary is the local version of the upper *virgula* Marls (cf. La Dôle section).

Sequence stratigraphy

At the base of the relatively open, high-energy lagoons of the Reuchenette Formation, large-scale sequence boundary SB $Kim5_{Boreal}$ is expressed as flasery dolomites, capping the patch reef at base of the section. Bernier (1984) reports root traces from this level. SB $Kim5_{Boreal}$ is followed by a major transgression that is primarily characterized by a substantial gain in accommodation space. This interval probably defines a period of maximum flooding in long-term (2^{nd}-order) sea-level evolution. Within this 2^{nd}-order MF, SB $Kim5_{Tethyan}$ (= SB $Kim7_{Boreal}$ = "*Calcaires de la Sémine*" = SB 140 of Strohmenger et al. 1991, Fookes 1995, and Enay 2000) is defined by a brief but marked excursion from oncoid- and ooid-rich bar environments to subaerial exposure and reworking.

Beginning with the base of medium-scale sequence 5, medium- and small scale sequences show a lower average thickness as below and are much more characterized by peritidal environments, repeated emersions, and sequence boundaries hidden in dolomite caps and/or with pronounced subaerial exposure. However, this decrease in average thickness is much less developed than, e.g., in the Dôle or Noirvaux sections. The SB between medium-scale sequences 5 and 6 is developed as dolomite cap, showing dedolomitization and karstification at the top. It is also interpreted to represent large-scale SB Ti1. Similar to most other platform sections described earlier, the top of medium-scale sequence 7 also consists of a pronounced dolomite cap, and the large-scale MF around medium-scale sequence 9 is emphasized by heavily bioturbated bedding planes. In addition, this interval also shows dark grey colour (probably caused by dysoxic conditions) in the Cirque des Avalanches section.

***Yenne** (Figs 4.18, 4.19)*

= upper part of the *La Balme* section of Bernier (1984)

approx. 10 km W of the Lac de Bourget, 30 km NW of Chambéry (France)

Institut Géographique National (IGN), TOP 25, sheet 3232 ET *Belley*, 1 : 25 000

Base of section: X: 865 000
Y: 2084 100

The *Yenne* section is also known under the name *La Balme* section from Bernier (1984), who worked on its entire stratigraphic range beginning from the Late Kimmeridgian. It is divided by a barrier-reef complex, probably of latest Kimmeridgian or earliest Tithonian age, into a lower part and an upper part. From the lower part ("*Calcaires de Tabalcon*" / "*Couches à silex*"), Bernier (1984) reports a succession of wackestones and packstones with common chert nodules yielding microfilaments, bivalves, rhynchonellid brachiopods, echinoderm debris, bryozoans, serpulids, *Globochaetes* sp., benthic foraminifera, *Globigerina* sp., radiolarians, aptychi, sponge spicules, and *Tubiphytes/Koskinobullina* microencruster associations – a faunal assemblage that is characteristic for fore-reef, deeper outer platform and/or ramp environments (cf. Chap. 2).

In all other platform sections of this study, the Late Kimmeridgian was deposited in back-reef facies. Unfortunately, the lower part of the section cannot be exactly correlated with the other measured sections due to a tectonic contact. Consequently, only the upper, Tithonian to Middle Berriasian part of entirely lagoonal origin was measured.

The section was primarily chosen because it makes the link with the Goldberg Formation (Strasser 1994). Log and microfacies data as well as palaeoenvironmental interpretation from the upper part of the section (Strasser 1994 and unpubl. data) were integrated and redrawn to fit with the newly measured base of the section (0-29 m).

Lithostratigraphy and sedimentology

The entire section consists of (highly) restricted lagoonal deposits, tidal-flat deposits, and dolomite caps. Emersion indicators such as multicoloured breccias,

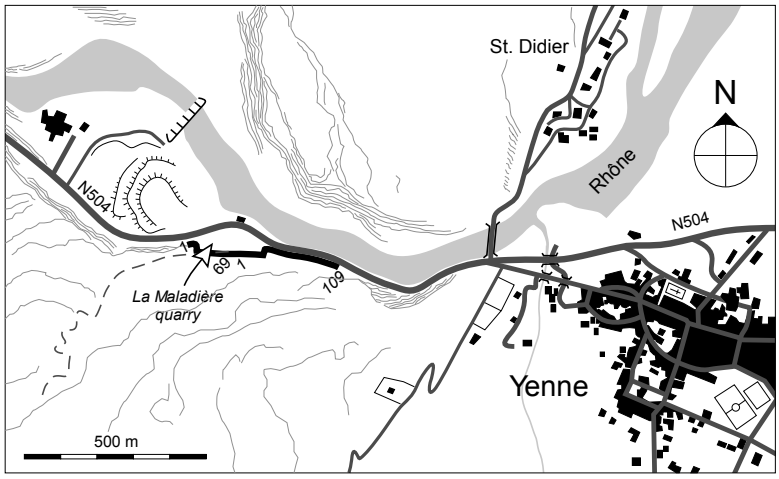

Fig. 4.18 - Location of the Yenne section. For legend see Fig. 4.6b.

desiccation cracks, circumgranular cracks, and bird's eyes are frequent. It was chosen to define the Twannbach/Goldberg boundary at the thick marl layer at 61 m. However, this position is highly speculative, also the marls layer at 34.5 m, respectively 44.3 m, both of them containing charophytes, could have been chosen. This uncertainty is related to the special facies of the Goldberg Formation in the relatively distal Yenne section that is nothing but a continuation of the facies characterizing the Twannbach Formation. Instead of a clear change to a succession of marlier sediments with abundant multicoloured breccias that usually shows a softer weathering ("*Combe purbeckienne*", cf. Lieu section), the change in Yenne is gradual. It is characterized by a step-by-step increase in abundance and thickness of marl layers and the abundance of charophytes that indicate continental conditions (presence of freshwater). Palaeosols and freshwater lakes only formed in the uppermost 10 m of the section, climaxing with a several dm thick multicoloured breccia in a marl matrix that forms a distinct depression in the cliff along the N504 (Pl. 20/4). It corresponds to a prolonged period of subaerial exposure that defines the top of the Goldberg Formation. The beginning of the high-energy bar system of the Pierre-Châtel Formation forms a well-developed crag over the top-Goldberg depression.

Biostratigraphy

The only organisms that are of biostratigraphic value in the peritidal facies of the Goldberg Formation are charophytes and ostracodes (Détraz & Mojon 1989). The biostratigraphic framework of the Yenne section was taken from Strasser (1994). Charophyte-ostracode assemblage zones M1b and M2/3 were found in samples taken by Strasser (1994). The approximate position of zone M1a is inferred from the correlations that are presented by Strasser (1994).

Sequence stratigraphy

Even if the Yenne section has the most distal location of the measured platform sections, it is also the one that exposes the youngest strata, i.e. sediments that were deposited during advanced long-term regression (cf. Fig. 1.9). Thus, non-deposition and erosion are common phenomena and the potential for sediment deposition and preservation is lowest, specifically in the interval from SB $Be2_{Tethyan}$ to SB Be3/4 (76-104 m). Below SB $Be2_{Tethyan}$, large-scale sequence boundaries are usually expressed as rather vague SBZs, defined by a repetition of emersion surfaces and vadose diagenesis, where as from SB $Be2_{Tethyan}$ onwards, SBs tend to be expressed in a clearly defined horizon, featuring emersion, reworking, and incipient pedogenesis.

An interesting feature concerning the stacking pattern in Yenne is the increase in thickness from medium-scale sequence 17 to medium-scale sequence 18. Medium-scale sequences then stay relatively thick until the top of medium-scale sequence 22 – a fact that seems to be completely in contradiction to the more and more restricted facies and a prograding shoreline on top of a shallow carbonate platform. However, this effect may be explained by the beginning of a long-term (2^{nd}-order) transgression that allows for the creation of more accommodation space but, at the same time, is not strong enough to force the sedimentary system into a retrogradational pattern ("backstepping") or even a platform drowning.

The pronounced dolomite cap between SB $Be2_{Boreal}$ and SB $Be2_{Tethyan}$ probably relate to a phase of strong seepage reflux triggered by the formation of massive evaporite deposits nearby (see Chap. 3 for explanation of dolomitizing mechanism). This is the inferred stratigraphic position where a major collapse breccia in the Dôle section proves the presence of such evaporites. If this hypothesis is developed further, the channelled breccia that defines SB $Be2_{Tethyan}$ might even be the reworked and transported remains of some collapse breccia that formed during the dissolution of nearby evaporites.

Together with SB $Ti3_{Tethyan}$ of the Dôle section, SB Be3/4 in Yenne is the most strongly expressed large-scale sequence boundary in the measured sections. Strasser & Hillgärtner (1998) already discussed the position of SB Be3 in their sequence-stratigraphic interpretation and the possibility of two SBs (SB Be3 and SB Be4) merged in this very pronounced interval. Considering the presence of charophyte-ostracode assemblage M2/3 in the multicoloured breccia in question and based on the detailed correlation (cf. Chap. 7), a merged SB Be3/4

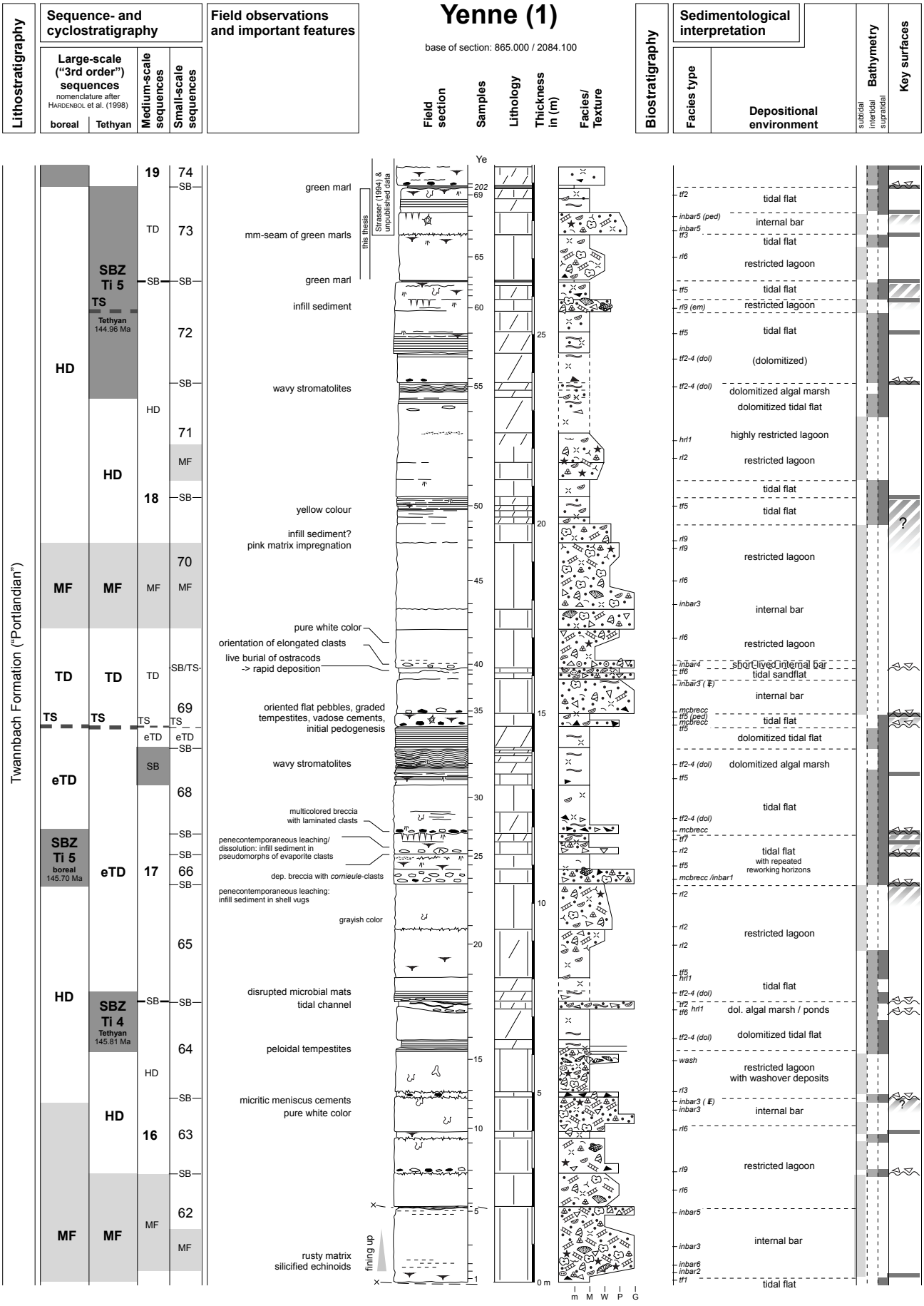

Fig. 4.19 - (this page and the three following pages) Sedimentological and sequence-stratigraphic interpretation of the Yenne section.

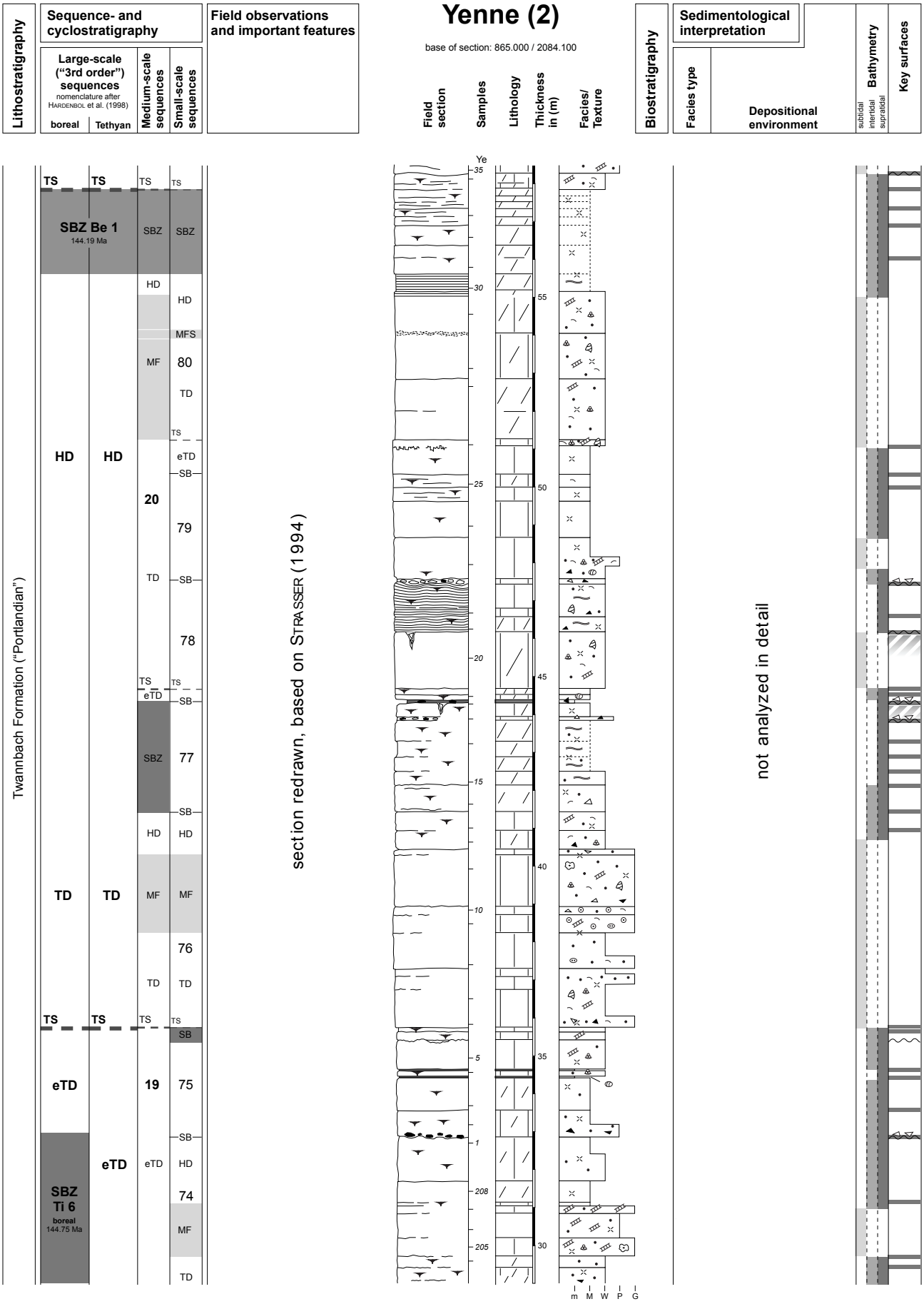
Yenne (2)
base of section: 865.000 / 2084.100
Lithostratigraphy
Sequence- and cyclostratigraphy
Large-scale ("3rd order") sequences
nomenclature after HARDENBOL et al. (1998)
boreal
Tethyan
Medium-scale sequences
Small-scale sequences
Field observations and important features
Field section
Samples
Lithology
Thickness in (m)
Facies/ Texture
Biostratigraphy
Sedimentological interpretation
Facies type
Depositional environment
Bathymetry
subtidal
intertidal
supratidal
Key surfaces
Twannbach Formation ("Portlandian")
SBZ Be 1
144.19 Ma
SBZ Ti 6
boreal
144.75 Ma
HD
TD
eTD
MF
MFS
SBZ
TS
SB
20
19
80
79
78
77
76
75
74
section redrawn, based on STRASSER (1994)
not analyzed in detail
m M W P G

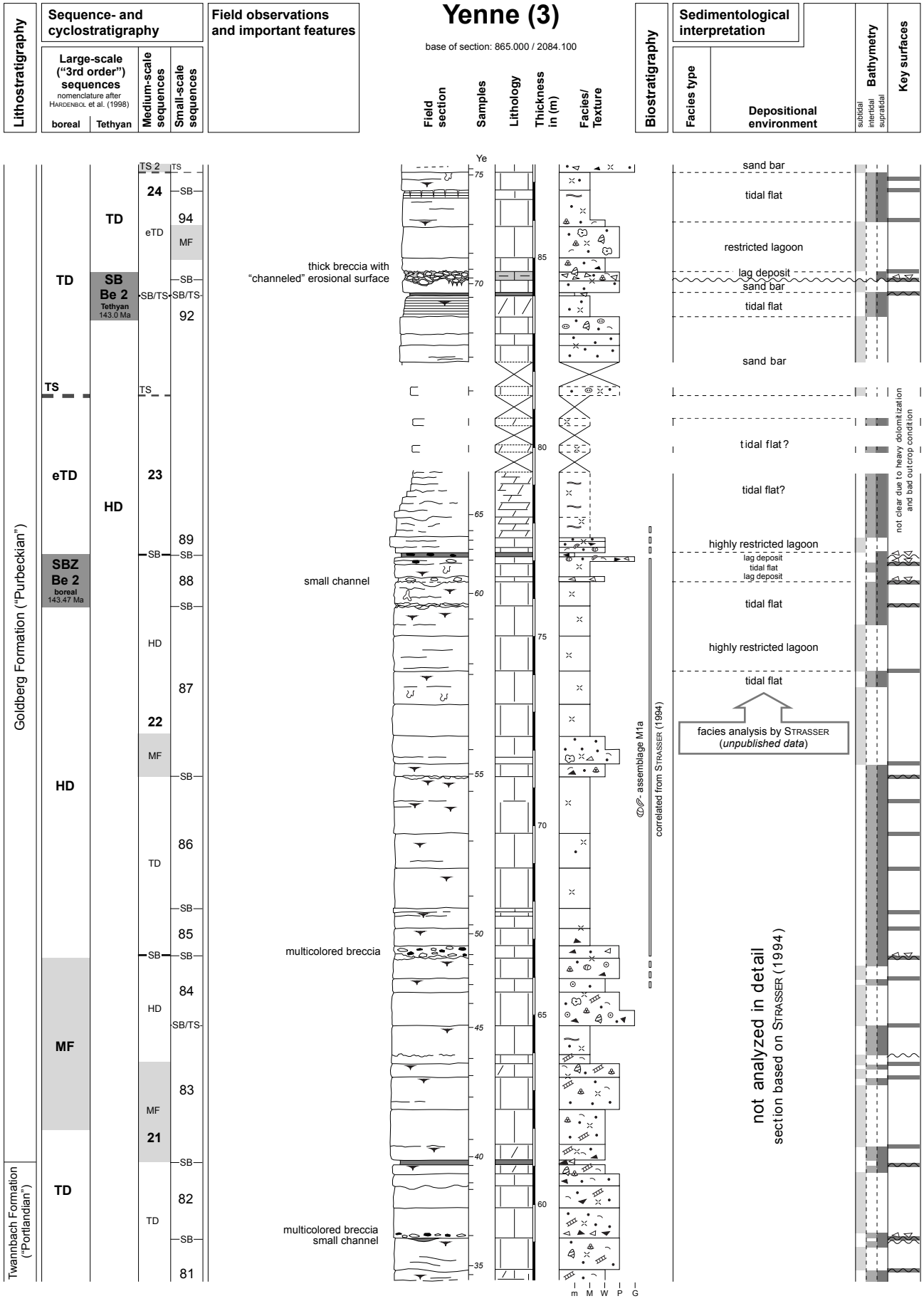
Yenne (3)
base of section: 865.000 / 2084.100
Lithostratigraphy
Sequence- and cyclostratigraphy
Large-scale ("3rd order") sequences
nomenclature after Hardenbol et al. (1998)
boreal
Tethyan
Medium-scale sequences
Small-scale sequences
Field observations and important features
Field section
Samples
Lithology
Thickness in (m)
Facies/ Texture
Biostratigraphy
Sedimentological interpretation
Facies type
Depositional environment
Bathymetry
subtidal
intertidal
supratidal
Key surfaces
Goldberg Formation ("Purbeckian")
Twannbach Formation ("Portlandian")
TD
SB Be 2
Tethyan
143.0 Ma
SBZ Be 2
boreal
143.47 Ma
eTD
HD
MF
TS
TS 2
SB
SB/TS
thick breccia with "channeled" erosional surface
small channel
multicolored breccia
multicolored breccia small channel
sand bar
tidal flat
restricted lagoon
lag deposit
tidal flat?
highly restricted lagoon
not clear due to heavy dolomitization and bad outcrop condition
facies analysis by Strasser (unpublished data)
correlated from Strasser (1994)
not analyzed in detail
section based on Strasser (1994)
m M W P G

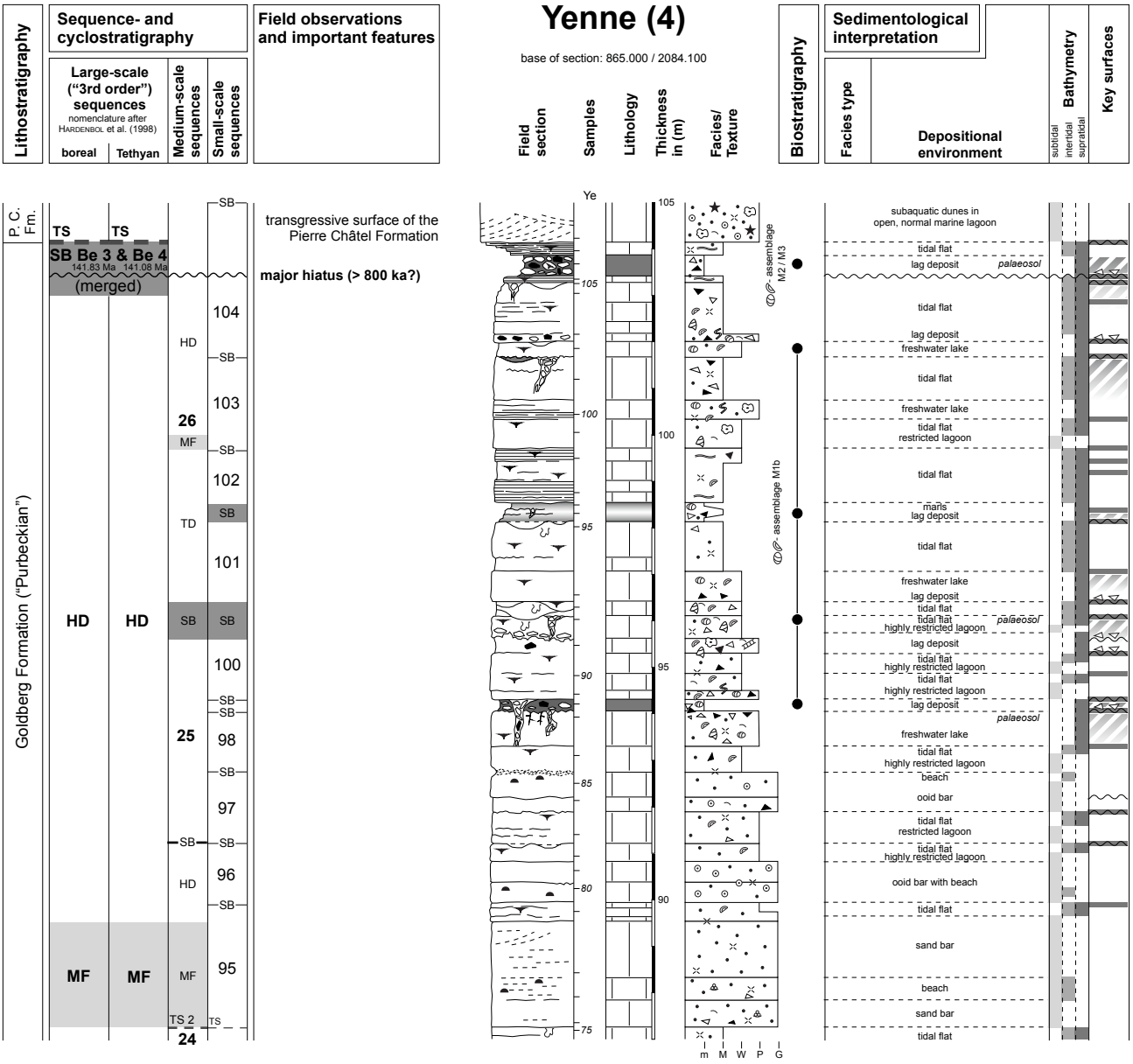

is the best-fitting and most probable solution for the Yenne section. This merged, large-scale "double" SB corresponds to the major disconformity DIIb mentioned by Détraz & Steinhauser (1988), respectively Détraz & Mojon (1989). On top of this major disconformity, the base of the Pierre-Châtel Formation marks the following large-scale transgression.

approx. 5 km S of Le Pouzin (western side of the French Rhône valley, halfway between Valence to the N and Montélimar to the S)

Institut Géographique National (IGN), Série Bleue, sheet 3037 O *La Voulte-sur-Rhône*, 1 : 25 000

Broyon Quarry X: 789 900
Y: 3272 450

Clue de la Payre X: 789 800
Y: 3272 900

4.3.2 Slope sections

Broyon – Clue de la Payre *(Figs 4.20, 4.21)*

The Broyon quarry is located about 2 km south of Le Pouzin, on the western side of the Rhône river,

along departmental road D22 (Fig. 4.20). The rocks exposed there at a thickness of about 40 m range from the Early Tithonian to Early Berriasian and are dated by calpionellids and ammonites (Le Hégarat 1973, Cecca et al. 1989). Earlier works on this section include Le Hégarat (1973), Cecca et al. (1989), Jan du Chêne et al. (1993), Strohmenger & Strasser (1993), and Dromart et al. (1993).

The Broyon section exposes hemipelagic slope deposits (Dromart et al. 1993, Strohmenger & Strasser (1993) and is characterized by strong reduction of thickness compared to all other measured platform and basin sections. This is due to a bypass-style of sedimentation (channel erosion, debris flows). For that reason, no high-resolution sequence analysis is possible, but from Jan du Chêne et al. (1993) and Strohmenger & Strasser (1993) a biostratigraphically calibrated framework of large-scale sequence boundaries can be drawn. The section was chosen to be investigated in order to understand the link between the Jura platform and the adjacent Vocontian Basin.

Unfortunately, during the field season of 2002, the Broyon quarry was off limits (and probably still is) due to the dangerous instability of the quarry walls. Thus, only some general observations could be made at the Clue de la Payre cliffs (Fig. 4.20), just outside of Le Pouzin, where essentially the same strata as in the Broyon quarry are exposed. Due to millennia of weathering, these cliffs have the advantage of a much better visibility of the stacking pattern (Pl. 21/1).

The logs, lithostratigraphic, and biostratigraphic data of Cecca et al. (1989), Jan du Chêne et al. (1993), and Strohmenger & Strasser (1993) from Broyon were compared with own observations from the La Payre cliffs and re-interpreted for an up-to-date sequence-stratigraphic framework.

Lithostratigraphy, sedimentology, and biostratigraphy

The Tithonian interval is represented by a base of bedded, fine-grained limestones with marl intercalations and three thin-bedded debris flows (beds 1a-8). The thick-bedded limestone cliff that shows a rather massive appearance on Pl. 21/1 begins with the "*Brêche de base*" (Cecca et al. 1989): channelled, massive breccias with erosive lower surfaces (bed 10, cf. Pl. 21/2) that are interpreted to be debris flows (Strohmenger & Strasser 1993). The interval between beds 12 and 17 is dominated by monomictic mudflow deposits with a minor grain-flow intercalation (base of bed 12). Most of the massive part corresponds to the "*Calcaires Blancs Formation*" of Cecca et al. (1989). The fossil assemblage is typical for a hemipelagic environment (radiolarians, calpionellids, foraminifera, sponge spicules, *Saccocoma*, calcispheres,

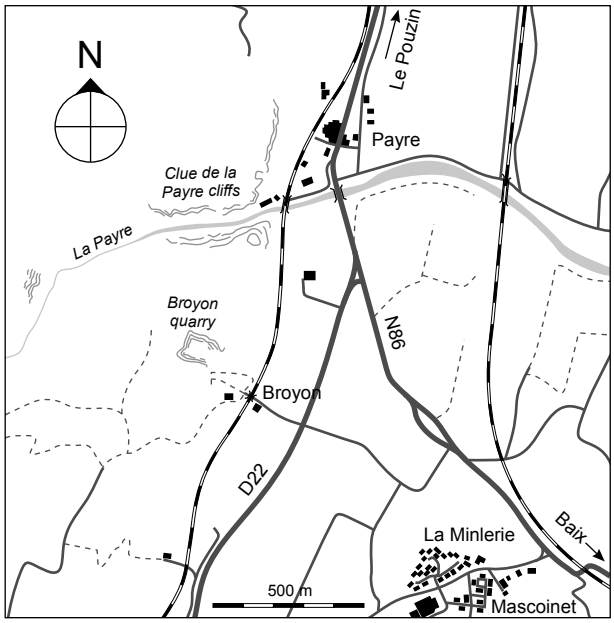

Fig. 4.20 - Location of the Broyon quarry and the Clue de la Payre cliffs. For legend see Fig. 4.6b.

filaments, aptychi, and globochaetids), but also shows some reworked, shallow-marine faunal elements such as pelecypods, echinoderm fragments, and gastropods (Strohmenger & Strasser 1993). The upper limit of the "*Calcaires Blancs Formation*" is defined by a prominent, Fe-encrusted and heavily bored hardground and also acts as upper edge of the quarry wall (Broyon), respectively of the massive cliff (Clue de la Payre).

The upper, Early Berriasian part of the section consists mainly of a limestone-marl alternation with a thickening-up trend of marlstones (Strohmenger & Strasser 1993). It is characterized by softer weathering and favourable conditions for microfossil preservation. Close to the top, outcrop conditions are rather bad and do not allow for sedimentologic interpretation. In Broyon, the section ends with a grain-flow deposit (bed 30) that is interpreted as fluxoturbidite (Strohmenger & Strasser 1993). A more detailed description of litho- and biostratigraphy, and specifically of the resediments is given in Cecca et al. (1989) and Strohmenger & Strasser (1993). All biostratigraphic data (calpionellid and ammonite zones, cf. Fig. 4.21) are taken from Cecca et al. (1989), Jan du Chêne et al. (1993), Strohmenger & Strasser (1993), and Dromart et al. (1993).

The Clue de la Payre section essentially shows the same succession as described above, the main difference being a lower abundance of gravitational deposits at the base of the "*Calcaires Blancs Formation*" and a less marly top. Cecca et al. (1989), who presented a regional study of the Ardèche area, mention that the lithological succession of the interval discussed above shows considerable lateral

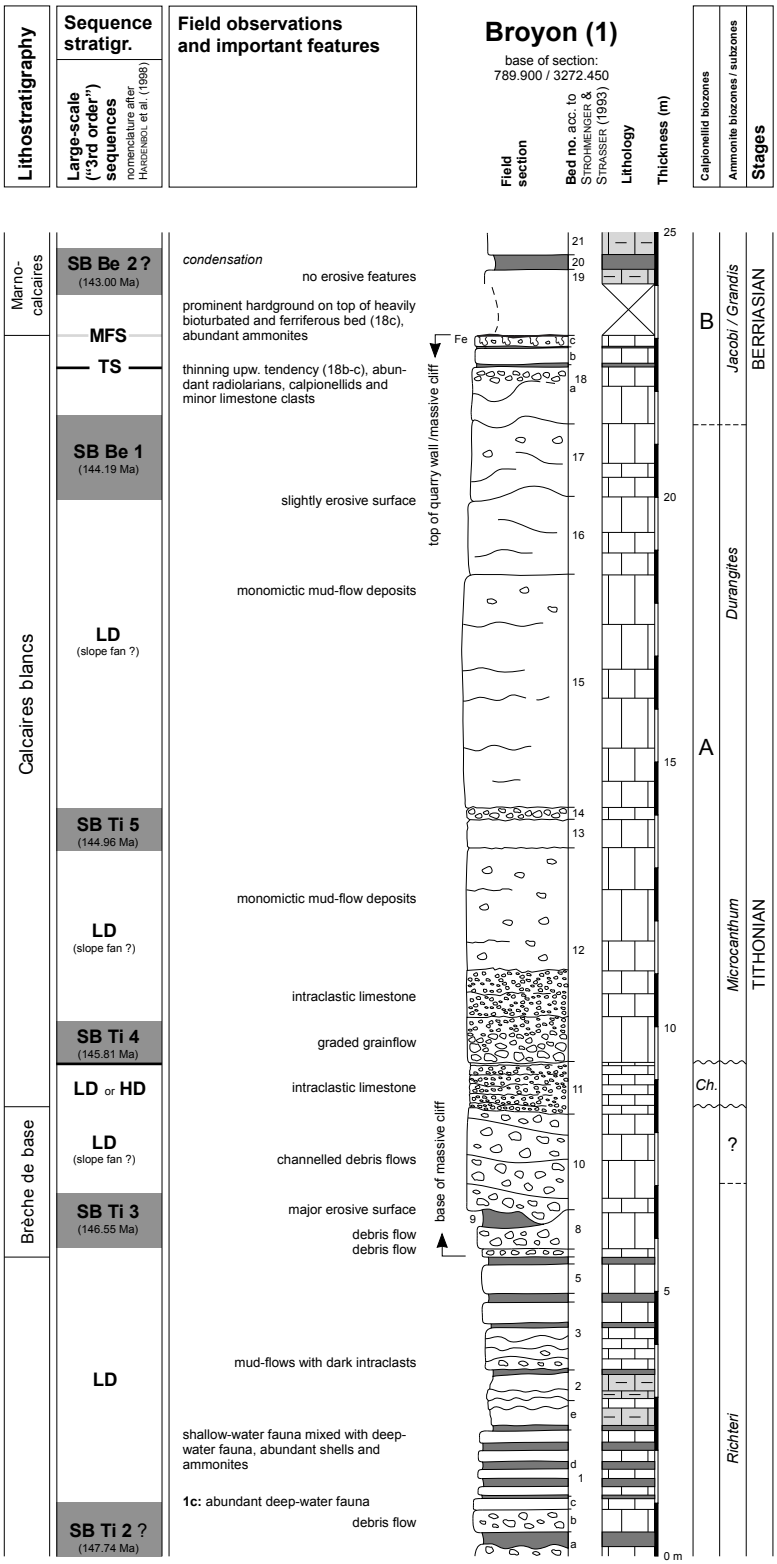

Fig. 4.21 - (this page and following page) Sedimentological and sequence-stratigraphic interpretation, and biostratigraphy of the Broyon section. Original sections by CECCA et al. (1989), JAN DU CHÊNE et al. (1993), and STROHMENGER & STRASSER (1993), re-drawn and re-interpreted.

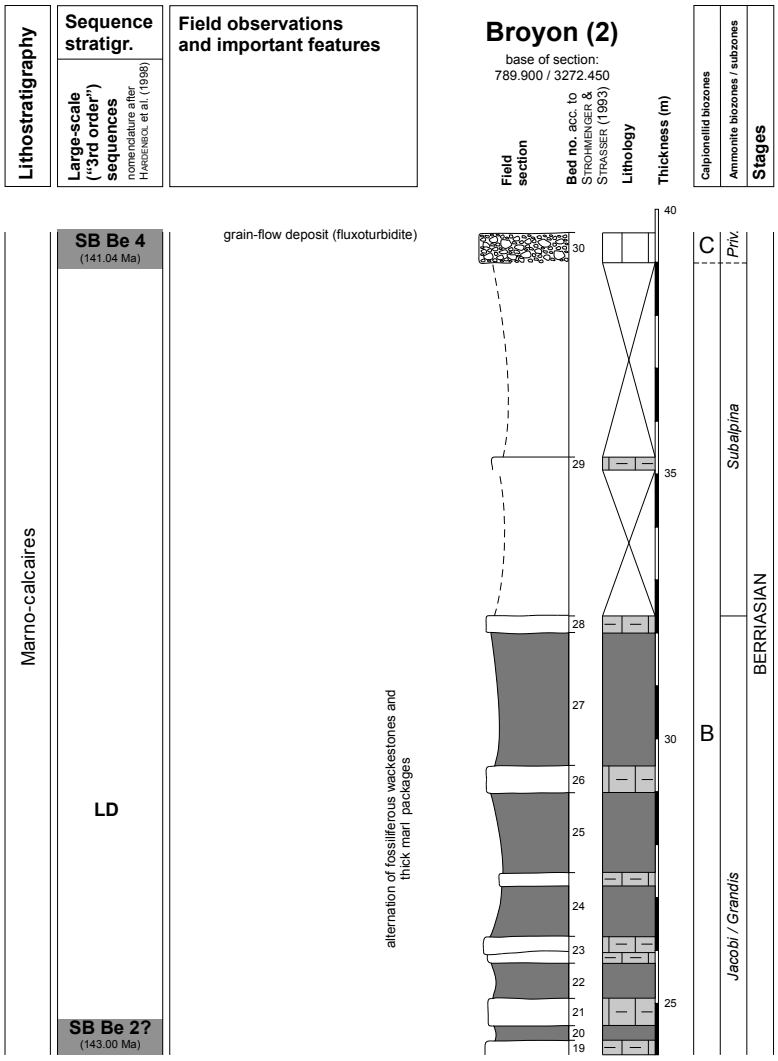

variation on longer distances. This observation fits well with an interpretation of the Broyon – Clue de la Payre area as wide-channelled slope-deposits. The Broyon section, displaying heavy resedimentation and a rather marly upper part, might have been relatively close to the channel axis, whereas the Clue de la Payre section is more likely to represent a more marginal position in a wide submarine channel.

The development of this bypass-slope is probably due to the Late Jurassic long-term regressive trend (Fig. 1.9). This would favour extensive platform progradation and resedimentation on the slope. Yet, eustatic sea-level changes can be attenuated or enhanced by tectonics. STROHMENGER & STRASSER (1993) propose that the rapid lithological changes are related not only to eustatic sea-level changes but also to tectonically induced changes in subsidence (DROMART et al. 1993), causing a predominance of mass-flow deposits throughout the Tithonian and an important creation of accommodation space in the earliest Berriasian. This interpretation is sustained by the plate tectonic models of STAMPFLI et al. (2002) and STAMPFLI & BOREL (2002) that suggest an extensional regime with a major strike-slip component (cf. Fig. 1.4). Such a fault could easily produce a kind of a small-scale "shelf break" that would promote the installation of a submarine canyon system running down the slope and then turning parallel to the basin axis, as already implied by REMANE (1970) and FOURCADE (1993). At the same time, an enhanced subsidence of the basin floor and high carbonate exportation rates would allow for the development of thick basin deposits in relatively shallow water depths (cf. SÉGURET et al. 2001, WHALEN et al. 2000).

Sequence stratigraphy

Due to the strong thickness reduction on the slope (erosion), no high-resolution sequence-stratigraphic

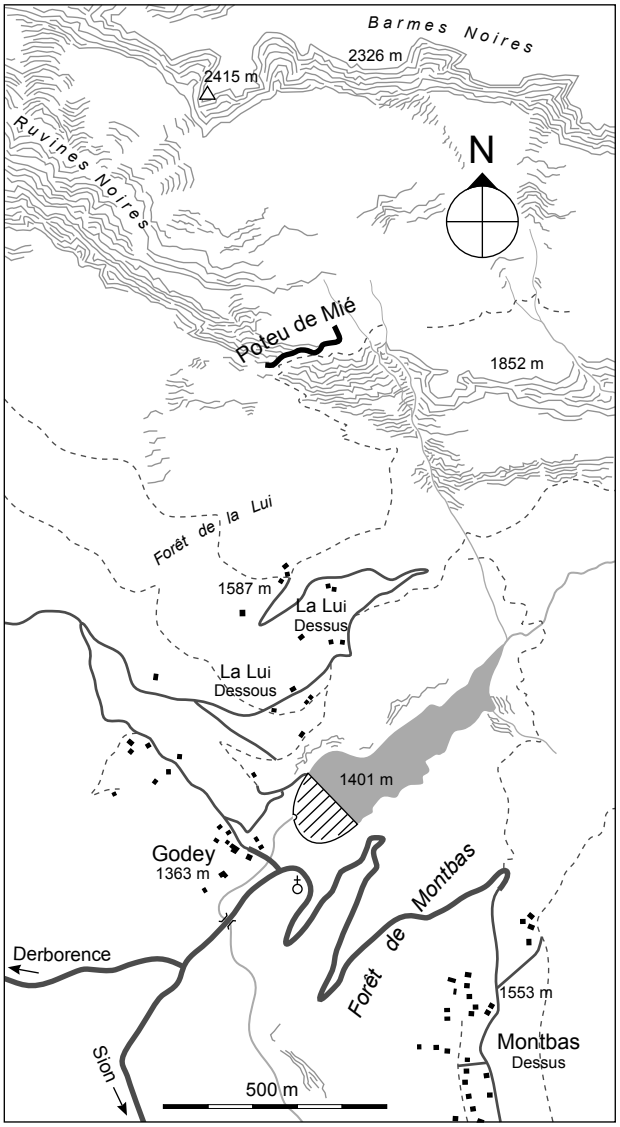

Fig. 4.22 - Location of the Poteu de Mié section. For legend see Fig. 4.6b.

analysis is possible in Broyon. Jan du Chêne et al. (1993) and Strohmenger & Strasser (1993) present a large-scale (3rd-order) sequence-stratigraphic framework that is re-interpreted here to fit with the chart of Hardenbol et al. (1998). Being located on a bypass-slope, the Broyon section mainly consists of gravitational, stacked lowstand deposits (LD), separated by major discontinuity surfaces with frequent indicators for erosion, representing large-scale sequence boundaries (SB). Beds 1a-8 are interpreted to represent a lowstand prograding wedge (Strohmenger & Strasser 1993, nomenclature after Vail et al. 1991). The channelized debris flows that consist of massive breccias (bed 10) may correspond to a slope-fan system, and the overlying, thin-bedded limestones (bed 11) either to a lowstand prograding wedge or to highstand deposits (Strohmenger & Strasser 1993). The massive interval from beds 12-17 probably consists of stacked lowstand slope-fan deposits developing into a lowstand prograding wedge (bed 18a) and finishes with a well-expressed maximum-flooding surface – the hardground of bed 18c (Strohmenger & Strasser 1993). After that, the sedimentary architecture switches to a thickening-up marl-limestone alternation that is interpreted as an interbed-dominated lowstand prograding wedge (Strohmenger & Strasser 1993, cf. Vail et al. 1991). The uppermost grain-flow deposit might represent a basin floor fan.

4.3.3 Basin sections

Poteu de Mié *(Figs 4.22, 4.23)*

located at the north-eastern end of the *Cirque de Derborence*, approx. 20 km NW of Sion (VS)

National topographic map of Switzerland 1 : 25 000, sheet 1285 *Les Diablerets*

Base of section X: 584 320
Y: 127 370

The Poteu de Mié section is located in the NE corner of the Cirque de Derborence, where the Late Jurassic is exposed along a steep, narrow mountain trail that climbs the vertical "*Malm*"-cliffs parallel to a fault-line (Fig. 4.22, Pl. 21/3).

Originally measured for a diploma thesis on the Helvetic Nappes of the Derborence-Sanetsch area (canton Valais) by Roulin (2001), the section represents the most distal of the studied basin sections. Existing data from the diploma thesis such as the log and thin sections were re-drawn, respectively re-interpreted and incorporated into this research project. Sampling was done by S. Roulin (2001) without a systematic approach but where it was possible while not getting in danger without using professional climbing equipment – a tribute that had to be paid to the steep and exposed conditions along the section.

Lithostratigraphy and sedimentology

The section starts close to the lower part of the "*Malm*"-cliffs, a massive cliff of about 100 m height that develops out of a marl-limestone alternation. It covers the entire Late Jurassic, up to the softer marl-limestone alternations of the "*Valanginien schisteux*" (= local formation that covers parts of the Berriasian and the Valanginian) on top (Pl. 21/3). The lithologic variety within the "*Calcaires bleutés massifs*", or "*Malm*", is very low: pelagic mud- to wackestones, with marly interbeds in the lower part.

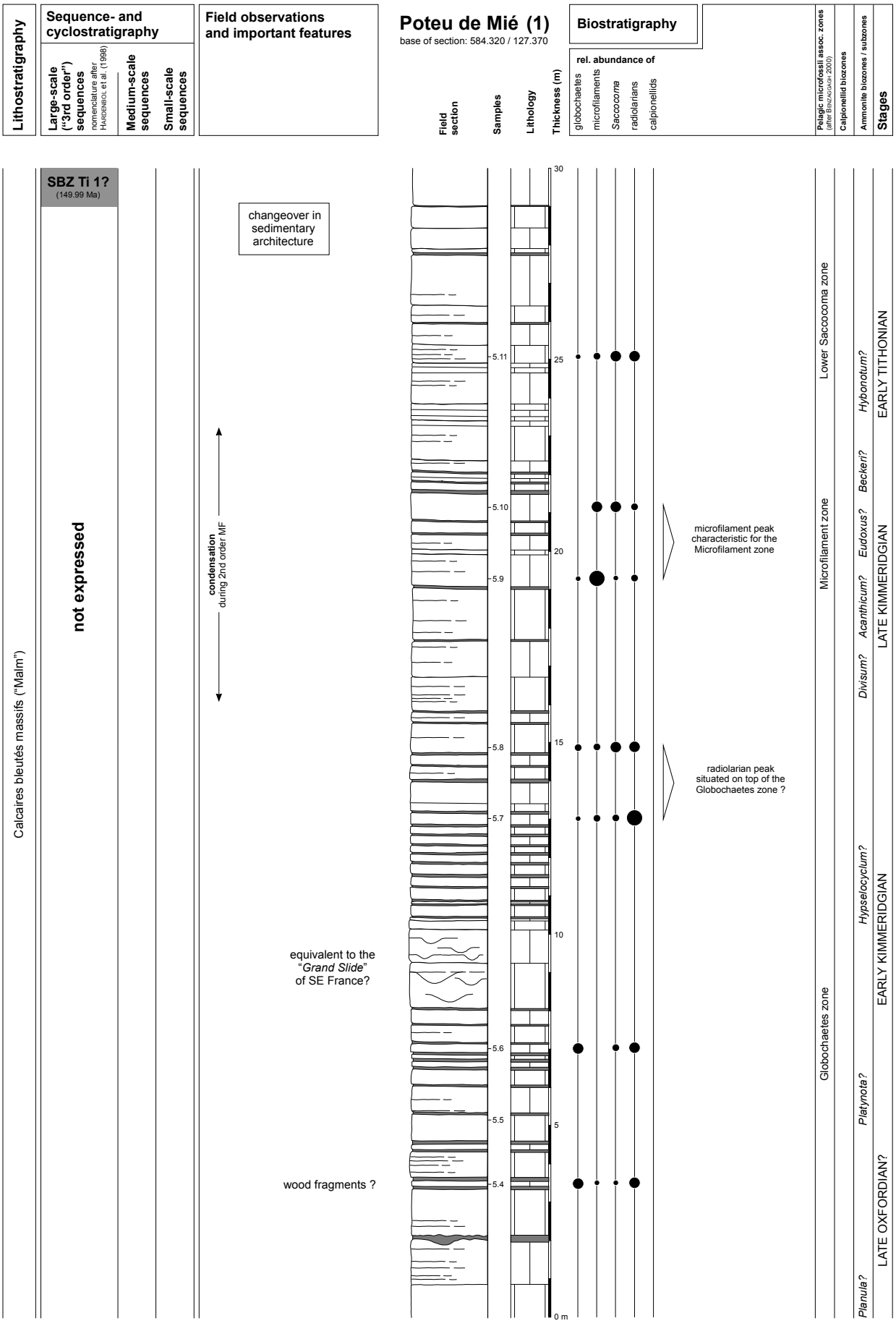

Fig. 4.23 - (this page and the three following pages) Sedimentological and sequence-stratigraphic interpretation, and biostratigraphy of the Poteu de Mié section. Original section from ROULIN (2001), re-drawn and re-interpreted.

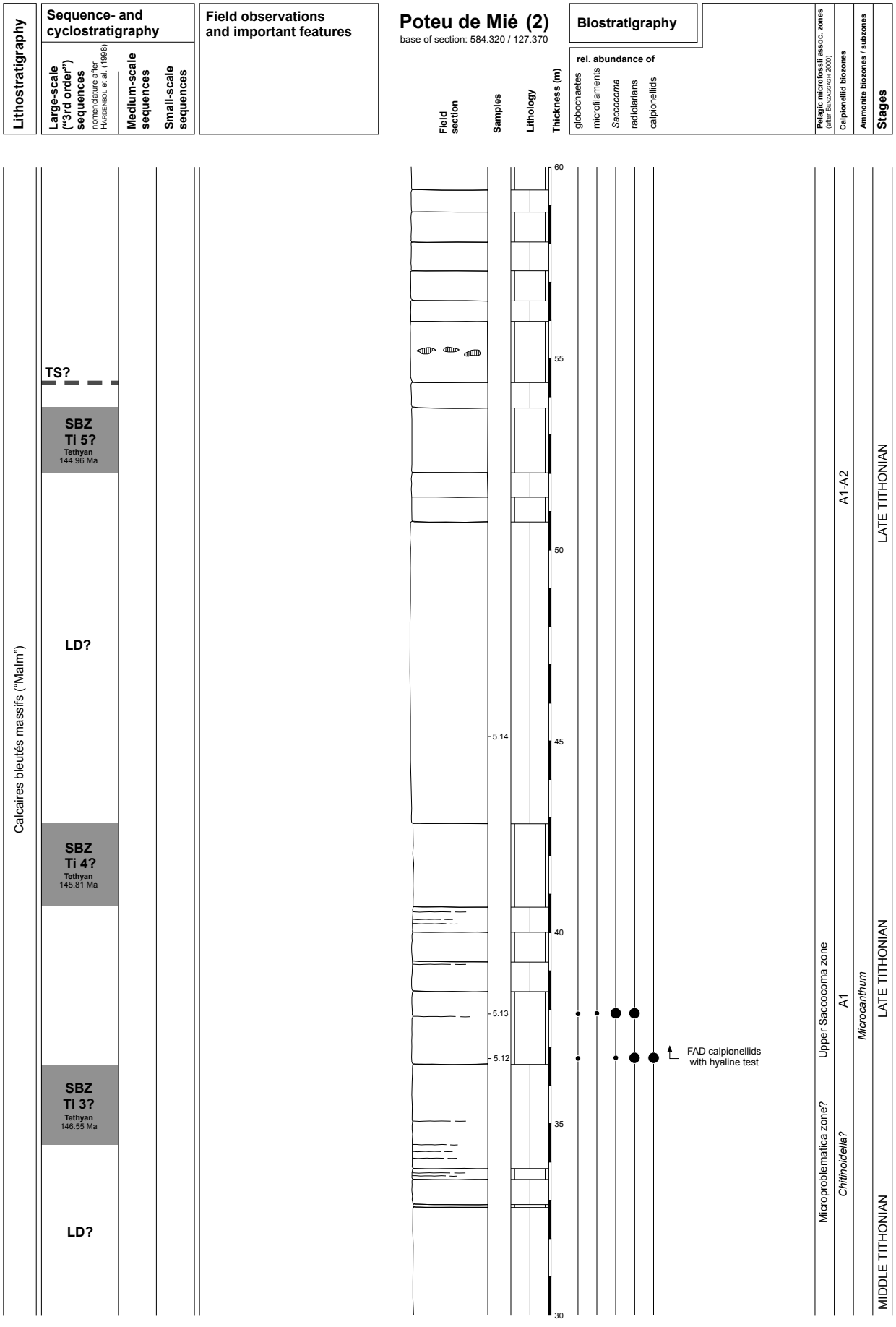
Lithostratigraphy
Sequence- and cyclostratigraphy
Large-scale ("3rd order") sequences
nomenclature after Hardenbol et al. (1998)
Medium-scale sequences
Small-scale sequences
Field observations and important features
Poteu de Mié (2)
base of section: 584.320 / 127.370
Biostratigraphy
Field section
Samples
Lithology
Thickness (m)
rel. abundance of
globochaetes
microfilaments
Saccocoma
radiolarians
calpionellids
Pelagic microfossil assoc. zones (after Benzaggagh 2000)
Calpionellid biozones
Ammonite biozones / subzones
Stages
Calcaires bleutés massifs ("Malm")
TS?
SBZ Ti 5?
Tethyan
144.96 Ma
LD?
SBZ Ti 4?
Tethyan
145.81 Ma
SBZ Ti 3?
Tethyan
146.55 Ma
LD?
5.14
5.13
5.12
60
55
50
45
40
35
30
FAD calpionellids with hyaline test
Microproblematica zone?
Upper Saccocoma zone
Chitinoidella?
A1
A1-A2
Microcanthum
MIDDLE TITHONIAN
LATE TITHONIAN
LATE TITHONIAN

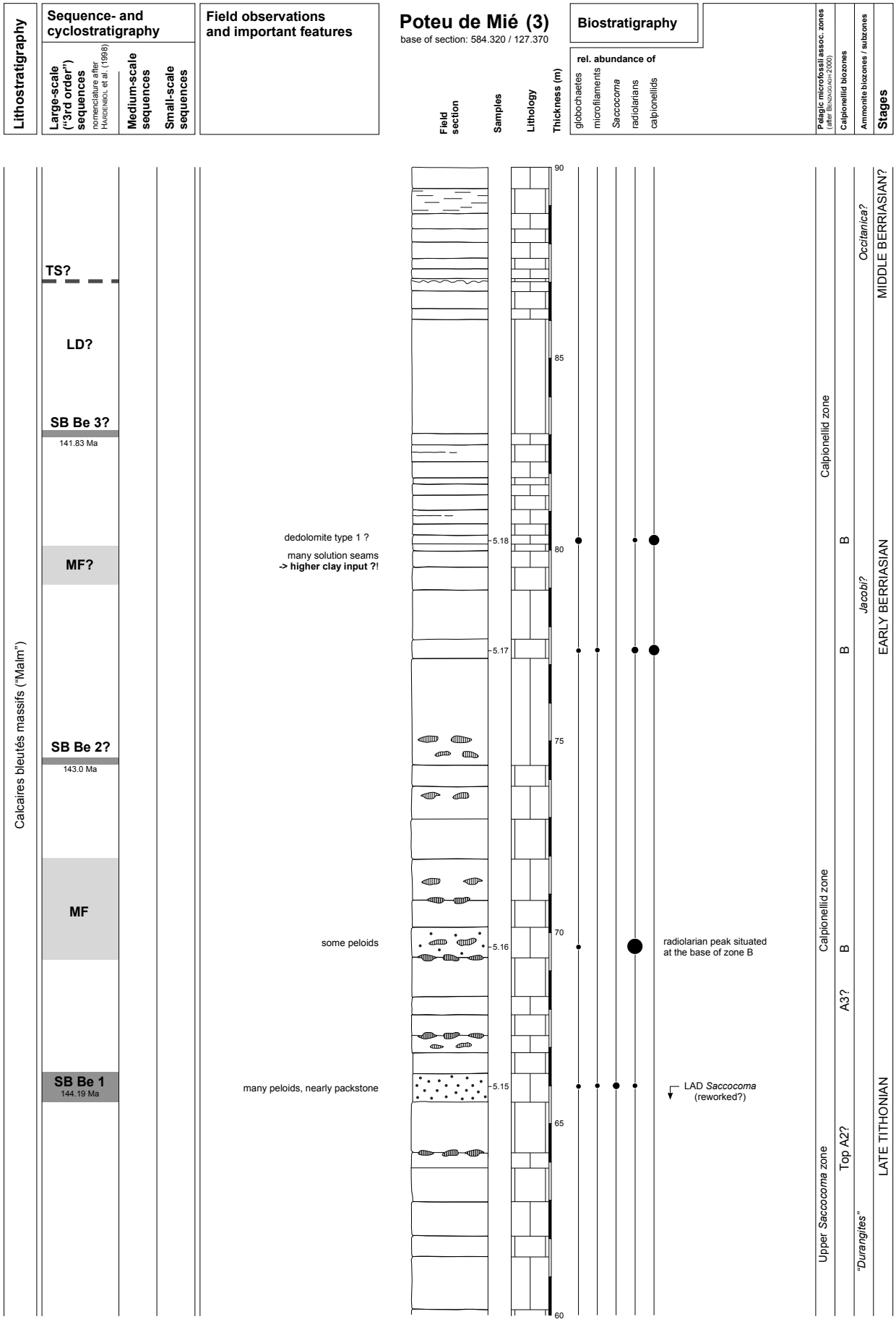
Lithostratigraphy
Sequence- and cyclostratigraphy
Large-scale ("3rd order") sequences
nomenclature after Hardenbol et al. (1998)
Medium-scale sequences
Small-scale sequences
Field observations and important features
Poteu de Mié (3)
base of section: 584.320 / 127.370
Biostratigraphy
Field section
Samples
Lithology
Thickness (m)
rel. abundance of
globochaetes
microfilaments
Saccocoma
radiolarians
calpionellids
Pelagic microfossil assoc. zones (after Benzaggagh 2000)
Calpionellid biozones
Ammonite biozones / subzones
Stages
Calcaires bleutés massifs ("Malm")
TS?
LD?
SB Be 3?
141.83 Ma
MF?
SB Be 2?
143.0 Ma
MF
SB Be 1
144.19 Ma
dedolomite type 1 ?
many solution seams
-> higher clay input ?!
some peloids
many peloids, nearly packstone
5.18
5.17
5.16
5.15
90
85
80
75
70
65
60
radiolarian peak situated at the base of zone B
LAD Saccocoma (reworked?)
Calpionellid zone
Upper Saccocoma zone
Top A2?
A3?
B
"Durangites"
Jacobi?
Occitanica?
LATE TITHONIAN
EARLY BERRIASIAN
MIDDLE BERRIASIAN?

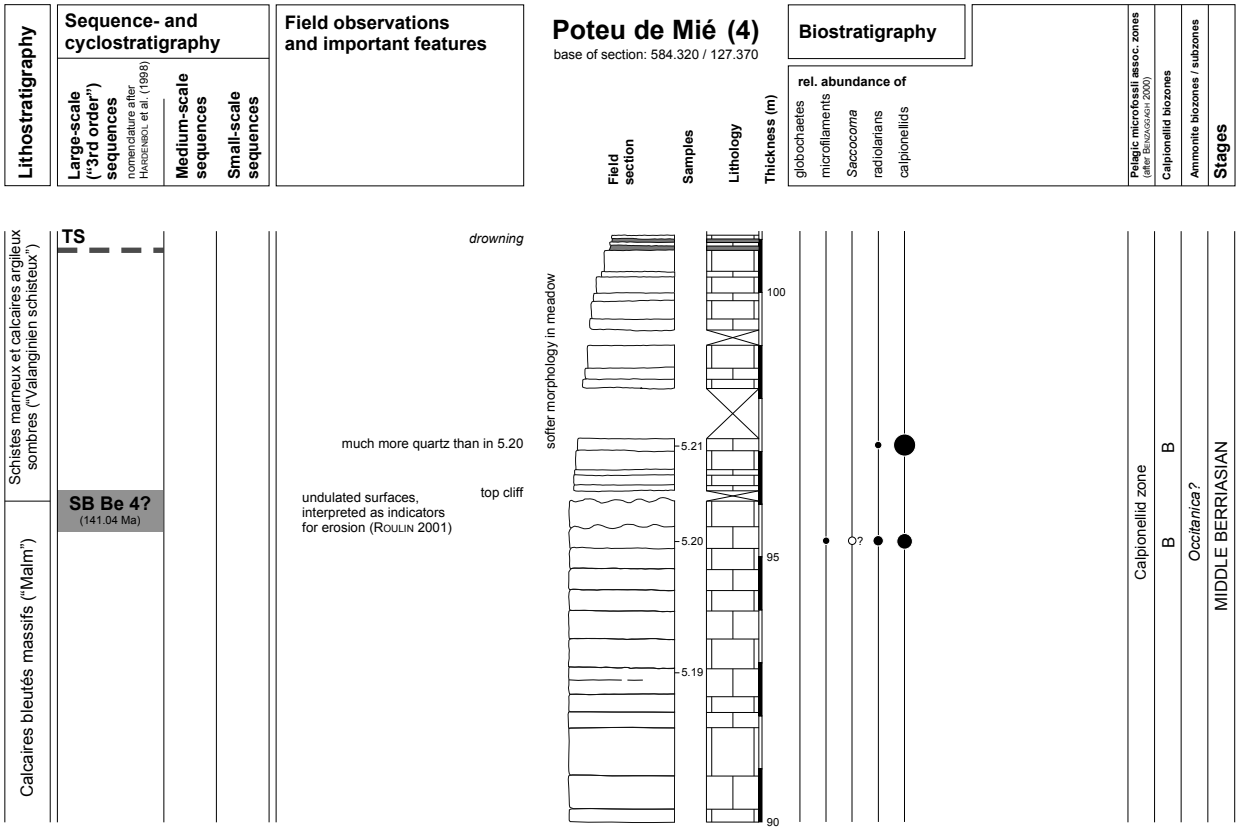

The only real changes that can be observed are in stacking pattern and microfossil assemblages.

The lower part of the section (0-29 m) consists of 20-40 cm thick limestone beds in alternation with thin (< 8 cm) marly intervals (Roulin 2001). Within this interval, there are two thicker beds (8.5-10.5 m) that are channelized. Regarding their position in the biostratigraphic framework (see paragraph below and Fig. 4.23), they might be an equivalent of the *Grand Slide* in the *Bassin du Sud-Est* of SE France (Debrand-Passard et al. 1984). At 29 m there is a change-over in sedimentation. At this point, the appearance of the cliff becomes very massive. Bed thicknesses increase dramatically (up to 8 m!) and the marly interbeds that are typical for the lower part are replaced by (mostly rather subtle) marly joints. From 55 m to 77.5 m chert nodules become apparent, while the beds stay rather thick (m-scale) but do not reach the maximum thicknesses of the underlying interval. From 77.5 m onwards, the previous persistence of stacking pattern is lost and average bed thickness decreases. This change is even more visible from 86 m upwards. Some beds show undulated upper surfaces, which are interpreted as possible signs of erosion (Roulin 2001). The abundance of solution seams observed in sample 5.18 may be a forerunner of the change to a marl-dominated sedimentation beginning at 96 m. At this level, the top of the cliff is reached, the outcrop becomes much softer, the slope diminishes rather abruptly, and the rocky cliff makes way for a meadow. This is caused by a change to more marly sediments, the "*Valanginien schisteux*" (Fig. 4.23, Pl. 21/3). Regarding microfacies, the exposed base of the "*Valanginien schisteux*" is very similar to the "*Calcaires bleutés massifs*", or "*Malm*", but the higher clay content causes the marly aspect. Also the fauna is essentially the same. Higher up in the formation, quartz content increases (fine grains, homogenous distribution in the sediment; Roulin 2001). This may be related to a higher continental influence (platform progradation), a climatic change in the hinterland (cf. Chap. 8), or a combination of both effects.

Biostratigraphy and sequence stratigraphy

The thin sections of Roulin's (2001) diploma thesis were re-examined and a biostratigraphic framework, based on calpionellids and microfossil assemblages (cf. Chap.1.3.3), was established. According to this new interpretation, the Poteu de Mié section exposes strata of Late Oxfordian to Middle Berriasian age (Fig. 4.23). In contrast to the platform and slope sections, the expression of sequence boundaries is very subtle in this distal section. Sequence stratigraphic interpretation is mainly based on changes of stacking pattern and erosional features.

Sequence boundaries are labelled in function of their biostratigraphic position.

Regarding biostratigraphy, it turns out that the lower 29 m of the section are rather condensed and expose rocks of Late Oxfordian to Early Tithonian age. Condensation reaches a maximum in the Late Kimmeridgian, where probably four ammonite zones (*divisum-beckeri*, dated indirectly by microfossil assemblages, cf. Fig. 1.8) are recorded in less than 10 m thickness. This condensation is due to the Late Kimmeridgian long-term maximum flooding (MF) situated in the *eudoxus* Zone (cf. Fig. 1.9).

In the upper part of the section (29 m – top), SB $Ti1_{Tethyan}$, SB $Ti3_{Tethyan}$ and SB $Ti4_{Tethyan}$ are interpreted to be located at the base of unusually thick, massive beds that are interpreted as lowstand deposits (LD). SB $Ti2?_{Tethyan}$ (cf. Fig. 1.9) is not expressed. The identification of SB $Ti3_{Tethyan}$ is additionally based on the first appearance of calpionellids with hyaline tests just above, whereas the position of SB $Ti5_{Tethyan}$ is inferred from the abundance of chert nodules from 55 to 77.5 m that may be related to the beginning of the latest Tithonian – Early Berriasian long-term transgression (cf. Fig. 1.9). SB $Be1_{Tethyan}$ is well expressed and relates to peloid wacke- to packstone that suggests platform export and might be compared to a basin-floor fan system (cf. e.g., Vail et al. 1991). The increase in the abundance of chert nodules above this sequence boundary thus marks the interval where the latest Tithonian – Early Berriasian long-term transgression really takes effect. This interval corresponds to the shift from massive limestone to marl-limestone alternations on the slope (Broyon – Clue de la Payre) and could be called a "minor drowning". SB $Be2?_{Tethyan}$ and SB $Be3_{Tethyan}$ again are placed at the base of thick beds that may represent lowstand deposits (LD), with SB $Be2?_{Tethyan}$ rather attenuated and badly expressed because it lies in the above-mentioned "minor drowning" event. Finally, SB $Be4_{Tethyan}$ is defined by undulated bed surfaces that are interpreted as markers for erosion (Roulin 2001). The following transgression causes a major change to a marl-limestone alternation, indicating a drowning respectively a retrogradation of the platform system located in the North.

Clue de Taulanne (Figs 4.24, 4.25)

Located in the Subalpine Chains of SE France, the Clue de Taulanne (Fig. 4.25, Pl. 21/4) section is palaeogeographically situated at the southern margin of the Vocontian Basin (cf. Fig. 1.3). Along the Route Nationale 85 some 300 m of section are exposed, covering Oxfordian to Berriasian age. Kilian (1889) provided a first, brief description of lithologic features. Remane (1970) studied the top of the section – around the boundary between calpionellid zones B/C, and Beaudoin (1977) measured the section with a focus on the resedimented carbonates. In their diploma thesis on the Late Jurassic of the Castellane region, Pellaton & Ullrich (1997) used a multifactor approach resulting in a "3rd-order" sequence-stratigraphic interpretation, integrating sedimentology, (micro)palaeontology, biostratigraphy, and palynofacies. Based on the log provided by Pellaton & Ullrich (1997), Schnyder (2003) additionally measured clay minerals, trace elements, and magnetic susceptibility in the upper part of the section.

approx. 8 km NW of Castellane,
35 km SE of Digne-les-Bains (France)

Institut Géographique National (IGN),
TOP 25, sheet 3542 OT *Castellane*
1 : 25 000

Base of section X: 929 900
Y: 3183 700

The section was completely re-logged from the Late

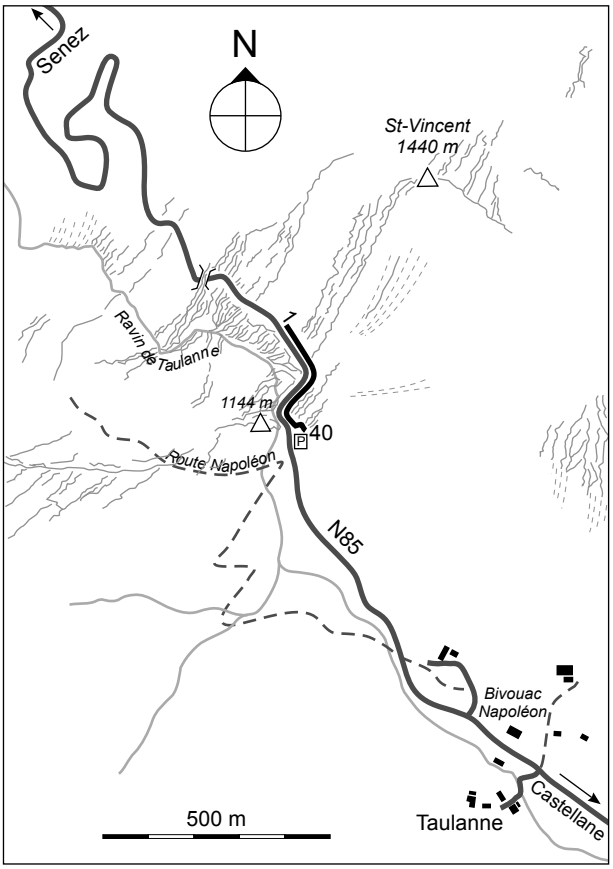

Fig. 4.24 - Location of the Clue de Taulanne section. For legend see Fig. 4.6b.

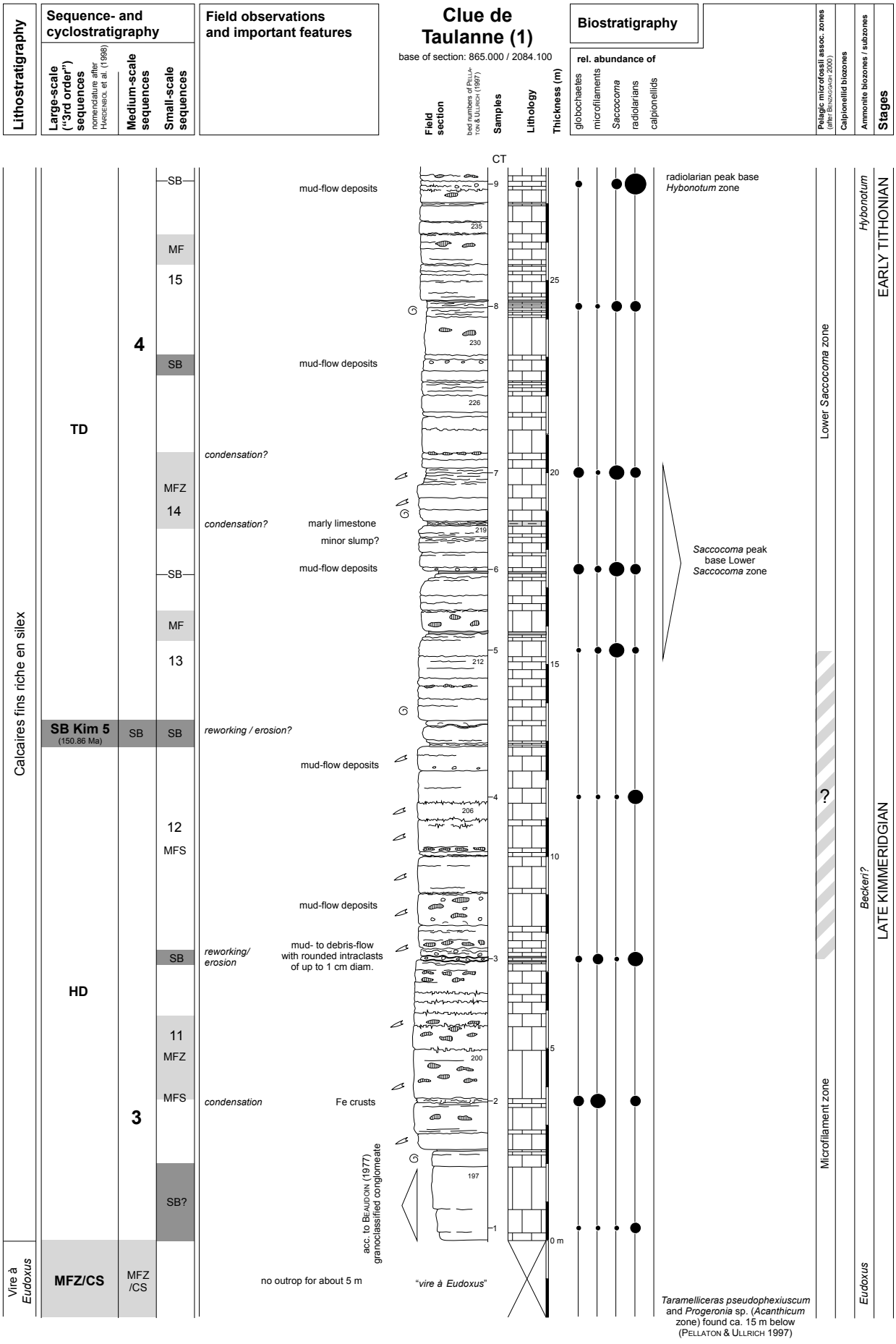

Fig. 4.25 - (this page and the four following pages) Sedimentological and sequence-stratigraphic interpretation, and biostratigraphy of the Clue de Taulanne section.

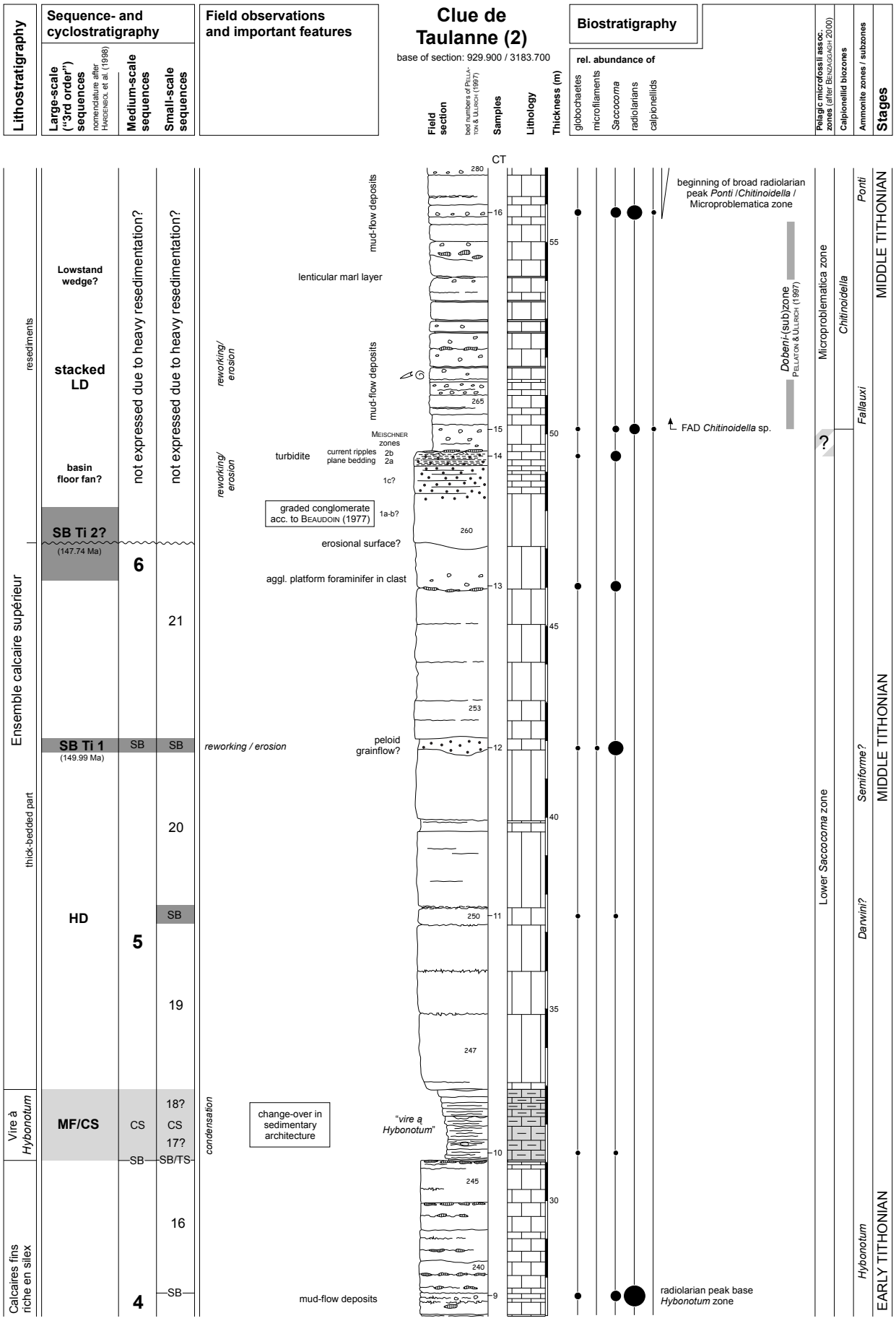
Lithostratigraphy
Sequence- and cyclostratigraphy
Large-scale ("3rd order") sequences
nomenclature after Hardenbol et al. (1998)
Medium-scale sequences
Small-scale sequences
Field observations and important features
Clue de Taulanne (2)
base of section: 929.900 / 3183.700
Field section
bed numbers of Pellaton & Ullrich (1997)
Samples
Lithology
Thickness (m)
Biostratigraphy
rel. abundance of
globochaetes
microfilaments
Saccocoma
radiolarians
calpionellids
Pelagic microfossil assoc. zones (after Benzaggagh 2000)
Calpionellid biozones
Ammonite zones / subzones
Stages
CT
Ensemble calcaire supérieur
resediments
thick-bedded part
Calcaires fins riche en silex
Lowstand wedge?
stacked LD
basin floor fan?
SB Ti 2?
(147.74 Ma)
SB Ti 1
(149.99 Ma)
HD
MF/CS
Vire à Hybonotum
not expressed due to heavy resedimentation?
not expressed due to heavy resedimentation?
6
5
4
SB
CS
SB/TS
21
20
19
18?
17?
16
mud-flow deposits
lenticular marl layer
mud-flow deposits
reworking/ erosion
reworking/ erosion
turbidite
current ripples
plane bedding
Meischner zones
2b
2a
1c?
graded conglomerate acc. to Beaudoin (1977)
1a-b?
erosional surface?
aggl. platform foraminifer in clast
peloid grainflow?
reworking / erosion
condensation
change-over in sedimentary architecture
"vire à Hybonotum"
mud-flow deposits
280
265
260
253
250
247
245
240
16
15
14
13
12
11
10
9
55
50
45
40
35
30
beginning of broad radiolarian peak Ponti /Chitinoidella / Microproblematica zone
Doben.-(sub)zone Pellaton & Ullrich (1997)
FAD Chitinoidella sp.
?
Microproblematica zone
Lower Saccocoma zone
Chitinoidella
Fallauxi
Ponti
Semiforme?
Darwini?
Hybonotum
radiolarian peak base Hybonotum zone
MIDDLE TITHONIAN
MIDDLE TITHONIAN
EARLY TITHONIAN

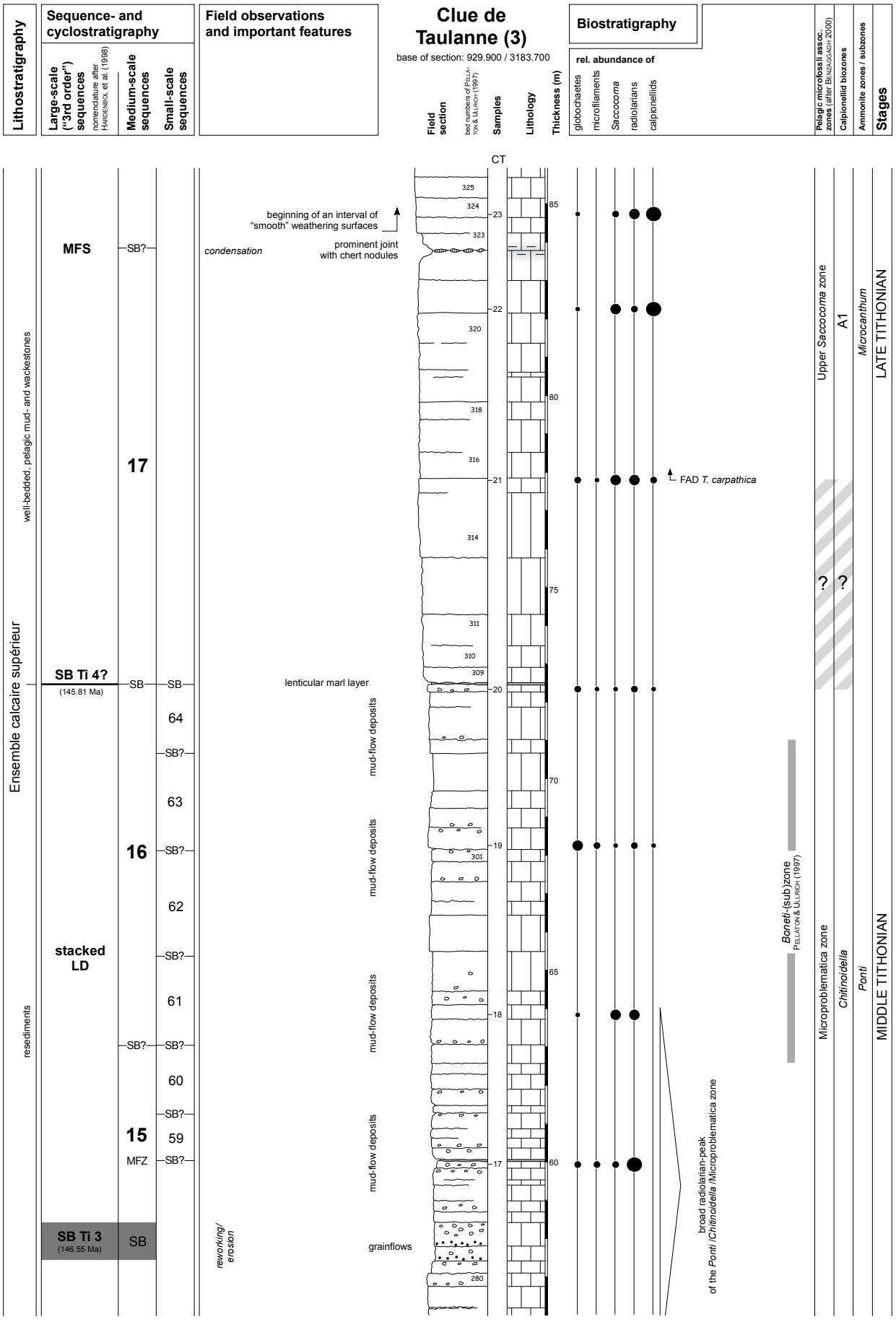
Lithostratigraphy
Sequence- and cyclostratigraphy
Large-scale ("3rd order") sequences
nomenclature after HARDENBOL et al. (1998)
Medium-scale sequences
Small-scale sequences
Field observations and important features
Clue de Taulanne (3)
base of section: 929.900 / 3183.700
Field section
bed numbers of PELLATON & ULLRICH (1997)
Samples
Lithology
Thickness (m)
Biostratigraphy
rel. abundance of
globochaetes
microfilaments
Saccocoma
radiolarians
calpionellids
Pelagic microfossil assoc. zones (after BENZAGGAGH 2000)
Calpionellid biozones
Ammonite zones / subzones
Stages
CT
Ensemble calcaire supérieur
well-bedded, pelagic mud- and wackestones
resediments
MFS
SB Ti 4?
(145.81 Ma)
SB Ti 3
(146.55 Ma)
SB
SB?
MFZ
17
16
15
stacked LD
64
63
62
61
60
59
beginning of an interval of "smooth" weathering surfaces
condensation
prominent joint with chert nodules
lenticular marl layer
mud-flow deposits
grainflows
reworking/ erosion
FAD T. carpathica
broad radiolarian-peak of the Ponti /Chitinoidella /Microproblematica zone
Boneti-(sub)zone
PELLATON & ULLRICH (1997)
Upper Saccocoma zone
A1
Microcanthum
Microproblematica zone
Chitinoidella
Ponti
MIDDLE TITHONIAN
LATE TITHONIAN

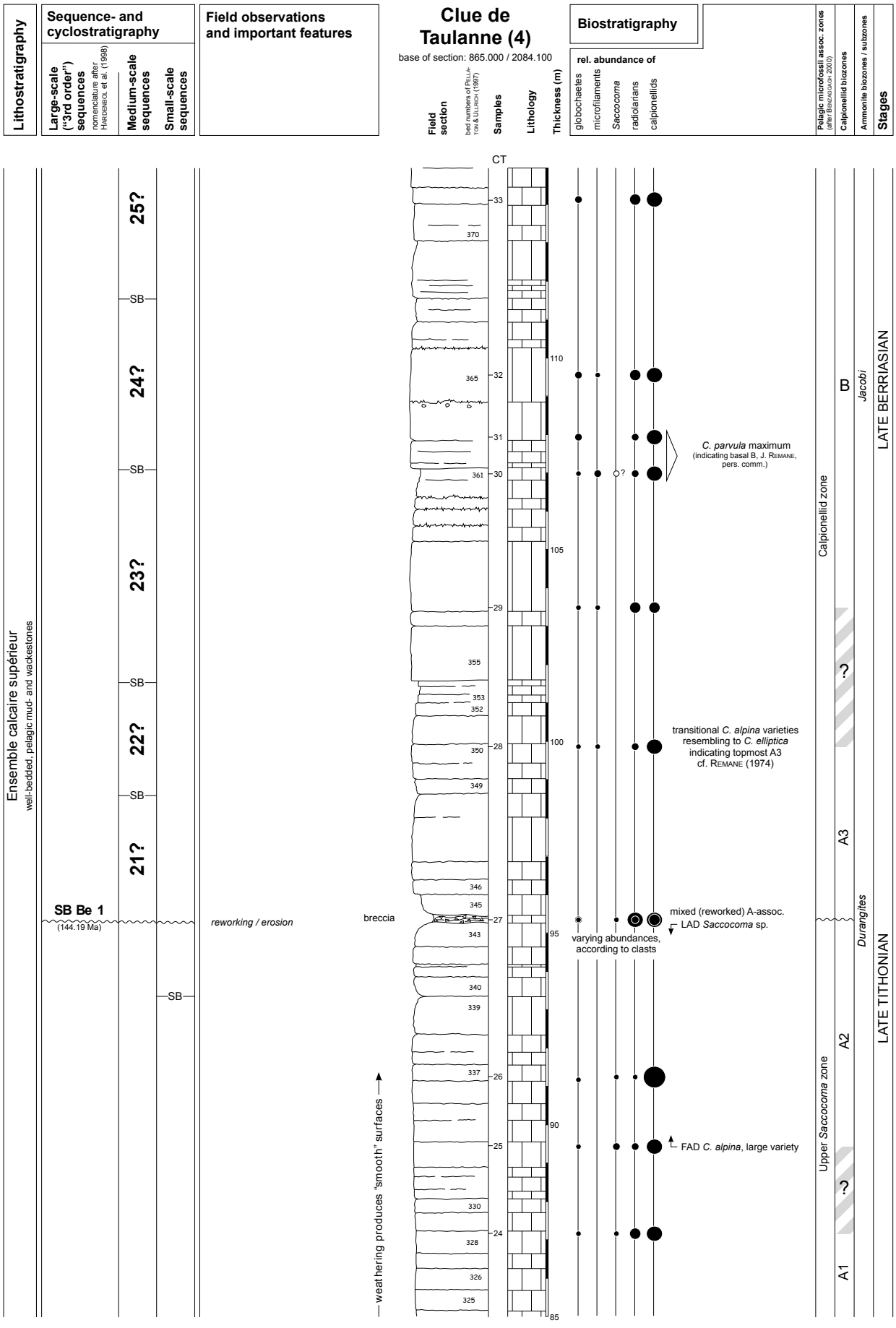
Lithostratigraphy
Sequence- and cyclostratigraphy
Large-scale ("3rd order") sequences
nomenclature after HARDENBOL et al. (1998)
Medium-scale sequences
Small-scale sequences
Field observations and important features
Clue de Taulanne (4)
base of section: 865.000 / 2084.100
Field section
bed numbers of PELLATON & ULLRICH (1997)
Samples
Lithology
Thickness (m)
Biostratigraphy
rel. abundance of
globochaetes
microfilaments
Saccocoma
radiolarians
calpionellids
Pelagic microfossil assoc. zones (after BENZAGHOU 2000)
Calpionellid biozones
Ammonite biozones / subzones
Stages
Ensemble calcaire supérieur
well-bedded, pelagic mud- and wackestones
21?
22?
23?
24?
25?
SB
SB Be 1
(144.19 Ma)
reworking / erosion
breccia
weathering produces "smooth" surfaces
CT
370
365
361
355
353
352
350
349
346
345
343
340
339
337
330
328
326
325
33
32
31
30
29
28
27
26
25
24
110
105
100
95
90
85
C. parvula maximum
(indicating basal B, J. REMANE, pers. comm.)
transitional C. alpina varieties
resembling to C. elliptica
indicating topmost A3
cf. REMANE (1974)
mixed (reworked) A-assoc.
LAD Saccocoma sp.
varying abundances,
according to clasts
FAD C. alpina, large variety
Calpionellid zone
Upper Saccocoma zone
A1
A2
A3
B
?
Jacobi
Durangites
LATE BERRIASIAN
LATE TITHONIAN

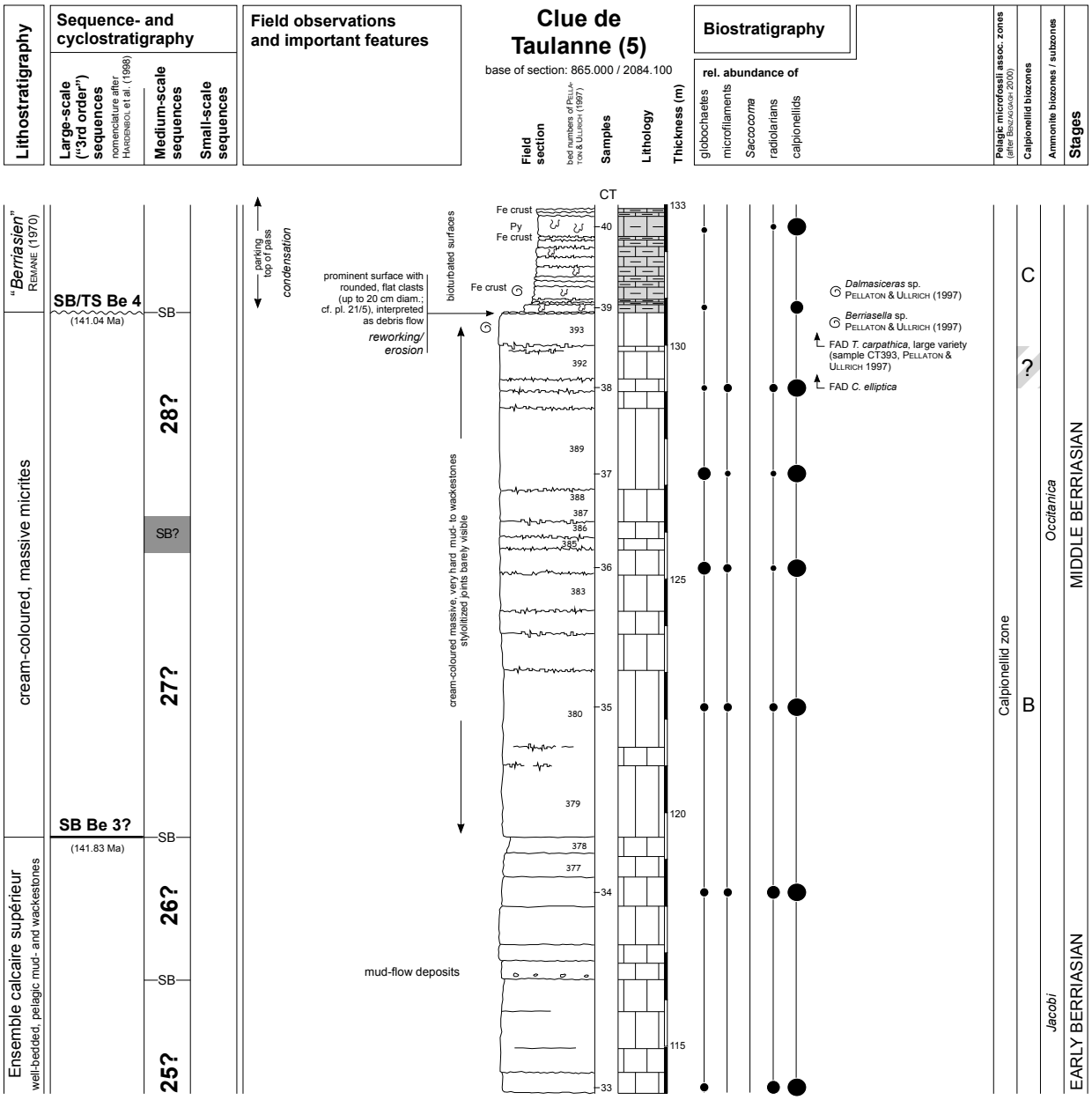

Kimmeridgian to the Middle Berriasian. The existing biostratigraphic framework from Pellaton & Ullrich (1997) was used as a basis and refined by a higher sampling density, specifically adapted to minimize biostratigraphic precision intervals.

Lithostratigraphy and sedimentology

The measured part of the section begins above the "*vire à Eudoxus*" (Pellaton & Ullrich 1997), representing a gap in the outcropping series, with the *Calcaires fins riches en silex* (0-31 m): a series of relatively thin-bedded pelagic mud- and wackestones that are rich in chert nodules and include some mud- and debris-flows. The end of the *Calcaires fins riches en silex* is defined by a sharp surface rich in chert nodules. Here, the *vire à Hybonotum* begins, a 2 m-thick succession of platy, marly mudstones with concretion-like nodules. Due to its accentuated weathering, the *vire à Hybonotum* is a valuable lithostratigraphic marker bed, similar to the *vire à Eudoxus* (Pellaton & Ullrich 1997). Additionally, it defines a major change-over in sedimentary architecture, from the thin-bedded, chert-rich *Calcaires fins riches en silex* to a thick-bedded limestone unit defining the base of the *Ensemble calcaire supérieur* (Pellaton & Ullrich 1997) that makes up most of the section's upper part. The *Ensemble calcaire supérieur* can, in turn, be further subdivided: its base is defined by the above mentioned thick-bedded limestone unit (33-47 m), followed by a succession dominated by gravitational deposits such as

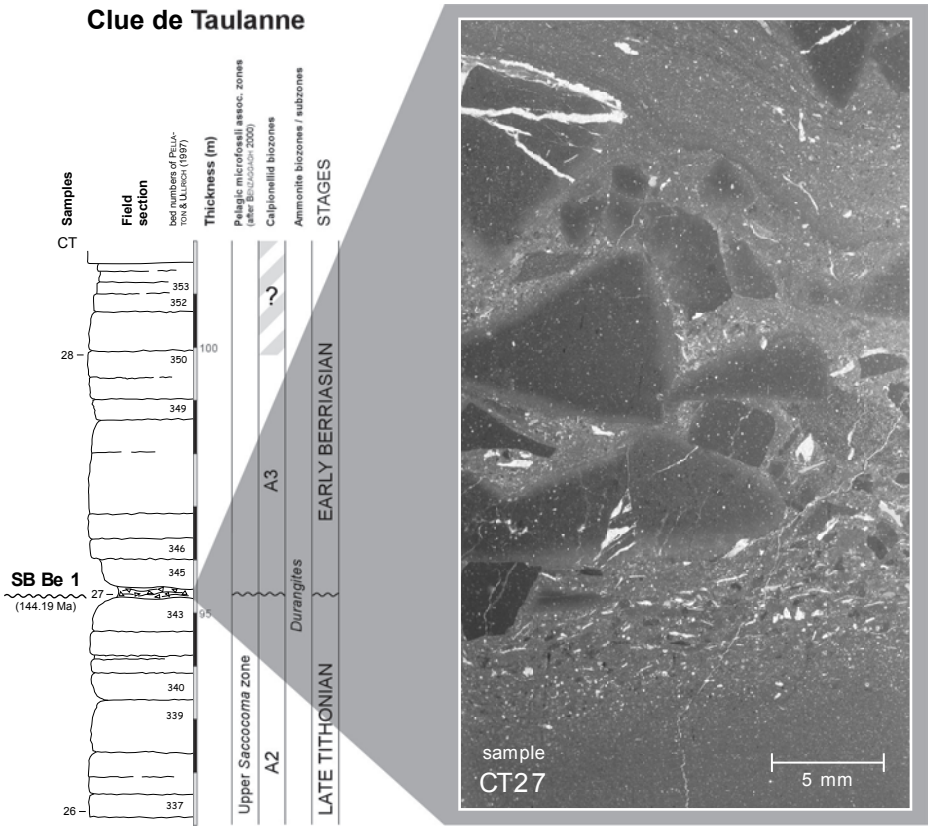

Fig. 4.26 - Erosion surface in the Clue de Taulanne section. In contrast to the intraclastic limestones (cf. Pl. 19/6), which are common in the lower part of the Clue de Taulanne section (cf. Chap. 2 and Pellaton & Ullrich 1997), these clasts are extremely angular and consist of basinal mud- and wackestones. Note also the relatively sharp lower surface (the mudstones at the lower edge of the photo are autochthonous Late Tithonian) and flow structures in the upper part of the image.

turbidites, mud- and grain-flows (47-72.5 m). The base of the gravitational unit is marked by a peloid-grainstone and clearly shows the zones 2a and 2b of a Meischner Sequence (cf. Flügel 2004; corresponds to Bouma divisions B and C: plane bedding and current ripples) over a sharp surface (Pl. 19/7). Consequently, it is interpreted as calcarenitic turbidite. Below this sharp surface, an (erosive?) surface with channel geometry is developed, overlain by mud-supported sediments that grade into platy peloid-grainstones. Beaudoin (1977) reports a graded breccia from this bed. If this is true, the succession would represent a complete Meischner-sequence:

1a-b) graded breccia (cf. Beaudoin 1977) with channel geometry

1c) platy peloid-grainstones

2a) plane bedding

2b) current ripples

This well-developed turbidite is overlain by a series of mud- and grain-flows that show a rather chaotic stacking pattern, which ends with a lenticular marl layer. Above this boundary, the third unit of the *Ensemble calcaire supérieur* begins (72.5-119.5 m): a succession of well-bedded pelagic mud- and wackestones, interrupted by rare mudflow deposits, a prominent joint with chert nodules (83.8 m), and a resedimented breccia horizon (95.3 m), the latter two forming well expressed depressions in the natural cliffs N and S of the section (Pl. 21/4). The upper, fourth unit consists of cream-coloured/yellowish, massive micrites (119.5-130.5 m) that are very hard and show conchoidal fracturing. Bedding planes are generally stylolitized and hardly recognizable in this interval.

Above a distinct surface with large, lenticular, reworked clasts (Pl. 21/5) that is perfectly exposed in the small parking lot at the section top (Fig. 4.24), the dark, marly limestones of the "*Berriasien*" (Remane 1970) begin. Abundant bioturbation, pyrite, and Fe crusts suggest condensation in a starved basin.

Biostratigraphy

The biostratigraphy of the Clue de Taulanne section shown here essentially builds on the biostratigraphic framework of ammonites and calpionellids as presented by Pellaton & Ullrich (1997). It was possible to refine the calpionellid zonation by a higher sampling density

and complete the biostratigraphy by adding a microfossil assemblage zonation after Dromart & Atrops (1988) and Benzaggagh (2000) (cf. Chap. 1.3.3). Due to a sufficiently high sample density, even some characteristic peaks in the abundance of certain microfossil group can be recognized (cf. Fig 1.8).

The *vire à Eudoxus* and the *vire à Hybonotum* are regionally correlatable lithostratigraphic units (Pellaton & Ullrich 1997). The newly set up microfossil assemblage zonation sustains the ages of theses marker beds.

Sequence stratigraphy

Over large parts of the section, neither small-scale nor medium-scale sequences can be determined because the stacking pattern – the only sedimentological means for sequence analysis in lithologically monotonous basin sections – is too irregular. Large-scale sequence boundaries, however, are recognizable by resedimented carbonates and/or a distinct change in stacking pattern.

The soft sediments of the *vire à Eudoxus* are related to the long-term (2^{nd}-order) maximum flooding of the *eudoxus* Zone (cf. Fig. 1.9). The early transgressive deposits of the long-term sequence are still characterized by considerable lack in carbonate import from the platform. This leads to a relative enrichment of autochtonous particles such as pelagic carbonate and notably sponge spicules, the concentration of the latter ones causing the observed abundance of chert nodules. The *vire à Hybonotum* represents a condensed interval due to large-scale maximum flooding. It is preceded by chert-rich bedding planes, the presence of which suggest decreasing carbonate import. In addition, the *vire à Hybonotum* probably correlates with the upper *virgula* Marls on the Jura platform (cf. Chap. 7), a crisis of the platform carbonate factory that is not only related to sea-level fluctuation but also to palaeoecological and palaeoclimatic changes has to be considered. The following thick-bedded micrites probably relate to highstand-shedding of carbonate mud (Schlager et al. 1994), until interrupted suddenly by the erosive base of carbonate resediments that are interpreted to represent stacked lowstand deposits ("lowstand flushing" during forced regression?). This interval reaches from SB $Ti2?_{Tethyan}$ to SB $Ti4_{Tethyan}$ and thus corresponds to the interval of maximum erosion and bypass-sedimentation on the slope (Broyon section, see above).

An interesting parallel to the stacking pattern of the Yenne section is the sudden change in lithofacies and increase in average thicknesses beginning with medium-scale sequence 17. Applying the same hypothesis as in Yenne – the beginning of a long-term (2^{nd}-order) transgressional trend that allows for the creation of more accommodation space on the platform – it makes sense to assume a switch from a general "lowstand flushing"- back to a "highstand shedding"-mode.

In the upper part of the *Ensemble calcaire supérieur* (72.5-130.7 m), large-scale sequence boundaries are not well expressed. SB $Ti5_{Tethyan}$ and SB Be3 are not expressed at all but the position of SB Be3 can be deduced from a significant change in lithofacies and stacking pattern (119.5 m, see below). Also large-scale SB Be1 shows no spectacular features in the field. On the first view, it seems to be just another marly joint. However, when examined in detail, microfacies analysis and calpionellid biostratigraphy indicate heavy erosion that probably eroded considerable parts of the upper A2 and lower A3 calpionellid zones (cf. Fig. 4. 26).

The top of the *Ensemble calcaire supérieur* (119.5-130.7 m) differs from the rest of the section by a very special lithology (cream-coloured/yellowish, hard, massive micrites). Judging from stacking pattern, the package is likely to consist of two medium-scale sequences. According to biostratigraphy, the surface with large, lenticular, reworked clasts that defines its upper limit (Pl. 21/5) is the sedimentary expression of large-scale SB Be4. From cyclostratigraphic analysis (Chap. 7), the time span that is covered by the massive interval can be estimated at about 800 ka, which again would mean that, according to the sequence chronostratigraphic chart of Hardenbol et al. (1998), the large-scale SB Be3 should be located somewhere near its lower limit. Eventually, if it is considered that in the Yenne section the large-scale SBs Be3 and Be4 are merged within an interval of prolonged subaerial exposure, it becomes rather obvious that the cream-coloured micrites in the Clue de Taulanne section may be the result of the basinal sedimentary system's reaction to the long-lasting emersion of the platform top. The subsequent major transgression in Yenne (base of the Pierre-Châtel Formation) would then correspond to the dark, marly limestones with frequent bioturbation, pyrite and Fe-crusts of the "*Berriasien*" (Remane 1970) that imply starved basin conditions.

* * *

5 - Clay mineralogy

The study of a sediment's clay mineral fraction allows for the investigation of climatic change, eustatic controls and tectonic activity in a given period of sedimentation (Millot 1970, Singer, 1984, Chamley 1989, Weaver 1989, Curtis, 1990, Velde 1995, Gawenda 1999, Thiry 2000). In this study, clay mineral assemblages are principally used as an invaluable tool for correlation (cf. Chap. 5) and as an indicator for a major climatic changeover during the Middle Tithonian.

5.1 The significance of clay mineral associations

5.1.1 The role of climate

The clay minerals that form in a soil are influenced by average annual temperature, average annual precipitation, seasonality, type of rock substrate and time available for soil maturation (Chamley 1989, Weaver 1989, Velde 1995). However, in order to preserve a climatic signal in a marine sedimentary rock, a characteristic soil must be eroded in a continental source area, then transported, and eventually deposited in diluted form as part of the sedimentary rock. Erosional and transportational processes can alter a climatic signal, e.g., by mixing horizons that indicate different degrees of alteration (Curtis 1990). Erosion and reworking of bed rock may also considerably modify the clay mineral association to produce an inherited signal.

Temperate conditions, low annual precipitations and limited time for soil development prevent intense chemical weathering and thus support the formation of illite, chlorite, and mixed-layer minerals (Fig. 5.1; cf. Chamley 1989, Curtis 1990). This mineralogical association is dominant in immature grounds, subjected to a weak chemical weathering (Robert & Kennet 1994). Thiry (2000) states that clay mineral associations forming in the temperate climate zone consist mainly of inherited and mixed-layer minerals and show only little differentiation.

Under hot or cold arid conditions (desert or tundra), no soil develops at all. The clay mineral associations in such areas thus primarily derive from the underlying bedrock or from reworked palaeosols (inherited associations). In the Mediterranean climate zone, however, soils will develop a shallow weathering profile that is characterized by the occurrence of smectite and palygorskite (Fig. 5.1).

The clay minerals that are of true interest for palaeoenvironmental reconstitutions result from intense chemical weathering mainly in the tropics (Thiry 2000): Kaolinite formation is supported by deep weathering associated with perennial precipitation and a soil temperature not dropping below 15°C. Another typical effect in tropical soils is the progressive depletion of cations and silica oxides that are washed out by percolating water (Curtis 1990, Robert & Kennet 1994, Gawenda 1999). Smectite forms preferentially under tropical and subtropical conditions that are characterized by an elevated seasonality of alternating wet and dry periods (Fig. 5.1). During the wet season, the solution of cations is activated, whereas an increased formation of authigenic clay minerals marks the dry season. Consequently, a badly drained area with modest relief supports the formation of smectite (Robert & Kennet 1994, Gawenda 1999).

5.1.2 Alteration after formation and/or deposition

However, the climatic conditions in the source area are not the only parameters that influence the final clay mineral association that passes into the geological record within a host sediment.

Illite and chlorite may derive from the erosion of unaltered bed rock. An increase in these minerals is often observed in areas with steep reliefs and/or a strong tectonic activity creating a pronounced relief, where rapid erosion does not allow for soil formation and maturation (Deconinck et al. 1985, Gawenda 1999). According to

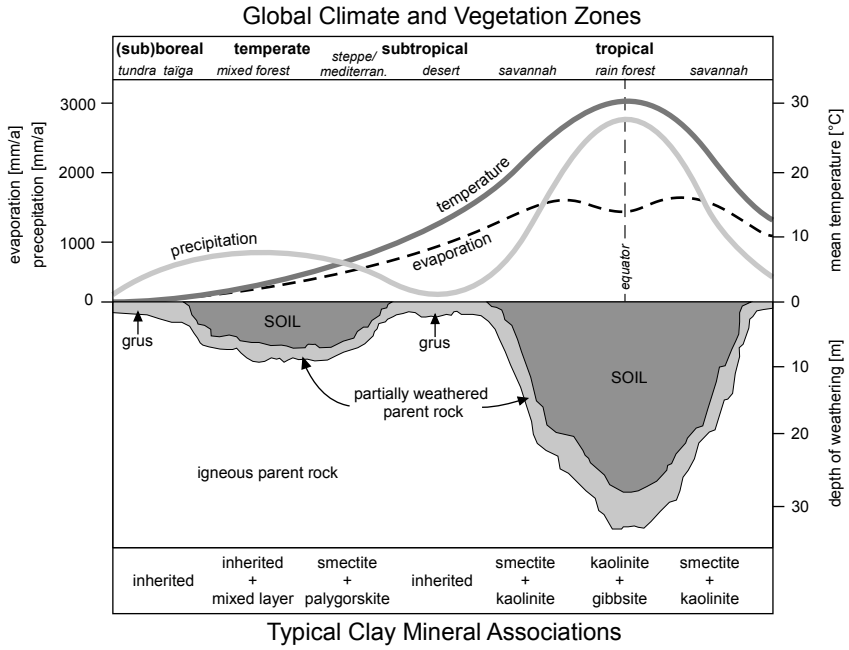

Fig. 5.1 - Schematic view of the silicate weathering system, showing the relations between precipitation, evaporation, temperature, depth of weathering, and nature of the residuum. Based on Lisitzin (1972), modified after Hay (1998) and Thiry (2000).

Deconinck (1993), lowstands in relative sea-level cause a higher relief energy, i.e. a higher erosion rate, thus the development of illite-rich sediments is favoured. Kaolinite, on the other hand, would come from the reworking of soils during platform flooding. Its abundance would therefore be highest around maximum flooding.

Additionally, once a clay mineral association arrives in a shallow marine sedimentation area, hydrodynamic control may influence the mineralogical spectrum of sediments, i.e. there may be links between (micro)facies and clay mineral assemblages (Bläsi 1980, Adatte 1988, Adatte & Rumley 1989, Singer 1990, Mouchet 1995, 1998).

Another widespread phenomenon is the alteration and neoformation of clay minerals. The most common process is the transformation of smectite to illite during burial diagenesis. It usually occurs at depths of 2-3 km, as e.g., Deconinck & Debrabant (1985) showed for basin sediments of Late Jurassic and Early Cretaceous age in the French Subalpine Ranges. However, this transformation may also happen under surface conditions: Deconinck et al. (1988, 2001) present sedimentological and radiometric evidence that synsedimentary (or early diagenetic) illite neoformation took place in the hypersaline Purbeckian lagoons of the Swiss and French Jura Mountains.

In short: the longer the transport distance, the higher the possibility that complex alteration processes happened during intermediate sediment storage, and the less clear the palaeoclimatic message of the deposited clay mineral association (Thiry 2000).

5.2 Methods

5.2.1 Sample preparation

Sample preparation and X-ray diffraction (XRD) analyses were carried out at the Institute of Geology of the University of Neuchâtel, Switzerland, on a SCINTAG XRD 2000 diffractometer. Sample preparation is based on the methods described by Kübler (1987): The crushed sediment is mixed with an ionized aqueous solution (pH 7-8) and agitated. The carbonate fraction is then eliminated by the addition of HCl 10% (1.25 N) at room temperature. During a reaction time of 20 minutes or more, physical disintegration is stimulated in an ultrasound bath every 3 minutes, until all carbonate is dissolved. The insoluble residue is then repeatedly concentrated in a centrifuge and washed (5-6 times) until obtaining a neutral suspension (pH 7-8). A separation of various particle sizes (< 2µm and 2-16µm) can be obtained using the relation between sedimentation time and the depth of pipettage based on Stokes' Law. The selected fraction is then transferred by pipette to a glass object tray and air-dried at room temperature. Additionally, the fraction < 2µm is analyzed after saturation with ethylene glycol and subsequent air drying. The intensities of the peaks that characterize each clay mineral (smectite, chlorite, illite, kaolinite, interstratified) are measured in *counts per second* (cps) for the semi-quantitative estimates of the proportions of clay minerals present.

5.2.2 Identification of peaks

Peak identification in XRD diffractograms is carried out by using the "SCINTAG DMS software package ". XRD peaks characteristic for one mineral can be superimposed on peaks of other minerals that have similar base distances in their crystallographic network. In case of a superposition, the SCINTAG DMS software uses Gaussian algorithms to correct peak morphology, until a better adjustment is obtained. Corrections due to such superpositions are often necessary to, e.g., separate the kaolinite (001) peak from the chlorite (002) peak (the

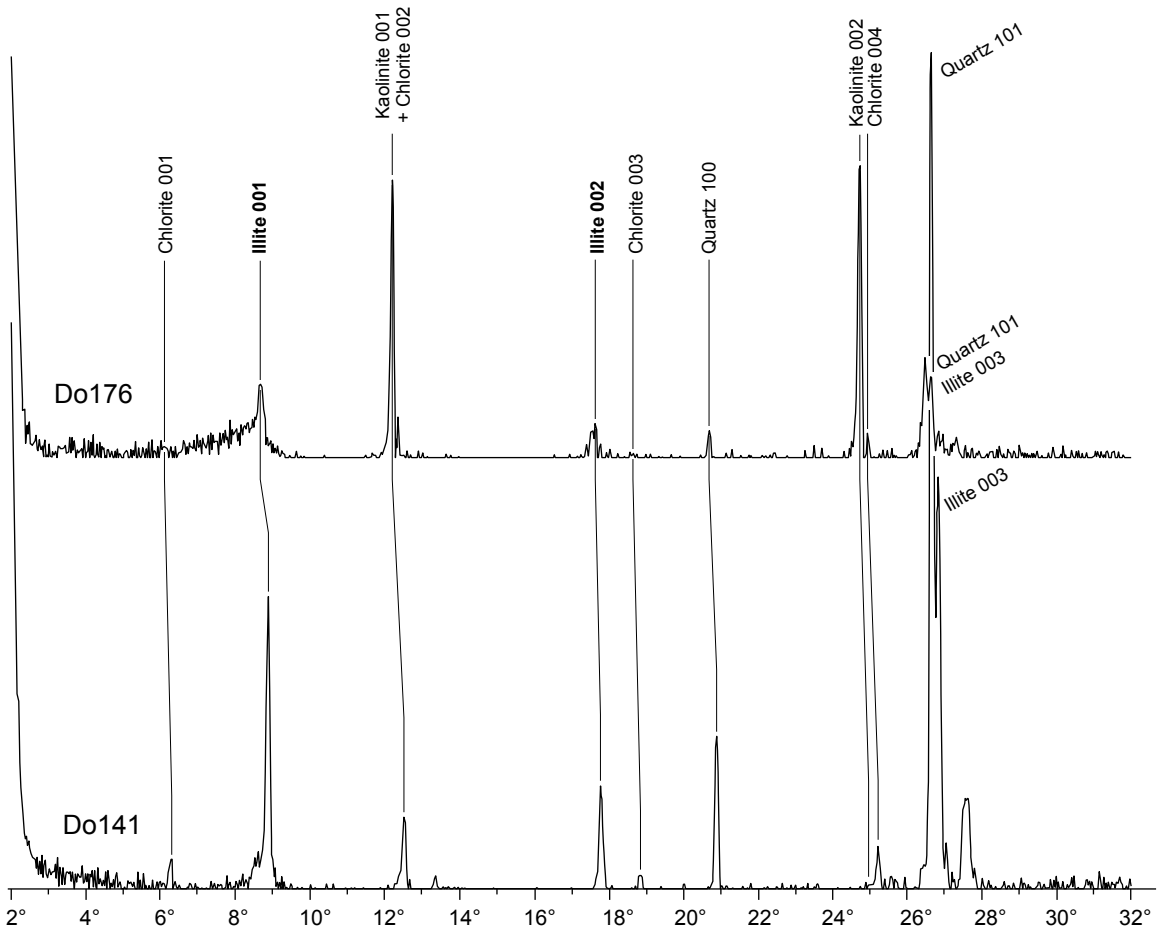

Fig. 5.2 - XRD plots of two samples that illustrate varying illite crystallinity. In sample Do141 the illite 001 and 002 peaks are sharply defined (detritic illite), whereas they are much broader and show a lower intensity in sample Do176 (authigenic illite). Note also that the clay-mineral assemblages are mainly composed of illite, kaolinite, and quartz. Chlorite is only an accessory mineral and may accompany detritic illite as in sample Do141.

two peaks are both located at approximately 12.2° on the diffractograms, cf. Fig. 5.2). The contribution of kaolinite and chlorite in this cumulated peak is calculated indirectly, starting from the peak intensities of the kaolinite (002) and the chlorite (004) peaks (24.9° and 25.2°, cf. Fig. 5.2). After the software successfully separated these two peaks, a relative abundance of the two minerals can be calculated, expressed as respective ratios R_1 and R_2.

$$R_1 = \frac{I_{KAO\,(002)}}{I_{KAO\,(002)} + I_{CHL\,(004)}}$$

$$R_2 = \frac{I_{CHL\,(004)}}{I_{KAO\,(002)} + I_{CHL\,(004)}}$$

with I = intensity in cps

These ratios are used to calculate the intensities of kaolinite and chlorite starting from the intensity of their cumulative peak at 12.2°. Finally, the intensities of smectite (001), chlorite (002), illite (001), interstratified clay minerals (001), and kaolinite (001) can be calculated to sum up to 100% (relative abundance).

5.2.3 Definition of parameters

Kaolinite/illite(K/I) ratio

The K/I-ratio is directly calculated from the intensities (in cps) of the kaolinite (001) and the illite (001) peaks. It represents the influence of climate and relief changes (tectonics) on chemical weathering and soil formation. A high K/I ratio generally indicates a humid, tropical climate. The more arid and desert-like the climate in the source area, the greater the effect that physical (illite delivering)

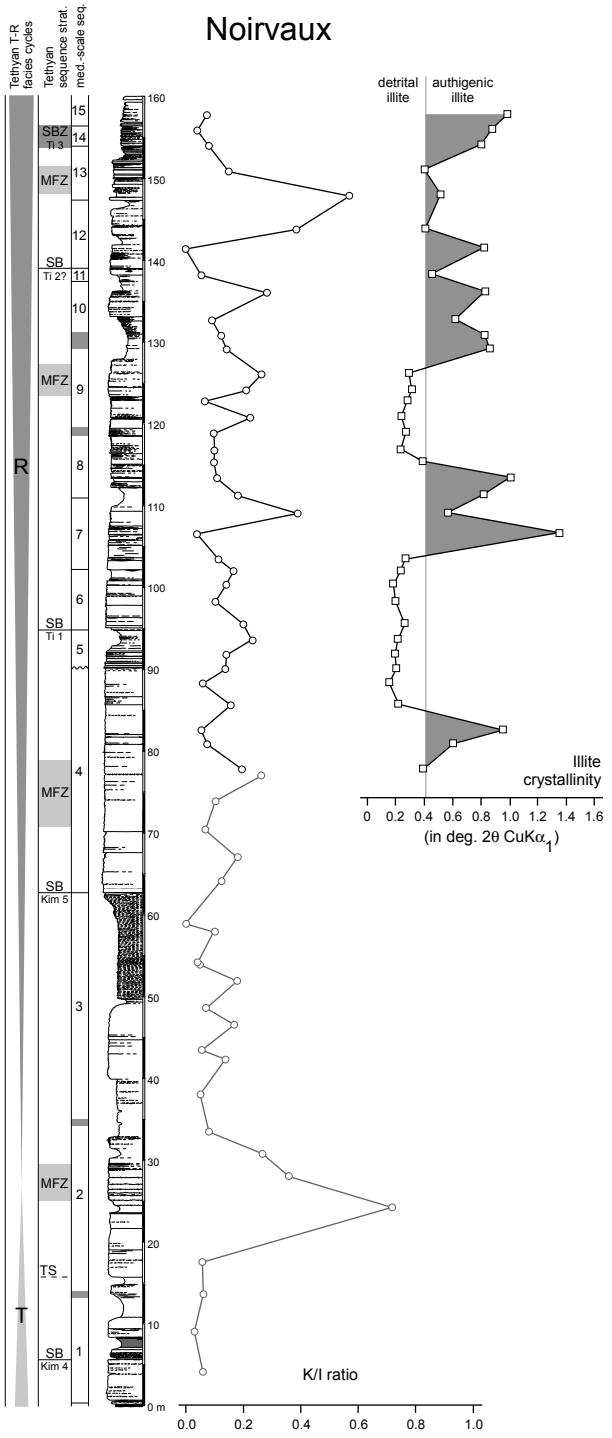

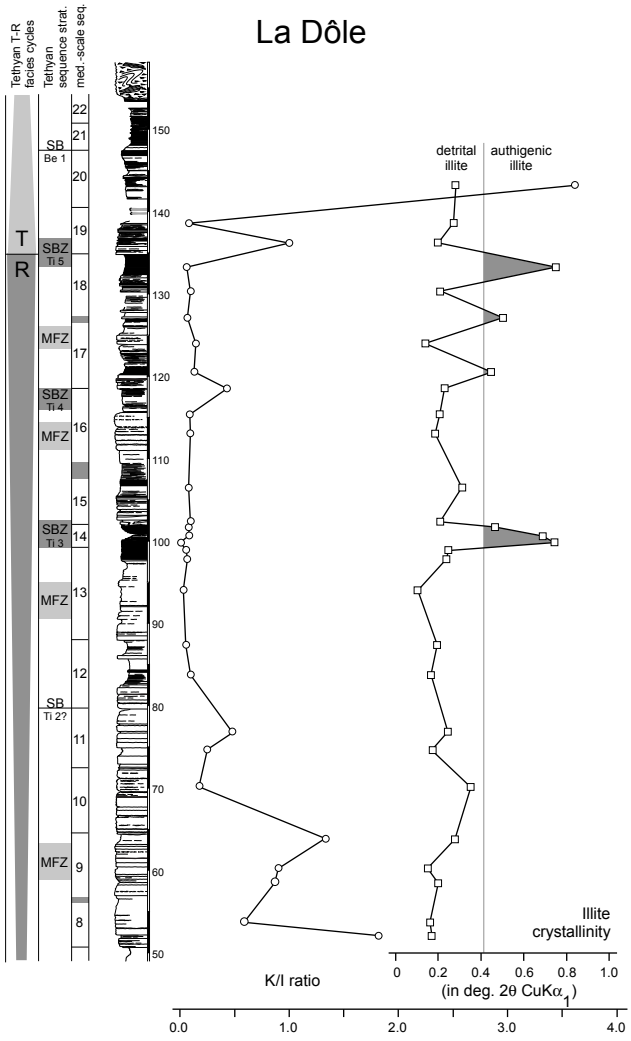

weathering has on the assemblage and the lower the K/I ratio will be. As the relief of the Late Jurassic landmasses was not very high and the Tithonian was a tectonically quiet period (cf. Chap. 1), the effects of tectonically induced relief-changes or steep slopes preventing soil maturation are regarded as negligible. Therefore, the main influences on the K/I-ratio are interpreted to be changes in climate and relative sea-level (cf. THIRY 2000, CURTIS 1990).

Illite crystallinity index

Detritic illites that are derived from eroded metamorphic or igneous rocks have obtained maximum crystallization during their process of formation and their composition approaches the ideal composition as calculated from the laws of crystallography. Grid spacing reaches a great regularity and the peaks show a maximum height in relation to a minimum of width (KÜBLER 1964; cf. Fig. 5.2). In contrast to that, authigenic clay minerals that form in shallow marine or peritidal environments are commonly degraded minerals, i.e. in a crystallographic sense they have no ideal structure and contain many foreign ions. The grid distances are thus disturbed, which results in widened XRD peaks at the expense of their absolute height (intensity) (Fig. 5.2).

The quality of crystallization can be defined by measuring the width (in degrees 2è $CuK\acute{a}_1$) of the illite (001) peak, at 50% height, of the air-dried samples of the < 2 ìm fraction (cf. MOUCHET 1995). This measurement is known under various abbreviations: e.g., IC (illite crystallinity) or

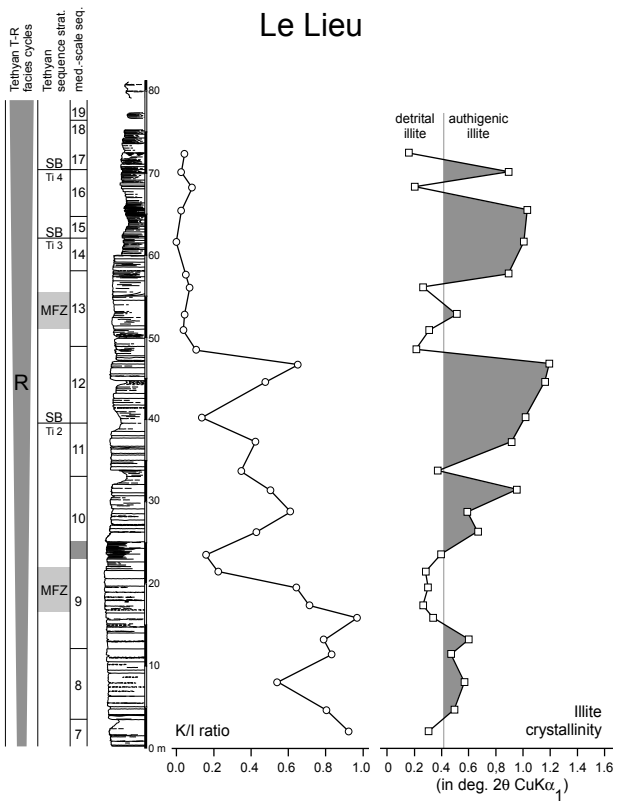

Fig. 5.3 - (this page and facing page) Kaolinite/illite ratio and illite crystallinity of the Noirvaux, Dôle, and Lieu sections (Noirvaux with data from Kettiger (1981) displayed in grey). The numbers in the column on the outer left refer to the medium-scale sequences defined in Chap. 4.

SW (Scherrer width) in English-speaking countries. The illite crystallinity is independent of the peak's intensity (height in cps; Kübler 1990). Note that the lower the illite crystallinity value (in degrees 2è CuKá$_1$), the closer an illite (or mica) is the ideal crystallographic composition. Illite crystallinity values below 0.25° are characteristic for metamorphic micas of the epizone. Illite crystallinity values ranging from 0.25° to 0.42° are characteristic for micas from the anchizone, whereas values higher than 0.42° are representative of poorly crystallized diagenetic micas (Kübler 1990).

However, if the intensity of the peak is too low, this method becomes unreliable (Kübler 1987). Persoz (1982) defines this limit at approx. 200 cps. However, most of the 93 analyzed samples are well above this limit, there are only 4 with intensities below 200 cps (No103: 109 cps; Do159: 149 cps; Do 163: 136 cps; Do176: 185 cps). The value of the peak width depends also on sample preparation techniques and equipment used. It is thus important not to compare the absolute values of samples that were not measured in the same laboratory.

5.3 Results, interpretation and discussion of XRD analyses

The clay minerals assemblages found in the analyzed samples are characterized mainly by illite, kaolinite and chlorite. Small amounts of mixed-layer clay minerals and smectite may also occur. The most striking differences in the studied sections are found in the illite crystallinity and the K/I ratio (Fig. 5.2).

Kaolinite/illite(K/I) ratios

The Noirvaux section (Fig. 5.3a) shows a bandwidth of K/I ratios from 0 to 0.57 (0.72 in the lower part, data of Kettiger 1981). The highest values are reached in medium-scale sequences 2 and 12/13. The curve starts rather flat and with values close to 0 in medium-scale sequence 1, but suddenly jumps to its maximum of 0.72 in medium-scale sequence 2. A series of well developed peaks starts at medium-scale sequence 7, with maxima in medium-scale sequences 7, 9, 10, and 12/13. The striking peak in medium-scale sequence 2 is probably linked to the major transgressive surface Kim 4 and the subsequent 2nd-order maximum flooding of the *Eudoxus* ammonite zone (cf. Fig. 1.9). Either climate conditions became more humid in parallel to the transgression, or, more probably, the peak is caused by the erosion of soils (Deconinck 1993) or reworking of intermediately stored sediment on the internal platform. Hug (2003) proposed a similar mechanism for high quartz abundance in transgressive sediments of the Jura Mountains' Late Oxfordian. Colombié (2002) accordingly interprets the gain in K/I ratio at this level as a result of reworking. Thus, the differing behaviour of the K/I ratio in the Gorges de Pichoux (Colombié 2002) and the Noirvaux section (Kettiger 1981, this work) during the Late Kimmeridgian could plausibly be explained as local effects during reworking. A major climate change would have produced a more uniform response.

The Dôle section (Fig. 5.3b) and the Lieu section (Fig. 5.3c) show a very similar evolution of K/I ratios (variation between 0 and 3.61). Values decline from 1.82 (La Dôle), respectively 0.93 (Le Lieu), at the base of medium-scale sequence 8 to a zone of K/I ratios close to zero (kaolinite minimum zone, KMZ), spanning over medium-scale sequences 13 to 18. At the base of medium-scale sequence 19 of the Dôle section, kaolinite reappears and in medium-scale sequence 20 values jump abruptly to their maximum of 3.61.

This kaolinite minimum zone is known all over Europe and associated with a major terminal Jurassic "dry event" (Deconinck et al. 1985, Deconinck & Debrabant 1985, Wignall & Ruffell 1990, Hallam et al. 1991, Abbink et al. 2001, Schnyder 2003).

The increase in kaolinite at the top of the Dôle section marks the end of the kaolinite minimum zone in the

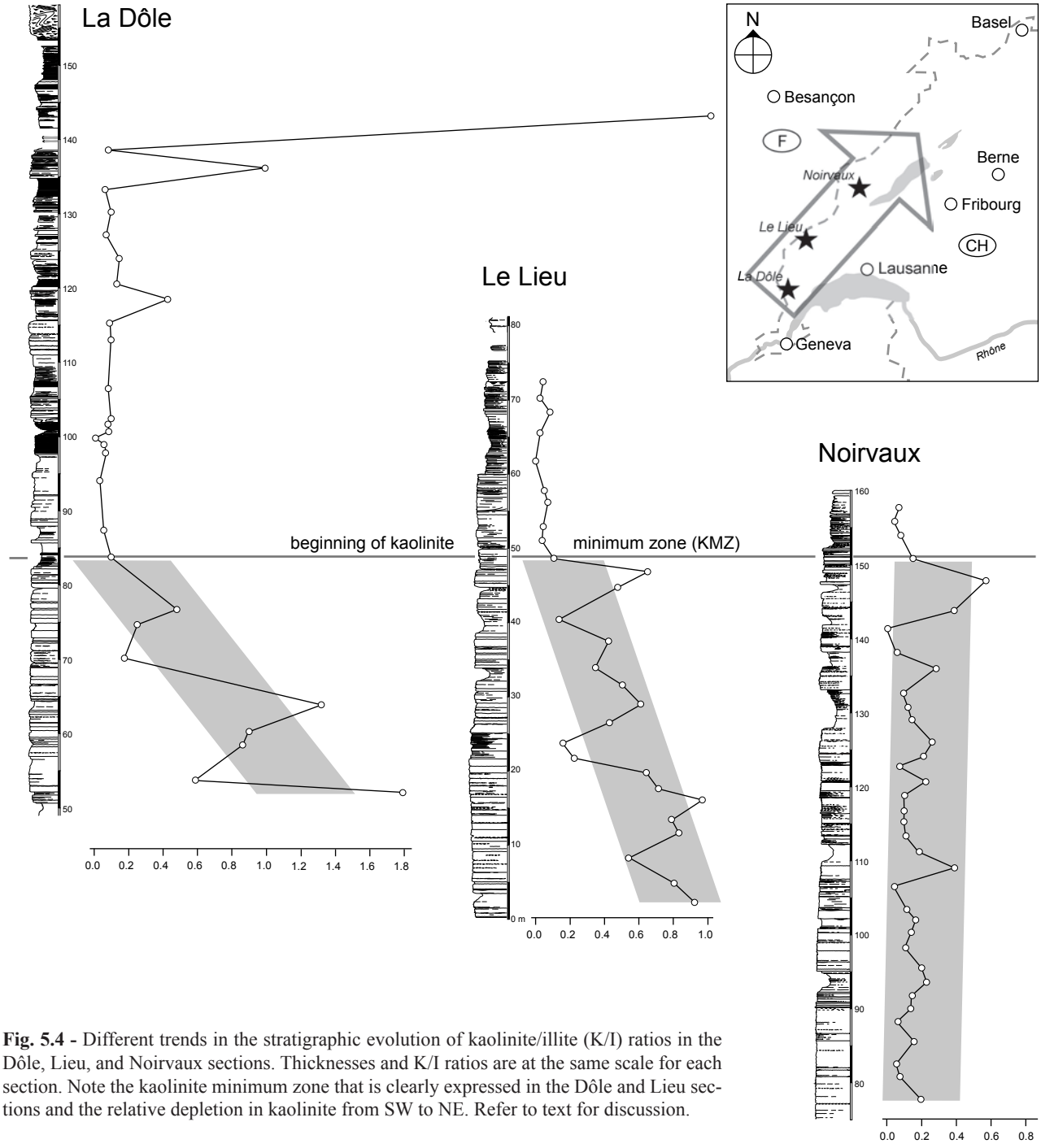

Fig. 5.4 - Different trends in the stratigraphic evolution of kaolinite/illite (K/I) ratios in the Dôle, Lieu, and Noirvaux sections. Thicknesses and K/I ratios are at the same scale for each section. Note the kaolinite minimum zone that is clearly expressed in the Dôle and Lieu sections and the relative depletion in kaolinite from SW to NE. Refer to text for discussion.

working area. This marks the end of the Late Jurassic "dry zone" *sensu stricto* and the beginning of a transitional climate before the change to a warm, humid climate with pronounced seasonality in the Late Berriasian. Sedimentological evidence supports this interpretation (cf. Chap. 8).

Just below the kaolinite minimum zone an eye-catching saw-tooth pattern is expressed in all three measured sections. The peaks lie in medium-scale sequences 7, 9/10, and 12/13. Again, it is not clear if these minor (and apparently cyclic) changes result from a combination of hydrodynamic sorting processes (cf. Bläsi 1980, Adatte 1988) and relative sea-level changes or from high-frequency climate changes as proposed, e.g., by Pittet & Strasser (1998b) for the Late Oxfordian.

Another interesting fact is that the three sections show very similar patterns of K/I-ratios between medium-scale sequences 7 to 13, but with differing absolute values (Fig.

5.4). The highest values occur in the SW (La Dôle) and the lowest in the NE (Noirvaux). There seems to be a gradient of increasing kaolinite content to the SW —exactly in the direction towards the Central Massif, a potential source area (Fig. 1.3). However, without a further, regional study relying on more sections this relationship cannot be more than a hypothesis.

Illite crystallinities

The illite crystallinities show no apparent correlation with the K/I ratios. In the Dôle section, they oscillate relatively constantly around a value of approximately 0.2° 2θ CuKα_1. The lowest values are regularly reached in large-scale maximum-flooding zones (MF Ti 1_{Tethys}, MF Ti $2?_{Tethys}$, MF Ti 4_{Tethys}), whereas the rare but well expressed peaks are linked to large-scale sequence boundaries (SB Ti 3_{Tethys}, SB Ti 5_{Tethys}). In contrast to this, the illite crystallinity graphs of the Lieu and Noirvaux sections show generally higher values of up to ca. 1.4° 2θ CuKα_1. However, the minimum values are reached around the same large-scale maximum-flooding zones as in the Dôle section (MF Ti 1_{Tethys}, MF Ti $2?_{Tethys}$).

In unaltered sedimentary rocks, illite is usually considered as a detrital mineral reworked from older rocks (including sedimentary and crystalline rocks). Such illite usually has an aluminous composition, a crystallinity index of less than 0.42°, and usually occurs together with other detrital minerals (e.g., chlorite, kaolinite, smectite, quartz), because the erosion commonly affects rocks and soils of various types and ages.

Another source for illite is the replacement of smectitic minerals during burial diagenesis (Chamley 1989). Detrital smectites derived from the gentle erosion of vertisols are common in the Purbeckian of the north-western Jura Mountains (Deconinck & Strasser 1987) and the traces of interstratified illite-smectite that were found may represent intermediate steps in the transformation of smectites into illites. The transformation usually occurs in depths of 2-3 km (Deconinck & Debrabant 1985). Diagenetic illite usually shows crystallinity indices higher than 0.42°, and the presence of smectite is inversely correlated with its occurrence. However, as indicated by the stratigraphy of the Jura, the burial depth of Tithonian carbonates did not exceed 1 km (Trümpy 1980). Moreover, regional studies on the clay mineralogy of Mesozoic sediments in the Jura Mountains also indicate relatively shallow burial depths (Persoz & Remane 1976, Persoz 1982). Therefore, the influence of deep burial on the illitization of smectite in the studied sediments seems to be negligible and smectite is more likely to have been converted to illite at surface temperature and pressure. Illitization was probably produced by repeated wetting by sea-water of elevated salinity and subsequent drying (Eberl et al. 1986, Deconinck & Strasser 1987, Deconinck et al. 1988) under a hot and arid climate. Deconinck et al. (2001) present K/Ar-ages for these illites, confirming that illite formation happened not during late burial but was in fact penecontemporaneous.

Consequently, high illite crystallinity indices can be regarded as an indicator for aridity, elevated evaporation and proximity of the land-sea interface. The measured illite crystallinities thus support the sequence stratigraphic-interpretation presented in chapter 4: during large-scale maximum flooding periods, only detrital, well crystallized illite (< 0.42° 2è CuKá$_1$) is deposited under relatively open-marine conditions. Towards a large-scale sequence boundary, the tidal flats prograde, and the mechanism of illite neoformation is activated. This scheme is particularly well expressed in the upper half of the Dôle section (from SB Ti 3_{Tethys} to SB Ti 5_{Tethys}). The graph of crystallinity indices show an oscillating geometry, reflecting regressive and transgressive phases of superimposed large- and medium-scale sequences. The overall trend is an increase in the occurrence of authigenic illite (> 0.42° 2è CuKá$_1$) towards an absolute maximum at SB Ti 5_{Tethys}, which is at the same time the peak of 2nd-order regression (cf. Fig. 1.9). With the subsequent large-scale TS combined with the switch back to a 2nd-order transgressive regime, the indices abruptly fall back to approx. 0.2° 2è CuKá$_1$ – the "background sedimentation value" of well crystallized, purely detrital illite.

Additionally to the sequence-stratigraphic information, the measured illite crystallinity indices can also serve as a proxy for proximal-distal facies trends. The sediments of the Dôle section are clearly dominated by detrital illite, whereas those of the Lieu section are clearly dominated by authigenic illite. Noirvaux takes an intermediate position. Le Lieu was situated in the platform interior (most of the time confined conditions and emersion) while La Dôle was closest to the platform rim (most of the time relatively open conditions). In fact, this reflects their palaeogeographic position with respect to the distance to the supposed platform rim (cf. Fig. 1.3).

* * *

6 - CYCLOSTRATIGRAPHY

"(Allocyclicity and autocyclicity on carbonate platforms represent) two alternative end-member models, one driven by relative sea-level change, the other driven by changes in transport rate and productivity controlled ultimately by climatic factors. Many carbonates systems may represent some combination of these end-member possibilities."

BURGESS (2001, p.1127)

At the end of the 19th century, Gilbert (1895) proposed that rhythms in a Late Cretaceous limestone-marl alternation in Colorado, U.S.A., are the result of astronomical forcing. Some thirty years later, Bradley (1929) recognized the precession cycle in oil-shale/dolomite sequences of the Eocene Green River Formation (Colorado, Wyoming, Utah, U.S.A.). While these publications went largely unnoticed, cyclostratigraphic bases were laid when Milutin Milankovitch published his groundbreaking monograph on insolation changes as controlling factor of the Pleistocene ice-ages (Milankovitch 1941). In 1947, Schwarzacher was the first to relate cyclic carbonates from shallow platform environments to orbital frequencies. With the advance in analytical methods and the possibility of analyzing large data-volumes, scientific interest in orbital forcing grew. In the late 20th century, Berger (1988) and Berger et al. (1989) made the theoretical astronomical basis accessible to the geoscience community by publishing calculated astronomical frequencies going back until the early Silurian.

Since then, numerous high-resolution sedimentological studies relate m-scale cyclicity to astronomically defined insolation variations that trigger changes in climate, oceanic circulation, and sea-level. The understanding of the mechanisms involved and their sedimentary signatures is a main domain of research today (e.g., FISCHER 1986, 1991, GOLDHAMMER et al. 1990, 1993, 1994, STRASSER 1994, READ et al. 1995, PITTET & STRASSER 1998a, 1998b, D'ARGENIO et al. 1999, BOSENCE et al. 2000, HINNOV 2000, STRASSER et al. 2000, PITTET et al. 2000, BUONOCUNTO et al. 2002, PAWELLEK & AIGNER 2003, STRASSER et al. 2004, WEEDON et al. 2004). Cyclical variations of sediment types and mineralogy, of palynofacies, and of geochemical, palaeoecologic, and various other markers are related to processes such as changes in oceanic productivity and redox potential on the sea floor (e.g., EINSELE & RICKEN 1991), shifting climate belts (e.g., PERLMUTTER & MATTHEWS 1989, 1992, HALLAM 1994, PITTET 1996, VALDES & GLOVER 1999), or short-term eustatic sea-level variations (e.g., MONTAÑEZ & OSLEGER 1993, D'ARGENIO et al. 1997, RAMEIL et al. 2000). These studies demonstrate that orbital signals recorded in a variety of environments in many different ways are the result of complex interactions of atmosphere, hydrosphere, biosphere, and lithosphere. The controlling orbital parameters (precession, obliquity, eccentricity; cf. Fig. 6.1) are well defined in terms of cycle duration back to Mesozoic times (BERGER et al. 1989, BERGER & LOUTRE 1994). The fact that they are often recorded in sedimentary environments, regardless of feedback mechanisms, make the corresponding sedimentological signatures a particularly good and independent chronostratigraphic tool (DE BOER & SMITH 1994, D'ARGENIO et al. 2004). The obtained high-resolution time framework allows for the quantification of sedimentary and tectonic processes (PITTET 1994, 1996, HILLGÄRTNER 1999, HUG 2003, STRASSER et al. 2004). It has to be mentioned, however, that some authors question the recording of orbital cycles

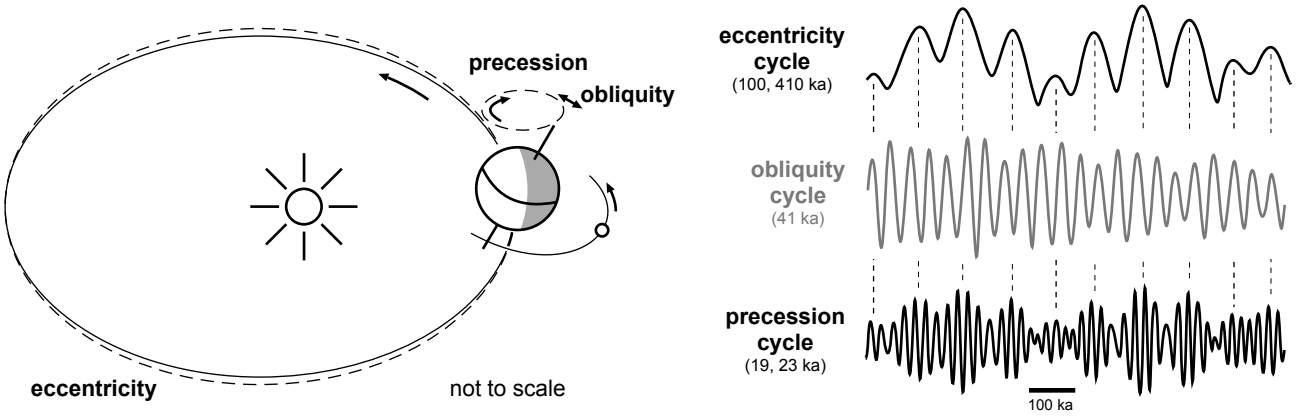

Fig. 6.1 - Orbital parameters and their major frequencies (modified after Einsele & Ricken 1991). Schematic insolation curves are given on the right. Note that the eccentricity cycles act as an amplitude modulation on the precession cycles. The obliquity cycle is not visible in the studied sediments (see text for details).

in sedimentary successions (e.g., Drummond & Wilkinson 1993, 1996, Wilkinson et al. 1996, 1997, Burgess 2001, Burgess et al. 2001, Burgess & Wright 2003, Wilkinson & Drummond 2004).

6.1 Advantages, annoyances, and pitfalls

6.1.1 The advantage: a high-resolution time window

A cyclostratigraphic timeframe has the enormous advantage of being (theoretically) completely independent of biostratigraphy and, additionally, allowing for a resolution as high as 20 ka under ideal conditions. Thus, it provides a high-resolution timescale for reconstructing platform and basin evolution and allows for the estimation of rates of ecological, sedimentary, and diagenetic processes (Strasser et al. 1999). As each sedimentary cycle represents a given duration (20, 40, 100, or 400 ka), the resulting timescale is very accurate but always relative ("*floating astronomical timescale*", Hilgen et al. 2004). Consequently, the full potential for high-resolution stratigraphy is only developed when the cyclostratigraphic timeframe is linked to biostratigraphic zones (or, at least, tie-points) and numerical ages (e.g., Gradstein et al. 1994). The more biostratigraphic and numerical data exist that allow for verifying the cyclostratigraphic interpretation, the more consistent and accurate the final result will be.

6.1.2 Annoyances and pitfalls

The following effects and mechanisms may prevent and/or distort the recording of orbitally forced high-frequency sedimentary sequences in shallow platform environments and thus have to be taken into account when setting up a cyclostratigraphic timeframe (cf. Strasser et al. 1999):

- Due to the platform emerging regularly, the incompleteness/completeness of the sedimentary record cannot be reliably assessed ("*missed beats*", Goldhammer et al. 1990), only an educated guess is possible.
- In shallow-water environments, autocyclic processes may be active that produce sedimentary successions very similar to high-frequency sequences that result from orbitally forced sea-level oscillations.
- Bed thickness and accommodation do not have a linear relationship. This is due to facies-dependent differential compaction. Consequently, the observed bed thicknesses do not correspond to the original accommodation space.
- A single cycle in environmental change may lead to the formation of multiple beds (Pittet & Strasser 1998) and, therefore, no simplistic assumptions on the time-span represented by each bed (or limestone-marl couplet) can be made.
- The estimation of accommodation potential is difficult when a sequence is composed entirely of subtidal facies.

- There is no record of high-frequency sea-level and/or climatic changes when sedimentological and/or biological thresholds were not passed and thus no facies contrast was created (e.g., "*amalgamation*" of subtidal cycles, Osleger 1991).
- Interference of long-term and short-term periodicities may lead to the enhancement or attenuation of high-frequency signals (cf. Fig. 4.5).
- Imprecise chronostratigraphic data introduce enormous error ranges into the calculation of mean cycle durations.

Among these, specifically the two main complications: (in)completeness of the sedimentary record, and autocyclicity vs. allocyclicity have to be critically and carefully assessed prior to the construction of an orbitally defined timeframe. Despite all these difficulties, cyclostratigraphy is the tool of choice for establishing a high-resolution timeframe on the Jura platform, because it simply is the only one available.

6.1.3 Completeness of the sedimentary record

When dealing with cyclostratigraphic interpretations of rhythmic sediment successions in platform environments, the question of the completeness of the sedimentary record arises inevitably. For shallow-marine high-frequency sequences, Strasser (1994), Strasser et al. (1999), Strasser & Samankassou (2003), and Mora (2004) showed that, despite of lateral variations in facies and sediment accumulation (cf. Rankey 2001, 2002, Burgess & Wright 2003), and despite of significant parts of the geological time-record lost in discontinuity surfaces (resulting from subaerial exposure and lag time: "*base cut-out*", or "*truncated*" cycles sensu Soreghan & Dickinson 1994), the rocks of a high-frequency sequence thus only representing a fraction of the geological time passed (cf. Burgess & Wright 2003), the final stacking pattern is representative of high-frequency changes in relative sea-level (Fig. 6.2). Obviously, this concept is only valid as long as each cyclic sea-level fluctuation creates a characteristic sediment succession that passes into the geological record. If, during a long-term emersion over several cycle-periods, sea-level stays below the platform top, no signal can be recorded ("*missed beats*" sensu Goldhammer et al. 1990).

Consequently, the crucial question is not if the sedimentary record is complete in general (it is not!), but if there are any longer-term hiatuses that produced missed beats. If such a missed beat can be deduced from sedimentological interpretation, irregularities in the stacking pattern and/or correlation, it is important to identify the duration of the missing cycle(s) (cf. Steinhauff & Walker 1995). E.g., even if several elementary cycles in a larger-scale composite cycle are missing, the larger-scale composite cycle they belong to may still be identifiable. Unfortunately, determining the exact duration of a hiatus is nearly impossible without the presence of high-quality bio/chronostratigraphic tie-points immediately below and above the discontinuity surface – a rare situation even in well-dated sections. Yet, by having a closer look at characteristic features of discontinuity surfaces created by subaerial exposure (Tab. 6.1), it is possible to separate major unconformities from short-termed ones that usually cap shallowing-upward cycles (Foos 1996). According to Esteban & Wilson (1993) and Wright (1994), it is possible to roughly estimate the duration of the subaerial exposure by evaluating the maturity of palaeosols, caliche and/or karst (if present). However, Budd et al. (2002) question the straightforward approach of linking macroscopic exposure features directly to exposure duration.

Major unconformity	Shallowing-upward carbonate cycles
Truncation of stratigraphic units	Multiple exposure surfaces within one stratigraphic unit
Low to high relief on unconformity surface	Exposure surfaces concordant with bedding
Well-developed cavern system and collapse breccias	Small-scale caves and solution features
Meteoric diagenesis up to 100 m below unconformity surface	Horizontal zones of meteorically enhanced porosity
Well-developed paleosols	Poorly developed paleosols
Solution features filled by sediments of subsequent transgression	Solution features filled by host sediment

Tab. 6.1 - Characteristics of subaerial exposure surfaces defining major unconformities and capping carbonate cycles (after Foos 1996).

Except for a major unconformity located at the top of the Yenne section, all observed subaerial exposure surfaces show exclusively characteristics of typical short-term emersions at the top of shallowing-upward carbonate cycles according to Foos (1996; cf. Tab. 6.1). This is perfectly in tune with the sequence stratigraphic model presented by Détraz & Mojon (1989) for the Late Jurassic and Early Cretaceous of the southern Jura platform.

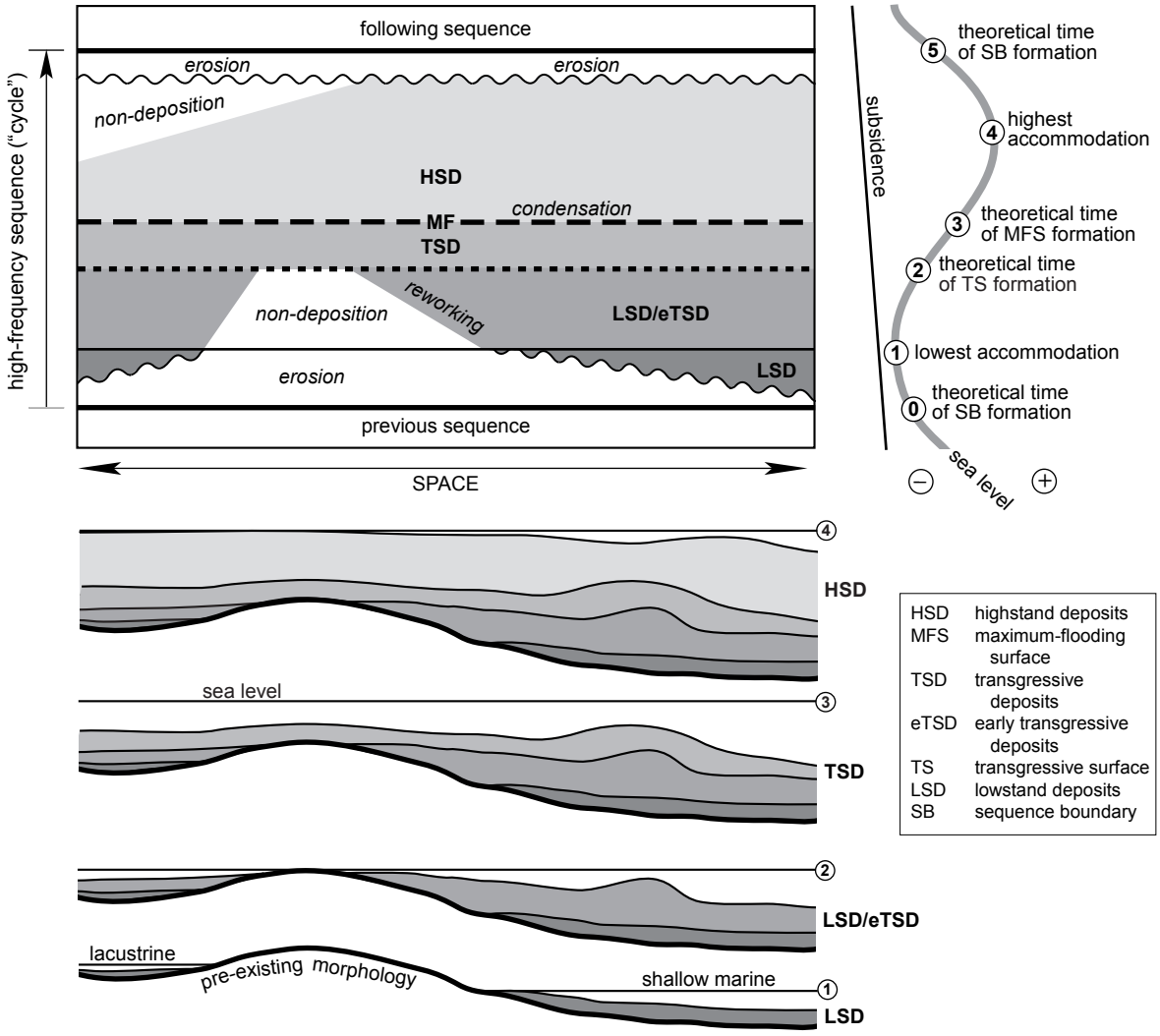

Fig. 6.2 - Hypothetical space-time diagram illustrating the different durations of sediment accumulation depending on platform morphology. As a result of erosion, reworking, and condensation, completeness of the sedimentary record and thickness of high-frequency sequences may vary considerably through time and space. However, even if the sedimentary record is incomplete, it may still allow for correctly identifying high-frequency sequences. Taken from Strasser & Samankassou (2003), modified.

Vadose diagenetic caps at cycle tops usually measure some 10s of cm in thickness. The only exception is an erosion surface in Noirvaux (90.2 m, Fig. 4.11), where vadose features are developed over a thickness of approximately 3 m. Yet, this is possibly the result of local tectonics. If it was due to a high-amplitude sea-level drop, correlatable vadose zones or pronounced sequence boundaries should occur also in other sections, which is not the case (cf. Chap. 7). Thin vadose zones indicate low-amplitude sea-level changes (Read & Horbury 1993, Read 1995, cf. Fig. 6.3). The thick vadose interval that defines the upper part of the Lieu section (Fig. 4.13) is interpreted to represent not one big, but a succession of several smaller sea-level drops.

Where it is present, karstification is only developed into its initial and early youth stages (microkarst and cavities of a few 10s of cm in diameter, cf. Pl. 10/5, 6). Consequently, the duration of subaerial exposure for these surfaces most probably did not exceed 10 ka (cf. Fig. 2.4). The absence of well-developed karst systems also suggests a low amplitude of sea-level changes (Read & Horbury 1993, Read 1995, cf. Fig. 6.3).

At the top of the Dôle section (top Twannbach Fm.), two thin, red-brown clay seams were found that are interpreted as incipient palaeosols. They mark the beginning of the Goldberg Formation, where caliche and palaeosols become rather frequent (cf. Fig. 4.19 and Strasser & Davaud 1982, Davaud et al. 1983). The development of caliche or palaeosols is both a function of climatic conditions (cf. Chap. 8) and exposure time (Wright 1994). Thick palaeosols featuring a well-structured soil profile indicate long exposure times – easily several 100 ka and

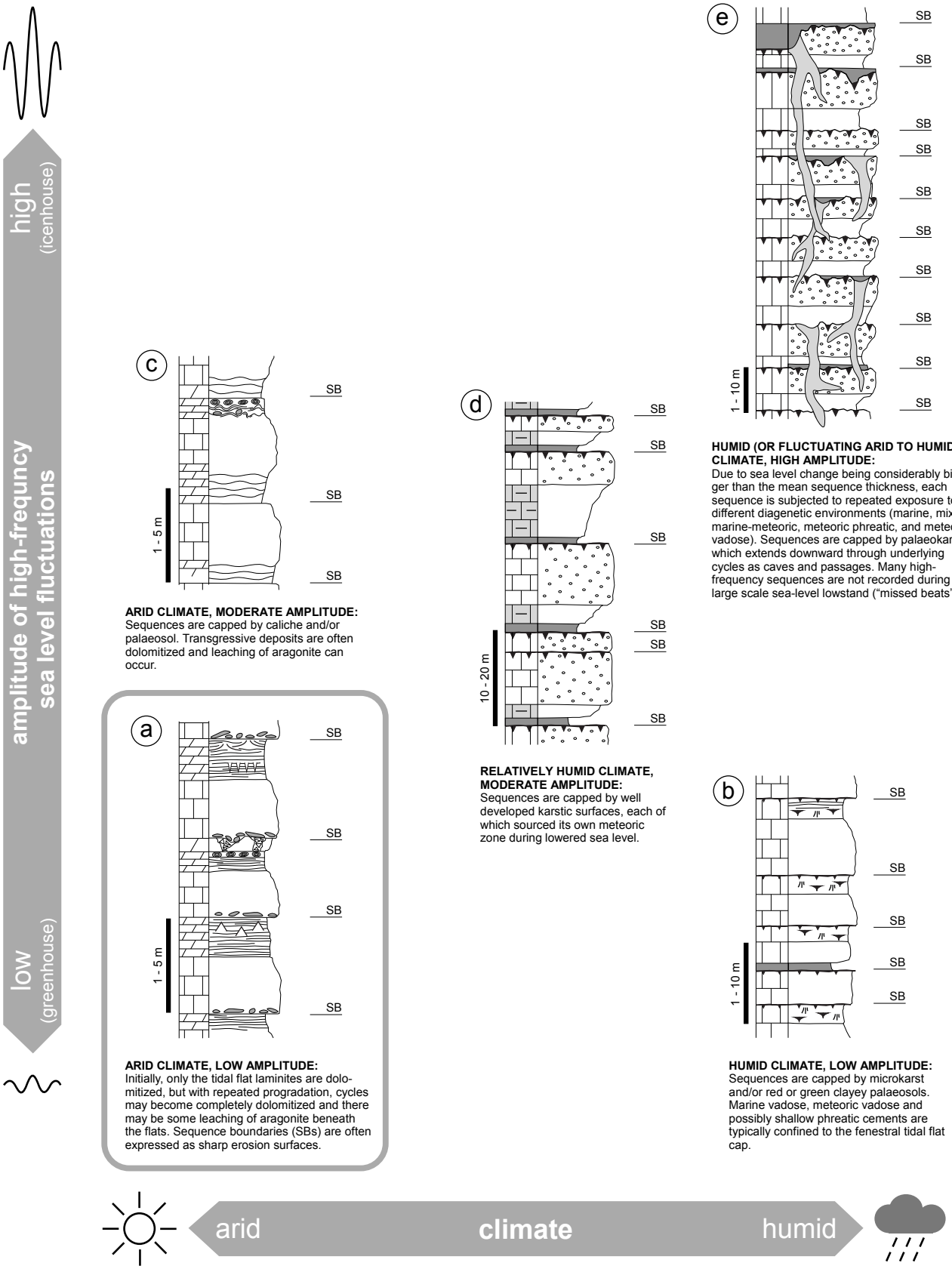

Fig. 6.3 - Idealized sections showing carbonate cycles generated under different climates and amplitudes of high-frequency sea level fluctuations. After Read & Horbury (1993) and Read (1995), modified. Low amplitude: m-scale, moderate: perhaps 20 to 50 m, high: glacioeustatic oscillation of 60 to >100 m amplitude. Scenario (a) is the most likely for the studied sections.

more, whereas thin, unstructured ("incipient") palaeosols reflect shorter exposure times. A mature caliche-level may represent 50-100 ka of exposure (pers. comm. A. Mindszenty, D'Argenio & Mindszenty 1995).

Every single caliche or palaeosol found in the studied sections can be classified as "incipient", thus indicating relatively short emersions that should not negatively affect the recording of a cyclostratigraphic signal on the 100 ka or 400 ka levels. Once again, the m-thick, soil-like interval at the top of the Yenne section is the exception to the rule.

Assessment of cycle preservation potential

In the studied sections, the observed features of subaerial exposure surfaces (thin vadose zones, only initial karstification and/or incipient palaeosols, cf. Tab. 6.1) indicate low-amplitude fluctuations in relative sea-level and relatively short durations of emersion. This is in accordance with Hallam (2001), who discusses different mechanisms for sea-level changes in the Jurassic and states that high-frequency sea-level changes would have been no more than metre scale.

Also, the overall sedimentary architecture of small- and medium-scale sequences (tidal-flat laminites, dolomite caps, sharp basal erosion surfaces overlain by lag deposits; cf. Chap. 4) permit the placement of the studied high-frequency sequences (or cycles) in a scheme that was developed by Read & Horbury (1993) and Read (1995) (Fig. 6.3). This places the observed cycle architecture in a model of low-amplitude high-frequency sea-level fluctuations in an arid climate setting.

High-frequency sea-level fluctuations of low amplitude were superimposed on the Late Jurassic long-term (2nd-order) regressive trend (cf. Figs 1.9 and 4.5). At the same time, the studied region was subject to accelerated subsidence since the Kimmeridgian (Stampfli et al. 2002). The resulting scenario is a delicate equilibrium between long-term eustatic trend, tectonic subsidence, and sediment accumulation, leading to numerous, regular short-term emersions that caused considerable condensation (or telescoping) of cycles due to "base cut-out", and/or "truncated" cycle geometries (cf. Soreghan & Dickinson 1994). Yet, the accelerated subsidence seems to have created enough accommodation space (cf. Zecchin 2005) that the potential for recording (and preserving) sedimentary cycles in the 100-400 ka band was high enough to create significant stacking patterns that can be correlated between all platform section (cf. Chap. 7). The Tithonian of the Jura platform is thus regarded as relatively complete in terms of recording the long and short eccentricity cycle. Congruently, Détraz & Mojon (1989) report major hiatuses exist from the Kimmeridgian and Tithonian of the Jura platform.

6.1.4 Autocyclicity vs. allocyclicity

A common argument against orbital forcing of sedimentary processes is that virtual sedimentary successions, showing stacking patterns that are very similar to those of natural sediment successions, can be created by a random-based, "autocyclic" process (e.g., Drummond & Wilkinson 1993, 1996, Wilkinson et al. 1996, 1997, Wilkinson & Drummond 2004). However, this is no proof against the possibility of a translation of Milankovitch cycles into the sedimentary record. Moreover, by using Markov-chain analyses, Lehrmann & Rankey (1999) demonstrated for cyclic carbonates of Permian age in New Mexico, U.S.A., that the facies succession of this specific carbonate platform is decidedly non-random.

A concept that implies autocyclic processes in sedimentary systems on a large scale is the shoreline "autoretreat" model of Muto & Steel (1997). Volumetric calculations which consider changing rates of accommodation versus sediment supply on a continental shelf suggest a varying effect of shoreline pro-and retrogradation on the architecture of large-scale depositional sequences. Yet, this model was developed for siliciclastic systems and does not consider in-situ carbonate production that intimately depends on accommodation changes. No other autocyclic processes are known that are capable to form regular large-scale stratigraphic patterns.

Some researchers also question the possibility of recording orbitally induced sea-level changes in sediments that were deposited during global greenhouse conditions and, consequently, relate all m-scale sedimentary cycles on carbonate platforms to non-linear, random processes. Yet, even in a Late Jurassic greenhouse world without major polar ice-caps there are a multitude of mechanisms for translating insolation changes into low-amplitude sea-level changes: even if major ice caps are absent, volume changes of mountain glaciers can make a small contribution (Fairbridge 1976, Valdes et al. 1995). Sea-level changes could also have been created by thermal expansion and retraction of ocean surface water (Gornitz et al. 1982), by thermally induced volume changes in deep-water circulation (Schulz & Schäfer-Neth 1997), and/or by water retention and release in lakes and aquifers (Jacobs & Sahagian 1993). In any of these scenarios, climate plays an important role.

Furthermore, Valdes et al. (1995) and Price et al. (1999) suggest modest, but significant (approximately one third the size of the present day) polar ice-caps for the studied interval. According to Valdes et al. (1995), the volume of the Kimmeridgian Antarctic ice-cap was linked to the 100 ka cycle in times of "*maximal seasonal forcing*". During these periods, its cyclical waxing and waning may have provided an additional mechanism for producing m-scale sea-level changes. Other evidence for

the possible existence of a (small) Antarctic ice cap comes from the Early Cretaceous (Stoll & Schrag 1996).

Random-based ("*autocyclic*"), m-scale sedimentary sequences can form on shallow-water carbonate platforms by combinations of vertical aggradation and progradation of tidal flats or lateral migration of islands, tidal channels and shifting carbonate shoals (e.g., Ginsburg 1971, Pratt & James 1986, Strasser 1991, Pratt et al. 1992, Burgess 2001, Burgess et al. 2001, Burgess & Wright 2003). In contrast to sedimentary cycles generated by external (orbital) forcing (= "*allocyclicity*"), these cycles originate from the intrinsic dynamics of sedimentary systems. Despite of their different origin, the resulting sequences are very similar to high-frequency sequences that are the product of orbitally induced sea-level changes.

These models, however, convince only for laterally discontinuous shallowing-up sequences but not in explaining subtidal cycles and/or sequences displaying significant vadose diagenetic overprinting (Osleger 1991, Strasser 1991; for a detailed discussion of problems and limitations of these models refer to Pratt et al. 1992). Yet, subtidal cycles as well as small- and medium-scale sequence boundaries that are underlain by intervals displaying vadose diagenesis were observed (cf. Figs 4.11 – 4.19) and are an unequivocal proof against autocyclic control in the sequences in question.

Additionally, depositional sequences on the Jura platform are physically traceable for up to 1 km in many cases (cf. Fig. 4.14 and Pl. 20/3, see also Hillgärtner 1999), and medium- and small-scale sequences usually can be correlated between the measured sections for distances of up to 100 km (this work, Colombié & Strasser 2005, 2003; Colombié 2002, Hillgärtner 1999, Pittet & Strasser 1998, Pittet 1996), which implies some kind of forcing on an at least regional scale.

Therefore, small-and medium-scale sequences are regarded as allocyclic in this study. However, not everywhere in the sections depositional sequences are evident: highly dynamic depositional environments, such as shifting carbonate sand bars, are subject to forcing factors intrinsic to the system (e.g., changes in current patterns through modified sea floor morphology) and thus, in many cases, do not display a regular sequence architecture on the small or elementary scales.

In contrast to shallow-water platform carbonates where random processes are mostly linked to a variety of different facies in high-energy systems, basin sediments are much more uniform and are deposited under rather calm conditions. Accordingly, the sedimentary record of deep-water carbonates is subject to different, basin-specific processes that can alter a potentially present allocyclic pattern or possibly create a random pattern from scratch. Probably the most important of these processes is related to differential diagenesis, caused by dissolution of aragonite needles imported from adjacent carbonate platforms (Munnecke & Samtleben 1996, Westphal et al. 2000, Munnecke et al. 2001, Westphal et al. 2002, Westphal & Munnecke 2002, Böhm 2003). However, one major criterion that helps filtering out autocycles from hierarchically stacked patterns related to orbital forcing on the platform is also valid in the basin – diagenetic self-organization alone is not sufficient to produce laterally extensive, correlatable beds.

6.2 A cyclostratigraphic timeframe for the Tithonian

The approach used in this study considers sequence stratigraphy and cyclostratigraphy as two end-members in the analysis of stratigraphic sequences (cf. Hilgen et al. 2004). Traditionally, sequence stratigraphy was concerned with large-scale stratigraphic sequences spanning thicknesses of tens to thousands of meters that were deposited in response to eustatic and tectono-eustatic cycles, and with durations of millions of years. Cyclostratigraphic studies, in contrast, initially described small, meter-scale depositional sequences (called "*cycles*" in these concepts) in basinal settings with regular facies or geochemical variations that formed in response to climatic and (glacio-)eustatic cycles with durations of 10-100 ka (e.g., Fischer et al. 1990, Weedon 1993). A classical, yet potentially misleading (Sadler et al. 1993) method to examine cyclic sedimentary successions on carbonate platforms and their accommodation changes are Fischer-Plots (e.g., Goldhammer et al. 1993). Cycle periodicities are usually calculated by dividing the duration of the interval between two chronostratigraphic tie-points by the number of sedimentary cycles, and/or by time-series analysis (e.g., Weedon et al. 1999).

However, time-series analysis is only valid in sedimentary systems that are well-dated and show a relatively simple stratigraphic architecture, i.e., featuring low facies variability, regular shallowing-up to a known bathymetric level, and the absence of significant hiatuses – most of which is not present on the shallow-water carbonate platform examined in this study.

The timescale provided by Gradstein et al. (1994) gives a duration of 6.5 Ma for the Tithonian stage (Kim/Ti boundary at 150.7 ± 3.0, J/K boundary at 144.2 ± 2.6). According to Pálfy et al. (2000a, b), the duration of the Tithonian is 8.7 Ma (Kim/Ti boundary at 150.5 ± 4.0 Ma, J/K boundary at 141.8 ± 4.0 Ma). However, the 8.7 Ma are to be regarded with scepticism as Pálfy et al. (2000a) state that "*the latest Jurassic isotopic database remains too sparse, therefore chronogram estimates are improved using interpolation based on magnetostratigraphy*."

(p. 923). In contrast to the significantly longer duration of Pálfy et al. (2000a, b) compared to Gradstein et al. (1994), Gradstein et al. (2004) calculate the duration of the Tithonian to 5.3 Ma (Kim/Ti boundary at 150.8 ± 4.0 Ma, J/K boundary at 145.5 ± 4.0 Ma).

So the duration of the Tithonian could be anywhere between 0 (Kim/Ti boundary at 150.8 - 4.0 Ma, J/K boundary at 145.5 + 4.0 Ma; Gradstein et al. 2004) and 16.7 Ma (Kim/Ti boundary at 150.5 + 4.0 Ma, J/K boundary at 141.8 - 4.0 Ma; Pálfy et al. 2000a, b). However, for the time being, the two more recent time scales are controversially discussed in the scientific community (pers. comm. A. Strasser). Consequently, the established sequence-chronostratigraphic timeframe of Hardenbol et al. (1998), based upon the chronostratigraphy of Gradstein et al. (1994), is selected as a reference in this study. Applying the timescale of Gradstein et al. (1994)

	141.6 Ma min. age
Top Tithonian at	144.2 ± 2.6 Ma
	146.8 Ma max. age
	147.7 Ma min. age
Base Tithonian at	150.7 ± 3.0 Ma
	153.7 Ma max. age

the minimum duration of the Tithonian would be 0.9 Ma (147.7 – 146.8 Ma) and the maximum duration 12.1 Ma (153.7 – 141.6 Ma). This implies average durations of small-scale sequences ranging from 13-14 ka (0.9 Ma divided by 66-68 small-scale sequences; cf. Tab. 6.2) to 178-183 ka (12.1 Ma divided by 66-68 small-scale sequences; cf. Tab. 6.2), which is well in the range of the Milankovitch spectrum (20 ka to 400 ka; cf. Fig. 6.1). The same type of calculation gives a lower limit for the average duration of 53 ka, and an upper limit of 712 ka when carried out for medium-scale sequences. The average duration of small-and medium-scale sequences is thus roughly in the Milankovitch spectrum, with the average duration of medium-scale sequences probably located towards the upper end of the spectrum.

The type of diagenetic alteration of several cycle tops (vadose diagenesis, palaeo(micro)karst) excludes a purely autocyclic genesis (Chap. 6.1.4) and from detailed correlation (cf. Chap. 7) it becomes evident that the formation of small- and medium-scale depositional sequences seems to have been controlled by a forcing factor that was effective at least on a regional scale. High-frequency sea-level oscillations are the most likely explanation for these observations.

Additionally, the high-resolution sequence-stratigraphic interpretation as described in Chap. 4 shows that medium-scale sequences are composed of 4 (or occasionally less) small-scale composite sequences (Fig. 4.2 and 4.3, Pl. 20/3). The 4:1 ratio is clearly dominant. If a medium-scale composite sequence consists of only 3 small-scale sequences, clear sedimentological evidence for erosion or non-deposition is always found, usually at the top and/or the base of the "reduced" medium-scale sequence. Each small-scale composite sequence comprises two to six elementary sequences (Fig. 4.2). This broader band-width is probably due to a combination of autocyclicity, amalgamation, missed beats, and erosion. Specifically the latter two factors are assumed to be responsible for the lowest ratios of elementary sequences to small-scale sequences during the Tithonian long-term regression. During a long-term transgression, however, like in Late Kimmeridgian times, it is most likely that the impact of missed beats and erosion on the sedimentary record is less important. Indeed, within this interval, the ratio usually only varies between 4:1 and 6:1 (cf. Fig. 4.2).

Consequently, the majority of the depositional sequences can be interpreted in terms of cyclostratigraphy. Considering the probably allocyclic nature of small- and medium scale sequences, their calculated average durations, the 4:1 ratio between the first and second eccentricity cycle, and approximately 5:1 between the second eccentricity cycle and the precession cycle(s), it is assumed as a working hypothesis that:

- medium-scale (composite) sequences were formed by sea-level changes related to the first eccentricity cycle (400 ka)
- small-scale (composite) sequences were formed by sea-level changes related to the second eccentricity cycle (100 ka)
- elementary sequences were partly formed by sea-level changes related to the eccentricity cycle (18.2 ka during the Early Tithonian acc. to Berger et al. 1989) and partly by autocyclic processes.

The obliquity cycle (cf. Fig. 6.1) seems not to be expressed in the sedimentary record of the Jura Mountains. This is probably due to the low-latitude position of the study area during the Late Jurassic to Early Cretaceous. The obliquity cycle tends to be better expressed in higher latitudes. Waterhouse (1995) and Weedon et al. (2004) have identified it in the Late Jurassic Kimmeridge Clay Formation of southern England. It is also present further north, in the Greenland-Norwegian Seaway (cf. Mutterlose et al. 2003, Swientek 2002).

These relations are also in perfect accordance with the results of the Fribourg working group, gathered during extensive studies in the Late Jurassic and Early Cretaceous of the Swiss and French Jura mountains (Strasser 1994, Pasquier 1995, Pittet 1996, Pasqier & Strasser 1997,

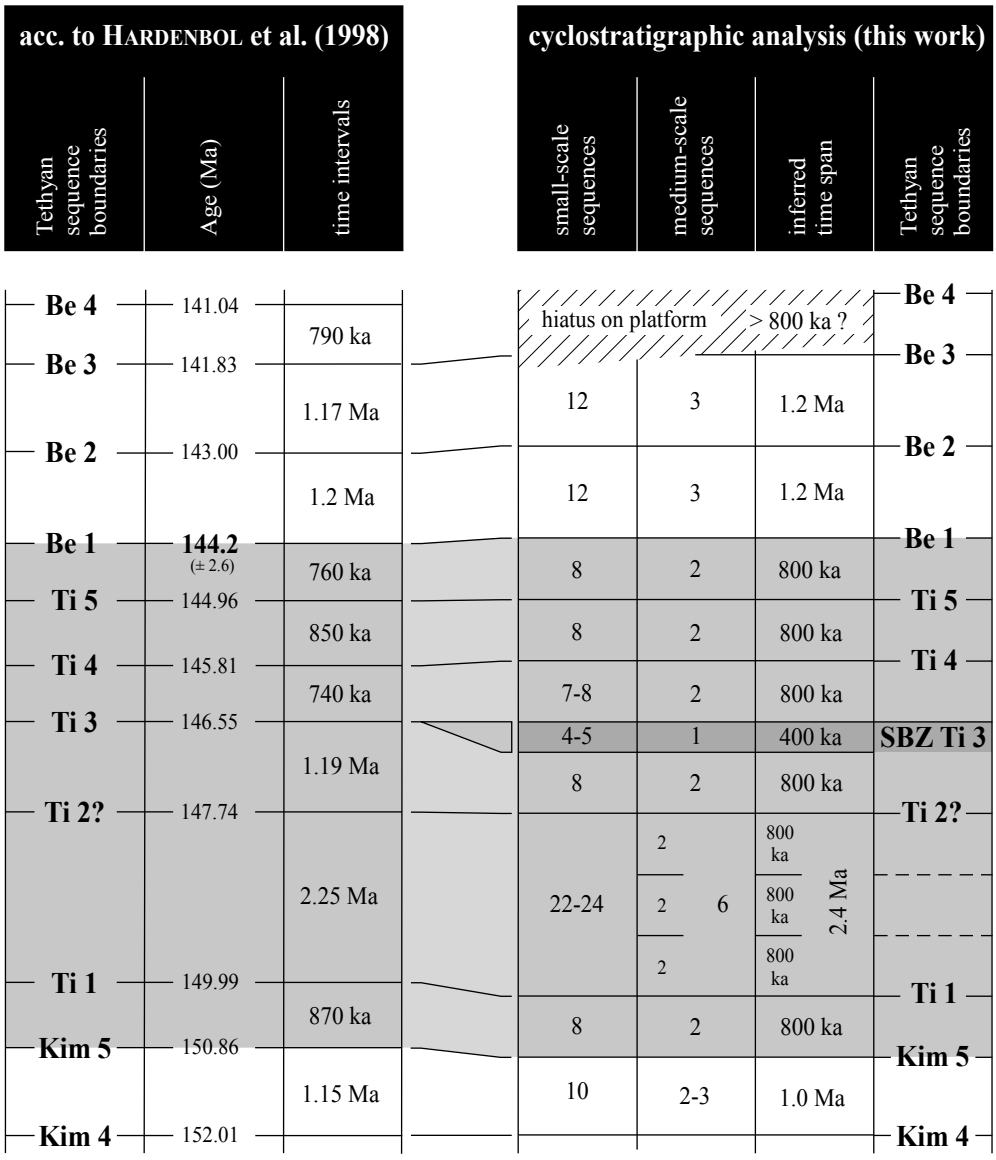

time span from **SB Kim 4** to **Be 3** according to HARDENBOL et al. (1998):

10.2 Ma

inferred time span from **SB Kim 4** to **Be 3**:

10.2 Ma

time span from **SB Kim 5** to **Be 1** (approx. duration of the Tithonian) according to HARDENBOL et al. (1998):

6.7 Ma

inferred time span from **SB Kim 5** to **Be 1** (approx. duration of the Tithonian):

6.8 Ma

Tab. 6.2 - Sequence-chronostratigraphic timing for the studied interval as given by HARDENBOL et al. (1998) compared to the estimation based on cyclostratigraphic analysis (this work).

Pittet & Strasser 1998a, 1998b, Hillgärtner 1999, Strasser et al. 1999, 2000, Colombié 2002, Colombié & Strasser 2003, 2005; Hug 2003, Strasser et al. 2004).

The stacking pattern in the Swiss and French Jura Mountains is thus assumed to reflect an orbitally forced cyclic organization on the level of medium- (400 ka) and small-scale (100 ka) sequences. The stacking pattern of elementary sequences may locally show a rather regular 5:1 ratio (with respect to small-scale sequences; cf. Fig. 4.2), but at the 20-ka scale, the Jura Platform's prevailing shallow-water conditions mostly led to an incomplete sedimentary record (erosion, non-deposition) and/or a disturbance of the allocyclic signal by autocyclic processes (cf. Chap. 6.1.4). In particularly protected, calm lagoons, however, also the precessional signal was recorded like, e.g., Park & Fürsich (2001) showed for the famous "*Solnhofener Plattenkalke*" (Early Tithonian) from the Swabian Alb (southern Germany).

Following these considerations, a cyclostratigraphic timeframe for the Tithonian of the Jura platform is proposed (Tab. 6.2). It is essentially based on the dominant 100- and 400-ka rhythm (small- and medium-scale sequences), whereas the 20-ka signal usually drowns in a high level of (autocyclic) "background noise".

This cyclostratigraphic timeframe correlates very well with the sequence-chronostratigraphic chart of Hardenbol et al. (1998) (Tab. 6.2). The numerical ages of this chart are based on Gradstein et al. (1994), who give a duration of 6.5 Ma for the Tithonian stage. For the interval between SB $Kim5_{Tethyan}$ and SB Be1 (that approximately represents the Tithonian, cf. Fig. 1.9), Hardenbol et al. (1998) give a time span of 6.7 Ma. The inferred time span from cyclostratigraphic analysis is 6.8 Ma for the same interval. Also the number, distribution, and relative timing of sequence boundaries are very similar to Hardenbol et al.'s (1998) chart (Tab. 6.2). Yet, from the sedimentary record of the Jura platform, it would be possible to derive two more large-scale sequences (located at the tops of medium-scale sequences 7, respectively 9, cf. Fig. 7.3) that would fill in the 2.25 (resp. 2.4) Ma interval between SB Ti1 and SB $Ti2?_{Tethyan}$, where the Tethyan part of the chart deviates from the otherwise rather regular distribution of large-scale (3rd-order) sequence boundaries in the Late Jurassic and Early Cretaceous. However, no evidence for these sequence boundaries was found in the basin sections (Clue de Taulanne, Poteu de Mié).

However, the lack of reliable time control such as biostratigraphy, the various diverging chronostratigraphic timeframes (Gradstein et al. 1994, 2004; Pálfy et al. 2000a, b), as well as the large error ranges given for each of the stages' numerical ages clearly show that the Jurassic/Cretaceous boundary interval is still one of the outstanding problems in global stratigraphy. Perhaps cyclostratigraphic timeframes may help here to verify (and refine) chronostratigraphic charts (cf. Hinnov 2000) as they do already in the Tertiary (Shackleton et al. 1999).

Comparison with other studies

Other European working groups have successfully applied similar combined sequence- and cyclostratigraphic approaches to Late Jurassic and Cretaceous carbonate platforms (e.g., D'Argenio et al. 1997, 1999, Buonocunto et al. 2000, Pawellek 2001, Pawellek & Aigner 2003a, b, Ruf et al. 2005a, b).

In the Iberian Basin of north-eastern Spain, Bádenas et al. (2003), report SB $Kim4_{Tethyan}$ and SB $Kim5_{Tethyan}$ to be separated by10.5 "sets of bundles", compared to 10 small-scale sequences in this study (Tab. 6.2). Bádenas et al. (2004) provide a sequence- and cyclostratigraphic timeframe for large parts of the Tithonian, also based on sections from the Iberian Basin. Apparently, SB $Ti2?_{Tethyan}$ is not expressed in north-eastern Spain, but the number of "parasequences" (that are interpreted to represent the 100 ka eccentricity cycle) separating its inferred position from SB $Ti3_{Tethyan}$ is comparable to the number of small-scale sequences found in this study (Tab. 6.2). For the interval from SB $Ti3_{Tethyan}$ to SB $Ti5_{Tethyan}$ the results of Bádenas et al. (2004) are perfectly in tune with this study: each sequence boundary is separated by 8 parasequences (respectively small-scale sequences) from the next one. The interval from SB $Ti5_{Tethyan}$ to SB $Be2?_{Tethyan}$, is composed by 18 (11 + 7) parasequences in the Iberian Basin (Bádenas et al. 2004), compared to 20 (8 + 12) small-scale sequences on the Jura platform (this work). Apparently, the sequence boundary that would correspond to SB Be1 according to Hardenbol et al. (1998) is shifted 400 ka (one medium-scale sequence) upwards in north-eastern Spain. This shift (and also the reduced number of parasequences?), might be due to strong local tectonic activity that influenced the long-term evolution of accommodation space (2nd-order regression) at sub-basin scale (Bádenas et al. 2004) and thus modified the physical expression and relative importance of medium- and large-scale sequence boundaries.

In Dorset (southern England), Weedon et al. (2004) have used magnetic susceptibility, photoelectric factor and total gamma-ray throughout the type Kimmeridge Clay Formation to identify sedimentary cycles. Spectral analysis demonstrates that these cycles record orbital obliquity and precession. By linking the cyclostratigraphic timing to the rich ammonite fauna, minimum durations of ammonite zones can be calculated. Weedon et al. (2004) give a minimum duration of 2.22 Ma for the Early

and Middle Tithonian (base *elegans* to top *pectinatus* Zone, Fig. 1.9). According to HARDENBOL et al. (1998), the same interval lasts some 4.7 Ma and is bounded by the sequence boundaries SB $Kim7_{Boreal}$ and $Ti4_{Boreal}$. In the Jura Mountains, the duration of the interval defined by the corresponding Tethyan sequence boundaries SB $Kim5_{Tethyan}$ and SB $Ti4_{Tethyan}$ is inferred to be 5.2 Ma (Tab. 6.2). It has to be mentioned, however, that the Tethyan-Boreal correlation of SB Ti4 is not well established (cf. Chap. 7).

* * *

7 - Stratigraphic correlations

The latest Jurassic of the Swiss and French Jura Mountains has resisted any attempt of detailed correlation for a long time due to absence of a solid biostratigraphic framework, and the laterally changing lithology of its peritidal deposits (cf. Tab. 1.1).

The only existing regional marker beds are the upper *virgula* Marls and the "*Grenznerineenbank*" that mark the boundary between the Reuchenette Formation ("Kimmeridgian") and the Twannbach Formation ("Portlandian") (Frei 1925, Aubert 1943, Thalmann 1966, Häfeli 1966, Schär 1967, Dauwalder & Remane 1979, Bläsi 1980). At the top, there is no sharp boundary to the Goldberg Formation ("Purbeckian"), but a gradual change to more and more intercalations of lacustrine and continental lithofacies. Locally, the so-called "*calcaire âpre*" (cell dolomites, *cornieules*, cf. Pl. 16/2a, b and Fig. 4.15) was used to define the upper limit of the "Portlandian" (e.g., Jaccard 1869), but this, too, is merely a change in facies on a prograding platform and thus diachronous, as Bernier (1984) suggested for the limit between the "*Couches du Chailley*" and the "*Tidalites de Vouglans*" in the southern French Jura.

Based on the extensive work already done during the last 150 years and some new developments in stratigraphic analysis since the 1980s – specifically sequence stratigraphy and cyclostratigraphy – a correlation is developed, which leads to the better understanding of the sedimentary and early diagenetic processes that caused the sequential patterns in the studied sediments.

7.1 Methods of correlation

7.1.1 Biostratigraphy

Like on most shallow-water carbonate platforms, biostratigraphy only furnishes some infrequent data that nevertheless help to tie some sections into a given biostratigraphic framework: e.g., the ammonites of Sur-Combe-Ronde, the biostratigraphic zonation for the Cirque des Avalanches section proposed by Enay (2000), and the charophyte-ostracode assemblages in Yenne (cf. Fig. 7.1). Yet, the correlation of the platform sections themselves demands for alternative correlation methods.

A low-resolution biostratigraphic correlation tool is the abundance of the hypercalcified sponge *Cladocoropsis mirabilis*. Being a facies-dependent dweller of Late Jurassic low-energy back-reef habitats of the western Tethys (cf. Chap. 2.3.2), its presence/absence has no exact biostratigraphic meaning. Yet, on a regional scale, a *Cladocoropsis mirabilis* interval in the upper Reuchenette Formation can be observed, contrasting with only sporadic occurrences below and above this interval (Fig. 7.1).

In contrast to the platform, the studied basin sections are well dated. Even if ammonites are relatively rare in the Tithonian strata of the Vocontian Basin, the abundance of microfossils allows for the development of a detailed biostratigraphic framework on the basis of calpionellids and certain microfossil assemblages (cf. Chap. 1.3.3). From this biostratigraphic framework, several correlation lines can be established that link the basin to the platform.

7.1.2 Lithofacies and stacking pattern

As already mentioned, correlations within the Tithonian strata of the Jura Mountains that were mainly based on lithostratigraphy were either unsuccessful or highly speculative due to lateral facies changes and the diachronous nature of facies zones on a prograding and retrograding carbonate platform. However, major changes in sedimentary architecture may be rooted in external forcing, such as changeovers in plate-tectonic regime that may influence subsidence rates on a regional scale. Also substantial climate changes and/or long-term sea-level changes are able to produce a virtually isochronous fingerprint that is traceable over large distances.

The only existing regional marker beds that are assumed to be isochronous are the upper *virgula* Marls,

and the "*Grenznerineenbank*" that mark the boundary between the Reuchenette Formation ("Kimmeridgian") and the Twannbach Formation ("Portlandian") (Frei 1925, Aubert 1943, Thalmann 1966, Häfeli 1966, Schär 1967, Dauwalder & Remane 1979, Bläsi 1980). Unfortunately, the upper *virgula* Marls are not present in all localities, and the correct identification of the "*Grenznerineenbank*" can be problematic (cf. discussion in Chap. 4, Noirvaux section). Despite these problems, this interval is of uttermost importance, because besides being a regional lithologic marker it also defines a major change-over in sedimentary architecture that is well expressed in both platform and basin sections and traceable all over the study area. This change-over is located in the lower part of medium-scale sequence 5 (Fig. 7.1). Although the exact time equivalence cannot be proven, this interval serves as a first approximation correlation level.

On the platform, the upper *virgula* Marls mark a switch from the thick-bedded succession of open-marine or restricted lagoonal carbonates of the upper Reuchenette Formation to the thinner bedded or platy beds of the Lower Twannbach Formation, representing mostly (heavily) restricted and peritidal environments. In parallel to decreasing average bed thickness, the same is true for the average thicknesses of small- and medium-scale sequences: medium-scale sequences 2 and 3 are unusually thick in Noirvaux and Cirques des Avalanches (Fig. 7.1), the thickness of 4 varies locally, and beginning with 5 the average thickness is definitively reduced, reaching a minimum around medium-scale sequences 14 and 15.

In the basin (Clue de Taulanne and Poteu de Mié sections) the thickness change is inversed. In both sections, the lower, relatively thin-bedded part gives evidence of sediment starvation (base of the Poteu de Mié section, chert nodules in Clue de Taulanne). Additionally, both basin sections also switch from a limestone-dominated limestone-marl alternation to a pure, thick bedded limestone succession.

7.1.3 Discontinuity surfaces and depositional sequences

The major change-over in depositional architecture mentioned above probably is the sedimentary expression of change in long-term trends in relative sea-level. During the Kimmeridgian long-term (2^{nd}-order) transgressive phase culminating in a MF in the *eudoxus* Zone (cf. Fig. 1.9), new accommodation space was created on the platform. Consequently, large volumes of organically produced carbonate accumulated in an aggradational pattern that kept up with the long-term relative sea-level rise (Colombié 2002). With the beginning long-term regression, decreasing accommodation space on the platform caused the development of thinner beds (and thinner small- and medium-scale sequences), simultaneously allowing for more sediment to be exported, leading to thicker beds in the basin.

This change in the creation of accommodation space is also recorded in the small- and medium-scale sequence architecture: in times with increased creation of accommodation space (catch-up and keep-up modes), small- and medium-scale sequences generally show pronounced transgressive deposits and well-expressed maximum floodings (TS and MF-sequences), whereas with the beginning of the long-term regression, transgressive and maximum-flooding deposits loose importance and regressive sediments, as well as sequence boundaries, are more pronounced (SB-sequences).

Large-scale sequence boundaries on the platform mostly consist of SB zones forming around pronounced medium-scale SBs (cf. Strasser et al. 2000) and are usually recognizable by a concentration of emersion surfaces and inter- to supratidal facies (rightmost two columns in the section logs, Chap. 4).

7.1.4 Clay minerals

In this study, clay-mineral analysis was an important tool to obtain an alternative method of correlation, independent of facies interpretation and the results of sequence/cyclostratigraphic analysis. The sequence- and cyclostratigraphic interpretation was compared to the vertical evolution of clay mineral distributions. However, the vertical evolutions of the two measured main-parameters (kaolinite/illite- ratio and illite crystallinity) are out of phase (Fig. 7.1). In order to obtain a correlation that is valid in a high-resolution timeframe, it is thus important to understand the processes that create the signals recorded by the clay minerals (cf. Chap. 5).

The K/I ratio mostly reflects climate changes in the hinterland. Erosion and transport processes can thus potentially alter and/or delay the record of the climatic signal in a given section (Curtis 1990). In contrast, the formation of poorly crystallized illite (> 0.42° 2è $CuKá_1$) that essentially influences the illite-crystallinity curve, is an in-situ process that depends on climate, geomorphology, and pro- and retrogradational patterns of the coastline. Consequently, the Middle Tithonian kaolinite minimum zone in the K/I-ratio curve was used to identify a general fit that was then refined by using the illite-crystallinity curve.

7.1.5 Early diagenesis

Dolomite caps are a prominent feature in the stacking pattern of the studied platform sections. As the formation of m-thick stratiform dolomite requires a considerable volume of meso- to hypersaline water that has to be

produced by evaporation (cf. Chap. 3), a large lagoon system that is periodically separated by a barrier from the open ocean is postulated for the Tithonian Jura platform. Depending on the degree of compartmentalization (e.g., by internal bars) of this lagoon system and different degrees of communication of these compartments with the open Tethys in the south, two end-members in possible platform configuration can be imagined: 1) a large-scale, platform-wide restricted lagoon that furnishes fluids for the creation of isochronous stratiform dolomite all over the Jura platform, and 2) isolated, small-scale lagoons that act as local sources for dolomitizing fluids and react to different (shorter-term) influences than the platform-wide system.

The majority of well-developed dolomite caps are located in the upper (regressive) part of medium- and large-scale sequences and can be correlated over 10s of km on the platform (cf. Figs 4.11-4.19 and 7.1). This would speak for a rather uniform, large-scale system that, besides some exceptions, mainly reacts to medium- and large-scale patterns in change of relative sea-level.

All the above-mentioned methods of correlation were combined in order to set up a best-fit correlation (Fig. 7.1) that accounts for a maximum of observed phenomena while, at the same time, raising a minimum of contradictions. The strategy followed was to develop at first an independent high-resolution sequence stratigraphic timeframe (large- to small-scale sequences) for the platform sections that eventually was correlated to the basin sections, by using the available bio- and sequence-stratigraphic guidelines. The high-resolution timeframe from the platform was thus linked to the biostratigraphically well-defined basin sections. Located in slope position, the Broyon / Clue de la Payre section played a central part in this step as it gives evidence of the mechanisms that link platform and basin domains.

7.2 Setting up a platform-to-basin correlation

7.2.1 Correlations on the platform

For each platform section, a high-resolution sequence stratigraphic interpretation was set up independently. These were then compared to each other. As biostratigraphic control is very poor, a few prominent sequence stratigraphic marker beds were used as reference levels:

1) the major transgressive surface above SB $Kim5_{Boreal}$ (Fig. 7.1) that marks the beginning of the long-term (2nd-order) maximum flooding in the *Eudoxus* ammonite zone, expressed in the thick-bedded, massive-appearing upper Reuchenette Formation in the lowermost part of the studied interval;
2) the upper *virgula* Marls (cf. Bläsi 1980), a level that also represents a drastic change in stacking pattern from the thick-bedded, lagoonal carbonates of the upper Reuchenette Formation to the thinner bedded, peritidal succession of the Twannbach Formation;
3) the zone around the large-scale sequence boundary $Ti3_{Tethys}$ that is marked by an outstanding package of tidal-flat deposits, a minimum gain in accommodation space (Fig. 7.1), subaerial exposure, as well as some erosion/non-deposition and resedimentation (cf. Pl. 9/2a, 9/3a, 10/6, 12/3b);
4) the major transgressive surface above SB Be4 that marks the beginning Pierre-Châtel Formation at the top of the studied interval (*Privasensis* subzone, Clavel et al. 1986).

The most import horizons for correlation are No. 2 and 3. Due to their position in the middle of the studied interval, they are present in most platform sections (Fig. 7.1). The result of this rough correlation fits with the sequence-chronostratigraphic charts provided by Hardenbol et al. (1998). Added to this are the correlations of the clay mineral curves, and of the stacking pattern of medium- and small-scale depositional sequences (dolomite caps).

The result represents the most consistent "*best-fit correlation*" for the platform sections (Fig. 7.1), integrating all investigated aspects such as facies changes, sequence- and cyclostratigraphy, dolomitization patterns, spatial and temporal distribution of evaporites, and climate changes.

Assuming that this best-fit correlation is the best that can be achieved with current data, it turns out that the beginning of the Middle Tithonian kaolinite minimum-zone is not isochronous (cf. Fig. 7.1). The correlation suggests that the negative K/I shift defining the beginning of the kaolinite minimum zone arrives first in the south-west (La Dôle section, base medium-scale sequence 12), then in the Lieu section (top medium-scale sequence 12), and last in the north-east (Noirvaux section, middle of medium-scale sequence 13) (for section locations see Fig. 1.2). According to cyclostratigraphic analysis (cf. Chap. 6), it arrives approximately one medium-scale sequence (400 ka) earlier in the Dôle than in the Noirvaux section. This can be explained by a relatively slow transport, probably from the south-west, or west (Massif Central landmass, cf. Fig. 1.3a). Interestingly, this transport hypothesis is consistent with the vertical evolution of K/I ratios (Fig.5.4) that also indicates a kaolinite depletion from SW to NE.

Another diachronous phenomenon made visible by the proposed sequence- and cyclostratigraphic timeframe is the progradation of evaporite deposits and massive type-2 dedolomitization due to subaerial exposure in the latest Tithonian and Early Berriasian. In the proximal Lieu section, massive dedolomitization starts in medium-scale

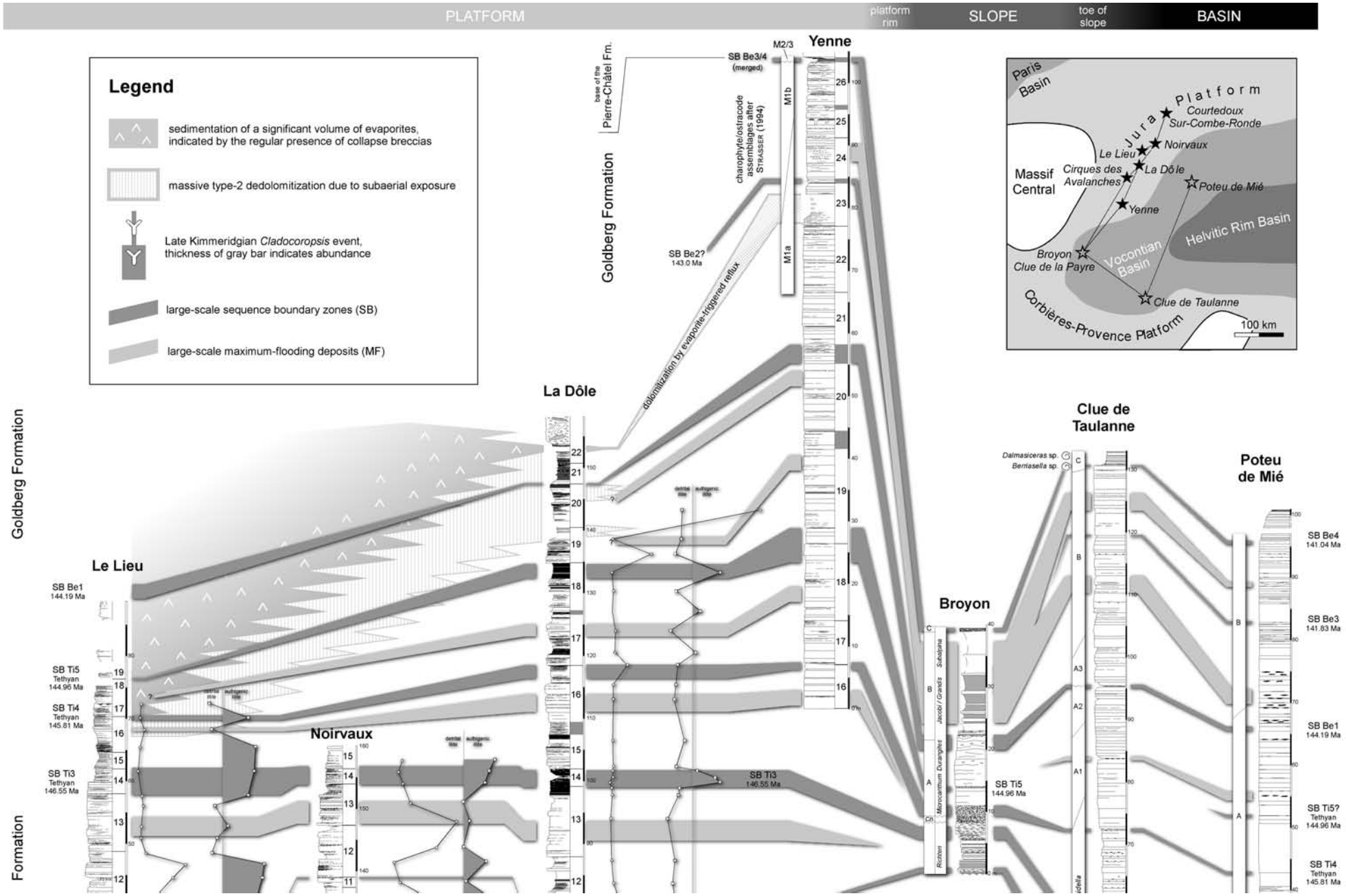
PLATFORM
platform rim
SLOPE
toe of slope
BASIN
Legend
sedimentation of a significant volume of evaporites, indicated by the regular presence of collapse breccias
massive type-2 dedolomitization due to subaerial exposure
Late Kimmeridgian Cladocoropsis event, thickness of gray bar indicates abundance
large-scale sequence boundary zones (SB)
large-scale maximum-flooding deposits (MF)
Paris Basin
Jura Platform
Courtedoux
Sur-Combe-Ronde
Noirvaux
Le Lieu
La Dôle
Cirques des Avalanches
Massif Central
Poteu de Mié
Yenne
Helvitic Rim Basin
Broyon
Clue de la Payre
Vocontian Basin
Clue de Taulanne
Corbières-Provence Platform
100 km
Yenne
Goldberg Formation
base of the Pierre-Châtel Fm.
SB Be3/4 (merged)
M2/3
M1b
M1a
charophyte/ostracode assemblages after Strasser (1994)
SB Be2?
143.0 Ma
dolomitization by evaporite-triggered reflux
La Dôle
Le Lieu
Noirvaux
Broyon
Clue de Taulanne
Poteu de Mié
Dalmasiceras sp.
Berriasella sp.
SB Be1
144.19 Ma
SB Ti5
Tethyan
144.96 Ma
SB Ti4
Tethyan
145.81 Ma
SB Ti3
Tethyan
146.55 Ma
SB Be4
141.04 Ma
SB Be3
141.83 Ma
SB Ti5?
Tethyan
144.96 Ma
detrital fills
authigenic fills
Goldberg Formation
Formation

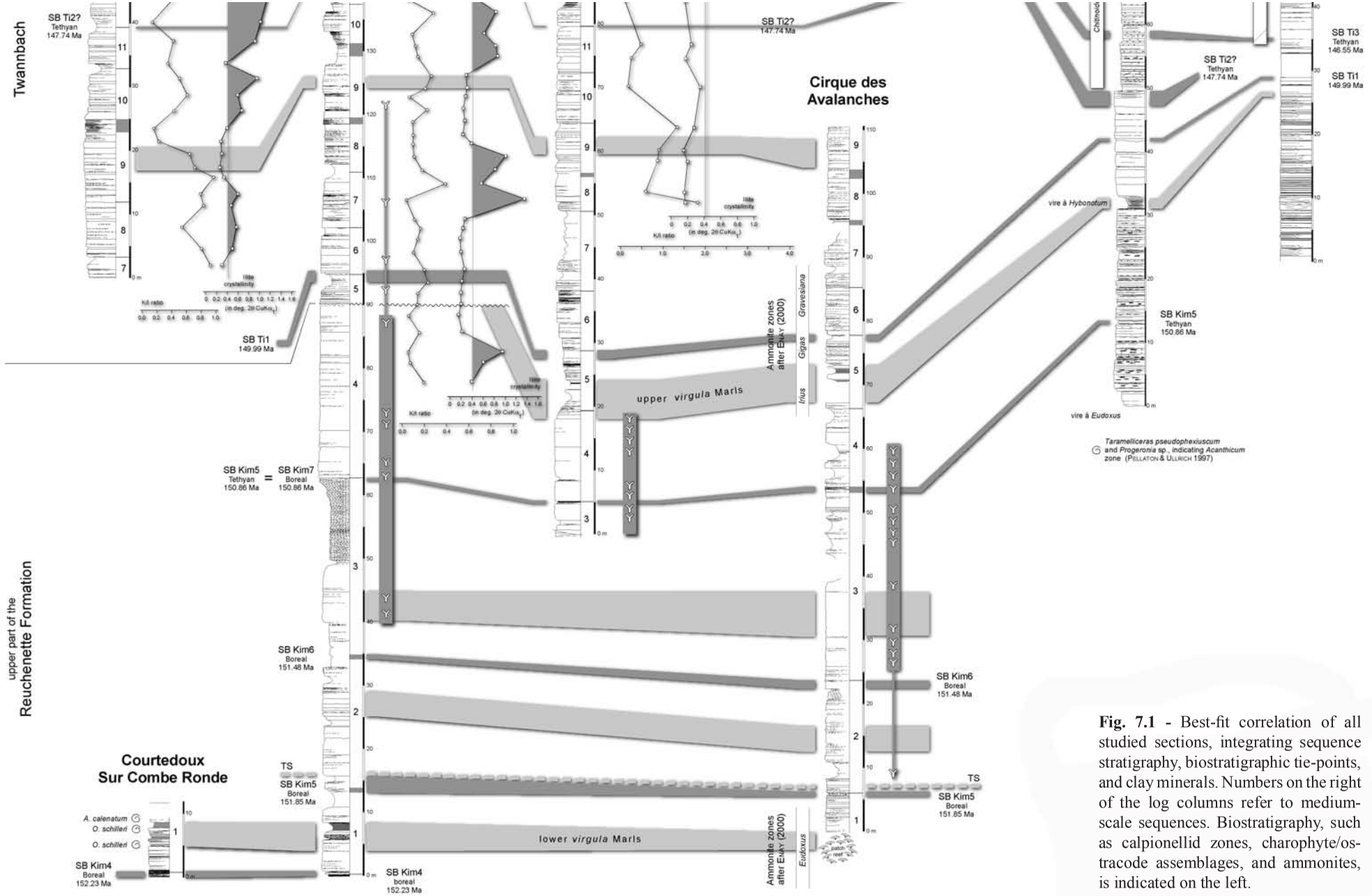

Fig. 7.1 - Best-fit correlation of all studied sections, integrating sequence stratigraphy, biostratigraphic tie-points, and clay minerals. Numbers on the right of the log columns refer to medium-scale sequences. Biostratigraphy, such as calpionellid zones, charophyte/ostracode assemblages, and ammonites, is indicated on the left.

sequence 16. Collapse breccias that indicate the deposition and subsequent dissolution of large volumes of evaporites start to appear at the base of medium-scale sequence 17. In the Dôle section, the first cornieule (porous type-2 dedolomite) occurs in medium-scale sequence 19 and the evaporites, the dissolution of which created the several m-thick collapse breccia at the section top, were deposited in medium-scale sequence 22 (or later). Interestingly, the Yenne section features a prominent dolomitized interval in medium-scale sequence 23 – not in the upper, regressive part of the sequence, as the dolomitization model (Chap.3) would predict, but in the lower, transgressive part. This may be explained by reflux action of hypersaline brines originating from evaporite deposits farther landward (as recorded, e.g., in Le Lieu and La Dôle) that percolated to platform areas that were located more seawards (e.g., Yenne).

7.2.2 Correlations in the basin

The biostratigraphic framework of the basin sections is mainly based on calpionellids (Remane 1985, 1998) and pelagic microfossil assemblages (Dromart & Atrops 1988, Benzaggagh & Atrops 1996). Some ammonites in the Late Kimmeridgian and Middle Berriasian of the Clue de Taulanne section (Pellaton & Ullrich 1997) give additional biostratigraphic tie points. Pellaton & Ullrich (1997) also provide a local litho-biostratigraphic correlation for marker beds in the Castellane area (Clue de Taulanne section). By this method, some horizons (e.g., the "*vire à Hybonotum*") can be dated even if they contain no ammonites in the Clue de Taulanne section. The "*vire à Hybonotum"* also coincides with the *Saccocoma* minimum located in the *Hybonotum* ammonite zone (cf. Figs 1.8 and 4.25).

Around this horizon, a major change-over in sedimentary architecture is observed in the two basin sections that can be correlated with the change-over known from the platform (Fig. 7.2). In both, the Clue de Taulanne and Poteu de Mié sections, the underlying, relatively thin-bedded part gives evidence of sediment starvation (condensation base of the Poteu de Mié section, frequent chert nodules in Clue de Taulanne). Above this level, both basin sections abruptly switch from the underlying limestone-dominated limestone-marl alternation to a pure, thick bedded limestone succession. Another key horizon for correlation is the Middle Berriasian drowning surface located at the top of each of the two basin sections (SB/TS Be4), well-dated by ammonites and calpionellids in Clue de Taulanne (cf. Figs 4.25 and 7.2).

Between these two key horizons, a framework of large-scale sequence boundaries and maximum-flooding zones, calibrated against the biostratigraphic framework, is set up. In some intervals the sedimentary changes are subtle and sequence boundaries and maximum-flooding zones are difficult to interpret (cf. Fig. 7.1). The interpretation of medium- and small-scale sequences was only possible in an interval in the lower part of the Clue de Taulanne section. Higher up, considerable resedimentation and erosion precludes a cyclostratigraphic interpretation. In the Poteu de Mié section, no medium- and small-scale sequences could be identified at all. Biostratigraphy reveals that the lower part is heavily condensed (Fig. 4.23). In the upper, thicker-bedded part, the stacking pattern reveals large-scale sequences but does not permit to identify medium- and small-scale sequences.

7.2.3 Linking the platform to the basin

Once the two correlation schemes for the platform and the basin are set up, they can be linked: the biostratigraphic zonation derived from the relatively well-dated basin sections can be traced onto the platform and compared to the cyclostratigraphic timeframe developed there. Vice-versa, effects of, e.g., sea-level drops and/or climatic changes recorded in the platform sediments – that react very sensitively to these signals – can be traced down into the basin. This cross-correlation allows for the establishment of a best-fit solution accommodating all aspects of bio-, litho-, sequence-, and cyclostratigraphy.

Four major correlative features were found that form the "backbone" of the platform-to-basin correlation. They correspond to the four prominent sequence-stratigraphic levels defined in Chap. 7.2.1:

1) The major transgressive surface above SB Kim4 that marks the beginning of the long-term (2^{nd}-order) maximum flooding in the *Eudoxus* ammonite zone. On the platform, it is expressed by the appearance of thick-bedded, limestones of massive appearance. In the Clue de Taulanne section, this major transgression corresponds to a zone of softer marls, the "*vire à Eudoxus*" (cf. Pellaton & Ullrich 1997).
2) A major change in sedimentary architecture, located around the Kimmeridgian/Tithonian boundary. On the platform, this level corresponds to the upper *virgula* Marls (cf. Bläsi 1980) and in the basin to the "*vire à Hybonotum*" (Clue de Taulanne section, cf. Pellaton & Ullrich 1997), respectively to the last marly interbeds in the Poteu de Mié section.
3) The zone around large-scale sequence boundary $Ti3_{Tethys}$ that is marked by an outstanding package of tidal-flat deposits, a minimum gain in accommodation space, and subaerial exposure on the platform and by the start of heavy resedimentation in sections that are located in (toe of) slope positions.

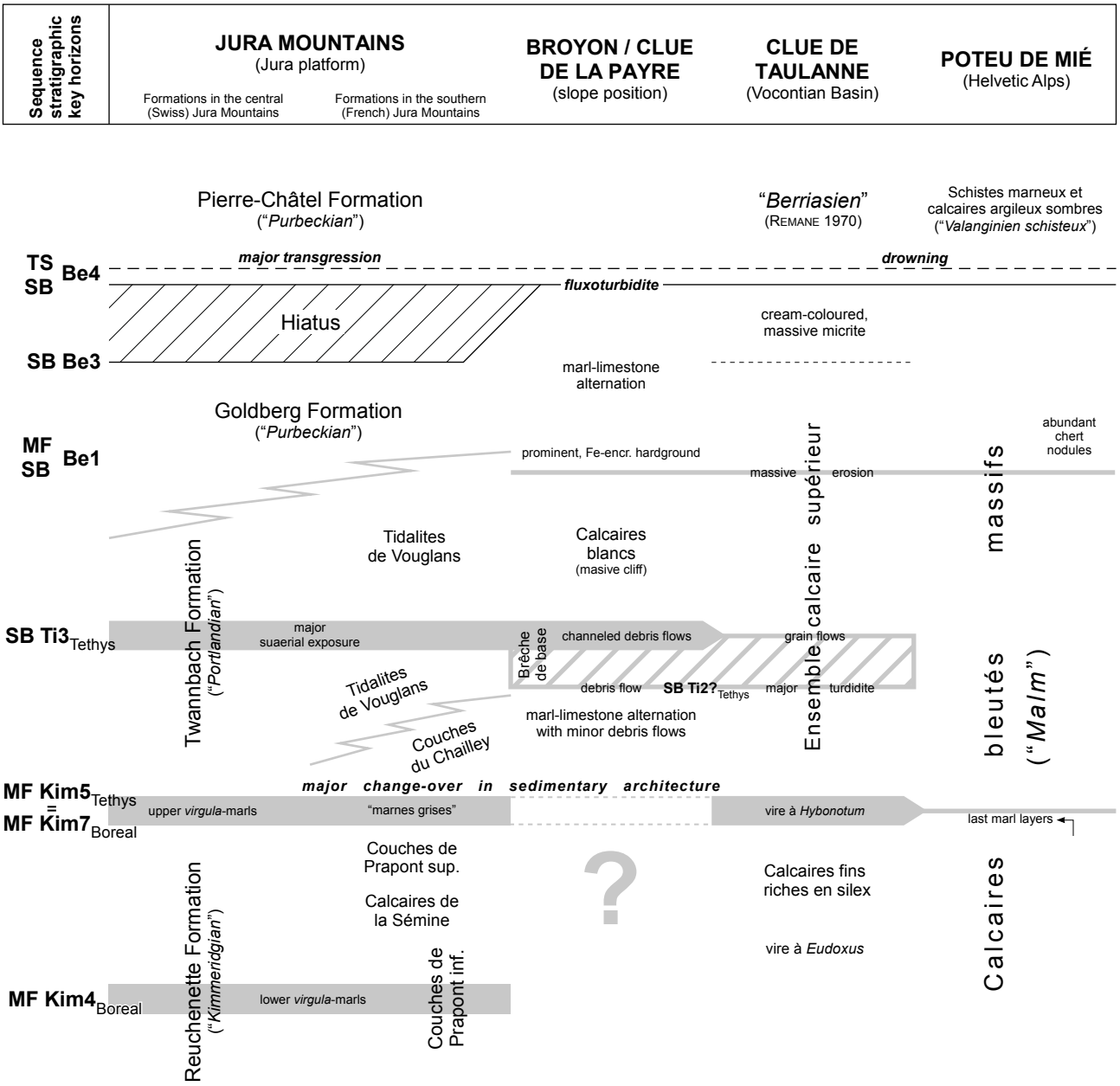

Fig. 7.2 - Platform-to-basin correlation of lithostratigraphic units and formations. Note that significant changes in lithostratigraphy, that serve traditionally for delimiting formations, are often equivalent to correlative discontinuities that define sequence stratigraphic surfaces.

4) The major transgressive surface following SB Be4 that marks the base of the Pierre-Châtel Formation on the platform is expressed as a drowning event in the basin.

Once having established these key horizons that are traceable all over the study area (Fig. 7.2) a correlation on the level of large-scale sequences can be carried out relatively easily. Based on the platform-to-basin correlation (Fig. 7.1), a sequence-stratigraphic scenario is developed that also explains the controlling factors (sea level, subsidence, ecology, and climate) and their effects on the platform and the basin sedimentation.

At the beginning of the studied interval, the long-term (2nd-order) maximum flooding during the Late Kimmeridgian *Eudoxus* zone created a maximum of accommodation space on the platform that led to the deposition of the tick-bedded upper part of the Reuchenette Formation. Meanwhile, the Vocontian Basin suffered sediment starvation ("*vire à Eudoxus*" and "*calcaires*

fins riches en silex" of the Clue de Taulanne section, cf. Pellaton & Ullrich 1997). Then, a long-term regressive trend began that defines the entire Tithonian (cf. Fig. 1.9).

The period of high accumulation rates on the platform and condensation in the basin ended with a crisis in the carbonate factory. On the platform, the dysoxic, heavily restricted upper *virgula* Marls witness a short but drastic change in environmental condition. In the basin, this interval corresponds to the quasi-abiotic, platy limestones of the "*vire à Hybonotum*".

At this level (lower part of medium-scale sequence 5; Fig. 7.1), also a major change-over in sedimentary architecture takes place that is well expressed in both platform and basin sections and traceable all over the study area. On the platform, thinner beds and frequent emersion indicate a decrease in the rate of creation of accommodation space. In parallel, the basin seems to have profited from an enhanced export of carbonate ooze from the platform: both basin sections switch from a limestone-dominated limestone-marl alternation to a thick-bedded limestone succession.

With a long-term trend of decreasing creation of accommodation space, the overall platform growth-trend lost most of the aggrading component characterizing the Late Kimmeridgian and switched to a generally more prograding pattern that eventually led to the development of heavy resedimentation on the prograding slopes as recorded in the Broyon / Clue de la Payre and the Clue de Taulanne sections in the Middle Tithonian.

There is an obvious link between the beginning of heavy erosion and resedimentation in (toe of) slope positions (Broyon / Clue de la Payre and Clue de Taulanne sections) and a major period of subaerial exposure on the platform. Such a period of prolonged subaerial exposure, characterized by a succession of laminated and dolomitic tidal-flat deposits, multicoloured breccias, and a very low creation of accommodation space exists around medium-scale sequence 14. Calpionellid biostratigraphy and microfossil assemblages in the slope and basin sections place the intervals with heaviest erosion and resedimentation in the *Chitinoidella* calpionellid zone, respectively the *Fallauxi* ammonite zone. The base of this interval is consequently interpreted to represent the well expressed large-scale SB Ti3 $_{\text{Tethyan}}$ (Hardenbol et al. 1998).

At the top of the studied interval, the platform is subject to another long subaerial exposure. In slope and toe-of-slope position, this prominent emersion is sharply defined by resediments, such as the fluxoturbidite in Broyon (cf. Fig. 4.21) and the clast-rich surface in Clue de Taulanne (Pl. 21/5). In the more distal basin (Poteu de Mié section) the expression is much more subtle: According to Roulin (2001), undulating bedding planes are interpreted as a sign of minor erosion. The duration of this major period of emersion is estimated to a minimum of 800 ka from cyclostratigraphic analysis (cf. Chap. 6), leading to a merging of large-scale sequence boundaries SB Be3 and SB Be4 on the platform (cf. Fig. 4.19). When comparing this with the sedimentary record of the Clue de Taulanne section, it turns out that the interval between SB Be3 and SB Be4 consists of cream-coloured, very hard mud- to wackestones with nearly absent bedding planes – a lithofacies that is found nowhere else in the measured parts of this section. This change in lithofacies is interpreted to result from a reaction of the sedimentary system on the prominent emersion on the platform that may have shut down (or, at least, extremely limited) the shallow-water carbonate factory and platform export of fine-grained carbonates. The following major transgression (TS Be4) finds its expression in the basin by a change to more marly sediments that is interpreted as a drowning event.

7.3 The examined sections in a regional/European context

7.3.1 Tethyan/submediterranean realm

When comparing the sequence-chronostratigraphic interpretation developed in this study with the one from Hardenbol et al. (1998) for the Tethyan realm (Fig. 7.3, right column), it stands out that the framework of large-scale (3rd-order) sequence boundaries correlates well, but that many large-scale maximum floodings (this study) correlate with 3rd-order transgressive surfaces of Hardenbol et al. (1998). One major drawback of Hardenbol et al.'s (1998) compilation is that it is not specified which data from which sections were used to set up the presented sequence-chronostratigraphic charts. However, it is assumed that the charts are based on deeper-water and basin sections where biostratigraphic information is available. Consequently, when compared to a platform-based study (like the one presented here) it is likely that there will be some differences caused by the internal logic of the sequence stratigraphic model: 3rd-order transgressions (according to Hardenbol et al. 1998) recorded in the basin could have created the interval of most open-marine facies on the Jura platform (this study) that, according to the definitions of outcrop-based high-resolution sequence stratigraphy (cf. Chap. 4), should be reflected in large-scale maximum flooding. When, after a certain lag time, massive carbonate production started up, the newly created accommodation space was filled rather rapidly and the platform switched to a "keep-up" mode. Thus, a rather restricted, or tidal-flat dominated highstand facies already characterized the platform sediments while the maximum flooding was recorded in the basin.

Bläsi (1980) did not a carry out a sequence stratigraphic interpretation *sensu stricto*, but worked with sedimentary

sequences that show shallowing-up trends and are correlatable between the sections he worked on. Moreover, the boundaries of these four "shallowing-up sedimentary sequences" (Fig. 7.3) all correspond to medium-scale sequence boundaries or large-scale transgressive surfaces (this study).

Compared to Strasser & Hillgärtner (1998), the sequence-stratigraphic interpretation of the Berriasian interval shows only minor changes. The relative timing, regarding the number of medium- and small-scale sequences stays exactly the same, but SB $Be3_{Tethyan}$ and SB $Be2?_{Tethyan}$ are lowered by one medium-scale sequence (Fig. 7.3). This possibility is already discussed in Strasser & Hillgärtner (1998) and, considering the new data accumulated in this study, it is the most consistent interpretation.

In all studied platform sections, the most important large-scale sequence boundary is located in the Middle Tithonian (SB $Ti3_{Tethyan}$). Its importance is also visible from the studied slope- and basin sections. Schlagintweit & Gawlick (2002), who worked on a carbonate platform some 100 km further to the north-east on the northern Tethyan rim (Plassen Formation of the Austrian Northern Calcareous Alps) also report a prominent interval with repeated emersions from the Middle Tithonian.

On the Aquitaine platform (south-western France), Hantzpergue (1979, 1983) places the Kimmeridgian/Tithonian boundary in a well-developed hardground that is dated by ammonites and located between the *Evolutissima* and *Gigas* horizons. It marks a prominent change in sedimentary architecture from a limestone-marl alternation (deeper water) to a shallow-water carbonate platform (Fig. 7.4). Moreover, Hantzpergue (1979, 1983) states that the hardground also marks a harsh break in morphological evolution of ammonites, separating the *Irius* from the *Gigas/Gravsiana* groups. Given the change-over in sedimentation regime and its position in the biostratigraphic framework, it is more than likely that this hardground corresponds to the maximum flooding preceding large-scale sequence boundary Ti1. In the Jura Mountains this level corresponds to the upper *virgula* Marls, also defined by an abrupt change-over in sedimentary environments reflecting a change from deeper to shallower (resp. more open-marine to restricted/tidal) conditions, usually with a well-developed hardground at their base, too (cf. Bläsi 1980).

Similarities in large-scale stacking pattern and sedimentary architecture also exist in the basinal sedimentary record – extending from the Vocontian Basin (Clue de Taulanne section, this study), over the deep shelf environments of the Valais trough (Poteu de Mié section, this study) to the eastern Helvetic nappes (Funk et al. 1993, Mohr & Funk 1995, Weissert & Mohr 1996, Hänni 1999, 2000). In both studied basin sections (Clue de Taulanne and Poteu de Mié), SB $Ti4_{Tethyan}$, located at the base of the Late Tithonian (cf. Fig. 1.9), defines a change to thicker beds. For the same stratigraphic level, Weissert & Mohr (1996) report a change to thicker beds in the "*Upper Quinten Limestone*" of the Helvetic Nappes of eastern Switzerland. Moreover, the drowning linked to the transgression following SB Be4 (Middle Berriasian, limit *Subalpina/Privasensis* subzones, cf. Fig. 1.9) that, by a change from hard limestones to softer marls, also translates well into outcrop morphology, is very similarly expressed in the Clue de Taulanne section (Pl. 21/4) and the limit between the "*Calcaires bleutés massifs*" and the "*Valanginien schisteux*" in the Poteu de Mié section (Pl. 21/3). This event seems to correspond to the limit between the "*Quinten Limestone*" and the "*Zementstein-Formation*" in the Helvetic Nappes of eastern Switzerland (Mohr 1992, Mohr & Funk 1995, Weissert & Mohr 1996, Hänni 1999).

For sections that are located relatively close to the platform slope, the frequency of major resedimentation events seems to bear a potential for regional correlation: e.g., the breccia at the A2/A3 boundary of the Clue de Taulanne section most probably correlates with a major debris flow in the nearby Angles section (Strohmenger & Strasser 1993).

7.3.2 Subboreal realm

Linking the Late Jurassic and Early Cretaceous rock record from southern to northern Europe is one of the long-standing problems in European stratigraphy. The strong provincialism shown by the northern and southern ammonite faunas that starts in the Middle-Late Oxfordian (Atrops et al. 1993) has resulted in the definition of two separate zonal schemes based on the different groups of ammonites, which occurred in the Boreal (arctic areas and northern Europe) and Tethyan (southern Europe and Tethys margin) palaeogeographic provinces, respectively (cf. Fig. 1.6).

Different correlations have been put forward (e.g., Gerasimov et al. 1975, Kutek & Zeiss 1975, Sachs et al. 1975, Shulgina 1975, Kutek & Zeiss 1994, G.F.E.J. 1997, Hardenbol et al. 1998, Gradstein et al. 2004), but correlating the Boreal with the Tethyan realm is still difficult (Explanatory note Int. Stratigr. Chart, 2000). As a matter of fact, a pure biostratigraphic correlation of these two realms is impossible. Integrated studies, however, aiming at a better understanding of the mechanisms that created the similarities and differences between northern and southern Europe, have already delivered promising results and may eventually be successful. (High-resolution) sequence stratigraphic studies, independently developed for the subboreal realm (e.g., Gallois & Cox 1976, Cox & Gallois 1979, 1981, Wignall 1991, Melynk

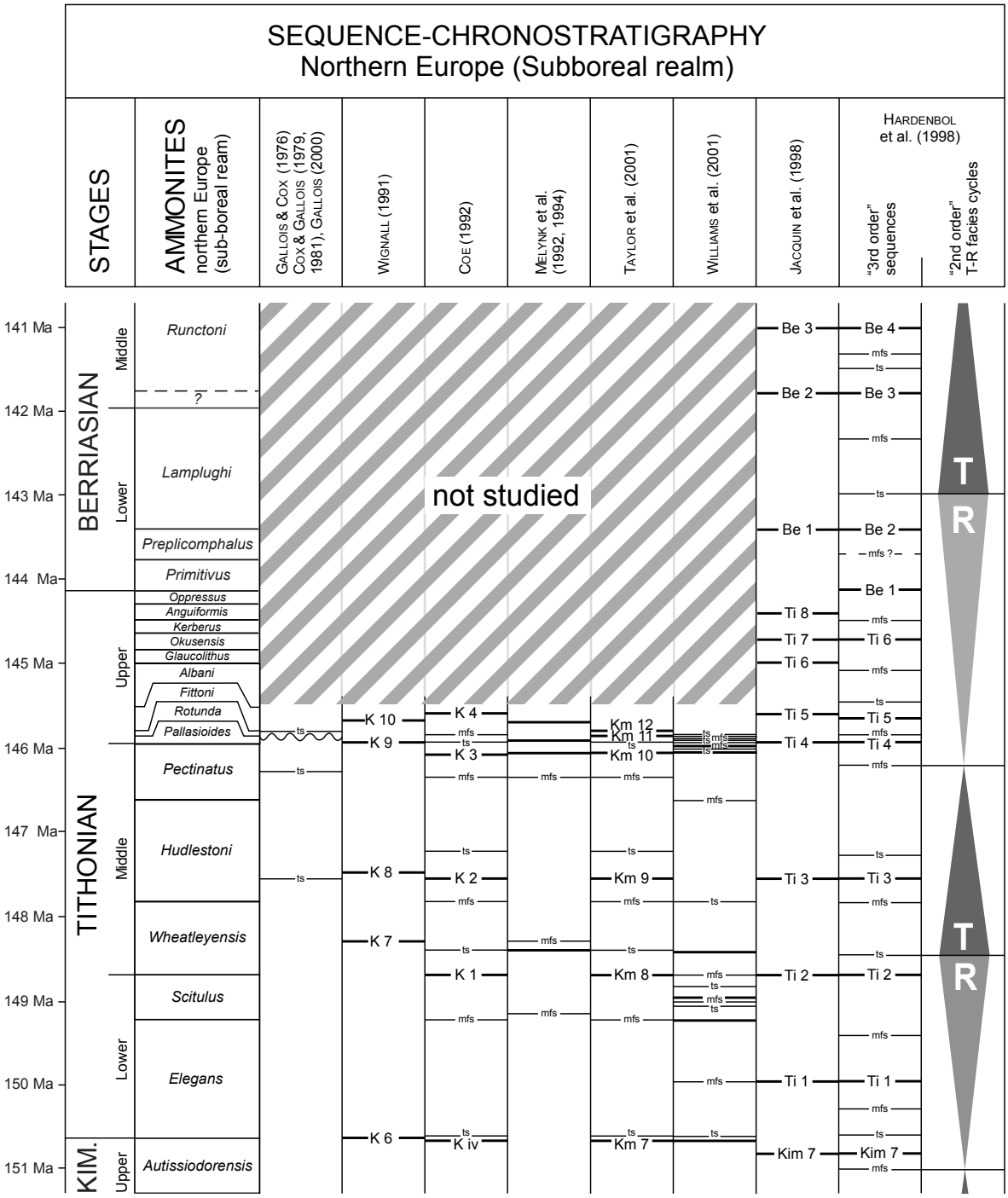

et al. 1992, 1994, Herbin et al. 1995, Proust et al. 1995, 2001, Gallois 2000, Taylor et al. 2001, Williams et al. 2001) and the Tethyan realm (e.g., Bläsi 1980, Strasser & Hillgärtner 1998, this study) can be compared and provide some sedimentary key surfaces that can be traced all over Europe.

For example, the Kimmeridge Clay Formation in Dorset contains coarser grained layers that correlate with sandstone packages in the Boulonnais succession of northern France (Williams et al. 2001). These packages seem to have been deposited at shallower depth than the underlying and overlying muddy units, and are thus interpreted as sequence boundaries. According to Taylor & Sellwood (2002), however, not each sandbed is necessarily related to a drop in relative sea-level. Even so, Williams et al. (2001) show that sequence boundaries in the Kimmeridgian of southern England correspond to abrupt increases in quartz content, transgressive surfaces

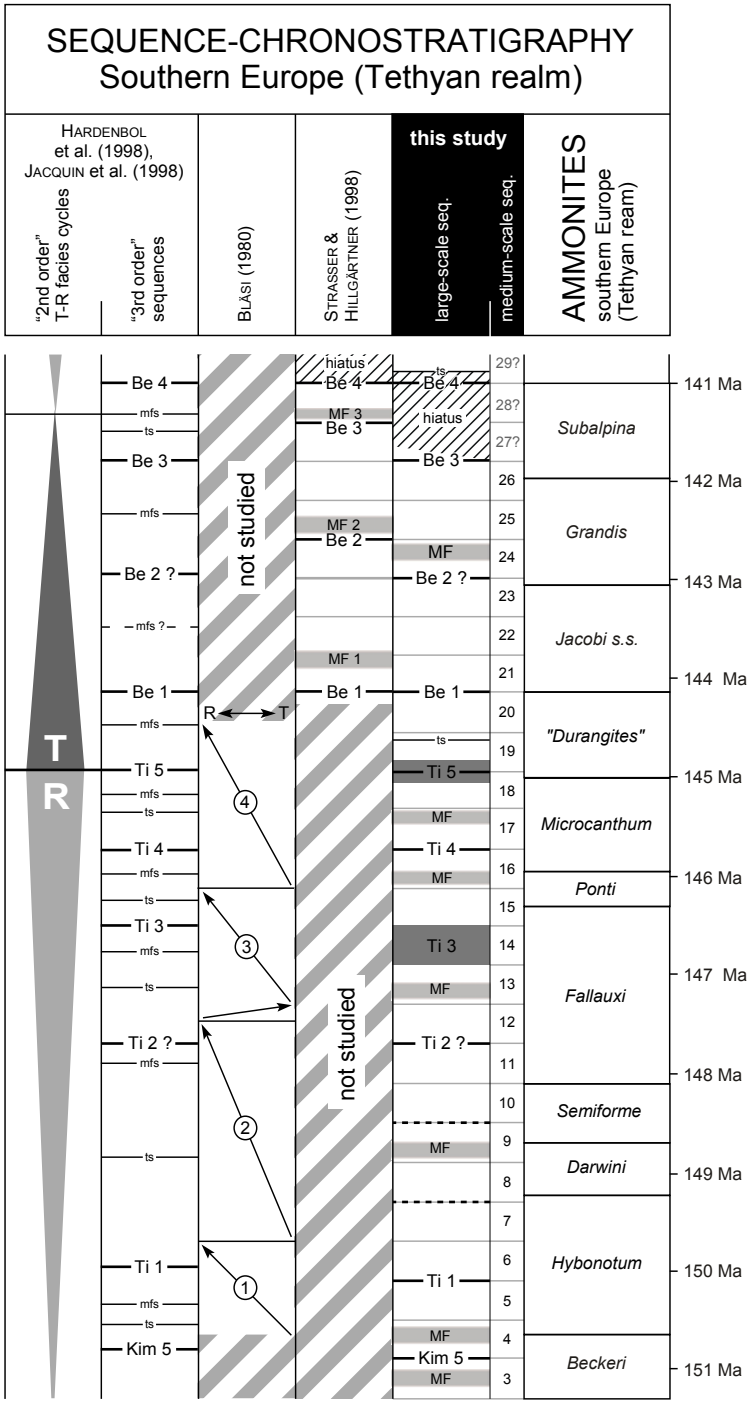

Fig. 7.3 - (this page and facing page) Comparison of different sequence-chronostratigraphic interpretations of the sub-boreal realm (southern England, French Channel coast) and the Tethyan/ submediterranean realm, compared to the working area in the Swiss and French Jura Mountains.

to abrupt decreases, and maximum-flooding surfaces coincide with the intervals of finest grain sizes. When analyzing the relative quartz content in the Kimmeridgian of the central Swiss Jura Mountains, COLOMBIÉ (2002) found a similar pattern. Considering these facts (among many others) it was possible to establish a Tethyan-Boreal correlation for the Kimmeridgian, based on a sequence- and cyclostratigraphic approach (for details see COLOMBIÉ & RAMEIL submitted).

Unfortunately, the northern and southern European sequence stratigraphic-frameworks show considerable divergence and "white areas" for the Tithonian (cf. HARDENBOL et al. 1998, JACQUIN et al. 1998). Nevertheless, by integrating clay-mineral analyses (e.g., PERSOZ & REMANE 1976, BLÄSI 1980, PERSOZ 1982, DECONINCK et al. 1985, DECONINCK & DEBRABANT 1985, HALLAM 1986, WIGNALL & RUFFELL 1990, HALLAM et al. 1991, DECONINCK 1993, PROUST et al. 1995, RUFFELL et al. 2002, SCHNYDER 2003, this work), information on palaeoclimatic changes (cf. Chaps 5 and 8) can be linked to a sequence/ bio/chrono-stratigraphic interpretation. As major climatic changes result from large-scale shifts in the Earth's atmosphere, they usually affect large areas and therefore are a valuable tool for adding reference levels to a correlation chart.

In the Weald Basin of SE England, WIGNALL & RUFFELL (1990) found a kaolinite minimum zone in bed 44 (*Hudlestoni* ammonite zone) that indicates a change from a semi-arid to arid climate. This interpretation is backed up by sedimentological, geochemical, and palaeontological evidence (cf. Fig. 8.4) and was confirmed by biogeographic (SCHUDACK 1999) and palynological data later on (ABBINK et al. 2001). This Late Jurassic "dry event" and the accompanying kaolinite minimum zone are known from large parts of Europe. However, duration and stratigraphic position of the kaolinite minimum zone are not equal on the European scale (cf. DECONINCK et al. 1985, DECONINCK & DEBRABANT 1985, HALLAM 1986, HALLAM et al. 1991).

In the Jura Mountains, the kaolinite minimum zone begins close to sequence boundary SB $Ti2?_{Tethyan}$ and ends with the reappearance of kaolinite around SB $Ti5_{Tethyan}$ (Fig. 5.3). This interval corresponds to approximately 2.8 Ma, according to both the chronostratigraphic data given by HARDENBOL et al. (1998) and this study's cyclostratigraphic interpretation (Tab. 6.2). The kaolinite minimum zone of southern England coincides relatively well with the *hudlestoni* ammonite zone, representing a duration of approximately 1.2 Ma

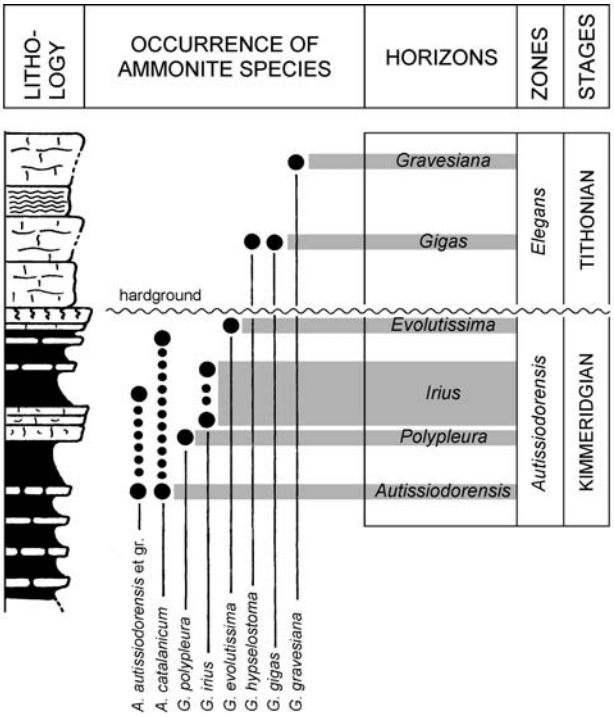

Fig. 7.4 - Litho- and biostratigraphy of the Kimmeridgian/ Tithonian boundary in the Aquitaine area, SW France. Note the changeover in sedimentary architecture and the hardground at that level. The hardground is interpreted as omission surface, which is confirmed by an observed "morphological hiatus" between the *Gravesia irius* and *Gravesia gigas/gravesiana* groups. From Hantzpergue (1983), modified.

according to Hardenbol et al. (1998), respectively a minimum duration of 0.6 Ma from cyclostratigraphic analysis (Weedon et al. 2004).

However, if we consider that the kaolinite minimum zone in the Jura Mountains is interrupted by a short humid "intermezzo" around SB $Ti3_{Tethyan}$ (cf. discussion in Chap. 8), the two inferred time spans match perfectly: approximately 1.2 Ma for the *hudlestoni* ammonite zone in southern England (see above), compared to approximately 1.2 Ma between SB $Ti2?_{Tethyan}$ and SB $Ti3_{Tethyan}$ in the Jura Mountains (Hardenbol et al. 1998 and cyclostratigraphic interpretation, cf. Tab. 6.2).

For Wignall & Ruffell (1990) it is evident that the clay minerals deposited in the Wessex-Weald Basin in southern England were eroded somewhere to the south, as the islands to the north and west (cf. Fig. 1.3) neither had enough landmass nor a relief steep enough to provide a significant clay-mineral signal. The only landmasses big enough were the Armorican and Central Massifs to the south, and the London-Brabant-Rhenish Massif to the (south-)east (cf. Fig. 1.3). These landmasses are the same that would have provided the clay minerals deposited on the Jura platform. Consequently, it is concluded that both, the Weald Basin in southern England and the Swiss and French Jura Platform, recorded the same change in clay mineral associations that was caused by a climatic change over the Armorican, London-Brabant, Central, and Rhenish Massifs. The slight difference in inferred timing may be due to inaccuracies in numeric ages and/or to differing transport distances and processes.

In southern England, Taylor et al. (2001) place the sequence boundary SB Km9 (= SB $Ti3_{Boreal}$ according to Hardenbol et al. 1998) at the base of bed 44. This level is simultaneously the beginning of the local kaolinite minimum zone (cf. Fig. 8.4). As stated already above, the kaolinite minimum zone of the Jura Mountains begins close to sequence boundary SB $Ti2?_{Tethyan}$. If it is accepted that the beginning of the kaolinite minimum zones in southern England and the Jura Mountains is more or less isochronous, these two large-scale (3^{rd}-order) sequence boundaries can be correlated, i.e. SB Km9 (= SB $Ti3_{Boreal}$; Hardenbol et al. 1998) would be the Boreal counterpart to SB $Ti2?_{Tethyan}$. Similar numeric ages (147.6, resp. 147.7 Ma) given by Hardenbol et al. (1998) also sustain this hypothesis.

* * *

8 - Palaeoclimatology and environmental change

8.1 Global climate around the J/K transition – an overview

Until well into the 1980s, the Jurassic and Cretaceous palaeoclimate was considered to be hot and uniform, with a total absence of polar ice caps ("*greenhouse conditions*", cf. Frakes 1979, Hallam 1981, 1985). The Late Jurassic in general was a period of climatic maximum (cf. Perlmutter & Matthews 1989). Compared to present settings, the subtropical high-pressure zone expanded to higher latitudes and pushed the subboreal low-pressure belts polewards (Fig. 8.1). As a result, the temperature gradient within the tropics and subtropics themselves was rather small and the N-S temperature differences were much smaller than today. More recent, palaeoclimate modelling indicated that both the average annual temperatures and humidity were probably significantly higher than today, with the higher humidity expressed by more cloud cover in the polar regions and greater rainfall over oceanic areas (Sellwood & Valdes 1997, Sellwood et al. 2000). This is supported by the distribution of thermophile fauna and flora, such as temperate floral biomes in polar regions (Rees et al. 2000) and dinosaurs in high latitudes (Siberia, Svalbard, southern Australia, and Antarctica; Rich et al. 2002) (Fig. 8.2).

The general rainfall patterns are also considered to have been different from today: during the Late Jurassic climatic maximum, the equatorial humid zone extended up to 20°, the subtropical arid zone was located at approximately 30-40°, and the subpolar humid zone at approximately 60-70° latitude (cf. Perlmutter & Mattews 1989). This is consistent with a bimodal distribution of dinosaur diversity with regard to palaeolatitude (highest diversity in the N and S mid-latitudes, with an equatorial minimum and peri-polar decline), as reported by Parrish (1993). However, this general scheme was disturbed by the effects a rather uniform landmass (Fig. 8.1) had on the general circulation pattern.

With an equatorial wet belt well developed over the oceans but quasi non-existent on the continents, most of the continental interiors were very dry, with hot summers and a rather strong seasonal contrast. Monsoonal precipitation was largely confined to coastal regions (Fig. 8.1).

After the first publications reported the existence of cold phases in the Jurassic and the Cretaceous (Embry 1984, Shearman & Smith 1985, Frakes & Francis 1988, Kemper 1983, 1987), the somewhat simplified image of a hot and uniform palaeoclimate was eventually corrected: amongst other indicators, high-latitude dropstones and tillites provide the main sedimentological evidence for the existence of ice-covered areas during the Jurassic and Cretaceous (Epshteyn 1978, Kaplan 1978, Kemper 1987, Frakes & Francis 1988, Frakes et al. 1992, 1995, Eyles 1993, Chumakov & Frakes 1997).

Reassessing these data, Price (1999) proposed an ice-free Callovian to Kimmeridgian "greenhouse" period (cf. Weissert & Mohr 1996), followed by a Tithonian/ Volgian "cool" phase. Isotopic data (belemnites from Germany, Morocco, England, and Russia) seem to confirm this interpretation: in 1998, Podlaha et al. published a synthesized Bajocian to Aptian ä^{18}O-curve, indicating a Callovian to Kimmeridgian hot phase, followed by less clear oscillations in Tithonian and Berriasian times. The data of Riboulleau et al. (1998) and of Ruffell et al. (2002) from the Russian platform show a similar pattern. They indicate hot temperatures for Callovian to Tithonian times, followed by a cooling and/or a stronger evaporation in the Volgian.

Despite these climatic changes that obviously also must have had an effect on the hydrologic cycle and erosion rates, the $^{87}Sr/^{86}Sr$ ratio does not show any rapid changes. It shows a steady increase during the Jurassic and Early Cretaceous (Jenkyns et al. 2002, Jones & Jenkyns 2001, Veizer et al. 1999, Jones et al. 1994), whereas the ä^{13}C curve is characterized by a continuing negative trend (Jenkyns et al. 2002, Veizer et al. 1999) (Fig.

Late Jurassic northern winter (Dec/Jan/Feb)

with Jan/Feb/Mar storm tracks

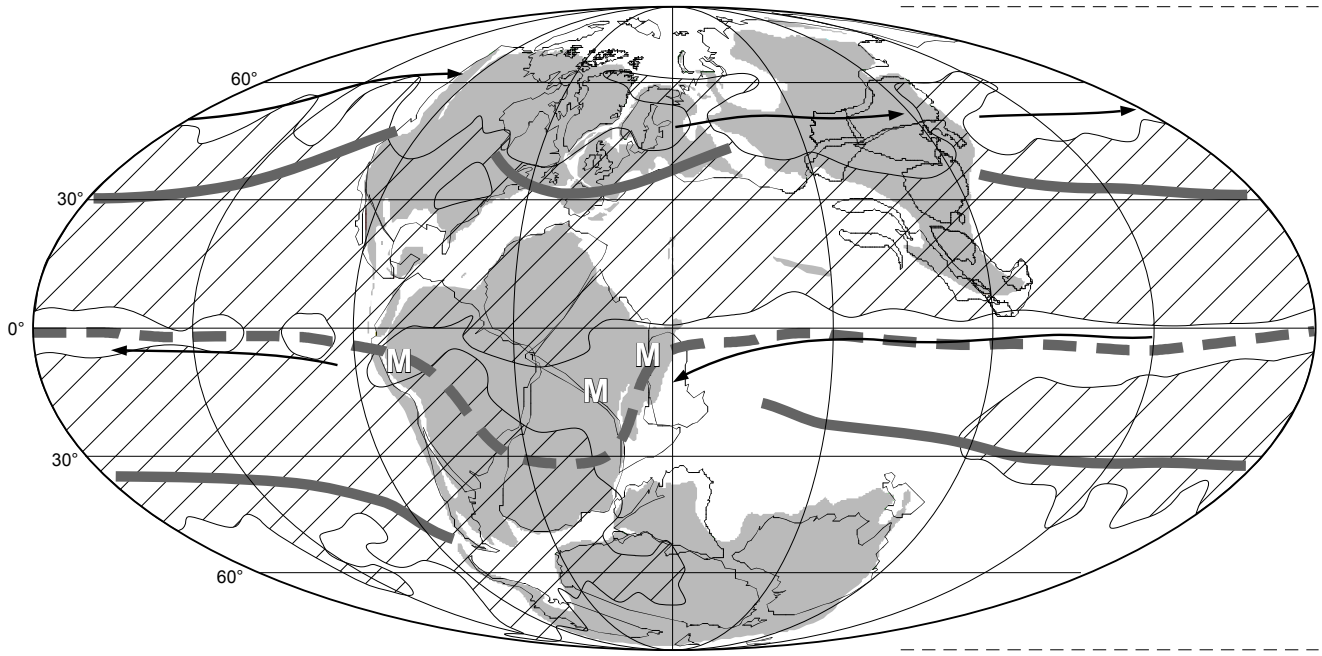

Late Jurassic northern summer (Jun/Jul/Aug)

with Aug/Sep/Oct storm tracks

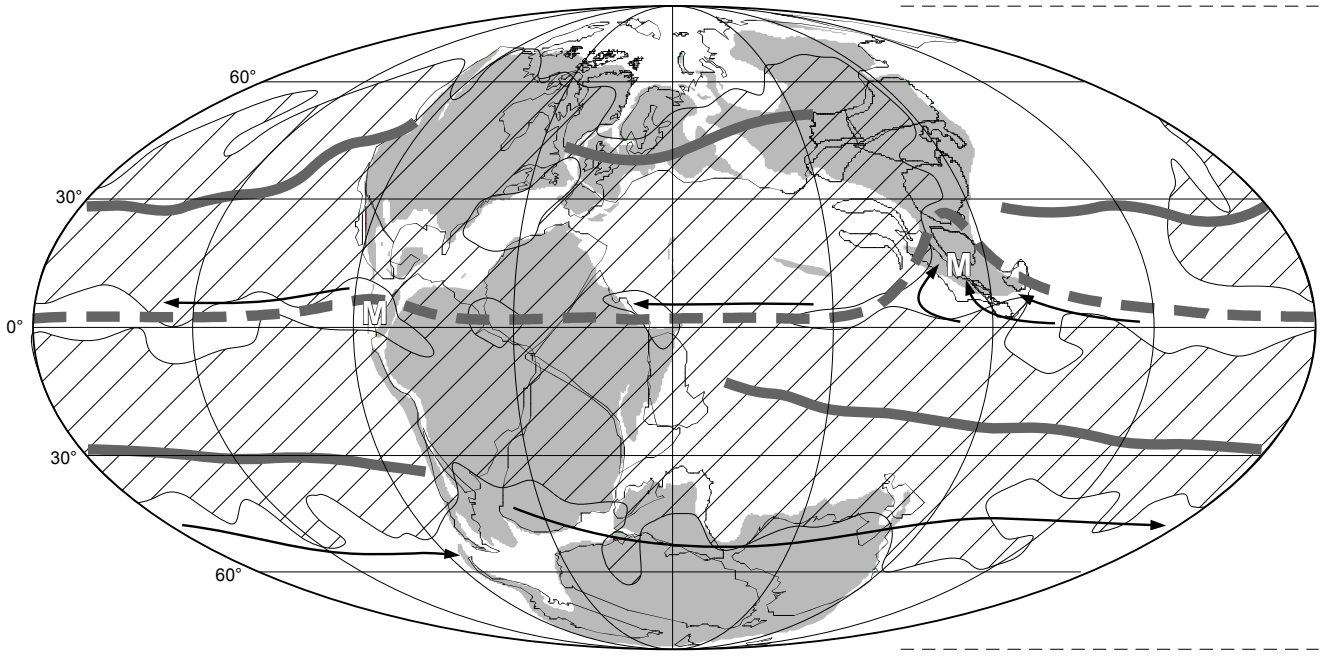

storm tracks

arid area (evaporation > precipitation)

Inter-Tropical Covergence (ITC)

subtropical high-pressure belt

M **monsoon climate:**
heavy rainfalls in Jun/Jul/Aug (northern hemisphere), respectively in Dec/Jan/Feb (southern hemisphere), after MOREet al. (1992), WILDES(1994)

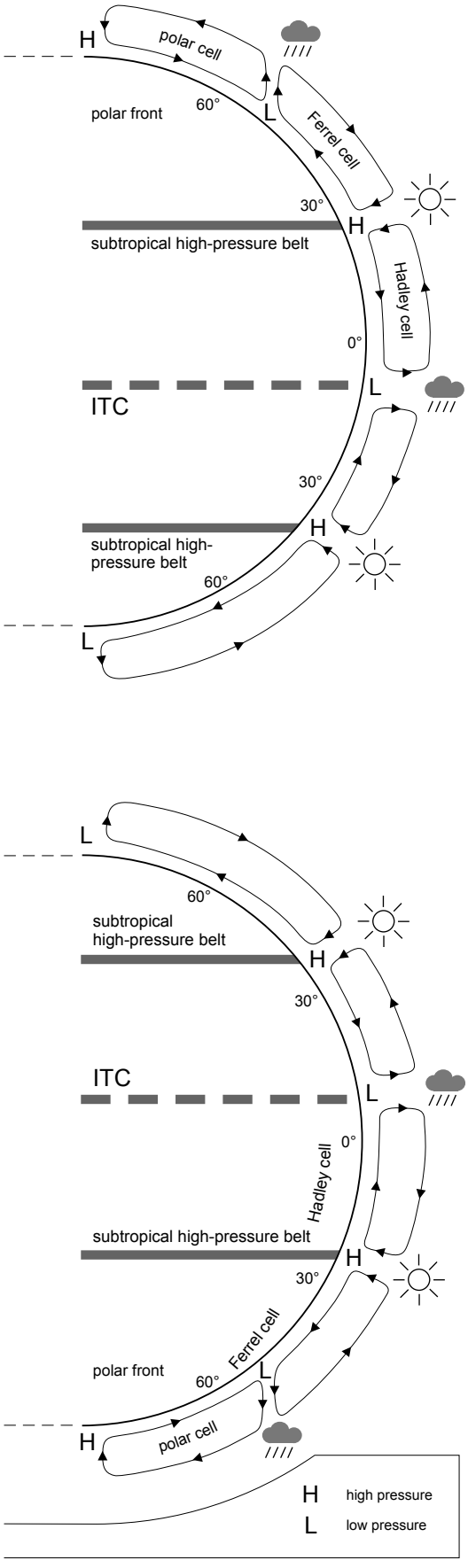

Fig. 8.1 - (this page and facing page) Schematic atmospheric circulation pattern for the Late Jurassic. After Rees et al. (2000), Valdes (1994), Moore et al. (1992), and Oschmann (1990).

8.3). On the first view, there is a problem – this development of the carbon-isotope curve is usually interpreted to reflect a slow-down of the hydrologic cycle (Weissert & Mohr 1996) but the trends towards more positive values in the Sr-isotope curve simultaneously indicates increasing import of erosion products to the oceans (Jenkyns et al. 2002). One can, however, observe a kind of a plateau in the Sr-isotope curve in the Middle Tithonian (Fig. 8.3), which might be associated with a decrease in the export of detritic material to the oceans, probably caused by a Late Jurassic dry-phase. This hypothesis is backed up by the fact that the Sr-isotope values increase again, with the ä^{13}C-curve showing a simultaneous positive excursion. Apparently, the factors controlling the development of the Sr-isotope curve seem to be complex and the $^{87}Sr/^{86}Sr$ ratio responds only imperfectly and/or delayed to fluctuations in detritic export from the landmasses (Schnyder 2003). Also, the similarity of ä^{13}C curves from South-Gondwana, the Tethyan realm, and the Russian platform favours a mechanism of global extent. Taking into account the entirety of data, this is relatively coherent with the model of Weissert & Mohr (1996).

Robinson (1973), Kutzbach & Gallimore (1989), Moore at el. (1992), and Parrish (1993) have, among many others, put forward a scenario of monsoon-type climate in the lower latitudes during a significant part of the Mesozoic, characterized by very dry conditions in the continental interiors, with hot summers and a rather strong seasonal contrast. In this scenario, precipitation is confined to the Tethyan coasts and some other continental margins. Thus, the equatorial wet belt would be essentially undisturbed over the oceans but almost non-existent on the continents (cf. Fig. 8.1). According to Parrish (1993), the monsoonal character of global climate ceased during the Jurassic and, due to the advancing break-up of the continents, was replaced by a more zonal climate pattern somewhere in the Late Jurassic or around the J/K boundary. The existing geological and palaeobotanical data (Fig. 8.2) generally confirm the existence of such climate zones for the Late Jurassic.

Berner et a1. (1983) and Berner (1994) estimate CO_2-levels several times higher than today for the Late Jurassic world, causing a pronounced greenhouse effect. Nevertheless, Frakes et al. (1992) have proposed the existence of cold zones that were geographically confined to high latitudes and did not affect the lower latitudes.

With developing computing power, numerical models of Mesozoic climate have become increasingly important since the beginning of the 1980s, introducing a more quantitative aspect to the palaeoclimatic studies (e.g., Moore et al. 1992; Valdes & Sellwood, 1992; Barron et al. 1993, Valdes et al. 1995, Price et al. 1995, 1997, 1998, Sellwood et al. 2000). Several of these models focus on the Late Jurassic, specifically

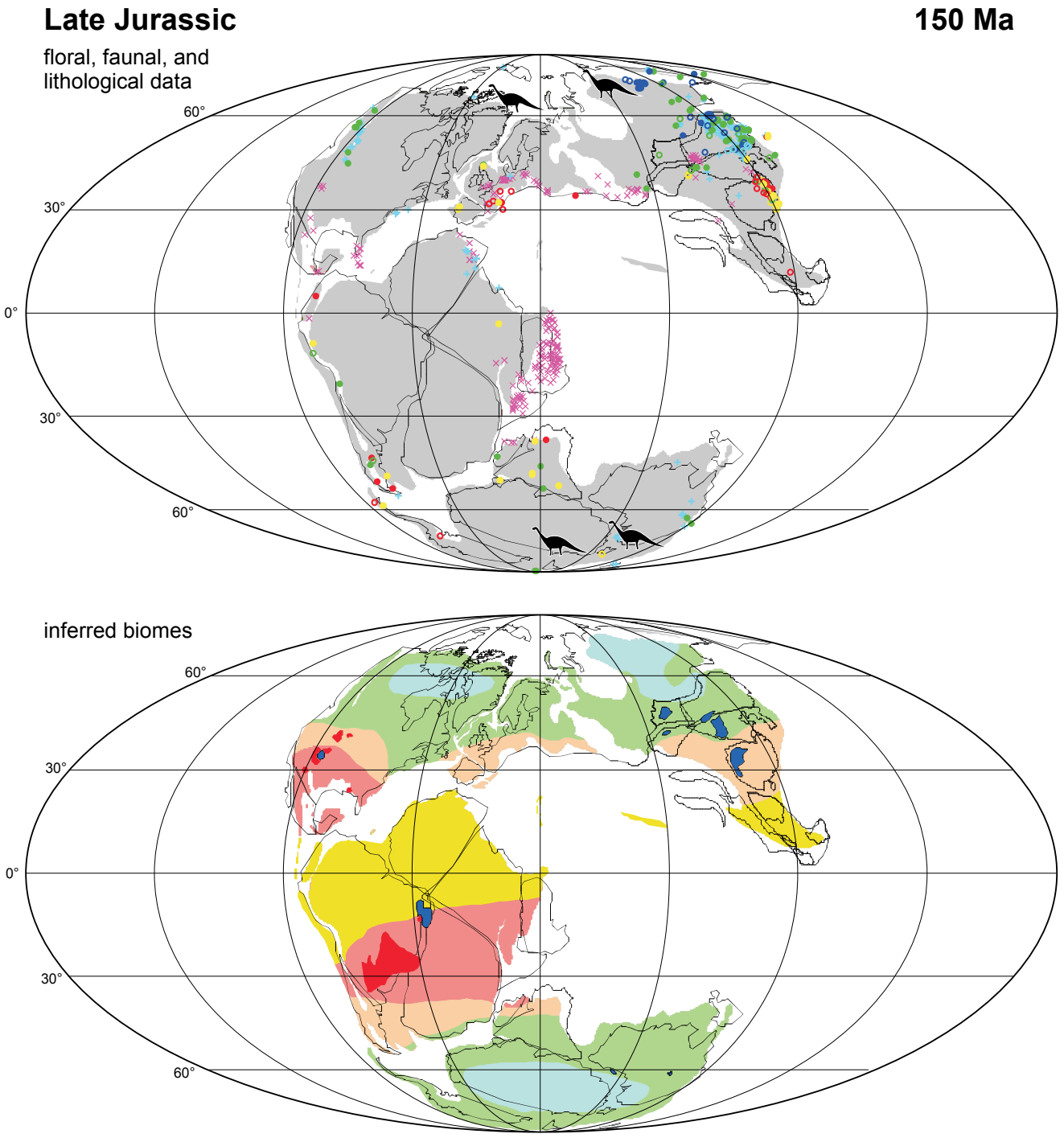

Fig. 8.2 - Late Jurassic (150 Ma) palaeogeographical maps, showing floral, faunal, and lithological data as well as inferred biomes (Rees et al. 2000, faunal data from Rich et al. 2002).

the Kimmeridgian. In general, the obtained results are in good agreement with the existing geological data: e.g. evaporites are localized in areas for with the models show negative precipitation-evaporation budgets and regions with intense precipitations in the models frequently show sedimentary evidence for runoff. However, it has to be mentioned that there are also significant differences between different models (e.g., Moore et al. 1992 vs. Valdes & Sellwood 1992 for the Kimmeridgian). Yet, many among these models predict very low temperatures in high latitudes that sustain the presence of sea ice and ice on land may also have occurred in restricted areas – even in greenhouse settings that were previously considered hot and climatically uniform. For example, Stoll & Schrag (1996) present evidence for the possible existence of an Antarctic ice cap during the Early Cretaceous. Valdes (1994) and Valdes et al. (1995) developed a model that predicts the existence of small, but significant, polar ice-caps during the Kimmeridgian, with waxing and waning rhythms primarily triggered by the 100 ka eccentricity cycle. This would have a significant impact on the interpretation of Late Jurassic eustatic variations and their possible amplitudes (Price 1999).

At the same time, however, model outputs regularly indicate temperatures for the continental interiors that have undoubtedly to be considered as too low when confronted with geological and palaeobotanical data (e.g., Valdes & Glover 1999, Price et al. 1995). This may be due to the applied numerical models, some of which are also used for predicting global change, having difficulties in assessing and coping with Mesozoic settings.

In summary, the idea of a hot and uniform climate during the Jurassic and the Cretaceous has definitely to be abandoned as evidence of colder conditions in certain periods and higher latitudes became apparent. However, the exact spatial and temporal extensions of these phases are still controversial. A relatively wet and hot phase during the Oxfordian and Kimmeridgian, with a relatively high sea-level and a high turnover in the hydrologic cycle, seems to have been replaced by a drier (and perhaps cooler?) phase towards the J/K boundary, accompanied by a long-term (2nd-order) trend of decreasing sea-level. This system was once again reversed in the Middle/Late Berriasian (Fig. 8.3).

In contrast to the "*cool J/K boundary*"-hypothesis (e.g., Price 1999, Schudack 1999), the recent palynological study of Abbink et al. (2001) proposes that the Late Jurassic dry phase in the subboreal realm was not related to a decrease but to an increase in average annual temperature. If, as suggested by this study, the conditions remained hot or even became drier and hotter during the Middle Tithonian, a new driving force has to be found that explains the postulated atmospheric changes in humidity and temperature.

8.2 Regional palaeoclimatic evolution

8.2.1 Literature data from western and central Europe

Being located at a palaeolatitude of some 30-35° N, the study area was under the influence of the northern subtropical high-pressure belt. According to the general circulation model of Moore et al. (1992), precipitation in the study area was about 1000 mm/a, with a negative precipitation-evaporation balance. This resulted in an arid, winterwet climate (Figs 8.1, 8.2). Monsoonal climates (= "summerwet climate" in Fig. 8.2), as proposed by several authors for the Late Jurassic of Central Europe, seem to have been restricted to Central America and SE Asia (Rees et al. 2000, Moore et al. 1992).

It has been suggested for the Kimmeridgian of the north-western Tethys coast that hurricanes were generated over the warm surface waters of the equatorial Tethys and moved to the NW during summer (Marsagalia & Klein 1983), similar to those of the modern Caribbean. Similarly, winter storms are thought to have moved ESE (Price et al. 1995). The direction of these storm tracks is supported by the storm-dominated sedimentation on ramps that developed preferentially on the windward side of the Iberian Basin (Bádenas et al. 2004, Aurell et al. 2003, Bádenas et al. 2003, Bádenas & Aurell 2001a, b).

However, as discussed above, the Late Jurassic and Early Cretaceous climate system was not static but showed some significant changes. The presence of evaporites is a solid indicator for arid climates in general. Thus, on the basis of distribution patterns of evaporites (Gordon 1975), the existence of dry conditions during the European Late Jurassic was known for a long time (Frakes 1979, Hallam 1984). Barale (1981) mentions that the Late Kimmeridgian and Early Tithonian palaeofloras of the Swabian Alb (southern Germany) are both characterized by a relative poverty in genera but high abundances of species. The presence of pteridosperm plants of the *Cycadopteris* group, many conifers of the *Brachyphyllum* and *Palaeocyparis* groups, and the absence of ferns and *Equisetaceae* in the Early Tithonian suggest a drier climate for the region compared to the Late Kimmeridgian.

Congruently, Deconinck et al. (1985) deduce a development from seasonally humid Oxfordian and Kimmeridgian climates to "more irregular" Tithonian conditions from the interpretation of clay mineral associations in the French Subalpine Ranges. A massive occurrence of kaolinite and smectite beginning in the Late Tithonian announces the reinstallation of a hot climate with well-expressed wet and dry seasons (cf. Chap. 5). Bläsi (1980) reports a kaolinite minimum from the

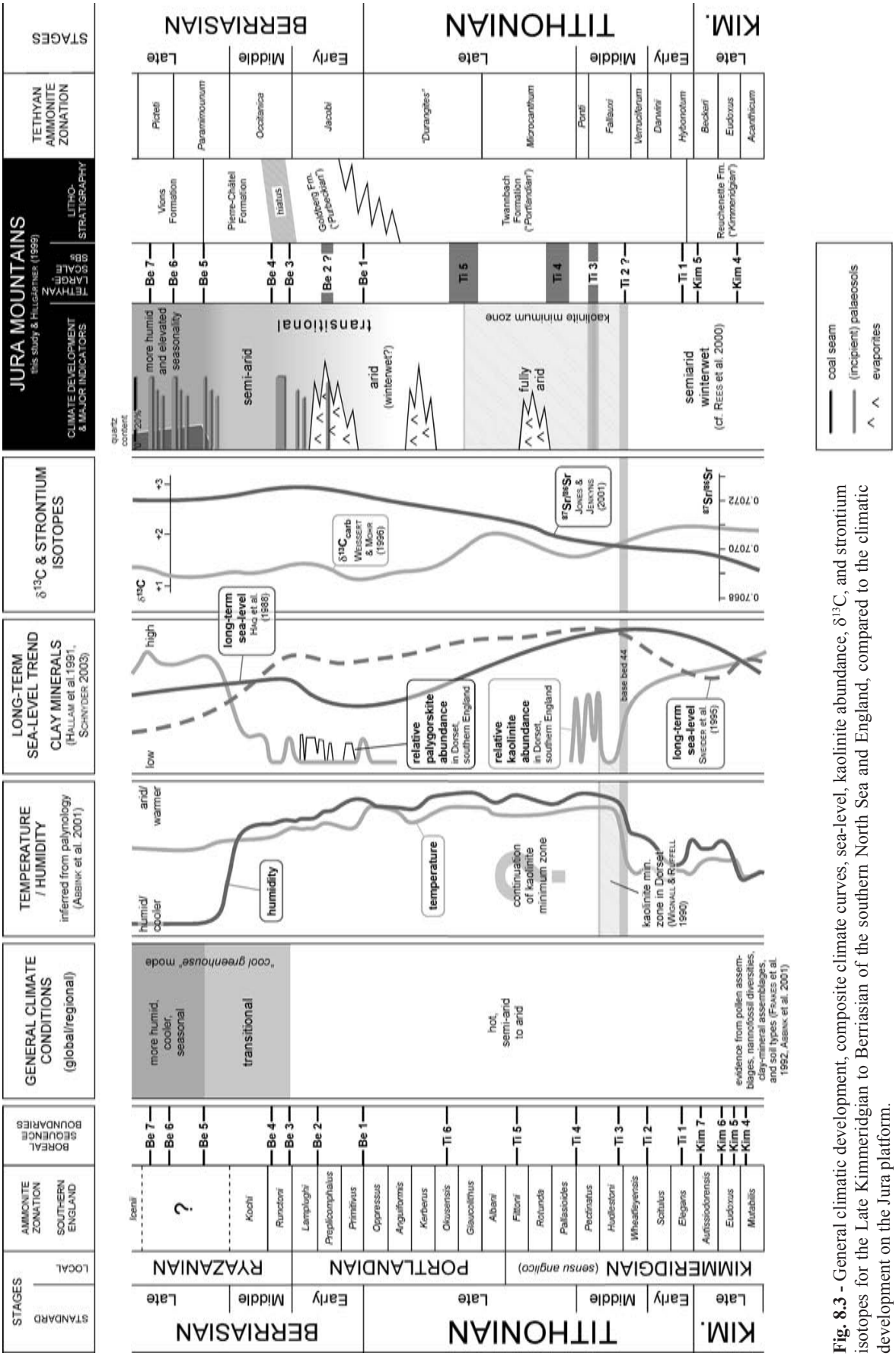

Fig. 8.3 - General climatic development, composite climate curves, sea-level, kaolinite abundance, $\delta^{13}C$, and strontium isotopes for the Late Kimmeridgian to Berriasian of the southern North Sea and England, compared to the climatic development on the Jura platform.

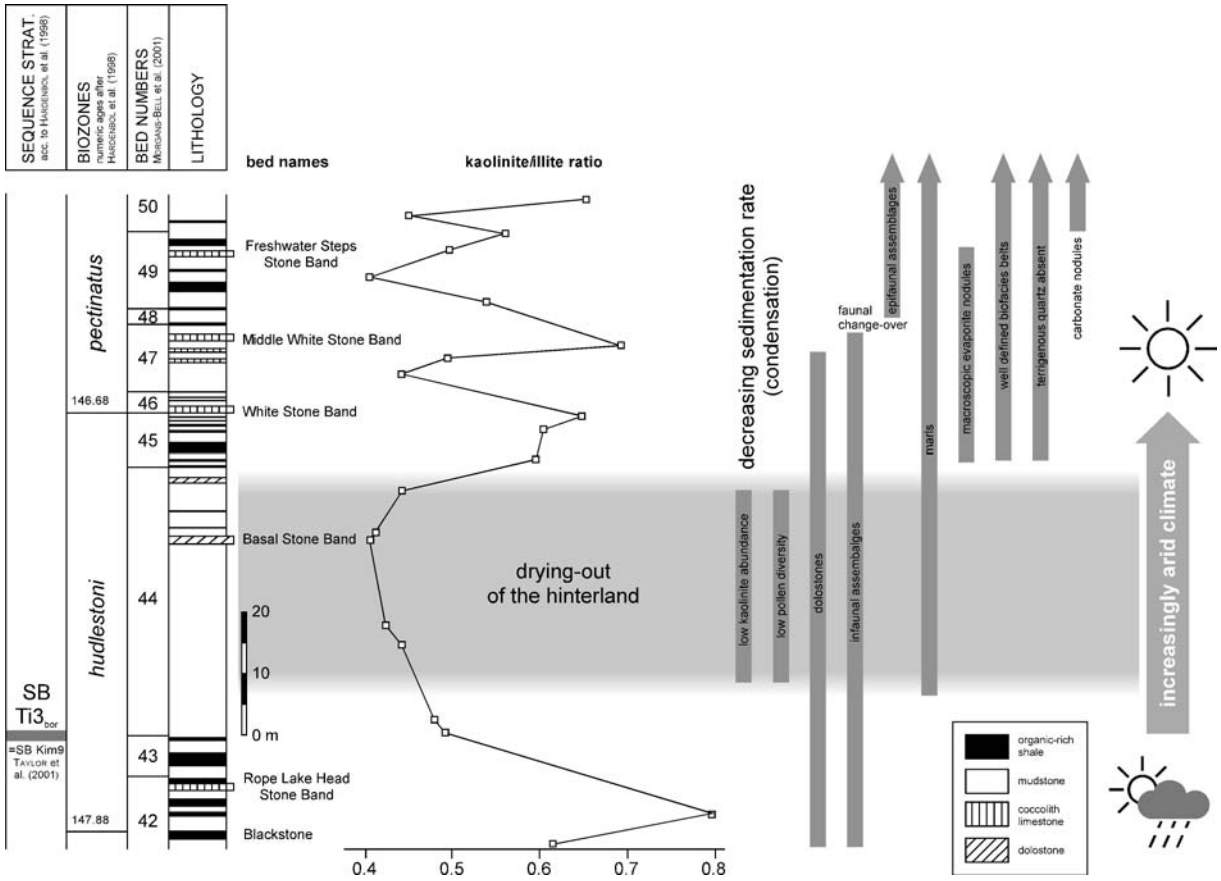

Fig. 8.4 - Kaolinite/illite ratio and several sedimentological and palaeontological indicators for a major climatic change-over in the Kimmeridge Clay (Rope Lake Head section. After WIGNALL & RUFFELL (1990).

Tithonian of northern Switzerland but interprets it to be caused by sorting processes. PERSOZ & REMANE (1976) and PERSOZ (1982) define different areas defined by absence respectively presence of "*inherited kaolinite*" but explain this with "*sedimentological reasons*".

WIGNALL & RUFFELL (1990) studied a lithologic and palaeoecologic change-over in the Upper Kimmeridge Clay Formation (Dorset, southern England, *hudlestoni* Zone, bed 44 of GALLOIS & COX 1976). Clay-mineralogical, sedimentological, and palaeontological data suggests that many aspects of these offshore mudrocks were influenced by a sudden climatic change to more arid conditions (Fig. 8.4). HALLAM et al. (1991) discuss the changes in clay mineralogy in western Europe and compare them to other climate indicators that show a latest Jurassic-earliest Cretaceous "dry phase".

ABBINK et al. (2001) confirmed this scenario by a palynological study carried out in southern England and the southern North Sea (cf. Fig. 8.3). In fact, by a detailed analysis of floral indicators, ABBINK et al. (2001) not only deduce a sudden change to drier conditions in the Middle Tithonian but also a parallel increase in mean temperature. By comparing their data from the Late Jurassic subboreal realm with modern environments, ABBINK et al. (2001) propose dry-phase conditions identical to the climate of today's Egypt (annual averages of 27°C and < 40 mm precipitation). After the re-installation of a cooler and more humid climate in the Berriasian (cf. Fig. 8.3), wet tropical characteristics (annual averages of 25°C and some 1700 mm precipitation) are assumed. SCHNYDER (2003), considering field data from the Purbeckian (Late Tithonian to Middle Berriasian) of southern England and northern France, questions these rather extreme conditions for the Late Jurassic dry-phase.

In contrast to ABBINK et al. (2001) who show a sudden change back to cooler and wetter conditions in the *Kochi* ammonite zone, ALLEN (1998) supposes a gradual transition from the Tithonian dry-phase to the Late Berriasian wet-phase for the English Purbeck. Climate is said to have gradually evolved from Mediterranean conditions featuring strong seasonal contrast (hot and dry summers versus cool and wet winters; annual averages of 15-25°C and < 500 mm precipitation) to warm temperate conditions (annual average of 15-25°C and precipitation ranging from 1250 to 1500 mm/a) in the Late Berriasian. Field data sustain seasonal alternation, e.g., by the

presence of tree rings in fossilized wood (Francis 1987). The contemporaneous presence of evaporite deposits and forests (Lulworth Cove, Francis 1984) also suggests that conditions were not extremely arid but rather semi-arid. Additional evidence comes from the presence of large reptiles that needed considerable amounts of water and the type of palaeosols (calcretes and rendzina-like palaeosols, Francis 1986) found in the English Purbeck Beds.

8.2.2 Implications from the study area

General considerations

The presence of coral reefs in or adjacent to the working area (Bernier 1984, Deville 1991, Fookes 1995, Meyer 2000) with a typical reefal faunal association implies warm water temperatures and oligotrophic conditions (cf. Philip 2003). This means either limited nutrient input by erosion and fluvial transport (i.e. an arid climate) or a sufficient distance to the rivermouths so that coral growth was not negatively affected by the rivers' sediment load (cf. Dupraz 1999, Dupraz & Strasser 2002). From the Middle Berriasian onwards, the Jura platform resembled more of a carbonate ramp than the earlier rimmed shelf. According to Hillgärtner (1999), this was mainly due to a major transgression at the base of the Pierre-Châtel Formation. However, also changes in climate and trophic levels may have played a role.

Clastic input

High contents of clastics are known from the Jura platform during certain intervals in the Late Oxfordian (Pittet 1996, Hug 2003) but the abundance of quartz gradually decreases during the Kimmeridgian (Colombié 2002), as well as the input of clays, iron, and nutrients. Fe-impregnated clasts and encrustations are still rather frequent in the Late Kimmeridgian of the Jura platform (specifically in the lower and upper *virgula* Marls, last appearance in medium-scale sequence 9). The uppermost dysoxic, clay-rich limestones that resemble the lithofacies of the *virgula* Marls are found in medium-scale sequence 10 (e.g., Noirvaux and Dôle sections, see also Colombié 2002).

After the Kimmeridgian and Tithonian, which are characterized by a relatively low abundance of clastics, clastic input increases during the Berriasian and Valanginian (Persoz 1982, Pasquier 1995, Hillgärtner 1999). This is also a basic condition for the formation of green marls and clayey palaeosols (see below).

In slope position (Broyon / Clue de la Payre), the change to marlier sedimentation is clearly expressed as a marl-limestone alternation, beginning between SB Be1 and SB Be2?$_{Tethyan}$ (Fig. 4.21). In the sections of the deeper basin (Clue de Taulanne and Poteu de Mié), the transgressive surface above SB Be4$_{Tethyan}$ defines a drowning event (cf. Chap. 7) that is followed by a marlier sedimentation. However, this may also be due to less carbonate export to the basin during a major transgression. Roulin (2001) found that, except for the higher clay content, the base of the *Valanginien schisteux* in the Poteu de Mié section (marl-limestone alternation above SB Be4) is very similar to the *Calcaires bleutés massifs* (massive limestone cliff below SB Be4, Pl. 21/3). Higher up in the *Valanginien schisteux* (SB Be5$_{Tethyan}$?) there is a significant rise in quartz content, consisting of fine grains that are homogenously distributed in the sediment. This is interpreted either as stronger continental influence (platform progradation) or a change to more humid climate in the hinterland, or both.

Evidence from clay minerals

The study of clay mineral associations (cf. Chap. 5) shows a gradual kaolinite loss during the Late Kimmeridgian (Fig. 5.3; see also Colombié 2002, Mouchet 1998, Kettiger 1981), ending in a well-defined kaolinite minimum zone that begins at about the top of medium-scale sequence 11 (= large-scale SB Ti2?$_{Tethyan}$). The first small reappearance of kaolinite is located around the boundary between medium-scale sequences 16 and 17 (= large-scale SB Ti4$_{Tethyan}$). The end of the kaolinite minimum zone in the Jura Mountains comes with the top of medium-scale sequence 18 (= large-scale SB Ti5$_{Tethyan}$) (Fig. 5.3). This is interpreted as a trend to drier climate during the Kimmeridgian and Early Tithonian, and to completely arid conditions during the kaolinite minimum zone.

Karst

The development of carbonate karst requires the presence of fresh (usually rain) water and an at least partially developed soil cover (James & Choquette 1988). Consequently, the presence of karst features can be used as palaeoclimatic indicator for a relatively humid, or at least semi-arid, seasonal climate (e.g., Wright 1988). The occurrence of karstified levels in the studied section is limited to Late Kimmeridgian and Early Tithonian times (medium-scale sequences 4, 5, 7, 8, 11, and 14; cf. Pl. 10/5, 6). Mouchet (1998) reports a major Kimmeridgian discontinuity (*divisum/acanthicum* Zone) in the Jura Mountains to be a karstified surface.

Green marls

Green marls form during emersion, either from detrital input caused by the erosion of smectite-rich soils which developed in the hinterland under a hot and

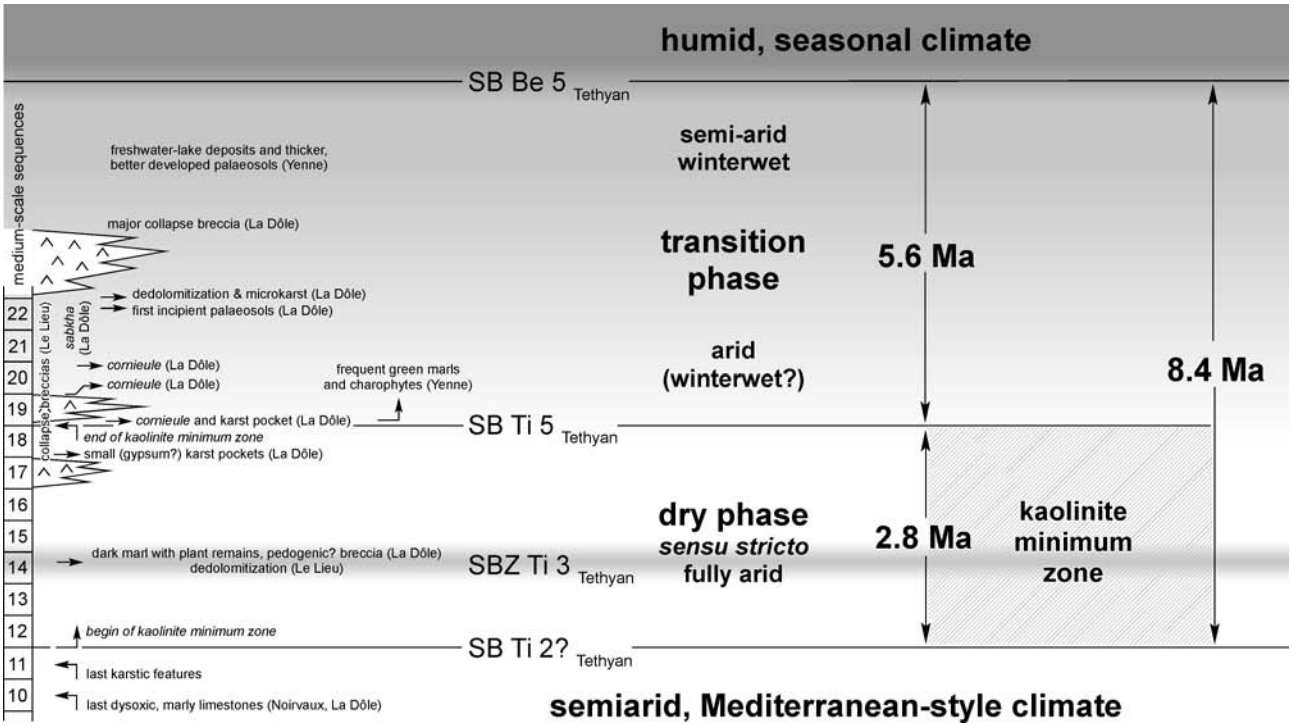

Fig. 8.5 - Field evidence for and timing of the Late Jurassic dry phase on the Jura platform as inferred from cyclostratigraphic analysis (Tab. 6.2, Hillgärtner 1999, Strasser & Hillgärtner 1998).

seasonally humid climate, or by in-situ transformation of Al-Fe smectite to Fe-illite during cyclic wetting by marine waters and drying (Deconinck & Strasser 1987). One single seam of green marls was found in the Early Tithonian (medium-scale sequence 7), whereas they are rather common in Berriasian times (top medium-scale sequence 18 and up; see also Deconinck & Strasser 1987).

(Incipient) palaeosols

The existence, or non-existence of palaeosols is basically a question of exposure time. If the climate is desert-like, no soil will develop at all. In all other cases, the climate determines the type of palaeosol (e.g., Wright 1986, Wright & Tucker 1991), with clayey palaeosols typical for more humid climates and carbonate palaeosols (calcretes) more typical for semiarid climates. Traces of incipient pedogenesis are found in the Late Kimmeridgian and Early Tithonian (medium-scale sequence 4, top of medium-scale sequences 7 and 11, base of medium-scale sequence 12; cf. Pl. 10/2-4). After their absence in the Middle Tithonian, they reappear in the Late Tithonian (top of medium-scale sequences 16). From the Early and Middle Berriasian onwards (medium-scale sequence 21 and up), incipient palaeosols and calcretes (cf. Strasser & Davaud 1982) become more and more abundant and thicker (Fig. 8.3). The thin, red-brown carbonaceous clays that are found at the top of the Dôle section together with thin, laminated cornieules (cf. Pl. 16/2a) show features similar to the "Basal Dirt Beds" of the English Purbeck. Francis (1986) interprets the red-brown colour as an indicator for a Mediterranean-style climate. Other incipient marly but thicker palaeosols are found higher up in the Early Berriasian (this study and Strasser 1994). According to E.J. Anderson (pers. comm.), also the boundary interval between the Goldberg and the Pierre-Châtel Formations (Fig. 4.19 and Pl. 20/4) is a relatively well-developed palaeosol. It consists of a dark grey to brown carbonaceous marl matrix with nodular texture, incorporating blackened and non-blackened limestone pebbles with a diameter of up to 20 cm. It thus resembles the "Great Dirt Bed" that marks the base of the Purbeckian *sensu anglico* in Dorset, southern England. Francis (1986) interprets this as a rendzina-like palaeosol. Moreover, Hillgärtner (1999) reports frequent incipient clayey palaeosols and even a coal seam from the Middle and Late Berriasian of the Swiss and French Jura Mountains (cf. Fig. 8.3).

Freshwater flora

In parallel to the temporal distribution of palaeosols and green marls in the upper part of the studied interval, the frequency of freshwater flora (charophytes) increases in Berriasian times, beginning with medium-scale sequence 19.

Evaporites

Sabkha deposits occur repeatedly during the Kimmeridgian and Tithonian. However, they are usually thin and mark the sequence boundaries or early transgressive deposits of small- or medium-scale sequences. A thick succession of sabkha deposits is found in the Early Berriasian of the Dôle section (medium-scale sequences 21 and 22), followed by a major collapse breccia that indicates the former existence of massive evaporites. Similar, but smaller, collapse breccias are found in the upper part of the Lieu section (medium-scale sequence 17 and up). The presence of evaporites, either in sabkha facies or massive deposits, is a sure indicator for at least seasonally arid conditions. In the sabkhas, arid conditions in the hinterland are additionally indicated by layers of windblown quartz silt (cf. Chap. 2.3.4).

Dedolomitization

The collapse breccias of the Dôle and Lieu sections are accompanied by massive type-2 dedolomitization. This type of dedolomitization is interpreted to have been caused by the flushing of sediments with meteoric waters during emersion (cf. Chap. 3). Type-2 dedolomitization is completely absent in the Late Kimmeridgian. This is probably due to the Kimmeridgian long-term transgressive trend that did not allow for longer emersions. Yet, some isolated dedolomitized beds are found in the Early and Middle Tithonian (medium-scale sequences 5 and 11).

Summary

The sum of these observations (karst, input of clastics, clay minerals) indicates a warm climate during the Late Kimmeridgian and Early/Middle Tithonian, with gradually increasing aridity. After Parrish (1993), this might indicate the gradual change from a monsoonal to a more Mediterranean-style, winterwet climate.

During the Late Kimmeridgian and earliest Tithonian (up to medium-scale sequence 10), medium- (and/or large-) scale maximum-flooding deposits are regularly represented by dark, dysoxic limestones with an elevated marl content (incl. the lower and upper *virgula* Marls; see Noirvaux, La Dôle, and Cirque des Avalanches sections). As medium-scale sequences are interpreted to reflect the 400 ka eccentricity cycle (cf. Chap. 6), it is possible to explain this pattern as high-frequency climate changes linked to orbital forcing. During the Late Kimmeridgian and earliest Tithonian, maximum-flooding deposits (high sea-level) would thus relate to more humid conditions, whereas sequence-boundary zones (low sea-level) might reflect more arid palaeoclimates. This is similar to the coupling of climate to high-frequency sea-level changes Pittet & Strasser (1998b) observed in the Late Oxfordian of Spain. Wignall & Ruffell (1990) report high-frequency alternations in the K/I ratio (cf. Chap. 5) from Tithonian basin sections in southern England that also might represent high-frequency climate alternations.

In the Late Kimmeridgian, the two *virgula* horizons stick out as the examples for more humid conditions during maximum-flooding. Elevated clay input, a high content of organic matter and pyrite (cf. Pl. 3/11 and 16/4), frequent occurrence of wood in the lower and upper *virgula* Marls (MFs of medium-scale sequences 1 and 5, data from Bläsi 1980, pers. comm. D. Marty and W. Hug, and own observations) indicate an enhanced input of clastics and nutrients, triggered by precipitation in the hinterland (probably the Massif Central). Also, the massive, monospecific appearance of oysters in these strata (own observations, Marty et al. 2003, Bläsi 1980) implies possible variations in the lagoon's salinity level. A rich vertebrate fauna and the existence of large, herbivorous sauropods in times of the deposition of the lower *virgula* Marls (Meyer 1993, Marty et al. 2003) proves the existence of both fresh water and a nearby flora that was sufficient to feed on. The distinct litho- and biofacies of both *virgula* horizons implies that these sediments reflect a change in the carbonate factory. Additionally, the fact that the upper *virgula* Marls define a level of changeover in sedimentation and correlate with distinctive levels such as the "vire à *Hybonotum*" in the Vocontian Basin or with a well developed hardground in the Aquitaine area, France (cf. Chap. 7.3) shows that this change had a widespread impact. Consequently, it is reasonable to assume that the lower and upper *virgula* Marls indicate crises of the carbonate factory (dilution and/or siliciclastic poisoning?) that may have been caused by short-lived, but significant climate changes to more humid conditions.

Around the top of medium-scale sequence 11 (= large-scale SB $Ti2?_{Tethyan}$), the last karst and pedogenetic features are observed before the beginning of the kaolinite minimum zone marks the beginning of the Late Jurassic "dry phase" (Fig. 8.5). During the kaolinite minimum zone, the climate seems to have been fully arid. No sedimentary features or early diagenetic overprints that demand the presence of meteoric water are observed in the studied sections, with one exception: in medium-scale sequence 14 (= SBZ $Ti3_{Tethyan}$), a band of green marls and a black clay seam with plant remains is found in the Dôle section. A bed of type-2 dedolomite marks this level in the Lieu section. This level is not accompanied by a regain in kaolinite (cf. Fig. 5.3). Nevertheless, these indicators suggest that during the kaolinite minimum zone, there was a short flip back to less arid conditions (Fig. 8.3). It is possible that this short period of less arid conditions corresponds to the beginning of Wignall & Ruffell's (1990) "*curious series of 'saw-tooth' fluctuations*" (p. 367)

of unknown origin that is located just above the kaolinite minimum zone (cf. Figs 8.3, 8.4). In Dorset, these high-frequency climate changes are located in the *pectinatus* ammonite zone (Wignall & Ruffell 1990, Hallam et al. 1991). According to the sequence-chronostratigraphic chart of Hardenbol et al. (1998), this coincides with the SBZ $Ti3_{Tethyan}$.

The first small reappearance of kaolinite is located around the boundary between medium-scale sequences 16 and 17 (= large-scale SB $Ti4_{Tethyan}$) (Fig. 5.3), followed by the first massive evaporites in the Lieu section (transgressive deposits overlying SB $Ti4_{Tethyan}$). Medium-scale sequence 18 (= large-scale SB $Ti5_{Tethyan}$) marks the end of the kaolinite minimum zone in the Jura Mountains (cf. Figs 5.3, 8.3). The regain in kaolinite represents the end of fully arid conditions. This is underlined by sedimentary evidence such as the reappearance of green marls (top medium-scale sequence 18), the increasing abundance of charophytes, and massive type-2 dedolomitization (both in medium-scale sequence 19). From medium-scale sequence 21 on up, incipient palaeosols become more and more frequent. However, between SB $Ti5_{Tethyan}$ and SB $Be2?_{Tethyan}$, there are still massive evaporites deposited on the Jura platform.

Later on, SB $Be5_{Tethyan}$ marks the beginning of a period that is defined by more frequent and better developed palaeosols and quartz contents of up to 20% (Hillgärtner 1999). This level represents a change to a hot, humid, and seasonal climate and defines the end of the Late Jurassic/Early Cretaceous "dry phase" (Fig. 8.3).

Schnyder (2003) gives an estimated duration of 9-11 Ma for the Late Jurassic/Early Cretaceous "dry phase". Inferred from cyclostratigraphy, the duration of the dry phase as defined on the Jura platform (SB $Ti2?_{Tethyan}$ to SB $Be5_{Tethyan}$) is 8.4 Ma (Fig. 8.5). However, from field observations and log interpretation, it is evident that the so-called "dry phase" is more complex than has been previously assumed: it can be subdivided into a dry phase *sensu stricto* that is equivalent to the kaolinite minimum zone (SB $Ti2?_{Tethyan}$ to SB $Ti5_{Tethyan}$), followed by a transition phase (SB $Ti5_{Tethyan}$ to SB $Be5_{Tethyan}$) (Fig. 8.5). The dry phase *sensu stricto* is fully arid and lasted about 2.8 Ma, whereas the transition phase is much longer (5.6 Ma) and marked by a gradual change from arid (winterwet?) to semi-arid conditions (cf. Fig. 8.3).

Comparing the desert-like temperature and precipitation data (27°C, < 40 mm/a) assumed by Abbink et al. (2001) to lithologic data from the Late Tithonian to Middle Berriasian of southern England and northern France, Schnyder (2003) questions their correctness. However, for the fully arid "dry phase *sensu stricto*" in the Middle and Late Tithonian, as postulated for the Jura platform, these assumed climate data make sense. Later on, in the transition phase, conditions were arid to semi-arid and winterwet ("Mediterranean"), exactly as proposed by Schnyder (2003) on the basis of his lithologic data.

This existence of two phases is also confirmed by the palynological data of Abbink et al. (2001). Both the temperature and the humidity curves show a gradual development back to less arid and cooler conditions, beginning in the *okusensis* Zone, followed by an abrupt change to more humid conditions in the Middle Berriasian. If it is assumed that palaeoclimatic changes in southern England and the Jura platform were in general simultaneous as proposed in Chapter 7, the Middle Berriasian abrupt drop should correlate with SB $Be5_{Tethyan}$ (cf. Fig. 8.3). However, an exact biostratigraphic correlation is problematic due to the provincialism of Tethyan and Boreal ammonite taxa.

8.3 Possible drivers for regional and local climate change

Between 155 and 135 Ma, i.e. from the base of Kimmeridgian to the base of the Valanginian (Gradstein et al. 1994), Central Europe migrated approximately 5° towards the north. The Russian platform did not move northwards. Yet, a change to drier climate is recorded there, too (Riboulleau et al. 1998, Ruffell et al. 2002). Consequently, the northward drift alone does not account for the climatic variations observed (Schnyder 2003).

If continental drift is not a significant driver for Late Jurassic and Early Cretaceous climate changes, perhaps changes in global circulation patterns were. Perlmutter & Mattews (1989) present a general model of different positions of atmospheric circulation cells during climatic minima and maxima. On the one hand, a temporal northward shift of the subtropical high-pressure belt, located between the Hadley and the Ferrel Cell, may account for a climate change that would have been able to affect both western and eastern Europe but, on the other hand, can not explain other contemporaneous events, e.g., the southward shift of the boundary between Tethyan and Boreal faunal provinces (Zakharov & Rogov 2003, Schudack 1999; cf. Fig. 8.6). The main reason for Late Jurassic faunal provincialism was a long-term (2^{nd}-order) regressive trend during the Tithonian (cf. Fig. 8.3) that had an impact on palaeogeography and created obstacles for free faunal exchange. Yet, also factors such as the distribution of continents, water temperature, and salinity are discussed as causes for provincialism (e.g., Dercourt et al. 1994, Cecca 1999, Price 1999).

Schnyder (2003), on the basis of the sea-level curve of Sneider et al. (1995), mentions a "parallel" evolution of sea level and climate (high sea level = arid climate, Fig.

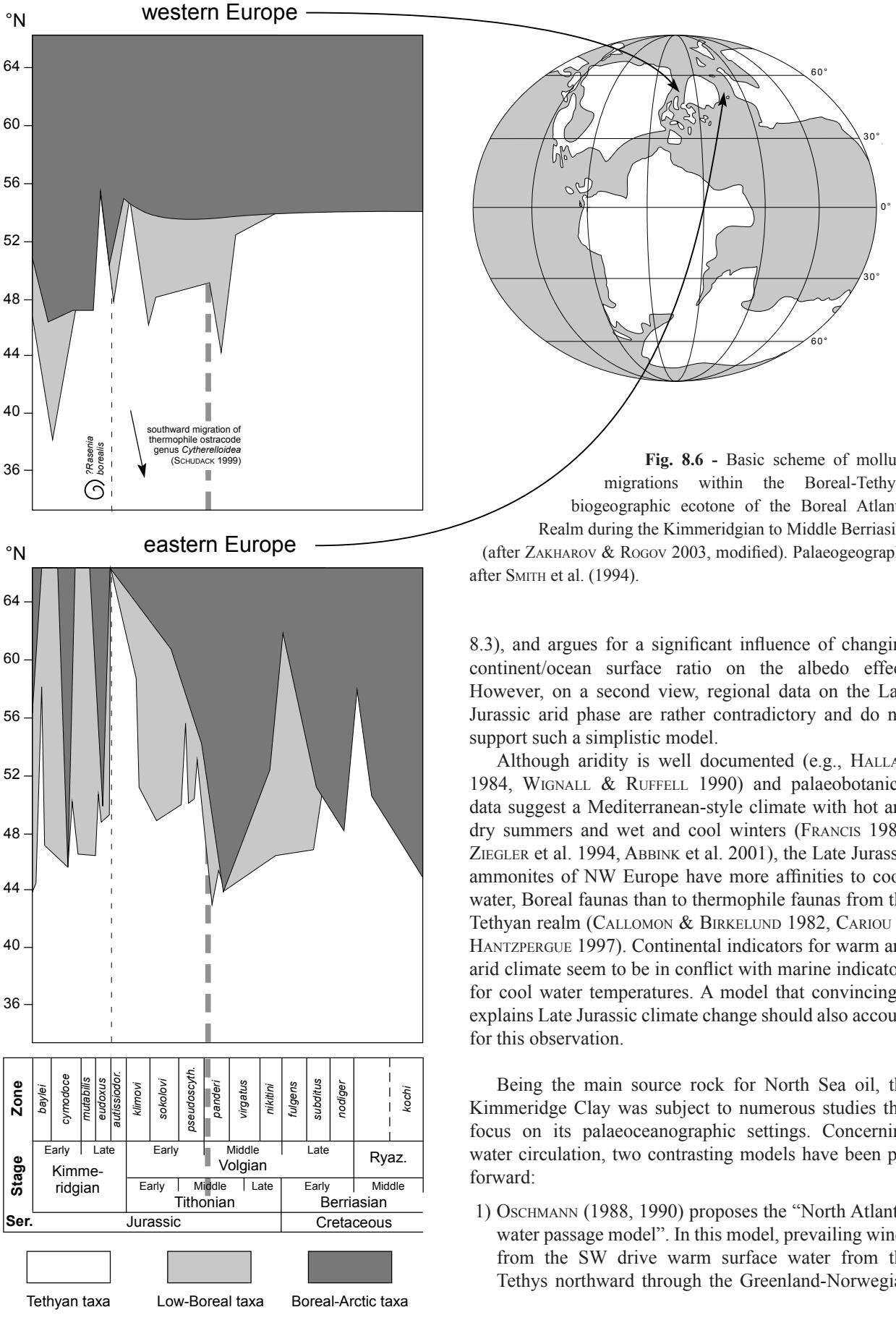

Fig. 8.6 - Basic scheme of mollusk migrations within the Boreal-Tethyan biogeographic ecotone of the Boreal Atlantic Realm during the Kimmeridgian to Middle Berriasian (after Zakharov & Rogov 2003, modified). Palaeogeography after Smith et al. (1994).

8.3), and argues for a significant influence of changing continent/ocean surface ratio on the albedo effect. However, on a second view, regional data on the Late Jurassic arid phase are rather contradictory and do not support such a simplistic model.

Although aridity is well documented (e.g., Hallam 1984, Wignall & Ruffell 1990) and palaeobotanical data suggest a Mediterranean-style climate with hot and dry summers and wet and cool winters (Francis 1984, Ziegler et al. 1994, Abbink et al. 2001), the Late Jurassic ammonites of NW Europe have more affinities to cool-water, Boreal faunas than to thermophile faunas from the Tethyan realm (Callomon & Birkelund 1982, Cariou & Hantzpergue 1997). Continental indicators for warm and arid climate seem to be in conflict with marine indicators for cool water temperatures. A model that convincingly explains Late Jurassic climate change should also account for this observation.

Being the main source rock for North Sea oil, the Kimmeridge Clay was subject to numerous studies that focus on its palaeoceanographic settings. Concerning water circulation, two contrasting models have been put forward:

1) Oschmann (1988, 1990) proposes the "North Atlantic water passage model". In this model, prevailing winds from the SW drive warm surface water from the Tethys northward through the Greenland-Norwegian

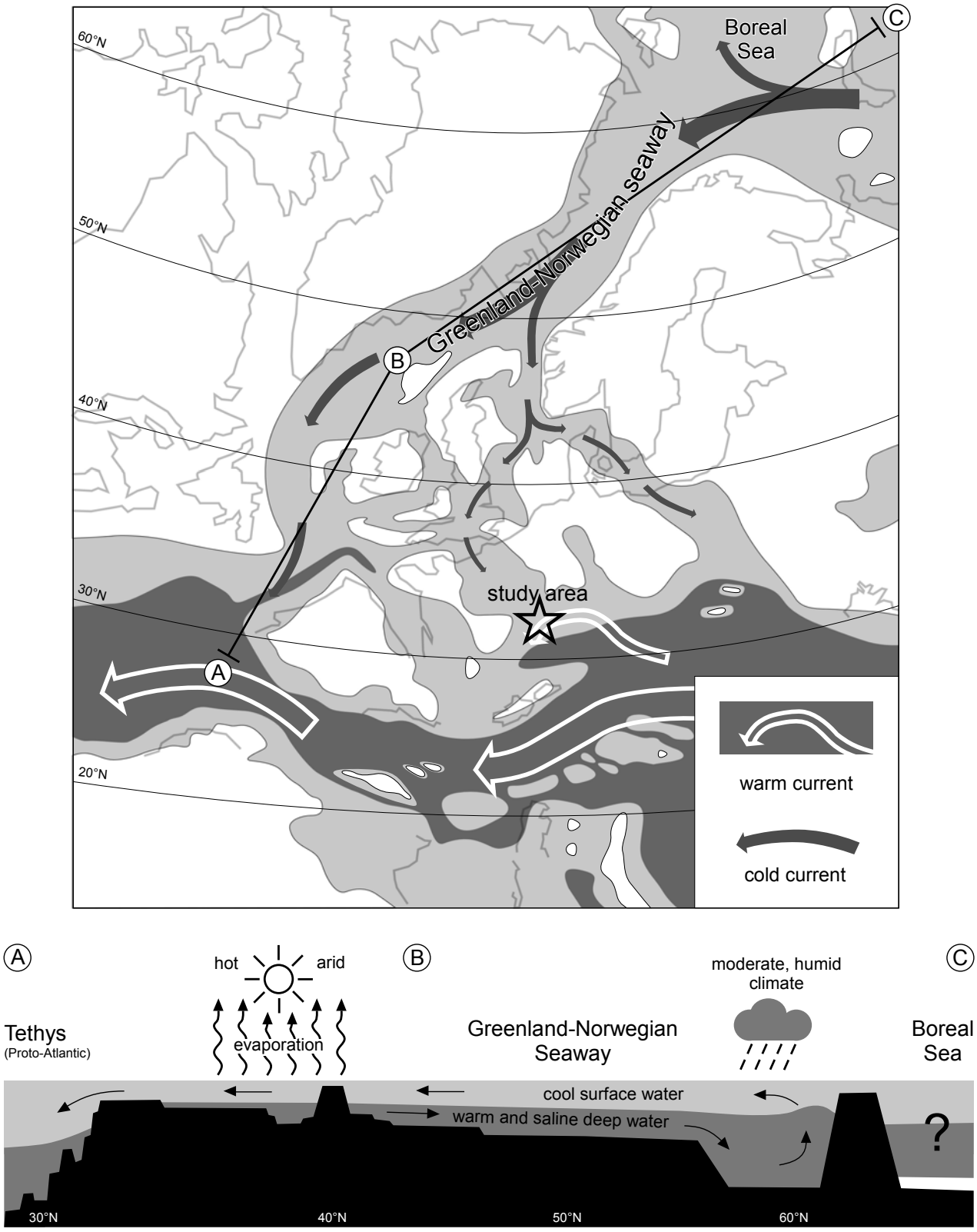

Fig. 8.7 - Palaeogeographic and palaeoceanographic reconstruction for the Early Tithonian (after Abbink et al. 2001). The Jura Platform is located at the northern Tethys margin, between the Vocontian Basin to the south and the Paris Basin to the north. With changing sea-level and/or current patterns, it can be either under the influence of the warm Tethyan current system, or of the cold currents from the north. Palaeogeographic data compiled from Ziegler (1988), Smith et al. (1994), and Thierry et al. (2000).

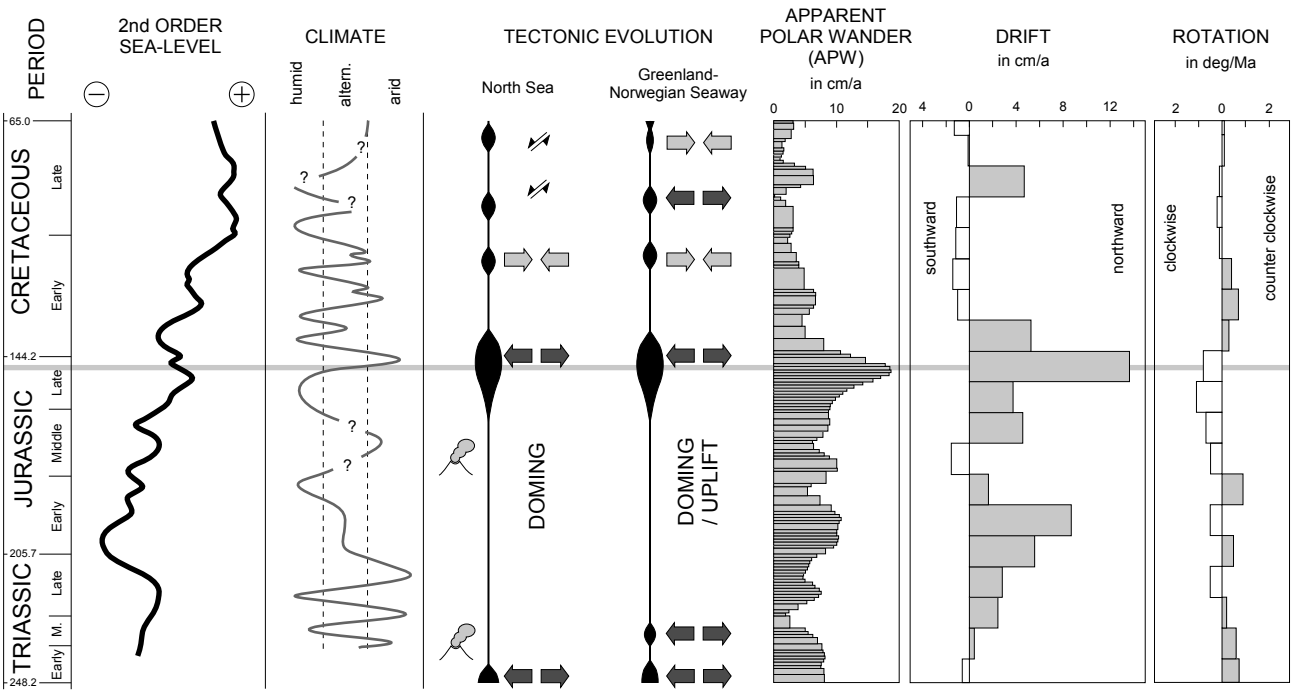

Seaway into the Boreal Sea. This is compensated by a counterflow of boreal, cool deep water to the south.

2) Miller (1991), in contrast, presents a model where cold surface water from the Boreal Sea flows southward to the Tethys. Due to the Coriolis effect, the main flow was concentrated on the western side of the basin (cf. Fig. 8.7). The cold surface flow was countered by a flow of warm and saline deep water to the north, the formation of which was linked to high evaporation in the European archipelago.

The model of Oschmann (1988, 1990) is consistent with seawater temperature estimates (cf. Oschmann 1988). However, low equator-pole temperature gradients do not favour the generation of winds strong enough to drive a water current northwards (Abbink et al. 2001). This model also fails to explain the observed ammonite migrations (Fig. 8.6).

The model favoured in this work is the one of Miller (1991). Southward directed currents transported cold surface water to the European archipelago (Fig. 8.7). There, it significantly affected regional climate: cold surface water, by cooling offshore winds, limits water transport by air and is able to produce an atmospheric inversion. The result would have been arid conditions downwind of the cold ocean. Present-day examples for this type of climate setting are the coastal deserts of Namibia and Nazca in Peru, respectively (Abbink et al. 2001). Miller (1991) and Abbink et al. (2001) argue for strong evaporation at 30-40° northern latitude, producing high-salinity, warm bottom water and humid conditions around 60°N, producing low-salinity, cold surface water, acting as a motor for the conveyor-belt like current pattern in the Greenland-Norwegian Seaway (cf. Fig. 8.7).

The proposed change in ocean current patterns corresponds not only well to the southward shift in the distribution of many ammonite and ostracode species as observed by Zakharov & Rogov (2003) and Schudack (1999) (Fig. 8.6) but also with the climate change from semi-arid winterwet (Kimmeridgian, Early Tithonian) to fully arid (Middle Tithonian) in Central and NW Europe (Wignall & Ruffell 1990, Hallam et al. 1991, Ruffell & Rawson 1994). With the European archipelago lying downwind of the westerly wind expected over the opening North Atlantic (Parrish & Curtis 1982, Moore et al. 1992a, b), it has been proposed that the Late Jurassic "dry phase" was the result of reduced moisture transport due to the cooling effect of the sea surface (Schudack 1999, Abbink et al. 2001).

Moreover, this scenario is consistent with regional clay-mineral data mentioned by Wignall & Ruffell (1990): the temporal evolution of kaolinite abundances in the northern and southern North Sea Basin are different, calling for different source areas (northern North Sea: Fennosarmatia – humid, southern North Sea: European archipelago – arid) but the entire North Sea shares the same subboreal ammonite fauna. According to palaeobotanical data of Barale (1981), Scotland (approx. 45°N, Thierry et al. 2000, cf. Fig. 8.7) was just out of the arid zone. Many plant species present in Scotland are also found in the Jura

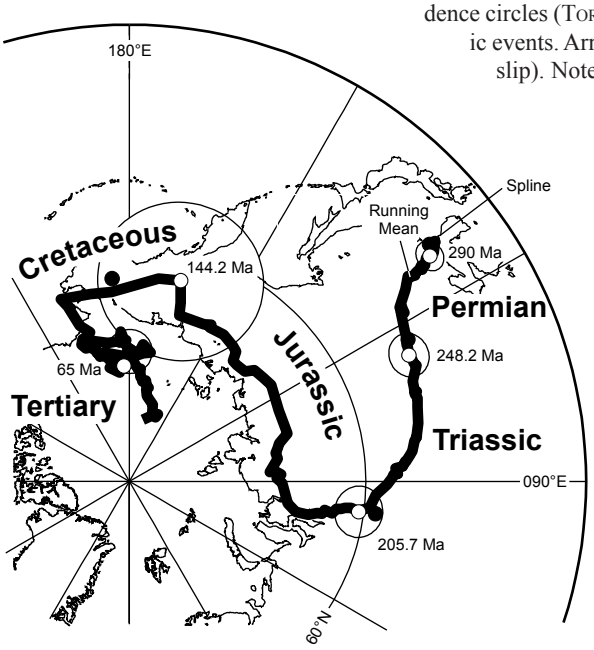

Fig. 8.8 – (this page and facing page) Tectonic evolution of the northern North Atlantic (Brekke et al. 2001), featuring selected relative plate movements (rotation and drift) of a reference point (45°N/270°E) in central North America and apparent polar wander path with selected 95% confidence circles (Torsvik et al. 2002). Black lenses indicate the timing and duration of tectonic events. Arrows indicate sense of tectonic movements (extension/compression/strike slip). Note the contemporaneous extreme events in all parameters, coinciding with the beginning of the Late Jurassic arid phase (gray line). Numerical ages after Gradstein et al. (1994).

Mountains. However, the Scottish flora shows a much higher abundance of pteridosperm and ginkgoal plants, implying less arid conditions there.

According to the current-pattern reconstruction of Abbink et al. (2001), the cold surface current began to influence the European archipelago somewhere during the Early Kimmeridgian *sensu anglico* (= Kimmeridgian *sensu gallico*, 154.1-150.7 Ma), peaked during the Late Kimmeridgian *sensu anglico* (= large parts of the Tithonian 150.7-144.2 Ma), and then collapsed at the base of the Ryazanian (= base Middle Berriasian, 142.0 Ma). This current pattern probably led to the well documented mixture of Boreal and Tethyan ammonite faunas in the Paris Basin from the Late Kimmeridgian until the Early Berriasian. In the Ajoie area of northern Switzerland, a *Rasenia Borealis* was found in the *banné* Member (*mutabilis* Zone) – a species that is usually reported from the east coast of Greenland (pers. comm. W. Hug, G. Schweigert). However, the correct determination of this ammonite is still under discussion (pers. comm. D. Marty).

In both models presented above, the Greenland-Norwegian Seaway plays a central role as a link between the Boreal Sea in the north (cold water reservoir) and the Tethys in the south (warm water reservoir). Consequently, Schudack (1999) proposed the "opening of the proto-North-Atlantic", beginning in the Late Jurassic, as a possible reason for the suggested change in the ocean current. The extensional tectonics that eventually culminate in the opening of the North Atlantic can be subdivided in three major phases: 1) Permian/Triassic, 2) Jurassic/Cretaceous, and 3) Tertiary. In the following, only the Jurassic/Cretaceous extensional phase is discussed in detail.

Initial movements of the Jurassic/Cretaceous extensional phase started at the end of the Middle Jurassic. The major rift process, however, began not before the Late Oxfordian/Early Kimmeridgian. The highest rates of subsidence and block rotations are known from the Middle Tithonian to Berriasian, and they continued intermittently until Berriasian/Valanginian times (Brekke et al. 2001, cf. Fig. 8.8). In East Greenland, the peak activity of the rift process is reported from Middle/Late Tithonian (Surlyk 1990, 1991, 2003). Yet, rifting was not continuous but comprised phases of more intense rifting and block rotation alternating with more tranquil periods of regional subsidence. Also, the main tectonic events appear to have started earlier in the south (Doré 1991, Mosar et al. 2002, Surlyk 2003).

Due to the clockwise rotation of Laurentia (Fig. 8.8), the Late Jurassic rift basins probably had an oblique slip component (Fig. 8.9). This effect is also visible from the small initial southward-drift of Greenland versus Europe in the plate reconstruction of Mosar et al. (2002). Yet, somewhere close to the J/K boundary, Laurentia changed to a counter-clockwise rotation. At the same time, maximum velocities of drift and apparent polar wander are measured, and the path of polar wander changes direction by a striking 90°-switch (Fig. 8.8). All this marks a change in the rifting direction that switches from a N-S oriented axis in the Late Jurassic to a more NE-SW oriented axis in the Early Cretaceous (Fig. 8.9), which goes hand in hand with a change in fabric and stress patterns (Doré et al. 1999).

However, major tectonic events were not exclusively restricted to the boundary region between the Laurentian and Baltic Shields but also concerned southern and eastern Europe: in the interval between the magnetostratigraphic chrons M25 (154.3 Ma, latest Oxfordian) and M21 (147.7 Ma, Middle Tithonian), Iberia began to separate from North America (150.0 Ma, Early Tithonian). This event caused the formation of a new transform plate boundary to the north, between Iberia and Eurasia (Fig. 1.4 and Fig. 8.9), and the progressive transfer of left-lateral motion from the southern boundary (the former shear zone

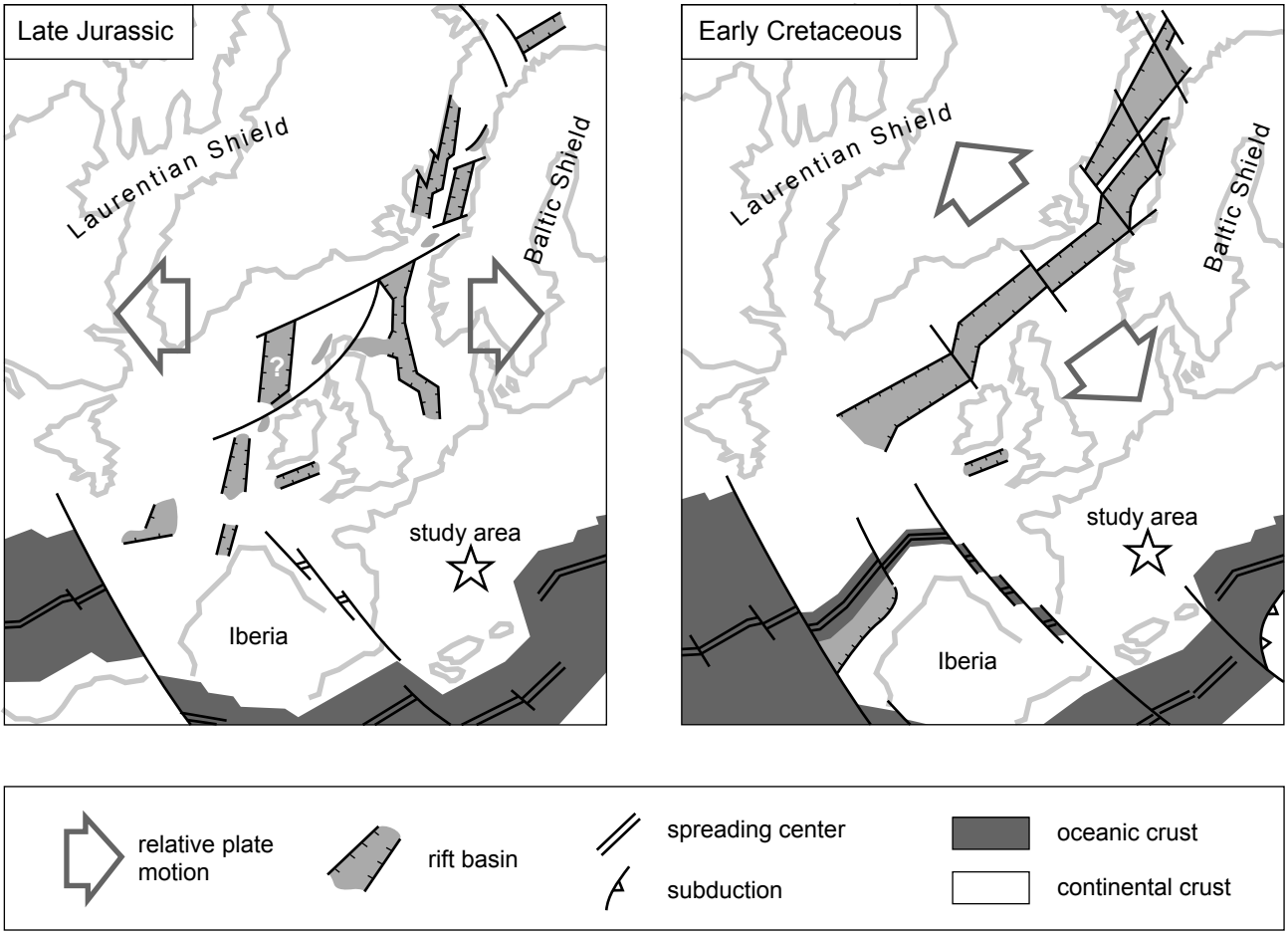

Fig. 8.9 - Plate tectonic sketch indicating the change in relative plate motion and the changes in extensional geometries that happened during the Tithonian. Based on Doré et al. (1999), with modifications in the lower half. The movements of Iberia, the exact location of the Alboran microplate (Corsica and Sardinia), and the geometry and plate kinematics of the Alpine Tethys are interpreted differently in different plate reconstructions (e.g., Stampfli et al. 2002, Schettino & Scotese 2002, Ziegler 1988).

between Iberia and Morocco) to this newly constituted fault system (Schettino & Scotese 2002). By the end of this interval, motion between Iberia and Africa ceased, the spreading center in the Alpine Tethys (Fig. 1.4 and Fig. 8.9) became extinct, and the tectonic regime switched to subduction (Ziegler 1990, Thierry et al. 2000, Stampfli & Borel 2002, Schettino & Scotese 2002).

It becomes clear that the Late Jurassic, and specifically the J/K boundary interval, was a time of major plate-tectonic reorganization and that all the events described above happened more or less contemporaneously to the Late Jurassic "dry phase" in NW and Central Europe (Fig. 8.8).

As mentioned above, the extensional tectonics led to a complex pattern of rotated blocks in the Greenland-Norwegian Seaway that surely influenced palaeoceanography and current patterns. Moreover, Surlyk (1990, 1991, 2003) reports the formation of deep half-grabens in East Greenland during the culmination of the rift process around the Middle/Late Tithonian. These half-grabens may have been capable of hosting and guiding the required flow of warm and saline deep water to the north that counterbalanced the southward flow of cold surface water (Abbink et al. 2001).

Even if it is difficult to correctly link a high-resolution study such as this work to the rather coarse timing of plate-tectonic reconstructions, it is evident that the very special plate tectonic situation around the J/K boundary, in conjunction with long-term sea-level changes, had the potential to inflict major influence on the oceanic current patterns that are thought to be responsible for the Late Jurassic "dry phase".

Another major impact on world-wide current patterns was caused by the disappearance of the Caribbean barrier in the Late Jurassic (probably somewhere between the Late Oxfordian and the Tithonian, Stephan et al. 1990). Without this barrier, a circumequatorial warm current was

able to build up that seems to have triggered profound modifications in pelagic sedimentation (De Wever et al. 1983). However, it apparently had less impact on climatic conditions in NW and Central Europe.

Considering all the plate-tectonic, palaeobiogeographic, and climate data, a possible scenario could have looked like this:

In Middle Jurassic times, the Greenland-Norwegian seaway was temporarily closed due to major regional uplift and doming (Doré 1991; cf. Fig. 8.8). Yet, from the Callovian onwards, rifting activity re-established a N-S marine connection that was probably not wider than the North Sea grabens (Fig. 8.9) and, due to the intense tectonic activity of the Late Jurassic, resulted in the development of marginal and intra-basinal highs of a complex geometry. The existence of this narrow and ever changing portal between the Baltic and Laurentian shields was the key factor for controlling marine links between Europe and the Boreal Sea (Doré 1991). The transgressive regime during the Oxfordian and Kimmeridgian created a relatively coherent seaway from the north to the south, resulting in faunal unity. In times of highest sea level and maximum extensional movements (Figs 8.3 and 8.8), N-S water exchange through the Greenland-Norwegian seaway was relatively unhindered and the conveyor-belt like current pattern as described by Miller (1991) and Abbink et al. (2001) started up. This caused both a southward migration of Boreal fauna (Schudack 1999, Zakharov & Rogov 2003; Fig. 8.6) and the Late Jurassic "dry phase" in the downwind areas of the European archipelago (Abbink et al. 2001; Fig. 8.7). During the Tithonian long-term regression, the connection became again more and more restricted. Also the progressive development of structural highs and/or lifting of the graben shoulders that increased erosion and thus the input of clastic sediments into the graben system (pers. comm. J. Mosar) probably played important roles.

Widespread emergence (deltaic deposits in England, East Greenland, and Svalbard) implies that the Greenland-Norwegian Seaway was probably closed from Late Berriasian times (mid-*kochi* Zone / *paramimounum* Zone) onwards (Doré 1991). Once more, this fits well with the palaeocurrent reconstruction of Abbink et al. (2001), who report the boreal cold-water influx into the European archipelago to have ceased at the base of the Ryazanian (= base Middle Berriasian, 142.0 Ma). Thus, the European basins fell again under the influence of warm Tethys waters, resulting in a shift back to (sub)tropical, humid climate (Fig. 8.3; see also Mutterlose et al. 2003). This climate shift is also observed on the Jura platform (Hillgärtner 1999).

* * *

9 - Conclusions and outlook

The examined interval reaches from SB $Kim4_{Boreal}$ (152.2 Ma) to SB Be3/4 (141.0 Ma) and covers some 11 Ma. Thus, the primary objective of this study – "filling the gap" between the studies of Colombié (2002) on the Kimmeridgian and Hillgärtner (1999) and Pasquier (1995) on the Early Cretaceous – was fulfilled. The main results of this study are:

1. The stratigraphic record of the measured sections can be subdivided in elementary, small-scale, medium-scale, and large-scale depositional sequences.

2. The upper part of medium- and small-scale sequences is frequently dolomitized ("dolomite caps").

3. Three different types of early diagenetic dolomite were observed in the studied sections that are interpreted to represent three different dolomitization mechanisms: type-1 dolomite ("*matrix dolomite*") makes up most of the volume of dolomite caps and is produced by a reflux-type mechanism. The presence of type-2 dolomite ("*burrow dolomite*") depends on the presence of organic matter in burrow systems and is probably related to microbial mediation. Penecontemporaneous type-3 dolomite ("*tidal-flat dolomite*") forms near the surface of tidal flats by evaporation. All three types can co-exist in one sample. However, the appearance of type-1 and type-3 dolomite is largely restricted to dolomite caps, whereas type-2 dolomite can be found in all stratigraphic positions.

4. Large-scale sequences are equivalent to 3rd-order sequences as defined by, e.g., Vail (1987) and Posamentier et al. (1988, 1992). Small-scale and medium-scale sequences show a stable 4:1 stacking pattern and are interpreted to represent the long and short orbital eccentricity-cycle, respectively (400 and 100 ka). Elementary sequences may in part represent the 20 ka precession cycle but in these high frequencies, the cyclostratigraphic signal is heavily distorted by autocyclic processes, erosion, and/or non-deposition.

5. The most important factors for creating well-developed sequence boundaries at all scales seem to be long-term (2nd-order) sea-level changes that are most probably of tectonoeustatic origin, and cyclic (orbitally forced) high-frequency sea-level fluctuations. Large-scale (3rd-order) sequence boundaries usually consist of well developed medium-scale sequence boundaries and were probably produced by the superposition of long- and short-term trends in sea-level change and/or by regional tectonics (cf. Strasser et al. 2000).

6. An integrated sequence- and cyclostratigraphic timeframe has been established for the Tithonian. The stratigraphic position of large-scale (3rd-order) sequence boundaries generally is in good accordance with the sequence chronostratigraphic chart of Hardenbol et al. (1998). Hardenbol et al. (1998), based on the numerical ages of Gradstein et al. (1994), give a duration of 6.5 Ma for the Tithonian, or a time span of 6.7 Ma for the interval between SB $Kim5_{Tethyan}$ and SB Be1. The duration of the latter interval inferred from cyclostratigraphic analysis (this work) is 6.8 Ma. The developed sequence- and cyclostratigraphic timeframe also shows strong similarities with the results of Bádenas et al. (2004) from NE Spain.

7. Two new large-scale (3rd-order) sequence boundaries can be defined on the Jura platform, filling the gap between $Ti1_{Tethyan}$ and $Ti2?_{Tethyan}$ (cf. Tab. 6.2). However, no correlative (un)conformities were found in the measured slope- and basin sections.

8. Biostratigraphically well-defined basin sections are linked to the sedimentary record of the Jura platform by a large-scale sequence-stratigraphic framework. This allows for a verification of the established sequence- and cyclostratigraphic timeframe.

9. A high-resolution correlation linked to the established sequence- and cyclostratigraphic timeframe gives evidence of isochronous events and changes in sedimentary architecture and of the diachronous nature of massive evaporite deposits on the Jura platform in the Late Tithonian/Early Berriasian. It is probable that on the regional scale (north-western margin of the Alpine Tethys), several key horizons correlate with outstanding stratigraphic horizons that are reported from other studies.

10. Judging from the high-resolution correlation and the cycle architecture, and considering accelerated subsidence rates and low amplitudes of orbitally induced high-frequency sea-level changes, the deposition- and preservation potential for high-frequency sequences ("cycles") is rather high. In terms of medium- and small-scale sequences, the stratigraphic record can be regarded as complete.

11. Clay mineral analysis reveals a Middle to Late Tithonian episode with very low abundance of kaolinite ("kaolinite minimum zone"). The low abundance of kaolinite is interpreted as the "Late Jurassic dry phase" that is known from all over Europe.

12. Sequence-, bio- and chronostratigraphic evidence support the theory that the beginning of the kaolinite minimum zone in the Jura Mountains is isochronous to the beginning of the kaolinite minimum zone in Dorset, southern England. Both depositional areas most probably share the same source area(s): the Massif Central/Armorican Massif and the London-Brabant-Rhenish Massif.

13. The different out-of-phase relationships of kaolinite/illite-ration and illite crystallinity in the three measured sections may be an additional hint to the Massif Central being the source area of clay minerals.

14. The duration of the Late Jurassic dry phase in the Jura Mountains is inferred to have lasted 8.4 Ma from cyclostratigraphy. Based on several sedimentological, diagenetic, geochemical, palaeontological, and pedologic indicators, the dry Late Jurassic phase can be subdivided into a dry phase *sensu stricto* and a transition phase. The dry phase *sensu stricto* lasted approximately from $Ti2?_{Tethyan}$ to $Ti5_{Tethyan}$ (2.8 Ma) and was characterized by a fully arid, probably desert-like climate. The transition phase lasted approximately from $Ti5_{Tethyan}$ to $Be5_{Tethyan}$ (5.6 Ma) and represents a gradual change from fully arid to (semi)arid (winterwet?) conditions.

15. The dramatic climatic shift that marks the beginning of the Late Jurassic dry phase was probably caused by a change in oceanic current patterns that resulted in the introduction of Boreal cold surface water to the proto-North-Atlantic and the European archipelago (Miller 1991, Abbink et al. 2001). Palynological data, as well as the penecontemporaneous southward migration of Boreal and thermophile taxa, support the scenario. These major changes in Earth's hydrological and atmospheric system were probably linked to plate tectonic processes during the Late Jurassic and Early Cretaceous that led to the opening of the North Atlantic.

Now that the present study is finished, a continuous high-resolution (100 ka, locally 20 ka) timeframe from the Late Oxfordian to the Early Valanginian can be set up for the Swiss and French Jura Mountains. However, due to the repeatedly mentioned problems with biostratigraphic control and outcrop availability, the Tithonian stage is probably the weakest link in the chain of PhD theses that stretches over 22 Ma from the Late Oxfordian to the Valanginian (cf. Fig. 1.1). Specifically the upper part of the studied interval (SB Be1 to SB Be3/4) is very difficult to interpret in terms of cyclostratigraphy. Consequently, additional platform sections in the upper part of the Twannbach and the Goldberg Formation would be of great use, but they are virtually non-existent, so that perhaps independent methods like magnetostratigraphy and Sr isotopes could help to back up the developed sequence- and cyclostratigraphic timeframe for this critical interval.

Nevertheless, the huge amount of sedimentologic and stratigraphic data available within this high-resolution timeframe will serve as an invaluable basis for detailed follow-up studies in the future. E.g., selected time intervals, where the durations of each depositional sequence are known, can now be studied in great detail in order to tackle palaeoecological questions like the influence of terrigenous run-off (siliciclastics and nutrients) on carbonate ecosystems, and how carbonate platforms relate to global biogeochemical cycling.

It is also a perfect basis for quantification and modelizations that will help to clarify, e.g., the amplitudes and rates of change of orbitally forced sea-level fluctuations under Mesozoic greenhouse conditions and the sediment fluxes across a shallow-water platform, as

well as from the platform into the basin. This goes hand in hand with questions about the potential of organic carbonate productivity to keep up with relative sea-level rise, about the influence of various palaeoecological settings, or about modelling early diagenesis and fluid flow driven by high-frequency sea-level changes. Studies that treat the huge volume of available microfacies data with multivariate statistics might lead to new insights into microfacies analysis, palaeoecology, and the change of depositional conditions through time.

It would also be interesting to use the Jura platform as a reference for high-resolution correlations. The comparison of the developed timeframe with sections from NE Spain (Bádenas et al. 2004) is a first encouraging example that can surely be repeated in other locations along the northwestern margin of the Alpine Tethys once local high-resolution studies have been established. In terms of neighbourhood and the existence of high resolution studies, the Swabian Jura (Pawellek 2001, Pawellek & Aigner 2003a, b, Ruf et al. *in press*) is definitely the most evident and promising candidate for correlations in the Oxfordian to lowermost Tithonian, as already shown by Pittet & Strasser (1998). However, for the Tithonian, there are other promising localities, e.g., the Helvetic Alps of eastern Switzerland (cf. Funk et al. 1993, Mohr & Funk 1995, Padden et al. 2002) or the Northern Calcareous Alps of Austria (Schagintweit & Ebli 1999, Missoni et al. 2001, Schlagintweit et al. 2002)

Tethyan-Boreal correlation is one of the long-standing problems in European stratigraphy. Its solution would surely lead to a better understanding of the factors – such as different subsidence, sediment production and accumulation patterns – which are probably responsible for the discrepancies that exist between the sequence stratigraphic interpretations of both realms. With the correlation potential of the base of the kaolinite minimum zone, the present study furnishes another stratigraphic tie point in the Middle Tithonian (cf. Colombié & Rameil *submitted*). As shown in Chapter 7 and 8, regional climate changes and their impact on the sedimentary record are a promising linking factor.

In order to better understand the deposition of clay minerals, the analysis of which is one of the most important tools for palaeoclimatology, it would be interesting to run a regional study around the Massif Central. This could give new insights into the delay between formation and deposition, and the transportation processes that inevitably differ between the Jura Mountains and Dorset. Yet, the essential problem of such a study would be the unfavourable outcrop situation in eastern France and Switzerland. Nevertheless, based on the high-resolution timeframe established in the Jura Mountains and similar studies, e.g., in the Kimmeridge Clay of southern England, it may become possible to reconstruct Mesozoic climate change (linked to orbital forcing and plate tectonics?) on a regional scale with a temporal resolution comparable to that of Tertiary/Quarternary studies.

As a closing remark, I want to say that it can not and has not been the scope of this study to solve all the problems related to Late Jurassic/Early Cretaceous stratigraphy but I hope to have posed some of the right questions, or at least to have given some new impulses to pose the right questions in the future. If in 25 years, the present work will be of the same use for future researchers as the work of Bläsi (1980) was for me, I will be very pleased.

"*Truth in science can be defined as the working hypothesis best suited to open the way to the next better one*."

Konrad Lorenz

* * *

References

Abbink, O., Taragona, J., Brinkhuis, H. & Visscher, H. (2001) Late Jurassic to earliest Cretaceous palaeoclimatic evolution of the southern North Sea. Global Planet. Change 30, 231-256.

Adams, J.E. & Rhodes, M.L. (1960) Dolomitization by seepage refluxion. AAPG Bulletin 44, 1912-1920.

Adatte, T. (1988) Etude sédimentologique, minéralogique, micropaléontologiqueet stratigraphique du Berrasien-Valanginien du Jura central. PhD thesis, University of Neuchâtel.

Adatte, T. & Rumley, G. (1989) Sedimentology and mineralogy of the Valanginian and Hauterivian in the stratotypic region. In: Wiedmann, E. (ed) Cretaceous of the Western Tethys: Proceedings of the 3rd Int. Cretaceous Syposium, Tübingen. (Schweizerbart)

Adatte, T. & Rumley, G. (1984) Microfaciès, minéralogie, stratigraphie et évolution des milieux de dépots de la plate-forme berriaso-valanginienne des régions de Ste-Croix (VD), Cressier et du Landeron (NE). Bull. Soc. neuchât. Sci. nat., 107, 221-239.

Allan, J.R. & Matthews, R.K. (1982) Isotope signatures associated with early meteoric diagenesis. Sedimentology 29, 797-817.

Allan, J.R. & Matthews, R.K. (1977) Carbon and oxygen isotopes as diagenetic and stratigraphic tools: surface and subsurface data, Barbados, West Indies. Geology 5, 16-20.

Allen, P. (1998) Purbeck-Wealden (Early Cretaceous) climates. Proc. Geol. Assoc. 109, 197-236.

Alonso-Zarza, A.M. (1999) Initial stages of laminar calcrete formation by roots: examples from the Neogene of central Spain. Sedimentary Geology 126, 177-191.

Al-Shaieb, Z. & Lynch, M. (1993) Palaeokarstic features and thermal overprints observed in some of the Arbuckle cores in Oklahoma. SEPM Core Workshop No. 18, 11-59.

Arnaud, M. et al. (25 co-authors) (1984) Jurassique supérieur: Malm. In: Debrand-Passard, S., Courbouleix, S. & Lienhardt, M.J. (eds) Synthèse géologique du Sud-Est de la France. Vol. I. Stratigraphie et paléogéographie. Mém. Bur. Rech. géol. min. 125, 223-286.

Arnott, R.W.C. (1995) The parasequence definition—are transgressive deposits inadequately addressed?

Atrops, F. (1994) Kimmeridgian. Géobios Mém. Spéc. 17, 767-769.

Atrops, F., Gygi, H.-R., Matyja, B.A. & Wierzbowski, A. (1993) The *Amoeboceras* faunas in the middle Oxfordian-lowermost Kimmeridgian, subMediterranean succession, and their correlation value. Acta Geol. Polonica 43, 213-227.

Aubert, D. (1950a) Un niveau à *Exogyra virgula*, Defr. à la vallée de Joux. Bull. Soc. Vaud. Sc. Nat. 57, 477-478.

Aubert, D. (1950b) Nouvelles observations sur le niveau à *Exogyra virgula*, dans le Jura. Bull. Lab. Géol. Min. Géophys. et Musée Géol. Univ. Lausanne 95, 6 pp.

Aubert, D. (1943) Monographie géologique de la Vallée de Joux (Jura Vaudois). Matér. Carte géol. Suisse N.S. 78.

Aubert, D. (1941) Vallée de Joux, Geologischer Atlas der Schweiz 1 : 25 000, Blatt 17.

Aurell, M., Robles, S., Bádenas, B., Rosales, I., Queseda, S., Meléndez, G. & García-Ramos, J.C. (2003) Transgressive–regressive cycles and Jurassic palaeogeography of northeast Iberia. Sed. Geol. 162, 239-271.

Azerêdo, A.C., Wright, V.P. & Ramalho, M.M. (2002) The Middle–Late Jurassic forced regression and disconformity in central Portugal: eustatic, tectonic and climatic effects on a carbonate ramp system. Sedimentology 49, 1339-1370.

Bádenas, B. & Aurell, M. (2001a) Kimmeridgian palaeogeography and basin evolution of northeastern Iberia. Palaeogeogr., Palaeoclim., Palaeoecol. 168, 291-310.

Bádenas, B. & Aurell, M. (2001b) Proximal–distal facies relationships and sedimentary processes in a storm dominates carbonate ramp (Kimmeridgian, northwest of the Iberian Ranges, Spain). Sed. Geol. 139, 319-340.

Bádenas, B., Aurell, M., Rodríguez-Tovar, F.J. & Pardo-Igúzquiza, E. (2003) Sequence stratigraphy and bedding rhythms of an outer ramp limestone succession (Late Kimmeridgian, Northeast Spain). Sed. Geol. 161, 153-174.

Bádenas, B., Salas, R. & Aurell, M. (2004) Three orders of regional sea-level changes control facies and stacking patterns of shallow platform carbonates in the Maestrat Basin (Tithonian-Berriasian, NE Spain). Int. J. Earth Sciences (Geol. Rundsch.) 93, 144-162.

Balog, A., Read, J.F. & Haas, J. (1999) Climate-controlled early dolomite, Late Triassic cyclic platform carbonates, Hungary, Journal of Sedimentary Research 69, 267-282.

Banner, J.L., Hanson, G.N. & Meyers, W.J. (1988) Determination of initial Sr isotopic compositions of dolostones from the Burlington-Keokuk Formation (Mississippian) constraints from cathodoluminescence, glauconite paragenesis, and analytical methods. J. Sed. Petr. 58, 673-687.

Barale, G. (1981) La paléoflore jurassique du Jura français: étude systématique, aspects stratigraphiques et paléoécologiques. Doc. Lab. Géol. Fac. Sci. Lyon 81, 467 pp.

Barron, E.J. & Moore, G.T. (1994) Climate model application in palaeoenvironmental analysis. SEPM Short Course No. 33.

Barron, E.J., Fawcett, P.J., Pollard, D. & Thompson, S. (1993) Model simulations of Cretacous climate: the role of geography and carbon dioxide. Phil. Trans. Soc. London B341, 307-316.

Bartolini, A., Baumgartner, P.O. & Hunziker, J. (1996) Middle and Late Jurassic carbon stable-isotope stratigraphy and radiolarite sedimentation of the Umbria-Marche Basin (Central Italy). Eclogae geol. Helv. 89, 811-844.

Bassoulet, J.P., Bernier, P., Conrad, M.A., Deloffre, R. & Jaffrezo, M. (1978) Les algues dasycladales du Jurassique et du Crétacé. Géobios Mém. Spec. 2, 21-329.

Bassoulet, J.P., Bernier, P., Deloffre, R., Genot, P., Jaffrezo, M. & Vachard, D. (1979) Essai de classification des dasycladales en tribus. In: Poignant, A.F. & Deloffre, R. (eds) Second International Symposium on Fossil Algae. Bull. Cent. Rech. Explor. Prod. Elf-Aquitaine 3, 429-442.

Bathurst, R.G.C. (1966) Boring algae, micrite envelopes and lithification of molluscan biosparites. Geological Journal 5, 15-32.

Beaudoin, B. (1977) Méthodes d'analyse sédimentaire et reconstitution du bassin : Le Jurassique terminal – Berriasien des chaînes subalpines méridionales. PhD thesis, Université de Caen, 339 pp. + 139 pp. annex.

Benzaggagh, M. (2000) Le Malm supérieur et le Berriasien dans le prérif interne et le Mésorif (Rif, Maroc): Biostratigraphie, lithostratigraphie, paléogéographie et évolution tectono-sédimentaire. Docum. Lab. Géol. Lyon 152, 347 pp.

Benzaggagh, M. & Atrops, F. (1995) Répartition stratigraphique des principales espèces de « microproblématiques » dans le Malm supérieur-Berriasien du Prérif interne et du Mésorif (Maroc). Biozonation et corrélation avec les zones d'ammonites et de calpionelles. C. R. Acad. Sci. Paris sér. IIa 322, 661-668.

Berger, A. (1988) Milankovitch theory and climate. Rev. Geophys. 26, 624-657.

Berger, A. & Loutre, M.F. (1994) Astronomical forcing through geological time. In: De Boer, P.L. & Smith, D.G. (eds) Orbital forcing and cyclic sequences. IAS Spec. Publ. 19, 15-25. (Blackwell)

Berger, A., Loutre, M.F. & Dehant, V. (1989) Astronomical frequencies for pre-Quarternary palaeoclimate studies. Terra Nova 1, 474-479.

Berner, R.A. (1994) GEOCARB II: a revised model of the atmospheric CO_2 over Phanerozoic times. Amer. J. Sci. 294, 56-91.

Berner, R.A. (1989) Biogeochemical cycles of carbon and sulfur and their effects on atmospheric oxygen over Phanerozoic times. Palaeogeogr., Palaeoclim., Palaeoecol. 75, 97-122.

Berner, R.A. & Lasaga, A.C. (1989) Modeling the geochemical carbon cycle. Scientific American March 1989, 54-61.

Berner, R.A., Lasaga, A.C. & Garrels, R.M. (1983) The carbonate-silicate geochemical cycle and its effect on atmospheric carbon dioxide over the past 100 million years. Amer. J. Sci. 283, 641-683.

Bernier, P. (1984) Les formations carbonatées du Kimméridgien et du Portlandien dans le Jura méridional. Stratigraphie, micropaléontologie, sédimentologie. – Thèse, Université de Lyon, Docum. Lab. Géol. Lyon 92, 803 pp.

Bernier, P. & Gaillard, C. (1980) Bioconstructions du Jura méridional. Géobios Mém. spécial 4, 55-75.

Bhattacharya, J.P. (1993) The expression and interpretation of marine flooding surfaces and erosional surfaces in core; examples from the Late Cretaceous Dunvegan Formation, Alberta foreland basin, Canada. SEPM Spec. Publ. 18, 125-160.

Bläsi, H. (1980) Die Ablagerungsverhältnisse im "Portlandien" des schweizerischen und französischen Juras. PhD Thesis, University of Berne, 153 pp.

Blau, J. & Grün, B. (1997) Late Jurassic/Early Cretaceous revised calpionellid zonal and subzonal division and correlation with ammonite and absolute time scales. Mineralia Slov. 29, 297-300.

Böhm, F. (2003) Required but disguised: environmental signals in limestone-marl alternations. Palaeogeogr., Palaeoclim., Palaeoecol. 189, 161-178.

Bolliger, W. & Burri, P. (1970) Sedimentologie von Schelf-Carbonaten und Beckenablagerungen im Oxfordien des zentralen Schweizer Jura. – Beitr. geol. Karte Schweiz (N. F.) 140.

Bombadiere, L. (1998) Distribution of dedimentary organic matter and sequence stratigraphy in the Late Jurassic carbonates of southeast France. Terre & Environnement 14, 145pp.

Bombadiere, L. & Gorin, G.E. (2000) Stratigraphical and lateral distribution of sedimentary organic matter in Late Jurassic carbonates of SE France. Sedimentary Geology 132, 177-203.

Bombadiere, L. & Gorin, G.E. (1998) Sedimentary organic matter in condensed sections from distal oxic environments: examples from the Mesozoic of SE France. Sedimentology 45, 771-788.

Bosence, D.W.J., Wood, J.L., Rose, E.P.F. & Qing, H. (2000) Low- and high-frequency sea-level changes control peritidal carbonate cycle facies and dolomitization in the Rock of Gibraltar (Early Jurassic, Iberian Peninsula). J. Geol. Soc. London 157, 61-74.

Bosscher, H. & Schlager, W. (1993) Accumulation rates of carbonate platforms, Journal of Geology 101, 345-355.

Bouchette, F., Séguret, M. & Moussine-Pouchkine, A. (2001) Coarse carbonate breccias as a result of water-wave cyclic loading (uppermost Jurassic - South-East Basin, France). Sedimentology 48, 767-789.

Bourgéat, E. (1888) Recherches sur les formations coralligènes du Jura méridional. 181 pp. (Savy & Lefort)

Bowen, G.J. & Wilkinson, B.H. (2002) Spatial distribution of ä^{18}O in meteoric precipitation. Geology 30, 315-318.

Bradley, W.H. (1929) The warves and climate of the Green River epoch. U.S. Geol. Survey Professional Paper 158, 87-110.

Brekke, H., Sjulstad, H.I., Magnus, C. & Williams, R.W. (2001) Sedimetary environments offshore Norway – an overview. In: Martinsen, O.J. & Dreyer, T. (eds) Sedimetary environments offshore Norway – Palaeozoic to Recent. . Norwegian Petroleum Soc. Spec. Publ. 10, 7-37. (Elsevier)

Budd, D.A. (1997) Cenozoic dolomites of carbonate islands: their attributes and origin. Earth Sci. Rev. 42, 1-47.

Budd, D.A., Gaswirth, S.B. & Oliver, W.L. (2002) Quantification of macroscopic subaerial exposure features in carbonate rocks. J. Sed. Res. 72, 917-928.

Budd, D.A., Saller, A.H. & Harris, P.M. (1995) Unconformities and porosity in carbonate strata. AAPG Memoir 63, 313pp.

Bulot, L.G. (1995) Les formations à ammonites du Crétacé inférieur dans le sud-est de la France (Berriasien à Hauterivien): biostratigraphie, paléontologie et cycles sédimentaires. PhD thesis, Université de Grenoble, 375 pp.

Buonocunto, F.P., D'argenio, B., Ferreri, V. & Sandulli, R. (2000) Orbital cyclostratigraphy and sequence stratigraphy of Late Cretaceous platform carbonates at Monte Sant'Erasmo, southern Apennines, Italy. Cretaceous Research 20, 81-95.

Burgess, P.M. (2001) Modeling carbonate sequence development without relative sea-level oscillations. Geology 29, 1127-1130.

Burgess, P.M. & Wright, V.P. (2003) Numerical forward modelling of carbonate platform dynamics: an evaluation of complexity and completeness in carbonate strata. J. Sed. Res. 73, 637-652.

Burgess, P.M., Wright, V.P. & Emery, D. (2001) Numerical forward modelling of peritidal carbonate parasequence development: implications for outcrop interpretation. Basin Res. 13, 1-16.

Burns, S.J., Mckenzie, J. & Vasconcelos, C. (2000) Dolomite formation and biogeochemical cycles in the Phanerozoic. Sedimentology 47 (SupPl. 1), 49-61.

Callomon, J.H. & Birkelund, T. (1982) The ammonite zones of the Boreal Volgian in East Greenland. In: Embry, A.F. & Balwill, H.R. (eds) Arctic geology and geophysics. Canadian Soc. Petrol. Geol. Mem. 8, 349-369.

Canter, K.L., Stearns, D.B., Geesaman, R.C. & Wilson, J.L. (1993) palaeostructural and related palaeokarst controls on reservoir development in the Lower Ordovician Ellenburger Group, Val Verde basin, Texas. SEPM Core Workshop No. 18, 61-99.

Carballo, J.D., Land, L.S. & Miser, D.E. (1987) Holocene dolomitization of supratidal sediments by active tidal pumping, Sugarloaf Key, Florida. J. Sed. Petr. 57, 153-165.

Cariou, E. & Hantzpergue, P. (coord.) (1997) Biostratigraphie du Jurassique ouest-européen et méditerranéen - zonations parallèles et distribution des invertébrés et microfossiles. Bull. Cent. Rech. Explor. Prod. Elf Aquitaine 17, 1-440.

Caron, V., Nelson, C.S. & Kamp, P.J.J. (2004) Transgressive surfaces of erosion as sequence boundary markers in cool-water shelf carbonates. Sed. Geol. 164, 179-189.

Cecca, F. (1999) Palaebiogeography of Tethyan ammonites during the Tithonian (latest Jurassic). Palaeogeogr., Palaeoclim., Palaeoecol. 147, 1-37.

Cecca, F. & Enay, R. (1991) Les ammonites des zones à Semiforme at à Fallauxi du Tithonique de l'Ardèche (Sud-Est de la France) : Stratigraphie, paléontologie, paléobiogéographie. Palaeontographica A219, 1-87.

Cecca, F., Enay, R. & Le Hégarat, G. (1989) L'Ardescien (Tithonique supérieur) de la région stratotypique: séries de référence et faunes (Ammonites, Calpionelles) de la bordure ardéchoise. Docum. Lab. Géol. Lyon 107, 115 pp.

Cecca, F. & Sanantonio, M. (1989) Kimmeridgian and Lower Tithonian ammonite assemblages in the Umbria-Marches-Sabine Apennines (Central Italy). In: Rocha, R.B. & Soares, A.F. (eds) 2nd Int. Symp. on Jurassic Stratigraphy, 1988, 525-542.

Cecca, F. & Zeiss, A. (1994) Kimmeridgian/Tithonian boundary. Géobios Mém. Spéc. 17, 771-772.

Cerling, T.E. (1984) The stable isotopic composition of modern soil carbonate and its relationship to climate. Earth planet. Sci. Letters 71, 229-240.

Chafetz, H.S. (1986) Marine peloids: a product of bacterially induced precipitation of calcite. J. Sed. Res. 56, 812-817.

Chamley, H. (1989) Clay sedimentology. 623 pp. (Springer)

Charollais, J., Davaud, E., Jamet, M. (1996) Evolution du bord oriental de la plate-forme jurassienne entre le Jurassique superieur et l'Oligocene; modele base sur trois forages petroliers (Haute-Savoie); Evolution of the southeastern Jura platform-margin between the Late Jurassic and the Oligocene; new data from three oil wells, Geologie de la France 1996, 25-42.

Chumakov, N.M. & Frakes, L.A. (1997) Mode of origin of dispersed clasts in Jurassi shales: southern part of the Yana-Kolyma fold belt, North East Asia. Palaeogeogr., Palaeoclim., Palaeoecol. 128, 77-85.

Clark, D.N. (1980) The sedimentology of the Zechstein 2 Carbonate Formation of Eastern Drenthe, The Netherlands. Contr. Sedimentology 9, 131-165.

Clavel, B., Charollais, J., Busnardo, R. & Le Hégarat, G. (1986) Précisions stratigraphiques sur le Crétacé inférieur basal du Jura méridional. Eclogae geol. Helv. 79, 319-341.

Cloething, S. (1988) Intraplate stresses: a tectonic cause for third-order cycles in apparent sea-level? In: Wilgus, C.E., Hastings, B.S., Kendall, Ch.G.St.C., Posamentier, H.W., Ross, C.A. & Van Wagoner, J.C. (eds) Sea-level changes – an integrated approach. SEPM Spec. Publ. 42, 21-29.

Colacicchi, R., Passeri, L. & Pialli, G. (1975) Evidences of tidal environment deposition in the Calcare Massiccio Formation (Central Apennines—Lower Lias). In: GINSBURG, R.N. Tidal deposits: a casebook of recent examples and fossil counterparts. 345-353. (Springer)

Colom, G. (1961) La paléoécologie des lacs du Ludien-Stampien inférieur de l'île de Majorque. Rev. Micropal. 1, 17-29.

Colombié, C. (2002) Sédimentologie, stratigraphie séquentielle et cyclostratigraphie du Kimméridgien du Jura Suisse et du Bassin vocontien (France): relations plate-forme – bassin et facteurs determinants. GeoFocus 4, 198pp.

Colombié, C. & Rameil, N. (submitted) Tethyan-to-Boreal correlation in the Kimmeridgian using high-resolution sequence stratigraphy (Vocontian Basin, Swiss Jura, Boulonnais, Dorset).

Colombié, C. & Strasser, A. (2005) Facies, cycles, and controls on the evolution of a keep-up carbonate platform (Kimmeridgian, Swiss Jura). Sedimentology 52, 1207–1227.

Colombié, C. & Strasser, A. (2003) Depositional sequences in the Kimmeridgian of the Vocontian Basin (France) controlled by carbonate export from shallow-water platforms. Géobios 36, 675-683.

Concheryo, A. & Wise Jr., S.W. (2001) Jurassic calcareous nannofossils from prerift sediments drilled during ODP Leg 173, Iberia Abyssal Plain, and their implications for rift tectonics. Proc. ODP, Sci. Results 173, 1-24.

Cotillon, P. (1968) Le Crétacé inférieur de l'Arc subalpin de Castellane, entre l'Asse et le Var: Stratigraphie et sédimentologie. . Mém. Bur. Rech. géol. min. 68, 315 pp.

Cotillon, P. (1974) Sédimentation rythmique et milieux de depot : données fournies par l'étude du Crétacé inférieur de l'Arc subalpin de Castellane (France, SE). Bull. Soc. géol. France 16, 583-592.

Cotillon, P., Ferry, S., Gaillard, C., Jautée, E., Latreille, G. & Rio, M. (1980) Fluctuation des paramètres du milieu marin dans le domaine vocontien (France Sud-Est) au Crétacé inférieur : mise en évidence pas l'étude des formation marno-calcaires alternantes. Bull. Soc. géol. France 22, 735-744.

Courtinat, B. (1989) Les Organoclastes des formations lithologiques du Malm dans le Jura méridional; systématique, biostratigraphie et éléments d'interprétation paléoécologique. Docum. Lab. Géol. Lyon 105, 361 pp.

Cox, B.M. & Gallois, R.W. (1981) The stratigraphy of the Kimmeridge Clay of the Dorset type area and its correlation with some other Kimmeridgian sequences. Inst. Geol. Sci. Report No. 80/4.

Cox, B.M. & Gallois, R.W. (1979) Description of the standard stratigraphical sequences of the Upper Kimmeridge Clay, Ampthill Clay and West Walton Beds. Inst. Geol. Sci. Report No. 78/19, 68-72.

Craig, H. & Gordon, L.I. (1965) Deuterium and oxygen-18 in the ocean and the marine atmosphere. in: Tongiorgi, E. (ed) Stable isotopes in oceanographic studies and palaeotemperatures. Consiglio Nazionale delle Ricerche, Loboratorio de Geologia Nucleare, Pisa, Italy 9-130.

Cross, T.A. (1991) High-resolution stratigraphic correlation from the perspectives of base-level cycles and sediment accommodation. In: Dolson, J. (ed.) Unconformity related hydrocarbon exploration and accumulation in clastic and carbonate settings. Rocky Mountain Assoc. Geol. Short Course Notes, 28-41.

Cross, T.A. & Lessenger, M.A. (1998) Sediment volume partitioning: rationale for stratigraphic model evaluation and high-resolution stratigraphic correlation. In: Gradstein, F.M., Sandvik, K.O. & Milton, N.J. (eds) Sequence stratigraphy – concepts and applications. . Norwegian Petroleum Soc. Spec. Publ. 8, 171-195.

Curtis, C.D. (1990) Aspects of climate influence on the clay mineralogy and geochemistry of soils, palaeosols and clastic sedimentary rocks. J. geol. Soc. London 147, 351-357.

D'Argenio, B. (2004) Cyclostratigraphy: Approaches and case histories. SEPM Spec. Publ. 81, 311pp.

D'Argenio, B., Ferreri, V., Amodio, S. & Pelosi, N. (1997) Hierarchy of high-frequency orbital cycles in Cretaceous carbonate platform strata. Sedimentary Geology 113, 169-193.

D'Argenio, B., Ferreri, V., Raspini, A., Amodio, S. & Buonocunto, F.P. (1999) Cyclostratigraphy of a carbonate platform as a tool for high-precision correlation. Tectonophysics 315, 357-385.

D'Argenio, B., Fischer, A.G., Premoli silva, I., Weissert, H. & Ferreri, V. (eds) (2004) Cyclostratigraphy: approaches and case histories. SEPM Spec. Publ. 81, 311 pp.

D'Argenio, B. & Mindszenty, A. (1995) Bauxites and related palaeokarst: tectonic and climatic event markers at regional unconformities. Eclogae geol. Helv. 88, 453-499.

D'Orbigny, A. (1842-51) Paléontologie Française. Terrain Jurassique, I (Céphalopodes). 642 pp. (Victor Masson)

Dahanayake, K. (1977) Classification of oncoids from the Late Jurassic carbonates of the French Jura. Sedimentary Geology 18, 337-353.

Dauwalder, P. & Remane, J. (1979) Etude du banc à Nérinées à la limite «Kimméridgien-Portlandien» dans le Jura neuchâtelois méridional. Paläont. Z. 53, 163-181.

Davaud, E., Strasser, A. & Charollais, J. (1983) Présence d'horizons calcrétisés dans le Purbeckien du Jura méridional: extension spatiale et conséquences paléogéographiques. C. R. Acad. Sci. Paris 296, 575-578.

De Boer, P.L. & Smith, D.G. (1994) Orbital forcing and cyclic sequences. IAS Spec. Publ. 19, 559 pp.

De Wever, P., Ricou, L.E. & Fourcade, E. (1986). La fin brutale de l'optimum radiolaritique au Jurassique terminal: l'effet de la circulation océanique. C. R. Acad. Sci. Paris, série II, 302, 665-670.

Debrand-Passard, S., Courbouleix, S. & Lienhardt, M.J. (eds) (1984) Synthèse géologique du Sud-Est de la France. Vol. I. Stratigraphie et paléogéographie. Mém. Bur. Rech. géol. min. 125.

Debrand-Passard, S., Courbouleix, S. & Lienhardt, M.J. (eds) (1984) Synthèse géologique du Sud-Est de la France. Vol. II. Atlas. Mém. Bur. Rech. géol. min. 126.

Deconinck, J.-F. (1993) Clay mineralogy of the Late Tithonian - Berriasian deep-sea carbonates of the Vocontian Trough (SE France): relationships with sequence stratigraphy. Bull. Cent. Rech.-ExPl. Elf-Aquitaine 17, 223-234.

Deconinck, J.-F., Beaudoin, B., Chamley, H., Joseph, P. & Raoult, J.-F. (1985) Contrôles tectonique, eustatique et climatique de la sédimentation argileuse du domaine subalpin français au Malm-Crétacé. Rev. Géol. Dyn. Géogr. Phys. 26 (5), 311-320.

Deconinck, J.-F. & Debrabant, P. (1985) Diagenèse des argiles dans le domaine subalpin: rôles respectifs de la lithologie, de l'enfouissement et de la surcharge tectonique. Rev. Géol. Dyn. Géogr. Phys. 26 (5), 321-330.

Deconinck, J.-F., Gillot, P.-Y., Steinberg, M. & Strasser, A. (2001) Syn-depositional, low temperature illite formation at the Jurassic-Cretaceous boundary (Purbeckian) in the Jura mountains (Switzerland and France): K/Ar and $d^{18}O$ evidence. Bull. Soc. géol. France 173, 343-348.

Deconinck, J.-F. & Strasser, A. (1987) Sedimentology, clay mineralogy and depositional environment of Purbeckian green marls (Swiss and French Jura). Eclogae geol. Helv. 80 (3), 753-772.

Deconinck, J.-F., Strasser, A. & Debrabant, P. (1988) Formation of illitic minerals at surface temperatures in Purbeckian sediments (Lower Berriasian, Swiss and French Jura). Clay Minerals 23, 91-103.

Demarest, J.M. & Kraft, J.C. (1987) Stratigraphic record of Quarternary sea-levels: implication for more recent strata. In: Nummedal,

D. (ed.) Sea-level fluctuation and coastal evolution. SEPM Spec. Publ. 41, 223-240.

Demicco, R.V. & Hardie, L.A. (1994) Sedimentary structures and early diagenetic features of shallow marine carbonate deposits. SEPM Atlas Series. 265 pp.

Dercourt, J., Fourcage, E., Cecca, F., Azéma, J., Enay, R., Bassoullet, J.-P. & Cotterau, N. (1994) Palaeoenvironment of the Jurassic system in the western and central Tethys (Toarcian, Callovian, Kimmeridgian, Tithonian): an overview. Géobios Mém. Spéc. 17, 625-644.

Détraz, H., Charollais, J. & Remane, J. (1987) Le Jurassique supérieur-Valanginien des chaînes subalpines septentrionales (massifs des Bornes et de Platé, Haute-Savoie; Alpes occidentales): Analyse des resédimentations, architecture du bassin et influences des bordures. Eclogae geol. Helv. 80 (1), 69-108.

Détraz, H. & Mojon, P.-O. (1989) Evolution paléogéographique de la marge jurassienne de la Téthys du Tithonique-Portlandien au Valanginien: corrélations biostratigraphique et séquentielle des faciès marins à continentaux. Eclogae geol. Helv. 82, 37-112.

Détraz, H. & Steinhauser, N. (1988) Le bassin delphino-helvétique et sa marge jurassienne sous contrôle tectonique entre le Kimmeridgien et le Valanginien. Eclogae geol. Helv. 81/1, 125-154.

Deville, Q. (1991) Stratigraphie, sédimentologie et environnements de depots, et analyse séquentielle dans les terrains entre le Kimméridgien supérieur et le Valanginian du Mont-Salève (Haute-Savoie, France). PhD Thesis, University of Geneva, 141pp.

Doré, A.G. (1991) The structural foundation and evolution of Mesozoic seaways between Europe and the Arctic. Palaeogeogr, Palaeoclimatol., Palaeoecol. 87, 441-492.

Doré, A.G., Lundin, E.R., Jensen, L.N., Birkeland, Ø., Eliassen, P.E. & Fichler, C. (1999) Principal tectonic events in the evolution of the northwest European Atlantic margin. In: Fleet, A.J. & Boldy, S.A.R. (eds) Petroleum geology of Northwest Europe: Proceedings of the 5th Conference. 41-61. (Geol. Soc. London)

Dromart, G. & Atrops, F. (1988) Valeur stratigraphique des biomicrofaciès pélagiques dans le Jurassique supérieur de la Téthys occidentale. C. R. Acad. Sci. Paris 306, 1365-1371.

Dromart, G., Ferry, S. & Atrops, F. (1993) Allochtonous deep-water carbonates and relative sea-level changes: the Late Jurassic - Lowermost Cretaceous of southeast France. SEPM Spec. Publ. 18, 295-305.

Drummond, C.N. & Wilkinson, B.H. (1996) Stratal thickness frequencies and the prevalence of ordererdnessin stratigraphic sequences. J. Geol. 104, 1-18.

Drummond, C.N. & Wilkinson, B.H. (1993) Aperiodic accumulation of cyclic peritidal carbonate. Geology 21, 1023-1026.

Dunham, R.J (1962) Classification of carbonate rocks according to depositional texture. In: Ham, W.E. (ed.) Classification of carbonate rocks. AAPG Mem. 1, 108-121.

Dupraz, C. (1999) Paléontologie, palécologie et évolution des faciès récifaux de l'Oxfordien Moyen-Supérieur (Jura suisse et français). GeoFocus 2, 200 pp.

Dupraz, C. & Strasser, A. (2002) Nutritional modes in coral-microbialite reefs (Jurassic, Oxfordian, Switzerland): evolution of trophic structure as a response to environmental change. palaios 17, 449-471.

Dupraz, C. & Strasser, A. (1999) Microbialites and micro-encrusters in shallow coral bioherms (Middle to Late Oxfordian, Swis Jura Mountains). Facies 40, 101-130.

Eberl, D.D., Srodon, J. & Northrop, H.R. (1986) Potassium fixation in smectite by wetting and drying. In: Davis, J.A. & Hayes, K.F. (eds) Geochemical Processes at Mineral Surfaces. Am. Chem. Soc. Symp. Ser. 323, 14, 296–326.

Einsele, G. (1991) Submarine mass flow deposits and turbidites. In: Einsele, G., Ricken, W. & Seilacher, A. (eds) Cycles and events in stratigraphy. 313-339. (Springer)

Einsele, G. & Ricken, W. (1991) Limestone-marl alternations – an overview. In: Einsele, G., Ricken, W. & Seilacher, A. (eds) Cycles and events in stratigraphy. 23-47. (Springer)

Emberger, L. (ed) (1968) Les plantes fossiles dans leurs rapports avec les végétaux vivants. 758 pp. (Masson & Cie)

Embry, A. (1995) Sequence boundaries and sequence hierarchies: problems and proposals. In: Steel, R. et al. (eds) Sequence stratigraphy on the Northwest European margin. . Norwegian Petroleum Soc. Spec. Publ. 5, 1-11.

Embry, A. (1993) Transgressive-regressive (T-R) sequence analysis of the Jurassic succession of the Sverdrup Basin, Canadian Arctic Archipeloago. Can. J. Earth Sc. 30, 301-320.

Embry, A.F. (1984) Late Jurassic to lowermost Cretaceous stratigraphy, sedimentology, and petroleum geology, Sverdrup Basin. CSPG-CSEG Nat. Conv., 49-50.

Embry, A. & Klovan, J.E. (1971) A Late Devonian reef tract on Northeastern Banks Island, N.W.T. Bull. Canadian Petrol. Geol. 19, 730-781.

Emery, D. & Myers, K.J. (eds) (1996) Sequence stratigraphy. 297pp. (Blackwell)

Enay, R. (2000) Recalage biostratigraphique et nouvelle datation de surfaces d'émersion du Kimméridgien-Tithonien dans le Jura méridional et conséquences sur leur interprétation séquentielle. Bull. Soc. géol. France 171, 665-671.

Enay, R. (1966) Le genre *Gravesia* (*Ammonitina* jurassique) dans le Jura français et les chaînes subalpines, Annales de Paléontologie – Invertébrés 52, 95-105.

Enay, R. (1965) Les formations coralliennes de Saint-Germain-de-Joux (Ain). Bull. Soc. Géol. France 7, 23-31.

Epshteyn, O.G. (1978) Mesozoic-Cenozoic climates of northern Asia and glacial-marine deposits. Int. Geol. Rev. 20, 49-58.

Esteban, M. & Klappa, C.F. (1983) Subaerial exposure environment. In: Scholle, P.A., Bebout, D.G. & Moore, C.H. (eds) Carbonate depositional environments. AAPG Mem. 33, 1-54.

Esteban, M. & Wilson, J.L. (1993) Introduction to karst systems and palaeokarst reservoirs. SEPM Core Workshop No. 18, 1-9.

Eyles, N. (1993) Earth's glacial record and its tectonic setting. Earth Sc. Rev. 35, 1-248.

Étallon, A. (1860) Recherches paléontostatiques sur la chaîne du Jura : Préliminaire à l'étude des polypiers. Arch. Sci. Bibl. Universelle, 32 pp.

Étallon, A. (1858-1859-1861) Etudes paléontologiques sur les terrains jurassiques du Haut-Jura : Monographie de l'étage corallien. Mém. Soc. Emul. Dép. Doubs série III, 1ère partie : vol. VI, 1-164, 2ème partie : vol. III, 1-153.

Étallon, A. (1857) Esquisse d'une description géologique du Haut-Jura et en particulier des environs de St-Claude. Am. Soc. Agric. Hist. Nat. Lyon, 247-354.

Favre, J. (1910) Déscription géologique des environs du Locle et de la Chaux-de-Fonds. Eclogae geol. Helv. 11.

Fischer, A.G. (1991) Orbital cyclicity in Mesozoic strata. In: Einsele, G., Ricken, W. & Seilacher, A. (eds) Cycles and events in stratigraphy. 48-62. (Springer)

Fischer, A.G. (1986) Climatic rhythms recorded in strata. Ann. Rev. Earth planet. Sci. 14, 351-376.

Fischer, A.G., Premoli Silva, I. & De Boer, P.L. (1990) Cyclostratigraphy. In: Ginsburg, R.N. & Beaudoin, B. (eds) Cretaceous resources, events, and rhythms. 139-172.

Flügel, E. (2004) Microfacies of carbonate rocks: Analysis, interpretation and application. 976 pp. (Springer)

Flügel, E. (1982) Microfacies analysis of limestones. 633 pp. (Springer)

Flügel, E. (1974) Fazies-Interpretation der Cladocoropsis-Kalke (Malm) auf Karaburun, W-Anatolien. Arch. Lagerstättenforsch. Ostalp. Sonderband 2 (Festschrift O.M. Friedrich), 79-94.

Flügel, E. (ed) (1977) Fossil algae: Recent results and developments. 375 pp. (Springer)

Flügel, E. & Steiger, T. (1981) An Late Jurassic sponge-algal buildup from the northern Frankenalb, West Germany. SEPM Spec. Publ. 30, 371-397.

Folk, R.L. (1962) Spectral subdivision of limestone types. In: Ham, W.E. (ed.) Classification of carbonate rocks. AAPG Mem. 1, 62-84.

Folk, R.L. & Chafetz, H.S. (2000) Bacterially induced microscale and nanoscale carbonate precipitates. Microbial Sediments 40-49.

Fookes, E. (1995) Development and eustatic control of an Late Jurassic reef complex (Saint Germain-de-Joux, Eastern France). Facies 33, 129-150.

Foos, A. (1996) Comparison of subaerial exposure surfaces at major unconformities and capping shallowing-upward cycles. In: WITZKE, B.J., LUDVIGSON, G.A. & DAY, J. Palaeozoic sequence stratig-

raphy: Views from the North American Craton. Geol. Soc. America Spec. Paper 306, 419-424.
Fouke, B.W., Zwart, E.W., Everts, A.J.W., Schlager, W. (1995) Carbonate platform stratal geometries and the question of subaerial exposure. Sedimentary Geology 97, 9-19.
Fourcade, E., Azema, J., Cecca, F., Dercourt, J., Guiraud, R., Sandulescu, M., Ricou, L.E., Vrielynck, B., Petzold, M. & Cotterau, N. (1993) Late Tithonian. In: Dercourt, J., Ricou, L.E. & Vrielynck, B. (eds) Atlas Tethys – Palaeoenvironmental Maps. (Gauthier-Villars)
Fourcade, E., Azema, J., Cecca, F., Dercourt, J., Guiraud, R., Vrielynck, B., Bellion, Y., Sandulescu, M., Ricou, L.E., Petzold, M. & Cotterau, N. (1993) Late Tithonian (138 to 145 Ma). Atlas Tethys palaeoenvironmental maps. Explanatory notes. 113-134.
Frakes, L.A. (1979) Climates through geologic time. 310 pp. (Elsevier)
Frakes, L.A., Alley, N.F. & Deynoux, M. (1995) Early Cretaceous ice-rafting and climate zonation in Australia. Int. Geol. Rev. 37, 567-583.
Frakes, L.A. & Francis, J.E. (1988) A guide to Phanerozoic cold polar climatesfrom high latitude ice-rafting in the Cretaceous. Nature 333, 547-549.
Frakes, L.A., Francis, J.E. & Sytkus, J.I. (1992) Climate modes of the Phanerozoic: the history of the earth's climate over the past 600 million years. (Cambridge University Press)
Francis, J.E. (1987) The palaeoclimatic significance of growth rings in Late Jurassic/Early Cretaceous fossil wood from southern England. In: Ward, R.G.W. (ed.) Applications of tree-ring studies – Current research in dendrochronology and related subjects. BAR Int. series 333.
Francis, J.E. (1986) The calcareous palaeosols of the basal Purbeck Formation (Late Jurassic), southern England. In: Wright, V.P. (ed.) Palaeosols: their recognition and interpretation. 112-138. (Blackwell)
Francis, J.E. (1984) The seasonal environment of the Purbeck (Late Jurassic) fossil forests. Palaeogeogr., Palaeoclim., Palaeoecol. 48, 285-307.
Frei, E. (1925) Zur Geologie des südöstlichen Neuenburger Jura. Beitr. Geol. Karte Schweiz N.F. 55.
Freytet, P. & Plaziat, J.-C. (1982) Continental carbonate sedimentation and pedogenesis – Late Cretaceous and Early Tertiary of southern France. Contrib. Sed. 12, 212 pp.
Freytet, P. & Verrecchia, E.P. (2002) Lacustrine and palustrine carbonate petrography: an overview. J. Palaeolimnol. 27, 221-237.
Freytet, P. & Verrecchia, E.P. (1998) Freshwater organisms that build stromatolites: a synopsis of of biocrystallization by prokaryotic and eukaryotic algae. Sedimentology 45, 535-563.
Fritz, P. & Smith, D.G.W. (1970) The isotopic composition of secondary dolomites. Geochim. Cosmochim. Acta 34, 1161-1173.
Funk, H., Föllmi, K.B. & Mohr, H. (1993) Evolution of the Tithonian-Aptian carbonate platform along the northern Tethys margin, Eastern Helvetic Alps. Cretaceous carbonate platforms. 56, 387-407.
Fürsich, F.T. (1979) Genesis, environments, and ecology of Jurassic hardgrounds. N. Jb. Geol. Paläont. Abh. 158 (1), 1-63.
Gallois, R.W. (2000) The stratigraphy of the Kimmeridge Clay Formation (Late Jurassic) in the RGGE boreholes at Swanworth Quarry and Metherhills, south Dorset. Proc. Geol. Assoc. 111, 265-280.
Gallois, R.W. & Cox, B.M. (1976) The stratigraphy of the Lower Kimmeridge Clay of eastern England. Proc. Yorkshire Geol. Soc. 41, 13-26
Galloway, W.E. (1989) Genetic stratigraphic sequences in basin analysis: I. Architecture and genesis of floodinf-surfave bounded depositional units. AAPG Bull. 73, 125-142.
Gawenda, P. (1999) Climatic and tectonic controls on turbiditic and pelagic sedimentation in the deep sea: the Palaeocene-Eocene Zumaia series. PhD thesis N°13110, ETH Zurich, 212 pp.
Gerasimov, P., Kuznetsova, K., Mikchailov, N.P. & Uspenskaya, E.A. (1975) Correlation of the Volgian, Portlandian and Tithonian stages. Colloque sur la limite Jurassique-Crétacé, Lyon, Neuchâtel, Sept. 1973, Mém. B.R.G.M. 86, 117-121.
Gignout, M. & Moret, L. (1952 Géologie dauphinoise (2ème éd.). 391 pp. (Masson)
Gilbert, G.K. (1895) Sedimentary measurement of geological time. J. Geology 3, 121-125.
Gingras, M.K., Pemberton, S.G., Muelenbachs, K. & Machel, H.G. (2004) Conceptual models for burrow-related, selective dolomitization with textural and isotopic evidence from the Tyndall Limestone, Canada. Geobiology 2, 21-30.
Ginsburg, R.N. (ed) (1975) Tidal deposits: a casebook of recent examples and fossil counterparts. (Springer)
Ginsburg, R.N. (1971) Landward movement of carbonate mud: new model for regressive cycles in carbonates. Abstract, AAPG Bull. 55, 340.
Gischler, E. & Zingeler, D. (2002) The origin of carbonate mud in isolated carbonate platforms of Belize, Central America. Int. J. Earth Scienes 91, 1054-1070.
Given, R.K. & Wilkinson, B.H. (1987) Dolomite abundance and stratigraphic age; constraints on rates and mechanisms of Phanerozoic dolostone formation, J. Sed. Petr. 57, 1068-1078.
Glover, W.A. (1975) Distribution by latitude of Phanerozoic evaporite deposits. J. Geol. 53, 671-684.
Goguel, J. (1944) Contribution à l'étude paléogéographique du Crétacé inférieur dans le S.E. de la France. Bull. Serv. Carte géol. France 44, n° 215, 62 pp.
Goguel, J. (1938) Glissements sous-marins dans le Crétacé inférieur. Bull. Soc. géol. France 8, 251-256.
Goldhammer, R.K., Dunn, P.A. & Hardie, L.A. (1990) Depositional cycles, composite sea-level changes, cycle stacking patterns, and the hierarchy of stratigraphic forcing: examples from Alpine Triassic platform carbonates. Geol. Soc. Am. Bull. 102, 535-562.
Goldhammer, R.K., Lehmann, P.J. & Dunn, P.A. (1993) The origin of high-frequency platform carbonate cycles and third-order sequences (Lower Ordovician El Paso Gp, West Texas): constraints from outcrop data and stratigraphic modeling. J. Sed. Res. 63, 318-359.
Goldhammer, R.K., Oswald, E.J. & Dunn, P.A. (1994) High-frequency, glacio-eustatic cyclicity in the Middle Pennsylvanian of the Paradox Basin: an evaluation of the Milankovich forcing. In: De Boer, P.L. & Smith, D.G. (eds) Orbital forcing and cyclic sequences. IAS Spec. Publ. 19, 243-283. (Blackwell)
Gordon W. A. (1975) Distribution by latitude of Phanerozoic evaporite deposits. J. Geol. 83, 671-684.
Gornitz, V., Lebedeff, S. & Hansen, J. (1982) Global sea level trend in the past century. Science 215, 1611-1614.
Gradstein, F.M., Agterberg, F.P., Ogg, J.G., Hardenbol, J., Van Veen, P., Thierry, J. & Huang, Z. (1994) A Mesozoic time scale. J. Geophys. Res. 99, 24051-24074.
Gradstein, F.M., Ogg, J.G. & Smith, A.G. (2004) Jurassic time scale. In: Gradstein, F.M., Ogg, J.G. & Smith, A.G. (eds) A geologic time scale 2004. 310. (Cambridge University Press)
Granier, B. & Deloffre, R. (1993) Inventaire critique des algues dasycladales fossiles IIe partie: Les algues dasycladales du Jurassique et du Crétacé. Revue Paléobiol. 12, 19-65.
Greppin, J.B. (1870) Description du Jura Bernois et quelques districts adjacents. Matér. Carte géol. Suisse 8.
Grün, B. & Blau, J. (1996) Phylogenie, Systematik und Biostratigraphie der Calpionellidae Bonet, 1956: Neue Daten aus dem Rosso Ammonitico superiore und dem Biancone (Oberjura/ Unterkreide: Tithon-Valangin) von Ra Stua (Prov. Belluno, Italien). Revue Paléobiol. 15, 571-595.
Grün, B. & Blau, J. (1997) New aspects of calpionellid biochronology: proposal for a revised calpionellid zonal and subzonal division. Revue Paléobiol. 16, 197-214.
Gygi, R.A. (1995) Datierung von Seichtwassersedimenten des Späten Jura in der Nordwestschweiz mit Ammoniten. Eclogae geol. Helv. 88/1, 1-58.
Häfeli, C. (1966) Die Jura/Kreide-Grenzschichten im Bielerseegebiet (Kt. Bern). Eclogae Geol. Helv. 59, 565-695.
Hallam, A. (2001) A review of the broad pattern of Jurassic sea-level changes and their possible causes in the light of current knowledge. Palaeogeogr., Palaeoclim., Palaeoecol. 167, 23-37.
Hallam, A. (1994) Jurassic climates as inferred from the sedimentary and fossil record. Palaeoclimates and their modelling. 79-88.
Hallam, A. (1993) Jurassic climates as inferred from the sedimentology and fossil record. Philosophical Transactions of the Royal Society (London) B341, 287-296.
Hallam, A. (1992) Phanerozoic sea-level changes. 224 pp. (Columbia Univ. Press)
Hallam, A. (1986) Role of climate in affecting Late Jurassic and Early

Cretaceous sedimentation in the North Atlantic. North Atlantic Palaeoceanography. 21, 277-281.

Hallam, A. (1985) A review of Mesozoic climates. J. Geol. Soc. London 142, 433-445.

Hallam, A. (1984) Continental humid and arid zones during the Jurassic and Cretaceous. Palaeogeogr., Palaeoclim., Palaeoecol. 47, 195-223.

Hallam, A. (1981) Facies interpretation and the stratigraphical record. 291pp. (Freeman)

Hallam, A., Grose, J.A. & Ruffell, A.H. (1991) Palaeoclimatic significance of changes in clay mineralogy across the Jurassic-Cretaceous boundary in England and France. Palaeogeogr., Palaeoclim., Palaeoecol. 81, 173-187.

Hallock, P. & Schlager, W. (1986) Nutrient excess and the demise of coral reefs and carbonate platforms. Palaios 1, 389-398.

Hänni, R. (1999) Der geologische Bau des Helvetikums im Berner Oberland. PhD thesis, University of Berne.

Hantzpergue, P. (1995) Faunal trends and sea-level changes; biogeographic patterns of Kimmeridgian ammonites on the western European shelf. Geol. Rundschau 84, 245-254.

Hantzpergue, P. (1983) Précisions nouvelles sur la limite Kimméridgien-Portlandien sensu gallico. C. R. Acad. Sci. Paris, Série II 296, 1803-1805.

Hantzpergue, P. (1979) Biostratigraphie du Jurassique supérieur nord-aquitain. Bull. Soc. géol. France 21, 715-725.

Haq, B.U. (1991) Sequence stratigraphy, sea-level change, and significance for the deep sea. In: Macdonald, D.I.M. (ed.) Sedimentation, tectonics and eustasy – Sea-Level changes at active margins. IAS Spec. Publ. 12, 3-39.

Haq, B.U., Hardenbol, J. & Vail, P.R. (1987) Chronology of fluctuating sea levels since the Triassic (250 million years ago to present). Science 235, 1156-1167.

Hardenbol, J., Thierry, J., Farley, M.B., Jacquin, T., De Graciansky, P.-C. & Vail, P.R. (1998) Cretaceous sequence chronostratigraphy. In: De Graciansky, P.C., Hardenbol, J., Jacquin, T. & Vail, P.R. (eds) Mesozoic and Cenozoic sequence stratigraphy of European basins. SEPM Spec. Publ. 60, charts.

Hardenbol, J., Thierry, J., Farley, M.B., Jacquin, T., De Graciansky, P.-C. & Vail, P.R. (1998) Jurassic sequence chronostratigraphy. In: De Graciansky, P.C., Hardenbol, J., Jacquin, T. & Vail, P.R. (eds) Mesozoic and Cenozoic sequence stratigraphy of European basins. SEPM Spec. Publ. 60, charts.

Hardie, L.A. (1987) Dolomitization: a critical view of some current views. J. Sed. Petr. 57 (1), 166-183.

Haug, E. (1891) Les chaînes subalpines entre Gap et Digne. Bull. Serv. Carte géol. France 3, n° 21, 1-197.

Hauser, M. (1994) Geologie der Region Péry-Reuchenette (Kanton Bern). Unpubl. diploma thesis, University of Berne, 209 pp.

Hay, W.W. (1998) Detrital sediment fluxes from continents to oceans. Chemical Geology 145, 287-323.

Herbin, J.P., Fernandez-Martinez, J.L., Geyssant, J.R., Albani, A.E., Deconinck, J.F., Proust, J.N., Colbeaux, J.P. & Vidier, J.P. (1995) Sequence stratigraphy of source rocks applied to the study of the Kimmeridgian/Tithonian in the North-West European shelf (Dorset/UK, Yorkshire/UK and Boulonnais/France). Mar. Petrol. Geology 12, 177-194.

Hilgen, F., Schwarzacher, W. & Strasser, A. (2004) Concepts and definitions in cyclostratigraphy (Second report of the cyclostratigraphy working group). In: D'Argenio, B., Fischer, A.G., Premoli silva, I., Weissert, H. & Ferreri, V. (eds) Cyclostratigraphy: approaches and case histories. SEPM Spec. Publ. 81, 303-305.

Hillgärtner, H. (1999) The evolution of the French Jura platform during the Late Berriasian to Early Valanginian: controlling factors and timing. GeoFocus 1, 203pp.

Hillgärtner, H. (1998) Discontinuity surfaces on a shallow-marine carbonate platform (Berriasian, Valanginian, France and Switzerland). J. Sed. Res. 68, 1093-1108.

Hillgärtner, H., Dupraz, C. & Hug, W. (2001) Microbially induced cementation of carbonate sands: are micritic meniscus cements good indicators of vadose cements? Sedimentology 48, 117-131.

Hinnov, L.A. (2000) New perspectives on orbitally forced stratigraphy. Annu. Rev. Earth Planet. Sci. 28, 419-475.

Horbury, A.D. & Qing, H. (2004) 'Pseudobreccias' revealed as calcrete mottling and bioturbation in the Late Dinantian of the southern Lake District, UK. Sedimentology 51, 19-38.

Hubbard, R.J. (1988) Age and significance of sequence boundaries on Jurassic and Early Cretaceous rifted continental margins. AAPG Bull. 72, 49-72.

Hug, W.A. (2003) Sequenzielle Faziesentwicklung der Karbonatplattform des Schweizer Jura im Späten Oxford und frühesten Kimmeridge. GeoFocus 7, 155 pp.

Hughes Clarke, M.W. & Keij, A.J. (1973) Organisms as producers of carbonate sediment and indicators of environment in the southern persian Gulf. In: PURSER, B.H. The Persian Gulf: Holocene carbonate sedimentation and diagenesis in a shallow epicontinental sea. 33-56. (Springer)

Hunt, D. & Tucker, M. (1995) Stranded parasequences and the forced regression wedge systems trakt: deposition during base-level fall – reply. Sed. Geol. 95, 147-160.

Hunt, D. & Tucker, M. (1992) Stranded parasequences and the forced regressive wedge systems tract: deposition during base-level fall. Sed. Geol. 81, 1-9.

Jaccard, A. (1869) Descrition géologique du Jura vaudois et neuchâtelois. Matér. Carte géol. Suisse 6.

Jaccard, A. (1869) Déscription géologique du Jura vaudois et neuchâtelois. Matér. Carte géol. Suisse 6.

Jaccard, M. (1990) Paléogéographie du Jurassique terminal de la région de Sainte-Croix (stratigraphie et sédimentologgie). Bull. Ass. Suisse Géol. Ing. Petr. 57, 37-51.

Jaccard, M. (1988) Paléogéographie du Jurassique terminal de la region de Ste-Croix (stratigraphie, sédimentologie). Unpubl. diploma thesis, University of Lausanne, 103 pp.

Jacobs, D.K. & Sahagian, D.L. (1993) Climate-induced fluctuations in sea level during non-glacial times. Nature 361, 710-712.

Jacquin, T., Dardeau, G., Durlet, C., De Graciansky, P.-C. & Hantzpergue, P. (1998) The North Sea Cycle: an overview of 2nd-order transgressive/regressive facies cycles in western Europe. Mesozoic and Cenozoic sequence stratigraphy of European basins. 60, 445-466.

James, N.P. & Choquette, P.W. (1988) Palaeokarst. (Springer)

Jan Du Chêne, R. et al. (16 co-authors) (1993) Sequence stratigraphic interpretation of Upper Tithonian-Berriasian reference sections in South-East France: a multidisciplinary approach. Bull. Cent. Rech.-ExPl. Elf-Aquitaine 17, 151-181.

Jenkyns, H.C., Jones, C.E., Gröcke, D.R., Hesselbo, S.P. & Parkinson, D.N. (2002) Chemostratigraphy of the Jurassic System: applications, limitations and implications for palaeoceanography. J. geol. Soc. London 159, 351-378.

Joachimski, M.M. (1994) Subaerial exposure and deposition of shallowing upward sequences: evidence from stable isotopes of Purbeckian peritidal carbonates (basal Cretaceous), Swiss and French Jura Mountains. Sedimentology 41, 805-824.

Jones, B. & Desrochers, A. (1992) Shallow platform carbonates. In: Walker, R.G. & James, N.P. (eds) Facies models, response to sea level change. Geol. Assoc. Canada, GeoText 1, 277 – 301.

Jones, C.E. & Jenkyns, H.C. (2001) Seawater Strontium isotopes, oceanic anoxic events, and seafloor hydrothermal activity in the Jurassic and Cretaceous. Amer. J. Sci. 301, 112-149.

Jones, C.E., Jenkyns, H.C., Coe, A.L. & Hesselbo, S.P. (1994) Strontium isotopic variations in Jurassic and Cretaceous seawater. Geochim. Cosmochim. Acta 58, 3061-3074.

Jones, G., Whitaker, F.F., Smart, P.L. & Sanford, W.E. (2004) Numerical analysis of seawater circulation in carbonate platforms: II. The dynamic interaction between geothermal and brine reflux circulation. Amer. J. Sci. 304, 250-284.

Jones, G., Whitaker, F.F., Smart, P.L. & Sanford, W.E. (2002) Fate of reflux brines in carbonate platforms. Geology 30, 371-374.

Jørgensen, B.B. (1983) The microbial sulfur cycle. In: Krumbein, W.E. (ed) Microbial geochemistry. 91-124. (Blackwell)

Joukovsky, E. & Favre, J. (1913) Monographie géologique et paléontologique du Salève (Haute-Savoie, France). Mém. Soc. Phys. Hist. nat. Genève, 37, 295-523.

Kaplan, M.E. (1978) Calcite pseudomorphoses in Jurassic and Early Cretaceous deposits of the northern area of eastern Siberia. Geol. Geofiz 19, 62-70.

Kaufman, J. (1994) Numerical models of fluid flow in cabonate plat-

forms: implications for dolomitization. J. Sed. Res. A64, 128-139.
Kazmierczak, J., Coleman, M.L., Gruszczynski, M. & Kempe, S. (1996) Cyanobacterial key to the genesis of micritic and peloidal limestones in ancient seas. Acta Palaeont. Polonica 41, 319-338.
Kemper, E. (1987) Das Klima der Kreidezeit. Geol. Jahrb. A96, 5-185.
Kemper, E. (1983) Über Kalt- und Warmzeiten der Unterkreide. Zitelliana 10, 359-369.
Kendall, C.G.S.C. & Schlager, W. (1981) Carbonates and relative changes in sea level. Mar. Geol. 44, 181-212.
Kettiger M. (1981) Microfacies, petrographie, minéralogie et évolution des milieux de dépots de l'Oxfordien de la Vraconnaz et du Malm supérieur des Gorges de Noirvaux. Unpubl. diploma thesis, IGUN, University of Neuchâtel, Neuchâtel, 71 pp. + annex.
Keupp, H. (1991) Fossil calcareous dinoflagellate cysts. In: Riding, R. (ed) Calcareous algae and stromatolites. 267-286. (Springer)
Kilian, W. (1895) Notes stratigraphiques sur les environs de Sisteron. Bull. Soc. géol. France 3, tôme 23.
Kilian, W. (1889) Description géologique de la Montagne de Lure (Basses-Alpes). 458 pp. (Éd. G. Masson)
Kirkland, D.W. & Evans, R. (1981) Source-rock potential of evaporitic environment. AAPG Bull. 65, 181–190.
Klappa, C.F. (1980) Rhizoliths in terrestrial carbonates: classification, recognition, genesis and significance. Sedimentology 27, 613-629.
Klappa, C.F. (1978) Biolithogenesis of *Microcodium*: elucidation. Sedimentology 25, 489-522.
Kobluk, D.R. & Risk, M.J. (1977) Calcification of exposed filaments of endolithic algae, micrite envelope formation and sediment production. J. Sed. Petr. 47, 517-528.
Kolla, V., Posamentier, H.W. & Eichenseer, H. (1995) Stranded parasequences and the forced regression wedge systems trakt: deposition during base-level fall – discussion. Sed. Geol. 95, 139-145.
Košir, A. (2004) *Microcodium* revisited: root calcification products of terrestrial plants on carbonate-rich substrates. J. Sed. Res. 74, 845-857.
Kübler, B. (1990) Cristallinité de l'illite, methods normalisées de préparations, méthodes normalisées de mesures. Cahiers Institut Géologie de Neuchâtel, Suisse, série ADX.
Kübler, B. (1987) "Cristallinité" de l'illite et mixed-layers: brève révision. Schweiz. Mineral. Petrogr. Mitt. 70.
Kübler, B. (1964) Les argiles, indicateurs de métamorphisme. Rev. Inst. Français Pétr. 19, 1093-1112.
Kutek, J. & Zeiss, A. (1994) Biostratigraphy of the highest Kimmeridgian and Lower Volgian of Poland. Géobios Mém. Spéc. 17, 337-341.
Kutek, J. & Zeiss, A. (1975) A contribution to the correlation of the Tithonian and Volgian stages: the ammonite fauna from Brzostokwa near Tomaszow Mozowiecki, central Poland. Colloque sur la limite Jurassique-Crétacé, Lyon, Neuchâtel, Sept. 1973, Mém. B.R.G.M. 86, 123-128.
Kutzbach, J.E. & Gallimore, R.G. (1989) Pangean climates: Megamonsoons of the megacontinent. J. Geophys. Res. 94, 3341-3357.
Lagotala, H. (1920) Etude géologique de la région de la Dôle. PhD thesis, University of Geneva 39 pp.
Land, L.S. (1980) The isotopic and trace element geochemistry of dolomite: the state of the art. In: Zenger, D.H., Dunham, J.B. & Ethington, R.L. (eds) Concepts and models of dolomitization. SEPM Spec. Publ. 28, 87-110.
Le Hégarat, G. (1980) Berriasien. In: Clavelier, J. & Roger, J. (eds) Les étages français et leur stratotypes. Mém. Bur. Rech. géol. min. 109, 96-105.
Le Hégarat, G. (1973) Le Berriasien du S.E. de la France. Doc. Lab. Géol. Fac. Sci. Lyon 43, 576 pp.
Le Hégarat, G. (1971) Le Berriasien du Sud-Est de la France. Doc. Lab. Géol. Fac. Sci. Lyon 43, 567 pp.
Le Hégarat, G. & Remane, J. (1968) Tithonique supérieur et Berriasien de l'Ardèche et de de l'Hérault - corrélation des ammonites et des calpionelles. Géobios 1, 7-70.
Lehrmann, D.J. & Rankey, E.C. (1999) Do meter-scale cycles exist? A statistical evaluation from vertical (1-D) and lateral (2-D) patterns in shallow-marine carbonates-siliciclastics of the "fall-in" strata of the Capitan Reef, Seven Rivers Formation, Slaughter Canyon, New Mexico. In: Saller, A.H., Harris, P.M., Kirkland, B.L. & Mazzullo, S.J. (eds) Geologic framework of the Capitan Reef. SEPM Special Publication 65, 51-62.
Leinfelder, R.R. (1993) Late Jurassic reef types and controlling factors – a preliminary report. Profil 5, 1-45.
Leinfelder, R.R., Nose, M., Schmid, D.U. & Werner, W. (1993) Microbial crusts of the Late Jurassic: composition, palaeoecological significance and importance in reef construction. Facies 29, 195-230.
Leinfelder, R.R. & Schmid, D.U. (2000) Mesozoic reefal thrombolites and other microbolites. Microbial Sediments 289-294.
Leinfelder, R.R., Werner, W., Nose, M., Schmid, D.U., Krautter, M., Laternser, R., Takacs, M. & Hartmann, D. (1996) Palaeoecology, growth parameters and dynamics of coral, sponge and microbolite reefs from the Late Jurassic. Global and regional controls on biogenic sedimentation. I. Reef Evolution. Research Reports. Sb2, 209-214.
Lippmann, F. (1973) Sedimentary carbonate minerals. (Springer)
Lisitzin, A.P. (ed.) (1972) Sedimentation in the World ocean – with emphasis on the nature, distribution and behavior of marine suspensions. SEPM Spec. Publ. 17, 218pp.
Loeblich, A. R. & Tappan, H. (eds) (1988) Foraminiferal genera and their classification. Vol. I & II. (Van Nostrand Reinhold)
Lohmann, K.C. (1988) Geochemical patterns of meteoric diagenetic systems and their application to studies of palaeokarst. In: James, N.P. & Philip, W.C. (eds) Palaeokarst. 58-80. (Springer)
Lombard, A. (1945) Attribution de microfossiles du Jurassique supérieur alpin à des Chlorophycées (Proto- et Pleurococcales). Eclogae Geol. Helv. 38, 163-173.
Machel, H.G. (2002) The dolomite problem — quo vadis? In: Hüssner, H., Hinderer, M., Götz, A.E. & Petschick, R. (eds) SEDIMENT 2002, 17. Sedimentologentreffen, Frankfurt a.M./Darmstadt, 29.-31. Mai 2002, Kurzfassungen und Programm. Schr. Deutsch. Geol. Ges. 17, 135-140.
Machel, H.G. & Mountjoy, E.W. (1986) Chemistry and environments of dolomitization — a reappraisal. Earth Sci. Rev. 23, 175-222.
Macintyre, I.A. (1985) Submarine cements—the peloidal question. In: Schneidermann, N. & Harris, P.M. Carbonate Cements. SEPM Spec. Publ. 36, 109-116.
Major, R.P., Lloyd, R.M. & Lucia, F.J. (1992) Oxygen isotope composition of Holocene dolomite formed in a humid hypersaline setting. Geology 20, 586-588.
Marsaglia, K.M., & deV. Klein, G. (1983) The palaeogeography of Palaeozoic and Mesozoic storm depositional systems. J. Geol. 91, 117-142.
Marshall, J.D. & Ashton, M. (1980) Isotopic and trace element evidence for submarine lithification of hardgrounds in the Jurassic of eastern England. Sedimentology 27, 271-289.
Marszalek, D. (1975) Calcisphere ultrastructure and skeletal aragonite from the alga *Acetabularia antillana*. J. Sed. Petr. 45, 266-271.
Marty, D. (2004) Rapport d'activités 2003 - Le Mésozoïque du Jura le long de la Transjurane: Prospection, sondages, fouilles et recherche. In: Section de Paléontologie - Rapport d'activités 2003. Paléontologie et Transjurane. 4, 104 pp.
Marty, D. (2003) Le Secondaire (Mésozoïque) du Jura le long de la Transjurane, avec recherche approfondie sur le site de Courtedoux - Sur Combe Ronde. In: Section de Paléontologie - Rapport d'activités 2002. Paléontologie et Transjurane 3, 1-52.
Marty, D., Hug, W.A., Iberg, A., Cavin, L., Meyer, C.A. & Lockley, M.G. (2003) Preliminary report in the Courtedoux dinosaur tracksite from the Kimmeridgian of Switzerland. Ichnos 10, 209-219.
Matthews, A. & Katz, A. (1977) Oxygen isotope fractionation during the dolomitization of calcium carbonate. Geochim. Cosmochim. Acta 41, 1431-1438.
Mattioli, E. & Pittet, B. (2002) Contribution of calcareous nannoplankton to carbonate deposition: a new approach applied to the Lower Jurassic of central Italy. Mar. Micropalaeontol. 45, 175-190.
Mazin, J. M., Hantzpergue, P., Lafaurie, G., Vignaud, P. (1995) Des pistes de ptérosaures dans le Tithonien de Crayssac (Quercy, France) C. R. Acad. Sci. Paris, Série II 321, 417-424.
Mazullo, S.J., Bischoff, W.D. & Teal, C.S. (1995) Holocene shallow subtidal dolomitization by near-normal seawater, northern Belize. Geology 23, 341-344.
Mazullo, S.J., Reid, A.M. & Gregg, J.M. (1987) Dolomitization of Holocene Mg-calcite supratidal deposits, Ambergris Cay, Belize. Geol. Soc. Am. Bull. 98, 224-231.

McKenzie, J.A. (1991) The dolomite problem: an outstanding controversy. In: Müller, D.W., Mckenzie, J.A. & Weissert, H. Controversies in modern geology. 37-54. (Academic Press)

McKenzie, J.A. (1981) Holocene dolomitization of calcium carbonate sediments from the coastal sabkhas of Abu Dhabi, U.A.E. J. Geol. 89, 185-198.

Melim, L.A. & Scholle, P.A. (2002) Dolomitization of the Capitan Formation forereef facies (Permian, west Texas and New Mexico): seepage reflux revisited. Sedimentology 49, 1207-1227.

Melim, L.A., Swart, P.K. & Eberli, G.P. (2004) Mixing-zone diagenesis in the subsurface of Florida and the Bahamas. J. Sed. Res. 74, 904-913.

Melynk, D.H., Athersuch, J. & Smith, D.G. (1992) Estimating the dispersion of biostratigraphic events in the subsurface by graphic correlation: an example from the Late Jurassic of the Wessex Basin, UK. Mar. Petrol. Geol. 8, 607-607.

Melynk, D.H., Smith, D.G. & Amiri-Garoussi, K. (1994) Filtering and frequency mapping as tools in subsurface cyclostratigraphy, with examples from the Wessex Basin, UK. In: De Boer, P.L. & Smith, D.G. (eds) Orbital forcing and cyclic sequences. IAS Spec. Publ. 19, 35-46. (Blackwell)

Meyer, C.A. (1993) A sauropod dinosaur megatracksite from the Late Jurassic of northern Switzerland. Ichnos 3, 29-38.

Meyer, C.A. & Pittman, J.G. (1994) A comparison between the Brontopodus ichnofazies of Portugal, Switzerland and Texas. Gaia, 125-133.

Meyer, M. (2000) Le complexe récifal kimméridgien-tithonien du Jura méridional interne (France), évolution multifactorielle, stratigraphie et tectonique. Terre & Environnement 24, 179 pp.

Miall, A.D. (1999) In defense of facies classifications and models. J. Sed. Res. 69, 2-5.

Miall, A.D. (1997) The geology of stratigraphic sequences. 421pp. (Springer)

Miall, A.D. (1992) EXXON global cycle chart: anevent for every occasion? Geology 20, 787-790.

Miall, A.D. (1991) Stratigraphic sequences and their chronostratigraphic correlation. J. Sed. Petr. 61, 497-505.

Miall, A.D. (1986) Eustatic sea-level changes interpreted from seismic stratigraphy: a critique of the methodology with particular reference to the North Sea record. Bull. amer. Assoc. Petrol. Geol. 70, 131-137.

Miall, A.D. & Miall, C.E. (2001) Sequence stratigraphy as a scientific enterprise: the evolution and persistence of conflicting paradigms. Earth Sci. Rev. 54, 321-348.

Milankovitch, M. (1941) Kanon der Erdbestrahlung und seine Anwendung auf das Eiszeitenproblem. Akad. Royal Serbe Spec. Publ. 132, Sect. Math. Nat. Sci. Vol. 33.

Miller, R.G. (1991) A palaeoceanographic approach to the Kimmeridge Clay Formation. In: (ED.), H.A.Y. Deposition of organic facies. AAPG Stud. Geol. 30, 13-26.

Millot, G. (1970) Geology of clays. 425 pp. (Springer)

Mirsal, I.A. & Zankl, H. (1985) Some phenomenological aspects of carbonate geochemistry: the control effect of transition metals. Geol. Rundschau 74, 367-377.

Missoni, S., Schlagintweit, F., Suzuki, H. & Gawlick, H.-J. (2001) Die oberjurassische Karbonatplattformentwicklung im Bereich der Berchtesgadener Kalkalpen (Deutschland) - eine Rekonstruktion auf der Basis von Untersuchungen polymikter Brekzienkörper in pelagischen Kieselsedimenten (Sillenkopf-Formation). Zbl. Geol. Paläont. Teil I 2000 (1/2), 117-143.

Mitchell, J.T., Land, L.S. & Miser, D.E. (1987) Modern marine dolomite cement in a north Jamaican fringing reef. Geology 15, 557-560.

Mitchum Jr., R.M. & Van Wagoner, J.C. (1991) High-frequency sequences and their stacking patterns: sequence stratigraphic evidence of high-frequency eustatic cycles. Sed. Geol. 70, 131-160.

Mohr, H. (1992) Der Helvetische Schelf der Ostschweiz am Übergang vom späten Jura zur Kreide. PhD thesis, University of Zurich, 221 pp.

Mohr, H. & Funk, H. (1995) Die Entwicklug der helvetischen Karbonatplattform in der Ostschweiz (Tithonian-Berriasian): Eine sequenzstratigraphischen Annäherung. Eclogae geol. Helv. 88/2, 281-320.

Mojon, P.O. (1989) Charophytes et ostracodes laguno-lacustres du Jurassique de la Bourgogne (Bathonien) et du Jura septentrional franco-suisse (Oxfordien). Remarques sur les discontinuités émersives du Kimméridgien du Jura. Rev. Paléobiol., Vol. Spéc. 3, 118.

Mojon, P.O. & Strasser A. (1987) Microfaciès, sédimentologie et micropaléontologie du Purbeckien de Bienne (Jura suisse occidental). Eclogae Geol. Helv. 80, 37-58.

Montañez, I.P. & Osleger, D.A. (1993) Parasequence stacking patterns, third-order accommodation events and sequence stratigraphy of Middle to Upper Cambrian platform carbonates, Bonanza King Formation, southern Great Britain. In: Loucks, R.G. & Sarg, J.F. (eds) Carbonate sequence stratigraphy. AAPG Mem. 57, 305-326.

Montañez, I.P. & Read, J.F. (1992) Eustatic control on early dolomitization of cyclic peritidal carbonates; evidence from the Early Ordovician upper Knox Group, Appalachians, Geol. Soc. Am. Bull. 104, 872-886.

Moore, C.H. (1989) Carbonate diagenesis and porosity. Developments in Sedimentology 42, 338 pp.

Moore, D. & Reynolds, R. (1989) X-ray diffraction and the identification and analysis of clay minerals. 332 pp. (Oxford University Press)

Moore, G.T., Hayashida, D.N., Ross, C.A. & Jacobson, S.R. (1992) Palaeoclimate of the Kimmeridgian/Tithonian (Late Jurassic) world: I. Results of a general circulation model. Palaeogeogr., Palaeoclim., Palaeoecol. 93, 113-150.

Moore, G.T., Sloan, L.C., Hayashida, D.N., & Umrirgar, N.P. (1992) Palaeoclimate of the Kimmeridgian/Tithonian (Late Jurassic) world: II. Sensitivity tests comparing three different palaeotopographic settings. Palaeogeogr., Palaeoclim., Palaeoecol. 95, 229-252.

Mora, R. (2004) Géologie de la région de Saint-Laurent-en-Grandvaux (Jura français) – étude latérale d'un dépot kimméridgien peu profond. Diploma thesis, Dept. de Géoscience - Géologie et Paléontologie, University of Fribourg, Fribourg, 75 pp.

Morin, N. (1993) Les *Microcodium*: Architecture, structure et composition. Comparaison avec des racines calcifiées. PhD thesis, University of Montpellier, 132 pp.

Mosar, J., Eide, E.A., Osmundsen, P.T., Sommaruga, A. & Torsvik, T.H. (2002) Greenland-Norway separation: a geodynamic model for the North Atlantic. Norwegian J. Geol. 82, 281-298.

Mouchet, P. (1998) Stratigraphy and mineralostratigraphy of the Kimmeridgian in the central Jura Mountains of Switzerland and eastern France. Eclogae geol. Helv. 91, 53-68.

Mouchet, P. (1995) Le Kimméridgien du Jura central. Microfaciès, minéralogie et interprétation séquentielle. PhD thesis, University of Neuchâtel. 204pp.

Munnecke, A. & Samtleben, C. (1996) The formation of micritic limestones and the development of limestone-marl alternations in the Silurian of Gotland, Sweden. Facies 34, 1598-176.

Munnecke, A. & Westphal, H. (2004) Shallow-water aragonite recorded in bundles of limestone-marl alternations – the Late Jurassic of WS-Germany. Sed. Geol. 164, 191-202.

Munnecke, A., Westphal, H., Elrick, M. & Reijmer, J.J.G. (2001) The mineralogical composition of precursor sediments of calcareous rythmites: a new approach. Int. J. Earth Sciences (Geol. Rundsch.) 90, 795-812.

Muto, T. & Steel, R.J. (1997) Principles of regression and transgression: the nature of of the interplay between accommodation and sediment supply. J. Sed. Res. 67, 994-1000.

Mutterlose, J., Brumsack, H., Flögel, S., Hay, W., Klein, C., Langrock, U., Lipinski, M., Ricken, W., Söding, E., Stein, R. & Swientek, O. (2003) The Greenland-Norwegian Seaway: a key area for understanding Late Jurassic to Early Cretaceous palaeoenvironments. Palaeoceanography 18, 1010-1035.

Mutti, M. & Simo, J.A. (1994) Distribution, petrography and geochemistry of early dolomite in cyclic shelf facies, Yates Formation (Guadalupian), Capitan Reef Complex, USA. Spec. Publs Int. Ass. Sediment. 21, 91-107.

Naish, T.R. & Kemp, P.J.J. (1997) Sequence stratigraphy of sixth-order (41 k.a.) Pliocene–Pleistocene cyclothems, Wanganui basin, New Zealand: a case for for the regressive systems tract. GSA Bull. 109, 978-999.

Neumann, A.C. & McIntyre, I.G. (1985) Reef response to sea-level: catch up, keep up, or give up. Proc. 5th Int. Coral Reef Congress,

Morea, French Polynesia, Antenne Museum-Ephe 3, 105-110.

Newell, N.D., Rigby, J.K., Fischer, A.G., Whiteman, A.J. Hilcox, J.E. & Bradley, J.S. (1953) The Permian reef complex of the Guadalupe Mountains region, Texas and New Mexico. 236 pp. (W.H. Freeman)

Nordeng, S.H. & Sibley, D. (2003) The induction period and dolomite kinetics in experimental and natural systems. 12th Bathurst Meeting – Int. Conference of Carbonate Sedimentologists, 8th-10th July 2003, Durham – Programme and Abstracts, 74.

Nummedal, D. & Swift, D.J.P. (1987) Transgressive stratigraphy at sequence-bounding unconformities: some principles derived from Holocene and Cretaceous examples. In: NUMMEDAL, D., PILKEY, O.H. & HOWARD, J.D. Sea-level fluctuation and coastal evolution. SEPM Spec. Publ. 41, 241-260.

Nystuen, J.P. (1998) History and development of sequence stratigraphy. In: Gradstein, F.M., Sandvik, K.O. & Milton, N.J. (eds) Sequence stratigraphy - concepts and applications. Norwegian Petroleum Soc. Spec. Publ. 8, 31-116.

Odin, G.S. (1994) Geological time scale. C. R. Acad. Sci. Paris, Série II 318, 59-71.

Oertli, H.J. (1959) Malm-Ostrakoden aus dem schweizerischen Jura-Gebirge. Denkschr. Schweiz. Natf. Ges. 83 (1), 44 pp.

Oschmann, W. (1990) Environmental cycles in the Late Jurassic northwest European epeiric basin: interaction with atmospheric and hydrospheric circulations. Aigner, T. & Dott, R.H. (eds.): Processes and patterns in epeiric basins. 69, 313-332.

Oschmann, W. (1988) Kimmeridge Clay sedimentation - a new cyclic model. Palaeogeogr., Palaeoclim., Palaeoecol. 65, 217-251.

Osleger, D.A. (1991) Subtidal carbonate cycles: implications for allocyclic vs. autocyclic controls. Geology 19, 917-920.

padden, m. (2001) Late Jurassic palaeoceanography: evidence from stable isotopes and carbonate sedimentology. PhD thesis Nr. 14094, ETH Zurich, 128 pp.

padden, m., weissert, h., funk, h., schneider, s. & gansner, c. (2002) Late Jurassic lithological evolution and carbon-isotope stratigraphy of the western Tethys. Eclogae geol. Helv. 95, 333-346.

Pálfy, J., Mortensen, J.K., Smith, P.L., Friedman, R.M., Mcnicoli, V. & Villeneuve, M. (2000) New U-Pb zircon ages integrated with ammonite biochronology from the Jurassic of the Canadian Cordillera. Can. J. Earth Sci. 37, 549-567.

Pálfy, J., Smith, P.L. & Mortensen, J.K. (2000) A U-Pb and $^{40}Ar/^{39}Ar$ time scale for the Jurassic. Can. J. Earth Sci. 37, 923-944.

Park, M.-H. & Fürsich, F. (2001) Cyclic nature of lamination in the Tithonian Solnhofen Plattenkalk of southern Germany and its palaeoclimatic implications. Int. J. Earth Sciences (Geol. Rundsch.) 90, 847-854.

Parrish, J.T. (1993) Climate of the supercontinent Pangea. J. Geol. 101, 215-233.

Parrish, J.T. & Curtis, R.L. (1982) Atmospheric circulation, upwelling, and organic-rich rocks in the Mesozoic and Cenozoic eras. Palaeogeogr., Palaeoclim., Palaeoecol. 40, 31-66.

Pasquier, J.-B. (1995) Sédimentologie, stratigraphie séquentielle et cyclostratigraphie de la marge nord-téthysienne au Berriasien en Suisse occidentale. PhD-Thesis No. 1088, University of Fribourg 274pp.

Pasquier, J.-B. & Strasser, A. (1997) Platform-to-basin correlation by high-resolution sequence stratigraphy and cyclostratigraphy (Berriasian, Switzerland and France). Sedimentology 44, 1071-1092.

Patterson, W.P. & Walter, L.M. (1994) Depletion of ^{13}C in seawater $ÓCO_2$ on modern carbonate platforms: significance for the carbon isotopic record of carbonates. Geology 22, 885-888.

Pawellek, T. (2001) Fazies-, Sequenz-, und Gamma-Ray-Analyse im höheren Malm der Schwäbischen Alb (SW-Deutscland) mit Bemerkungen zur Rohstoffgeologie (hochreine Kalke). Tübinger Geowiss. Arb., Reihe A 61, 244 pp.

Pawellek, T. & Aigner, T. (2003a) Stratigraphic architecture and gamma ray logs of deeper ramp carbonates (Late Jurassic, SW Germany). Sed. Geol. 159, 203-240.

Pawellek, T. & Aigner, T. (2003b) Apparently homogenous "reef"-limestones built by high-frequency cycles: Late Jurassic, SW.Germany. Sed. Geol. 160, 259-284.

Pellaton, C. & Ullrich, S. (1997) Etude multidisciplinaire du Jurassique supérieur de la région de Castellane (SE France). Diploma thesis, University of Geneva, 190 pp. + annex.

Pelletier, M. (1953a) Observations stratigraphiques sur les formations coralligènes du Bugey (Ain), Compte Rendus Hebdomadaires des Séances de l'Academie des Sciences, 237 (23), p. 1540-1542

Pelletier, M. (1953b) Sur l'existence d'un calcaire dolomitique fossilifère dans le Séquanien supérieur du Jura méridional, C. R. Acad. Sci. Paris 15-16, 349-350.

Perlmutter, M.A. & Mattews, M.D. (1992) Global cyclostratigraphy. Encyclopedia of Earth System Science 2, 379-393.

Perlmutter, M.A. & Mattews, M.D. (1989) Global cyclostratigraphy—a model. In: Cross, T.A. (ed) Quantitative dynamic stratigraphy. 233-260. (Prentice Hall)

Persoz, F. (1982) Inventaire minéralogique, diagenèse des argiles et minéralostratigraphie des séries jurassiques et crétacées inférieures du Plateau suisse et de la bordure sud-est du Jura entre les lacs d'Annecy et de Constance. Mat. Carte Géol. Suisse N.S. 155, 52 pp.

Persoz, F. & Remane, J. (1976) Minéralogie et géochimie des formations à la limite Jurassique-Crétacé dans le Jura et le Bassin vocontien. Eclogae geol. Helv. 69, 1-38.

Persoz, F. & Remane, J. (1973) Evolution des milieux de dépôt au Dogger supérieur et au Malm dans le Jura neuchâtelois méridional. – Eclogae Geol. Helv. 66, 41-70.

Peterhänsel, A. (2003) Depositional dynamics of a giant carbonate platform—the Famennian Palliser Formation of western Canada. PhD thesis, Dept. of Geological Sciences, University of Saskatchewan, Saskatoon, 220 pp.

Péwé, T.L. (1981) Desert dust: an overview. In: Péwé, T.L. Desert dust: origin, characteristics, and effect on man. GSA Spec. Paper 186, 1-10.

Philip, J. (2003) Peri-Tethyan neritic carbonate areas: distribution through time and driving factors. Palaeogeogr., Palaeoclim., Palaeoecol. 196, 19-37.

Pidancet, M.M. & Lory, Ch. (1847) Sur le phénomène erratique dans les hautes vallées du Jura. C. R. Acad. Sci. Paris 25A, 718-720.

Pittet, B. (1996) Contrôles climatiques, eustatiques et tectoniques sur des systèmes mixtes carbonates-siliciclastiques de plate-forme: exemples de l'Oxfordien (Jura suisse, Normandie, Espagne). PhD-Thesis No. 1124, University of Fribourg, Fribourg, 258pp.

Pittet, B. (1994) Modèle d'estimation de la subsidence et des variations du niveau marin: un exemple de l'Oxfordien du Jura suisse. Eclogae geol. Helv. 87, 513-543.

Pittet, B. & Gorin, G. (1997) Distribution of sedimentary organic matter in a mixed carbonate-siliciclastic platform environment: Oxfordian of the Swiss Jura Mountains. Sedimentology 44, 915-937.

Pittet, B. & Mattioli, E. (2002) The carbonate signal and calcareous nannofossil distribution in an Late Jurassic section (Balingen-Tieringen, Late Oxfordian, southern Germany). Palaeogeogr., Palaeoclim., Palaeoecol. 179, 71-96.

Pittet, B. & Strasser, A. (1998a) Depositional sequences in deep-shelf environments formed through carbonate-mud import from the shallow platform (Late Oxfordian, German Swabian Alb and eastern Swiss Jura). Eclogae geol. Helv. 91, 149-169.

Pittet, B. & Strasser, A. (1998b) Long-distance correlations by sequence stratigraphy and cyclostratigraphy: examples and applications (Oxfordian from the Swiss Jura, Spain, and Normandy). Geol. Rundsch. 86, 852-874.

Pittet, B., Strasser, A. & Mattioli, E. (2000) Depositional sequences in deep-shelf environments; a response to sea-level changes and shallow-platform carbonate productivity (Oxfordian, Germany and Spain). J. Sed. Res. 70 (2), 392-407.

Plint, A.G., Eyles, N., Eyles, C.H. & Walker, R.G. (1992) Control of sea level change. In: Walker, R.G. & James, N.P. (eds) Facies models – response to sea level change. 15-25.

Plunkett, J.M. (1997) Early diagenesis od shallow platform carbonates in the Oxfordian of the Swiss Jura Mountains. PhD Thesis, University of Fribourg, 168pp.

Podlaha, O.G., Mutterlose, J. & Veizer, J. (1998) Preservation of $d^{18}O$ and $d^{13}C$ in belemnite rostra from the Jutassic/Early Cretaceous successions. Amer. J. Sci. 298, 324-347.

Poignant, A.F. & Deloffre, R. (eds) (1979) Second International Symposium on Fossil Algae. Bull. Cent. Rech. Explor-Prod. Elf-Aquitaine 3, 385-885.

Pomoni-Papaioannou, F. & Karakitsios, V. (2002) Facies analysis of the Trypali carbonate unit (Upper Triassic) in central-western Crete (Greece): an evaporite formation transformed into solution-collapse breccias. Sedimentology 49, 1113-1132.

Pop, G. (1997) Tithonian to Hauterivian praecalpionellids and calpionellids: bioevents and biozones. Mineralia Slov. 29, 304-305.

Posamentier, H.W. & Allen, G.P. (1993) Variability of the sequence stratigraphic model: effects of local basin factors. Sed. Geol. 86, 91-109.

Posamentier, H.W., Allen, G.P., James, D.P. & Tesson, M. (1992) Forced regressions in a sequence stratigraphic framework: concepts, examples and exploration significance. AAPG Bull. 76, 1687-1709.

Posamentier, H.W. & James, D.P. (1993) An overview of sequence-stratigraphic concepts: uses and abuses. Spec. Publ. Int. Assoc. Sedimentol. 18, 3-18.

Posamentier, H.W., Jervey, M.T. & Vail, P.R. (1988) Eustatic controls on clastic deposition I - conceptual framework. In: Sea-level changes - an integrated approach. SEPM Spec. Publ. 42, 109-124.

Posamentier, H.W. & Vail, P.R. (1988) Eustatic controls on clastic deposition II - sequence and systems tract models. In: Sea-level changes - an integrated approach. SEPM Spec. Publ. 42, 125-154.

Pratt, B.R. & James, N.P. (1986) The St George Group (Lower Ordovician) of western Newfoundland: tidal flat island maodel for carbonate sedimentation in shallow epeiric seas. Sedimentology 33, 313-343.

Pratt, B.R., James, N.P. & Covan, C.A. (1992) Peritidal carbonates. In: Walker, R.G. & James, N.P. (eds) Facies models: a response to sea-level change. 303-322. (Geol. Assoc. Canada)

Price, G.D. (1999) The evidence and implications of polar ice during the Mesozoic. Earth Sci. Rev. 48, 183-210.

Price, G.D., Sellwood, B.W. & Valdes, P.J. (1995) Sedimentological evaluation of general circulation model simulations for the "greenhouse" Earth: Cretaceous and Jurassic case studies. Sed. Geol. 100, 159-180.

Price, G.D., Valdes, P.J. & Sellwood, B.W. (1998) A comparison of CGM simulated Cretaceous 'greenhouse' and 'icehouse' climates: implications for the sedimentary record. Palaeogeogr., Palaeoclim., Palaeoecol. 142, 123-138.

Price, G.D., Valdes, P.J. & Sellwood, B.W. (1997) Quantitative palaeoclimate CGM validation: late Jurassic and mid Cretaceous case studies. J. Geol. Soc., London 154, 769-772.

Proust, J.N., Deconinck, J.-F., Geyssant, J.R., Herbin, J.P. & Vidier, J.P. (1995) Sequence analytical approach to the Upper Kimmeridgian-Lower Tithonian storm-domiated ramp deposits of the Boulonnais (Northern France). A landward time-equivalent to offshore marine source rocks. Geol. Rundsch. 84, 255-271.

Proust, J.-N., Mahieux, G. & Tessier, B. (2001) Field and seismic images of sharp-based shoreface deposits: implications for sequence stratigraphic analysis. J. Sed. Res. 71, 944-957.

Purser, B.H. (1975) Tidal sediments and their evolution in the Bathonian carbonates of Burgundy, France. In: GINSBURG, R.N. Tidal deposits: a casebook of recent examples and fossil counterparts. 335-343. (Springer)

Purser, B.H. (ed) (1973) The Persian Gulf: Holocene carbonate sedimentation and diagenesis in a shallow epicontinental sea. 471 pp. (Springer)

Purser, B.H., Brown, A. & Aissaoui, D.M. (1994) Nature, origins and evolution of porosity in dolomites. In: .Purser, B.H., Tucker, M.E. & Zenger, D.H. (eds) Dolomites – a volume in honour of Dolomieu. IAS Spec. Publ. 21, 283-308.

Purser, B.H., Tucker, M.E. & Zenger, D.H. (1994) Problems, progress and future research concerning dolomites and dolomitization. In: Purser, B.H., Tucker, M.E. & Zenger, D.H. (eds) Dolomites – a volume in honour of Dolomieu. IAS Spec. Publ. 21, 3-20.

Qing, H., Bosence, D.W.J. & Rose, E.P.F. (2001) Dolomitization by penesaline sea water in Early Jurassic peritidal platform carbonates, Gibraltar, western Mediterranean. Sedimentology 48, 153-163.

Radke, B.M. & Mathis, R.L. (1980) On the formation and occurrence of saddle dolomite. J. Sed. Petr. 50, 132-148.

Raja Gabaglia, G.P. (1995) Stratigrphie et faciès de tempête de la rampe carbonatée du Jurassique supérieur du centre du Bassin du Sud-Est (France) : Calcarenites, brèches, corps glissés. PhD thesis, Université Montpellier II, vol. 1 (text, 239 pp.) & vol. 2 (figures).

Rameil, N., Götz, A.E. & Feist-Burkhardt, S. (2000) High-resolution sequence interpretation of epeiric shelf carbonates by means of palynofacies analysis: an example from the Germanic Triassic (Lower Muschelkalk, Anisian) of East Thuringia, Germany. Facies 43, 123-144.

Rankey, E.C. (2002) Spatial patterns of sediment accumulation on a Holocene carbonate tidal flat, Northwest Andros Island, Bahamas. J. Sed. Res. 72, 591-601.

Rankey, E.C. (2001) Patterns of sediment accumulation on a modern tidal flat: Three Creeks area, Andors Island, Bahamas. 11 pp.

Read, J.F. (1995) Overview of carbonate platform sequences, cycle stratigraphy and reservoirs in greenhouse and icehouse worlds. In: Read, J.F., Kerans, C., Weber, L.J. Sarg, J.F. & Wright, F.M. (eds) Milankovitch sea-level changes, cycles, and reservoirs on carbonate platforms in greenhouse and icehouse worlds. SEPM Short Course Notes 35, 1-102.

Read, J. F. & Horbury, A.D. (1993) Eustatic and tectonic controls on porosity evolution beneath sequence-bounding unconformities and parasequence disconformities on carbonate platforms. In: Horbury, Andrew D. & Robinson, Andrew (eds) Diagenesis and basin development. AAPG Studies in Geology 36, 155-197.

Read, J.F., Kerans, C., Weber, L.J. Sarg, J.F. & Wright, F.M. (1995) Milankovitch sea-level changes, cycles, and reservoirs on carbonate platforms in greenhouse and icehouse worlds. SEPM Short Course Notes 35.

Rees, P.M., Ziegler, A.M. & Valdes, P.J. (2000) Jurassic phytogeography and climates: new data and model comparisons. In: Huber, B.T., Macleod, K.G. & Wing, S.L. (eds) Warm climates in Earth history. 297-318. (Cambridge University Press)

Reid, R.P. & Macintyre, I.G. (1998) Carbonate recrystallization in shallow marine environments: a widespread diagenetic process forming micritized grains. J. Sed. Res. 68, 928-946.

reid, r.p. & macintyre, I.G. (2000) Microboring versus recrystallization: further insight into the micritization process. J. Sed. Res. 70, 24-28.

Reid, R.P., Macintyre, I.G. & James, N.P. (1990) Internal precipitation of microcrystalline carbonate: a fundamental problem for sedimentologists. Sedimentary Geology 68, 163-170.

Reid, R.P., Macintyre, I.G. & Post, J.E. (1992) Micritized grains in northern Belize lagoon: a major source of Mg-calcite mud. J. Sed. Petr. 62, 145-156.

Reinhold, C. (1998) Multiple episodes of dolomitization and dolomite recrystallization during shallow burial in Late Jurassic shelf carbonates: eastern Swabian Alb, southern Germany. Sedimentary Geology 121, 71-95.

Remane, J. (1998) Les calpionelles : possibilités biostratigraphiques et limitations paléobiogéographiques. Bull. Soc. géol. France 169, 829-839.

Remane, J. (1991) The Jurassic-Cretaceous boundary: problems of definition and procedure. Cretaceous Res. 12, 447-453.

Remane, J. (1985) Calpionellids. In: Bolli, H.M., Saunders, J.B. & Perch-Nielsen, K. Plankton stratigraphy. 555-572. (Cambridge University Press)

Remane, J. (1970) Die Entstehung der resedimentären Breccien im Obertithon der subalpinen Ketten Frankreichs. Eclogae geol. Helv. 63, 685-740.

Remane, J. (1967) Les possibilités actuelles pour une utilisation stratigraphique des Calpionelles (Protozoa *incertae sedis*, Ciliata?). Proc. 1st Int. Conf.planktonic microfossils, Geneva, 559-573.

Remane, J. (1966) Note préliminaire sur la paléogéographie du Tithonique des chaînes subalpines. Bull. Soc. géol. France (7) VIII, 448-453.

Remane, J. (1960) Les formations brèchiques dans le Tithonique du S.E, de la France. Trav. Lab. Géol. Fac. Sci. Grenoble 36, 75-114.

Riboulleau, A., Baudin, F., Daux, V., Hantzpergue, P., Renard, M. & Zakharov, V. (1998) Evolution de la paléotempérature des eaux de la plate-forme russe au cours du Jurassique supérieur. C. R. Acad. Sci. Paris 326, 239-246.

Rich, T.H., Vickers-Rich, P. & Gangloff, R.A. (2002) Polar dinosaurs. Science 295, 979-980.

Richter, D.K. (1983) Calcareous ooids: a synopsis. In: Peryt, T.M. (ed.) Coated Grains. 71–99. (Springer)

Ricken, W. (1986) Diagenetic Bedding –A Model for Marl-Limestone

Alterations. Lecture Notes in Earth Sciences 6, 210 pp. (Springer)
Riding, R. (2000) Microbial carbonates: the geological record of calcified bacterial-algae mats and biofilms. Sedimentology 47 (SupPl. 1), 179-214.
Riding, R. (1999) The term stromatolite: towards an essential definition. Lethaia 32, 321-330.
Riding, R. (ed) (1991) Calcareous algae and stromatolites. 571 pp. (Springer)
Riding, R. & Guo, L. (1992) Affinity of *Tubiphytes*. Palaeontology 35, 37-49.
Rittener, T. (1902) Etude géologique de la Côte aux Fées et des environs de Ste-Croix et des Baulmes. Matér. Carte Géol. Suisse, N.S. 13.
Robert, C. & Kennet, J.P. (1994) Antarctic continental weathering changes during Eocene-Oligocene boundary: clay mineral evidence. Geology 22, 211-214.
Robinson, P.L. (1973) Palaeoclimatology and continental drift. In: Tarling, D.H. & Runcorn, S.K. (eds) Implications of continental drift to the Earth Sciences, I. 449-476. (Academic Press)
Rollier, L. (1888) Etude stratigraphiue sur le Jura bernois : Les faciès du Malm jurassien. Arch. Sci. phys. nat. Genève, 3/19.
Roulin, S. (2001) Géologie de la région Derborence-Sanetsch (Valais, Suisse) et étude séquentielle et cyclostratigraphique du Malm. Unpubl. diploma thesis 70 pp.
Ruf, M., Link, E., Pross, J. & Aigner, T. (2005a) Integrated sequence stratigraphy: Facies, stable isotope and palynofacies analysis in a deeper epicontinental carbonate ramp (Late Jurassic, SW Germany). Sed. Geol. 175, 391–414.
Ruf, M., Link, E., Pross, J. & Aigner, T. (2005b) A multi-proxy study of deeper-water carbonates (Late Jurassic, southern Germany): combining sedimentology, chemostratigraphy and palynofacies. Facies. (online first)
Ruffell, A.H., Price, G.D., Mutterlose, J., Kessels, K., Baraboshkin, E. & Gröcke, D.R. (2002) Palaeoclimate indicators (clay minerals, calcareous nannofossils, stable isotopes) compared from two successions in the late Jurassic of the Volga Basin (SE Russia). Geol. J. 37, 17-33.
Ruffell, A.H. & Rawson, P.F. (1994) Palaeoclimate controls on sequence stratigraphic patterns on the late Jurassic to mid-Cretaceous, with a case study from Eastern England. Palaeogeogr., Palaeoclim., Palaeoecol. 110, 43-54.
Sachs, V.N., Basov, V.A., Zakharov, V.A., Nalnjaeva, T.I. & Shulgina, N.I. (1975) Jurassic-Cretaceous boundary, position of Berriasian in the Boreal realm and correlation with Tethys. Colloque sur la limite Jurassique-Crétacé, Lyon, Neuchâtel, Sept. 1973, Mém. B.R.G.M. 86, 135-141.
Sadler, P.M., Osleger, D.A. & Montañez, I.P. (1993) On the labeling, length, and objective basis of Fischer Plots. J. Sed. Petr. 63, 360-368.
Salfeld, H. (1913) Certain Upper Jurassic strata of England. J. Geol. Soc. London 69, 423–432.
Samankassou, E., Tresch, J. & Strasser, A. (2005) Origin of peloids in Early Cretaceous deposits, Dorset, South England. Facies 51, in press.
Sarg, J.F. (2003) Saline giants and carbonate-evaporite transitions. Abstract 12th Bathurst Meeting – Int. Conference of Carbonate Sedimentologists, 8-10 July 2003, Durham, 97.
Sarg, J.F. (1988) Carbonate sequence stratigraphy. In: Wilgus, C.K., Hastings, B.K., Posamentier, H., Van Wagoner, J., Ross, C.A. & Kendall, C.G.St.C. (eds) Sea-level changes - an integrated approach. SEPM Spec. Publ. 42, 155-181.
Schär, U. (1967) Geologische und sedimentpetrographische Untersuchungen im Mesozoikum und Tertiär des Bielerseegebiets (Kt. Bern). Beitr. geol. Karte Schweiz N.F. 133.
Schardt, H. (1891) Études géologiques sur l'extrémité méridionale de la première chaîne du Jura (Chaîne du Reculet-Vuache), Bull. Soc. vaud. Sci. nat. 27, 69-158.
Scherzinger, A. & Schweigert, G. (1999) Die Ammoniten-Faunenhorizonte der Neuburg-Formation (Oberjura, Südliche Frankenalb) und ihre Beziehungen zum Volgium. Mitt. Bayer. Staatsslg. Paläont. hist. Geol. 39, 3-12.
Schettino, A. & Scotese, C. (2002) Global kinematic constraints to the tectonic history of the Mediterranean region and surrounding areas during the Jurassic and Cretaceous. In: Rosenbaum, G. & Lister, G.S. (eds) Reconstruction of the evolution of the Alpine-Himalayan Orogen. J. Virtual ExPl. 8, 149-168.
Schlager, W. (1999) Scaling of sedimentation rates and drowning of reefs and carbonate platforms, Geology 27, 183-186.
Schlager, W. (1999) Sequence stratigraphy of carbonate rocks. The Leading Edge 18, 901-907.
Schlager, W. (1999) Type-3 sequence boundaries. In: Harris, P.M., Saller, A.H., Arthur H. & Simo, J.A. (eds) Advances in carbonate sequence stratigraphy: Application to reservoirs, outcrops and models. SEPM Spec. Publ. 63, 35-45.
Schlager, W. (1993) Accomodation and supply — a dual control on stratigraphic sequences. Sedimentary Geology 86, 111-136.
Schlager, W. (1991) Depositional bias and environmental change — important factors in sequence stratigraphy. Sedimentary Geology 70, 109-130.
Schlager, W. (1989) Drowning unconformities on carbonate platforms. In: Controls on carbonate platform and basin development. SEPM Spec. Publ. 44, 15-25.
Schlager, W., Marsal, D., van der Geest, P.A.G., Sprenger, A., Fouke, B.W. (1995) Platform drowning, scaling of sedimentation rates and environmental change. In: Hine, A.C. & Halley, R.B. (prefacers) Linked Earth systems, St. Pete Beach, FL, United States, Aug. 13-16: Congress program and abstracts Vol. 1, 110.
Schlager, W., Reijmer, J.J.G. & Droxler, A. (1994) Highstand shedding of carbonate platforms, J. Sed. Res. 64, 270-281.
Schlager, W. & Schlager, M. (1973) Clastic sediments associated with radiolarites (Tauglboden-Schichten, Late Jurassic, Eastern Alps). Sedimentology 20, 65-89.
Schlagintweit, F. & Ebli, O. (1999) New results on microfacies, biostratigraphy and sedimentology of Late Jurassic - Early Cretaceous platform carbonates of the Northern Calcareous Alps. Abh. Geol. B.-A. 56 (2), 379-418.
Schlagintweit, F. & Gawlick, H.-J. (2002) Biostratigraphy of the Alpine Plassen Formation (Kimmeridgian - Berriasian) – new aspects on base of analysis of the type-locality (Plassen, Austria) and occurrences near Lofer (Salzburg, Austria). In: Hüssner, H., Hinderer, M., Götz, A.E. & Petschick, R. (eds) SEDIMENT 2002, 17. Sedimentologentreffen, Frankfurt a.M./Darmstadt, 29.-31. Mai 2002, Kurzfassungen und Programm. Schr. Deutsch. Geol. Ges. 17, 185-186.
Schmid, D.U. (1996) Marine Mikrobolithe und Mikroinkrustierer aus dem Oberjura. Profil 13, 101-251.
Schmid, D.U. (1995) "*Tubiphytes*" *morronensis* – eine fakultativ inkrustierende Foraminifere mit endosymbiontischen Algen. Profil 8, 305-317.
Schmid, D.U. & Jonischkeit, A. (1995) The Late Jurassic São Romão limestone (Algarve, Portugal): an isolated carbonate ramp. Profil 8, 319-337.
Schmid, D.U. & Leinfelder, R.R. (1996) The Jurassic *Lithocodium aggregatum-Troglotella incrustans* foraminiferal consortium. Palaeontology 39, 21-52.
Schnyder, J. (2003) Le passage Jurassique/Crétacé: Evénements instantanés, variations climatiques enregistrées dans les faciès purbeckiens français (Boulonnais, Charentes) et anglais (Dorset) - Comparaison avec le domaine téthysien. PhD thesis, Laboratoire PBDS, Université de Lille 1, 388 pp.
Scholle, P.A., Bebout, D.G. & Moore, C.H. (eds) (1983) Carbonate depositional environments. AAPG Mem. 33, 708 pp.
Scholle, P.A., Stemmerik, L., Ulmer-Scholle, D., Di Liegro, G. & Henk, F.H. (1993) Palaeokarst-influenced depositional and diagenetic patterns in Upper Permian carbonates and evaporites, Karstryggen area, central East Greenland. Sedimentology 40, 895-918.
Scholle, P.A., Ulmer, D.S. & Melim, L.A. (1992) Late-stage calcites in the Permian Capitan Formation and its equivalents, Delaware Basin margin, west Texas and New Mexico: evidence for replacement of precursor evaporites. Sedimentology 39, 207-234.
Schreiber, B.C. & El Tabakh, M. (2000) Deposition and early alteration of evaporites. Sedimentology 47 (SupPl. 1), 215-238.
Schudack, M.E. (1999) Ostracoda (marine/nonmarine) and palaeoclimate history in the Late Jurassic of Central Europe and North America. Mar. Micropalaeontol. 37, 273-288.
Schulz, M. & Schäfer-Neth, C. (1997) Translating Milankovitch climate forcing into eustatic fluctuations via thermal deep water ex-

pansion: a conceptual link. Terra Nova 9, 228-231.

Schwarzacher, W. (1947) Über die sedimentäre Rhythmik des Dachsteinkalkes von Lofer. Geol. Bundesanstalt, Verh. H10-12, 175-188.

Schweigert, G. (1993) Subboreale Faunenelemente (Ammonoidea) im oberen Weißjura (Oberkimmeridgium) der Schwäbischen Alb. Profil 5, 141-155.

Séguret, M., Moussine-Pouchkine, A., Raja Gabaglia, G. & Bouchette, F. (2001) Storm deposits and storm-generated coarse carbonate breccias on a pelagic outer shelf (South-East Basin, France). Sedimentology 48, 231-254.

Sellwood, B.W. & Sladen, C.P. (1981) Mesozoic and Tertiary argillaceous units; distribution and composition. J. Engin. Geol. & Hydrogeol., 14, 263-275

Sellwood, B.W. & Valdes, P.J. (1997) Geological evaluation of climate General Circulation Models and model implications for Mesozoic cloud cover. Terra Nova 9, 75-78.

Sellwood, B.W., Valdes, P.J. & Price, G.D. (2000) Geological evaluation of multiple general circulation model simulations of Late Jurassic palaeoclimate. Palaeogeogr., Palaeoclim., Palaeoecol. 156, 147-160.

Septfontaine, M. (1981) Les foraminifères imperforés des milieux de plate-forme au Mésozoïque: Détermination pratique, interprétation phylogénétique et utilitation biostratigraphique. Rev. Micropaléont. 23, 169-203.

Shackleton, N.J., Mccave, I.N. & Weedon, G.P. (1999) Astronomical (Milankovitch) calibration of the geological time-scale. Phil. Trans. R. Soc.Lond. A 357.

Shearman, D.J. & Smith, A.J. (1985) Ikaite, the parent mineral of Jarrowite-type pseudomorphs. Proc. Geol. Assoc. 96, 305-314.

Shinn, E.A. (1983a) Birdseyes, fenestrae, shrinkage pores, and loferites: a reevaluation. J. Sed. Petr. 53, 619-628.

Shinn, E.A. (1983b) Tidal flat. In: Scholle, P.A., Bebout, D.G. & Moore, C.H. (eds) Carbonate depositional environments. AAPG Mem. 33, 171-210.

Shinn, E.A. (1969) Submarine lithification of Holocene carbonate sediments in the Persian Gulf. Sedimentology 12, 109-144.

Shinn, E.U., Ginsburg, R.N. & Lloyd, R.M. (1965) Recent supratidal dolomite from Andros Island, Bahamas. Dolomitization and Limestone Diagenesis. 13, 112-123.

Shulgina, N.I. (1975) Boreal ammonites at the turn of the Jurassic and Cretaceous and their correlation with Tethyan ammonites. Colloque sur la limite Jurassique-Crétacé, Lyon, Neuchâtel, Sept. 1973, Mém. B.R.G.M. 86, 142-148.

Sibley, D.F. & Gregg, J.M. (1987) Classification of dolomite rock textures. J. Sed. Petr. 57 (6), 967-975.

Simms, M.A. (1984) Dolomitization by groundwater-flow systems in carbonate platforms. Trans. Gulf Coast Assoc. Geol. Soc. 34, 411-420.

Singer, A. (1984) The palaeoclimatic interpretation of clay minerals in sediments - a review. Earth Sci. Rev. 21, 251-293.

Sloss, L.L. (1963) Sequences of the cratonic interior of North America. GSA Bull. 74, 93-114.

Smith, A.G., Smith, D.G. & Funnell, B.M. (1994) Atlas of Mesozoic and Cenozoic coastlines. 99 pp. [Cambridge University Press]

Sneider et al. (1995) Sequence stratigraphy of the Middle to Late Jurassic, Viking Graben, North Sea. In: Steel, R.J. (ed) Sequence stratigraphy on the Northwest European margin. . Norwegian Petroleum Soc. Spec. Publ. 5, 167-197.

Soreghan, G.S. & Dickinson, W.R. (1994) Generic types of stratigraphic cycles controlled by eustasy. Geology 22, 759-761.

Spence, G.H. & Tucker, M.E. (1999) Modeling carbonate microfacies in the context of high-frequency dynamic relative sea-level and environmental changes. J. Sed. Res. 69, 947-961.

Stampfli, G.M. & Borel, G.D. (2002) A plate tectonic model for the Palaeozoic and Mesozoic constrained by dynamic plate boundaries and restored synthetic oceanic isochrons. Earth planet. Sci. Letters 196, 17-33.

Stampfli, G.M., Borel, G.D., Marchant, R. & Mosar, J. (2002) Western Alps geological constraints on western Tethyan reconstructions. In: ROSENBAUM, G. & LISTER, G.S. Reconstruction of the evolution of the Alpine-Himalayan Orogen. J. Virtual ExPl. 8, 77-106.

Steinhauff, D.M. & Walker, K.R. (1995) Recognizing exposure, drowning, and "missed beats": platform-interior to platform-margin sequence stratigraphy of Middle Ordovician limestones, East Tennessee. J. Sed. Res. B65, 183-207.

Steinhauser, N. & Lombard, A. (1969) Définition de nouvelles unites lithostratigraphiques dans le Crétacé inférieur du Jura méridional (France). C. R. Soc. Phys. Hist. nat. Genève N.S. 4, 100-113.

Stephan, J.-F. et al. (14 co-authors) (1990) Palaeogeodynamic maps of the Caribbean: 14 steps from Lias to Present. Bull. Soc. Géol. France 8, 915-919.

Stoll, H.M. & Schrag, D.P. (1996) Evidence for glacial control of rapid sea level changes in the Early Cretaceous. Science 272, 1771-1774.

Strasser, A. (1994) Milankovitch cyclicity and high-resolution stratigraphy in lagoonal-peritidal carbonates (Upper Tithonian-Lower Berriasian, French Jura Mountains). In: De Boer, P.L. & Smith, D.G. Orbital forcing and cyclic sequences. Spec. Publ. Int. Assoc. Sedimentol. 19, 285-301. (Blackwell)

Strasser, A. (1991) Lagoonal-peritidal sequences in carbonate environments: autocyclic and allocyclic processes. In: Einsele, G., Ricken, W. & Seilacher, A. (eds) Cycles and events in stratigraphy. 709-721. (Springer)

Strasser, A. (1988) Shallowing-upward sequences in Purbeckian peritidal carbonates (lowermost Cretaceous, Swiss and Frech Jura, Switzerland). Sedimentology 35, 369-383.

Strasser, A. (1986) Ooids in Purbeck limestones (lowermost Cretaceous) of the Swiss and French Jura. Sedimentology 33, 711-727.

Strasser, A. (1984) Black-pebble occurrence and genesis in Holocene carbonate sediments (Florida Keys, Bahamas, and Tunisia). J. Sed. Petr. 54, 1097-1109.

Strasser, A. & Davaud, E. (1982) Les croûtes calcaires (calcretes) du Purbeckien du Mont-Salève (Haute-Savoie, France). Eclogae geol. Helv. 75 (2), 287-301.

Strasser, A. & Davaud, E. (1983) Black pebbles of the Pubeckian (Swiss and French Jura): lithology, geochemistry and origin. Eclogae geol. Helv. 76 (3), 551-580.

Strasser, A. & Hillgärtner, H. (1998) High-frequency sea-level fluctuations recorded on a shallow carbonate platform (Berriasian and Lower Valanginian of Mount Salève, French Jura). Eclogae geol. Helv. 91, 375-390.

Strasser, A., Hillgärtner, H., Hug, W. & Pittet, B. (2000) Third-order depositional sequences reflecting Milankovitch cyclicity. Terra Nova 12, 303-311.

Strasser, A., Hillgärtner, H. & Pasquier, J.-B. (2004) Cyclostratigraphic timing of sedimentary processes: an example from the Berriasian of the Swiss and French Jura Mountains. In: D'argenio, B. (ed.) Cyclostratigraphy: Approaches and case histories. SEPM Spec. Publ. 81, 135-151.

Strasser, A., Pittet, B., Hillgärtner, H. & Pasquier, J.-B. (1999) Depositional sequences in shallow carbonate-dominated sedimentary systems: concepts for a high-resolution analysis. Sedimentary Geology 128, 201-221.

Strasser, A. & Samankassou, E. (2003) Carbonate sedimentation rates today and in the past: Holocene of Florida Bay, Bahamas, and Bermuda vs. Late Jurassic and Early Cretaceous of the Jura Mountains (Switzerland and France). Geol. Croat. 56, 1-18.

Strohmenger, C., Deville, Q. & Fookes, E. (1991) Kimmeridgian/Tithonian eustacy and its imprints on carbonate rocks from the Dinaric and the Jura carbonate platforms. Bull. Soc. Géol. France 162, 661-671.

Strohmenger, C. & Strasser A. (1993) Eustatic controls on the depositional evolution of Upper Tithonian and Berriasian deep-water carbonates (Vocontian Trough, SE France). Bull. Cent. Rech.-Expl. Elf-Aquitaine 17/1, 183-203.

Sudan, P. (1997) Géologie de la rive gauche du Lac de Joux (VD, Suisse) et analyse séquentielle de coupes stratigraphiques Portlandien - Berriasien. Unpubl. diploma thesis, University of Fribourg, Fribourg, 109pp.

Sun, S.Q. (1994) A reappraisal of dolomite abundance and occurrence in the Phanerozoic. J. Sed. Res. A64, 396-404.

Sun, S.Q. & Wright, V.P. (1989) Peloidal fabrics in Late Jurassic reefal limestones, Weald Basin, southern England. Sed. Geol. 65, 165-181.

Surlyk, F. (2003) The Jurassic of East Greenland: a sedimentary record

of thermal subsidence, onset and culmination of rifting. In: Ineson, J.R. & Surlyk, F. (eds) The Jurassic of Denmark and Greenland. Geol. Survey Denmark Greenland Bull. 1, 659-722.

Surlyk, F. (1991) Sequence stratigraphy of the Jurassic-Lowermost Cretaceous of East Greenland. AAPG Bull. 75, 1468-1488.

Surlyk, F. (1990) Timing, style and sedimentary evolution of Late Palaezoic-Mesozoic extensional basins of East Greenland. In: Hardman, R.F.P. & Brooks, J. (eds) Tectonic events responsible for Britain's oil and gas reserves. Geol. Soc. London Spec Publ. 55, 107-125.

Swientek, O. (2002) The Greenland Norwegian seaway: climatic and cyclic evolution of Late Jurassic-Early Cretaceous sediments. PhD thesis, University of Cologne, 119pp. + appendix.

Swift, D.J.P. (1968) Coastal erosion and transgressive stratigraphy. J. Geol. 76, 444-456.

Tavera, J.M. (1985) Les ammonites del Tithonico superior-Berriasense da la Zone Subbética. PhD thesis, University of Granada, 381 pp.

Taylor, S.P. & Sellwood, B.W. (2002) The context of lowstand events in the Kimmeridgian (Late Jurassic) sequence stratigraphic evolution in the Wessex-Weald Basin, Southern England. Sedimentary Geology 151, 89-106.

Taylor, S.P., Sellwood, B.W., Gallois, R.W. & Chambers, M.H. (2001) A sequence stratigraphy of the Kimmeridgian and Bolonian stages (late Jurassic): Wessex-Weald Basin, southern England. J. geol. Soc. London 158, 179-192.

Tempier, C. (1966) Les faciès du Jurassique terminal en Provence. C. R. Acad. Sci. Paris 262, 958-960.

Termier, H. & Termier, G. (1977) Rôle des éponges hypercalcifiées en palécologie et en paléobiogéographie. Bull. Soc. géol. France XVII, n° 5, 803-819.

Termier, G., Termier, H. & Vachard, D. (1977) Etude comparative de quelques ischyrosponges. Géologie Méditerranéenne Tome IV, n° 2, 139-180.

Thalmann, H.K. (1966) Zur Stratigraphie des oberen Malm im südlichen Berner und Solothurner Jura. PhD thesis, University of Berne, 126 pp.

Thierry, J. (2000) Early Tithonian. In: Crasquin, S. (coord.) Atlas Peri-Tethys: Palaegeographical maps – Explanatory notes. CCGM/CGMW, Paris, 99-110.

Thierry, J. et al. (41 co-authors) (2000) Early Tithonian. In: Dercourt, J., Gaetani, M., Vrielynck, B., Barrier, E., Biju-Duval, B., Brunet, M.F., Cadet, J.P., Crasquin, S. & Sandulescu, M. (eds) Atlas Peri-Tethys: Palaegeographical maps. CCGM/CGMW, Map 11.

Thiry, M. (2000) Palaeoclimatic interpretation of clay minerals in marine deposits: an outlook from the continental origin. Earth Sci. Rev. 49, 201-221.

Thorne, J.A. & Swift, D.J.P. (1991a) Sedimentation on continental margins, II. Application of the regime concept. In: Swift, D.J.P. et al. (eds) Shelf sand and sandstone bodies. IAS Spec. Publ. 14, 33-58.

Thorne, J.A. & Swift, D.J.P. (1991b) Sedimentation on continental margins, VI. A regime model for depositional sequences, their component systems tracts, and bounding surfaces. In: Swift, D.J.P. et al. (eds) Shelf sand and sandstone bodies. IAS Spec. Publ. 14, 189-255.

Thurmann, J. (1832) Essai sur les soulèvements jurassiques de Porrentruy – Description géognostique de la série jurassique et théorie orographique du soulèvement. Mém. Soc. Hist. nat. Strasbourg.

Thurmann, J. & Étallon, A. (1861-64) *Lethea bruntrutana* ou études paléontologiques et stratigraphiques sur le Jura bernois. Neue Denkschr. schweiz. naturf. Ges. 21, 18-20.

Tribovillard, N.-P. (1998) Cyanobacterially generated peloids in laminated, organic-matter rich limestones: an unobstrusive presence. Terra Nova 10, 126-130.

Trümpy, R. (1980) Geology of Switzerland — A guidebook. Part A: An outline of the geology of Switzerland.

Tucker, M.E. (1999) Evaporites in a sequence stratigraphic context. Abstract IAS Int. Conference on Carbonate-Evaporite Transitions, Lviv, Ukraine.

Tucker, M.E. (1993) Carbonate diagenesis and sequence stratigraphy, Sedimentology Review 1, 51-72.

Tucker, M.E. & Wright, V.P. (1990) Carbonate Sedimentology. 482 pp. (Blackwell)

Vail, P.R., Audemard, F., Bowman, S.A., Eisner, P.N. & Perez-Cruz C. (1991) The stratigraphic signatures of tectonics, eustasy and sedimentology – an overview. In: Einsele, G., Ricken, W. & Seilacher, A. (eds) Cycles and events in stratigraphy. 617-659. (Springer)

Vail, P.R., Hardenbol, J. & Todd, R.G. (1984) Jurassic unconformities, chronostratigraphy, and sea-level changes from seismic stratigraphy and biostratigraphy. In: Schlee, J.S. (ed.) Interregional unconformities and hydrocarbon accumulation. AAPG Mem. 36, 129-144.

Vail, P.R., Mitchum, R.M. & Thompson, S. (1977) Seismic stratigraphy and global changes of sea level, part 3: Relative changes of sea level from coastal onlap. In: Clayton, C.E. (ed.) Seismic stratigraphy – applications to hydrocarbon exploration. AAPG Mem. 26, 63-81.

Valdes, P. (1994) Atmospheric general circulation models of the Jurassic. In: Allen, J.R.L., Hoskins, B.J., Sellwood, B.W., Spicer, R.A & Valdes, P.J. (eds) Palaeoclimates and their modelling. 109-118.

Valdes, P.J. & Glover, R.W. (1999) Modelling the climate response to orbital forcing. In: Shackleton, N.J., Mccave, I.N. & Weedon, G.P. (eds) Astronomical (Milankovitch) calibration of the geological time-scale. Phil. Trans. R. Soc.Lond. A 357, 1873-1890.

Valdes, P.J. & Sellwood, B.W. (1992) A palaeoclimate model for the Kimmeridgian. Palaeogeogr., Palaeoclim., Palaeoecol. 95, 47-72.

Valdes, P.J., Sellwood, B.W. & Price, G.D. (1995) Modelling Late Jurassic Milankovitch climate variations. In: House, M.R. & Gale, A.S. (eds) Orbital forcing timescales and cyclostratigraphy. Geol. Soc. Spec. Publ. 85, 115-132.

van Houten, F.B. & Purucker, M.E. (1984) Glauconitic peloids and chamositic ooids – favourable factors, constraints, and problems. Earth Sci. Rev. 20, 211-243.

van Lith, Y., Warthmann, R., Vasconcelos, C. & Mckenzie, J.A. (2003a) Sulphate-reducing bacteria induce low-temperature Ca-dolomite and high Mg-calcite formation. Geobiology 1, 71-79.

van Lith, Y., Warthmann, R., Vasconcelos, C. & Mckenzie, J.A. (2003b) Microbial fossilization in carbonate sediments: a result of the bacterial surface involvement in dolomite precipitation. Sedimentology 50, 237-245.

Van Wagoner, J.C., Mitchum, R.M., Campion, K.M. & Rahmanian, V.D. (1990) Siliciclastic sequence stratigraphy in well logs, cores, and outcrops. AAPG Methods in Exploration 7, 55 pp.

Van Wagoner, J.C., Posamentier, H.W., Mitchum, R.M., Vail, P.R., Sarg, J.F., Loutit, T.S. & Hardenbol, J. (1988) An overview of the fundamentals of sequence stratigraphy and key definitions. Sea-level changes - an integrated approach. 42, 38-45.

Vasconcelos, C. & Mckenzie, J.A. (1997) Microbial mediation of modern dolomite precipitation and diagenesis under anoxic conditions (Lagoa Vermelha, Rio de Janeiro, Brazil). J. Sed. Res. 67 (3), 379-390.

Veizer, J. et al. (14 co-authors) (1999) $^{87}Sr/^{86}Sr$, delta^{13}C and delta^{18}O evolution of Phanerozoic seawater. Chemical Geology 161, 59-88.

Velde, B.C. (1995) Compaction and diagenesis. In: Velde, B.C. (ed) Origin and mineralogy of clays – Clays and the environment. 220-246. (Springer)

Vercoutere, C. & van den Haute, P. (1993) Post-Palaeozoic cooling and uplift of the Brabant Massif as revealed by apatite fission track analysis. Geol. Mag. 130, 639-646.

Videtich, P.E. & Matthews, R.K. (1980) Origin of discontinuity surfaces in limestones: isotopic and petrographic data, Pleistocene of Barbados, West Indies. J. Sed. Petr. 50, 971-980.

Waehry, A. (1989) Faciès et séquences de dépot dans la formation de Pierre-Châtel (Berriasien moyen, Jura éridional/France). Unpubl. diploma thesis, Université de Genève, 78 pp.

Walker, R.G. & James, N.P. (eds) (1992) Facies models, response to sea level change. Geol. Assoc. Canada, GeoText 1, 409 pp.

Wanless, H.R., Tedesco, L.P. & Tyrell, K.M. (1988) Production of subtidal tubular and surficial tempestites by hurricane Kate, Caicos platform, British West Indies. J. Sed. Petr. 58 (4), 739-750.

Warrak, M. (1974) The petrography and origin of dedolomitized, veined or brecciated carbonate rocks, the 'cornieules', in the Fréjus region, French Alps. J. geol. Soc. London 130, 229-247.

Warren, J. (2000) Dolomite: occurrence, evolution and economically important associations. Earth Sci. Rev. 52, 1-81.

Waterhouse, H.K. (1995) High-resolution palynofacies investigation of Kimmeridgian sedimentary cycles. Orbital forcing timescales and cyclostratigraphy. 85, 115-132.

Weaver, C.E. (1989) Clays, muds and shales. 819 pp. (Elsevier)

Weedon, G.P. (1993) The recognition and stratigraphic implications of orbital-forcing of climate and sedimentary cycles. Sedimentology Reviews 1, 31-50.

Weedon, G.P., Coe, A.E. & Gallois, R.W. (2004) Cyclostratigraphy, orbital tuning and inferred productivity for the type Kimmeridge Clay (Late Jurassic), Southern England). J. geol. Soc. London 161, 655-666.

Weedon, G.P., Jenkyns, H.C., Coe, A.L. & Hesselbo, S.P. (1999) Astronomical calibration of the Jurassic time-scale from cyclostratigraphy in British mudrock formations. In: Shackleton, N.J., Mccave, I.N. & Weedon, G.P. Astronomical (Milankovitch) calibration of the geological time-scale. Phil. Trans. R. Soc. Lond. A 357, 1787-1813.

Weissert, H. & Mohr, H. (1996) Late Jurassic climate and its impact on carbon cycling. Palaeogeogr., Palaeoclim., Palaeoecol. 122, 27-43.

Westphal, H., Böhm, F. & Bornholt, S. (2004) Orbital frequencies in the carbonate sedimentary record: distorted by diagenesis? Facies 50, 3-11.

Westphal, H., Head, M.J. & Munnecke, A. (2000) Differential diagenesis of rhythmic limestone alternations supported by palynological evidence. J. Sed. Res. 70, 715-725.

Westphal, H. & Munnecke, A. (2002) What the spatial and temporal distribution of limestone-marl alternations is telling us. In: Hüssner, H., Hinderer, M., Götz, A.E. & Petschick, R. (eds) SEDIMENT 2002, 17. Sedimentologentreffen, Frankfurt a.M./Darmstadt, 29.-31. Mai 2002, Kurzfassungen und Programm. Schr. Deutsch. Geol. Ges. 17, 218.

westphal, h., munnecke, a., pross, j. & herrle, j. (2002) Pelagic limestone-marl alternations from the Cretaceous North Atlantic — do they reflect sea-level fluctuations? In: Hüssner, H., Hinderer, M., Götz, A.E. & Petschick, R. (eds) SEDIMENT 2002, 17. Sedimentologentreffen, Frankfurt a.M./Darmstadt, 29.-31. Mai 2002, Kurzfassungen und Programm. Schr. Deutsch. Geol. Ges. 17, 219.

Westphal, H., Munnecke, A., Pross, J. & Herrle, J.O. (2004) Multiproxy approach to understanding the origin of Cretaceous pelagic limestone-marl alternations (DSDP site 391, Blake-Bahama Basin). Sedimentology 51, 109-126.

Whalen, M.T., Eberli, G.P., Van Buchem, F.S.P., Mountjoy, E.W. & Homewood, P.W. (2000) Bypass margins, basin-restricted wedges, and platform-to-basin correlation. Upper Devonian, Canadian Rocky Mountains: implications for sequence stratigraphy of carbonate platforms. J. Sed. Res. 70, 913-936.

Whitaker, F.F. & Smart, P.L. (1993) Circulation of saline ground water in carbonate platforms - a review and case study from the Bahamas.

Wignall, P.B. (1991) Test of the concepts of sequence stratigraphy in the Kimmeridgian (Late Jurassic) of England and northern France. Mar. Petrol. Geol. 8, 430-441.

Wignall, P.B. & Ruffell, A.H. (1990) The influence of a sudden climatic change on marine deposition in the Kimmeridgian of northwest Europe. J. Geol. Soc. London 147, 365-371.

Wilkinson, B.H., Diedrich, N.W. & Drummond, C.N. (1996) Facies successions in peritidal carbonate sequences. J. Sed. Res. 66, 1065-1078.

Wilkinson, B.H. & Drummond, C.N. (2004) Facies mosaic across the Persian Gulf and around Antigua: stochastic and dterministic pructs of shallow-water sediment accumulation. J. Sed. Res. 74, 513-526.

Wilkinson, B.H., Drummond, C.N., Rothman, E.H. & Diedrich, N.W. (1997) Stratal order in peritidal carbonate sequences. J. Sed. Res. 67, 1068-1082.

Williams, C.J., Hesselbo, S.P., Jenkyns, H.C. & Morgans-Bell, H.S. (2001) Quartz silt in mudrocks as a key to sequence stratigraphy (Kimmeridge Clay Formation, Late Jurassic, Wessex Basin, UK). Terra Nova 13, 449-455.

Wilson, J.L. (1975) Carbonate facies in geologic history. 471 pp. (Springer)

Wright, V.P. (1994) Paleosols in shallow marine carbonate sequences. Earth Sci. Rev. 35, 367-395.

Wright, V.P. (1988) Palaeokarst and palaeosols as indicators of palaeoclimate and porosity evolution: a case study from the Carboniferous of South Wales. In: JAMES, N.P. & CHOQUETTE, P.W. (eds) Palaeokarst. 329-341. (Springer)

Wright, V.P. (ed) (1986) Palaeosols: Their recognition and interpretation. 315 pp. (Blackwell)

Wright, V.P. & Tucker, M.E. (eds) (1991) Calcretes. IAS Reprint Series Vol. 2, 352 pp. (Blackwell)

Yang, W. (2001) Estimation of duration of subaerial exposure in shallow-marine limestones - an isotopic approach. J. Sed. Res. 71 (5), 778-789.

Zakharov, V.A. & Rogov, M.A. (2003) Boreal-Tethyan mollusk migrations at the Jurassic-Cretaceous boundary time and biogeostratigraphic ecotone position in the northern hemisphere. Stratigr. Geol. Correl. 11, 152-171.

Zecchin, M. (2005) Relationships between fault-controlled subsidence and preservation of shallow-marine small-scale cycles: example from the Lower Pliocene of the Crotone Basin (southern Italy). J. Sed. Res. 75, 300-312.

Zeiss, A. (2003) The Late Jurassic of Europe: its subdivision and correlation. In: INESON, J.R. & SURLYK, F. The Jurassic of Denmark and Greenland. Geol. Survey Denmark Greenland Bull. 1, 75-114.

Ziegler, A.M., Parrish, J.M., Jiping, Y., Gyllenhaal, E.D., Rowley, D.B., Totman Parrish, J., Shangyou, N., Bekker, A. & Hulver, M.L. (1994) Early Mesozoic phytogeography and climate. In: Allen, J.R.L., Hoskins, B.J., Sellwood, B.W., Spicer, R.A & Valdes, P.J. (eds) Palaeoclimates and their modelling. 89-97.

Ziegler, P.A. (1990) Geological atlas of western and central Europe – 2nd and completely revised edition. 239 pp., 56 enclosures. (Shell Intern. Petrol. Maatschappij B.V. / Geol. Soc.)

Ziegler, P.A. (1988) Evolution of the Arctic-North Atlantic and the western Tethys. AAPG Mem. 43, 198pp.

PLATES

Plate 1 – Non-bioclastic grains

1 – Transgressive surface on tidal flat (facies tf3) overlain by an intra-pelsparite (MF inbar1). Note imbrication of larger clasts in the upper part indicating palaeocurrent direction from left to right. Sample Av188, thin section, normal light.

2 – Course, cross-bedded intraclastic grainstone (facies exbar1). Grains are well rounded and arranged in cm-scale sheets, each showing a fining-upward trend. Dip direction of foresets indicates shoal migration from right to left. Well rounded black pebbles are interpreted as reworked remains of an older emersive horizon not far away. Sample No61, etched slab.

3 – Pel-biomicrite consisting mainly of type-2 peloids (facies rl2). Sample P37, thin section, normal light.

4 – Pelsparite consisting of type-2 and type-1 peloids (facies inbar1). Note the clear difference in diameter and definition of grain surfaces: small, "cloudy" type-1 peloids fill the intergranular pore-space between large type-2 peloids characterized by a clearly defined and commonly dark edge. Sample P60-2, thin section, normal light.

5 – Oo-biomicrite (facies inbar4/rl8). The predominance of type-4 ooids ("*superficial ooids*", Strasser 1986) indicates restricted and low-energy lagoonal environments. Sample P85-3, thin section, normal light.

6 – Well sorted oosparite (facies inbar4). The absence of a muddy matrix and ooids of type 3(-4) indicate more open and agitated conditions when compared to pl. 1/5. Sample P88, thin section, normal light.

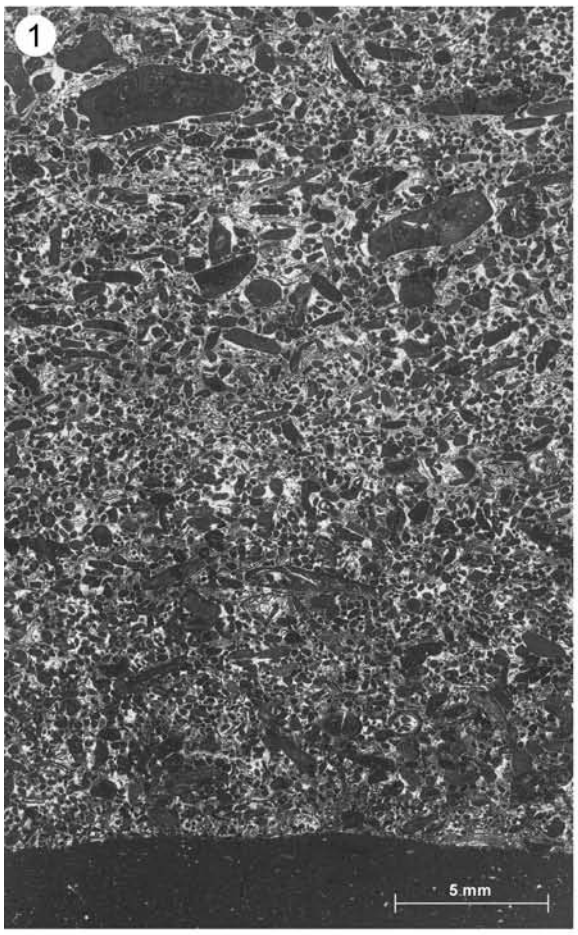
1
5 mm

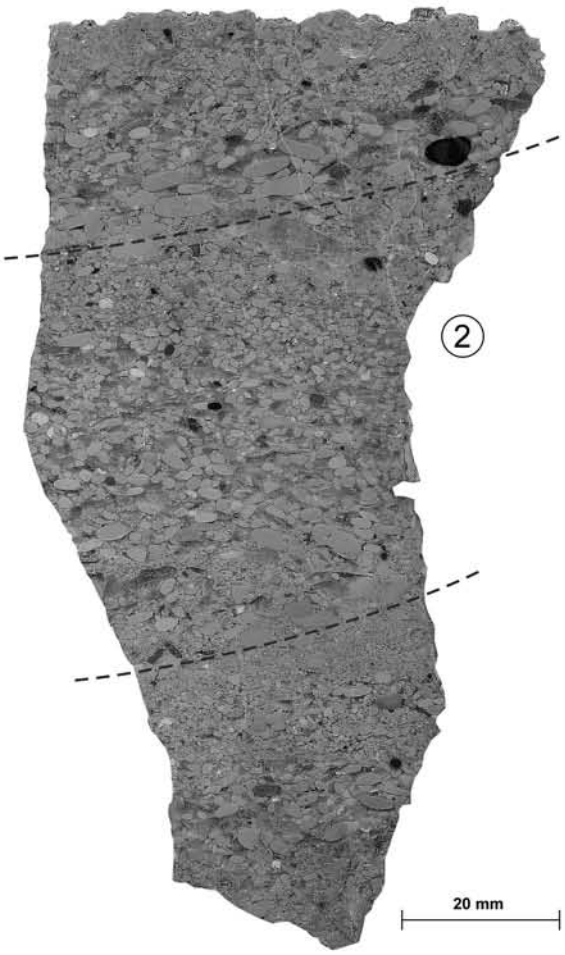
2
20 mm

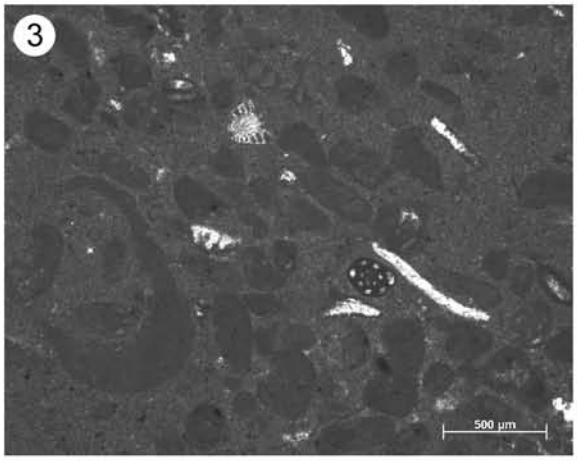
3
500 µm

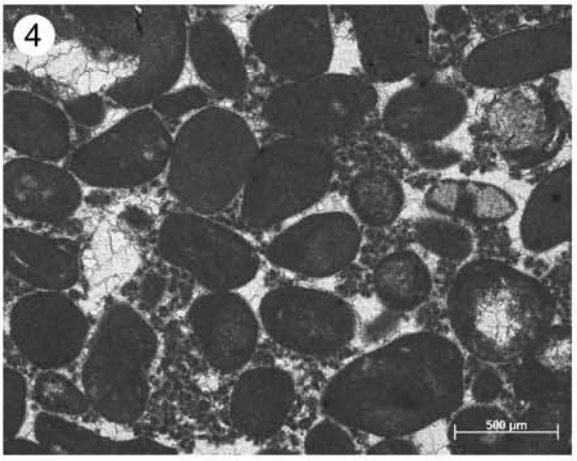
4
500 µm

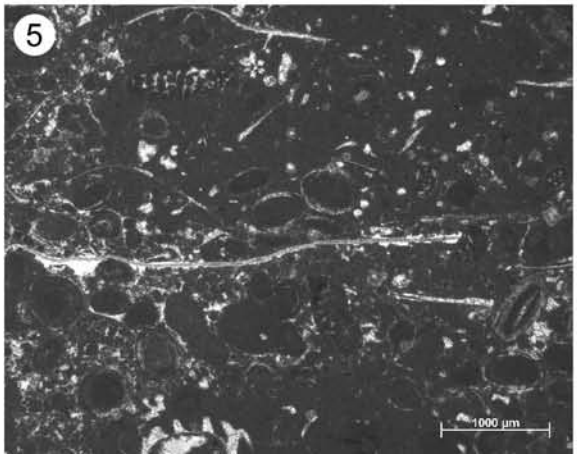
5
1000 µm

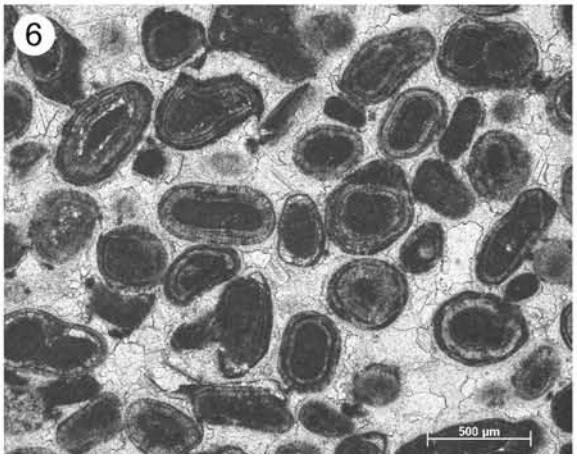
6
500 µm

Plate 2 – Bioclastic grains

1 – Subrounded coral fragment. Sample Ye2, thin section, normal light.

2 – Entire sea-urchin plate. Sample No279, thin section, normal light.

3 – Bio-pelsparite (facies wash), consisting nearly exclusively of gastropods and type-2 peloids. Note geopetal infill structures in intact gastropod shells. Sample No207, thin section, normal light.

4 – Tetraxone and monaxone sponge spicules, (a) with and (b) without preserved central cavity (facies lowEl1). Sample P44, thin section, normal light.

5 – *Cladocoropsis mirabilis* Felix. Most of the skeletal cavities are filled by muddy sediment, except for the extreme left. Note also the obliquely cut echinoid spine in the lower middle. Sample No89, thin section, normal light.

6 – *Favreina* sp. (faecal pellets of decapod crabs) in pel-biosparite (facies inbar4). (a) cross-section, (b) longitudinal section. Sample Do138, thin section, normal light.

7 – Charophyte oogon. Sample Do149, thin section, normal light.

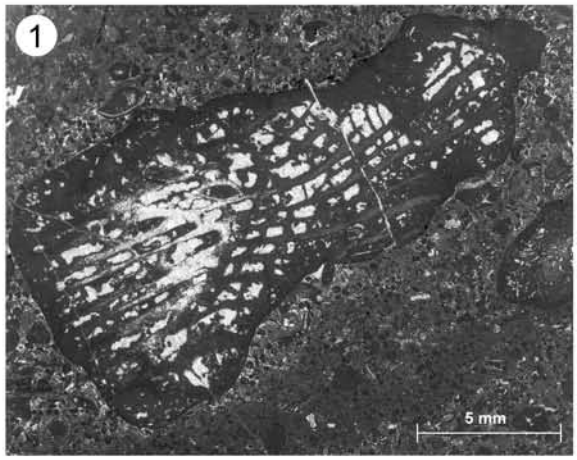
1
5 mm

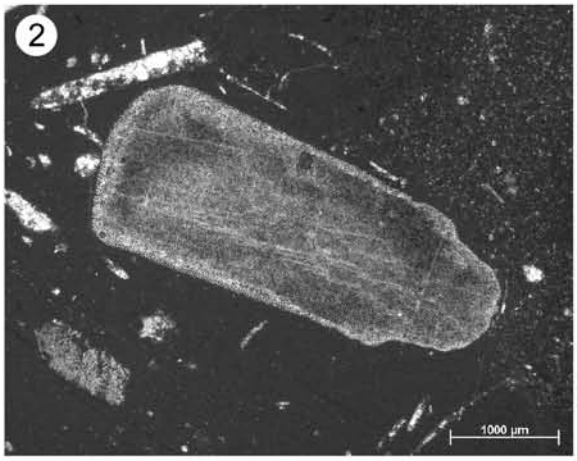
2
1000 µm


3
5 mm

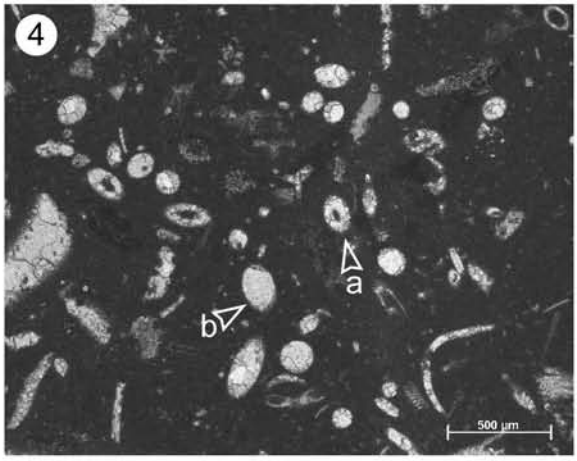
4
a
b
500 µm

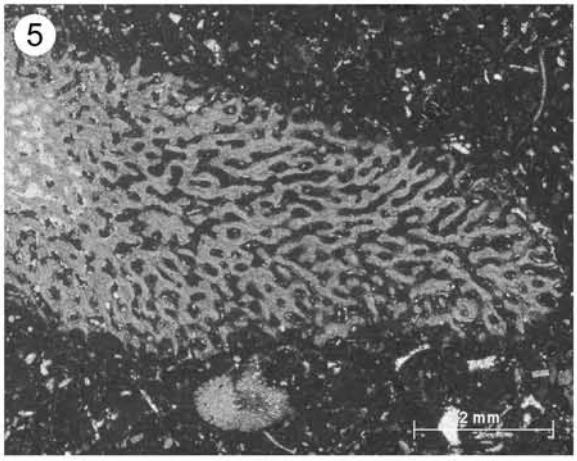
5
2 mm

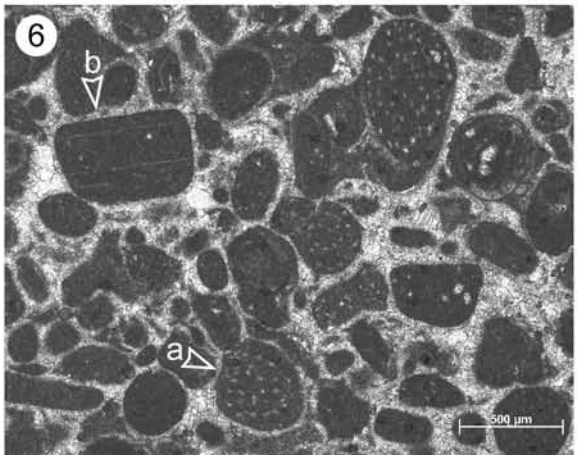
6
b
a
500 µm

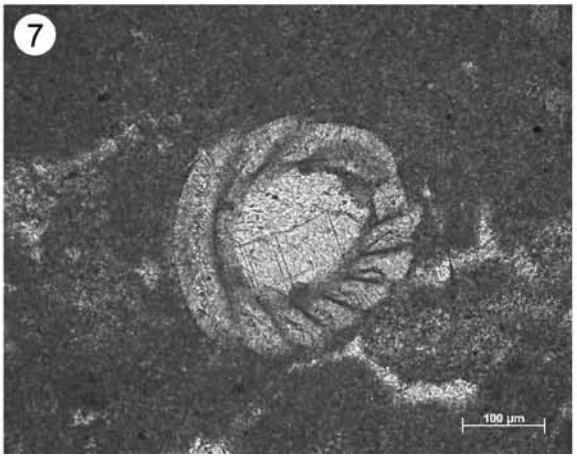
7
100 µm

Plate 3 – Bioclastic grains: forminifera

1a-c – *Kurnubia* sp. (a) Tangential section, Late Reuchenette Fm., Late Kimmeridgian, sample No98. Scale bar is 100 μm. (b) Tangential section, Late Reuchenette Fm., Late Kimmeridgian, sample No99. Scale bar is 200 μm. (c) Subaxial section, Late Reuchenette Fm., Late Kimmeridgian, sample Do80. Scale bar is 200 μm. Thin sections, normal light.

2a, b – *Lenticulina* sp. (a) Subequatorial section, Twannbach Fm., Early/Middle Tithonian, sample P11. (b) Tangential section, Twannbach Fm., Middle Tithonian, sample P39. Thin sections, normal light. Scale bar is 100 μm.

3 – *Conicospirillina* sp., axial section, Twannbach Fm., Middle Tithonian. Sample P37, thin section, normal light. Scale bar is 100 μm.

4 – *Nautiloculina oolithica*, equatorial section (left) and axial section (right). Twannbach Fm., Middle Tithonian, sample P62-1, thin section, normal light. Scale bar is 200 μm.

5 – *Valvulina lugeoni*, axial section. Twannbach Fm., Late Tithonian, sample Ye46, thin section, normal light. Scale bar is 200 μm.

6 – Quartz-agglutinating foraminifer, Twannbach Fm., Middle Tithonian. Sample P48, thin section, normal light. Scale bar is 100 μm.

7 – *Anchispirocyclina lusitanica*, tangential section, Twannbach Fm., Middle Tithonian. Sample P65, thin section, normal light. Scale bar is 500 μm.

8 – *Parurgonia* sp. (?), tangential section, Late Reuchenette Fm., Late Kimmeridgian. Sample Do80, thin section, normal light. Scale bar is 200 μm.

9 – *Everticyclammina* sp., tangential section, Twannbach Fm., Early Tithonian. Sample No167, thin section, normal light. Scale bar is 200 μm.

10 – Biopelmikrit (MF rl2) with miliolid foraminifers, axial section (lower left) and equatorial section (upper right). Twannbach Fm., Middle Tithonian. Sample P37, thin section, normal light.

11 – Biomikrit (MF rl4) with blackened *Everticyclammina* sp. and oysters. Upper *virgula* Marls, top Reuchenette Fm., latest Kimmeridgian / earliest Tithonian. Sample Do98, thin section, normal light.

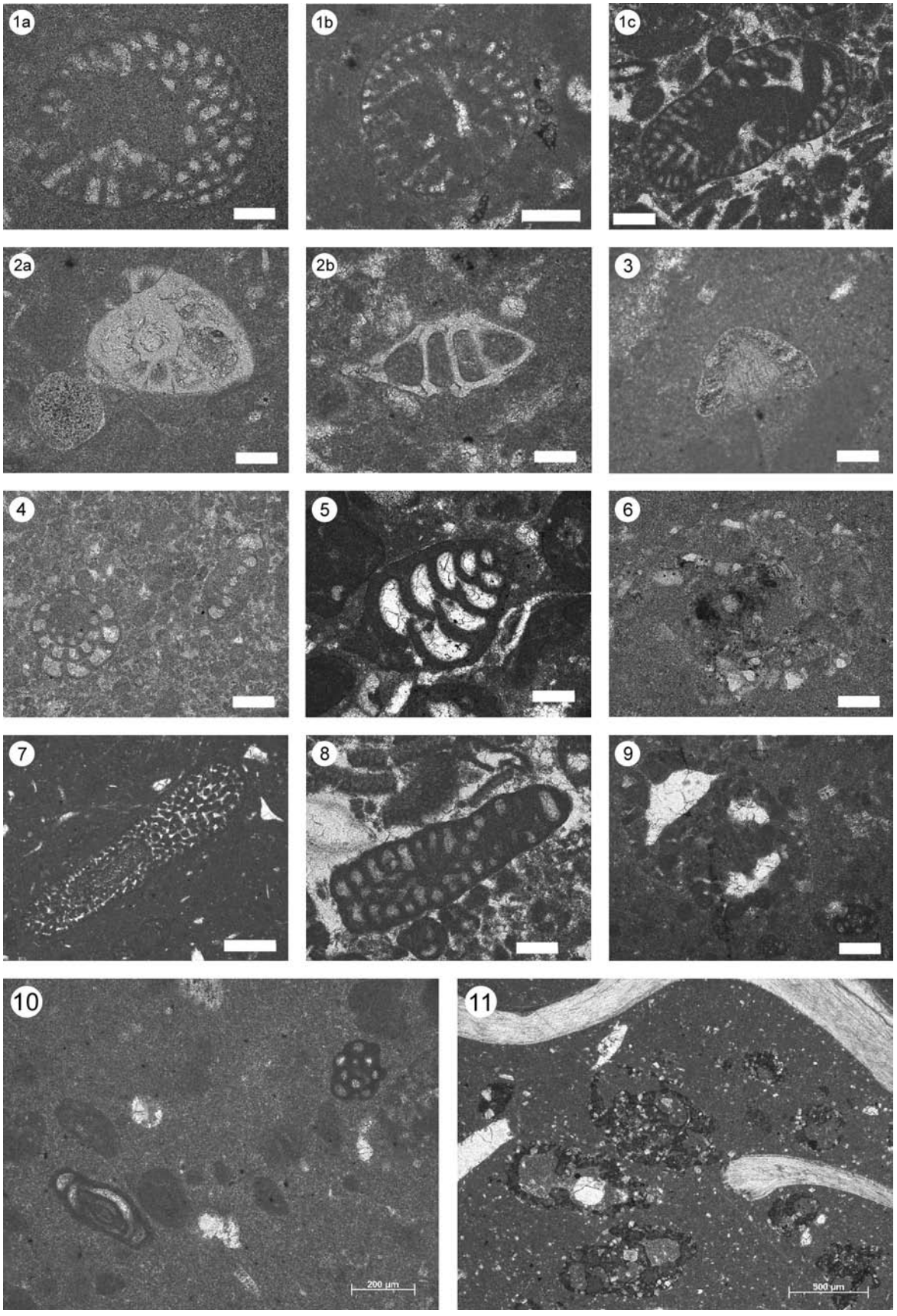
1a
1b
1c
2a
2b
3
4
5
6
7
8
9
10
200 µm
11
500 µm

Plate 4 – Bioclastic grains: dasycladacean algae

1a, b – *Clypeina sulcata* (ex *C. jurassica*), (a) subaxial and (b) subtransversal section. Twannbach Fm., Late Tithonian, sample Ye42, thin sections, normal light.

2a, b – *Campbelliella striata*. (a) tangential section, Twannbach Fm., Middle Tithonian, sample No226 and (b) transversal section, Upper Reuchenette Fm., Late Kimmeridgian, sample Av96, thin sections, normal light.

3a, b – *Macroporella espichelensis*. (a) subaxial section, Twannbach Fm., Middle Tithonian, sample P44 (b) oblique section, Twannbach Fm., Middle Tithonian, sample P43-2. Thin sections, normal light.

4 – *Heteroporella* sp. (?), transversal section. Twannbach Fm., Middle Tithonian, sample P43-2, thin section, normal light.

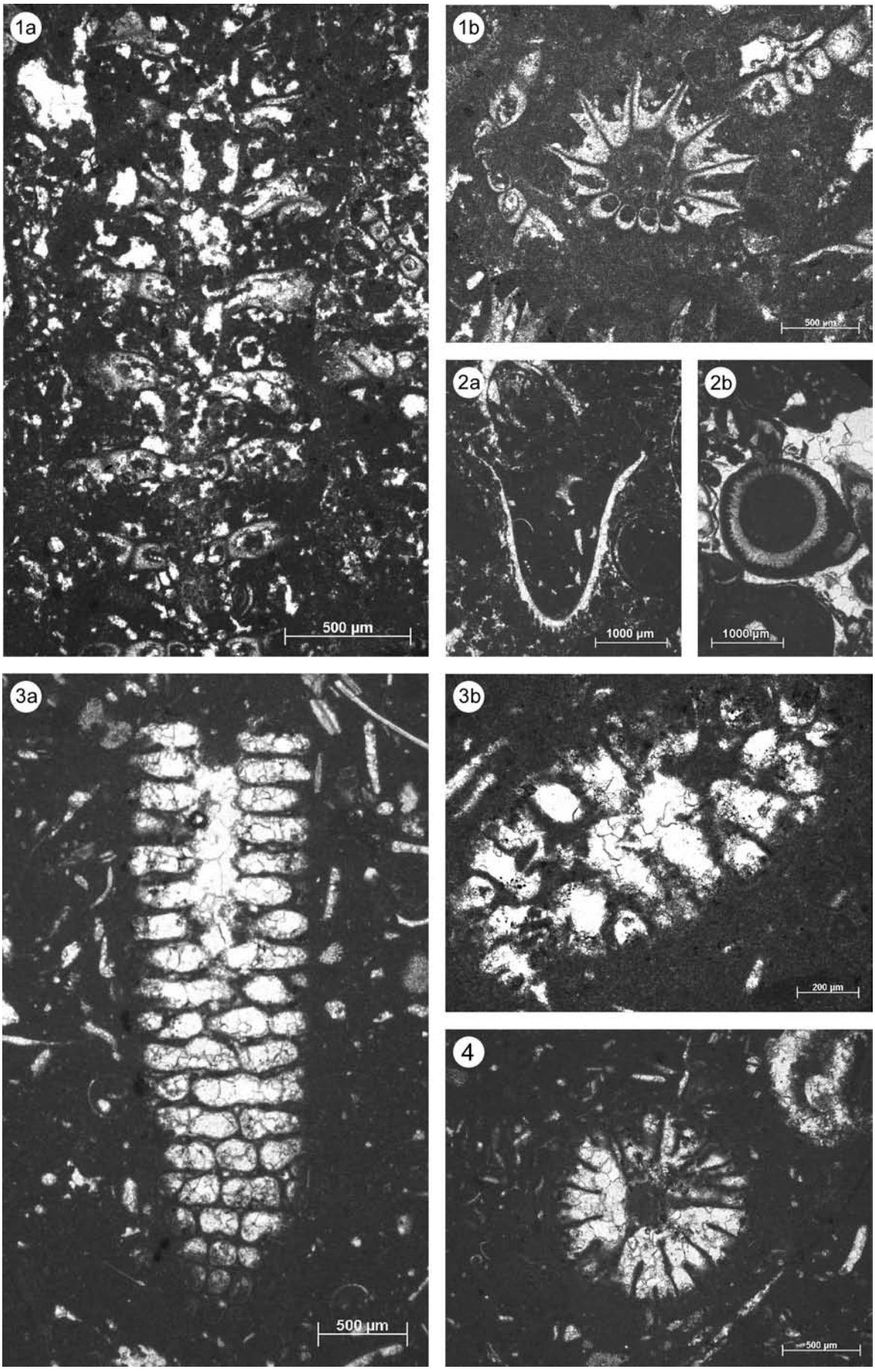
1a
500 µm
1b
500 µm
2a
1000 µm
2b
1000 µm
3a
500 µm
3b
200 µm
4
500 µm

Plate 5 – Bioclastic grains: dasycladacean algae

1a, b – *Salpingoporella* sp. (a) axial section, sample Av86, and (b) transversal section, sample Av99. Upper Reuchenette Fm., Late Kimmeridgian. Thin sections, normal light.

2 – *Acicularia* sp., Twannbach Fm., Early Tithonian, sample No208, thin section, normal light.

3, 4 – The vast majority of dasycladacean algae accumulations shows a clear tendency towards monospecific occurrence: (3) shows a nearly monospecific *Campbelliella*-wackestone with only two *Salpingoporella* specimens (arrows), facies rl6, Twannbach Fm., Middle Tithonian, sample No226, and (4) is a completely monospecific *Clypeina*-wackestone, facies rl6, Twannbach Fm., Late Tithonian, sample Ye42. Thin sections, normal light.


1a
200 µm

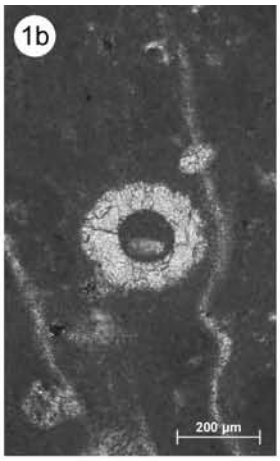
1b
200 µm

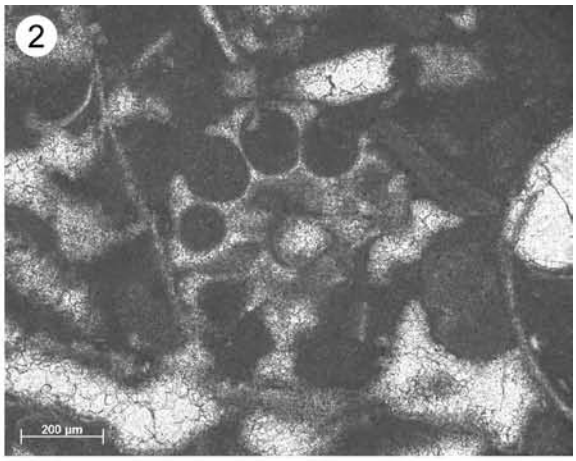
2
200 µm

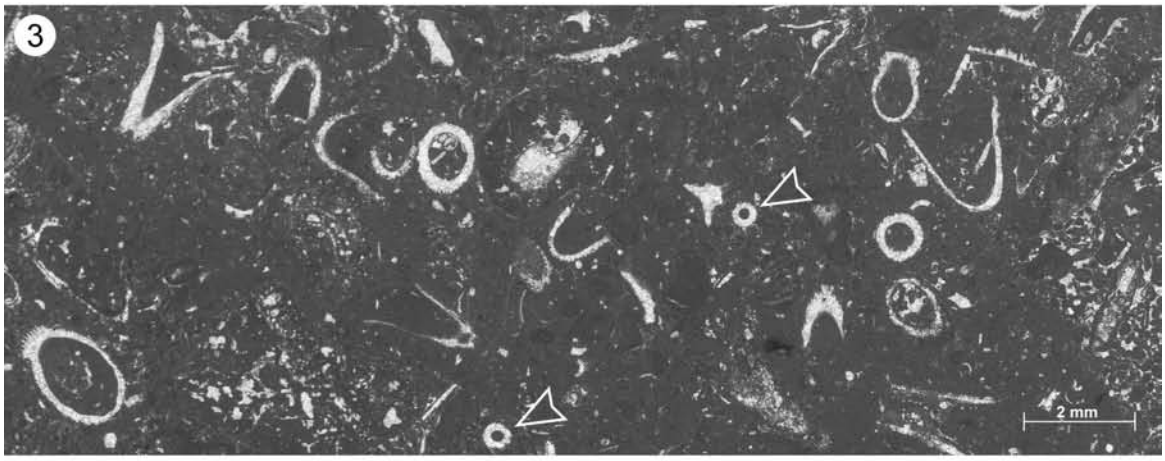
3
2 mm

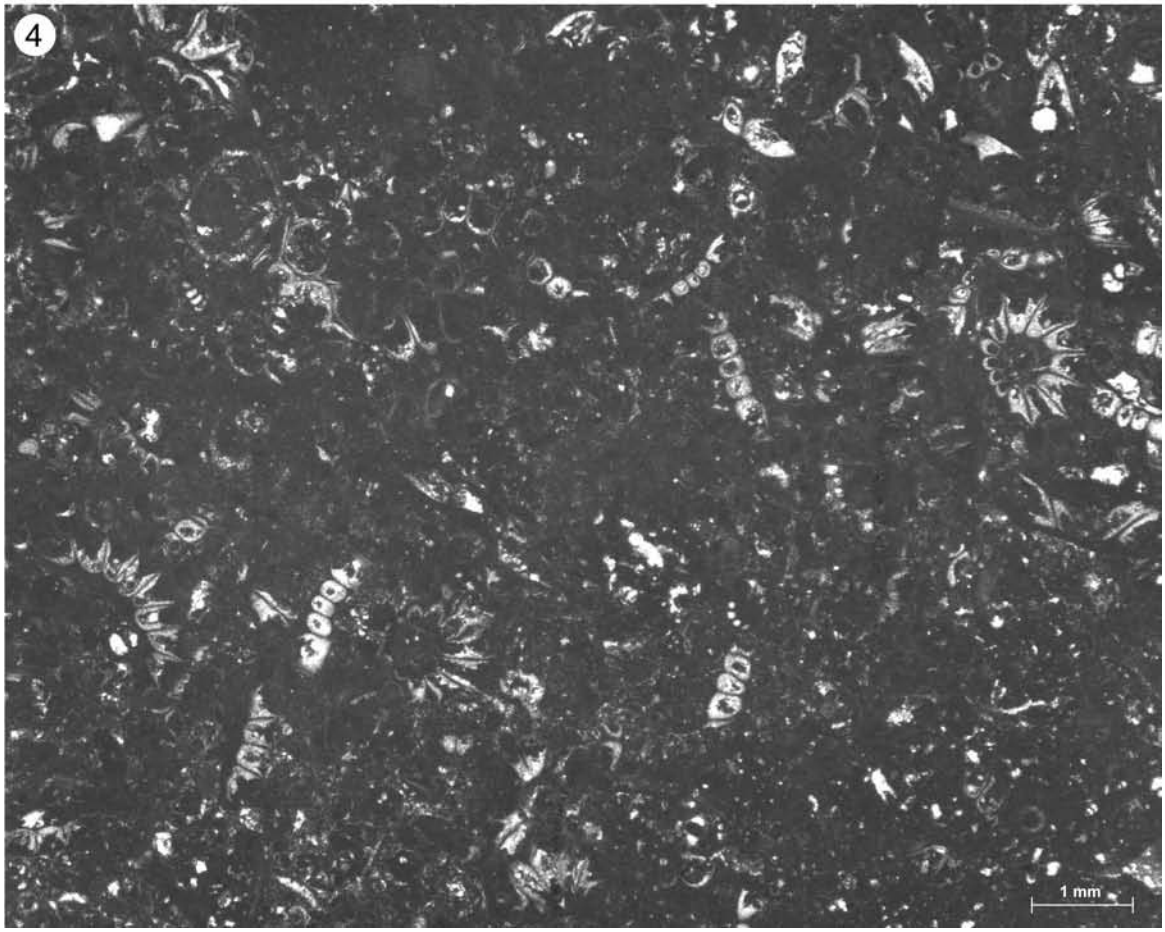
4
1 mm

Plate 6 – Encrusting organisms

1 – *Thaumatoporella* sp. (arrows) encrusting the inner wall of a gastropod shell (that was dissolved during later diagenesis). Note also the fragmented micritic envelope and geopetal structure in the infilled grainstone (white circle) and that the *Thaumatoporella*–encrustation is clearly older than the infill sediment. Sample Do102, thin section, normal light.

2 – *Cayeuxia* sp. Cayeuxia is typically found in rather calm, muddy lagoonal deposits. Sample Do102, thin section, normal light.

3 – Unknown algae. Sample No116, thin section, normal light.

4 – Microbially stabilized surface in a peloid grainstone (facies inbar3↓E), indicating a temporary drop of depositional energy and/or sediment supply. Sample Ye37, thin section, normal light.

5 – Serpulid tubes attached to an oyster shell. Sample Av200, thin section, normal light.

6 – Part of a small mound structure composed of peloidal thrombolite (facies hr4). The mound was "buried" under peloid grainstone. Note the grainstone's onlap on the mound surface (sloping to the left). Sample Av117, thin section, normal light.

7 – Partially micritized brachiopod shell. Micritization fronts penetrating from the inner and outer shell surface are clearly visible. The geometry of micritized parts strongly suggests perforation by microborers (algae, fungi mycellum, or sponges, cf. Bathurst 1975, Reid & Macintyre 2000). Sample Av255, thin section, normal light.


1
1000 µm

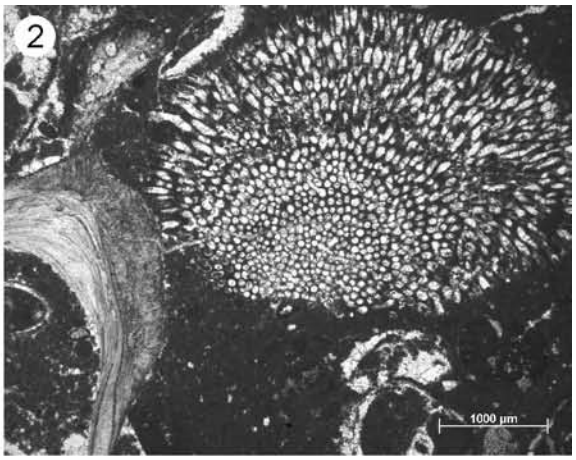
2
1000 µm

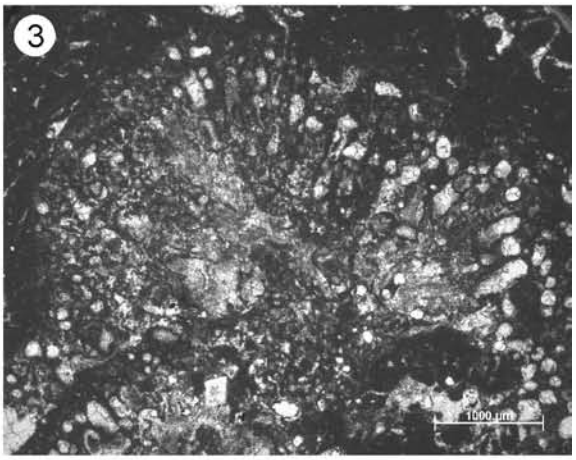
3
1000 µm

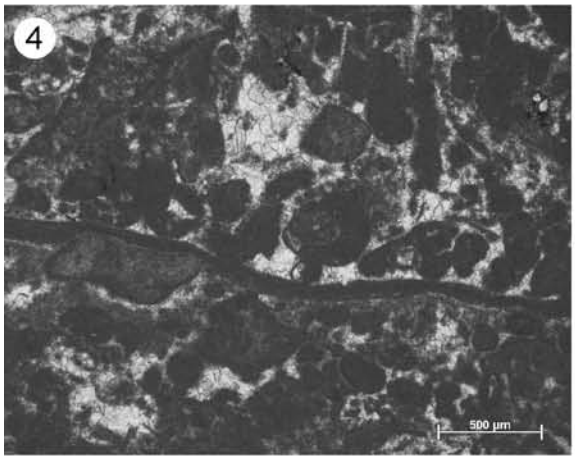
4
500 µm

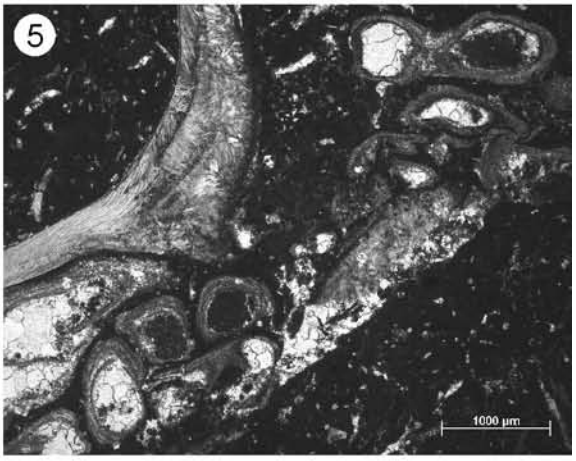
5
1000 µm

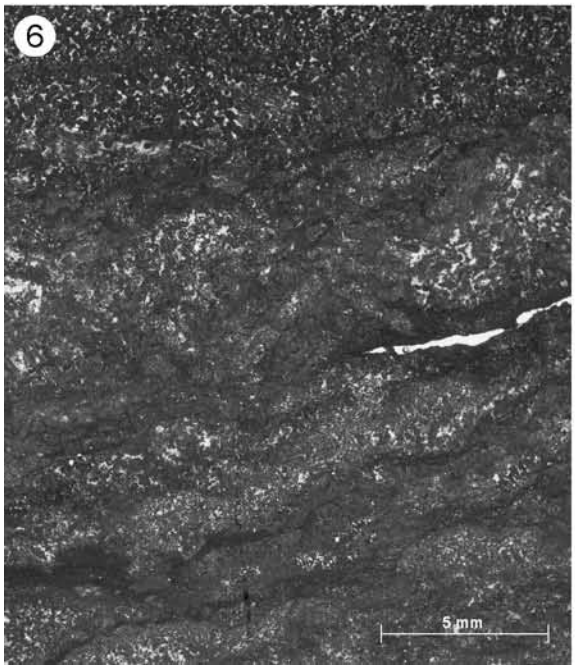
6
5 mm

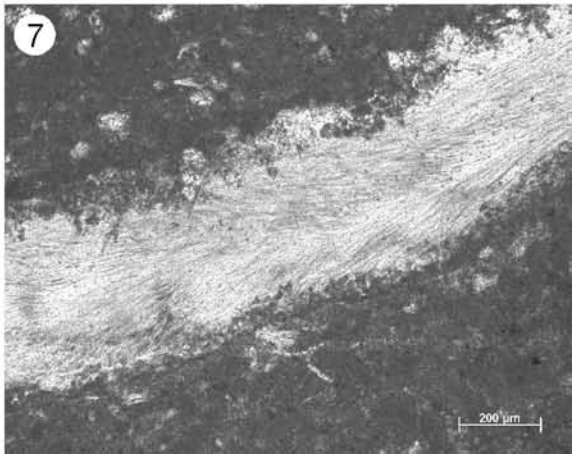
7
200 µm

Plate 7 – Oncoids

1 – **Type-1 oncoid**: Cortex is made up of diverse encrusting organisms, such as *Lithocodium* sp., *Baccinella* sp., *Cayeuxia* sp. (a), *Thaumatoporella* sp. (b). In the outer part of the cortex, some dolomite rhombs are found (c). The nucleus consists of a well-rounded *Cladocoropsis mirabilis* clast. Sample Av69, thin section, normal light.

2 – **Type-2 oncoid** (center of image): Note the irregular shape of the nucleus and the very thin cortex consisting only of one or two laminae. Sample Av69, thin section, normal light.

3 – **Type-3 oncoids**. Sample No1, thin section, normal light.

4 – Oncoid-wackestone (MF rl9) with large type-1 oncoids and dolomitized matrix. Sample Av44, etched slab.

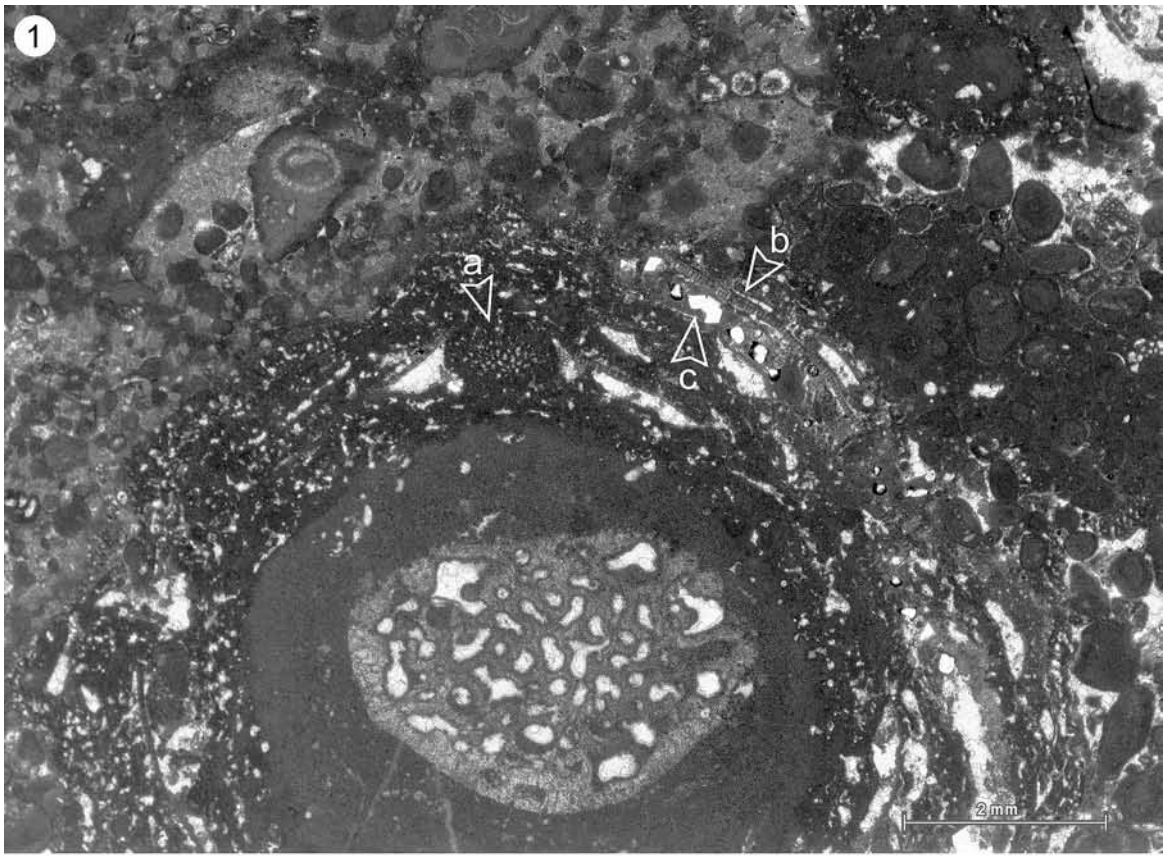
1
a
b
c
2 mm

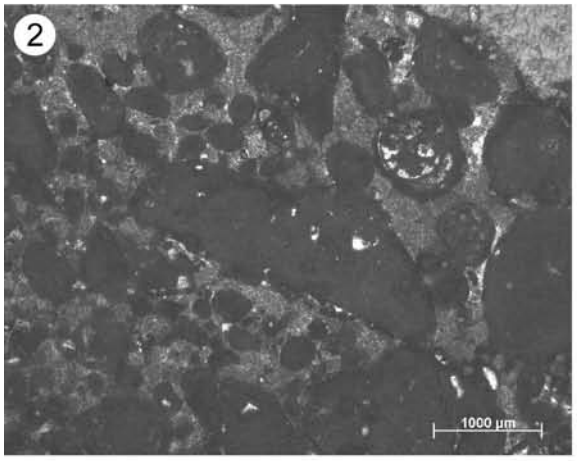
2
1000 µm

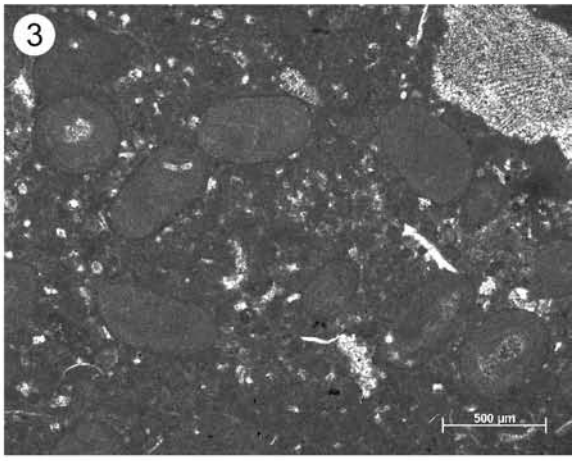
3
500 µm

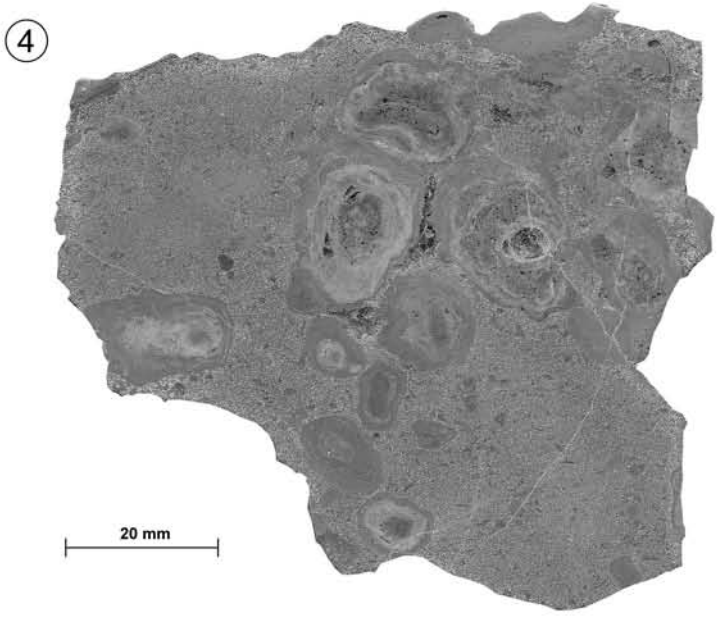
4
20 mm

Plate 8 – Sedimentary structures

1 – Geopetal structure in a bioclastic grainstone (facies inbar4 ↓E). Some cm above this sample, a microbially stabilized surface (cf. pl. 6/4) indicates a decrease in depositional energy. The small peloids in the intergranular pore space are thus interpreted as infill sediment, probably infiltrating the coarse grainstone during a period of lesser agitation, immediately before the growth of the microbial mat. Sample Av110, thin section, normal light.

2 – Truncation surfaces in tidal flat tempestites (facies tf4). Sample Av110, thin section, normal light.

3 – Keystone vugs (facies bch). Sample Av28, thin section, normal light.

4 – Perforated hardground (small-scale MFS) and bioturbation. Dark spots in the upper half of the picture (naturally weathered rock surface) are predominantly *Thalassinoides*-burrows. Nodular appearance above the small-scale SB/TS is due to heavy bioturbation. The darker rocks underlying the small-scale SB/TS are completely dolomitized ("dolomite cap", lHD of the underlying small-scale sequence). Cirque des Avalanches section, 88.5-90.5 m (picture approx. 2 m high).

5 – Pelsparite (peloid grainstone, facies inbar3 em?) showing mensicus-type grain bridges that probably originate from microbial mucilage binding. This type of meniscus "cement" is not necessarily a sign of vadose diagenesis (cf. Hillgärtner et al. 2001)! Sample Av83, thin section, normal light.

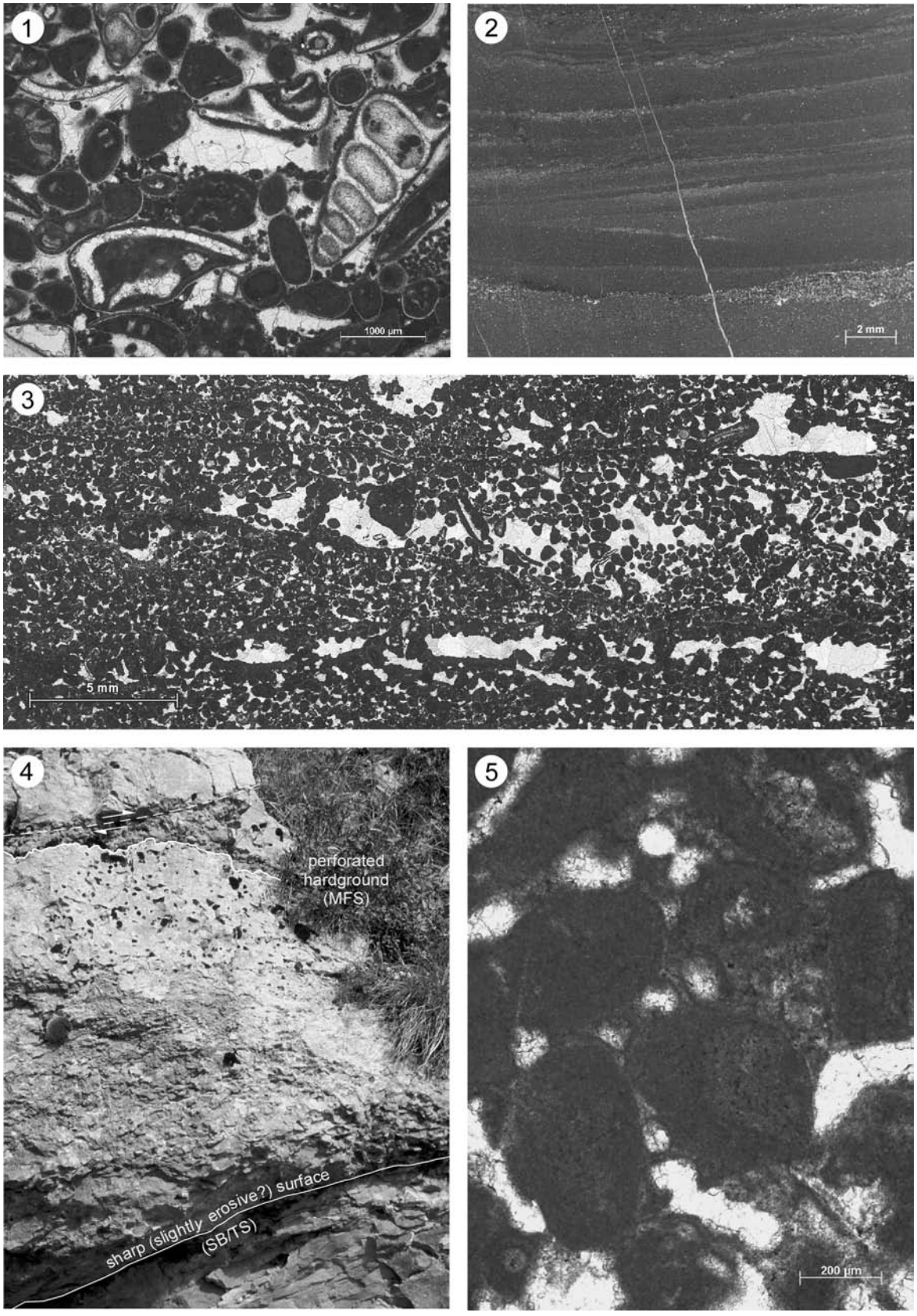
1
1000 µm
2
2 mm
3
5 mm
4
perforated
hardground
(MFS)
sharp (slightly erosive?) surface
(SB/TS)
5
200 µm

Plate 9 – Sedimentary structures: desiccation

1a, b – Large polygonal mudcracks (intertidal): (a) Le Lieu section, 59.7 m, bedding plane from above. (b) Recent example from Bahar Alouane, Tunisia. Polygons in the foreground are approx. 0.5 m in diameter (Photo by A. Strasser 2002).

2a, b – Teepee-like "pressure ridges" at the rim of large polygonal mudcracks: (a) Le Lieu section, 60.0 m. The left clod of algal laminite was thrusted over the right one (beds dip steeply to the left). (b) Dug out rim of one of the polygons shown in 1b. The algal laminites on the right side are thrusted back and rolled over. Bahar Alouane, Tunisia, 2002.

The polygonal crack pattern as shown in 1 and 2 originated most probably from repeated periods of desiccation, whereas the pressure ridges in 2a and 2b are interpreted to be the result of lateral growth of algal laminite.

3a-c – Supratidal mudcracks: (a) Noirvaux section, ca. 156 m, bed surface from above. (b) Shallow mudcracks may only effect the uppermost sediment layer of a few mm thickness whereas deeper mudcracks usually have a V-shaped geometry (arrows). They are typically filled with sediment from above. However, in this example they are cemented with sparry calcite. Sample P96b, etched slab. (c) Example of supratidal mudcracks in a modern carbonate tidal flat. Three Creeks, W-coast of Andros Island, Bahamas, 2001. *Pen for scale*.

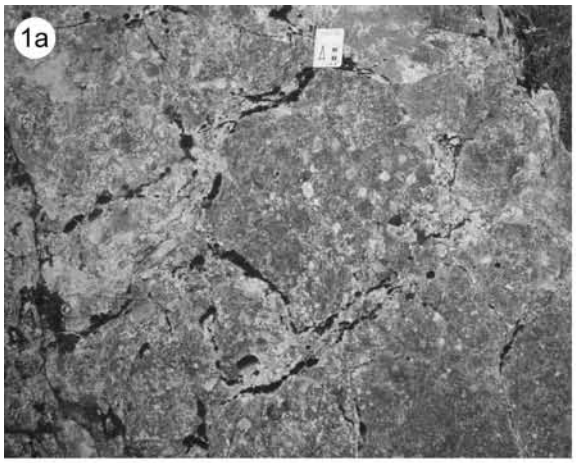
1a


1b

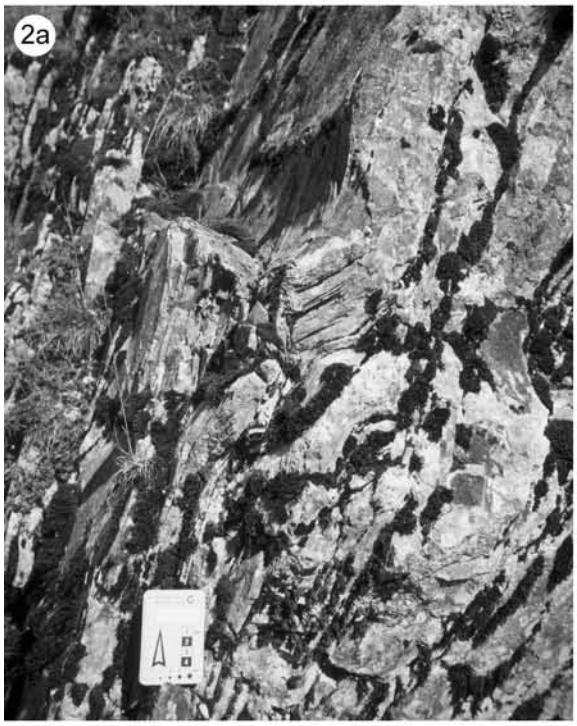
2a


2b
1 cm
2
3
4

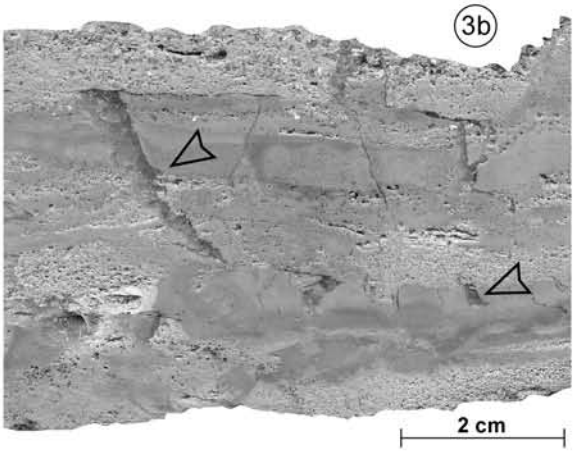
3b
2 cm

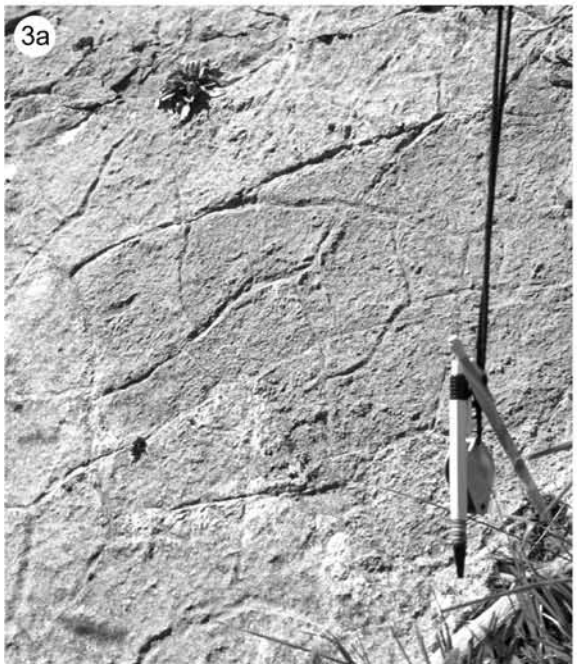
3a


3c

Plate 10 – emersion, vadose diagenesis and karstification

1 – Pendant cements and micritic infill sediment in a grainstone (facies inbar4 em). Sample Av185, thin section, normal light.

2 – Continental stromatolite. Note the typical fibro-radial calcite crystals with undulating alternations of dark and light (growth) layers. Sample No265, thin section, normal light.

3 – *Microcodium* in a brecciated limestone. The typical corn-cob (longitudinal section, upper left) and rosette (transversal sections, right) structure is clearly visible. Note quartz grains floating in matrix (arrows). Sample No269, thin section, normal light.

4 – Root cast with attached *Microcodium*. Sample No271, thin section, normal light.

5 – Microkarst cavities with infill sediment (bright), local brecciation, and cementation. The original fissures were probably mudcracks (vertical), respectively sheet cracks (horizontal) in a tidal flat laminite. Under vadose conditions, the existing fissures were later widened by dissolution, as visible in the lower half of the picture. Sample No200, etched slab.

6 – Large karst pocket with breccia fill (marked with white line). The thick bed (middle right) consists of tidal sandflat deposits (facies tf6) and is underlain by a yellow marl band. This yellow marl was deposited on a disrupted, stromatolitic surface with teepee structures (note tilted block in the lower left). La Dôle section at 102.5 m (SBZ $Ti3_{Tethyan}$).

7 – Channeled breccia deposit. The lower contact surface is mudcracked (not visible on photograph). Platy limestone in the lower half represents tidal flat laminites. Yenne section at 84.5 m (SB $Be2_{Tethyan}$). *Hammer for scale*.

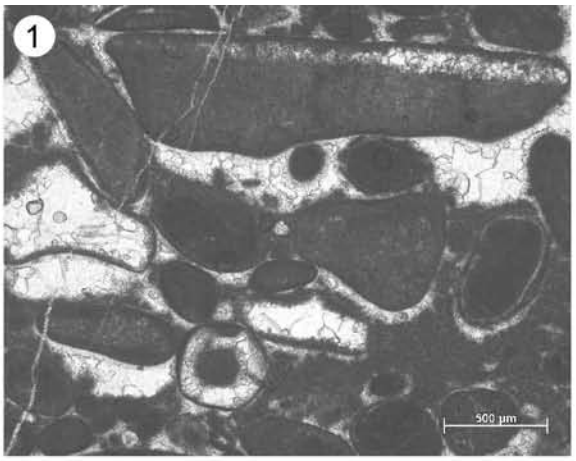
1
500 µm

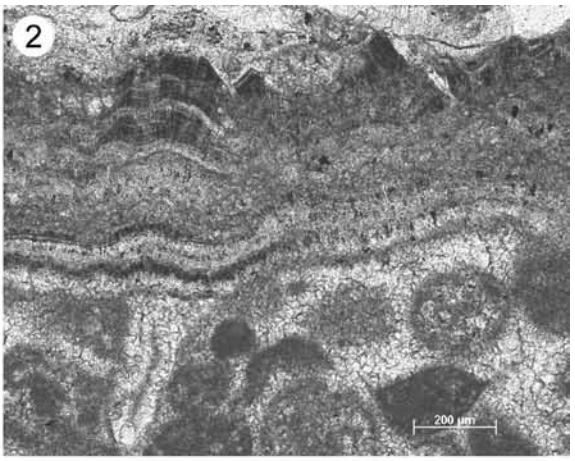
2
200 µm

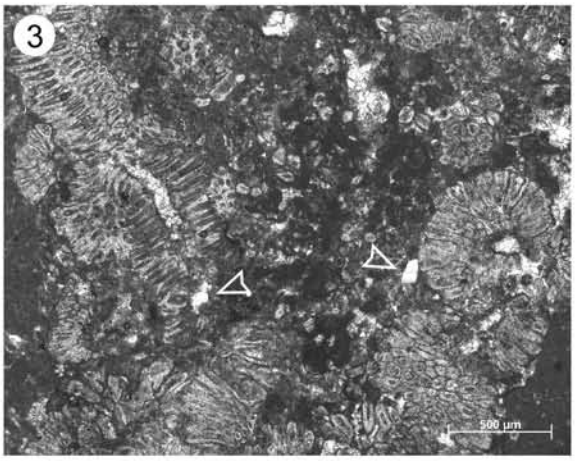
3
500 µm

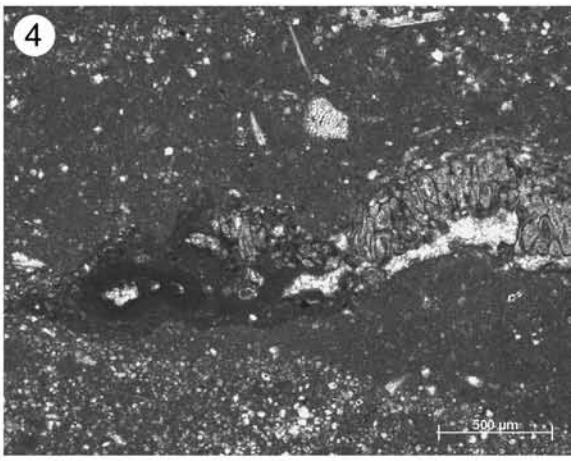
4
500 µm

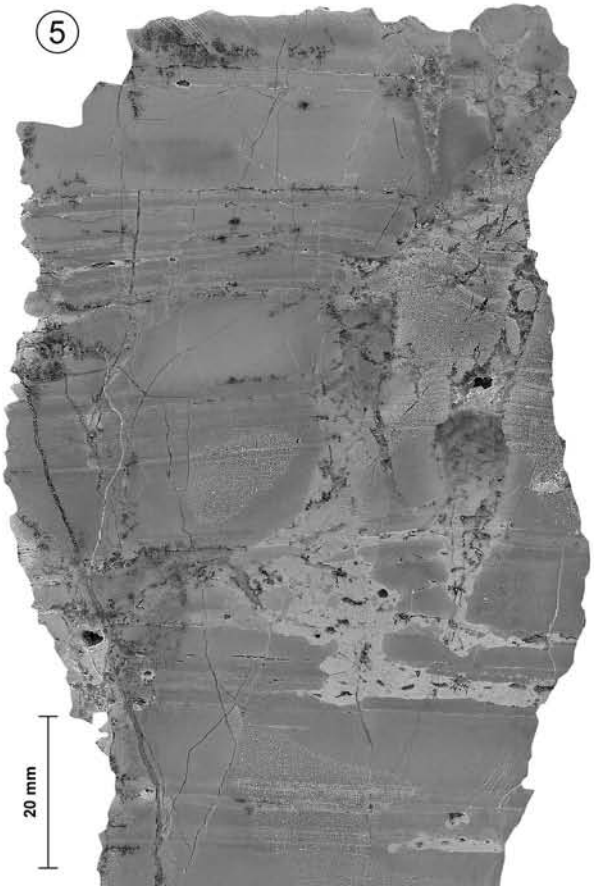
5
20 mm


6


7

Plate 11 – Tidal flat: lithofacies

1 – Laminated tidal flat deposit (supratidal, facies tf2). Lamination consists of an alternation of relatively thick layers of well sorted peloid grainstones (interpreted as tempestites) and thin laminae of clotted mud (microbial mats, "stick-on layers"). On modern carbonate tidal flats, these features are typical for deposits on (or near) the crests of tidal channel levees. Sample P68-1, thin section, normal light.

2 – Laminated tidal flat deposit (upper intertidal, facies tf3). Lamination mainly due to a succession of tempestitic layers of different grain size. The undulated surface in the middle is interpreted as a microbial mat. Sample P81, thin section, normal light.

3 – Tidal flat deposit with parallel texture (upper? intertidal, facies tf3). In a monotonous micrite, no lamination is visible. However, layers of parallel oriented oyster shells indicate the ancient sedimentary surfaces. Sample Av137, thin section, normal light.

4 – Tidal sandflat deposit with parallel texture / flaser texture (lower intertidal, facies tf6). Note the relatively high number of ostracodes with both valves preserved, indicating rapid burial. Sample Do139, thin section, normal light.

5 – Flat-pebble conglomerate, lower bed surface. Le Lieu section, 27.6 m.

6 – Algal mudchips ("flat pebbles") on a modern carbonate tidal flat. Three Creeks, W-coast of Andros Island, Bahamas, 2001.

7 – Dolomitized flat-pebble conglomerate with burrows in upper half. Lenticular bedding indicates deposition in tidally influenced environment. Sample No172, etched slab.

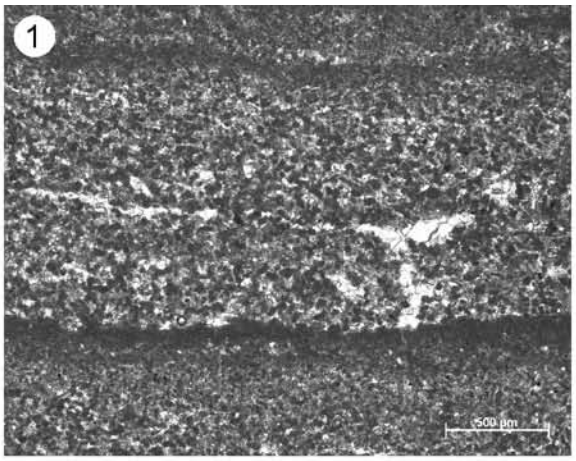
1
500 µm

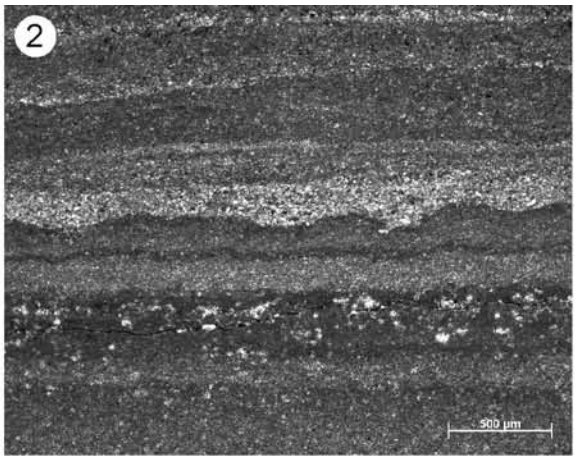
2
500 µm

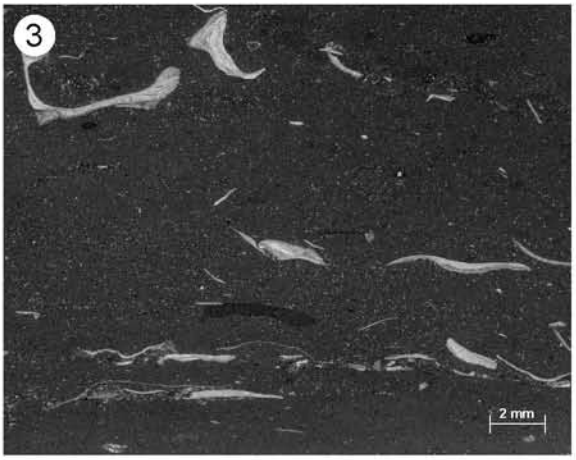
3
2 mm

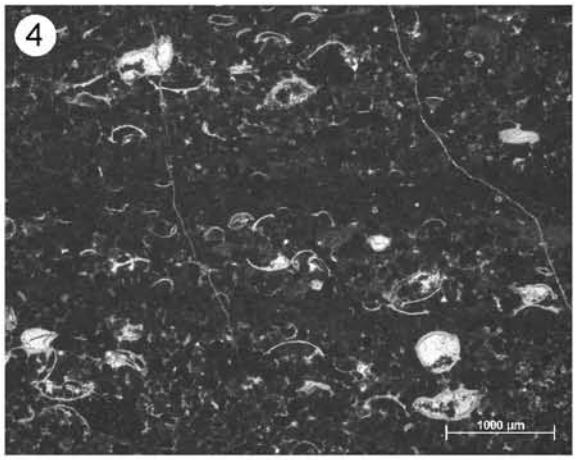
4
1000 µm


5
1
cm
2
3
4
4
5 mm

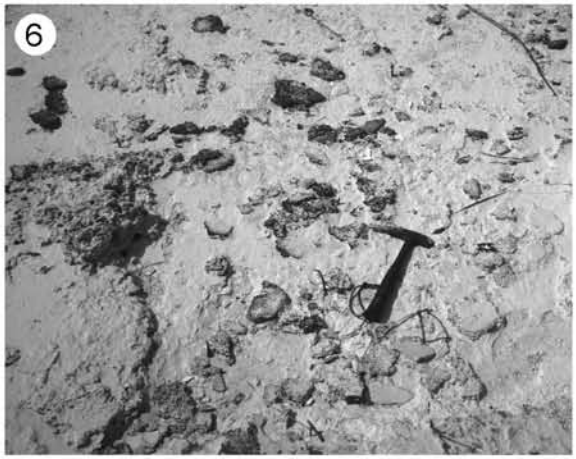
6

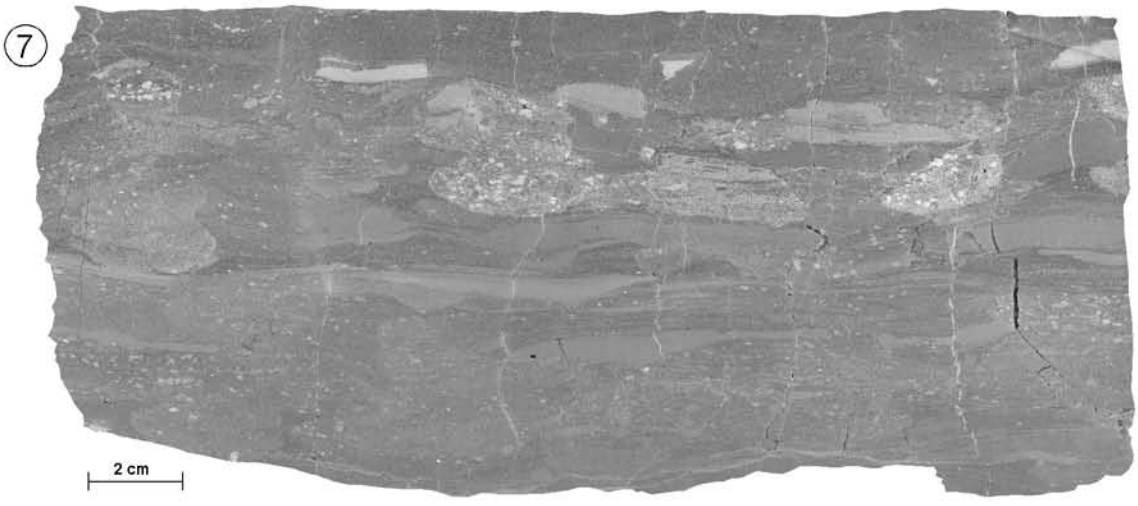
7
2 cm

Plate 12 – Tidal flat: emersion features

1 – Supratidal flat deposit: sheet-cracked ("horizontal joint planes") algal laminite (facies tf2) with bird's eyes. Worm tube in upper half of the picture. Sample No195, thin section, normal light.

2 – Transgressive tidal flat → lagoonal sequence expressed in one bed: The basal multicoloured breccia is overlain by tidal-flat laminites – note the worm tube filled with fine multicoloured breccia (arrow) – that develop into highly bioturbated, restricted lagoonal facies. *Badly visible: the top of the bed is a bored hardground surface (MFS of an elementary sequence) with slight Fe-staining that also infiltrates into the subvertical burrows*. Sample No209, etched slab.

3a, b – Multicoloured breccia (facies mcbrec). Note (a) the corroded rims of most black pebbles (cf. Bläsi (1980); sample No202, thin section, normal light) and (b) the existence of bored clasts (arrows; sample Do144, etched slab).

4 – Supratidal flat deposit (facies tf2) with bird's eyes and incipient circumgranular cracks. Sample No179, thin section, normal light.

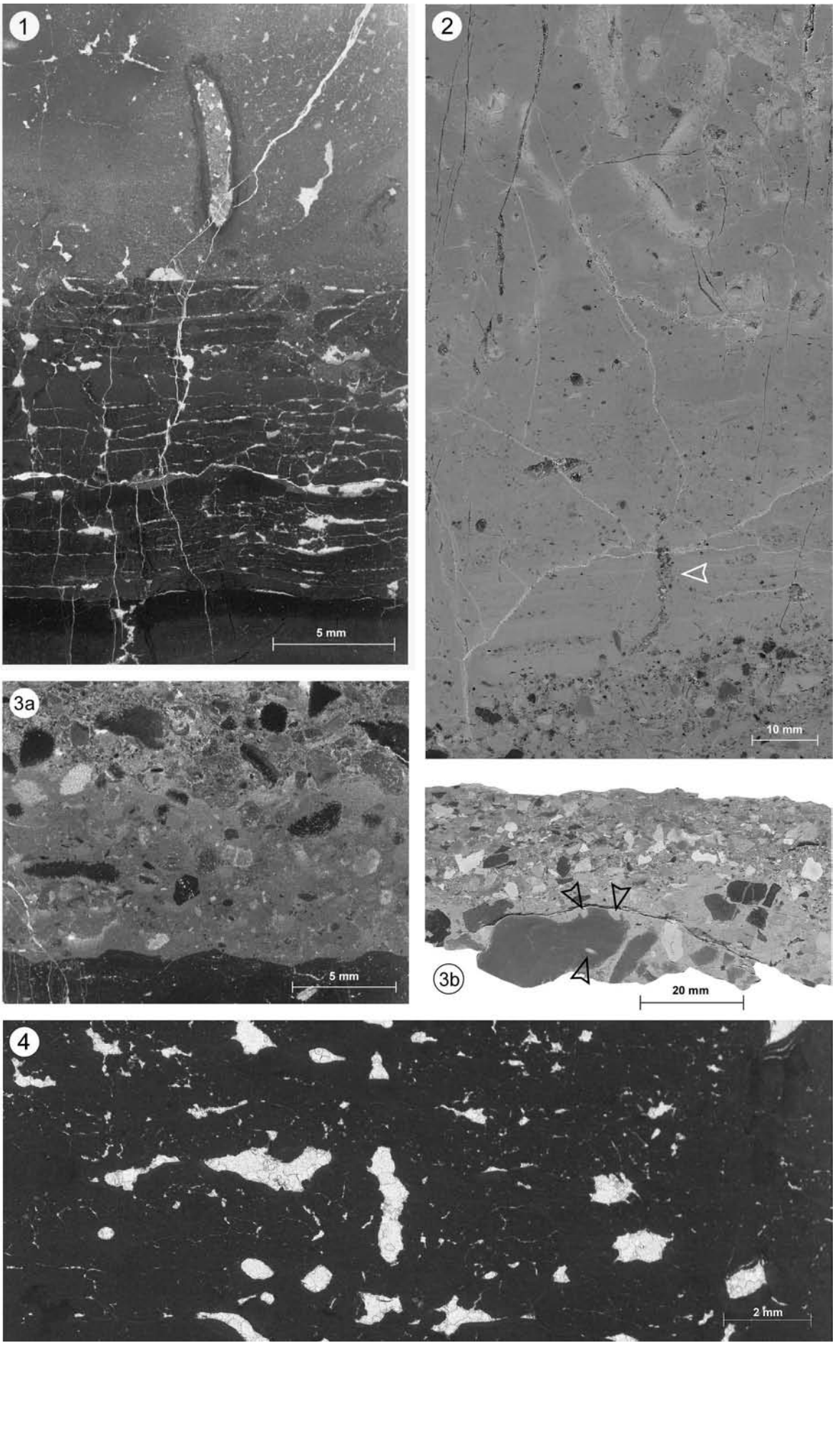
1
5 mm
2
10 mm
3a
5 mm
3b
20 mm
4
2 mm

Plate 13 – Tidal flat: Stromatolithes

1 – Dolomitized undulating ("wavy") stromatolite (facies tf2 dol). A lamina with some reworking features can be seen at the bottom of the photo. Sample Do153, etched slab.

Tidal flat: sabkha

2 – Dolomitized algal laminite (facies tf2 dol). Dark laminae represent remains of organic matter. Sample Ye17, thin section, normal light.

3a, b – Graded evaporite tempestite (facies tf1). (a) Relatively light evaporite crystals (now pseudomorphs) float over a quartz-containing "bedload" (close-up in b). Sample P78, thin section, normal light.

4 – Gypsum pseudomorphs. Rosette-like clusters of intergrown crystals and "discoidal" or "lenticular" morphology of rosette-"leaves" suggest displacive in-sediment growth (Demicco & Hardie 1994). Sample P82-2, thin section, normal light.

5 – Partially cement-filled crystal molds interpreted to be pseudomorphs after displacive, in-sediment grown halite. Note also the *Favreina* coprolites on the outer right and left of the picture. Sample No171, thin section, normal light.

6 – Cement-filled molds interpreted to be pseudomorphs after anhydrite (or gypsum?) nodules that are characteristic for sabkha environments (cf. Demicco & Hardie 1994) (facies sbk2). Sample Do181, thin section, normal light.

7 – Collapse breccia. Brecciation is interpreted to have been caused by massive dissolution of evaporites in underlying strata. Sample P93-2, etched slab.

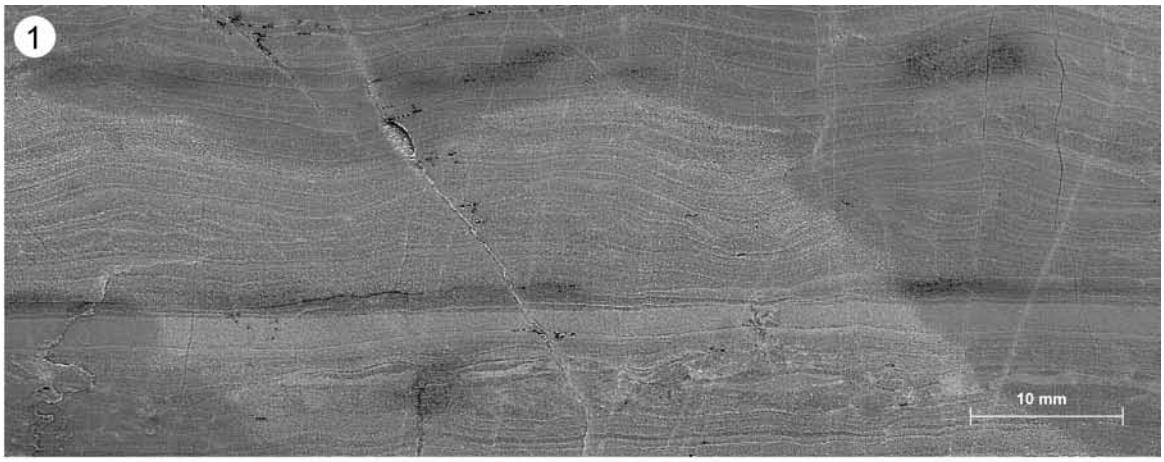
1
10 mm

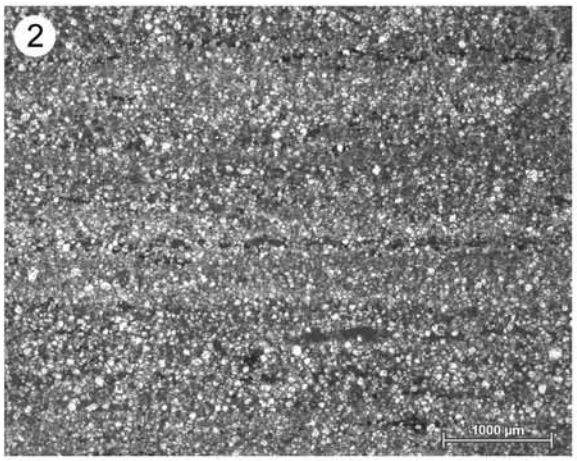
2
1000 µm

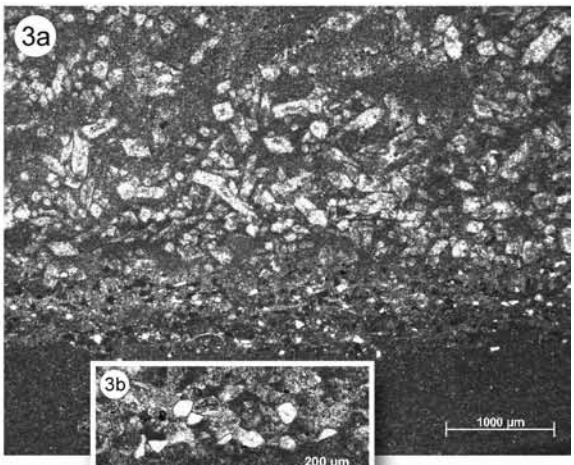
3a
1000 µm

3b
200 µm

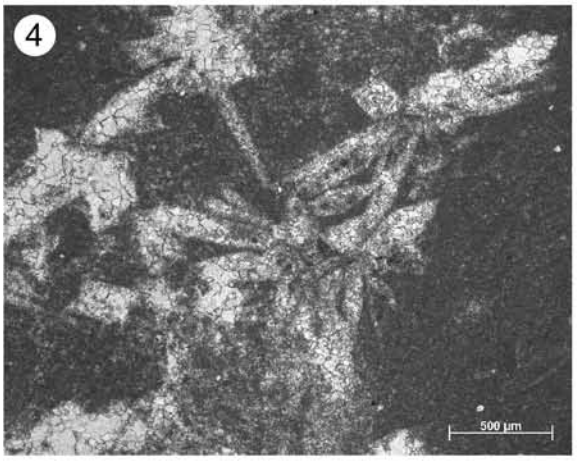
4
500 µm

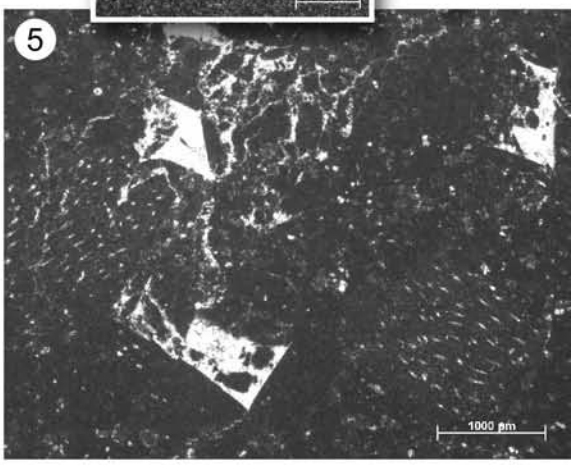
5
1000 µm

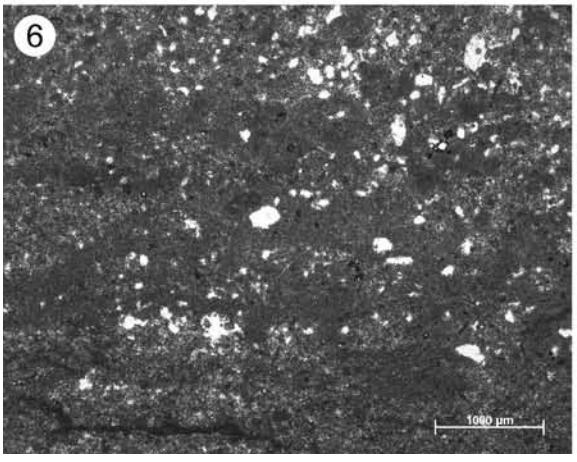
6
1000 µm

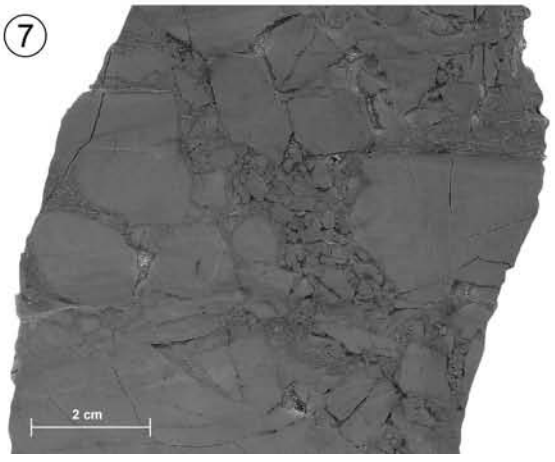
7
2 cm

Plate 14 – Dolomitization

1 – "*Matrix dolomite*": Medium-grained, idiotopic dolomite (planar-e type, "floating/packed rhombs"), commonly with zoned crystals, occur predominantly in stratiform packages of several dm to m thickness that show a sharply defined top and a diffuse "fading" of dolomitization intensity to underlying strata. ("dolomite caps"). This type of dolomite is interpreted to originate mainly from a reflux-type dolomitization mechanism. Sample Ye18, thin section, normal light.

2 – "*Burrow dolomite*": Many burrows are filled by medium- to fine-grained, hypidiotopic dolomite (planar-s type), commonly in association with pyrite grains (dark patches). This type of dolomite is interpreted to have precipitated from dolomitizing fluids during shallow burial under anaerobic conditions, probably mediated by organic material present in the burrows. Note the idiotopic, floating rhombs in the matrix on the lower left: dolomitized burrows often show a halo of matrix dolomite that fades out after some mm to cm (cf. Pic. 5, this plate). Sample No107, thin section, normal light.

3 – "*Tidal flat dolomite*": Small-grained, badly defined dolomite rhombs that are always associated with tidal flat features (e.g. microbial lamination in this example) are interpreted to be of syndepositional origin, with their precipitation linked to evaporation on tidal flats, involving storm recharge and/or evaporitic pumping. Note the organic matter in the middle of the photo, representing the remains of a microbial mat. Sample Ye17, thin section, normal light.

4 – Visible lamination in dolomitized strata is generally caused by changes in dolomitization intensity and/or crystal diameter. Sample Ye18, thin section, normal light.

5 – Dolomitization halo linked to "*burrow dolomite*". The burrow (not on the picture) is located to the left. In the centre, the dolomitization front was abruptly blocked by a bivalve shell, whereas it is clearly of diffuse character above and below the obstacle. Sample No277, thin section, normal light.

6 – Oncoid wackestone to packstone (facies rl9 dol), matrix dolomitized by medium-grained, idiotopic, zoned dolomite rhombs ("*matrix dolomite*"). Note that only the outer laminae of the shown oncoid's cortex are affected by dolomitization (arrows). I.e. either, that the oncoid was still in active growth when dolomitization started, or that the cortex was not fully cemented then and thus permeable for the dolomitizing fluid. In any case, it underlines that the timing of the reflux dolomitization process was quasi syndepositional, or at least *very* early with respect to diagenetic history. Sample Av54, thin section, normal light.

7 – Saddle dolomite. Sample CT11, thin section, normal light.

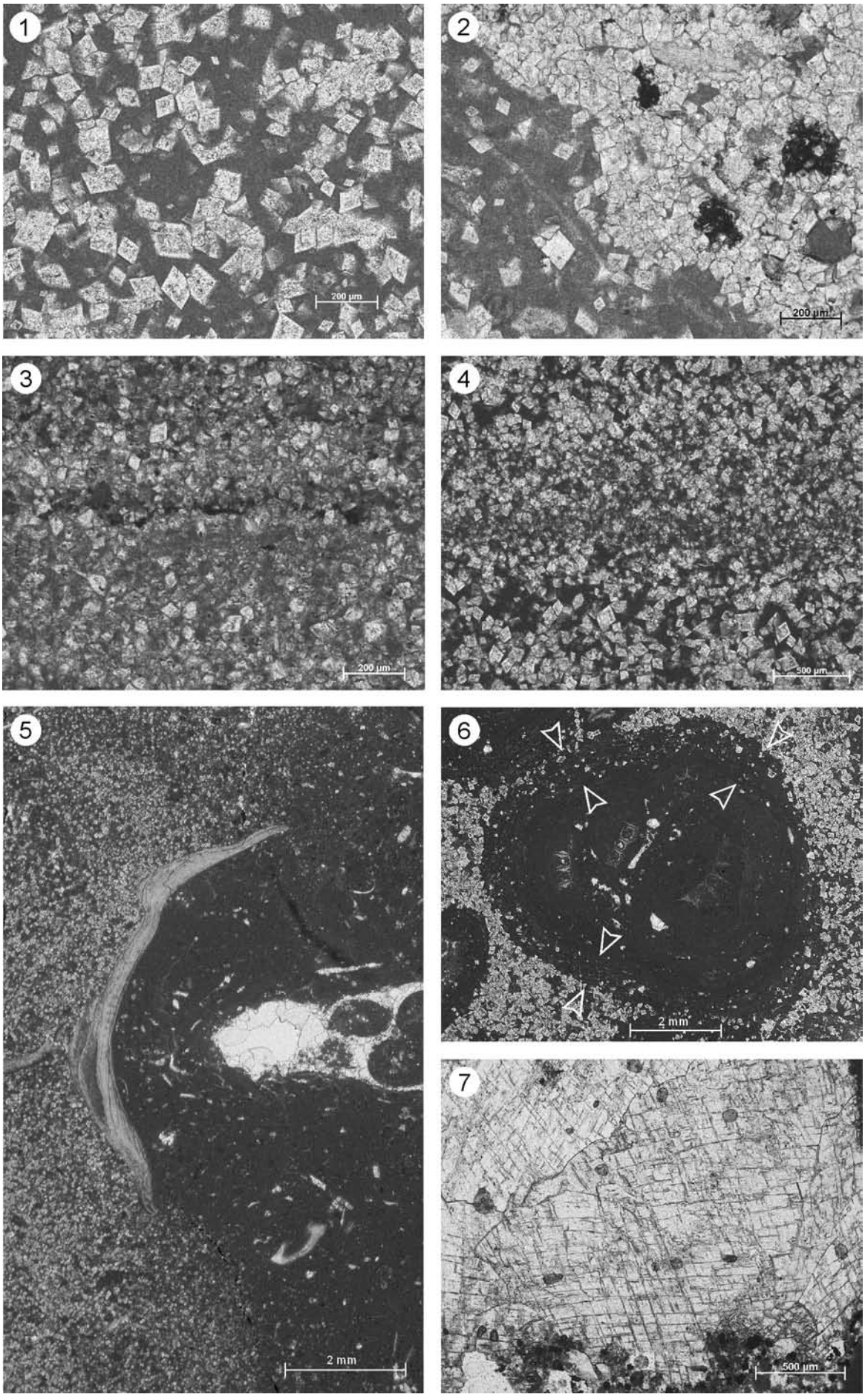
1
200 µm
2
200 µm
3
200 µm
4
500 µm
5
2 mm
6
2 mm
7
500 µm

Plate 15 – Dedolomitization

1 – Type-1 dedolomite. Sample No84, thin section, normal light.

2 – Structureless, “sucrosic” type-2 dedolomite. Sample Do196, thin section, normal light.

3 – Type-2 dedolomite, showing ghost structures of an ancient (oo?-)pel sparite. Sample P96-2, thin section, normal light.

4 – Type-2 dedolomite, showing ghost structures of an ancient algal laminite. Sample Do189, thin section, normal light.

5 – Spatial relations between dolomitized limestone, type-1 dedolomite and type-2 dedolomite. Sample No200, thin section, normal light.

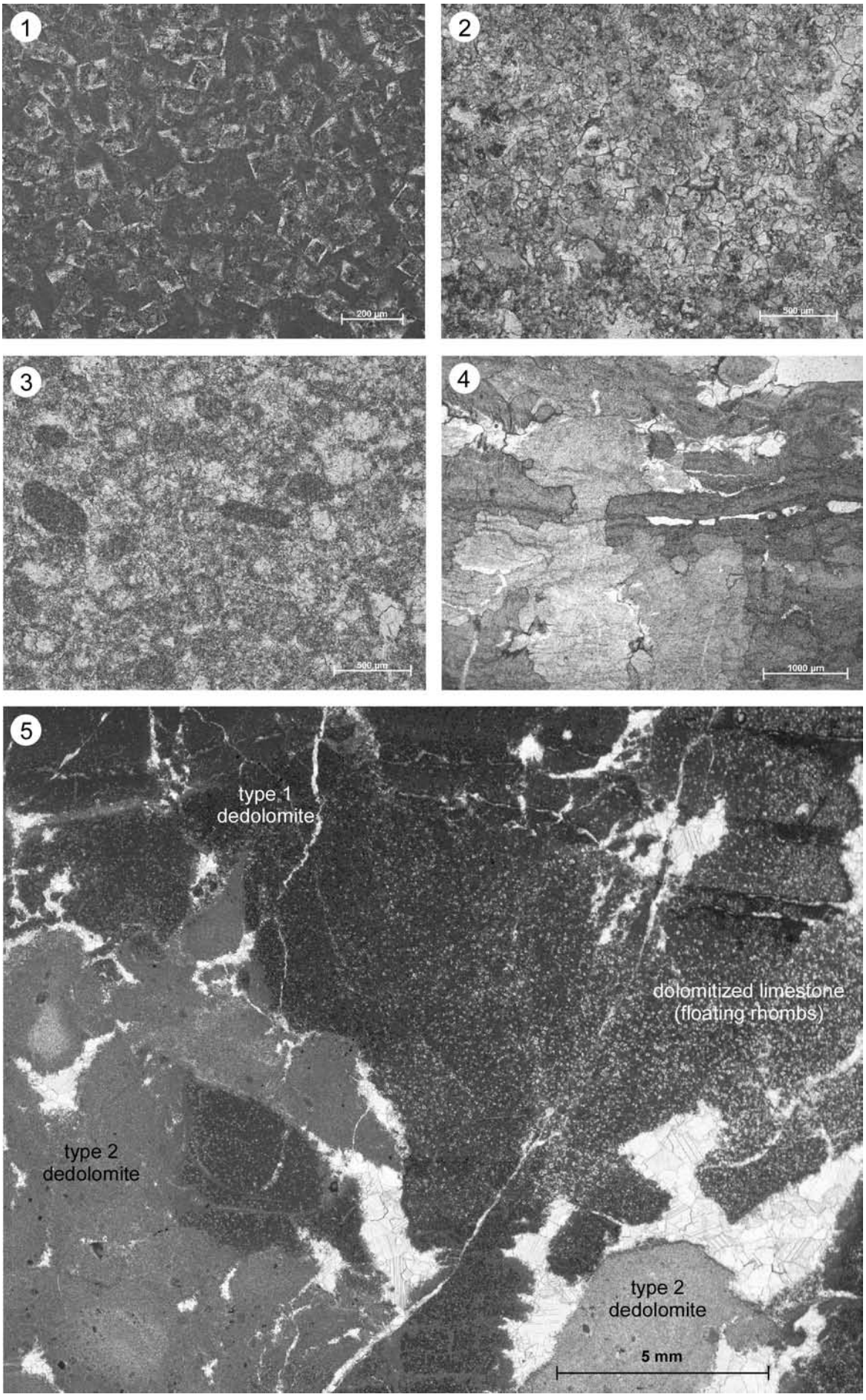
1
200 µm
2
500 µm
3
500 µm
4
1000 µm
5
type 1
dedolomite
dolomitized limestone
(floating rhombs)
type 2
dedolomite
type 2
dedolomite
5 mm

Plate 16 – Emersion features

1a, b – (a) Breccia with large, unrounded clasts. In outcrop, lower contact with tidal flat facies (MF tf4) shows an edgy morphology. The breccia matrix is of a distinct, reddish colour and (b) consists mainly of *Microcodium* growing between, and partly into, the clasts. The typical corn-cob (longitudinal section, lower left) and rosette structures (transversal section(s), central upper part) are clearly visible. Note also the root cast in the upper left (arrow). Sample No269, (a) etched slab, (b) thin section, normal light.

2a, b – Two different types of *cornieule* from the Upper Twannbach Formation and Lower Goldberg Formation of the Dôle section; (a) showing rests of a primarily laminated structure (sample Do195) and (b) without remnants of lamination or bedding planes (sample Do183). Solution vugs in (b) are filled with red-brown, only partly lithified clay. Etched slabs.

Lagoonal facies

3 – Lagoonal packstone (MF lowEl3), heavily bioturbated by *Thalassinoides*-like burrows. Burrow fillings are dark grey due to a high pyrite content and are dolomitized. Red staining of cream-coloured matrix may be related to partial pyrite dissolution, Fe-ion migration, and later precipitation under oxidizing conditions. The contrasts in colour and mineralogy between matrix and burrow fill lead to a very distinctive, "mottled" or "pseudobreccia" texture (pl. 8/4; cf. Horbury & Qing 2004). This lithofacies is rather common in the Upper Reuchenette and Lower Twannbach Formations and was used in the French Jura to define a lithological unit known as *Calcaire à tubulures* or *Couches du Chailley* (cf. Bernier 1984, Enay 2000). Sample No107, etched slab.

4 – Dark, marly limestone from the "upper *virgula*-beds" (Top Reuchenette Formation). Dark colour is due to a relatively high content of pyrite and/or organic matter. Black dots are pyritized agglutinating foraminifera (*Everticyclammina* sp., cf. pl. 3/11). Note the well-preserved bone fragment (arrow) and the reddish "halo" resulting from oxidation of pyrite during recent weathering processes near the outcrop surface. Sample Do98, etched slab.

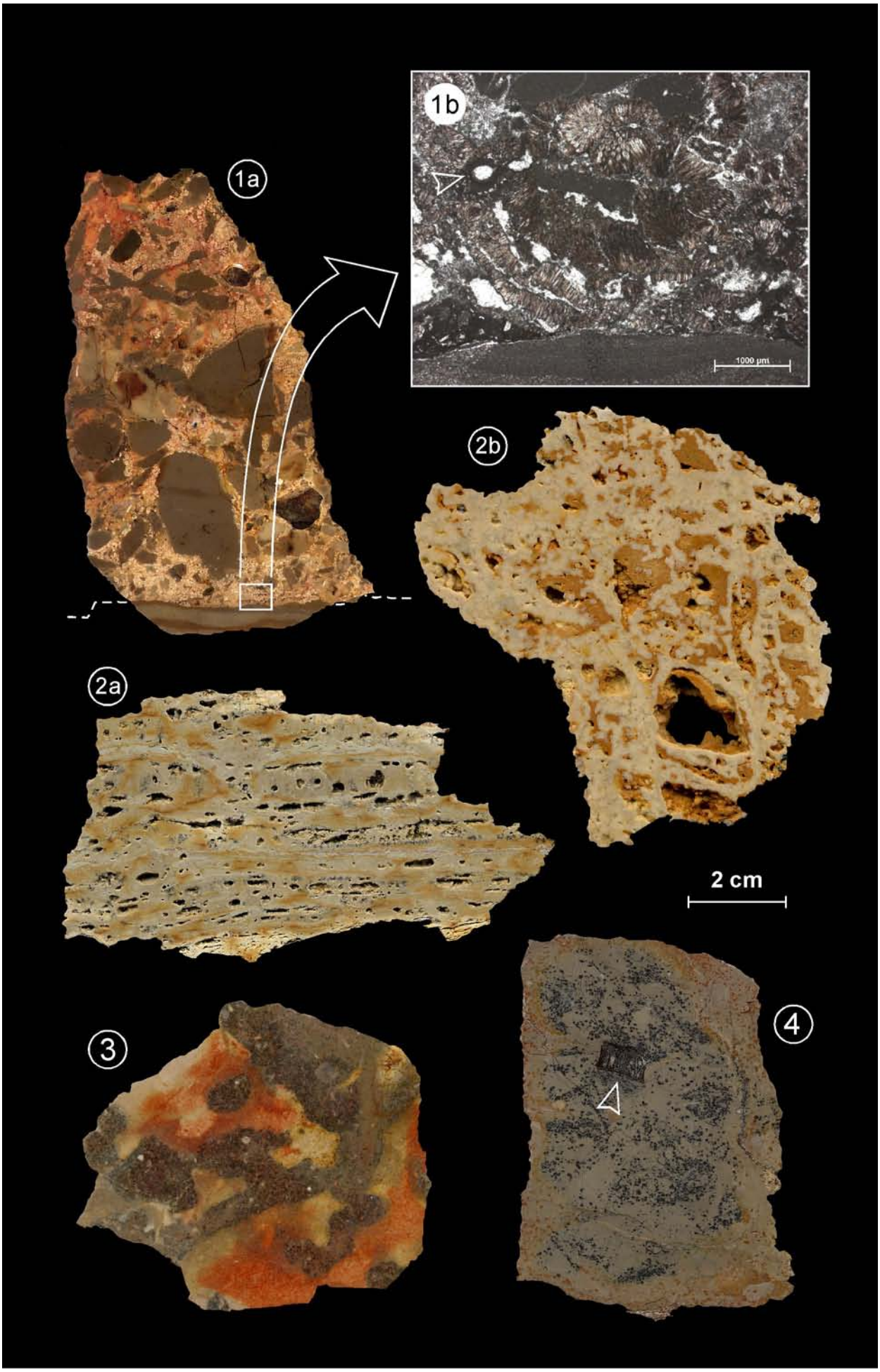
1a
1b
1000 µm
2a
2b
2 cm
3
4

Plate 17 – Basin: bioclastic grains

1 – Radiolarians. Several *Spumellaria* sp., one with clearly visible spines, and one *Nassellaria* sp. (arrow). Sample CT9, thin section, normal light.

2 – Protoglobigerinid planctic foraminifer. Sample CT2, thin section, normal light.

3a, b – *Globochaetes* sp. Sample CT7, thin section, (a) normal light, (b) crossed nichols.

4 – Calcisphere. Sample CT7, thin section, normal light.

5 – Microproblematicum. Sample CT7, thin section, normal light.

6 – *Saccocoma* sp. Sample CT5, thin section, normal light.

7 – Ammonite aptychus. Sample CT23, thin section, normal light.

8 – *Tubiphytes* sp. Sample CT12, thin section, normal light.

9 – Sponge fragment, with perfectly visible internal cavities. Sample CT32, thin section, normal light.

10 – Pyritized hexactinellid sponge skeleton. Sample CT8, thin section, normal light.

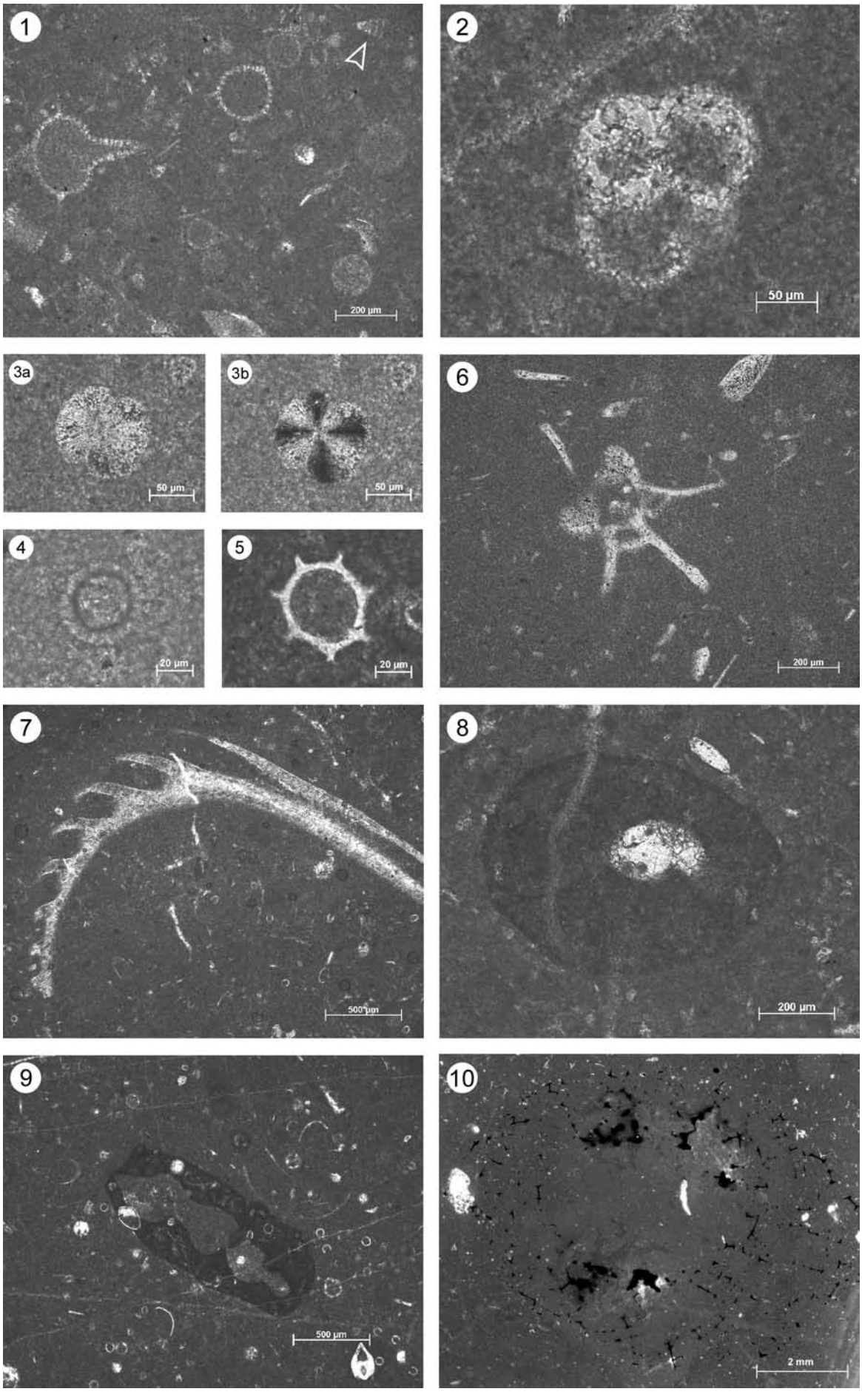
1
200 µm
2
50 µm
3a
50 µm
3b
50 µm
4
20 µm
5
20 µm
6
200 µm
7
500 µm
8
200 µm
9
500 µm
10
2 mm

Plate 18 – Basin: calpionellids

1 – *Chitinoidella* sp. "*Chitinoidella* zone", Middle/Late Tithonian boundary interval. Sample CT18, thin section, normal light.

2 – *Calpionella elliptica*. Calpionellid zone C, Middle Berriasian. Sample CT40, thin section, normal light.

3a-c – *Calpionella alpina*. (a) Large variety. Calpionellid zone A2, Late Tithonian. Sample CT26, (b) Transitional variety, easily mistaken for *C. elliptica* (cf. pl. 18/2)! Characteristic for topmost calpionellid zone A3, Tithonian/Berriasian boundary interval. Sample CT28. (c) Small, "spherical" variety. Calpionellid zone B, Early Berriasian. Sample CT34. Thin sections, normal light.

4 – *Crassicollaria intermedia*. Calpionellid zone A2, Late Tithonian. Sample CT25, thin section, normal light.

5 – *Crassicollaria brevis*. Calpionellid zone A2, Late Tithonian. Sample CT26, thin section, normal light.

6 – *Crassicollaria parvula*. Calpionellid zone B, Early Berriasian. Sample CT31, thin section, normal light.

7 a-c – *Tintinnopsella carpathica*. (a) Small variety. Calpionellid zone A2, Late Tithonian. Sample CT26. (b) Transitional variety. Calpionellid zone B, Middle Berriasian. Sample CT38. (c) Large variety. Calpionellid zone C, Middle Berriasian. Sample CT40. Thin sections, normal light.

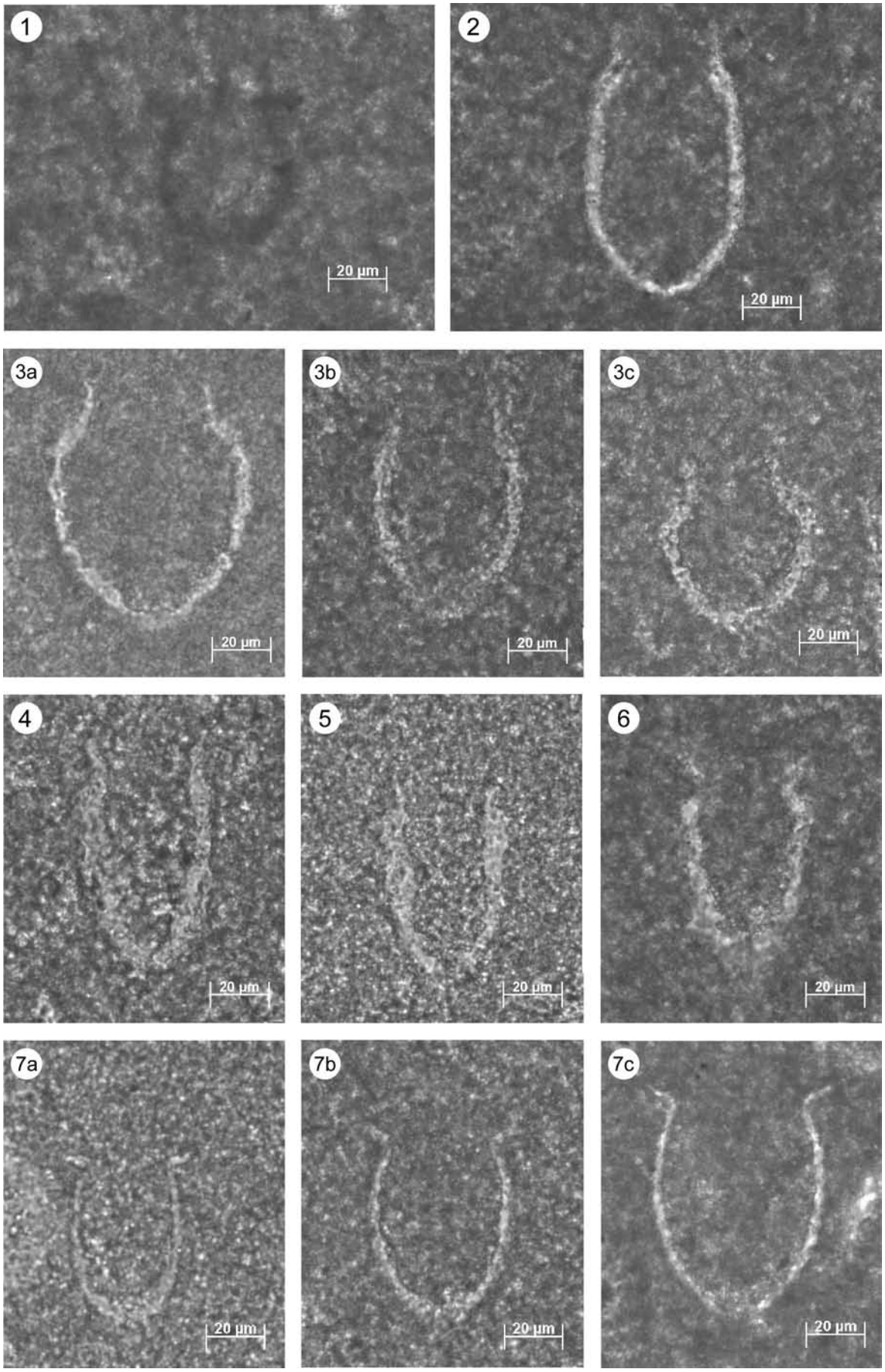
1
20 µm
2
20 µm
3a
20 µm
3b
20 µm
3c
20 µm
4
20 µm
5
20 µm
6
20 µm
7a
20 µm
7b
20 µm
7c
20 µm

Plate 19 – Basin: microfacies

1 – Filament-dominated wackestone. Microfilament zone, Late Kimmeridgian. Sample CT2, thin section, normal light.

2 – *Saccocoma*-dominated wackestone. *Saccocoma* peak base lower *Saccocoma* zone, Early Tithonian. Sample CT7, thin section, normal light.

3 – Radiolarian-dominated wackestone. Topmost Microfilament zone / basal lower *Saccocoma* zone?, Late Kimmeridgian. Sample CT4, thin section, normal light.

4 – Calpionellid-dominated wackestone. Upper Saccocoma zone, Late Tithonian. Sample CT26, thin section, normal light.

5 – Lithoclast containing an agglutinating foraminifer (*Pseudocyclammina/Everticyclammina* sp.?) that lived predominantly in lagoonal environments. Sample CT13, thin section, normal light.

6 – Intraclastic limestone. Sample CT15, etched slab.

7 – Plane-bedded, calcarentic turbidite. Sample CT14, thin section, normal light.

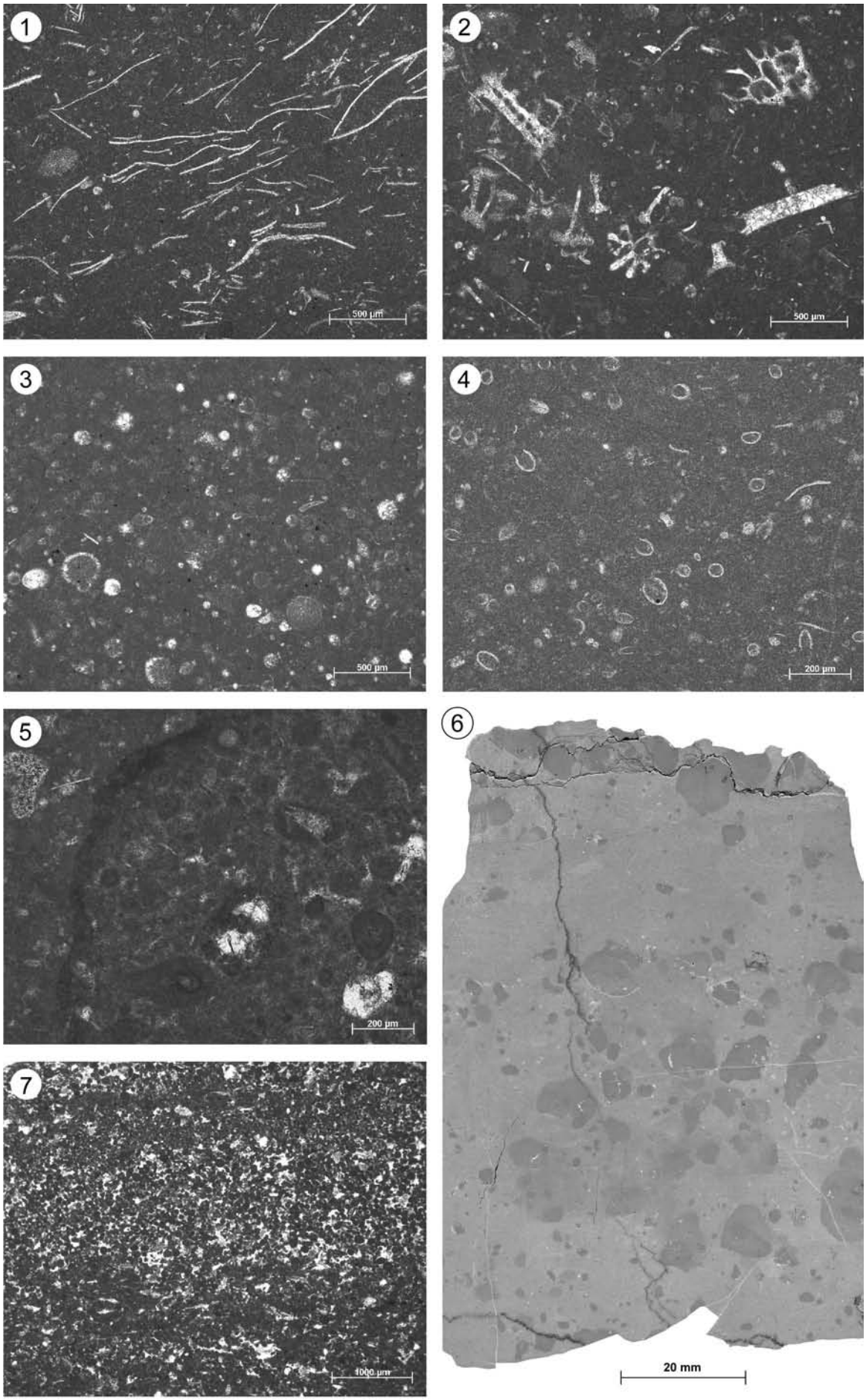
1
500 µm
2
500 µm
3
500 µm
4
200 µm
5
200 µm
6
20 mm
7
1000 µm

Plate 20 – Platform sections

1 – In the Noirvaux section, the boundary between the Reuchenette Formation and the Twannbach Formation (90.3 m) is expressed as a sharply defined erosion surface, easily recognizable in outcrop due to different weathering colour (Upper Reuchenette Formation grey, basal Twannbach Formation cream-coloured) and an abrupt change in sedimentary architecture. Also note SBZ $Ti1_{Tethyan}$, lithologically expressed as a soft-weathering dolomite cap.

2 – Top of the Noirvaux section (ca. 152-155 m). The step in the center of the image consists mainly of laminated tidal flat deposits (SBZ $Ti3_{Tethyan}$).

3 – La Dôle section (ca. 115-133 m). The Dôle section is the only measured platform section that consists to a 100% of a natural cliff and by thousands of years of weathering. Here, the stacking pattern of superimposed depositional sequences of different scales translated nearly perfectly into outcrop morphology: Small-scale sequence 64 begins with an erosional surface and consists mainly of thinning-up, dolomitized tidal-flat deposits. Small-scale sequence 65 begins with an abrupt lithology change linked to a SB/TS (both small- and medium-scale). The overlying limestone-bundle is capped by a surface showing features of early cementation (MFS). The rest of the sequence is a dolomitized shallowing-up succession that terminates with wavy stromatolites. Small-scale sequence 66 consists mainly of tidal-flat deposits. Yet, it shows a thickening-up trend that is due to its position just below a medium-scale MF. Small-scale sequence 67 begins with a SB/TS, directly followed by the most open-marine facies (medium-scale MF). Small-scale sequences 68 and 69 are completely dolomitized, much reduced in thickness, and separated by a karstified surface that also acts as medium-scale sequence boundary

4 – Upper part of the Yenne section, with the prominently marked boundary between the Goldberg Formation and the Pierre-Châtel Formation. The formation boundary is an approximately 1m-thick, soft-weathering interval showing signs of emersion, pedogenesis, and reworking. Based on cyclostratigraphic analysis (correlations and reinterpretation of Strasser 1994), it is assumed to represent two merged sequence boundaries (SB Be3 and SB Be4), i.e. a hiatus of 800 ka or more.

5 – Le Lieu section around electric pole n° 21.

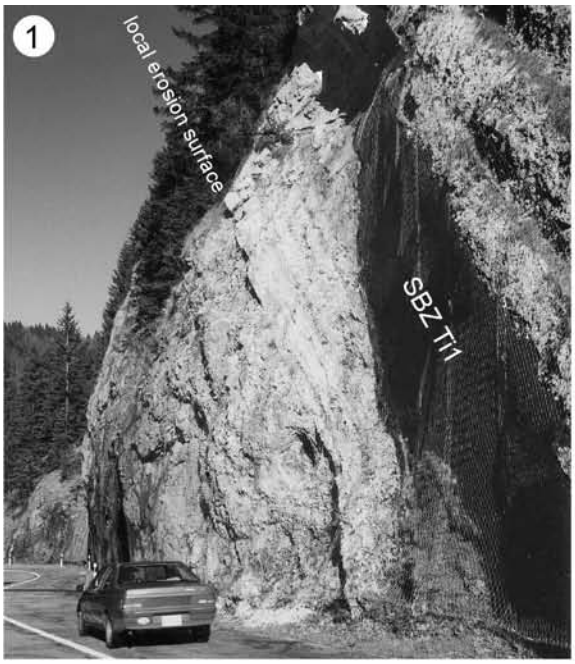
1
local erosion surface
SBZ Ti1


2

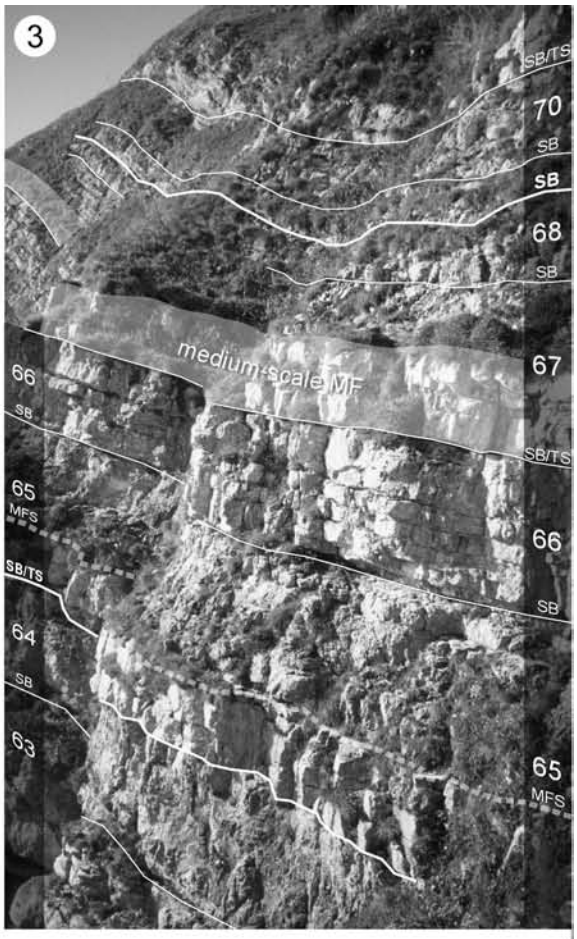
3
SB/TS
70
SB
SB
68
SB
medium-scale MF
66
SB
67
SB/TS
65
MFS
66
SB/TS
SB
64
SB
63
65
MFS


4
base Pierre-Châtel Fm.
merged SBs Be3 & Be4
Goldberg Fm.
"Purbeckian"


5

Plate 21 – Slope & basin sections

1 – Clue de la Payre cliffs. Photo taken from the riverside footpath at the bottom of the Payre valley, looking north.

2 – Broyon quarry. Channeled debris-flow deposits at the foot of the quarry wall (Photo by A. Strasser).

3 – Poteu de Mié section, view from Montbas-Dessus.

4 – Northern flank of the Clue de Taulanne section. Photo taken from the N85, looking north-east.

5 – Clue de Taulanne section. Bedding plane (view from above) with large, subrounded, resedimented clasts and clods (SB/TS Be4, 130.8 m - northern end of the parking lot at the gap in the cliff through which the N85 and the Taulanne River pass).

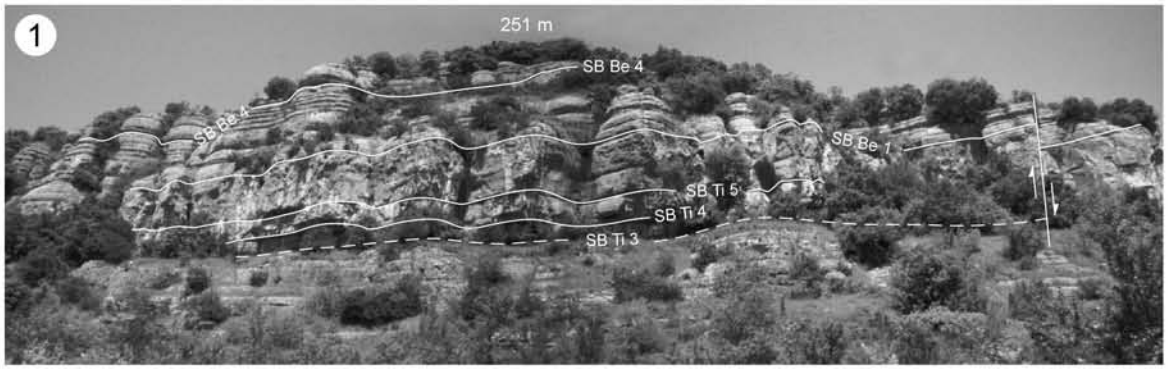
1
251 m
SB Be 4
SB Be 4
SB Be 1
SB Ti 5
SB Ti 4
SB Ti 3

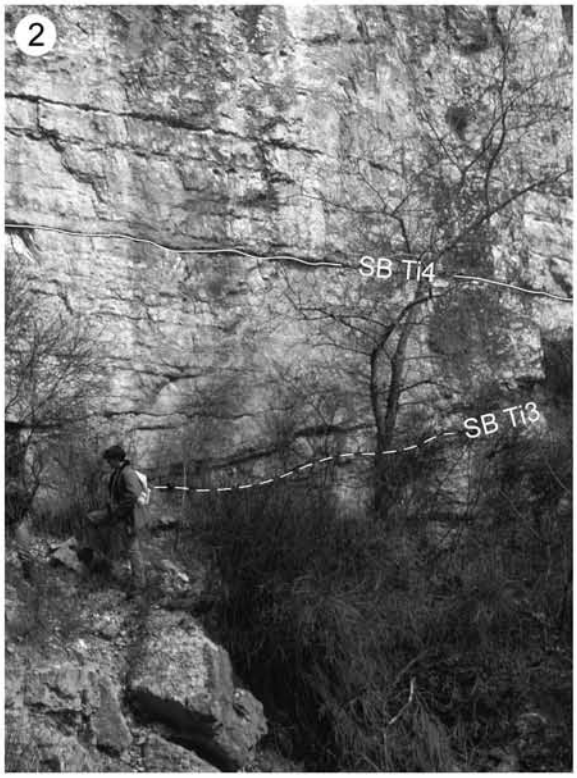
2
SB Ti4
SB Ti3

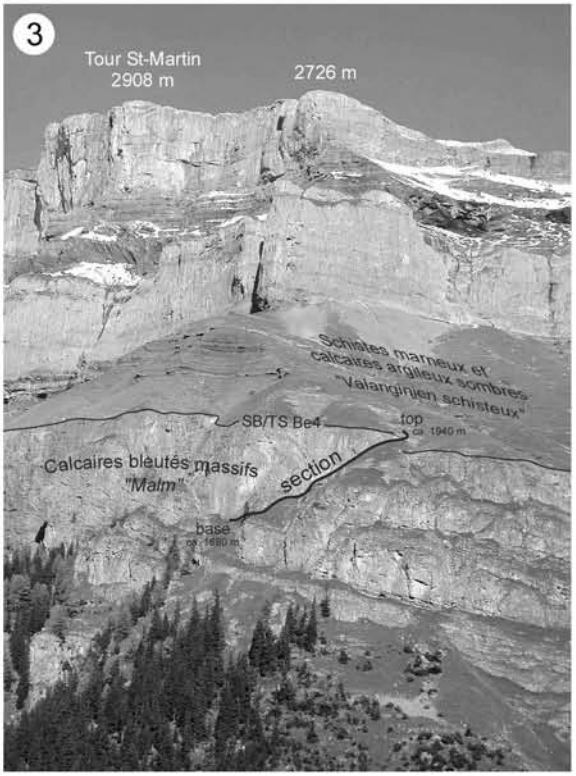
3
Tour St-Martin
2908 m
2726 m
Schistes marneux et
calcaires argileux sombres
"Valanginien schisteux"
SB/TS Be4
top
ca. 1940 m
Calcaires bleutés massifs
"Malm"
section
base
ca. 1680 m


4
St-Vincent
1440 m
SB/TS Be4
SB Be1
joint with chert nodules
lenticular marl layer
SBZ Ti 3
SB Ti 2?
MF/CS
Kim5
N 85 (ca. 1010 m)


5

ANNEX

Sample no.	**Mica001** 8.8°	**K001-C002** 12.2°	**K001** 12.1-2°	**C002** 12.2-3°	**K002** 24.8-9°	**C004** 25.1-2°	**K001 calc**	**C002 calc**	**K/I ratio** K001 / Mica001	**illite crystallinity index** (deg)
No103	109	34			43	25	21.48	12.40	0.20	0.39
No111	406	59	59	57	46	42	31.09	27.91	0.08	0.61
No115	565	52			33	25	29.83	22.60	0.05	0.95
No120	392	97			85	48	61.87	34.68	0.16	0.22
No125	302	42			13	18	17.71	24.51	0.06	0.15
No132	351	88	88	85	55	45	48.19	39.43	0.14	0.21
No141	288	54			37	13	40.28	14.15	0.14	0.20
No148	495	183	183	108	105	62	115.10	67.90	0.23	0.21
No157	633	196			126	68	127.07	68.70	0.20	0.27
No164	478	108	97	108	46	54	49.54	58.79	0.10	0.20
No170	432	121	103	121	83	83	60.48	60.52	0.14	0.18
No174	523	188	125	188	86	100	86.72	100.86	0.17	0.23
No178	737	147			85	63	84.48	62.79	0.11	0.27
No183	923	100			18	32	35.95	63.92	0.04	1.35
No188	722	371			338	108	280.68	89.87	0.39	0.57
No192	529	136			141	60	95.72	40.70	0.18	0.82
No199	1109	241			142	141	120.59	119.93	0.11	1.01
No205	692	127	63	127	53	47	67.00	60.00	0.10	0.39
No212	378	120	71	120	30	66	37.50	82.50	0.10	0.24
No219	470	164	78	164	38	98	45.82	118.18	0.10	0.27
No225	278	289			56	202	62.70	226.18	0.23	0.24
No229	948	216			46	112	62.92	153.18	0.07	0.28
No235	837	272			177	99	174.70	97.57	0.21	0.31
No238	475	191	191	88	168	89	124.83	66.17	0.26	0.29
No244	1112	253	253	115	191	114	158.23	94.77	0.14	0.86
No247	1423	279			159	95	174.58	104.69	0.12	0.82
No251	1011	172	172	82	68	59	92.09	79.91	0.09	0.62
No259	706	289			203	94	198.27	91.13	0.28	0.83
No265	423	80	25	80	24	60	22.86	57.14	0.05	0.46
No274	649	64			0	50	0.00	63.58	0.00	0.82
No278	514	276			185	73	197.67	78.15	0.38	0.41
No283	1039	676			591	85	591.42	85.06	0.57	0.52
No293	1427	286			243	82	213.34	72.33	0.15	0.40
No305	1028	188			81	105	82.24	106.09	0.08	0.80
No309	1079	165			26	74	42.86	121.97	0.04	0.88
No314	1243	161			98	78	89.34	71.16	0.07	0.98

Annex 1 - Clay mineral data (fraction < 2 μm) from the Noirvaux section.

Sample no.	**Mica 001** 8.8°	**K001-C002** 12.2°	**K001** 12.1-2°	**C002** 12.2-3°	**K002** 24.8-9°	**C004** 25.1-2°	**K001 calc**	**C002 calc**	**K/I ratio** K001 / Mica001	**illite crystallinity index** (deg)
P1.3	1045	1092			992	124	971.00	121.38	0.93	0.30
P2.3	1016	994			847	178	821.18	172.95	0.81	0.50
P5	958	704			552	191	523.30	181.13	0.55	0.57
P9.1	818	832			739	156	686.68	144.95	0.84	0.47
P11	809	794			633	149	642.57	151.31	0.79	0.60
P14	909	963			833	75	883.78	79.57	0.97	0.34
P17	754	625			545	84	541.85	83.52	0.72	0.27
P20.1	382	317			284	79	247.95	68.97	0.65	0.30
P22.1	612	173			144	36	138.66	34.67	0.23	0.28
P22.3	628	176			124	88	102.46	73.21	0.16	0.40
P24	671	346			389	75	289.86	55.89	0.43	0.67
P28	891	702			622	175	547.46	154.07	0.61	0.59
P31	780	444			478	57	396.61	47.27	0.51	0.95
P34	483	244			160	71	169.72	74.61	0.35	0.37
P40.1	601	319			238	59	256.09	63.11	0.43	0.92
P43.2	984	204			145	73	135.76	68.46	0.14	1.02
P46	1095	593			527	69	524.33	68.60	0.48	1.16
P51.2	1059	773			771	87	694.56	78.37	0.66	1.19
P53.2	384	81			17	16	41.50	39.05	0.11	0.21
P58	658	51			0	0	25.55	25.55	0.04	0.31
P60.1	518	54			17	21	24.10	29.78	0.05	0.51
P62.3	449	51			45	24	33.03	17.62	0.07	0.27
P64	1014	136			67	92	57.31	78.62	0.06	0.90
P71	709	82			0	39	0.00	81.67	0.00	1.01
P82.1	964	36	31	36	24	8	27.00	9.00	0.03	1.03
P86	242	30			18	8	21.00	9.33	0.09	0.20
P90	353	21			18	21	9.69	11.31	0.03	0.90
P93.2	244	34	23	34	9	19	10.93	23.07	0.04	0.16

Annex 2 - Clay mineral data (fraction < 2 µm) from the Lieu section.

Sample no.	Mica 001 8.8°	K001-C002 12.2°	K001 12.1-2°	C002 12.2 3°	K002 24.8-9°	C004 25.1-2°	K001 calc	C002 calc	K/I ratio (K001 / Mica001)	illite crystallinity index (deg)
Do119	208	429	429	86	441	59	378.38	50.62	1.82	0.17
Do120	384	292	301	36	225	67	225.00	67.00	0.59	0.16
Do122	356	341	358	10	301	33	307.31	33.69	0.86	0.20
Do123	328	363			344	81	293.82	69.18	0.90	0.15
Do125	445	679			535	78	592.60	86.40	1.33	0.28
Do128	850	207	217	92	138	56	147.25	59.75	0.17	0.35
Do131	203	74			59	30	49.06	24.94	0.24	0.17
Do132	437	270	261	50	188	56	208.03	61.97	0.48	0.24
Do135	362	52			57	28	34.87	17.13	0.10	0.17
Do137	565	112	68	128	28	72	31.36	80.64	0.06	0.19
Do141	751	189			11	92	20.18	168.82	0.03	0.10
Do142	882	134			25	32	58.77	75.23	0.07	0.24
Do143	592	72			32	36	33.88	38.12	0.06	0.25
Do144	537	39	11	39	0	26	0.00	39.00	0.00	0.74
Do146	432	41	35	38			35	38	0.08	0.69
Do148	243	33			24	22	17.22	15.78	0.07	0.47
Do150	427	74	79	69	29	28	37.65	36.35	0.09	0.21
Do153	710	97			60	55	50.61	46.39	0.07	0.31
Do157	402	67	67	50	48	38	37.40	29.60	0.09	0.18
Do158	274	40			34	24	23.45	16.55	0.09	0.21
Do159	149	86	93	41	92	32	63.81	22.19	0.43	0.23
Do160	335	96	85	86	52	64	43.03	52.97	0.13	0.45
Do163	136	34			31	23	19.52	14.48	0.14	0.14
Do164	496	68	67	55	48	50	33.31	34.69	0.07	0.50
Do166	257	60	25	66	27	40	24.18	35.82	0.09	0.21
Do168	570	64	46	66	19	21	30.40	33.60	0.05	0.75
Do170	304	391	404	67	356	106	301.29	89.71	0.99	0.20
Do174	293	54	29	55	23	31	23.00	31.00	0.08	0.27
Do176	185	722	747	73	783	63	668.23	53.77	3.61	0.28

Annex 3 - Clay mineral data (fraction < 2 μm) from the Dôle section.

Sample no.	$\delta^{18}O$	$\delta^{13}C$
Av130	-1.82	2.03
Av132	-1.96	2.30
Av134	-2.11	2.31
Av137	-1.18	1.88
Av138	2.04	2.33
Av140	-2.22	1.67
Av141	-1.12	2.05
Av142	-4.80	-3.88
Av143	0.09	1.33
Av144	-2.76	1.61
Av146	-2.10	2.32
Av218 burrow	-0.26	2.83
Av218 matrix	-1.97	2.20
Do100	-0.83	2.25
Do113 burrow	1.48	2.96
Do113 matrix	-1.94	2.63
Do140 burrow	0.66	2.79
Do140 matrix	-2.36	1.95
Do189	-6.07	-5.60
Do193	2.19	2.15
Do197	-6.09	-2.21
Do98	-2.10	2.28
Do99	-1.52	2.28
No106 burrow	0.26	3.06
No106 matrix	-4.27	1.96
No126	-5.04	0.83
No128	-4.97	0.47
No131	-5.96	1.50
No132	-3.89	1.93
No134	-3.52	1.74
No136	-5.10	-2.00
No138	-3.85	1.25

Sample no.	$\delta^{18}O$	$\delta^{13}C$
No140	-4.02	1.29
No143	-3.52	1.68
No145	-0.84	2.11
No146	-1.54	1.83
No147	1.89	2.61
No150	-1.16	2.16
No152	-1.60	2.00
No153	1.85	2.56
No155	-2.79	1.85
No156	-4.28	0.57
No157	-4.67	0.61
No159	-4.44	0.77
No161	-4.95	-0.10
No162	-3.34	0.71
No235	-3.35	1.62
No236	-2.41	1.66
No239	0.69	2.55
No240	0.26	2.62
No242	0.69	2.70
No243	1.85	3.13
No245	0.60	2.30
No248	1.78	3.08
No249	1.20	2.85
No250	1.61	2.84
No251	-0.64	2.33
No252 burrow	-0.03	2.24
No252 matrix	-2.76	1.99
No253	-3.01	1.21
No255	-3.09	0.85
P89	-6.42	-0.89
P96b	-3.57	-2.33
P98-3	-6.14	0.92

Annex 4 - Stable isotope data.

Curriculum vitae

I was born in Frankfurt a.M., Germany, on the 16th of October, 1971 to Helmut and Susanne Rameil (born Böttner). I am quite sure that the fascination for geosciences struck me already in my early years, although I was not aware of it then. Perhaps it developed because I stuck my nose into the mud more frequently than other children did and those who are not allowed to play in mud holes rather tend to study economics, law, or computer science when they grow up eventually. My parents may even have taken a more direct influence when they took me along for mountain hiking as soon as I was able to walk longer distances (not to mention some vague memories of having been carried around before). Anyway, the fascination has not faded yet, this is the central issue.

After obtaining the *Abitur* (German university entrance degree) from the Friedrich-Dessauer-Gymnasium in 1991 and the following 15 months of community service at the Bavarian Red Cross (both in Aschaffenburg, Germany), I was temporarily side-dragged by "hard science" and enrolled in October 1992 as a student of physics at the Darmstadt University of Technology (Germany). However, I abandoned the vague idea of studying geophysics as principal subject rather quickly and found myself as a full-time student of geology as soon as spring 1993. Having passed the *Vordiplom* (intermediate exams) in 1995, I began my graduate studies, which finally led to the diploma degree in geology (German MSc equivalent), issued at the Darmstadt University of Technology in April 1999. My diploma thesis entitled "*Palynofacies, sedimentology and sequence analysis in the Lower Muschelkalk (Middle Triassic, Anisian) of East Thuringia (Steudnitz quarry near Jena, Germany)*" (written in German language) was carried out under the guidance of Dr Susanne Feist-Burkhardt and Dr Annette E. Götz.

After working a few months in a consulting engineer's office for soil mechanics and dangerous waste and some subsequent travelling, I began my PhD thesis on sedimentology, sequence- and cyclostratigraphy of the Tithonian of the Swiss and French Jura Mountains under the direction of Prof. André Strasser in Fribourg (Switzerland) in October 1999. I occupied the position of a research and teaching assistant at the Department of Geosciences of the University of Fribourg, financed by the Swiss National Science Foundation (projects no. 20-56491.99 and 20-67736.02) and the University of Fribourg.

Fribourg, 22. August 2005

Already published:

vol 1 **HILLGÄRTNER, Heiko** (1999) The evolution of the French Jura platform during the Late Berriasian to Early Valanginian: controlling factors and timing. (203 pp.)

vol 2 **DUPRAZ, Christophe** (1999) Paléontologie, paléoécologie et évolution des faciès récifaux de l'Oxfordien Moyen-Supérieur (Jura suisse et français). (247 pp.)

vol 3 **BASSANT, Philip** (1999) The high-resolution stratigraphic architecture and evolution of the Burdigalian carbonate-siliciclastic sedimentary systems of the Mut Basin, Turkey. (278 pp. + annex in colour)

vol 4 **COLOMBIÉ, Claude** (2002) Sédimentologie, stratigraphie séquentielle et cyclostratigraphie du Kimméridgien du Jura suisse et du Bassin vocontien (France) : relations plate-forme – bassin et facteurs déterminants. (198 pp.)

vol 5 **PICOT, Laurent** (2002) Le Paléogène des synclinaux du Jura et de la bordure sud-rhénane : paléontologie (Ostracodes), paléoécologie, biostratigraphie et paléogéographie. (240 pp.)

vol 6 **DAPPLES, Florence** (2002) Instabilités de terrain dans les Préalpes fribourgeoises (Suisse) au cours du Tardiglaciaire et de l'Holocène : influence des changements climatiques, des fluctuations de la végétation et de l'activité humaine. (158 pp.)

vol 7 **HUG, Wolfgang Alexander** (2003) Sequenzielle Faziesentwicklung der Karbonatplattform des Schweizer Jura im Oberoxford und unterstem Kimmeridge. (154 pp.)

vol 8 **OSWALD, Daniel** (2003) Analyse de l'activité de glissements de terrain et relation avec les conditions climatiques : Exemples dans les Préalpes fribourgeoises (Suisse). (147 pp.)

vol 9 **BECKER, Damien** (2003) Paléoécologie et paléoclimats de la Molasse du Jura (Oligo-Miocène) : apport des Rhinocerotoidea (Mammalia) et des minéraux argileux. (327 pp.)

vol 10 **DELALOYE, Reynald** (2005) Contribution à l'étude du pergélisol de montagne en zone marginale. (240 pp.)

vol 11 **FREUDIGER-BONZON, Jeanne** (2005) Archaeometrical study (petrography, mineralogy and chemistry) of Neolithic Ceramics from Arbon Bleiche 3 (Canton of Thurgau, Switzerland). (187 pp.)

vol 12 **STOFFEL, Markus** (2005) Spatio-temporal variations of rockfall activity into forests - results from tree-ring and tree analysis. (188 pp.)

GeoFocus is the publication series of the Department of Geosciences, Geology and Paleontology, University of Fribourg, Switzerland, and can be ordered at:

Department of Geosciences - Geology and Paleontology
University of Fribourg
1700 Fribourg, Switzerland
http: //www.unifr.ch/geoscience/geology

ISSN 1424 - 1463